Attachment S-1

References

Hydration and Cation Exchange during Subgrade Hydration and Effect on Hydraulic Conductivity of Geosynthetic Clay Liners

Sabrina L. Bradshaw, A.M.ASCE[1]; Craig H. Benson, F.ASCE[2]; and Joseph Scalia IV, M.ASCE[3]

Abstract: Experiments were conducted to evaluate cation exchange during hydration of geosynthetic clay liners (GCLs) used in composite hydraulic barriers and the effect on their hydraulic conductivity. GCLs arranged in a composite barrier configuration were hydrated by contact with moist compacted subgrades (two clays, one silt, and one sand) under a confining stress of 10 kPa for 30 days to 1 year. No measurable exchange occurred in GCLs hydrated for 30 days. For hydration periods longer than 30 days, the exchange increased as the duration of hydration increased. The exchange during subgrade hydration had no measurable effect on the hydraulic conductivity to deionized (DI) water. However, if the GCL was desiccated after hydration, the hydraulic conductivity increased more than 1,000-fold. Dissolution of calcite within the bentonite during permeation with DI water also induced the replacement of sodium by calcium; however, this additional exchange had no measurable effect on the hydraulic conductivity to DI water. Data from two case histories indicate that calcium and/or magnesium in the subgrade, or in calcite within the GCL, eventually will replace nearly all sodium in GCLs used in composite barriers. The data also indicate that cover soil should be deployed expediently on composite barriers with GCLs to prevent wet-dry cycling and corresponding impacts on hydraulic conductivity. **DOI: 10.1061/(ASCE)GT.1943-5606.0000793.**

CE Database subject headings: Subgrades; Geosynthetics; Clay liners; Bentonite; Hydration; Hydraulic conductivity; Water content; Barriers.

Author keywords: Geosynthetic clay liner; Bentonite; Cation exchange; Subgrade hydration; Hydraulic conductivity; Water content; Landfill; Barrier; Composite liner.

Introduction

Composite hydraulic barriers consisting of a fine-grained soil barrier overlain by a geomembrane are commonly used in liners and covers in waste containment systems. In many cases, a geosynthetic clay liner (GCL) is used as the soil barrier. GCLs consist of a thin layer of granular or powdered bentonite clay encased between two geotextiles or glued to a geomembrane. Hydraulic conductivity of the bentonite is the most important factor affecting the hydraulic efficacy of a GCL. Montmorillonite is the predominant clay mineral in bentonite and is characterized by high cation exchange capacity (CEC), large specific surface area, and the potential to develop a thick layer of bound water (Grim 1968; Mitchell and Soga 2005; Meer and Benson 2007; Scalia and Benson 2011). This bound water layer, manifested as bentonite swell, contributes to the very low hydraulic conductivity of bentonite to water (Jo et al. 2001; Kolstad et al. 2004; Lee et al. 2005; Meer and Benson 2007; Scalia and Benson 2011).

[1]Research Scientist and Outreach Coordinator, Geological Engineering, Univ. of Wisconsin, 1415 Engineering Dr., Madison, WI 53706 (corresponding author). E-mail: sbradshaw@wisc.edu

[2]Wisconsin Distinguished Professor and Chair, Geological Engineering, and Director of Sustainability Research and Education, Office of Sustainability, Univ. of Wisconsin, 1415 Engineering Dr., Madison, WI 53706. E-mail: chbenson@wisc.edu

[3]Ph.D. Candidate, Geological Engineering, Univ. of Wisconsin, 1415 Engineering Dr., Madison, WI 53706. E-mail: scalia@wisc.edu

Note. This manuscript was submitted on January 4, 2012; approved on June 19, 2012; published online on August 1, 2012. Discussion period open until September 1, 2013; separate discussions must be submitted for individual papers. This paper is part of the ***Journal of Geotechnical and Geoenvironmental Engineering***, Vol. 139, No. 4, April 1, 2013. ©ASCE, ISSN 1090-0241/2013/4-526–538/$25.00.

Bentonite swell and hydraulic conductivity are strongly influenced by the cation occupying the interlayer region of the montmorillonite mineral. When monovalent cations such as Na^+ are predominant in the interlayer region, bentonites undergo both crystalline and osmotic swell during hydration, which maximizes the bound water fraction and minimizes the hydraulic conductivity. In contrast, when polyvalent cations (e.g., calcium and magnesium) are predominant in the interlayer region, bentonites only undergo crystalline swell during hydration (Norrish 1954; Norrish and Quirk 1954), which limits the bound water fraction and results in higher hydraulic conductivity (Mesri and Olson 1971; Jo et al. 2001, 2004; Kolstad et al. 2004; Guyonnet et al. 2005; Meer and Benson 2007; Scalia and Benson 2011). Here, for conciseness the cations are shown with their atomic symbol but without the charge superscript; i.e., Na^+ = Na, Ca^{2+} = Ca, and Mg^{2+} = Mg.

In most cases, Na is the primary interlayer cation present when a GCL is manufactured (Jo et al. 2001; Kolstad et al. 2004). After installation, the Na cations are susceptible to exchange by divalent cations present in the surrounding pore water and from dissolution of calcite within the GCL itself (James et al. 1997; Guyonnet et al. 2005; Rauen 2007). These exchange reactions are thermodynamically favorable (Sposito 1981) and can alter the hydraulic conductivity. Examples exist where near complete replacement of Na by Ca and Mg has occurred in situ (Melchior 2002; Egloffstein 2002; Benson et al. 2007, 2010; Meer and Benson 2007; Scalia and Benson 2011).

Meer and Benson (2007) and Scalia and Benson (2011) indicated that these exchange reactions can occur when a GCL hydrates on a subgrade because cations move upward into the GCL in response to advective and diffusive gradients during hydration. Based on an analysis of field data, Scalia and Benson (2011) suggested that cation exchange caused by subgrade hydration is inevitable in

environments were Ca and Mg are abundant in the subgrade. They also hypothesized that this exchange has minimal impact on the hydraulic conductivity of the GCL to water if the GCL is hydrated on a subgrade prepared with a water content greater than optimum, which promotes osmotic swelling (Scalia and Benson 2011).

In this study, cation exchange during subgrade hydration was studied systematically using experiments mimicking the in situ condition of a GCL in a composite barrier where bentonite in the GCL was hydrated by contact with a moist subgrade without the influence of water entering from overlying soil layers. The water content, relative abundance of cations in the exchange complex, swell index of the bentonite, and hydraulic conductivity of the GCL were evaluated at various times over a 365-day period. The influence of the effective stress on the hydraulic conductivity of GCLs exposed to varying amounts of cation exchange has been evaluated. Inferences regarding the field-scale conditions are drawn using data from these experiments along with field data from two case histories.

Background

When a GCL is installed, the bentonite is usually dry relative to the atmosphere and surrounding soils. Hydration of the bentonite begins immediately as moisture from the atmosphere and from adjacent soils is drawn in by gradients in the water vapor pressure and matric potential.

The U.S. Environmental Protection Agency (USEPA 1996a, b) examined the hydration of a needle-punched GCL in the laboratory under a confining stress of 10 kPa on a low-plasticity clay compacted at three different water contents (16, 20, and 24%). The water content of the GCL increased rapidly for approximately the first 20 days and then the rate of increase slowly diminished. At the end of testing (75 days), the water content of the GCL ranged from 45 to 100%, with higher final water content corresponding to subgrades compacted with higher water content. Thiel and Criley (2005), Rayhani et al. (2011), and Rowe and Abdelatty (2011) reported similar temporal evolution of water content.

Rayhani et al. (2011) hydrated three different needle-punched GCLs in the laboratory under a confining stress of 2 kPa on a silty sand compacted to 5, 10, 16, and 21% water content. The water content of the GCLs was determined periodically over 30 weeks. For GCLs hydrated on the silty sand for 30 weeks, the final water content was 34–141% for GCL 1, 40–116% for GCL 2, and 83–119% for GCL 3. The final water content of the GCLs was proportional to the subgrade water content (i.e., higher subgrade water content equated to higher GCL water content). GCLs hydrated on the silty sand compacted at 10% (near an optimum water content of 11.4%) had water contents ranging from 85 to 102% after 30 weeks.

Rowe and Abdelatty (2011) hydrated a Na-bentonite GCL in the laboratory under a confining stress of 15 kPa on a silty-sand subgrade compacted at a water content of 13.9%. The subgrade was moistened with a 13.5-mM calcium chloride solution to simulate calcium-rich soil. The water content and swell of the GCL were measured periodically over 625 days. The GCL had a maximum water content of 86% at 279 days of hydration and a final GCL water content of 68% at 625 days. The loss in water content in the GCL was attributed to the loss of bound water when Ca replaced Na in the bentonite. The swell index decreased with increasing hydration time, indicating that Ca was replacing Na in the bentonite during subgrade hydration. The hydraulic conductivity of the GCLs increased from 1 to 3×10^{-9} cm/s (no subgrade hydration) to 2×10^{-8} cm/s after 625 days of subgrade hydration.

Meer and Benson (2007) and Scalia and Benson (2011) exhumed GCLs in composite barriers in landfill covers that had been in service for 3.1–6.7 years. Because these GCLs were covered by intact geomembranes (no defects were evident in the geomembranes during the exhumations in either study) and were firmly in contact with the subgrade, pore water migrating upward from the subgrade was responsible for hydration of the bentonite and contributed to the cation exchange. Meteoric water percolating through the cover and contacting the overlying geomembrane probably had little or no contribution to the hydration or cation exchange.

The GCL samples exhumed by Meer and Benson (2007) were from the final cover of a Wisconsin landfill (Site S in Meer and Benson 2007) where the GCL had been in service for 4.1 years. The cover consisted of 900 mm of well-graded silty sand over a 1.5-mm-thick textured high-density polyethylene geomembrane, needle-punched GCL, and a compacted clayey-sand subgrade (water content = 13%; calcite content = 1%). The water content of the exhumed GCL ranged from 57.9 to 60.9%, the swell index of the bentonite averaged 9.4 mL/2g, and the mole fraction of Na in the exchange complex (X_{Na}) decreased from 0.65–0.74 (as built) to 0.18–0.22 (exhumation); Ca ($X_{Ca} = 0.61-0.68$) and Mg ($X_{Mg} = 0.09-0.13$) replaced the Na. The hydraulic conductivity of the exhumed GCL samples to deionized (DI) water and to 10-mM $CaCl_2$ solution ranged between 10^{-5} and 10^{-4} cm/s, whereas the hydraulic conductivity was $\approx 10^{-9}$ cm/s when the GCL was installed.

Scalia and Benson (2011) exhumed GCLs from four landfill final covers with composite barriers that were in service for 3.1–6.7 years. Each composite barrier had a cover soil layer over a geomembrane and a needle-punched GCL. Two landfills had a geosynthetic drainage layer between the cover soil and the geomembrane. The cover soil layer thickness ranged from 300 to 1,200 mm, with a typical cover thickness of 900 mm. The water content of the exhumed GCLs increased systematically with increasing subgrade water content. Na replacement by Ca or Mg was more extensive in the GCLs placed adjacent to the subgrades with higher water content.

The GCLs that had exhumed water contents greater than 50% had low hydraulic conductivities ($\approx 10^{-9}$ cm/s) when permeated with a 10-mM $CaCl_2$ solution and were adjacent to subgrades placed at or above optimum. The GCLs with exhumed water contents of less than 50% were adjacent to subgrades placed at water contents less than optimum and had higher hydraulic conductivities ($>10^{-7}$ cm/s). The higher hydraulic conductivities of the GCLs placed on drier subgrades was attributed to nonexistence or incomplete osmotic swell of the bentonite prior to replacement of Na by Ca and Mg.

Scalia and Benson (2011) hypothesized that the hydration and swell of bentonite in GCLs placed on subgrades prepared wet of optimum occurred rapidly relative to cation exchange, which induced the osmotic swell and provided tightly bound water molecules in the interlayer that retained a swollen structure and maintained low hydraulic conductivity, even if the cation exchange occurred subsequently; in contrast, cation exchange occurred concomitant with hydration when the GCLs were placed on drier subgrades because the rate of hydration was slower. If sufficient replacement of Na occurs prior to appreciable hydration, osmotic swell is precluded and the hydraulic conductivity of the GCL is much higher.

Some of the GCLs from composite barriers that were examined by Meer and Benson (2007) and Scalia and Benson (2011) contained preferential flow paths and high hydraulic conductivity, even though they were placed on subgrades compacted wet of optimum. Scalia and Benson (2010) reported that these preferential flow paths coincided with MnO precipitates that formed along needle-punching fibers in the GCLs. Meer and Benson (2007) did not

J. Geotech. Geoenviron. Eng. 2013.139:526-538.

proffer an explanation for the preferential flow paths they observed. However, anecdotal reports indicated that the geomembrane remained exposed for an extended period after installation (i.e., no cover soil placement), and that condensation in the gap between the geomembrane and GCL may have caused wet-dry cycling of the GCL, resulting in cracking of the bentonite and preferential flow in the cracks.

Materials

Subgrades

Four subgrades (Torpedo sand, Red Wing clay, Boardman silt, and Cedar Rapids clay) were selected to represent various soil types (sand, silt, and clay) and pore water chemistries that may be encountered in subgrades on which GCLs hydrate. The properties of the four subgrades are shown in Table 1.

The major cations and chemical indicators for the pore water of each subgrade were determined by batch elution tests performed according to Section 7 of ASTM D6141 (ASTM 2008) and Meer and Benson (2007). DI water and dry soil were combined at a 1.3:1 liquid-to-solid ratio and tumbled at 30 rpm for a minimum of 24 h. The slurry was centrifuged to separate the liquid and solid phases. Supernatant was filtered through a 0.2-μm filter and then analyzed for concentrations of major cations (Na, Ca, Mg, and K) by inductively coupled plasma/optical emission spectrophotometry (ICP-OES) following USEPA Method 6010B.

The cation concentrations and chemical characteristics including pH, electrical conductivity, redox potential (E_h), cationic strength (I_c), and the ratio of monovalent to divalent cations (RMD) of the pore water are summarized in Table 2. Cationic strength is analogous to ionic strength; however, it is based solely on the contributions of the cations in solution as follows (Rauen and Benson 2008):

$$I_c = \frac{1}{2}\sum C_i z_i^2 \quad (1)$$

where C_i = molar concentration of the ith cation and z_i = valence of the ith cation. The cationic strength was calculated using the molar concentration of four major cations (Na^+, Ca^{2+}, Mg^{2+}, K^+). The RMD is a measure of the relative abundance of monovalent and polyvalent cations in a solution, and is defined as (Kolstad et al. 2004)

$$\text{RMD} = \frac{M_M}{\sqrt{M_D}} \quad (2)$$

where M_M = molar concentration of monovalent cations and M_D = molar concentration of divalent and multivalent cations. Kolstad et al. (2004) indicated that ionic or cationic strength, RMD, and pH are master variables controlling the cation exchange, swelling, and hydraulic conductivity of bentonite.

Cationic strength I_c and RMD for the subgrade pore waters are shown in Fig. 1 along with data for cover soils reported by Meer and Benson (2007) and Scalia and Benson (2011). The data from Meer and Benson (2007) and Scalia and Benson (2011) were obtained using the same batch extraction method used in this study. Here, I_c ranges from 2.2 to 3.7 mM and RMD between 0.0065 and 0.12 $M^{1/2}$. The range of RMD is comparable to the range reported by Meer and Benson (2007) and Scalia and Benson (2011) (RMD = 0.01−0.08 $M^{1/2}$). The I_c for the subgrades tended to be higher than the I_c for the cover soils (I_c = 0.4−3.2 mM) reported by Meer and Benson (2007) and lower than the I_c for cover soils (I_c = 3.0−5.6 mM) reported by Scalia and Benson (2011). Red

Table 1. Properties of the Four Subgrades Used in this Study

Property	Method	Subgrade			
		Torpedo sand	Cedar Rapids clay	Boardman silt	Red Wing clay
USCS classification	ASTM D2487 (ASTM 2008)	SP	CL	ML	CL
Plasticity index	ASTM D4318 (ASTM 2008)	NP	19	3	11
Liquid limit	ASTM D4318 (ASTM 2008)	NP	34	23	28
Percent fines	ASTM D422 (ASTM 2008)	2	52	88	88
Optimum water content (%) per standard Proctor	ASTM D698 (ASTM 2008)	—	12.3	16.4	14.0
Maximum dry unit weight (kN/m^3) per standard Proctor	ASTM D698 (ASTM 2008)	18.6	19.1	17.0	17.9
Percent calcite	Dreimanis (1962)	6.5	4.2	4.4	5.7

Note: Torpedo sand does not have a bell-shaped compaction curve and therefore the optimum water content is not reported. NP = nonplastic.

Table 2. Chemical Characteristics of Pore Water for the Four Subgrades

Property	Method	Subgrade			
		Torpedo sand	Cedar Rapids clay	Boardman silt	Red Wing clay
USCS classification	ASTM D2487 (ASTM 2008)	SP	CL	ML	CL
Plasticity index	ASTM D4318 (ASTM 2008)	NP	19	3	11
Liquid limit	ASTM D4318 (ASTM 2008)	NP	34	23	28
Percent fines	ASTM D422 (ASTM 2008)	2	52	88	88
Optimum water content (%) per standard Proctor	ASTM D698 (ASTM 2008)	—	12.3	16.4	14.0
Maximum dry unit weight (kN/m^3) per standard Proctor	ASTM D698 (ASTM 2008)	18.6	19.1	17.0	17.9
Percent calcite	Dreimanis (1962)	6.5	4.2	4.4	5.7

Note: Torpedo sand does not have a bell-shaped compaction curve and therefore the optimum water content is not reported. NP = nonplastic.

J. Geotech. Geoenviron. Eng. 2013.139:526-538.

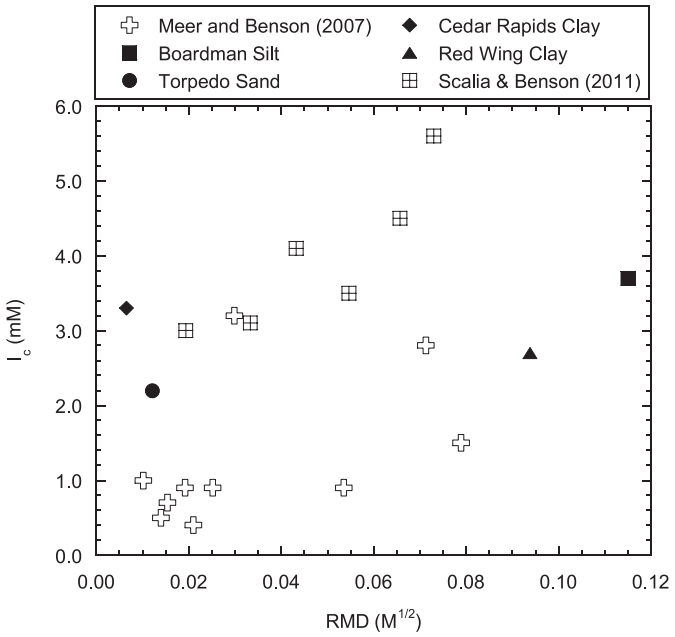

Fig. 1. Cationic strength (I_c) and RMD for cover soils reported by Meer and Benson (2007) and Scalia and Benson (2011) along with I_c and RMD for the pore water of the subgrades in this study

Table 3. CEC, Bound Cation Concentrations, and Soluble Cation Concentrations of the GCL

		Cation concentration ($cmol^+/kg$)[a]				CEC
Occupation site	Cation	Na	Ca	Mg	K	($cmol^+/kg$)
GCL	Bound	33.5	20.7	5.8	0.7	75.8[b]
	Soluble	19.8	0.1	0.1	0.1	

[a]Average of two tests.
[b]Average of 30 tests.

Wing clay and Boardman silt are at the higher end of the range in RMD and are more sodic (Na rich) than Torpedo sand or Cedar Rapids clay.

Geosynthetic Clay Liner

The GCL contained granular Na-bentonite encased by two geotextiles (slit-film woven geotextile and nonwoven staple fiber geotextile) bonded by needle punching. The mass per unit area of the bentonite was 3.66 kg/m^2, the initial thickness of the GCL ranged from 4.3 to 6.2 mm, and the average initial water content of the bentonite was 4.5%. The bentonite granules were predominantly sand sized with 50% of the granules larger than 0.2 mm. X-ray diffraction done by Mineralogy, Inc. (Tulsa, Oklahoma) using a method adapted from Moore and Reynolds (1989) showed that the bentonite contained 51% montmorillonite and 4% calcite. The average CEC was 75.8 ± 4.0 $cmol^+/kg$, with $X_{Na} = 0.55$, $X_{Ca} = 0.34$, $X_{Mg} = 0.10$, and $X_K = 0.01$ (see Table 3).

Methods

Preparation of Subgrades

Subgrade soils were initially oven dried at 105°C and then hydrated with DI water to target water contents of 1% wet of standard Proctor optimum water content for the silt and clays and at the field capacity for the sand (8% water content). The soil was allowed to hydrate for at least 24 h to ensure uniform hydration. After hydration, the soil was compacted following the procedure described in ASTM D698 Method A (ASTM 2008).

Preparation of Geosynthetic Clay Liner Specimens

Rectangular sections of GCL (420×200 mm) were removed from a roll of GCL in a region where the thickness appeared uniform. An arbor press equipped with a steel ring (diameter = 105 mm) was used to punch GCL specimens from the rectangular section. Before the cutting ring was removed, the perimeter of the specimen was wetted with a small amount of DI water to avoid loss of bentonite. The initial weight and thickness of each GCL specimen were measured within 0.1 g and 0.01 mm, respectively, with a laboratory scale and a caliper.

Subgrade Hydration

The GCL subgrade hydration experiments were conducted in flexible-wall permeameters in which the effluent and influent lines were dry and closed. A nonwoven geotextile (mass/area = 240 g/m^2) was placed on an acrylic base plate followed by the extruded compacted subgrade specimen (the sand subgrades were carefully extruded to maintain the shape for experimental assembly), GCL specimen, 1.5-mm geomembrane disk, geotextile disk, and acrylic top plate. The nonwoven face of the GCL was in contact with the subgrade. A latex membrane was placed around the entire assemblage and sealed to the top and bottom plates with three O-rings on each plate. The cell was filled with water and a 10-kPa confining stress was applied to simulate the presence of a leachate collection system or the surface layer in a final cover. A schematic and photographs of the test setup are given in Bradshaw and Benson (2011).

The GCL specimens were hydrated for 30 or 90 days on each subgrade soil, with additional tests performed over 180 and 365 days for Cedar Rapids clay and Red Wing clay. Hydration tests were also conducted for 0.75, 1, 2, and 7 days on Red Wing clay to define the temporal evolution of hydration at short time scales. Two replicate hydration experiments were conducted for each hydration condition. One of the GCLs from the replicate experiments was analyzed immediately after completion of the hydration phase to determine the bound and soluble cation composition and swell index of the bentonite. The other was permeated with DI water to determine the hydraulic conductivity. When the hydraulic conductivity tests were completed, the bentonite from the GCLs was analyzed for bound cations and the swell index.

Additional hydration tests were conducted where the GCL was hydrated solely with water vapor to assess the contributions of liquid- and vapor-phase hydration. A 100-mm-diameter GCL was placed on a perforated plastic plate located above the DI water in a sealed reservoir. The edge of the GCL was covered with a latex membrane and the upper surface was covered with a geomembrane overlain by geotextile. A steel plate (8 kg) was placed on top of the geotextile to apply a 10-kPa dead load. Periodically, the GCL was weighed to determine the water content.

Hydraulic Conductivity Tests

Hydraulic conductivity tests on the GCL were initiated immediately after the hydration phase was complete. Prior to permeation, the geomembrane and subgrade soil were removed and the weight and thickness of each hydrated GCL specimen was measured to ± 0.1 g

J. Geotech. Geoenviron. Eng. 2013.139:526-538.

and 0.01 mm, respectively. The hydraulic conductivity tests were conducted in flexible-wall permeameters using the falling-head-water constant-tail-water method described in ASTM D6766 (ASTM 2008). DI water was used as the permeant liquid with the intention of limiting the cation exchange to subgrade contact only. The GCL specimens were placed between two geotextiles (mass/area = 240 g/m^2) to evenly distribute the permeant liquid. Fresh bentonite paste prepared with DI water was applied along the perimeter of the GCL to ensure an adequate seal between the membrane and GCL.

Overburden stresses of 10, 70, 270, and 520 kPa were applied incrementally to evaluate how effective stress affects hydraulic conductivity. The hydraulic gradient was between 120 and 295. Gradients of this magnitude are not typical in the field; however, they are common when testing GCLs in the laboratory. Shackelford et al. (2000) showed that elevated hydraulic gradients have a much smaller impact on the effective stress and hydraulic conductivity of GCLs because GCLs are thin compared with conventional specimens of clay. Backpressure was not applied to better simulate in situ conditions.

Swell Index

The swell index was measured according to ASTM D5890 (ASTM 2008) using 2 g of oven-dried bentonite added in 0.1-g increments to 90 mL of DI water in a 100-mL graduated cylinder. Bentonite particles adhering to the side of the graduated cylinder were rinsed into the solution using DI water until the total volume reached 100 mL. The volume of hydrated bentonite was measured after 24 h of hydration.

Bound Cations, Soluble Cations, and Cation Exchange Capacity

The bound cations, soluble cations, and CEC were determined according to ASTM D7503 (ASTM 2008). The soluble and bound cation concentrations were determined for the major cations (Na, Ca, Mg, and K) by ICP-OES following USEPA Method 6010B. The CEC was determined using the procedure in ASTM D7503 (ASTM 2008) with the extracted ammonium measured using a Spectronic 20 Genesys spectrophotometer (ThermoFisher Scientific, Waltham, Massachusetts) with the salicylate method (Hach Method 10031; Hach Company 2003).

Results and Discussion

Hydration

The water content of the GCLs hydrated on the subgrades is shown in Fig. 2 as a function of hydration time. The water content increased rapidly for the first 10 days, which was followed by tapering of the hydration rate. The GCL water content increased from 5 to 65% on average during the first 30 days, 65–70% during 30–90 days, and 70–85% between 90 and 365 days.

Data from similar tests performed by USEPA (1996a, b), Thiel and Criley (2005), Rayhani et al. (2011), and Rowe and Abdelatty (2011) are also shown in Fig. 2. Thiel and Criley (2005) hydrated a needle-punched GCL on a silty sand (water content = 27%) without a confining stress. The USEPA tests were conducted on the same brand of needle-punched GCL used in the current study using a confining stress of 10 kPa on low-plasticity clay compacted at optimum (20%) following the standard Proctor effort. USEPA (1996a, b) also evaluated GCLs hydrated on subgrades prepared at other water contents; however, only data from the optimum water content are presented in Fig. 2 to be consistent with the data from the current study.

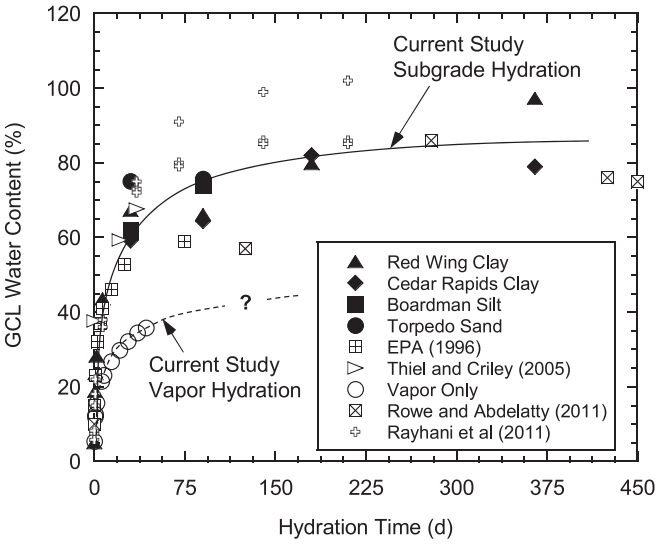

Fig. 2. Gravimetric water content of GCLs hydrated from subgrades or by vapor as a function of time [USEPA (1996a, b) data for the same GCL type as in the current study]

Rayhani et al. (2011) hydrated three different needle-punched Na-bentonite GCLs under a confining stress of 2 kPa on a silty-sand subgrade compacted at 5, 10, 16, and 21% water content (the optimum water content per standard Proctor for the silty-sand was 11.4%). The data presented in Fig. 2 from Rayhani et al. (2011) are for GCLs hydrated on silty sand compacted at 10% (1.4% dry of optimum per standard Proctor) to compare with the data from this study. Rowe and Abdelatty (2011) hydrated a GCL on a silty sand moistened to optimum per standard Proctor (13.9%) with a 13.5-mM calcium chloride solution to simulate calcium-rich soil. The data from the other studies were similar.

Water content as a function of time as a result of vapor-phase hydration at ~100% relative humidity is shown as open circles in Fig. 2. As with subgrade hydration, the water content of the GCL initially increased quickly in response to vapor-phase hydration, and then began to level off. However, the rate of hydration was slower with vapor, and the final water content was lower (38% versus 65–70% at the same time). Likos and Wayllace (2010) found a slightly lower vapor-phase contribution to bentonite water content at equilibrium (water content = 25%) in loosely compacted Wyoming sodium bentonite (void ratio = 1.28) at 97% relative humidity. These findings suggest that both liquid- and vapor-phase processes are involved in GCL hydration and that up to half of the GCL-subgrade hydration process may be a result of water supplied by the vapor phase.

Swell Index

The swell index of bentonite from the GCLs hydrated for 30, 90, 180, or 365 days on the four subgrades is shown in Fig. 3. The data corresponding to the end of hydration (EOH) are labeled in Fig. 3. The swell index in DI water as measured by ASTM D5890 (ASTM 2008) is often used as an indicator of cation exchange (Shackelford et al. 2000; Jo et al. 2001, 2004) because free swell diminishes when bound Na is replaced by divalent cations. The EOH swell indices (19.5–25 mL/2 g) were consistently lower than the swell index for the new GCL (28 mL/2 g) (upper dashed line in Fig. 3), indicating that the subgrade hydration affected the swelling of the bentonite. However, the duration of subgrade hydration, or the

J. Geotech. Geoenviron. Eng. 2013.139:526-538.

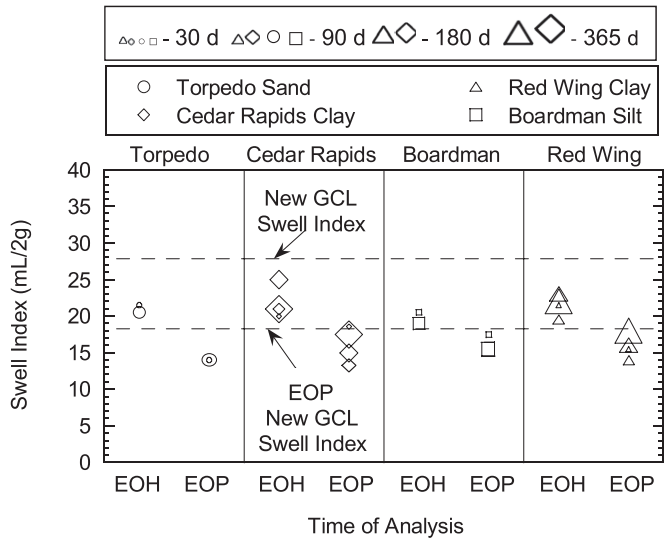

Fig. 3. Swell index for bentonite from GCLs hydrated on Torpedo sand, Cedar Rapids clay, Boardman silt, and Red Wing clay for 30, 90, 180, and 365 days at EOH and EOP (larger symbols correspond to longer hydration times)

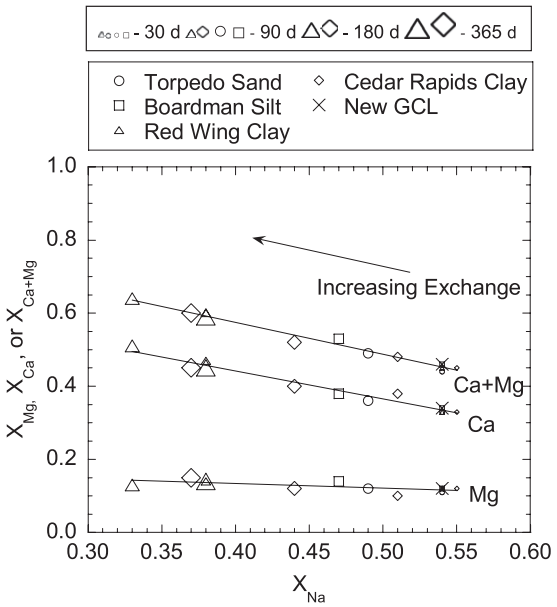

Fig. 4. Mole fractions of bound Ca (X_{Ca}), Mg (X_{Mg}), and Ca + Mg (X_{Ca+Mg}) in the exchange complex of bentonite as a function of mole fraction of bound Na for GCLs hydrated on Torpedo sand, Cedar Rapids clay, Red Wing clay, or Boardman silt for 30 or 90 days (the new GCL is the specimen not subjected to hydration or permeation)

subgrade on which the GCL was hydrated, did not have a systematic effect on the swell index.

Cation Exchange during Hydration

Mole fractions of bound Ca (X_{Ca}), Mg (X_{Mg}), and combined Ca and Mg (X_{Ca+Mg}), computed based on the sum of the major bound cations (Na, Ca, Mg, and K) satisfying the CEC, are shown in Fig. 4 as a function of the mole fraction of Na (X_{Na}). Bentonite from the new GCL (not hydrated or permeated) is also shown in Fig. 4 (X symbol). The symbol size in Fig. 4 varies with the hydration time, with larger symbols corresponding to longer hydration times. The concentrations of the major bound cations (Na, Ca, Mg, and K) in the bentonite immediately after subgrade hydration (EOH) are summarized in Table 4. The mole fractions of bound Na, Ca, and Mg after the first 30 days of subgrade hydration were essentially the same as those for the new GCL (Table 4, Fig. 4), indicating that essentially no exchange occurred during the first 30 days even though liquid-phase water from the subgrade was contributing to hydration of the GCL. In contrast, exchange occurred between 30 and 90 days, and continued through 365 days of hydration.

The solid lines in Fig. 4 represent the exchange of Na by another cation (or cations), and are referred to as exchange lines, where the slope of each exchange line represents the fraction of Na replaced by that cation or combination of cations. In Fig. 4, the exchange line for Mg has a shallow slope of −0.15, indicating that Mg contributed to 15% of the exchange for Na. The Ca line has a slope of −0.80, indicating that 80% of the Na exchange was Ca for Na replacement. Together, Ca and Mg were responsible for 95% of the exchanged Na. Ca had a greater role in the exchange because Ca is favored over Mg in the lyotropic series (Mitchell and Soga 2005), and had higher concentrations in the subgrade pore water relative to Mg for all subgrades except Torpedo sand (Mg and Ca had a comparable concentration in the subgrade pore water for Torpedo sand) (see Table 2).

The mole fractions of bound Na (X_{Na}) in the exchange complex of GCLs hydrated on Torpedo sand, Cedar Rapids clay, Red Wing clay, or Boardman silt are shown as function of hydration duration in Fig. 5. The mole fraction of Na decreased with increasing hydration time (the modest increase in X_{Na} between 180 and 365 days for Red Wing clay is an exception that cannot be explained). By 365 days of subgrade hydration, approximately 31% of the Na was replaced in GCLs hydrated on Red Wing clay and Cedar Rapids clay.

The mole fraction of Na in the exchange complex at various hydration times as a function of I_c and RMD of the subgrade pore water is shown in Fig. 6. Greater exchange was anticipated for GCLs hydrated on the Cedar Rapids clay because the pore water had a greater relative abundance of divalent cations and higher cationic strength (RMD = 0.007 $M^{1/2}$, I_c = 3.3 mM) relative to the other subgrades (Table 2). The GCL hydrated on Cedar Rapids clay for 365 days did have the greatest amount of Na replaced (31%). However, no systematic relationship was observed between Na replacement and RMD or I_c (Fig. 6). For example, at 90 days the most exchange occurred in the GCLs hydrated on Red Wing clay (30% of Na replaced) and Boardman silt (14% of Na replaced), which had higher RMD (0.094 and 0.12 $M^{1/2}$, respectively) than Cedar Rapids clay. The least exchange at 90 days occurred in the GCL hydrated on Cedar Rapids clay (6% of Na replaced).

The relationship between the fraction of Na replaced and percent calcite (a source of Ca) in the subgrade soil is shown in Fig. 7. For the subgrades used in this study, no systematic relationship between Na replaced in the bentonite and calcite content of the subgrade was observed, and for the longest tests (365 days), the greatest Na replacement was observed with the subgrade having the lowest calcite content (Cedar Rapids, 4.2% calcite). This absence of a trend may be a result of the narrow range of calcite contents (4.2–6.7%). Subgrades having higher carbonate content (>6.7%) may have a greater influence on Na replacement and hydraulic conductivity of GCLs; however, these conditions were not tested in this study.

J. Geotech. Geoenviron. Eng. 2013.139:526-538.

Table 4. GCL Water Content at EOH, Swell Index, and Concentrations of Bound Cations in the Exchange Complex of Bentonite after Completion of Hydration Experiments (EOH)

Subgrade	Hydration duration (d)	Final water content (%)	Swell index (mL/2 g)	Bound cation concentration ($cmol^+/kg$)			
				Na	Ca	Mg	K
None	None	NA	28.0	32.1	20.2	6.8	0.1
Torpedo sand	30	75.1	21.5	31.5	19.3	6.6	1.0
	90	75.7	20.5	27.4	20.1	6.9	1.0
Cedar Rapids clay	30	59.2	20.0	32.9	19.7	7.0	<0.001
	90	64.4	21.0	29.7	22.2	5.5	0.9
	180	82.0	25.0	22.1	19.8	6.1	1.7
	365	78.9	21.0	18.8	22.3	7.3	1.1
Boardman silt	30	61.9	20.5	32.0	19.9	7.0	<0.001
	90	73.9	19.0	28.2	23.1	8.7	0.2
Red Wing clay	30	67.3	21.5	31.9	19.8	6.8	0.9
	90	66.1	19.5	23.4	28.7	8.4	1.0
	180	79.8	23.0	19.2	29.3	7.3	1.1
	365	97.2	22.0	21.2	24.8	7.8	1.3

Note: < = lower than method detection limit; NA = data not available.

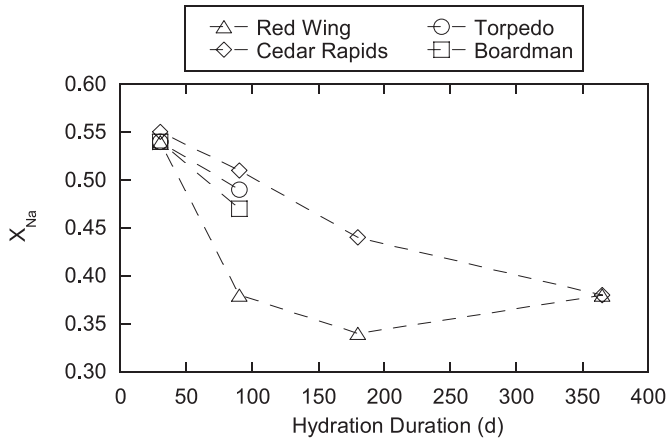

Fig. 5. Mole fractions of bound Na (X_{Na}) in the exchange complex of bentonite as a function of hydration duration for GCLs hydrated on Torpedo sand, Cedar Rapids clay, Red Wing clay, or Boardman silt (tests with Torpedo sand and Boardman silt conducted for 30 and 90 days only)

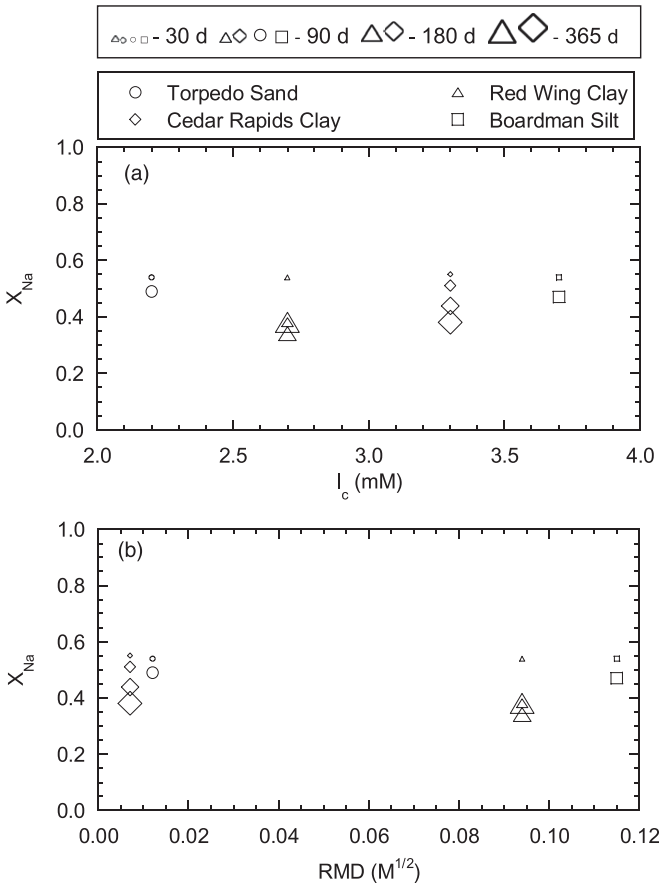

Fig. 6. Fraction of sodium (X_{Na}) in the exchange complex of bentonite in GCLs after subgrade hydration as a function of pore water (larger symbols correspond to longer hydration times): (a) I_c; (b) RMD

Hydraulic Conductivity to Deionized Water

The hydraulic conductivity to DI water of the GCLs hydrated on the subgrade soils at low stress (10 kPa) is summarized in Table 5 and is shown as a function of the effective stress applied during permeation in Fig. 8. The larger symbols in Fig. 8(a) correspond to longer hydration times. The hydraulic conductivities of the new GCL permeated directly with DI water (not hydrated on subgrade) and hydraulic conductivities of new needle-punched GCLs with granular bentonite permeated with DI water by other investigators (Petrov et al. 1997; D. Daniel, personal communication, August 2008) are shown in Fig. 8(b) along with the data from Fig 8(a).

The variation in hydraulic conductivity at a given stress in Fig. 8(a) is within a factor of 2.2, which falls within the range of reproducibility (3×) identified by Daniel et al. (1997) in their round-robin study on hydraulic conductivity testing of GCL (shown as error bars in Fig. 8). The hydraulic conductivities of the GCLs hydrated on subgrades through 365 days of hydration were indistinguishable from the hydraulic conductivities of the new GCL permeated directly with DI water at all stresses [Fig. 8(a)], and were similar to the hydraulic conductivity reported by others in Fig. 8(b). Thus, replacement of Na by Ca during subgrade hydration apparently had no measurable effect on the hydraulic conductivity of the bentonite to DI water, as hypothesized by Scalia and Benson (2011) for GCLs placed on subgrades compacted wet of optimum.

The trend line in Fig. 8(b) is for needle-punched GCLs only and is described by

$$\log K = -8.42 - 0.06\sqrt{\sigma'} \quad (3)$$

where K = hydraulic conductivity in cm/s and σ' = effective stress in kPa. Eq. (3) was obtained by least-squares regression and has $R^2 = 0.976$.

Rowe and Abdelatty (2011) reported various findings for a GCL hydrated on a moist subgrade with calcium-rich pore water. After 279 days of subgrade hydration, the hydraulic conductivity of the GCL increased 1.7–5.0 times the hydraulic conductivity of a new GCL, and after 421 days of hydration, the hydraulic conductivity increased 3.7–11.0 times. The increase in hydraulic conductivity observed by Rowe and Abdelatty (2011) may be related to the high Ca concentration (13.5 mM) in their subgrade, which was elevated artificially, compared with the Ca and Mg concentrations in the subgrade pore waters in the current study (0.75−1.6 mM).

Jo et al. (2004) observed a relationship between the hydraulic conductivity of GCLs to the fraction of bound Na replaced by Ca, in which GCLs with dilute $CaCl_2$ solutions were permeated and the exchange complex of the bentonite was periodically evaluated to determine the fraction of Na replaced by Ca. The hydraulic conductivity of the GCLs increased by factor of 1.1 when less than 30% of the Na was replaced by Ca (i.e., similar to the replacement observed in the current study) and the permeant liquid was a dilute solution, which is within the testing reproducibility reported by Daniel et al. (1997). The observations of Jo et al. (2004) are consistent with the degree of exchange and hydraulic conductivities measured in this study.

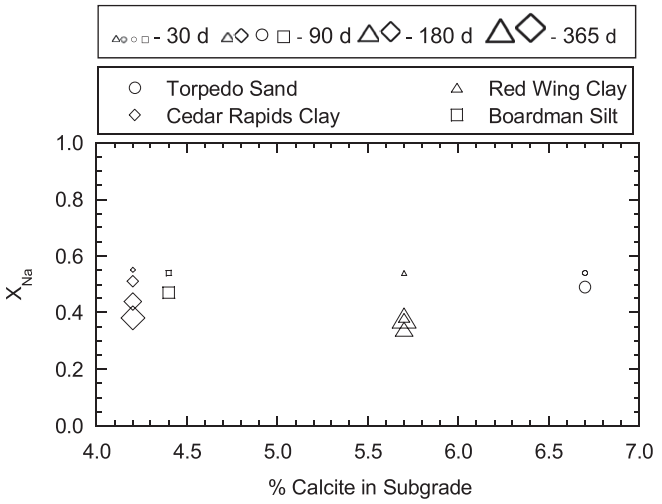

Fig. 7. Fraction of sodium (X_{Na}) in the exchange complex of bentonite in GCLs after subgrade hydration as a function of the percent of calcite in the subgrade (larger symbols correspond to longer hydration times)

Cation Exchange during Deionized Water Permeation

A summary of the major bound cations at the end of permeation (EOP) with DI water is given in Table 6. On average, permeation with DI water resulted in 7.5 $cmol^+$/kg of additional Ca exchange, which corresponds to approximately 50 mg of Ca in a 100-mm-diameter GCL specimen. The relative amounts of Ca-for-Na exchange that occurred during permeation and hydration are shown in Fig. 9(a) in terms of the exchange fraction, which is defined as the mole fraction of bound Na replaced during hydration or permeation ($|X_{Na\text{-EOH or EOP}} - X_{Na\text{-Initial}}|$) normalized by the mole fraction of bound Na in fresh bentonite from a new GCL ($X_{Na\text{-Fresh}}$). The data that fall above the 1:1 line in Fig. 9(a) correspond to more exchange during permeation than during subgrade hydration, whereas the data falling below the line correspond to more exchange during hydration.

Greater exchange occurred during permeation than during hydration for all GCLs hydrated for less than 180 days, except for the GCL hydrated on Red Wing clay for 90 days. This additional exchange of Ca for Na that occurred during permeation was not anticipated given that DI water was used as the permeant liquid specifically to preclude exchange during permeation. The swell indices corresponding to EOP in Fig. 3 exhibit a similar effect; they are consistently lower than swell indices at EOH for the same subgrade hydration conditions, and a similar drop in the swell index occurred for the GCL permeated directly with DI water (i.e., no subgrade hydration).

Several sources of Ca for the exchange during permeation were considered: (1) Ca below detection limits (<0.005 mM) in the DI water used as the permeant liquid; (2) residual salts on the surface of the geotextile placed on the GCL to distribute flow; and (3) dissolution of calcite within the bentonite. The amount of Ca that

Table 5. Hydraulic Conductivities of GCLs Permeated with DI Water after Hydration for 30, 90, 180 or 365 days on Subgrades (Tests at Overburden Stresses of 10, 70, 270, and 520 kPa)

		Hydraulic conductivity (cm/s)			
Subgrade	Hydration duration (d)	10 kPa	70 kPa	270 kPa	520 kPa
None	None	2.6×10^{-9}	1.3×10^{-9}	3.9×10^{-10}	1.9×10^{-10}
Torpedo sand	30	2.9×10^{-9}	1.2×10^{-9}	3.7×10^{-10}	1.5×10^{-10}
	90	3.9×10^{-9}	1.1×10^{-9}	4.9×10^{-10}	1.8×10^{-10}
Cedar Rapids clay	30	5.6×10^{-9}	2.0×10^{-9}	3.8×10^{-10}	1.5×10^{-10}
	90	3.0×10^{-9}	1.1×10^{-9}	4.4×10^{-10}	1.5×10^{-10}
	180	NT	1.6×10^{-9}	3.8×10^{-10}	2.1×10^{-10}
	365	4.6×10^{-9}	1.9×10^{-9}	6.4×10^{-10}	2.2×10^{-10}
Red Wing clay	30	2.5×10^{-9}	1.1×10^{-9}	3.6×10^{-10}	1.3×10^{-10}
	90	3.4×10^{-9}	1.2×10^{-9}	4.2×10^{-10}	1.4×10^{-10}
	180	NT	1.9×10^{-9}	5.2×10^{-10}	3.6×10^{-10}
	365	3.7×10^{-9}	1.7×10^{-9}	6.5×10^{-10}	9.8×10^{-11}
Boardman silt	30	3.0×10^{-9}	1.1×10^{-9}	5.0×10^{-10}	2.1×10^{-10}
	90	3.4×10^{-9}	1.5×10^{-9}	4.4×10^{-10}	1.6×10^{-10}

Note: Hydraulic conductivity tests at 10 kPa were not conducted on GCLs hydrated for 180 days because of time constraints. NT = no test.

J. Geotech. Geoenviron. Eng. 2013.139:526-538.

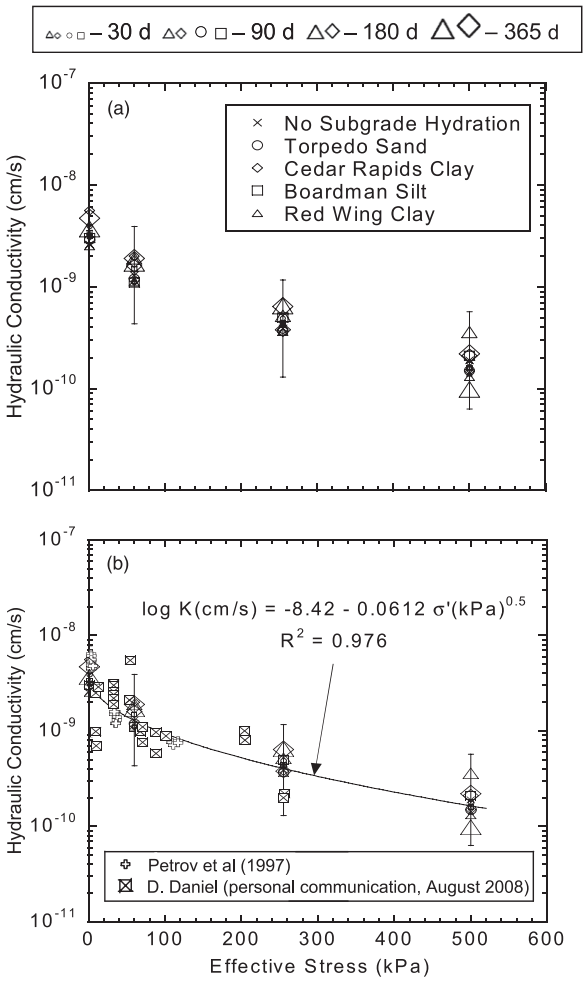

Fig. 8. Hydraulic conductivity to DI water as a function of the effective stress for the new GCL (error bars indicate range of reproducibility) and GCLs hydrated on subgrade soils for 30, 90, 180, and 365 days: (a) data from Petrov et al. (1997) and Daniel (personal communication, August 2008) are from GCLs permeated directly with distilled or DI water (no subgrade hydration); (b) error bars indicate range of reproducibility (3×)

could enter 100-mm-diameter GCL specimens through the permeant water (DI water) was calculated using the detection limit for Ca (0.005 mM), the maximum pore volumes of flow (9.0), the average GCL volume (60 mL), and the average porosity (0.8). Batch tests were performed with the stock geotextile used to distribute the permeant liquid across the GCL during permeation. Two 100-mm-diameter geotextiles were tumbled in a rotator for 24 h with 100 mL of DI water. The extract was filtered and preserved with nitric acid, Ca concentrations in the eluent were determined with ICP-OES, and the total Ca available was computed. X-ray diffraction was used to determine the calcite content in bentonite from the GCL roll (no subgrade hydration or permeation) and bentonite from GCLs after hydration and permeation with DI water.

Calculations showed that at most 0.1 mg of Ca was available in the permeant water for exchange and extraction of salts from the geotextiles showed that at most 0.5 mg of Ca was available from the geotextile. X-ray diffraction indicated that the bentonite originally contained 4% calcite, and the computations conducted using *Visual MINTEQ*, version 2.53 (USEPA 1991), indicated that 96% of this calcite is soluble at the pH (6.5) of the DI water used as the permeant liquid and 25°C (laboratory temperature). Complete dissolution of calcite would yield 500 mg of Ca per each 100-mm GCL specimen, or 10 times the Ca that replaced Na in the GCL specimens. The X-ray diffraction analyses of the bentonite postpermeation showed 1–3% calcite remaining. Thus, the DI water used as the permeant liquid and the residual salts on the geotextile were insignificant sources of the Ca involved in the exchange, whereas the calcite within the bentonite probably was the major source.

James et al. (1997) and Guyonnet et al. (2005) suggested that dissolution of Ca within bentonite can result in considerable replacement of Na. Exchange of Ca for Na during permeation with permeant liquids devoid of Ca is also evident from the laboratory data in Guyonnet et al. (2005) and Rauen (2007). Rauen (2007) observed 27% of Na being replaced by Ca in a new GCL containing natural Na-bentonite after permeation with DI water for 502 days and 6.7 pore volumes of flow (PVF). Similarly, Guyonnet et al. (2005) report 9–57% of Na being replaced by Ca and Mg after permeation of GCLs containing natural and activated Na-bentonites with at least 3.0 PVF of dilute (1.2-mM) NaCl solution.

Additional evidence suggesting that calcite dissolution is responsible for replacement of Na by Ca during permeation is shown

Table 6. GCL Water Content at EOP, Swell Index, and Concentrations of Bound Cations in the Exchange Complex of Bentonite Analyzed after Permeation with DI Water (EOP)

Subgrade	Hydration duration (*d*)	Final water content (%)	Swell index (mL/2 g)	Bound cation concentration ($cmol^+/kg$)			
				Na	Ca	Mg	K
None	None	65.9	18.0	27.9	29.3	7.9	1.5
Torpedo sand	30	61.9	14.0	25.1	28.7	7.7	1.2
	90	53.5	14.0	25.1	28.4	7.6	1.1
Cedar Rapids clay	30	74.2	18.5	30.6	22.5	6.6	1.2
	90	62.3	13.5	27.2	27.8	7.3	1.2
	180	NA	15.0	32.6	27.0	7.2	2.4
	365	59.6	17.5	24.3	22.9	6.8	1.3
Boardman silt	30	62.8	17.5	25.9	29.6	7.8	1.2
	90	62.9	15.0	22	30.6	8.3	1.2
Red Wing clay	30	61.8	15.5	26	29.2	7.0	1.2
	90	51.9	14.0	17.7	34.8	7.8	1.1
	180	NA	16.0	29.9	31.1	7.6	2.3
	365	54.3	18.0	21.2	27.0	7.5	1.3

Note: NA = data not available.

J. Geotech. Geoenviron. Eng. 2013.139:526-538.

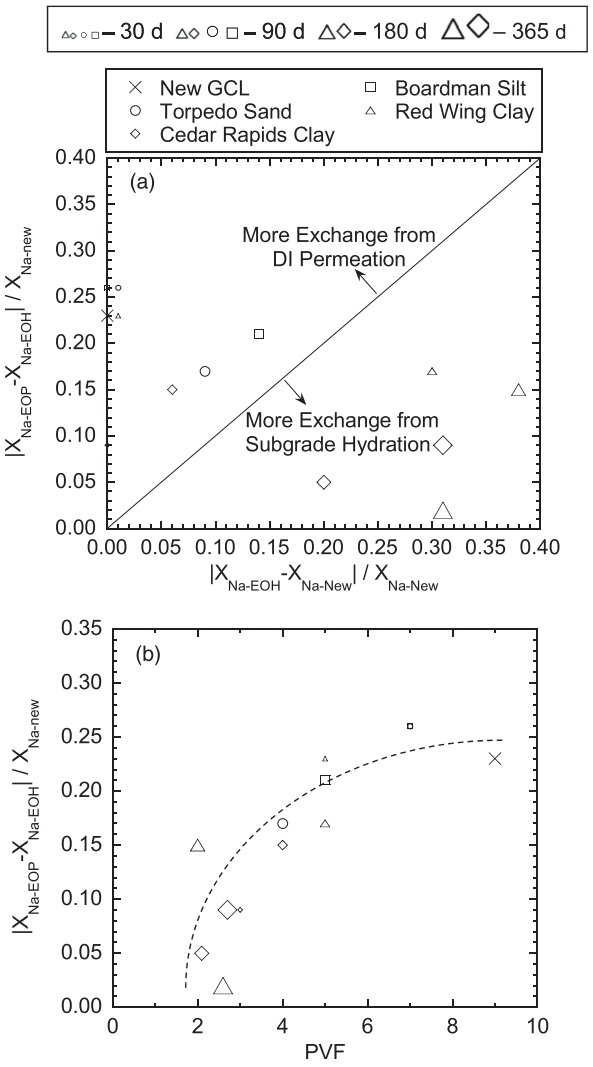

Fig. 9. Comparison of the exchange fraction, $[X_{Na\text{-new or EOH}} - X_{Na\text{-EOH or EOP}}]/X_{Na\text{-new}}$: (a) at EOP and EOH; (b) at EOP as a function of the PVF of DI water for GCLs hydrated on the subgrades

in Fig. 9(b), which shows the exchange fraction at EOP versus the total PVF during permeation. The exchange fraction increases with increasing PVF, which suggests that local equilibrium exists between the calcite and dissolved phase, and that additional Ca-for-Na exchange occurs as more DI water is made available for dissolution of calcite. Fig. 9(b) also illustrates why the new GCL specimens and the specimens hydrated for 30 days experienced more exchange during permeation than the specimens hydrated for 90 days. The GCL specimens hydrated for 30 days were permeated for more PVF than the specimens hydrated for 90 days, and therefore were exposed to more Ca from the dissolution of calcite.

Comparison with Field Studies

Scalia and Benson (2011)

The findings presented in this study are consistent with those reported by Scalia and Benson (2011). The GCLs exhumed by Scalia and Benson (2011) were hydrated on subgrades placed at optimum water content (or greater) and had low hydraulic conductivity ($\approx 10^{-9}$ cm/s), despite having some or all of the Na replaced by Ca and Mg. Scalia and Benson (2011) also found that the bentonite water content was in excess of 50% for all exhumed GCLs that had low hydraulic conductivity. The GCLs hydrated on drier subgrades with comparable or less Na replaced had lower bentonite water content and much higher hydraulic conductivity. In the current study, all of the GCLs that were hydrated on subgrades compacted 1% wet of optimum consistently had bentonite water content in excess of 50% (Table 4) and maintained low hydraulic conductivity despite replacement of Na by Ca and Mg.

Large column tests were assembled representing conditions existing at Site E in Scalia and Benson (2011) to provide additional confirmation of these findings. A 305-mm-thick layer of silty clay from Site E was compacted in a 254-mm-diameter section of pipe to represent the actual subgrade at Site E (Fig. 10). The clay was placed in three lifts of equal thickness at a water content of 13.9% (optimum water content) and a dry unit weight of 17.6 kN/m^3 (i.e., field condition). A GCL sample with a diameter of 250 mm was placed on the subgrade and then overlain by a geomembrane and an acrylic cap. The GCL and subgrade were then sealed with a latex membrane, as shown in Fig. 10.

The assembly of pipe, silty-clay subgrade, GCL, geomembrane, and acrylic caps was placed inside a larger pipe (inside diameter = 305 mm). Clean and dry sand was then placed on top of the assembly in the larger pipe to simulate the overburden stress existing in the field at Site E. The stress applied to the top acrylic plate was measured with earth pressure cells. Three columns were assembled for decommissioning after 50, 125, and 365 days of hydration. When decommissioned, the water content, bound cation concentrations, and hydraulic conductivity of the GCL were measured. DI water was used as the permeant liquid.

The water contents and X_{Na} of the GCLs in the columns are shown as a function of time in Fig. 11 along with the data from Site E. The water contents increased rapidly in a manner similar to those shown in Fig. 2, and then leveled off near 70%. Similar water contents were observed in the field after 4.7 years [Fig. 11(a)]. A reduction in X_{Na} also occurred over time as Ca and Mg replaced Na, which was similar to the reduction in X_{Na} observed in the bench-scale experiments. The shape of the X_{Na} trend can be extrapolated to the field condition [Fig. 11(b)], where nearly all of the Na was replaced ($X_{Na} = 0.03-0.06$) after 4.7 years. This suggests that complete replacement of Na by Ca and/or Mg is likely to occur in the field in most cases, given sufficient time and the presence of Ca and Mg in the subgrade (or calcite in the GCL).

When decommissioned, the GCLs had hydraulic conductivities of 1.5×10^{-9} cm/s (50 days), 1.1×10^{-9} cm/s (125 days), and 1.3×10^{-9} cm/s (365 days). Of the 11 GCL samples exhumed from Site E, five had hydraulic conductivities between 2.3 and 4.0×10^{-9} cm/s; i.e., comparable to the initial hydraulic conductivity of the GCL. Thus, low hydraulic conductivity can be maintained even in the presence of complete cation exchange provided that the GCL is hydrated on a subgrade placed at optimum or higher.

Even with these conditions, low hydraulic conductivity will not necessarily be ensured; the other six samples from Site E contained unusual MnO precipitates embedded in bundles of needle-punching fibers that resulted in preferential flow and hydraulic conductivities between 6.5×10^{-7} and 1.3×10^{-5} cm/s (Scalia and Benson 2010). The MnO precipitates were not a result of the cation exchange, and the mechanism controlling their formation remains unknown. Nevertheless, they did cause an increase in hydraulic conductivity. These precipitates appear to be a highly unusual anomaly and have not been observed elsewhere.

J. Geotech. Geoenviron. Eng. 2013.139:526-538.

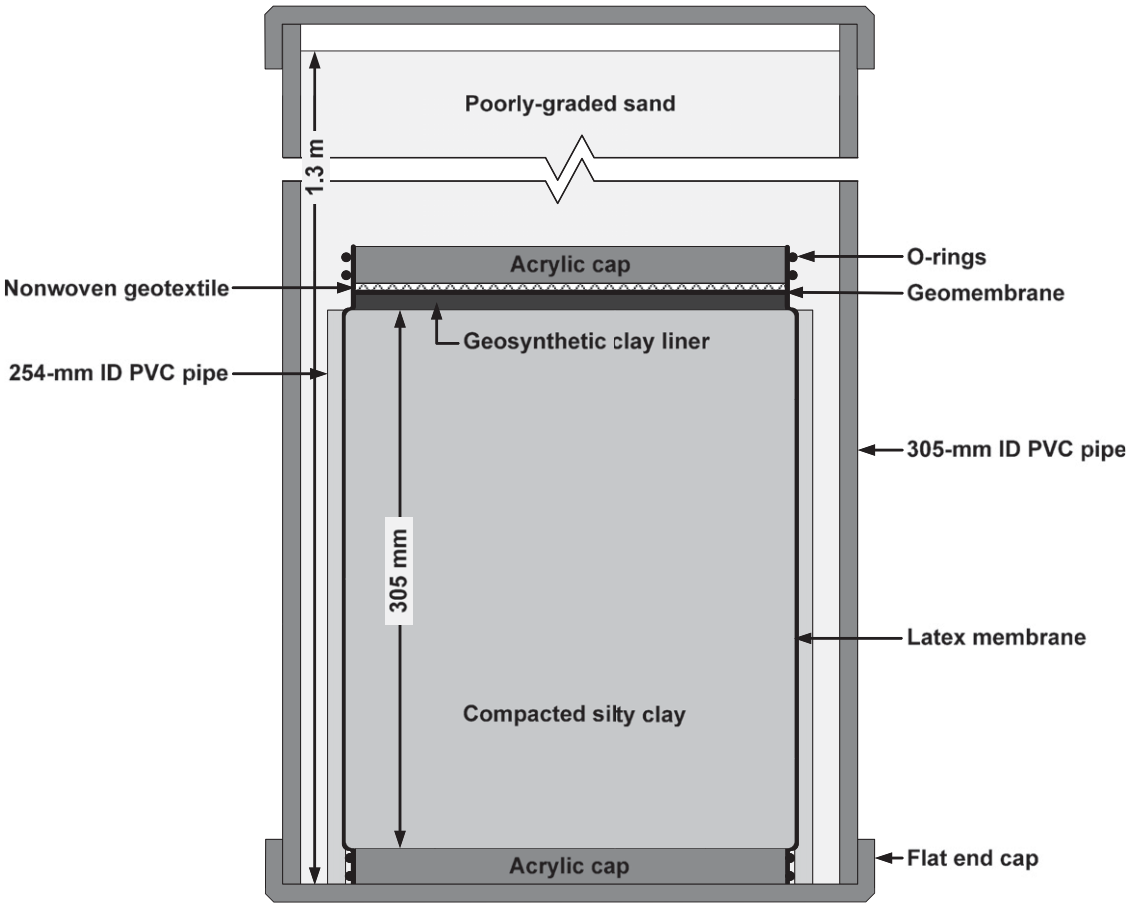

Fig. 10. Schematic of the large-scale hydration column simulating conditions at Site E

Meer and Benson (2007)

The GCL that Meer and Benson (2007) exhumed from a composite barrier had water content in excess of 50% and was installed on a subgrade placed wet of optimum. Thus, the high hydraulic conductivity (10^{-5} to 10^{-4} cm/s) observed by Meer and Benson (2007) for the GCL exhumed from a cover with a composite barrier may have been a result of factors other than Ca-for-Na exchange during hydration on a subgrade with water content lower than optimum. The bentonite contained cracks (Scalia and Benson 2011), and anecdotal reports indicated that cover soil was not placed promptly over the geosynthetics, which can induce wet-dry cycling of the GCL as the dark overlying geosynthetics heat and cool diurnally (e.g., as in Rowe et al. 2011). Wet-dry cycling of GCLs that have also undergone Ca-for-Na exchange has been shown to result in hydraulic conductivities on the order of 10^{-5} cm/s (Lin and Benson 2000; Meer and Benson 2007; Benson and Meer 2009).

To evaluate the impact of desiccation after subgrade hydration, the GCL hydrated on Red Wing clay for 90 days was subjected to one wet-dry cycle. After subgrade hydration, the GCL was air dried until the water content ceased changing (~5%) and then permeated with DI water under an overburden pressure of 20 kPa, simulating the cover scenario at Site S in Meer and Benson (2007). The hydraulic conductivity after one desiccation cycle was 9×10^{-5} cm/s, which falls into the range of hydraulic conductivity reported by Meer and Benson (2007) for GCLs exhumed from a composite cover barrier (10^{-5}–10^{-4} cm/s). Although the desiccation used in this study was more severe than would likely occur in the field, this experiment illustrates how desiccation after cation exchange can alter hydraulic conductivity. Subsequent permeation with Rhodamine WT dye demonstrated that no sidewall leakage had occurred, and that flow was occurring through cracks in the bentonite.

The exchange complex of the bentonite was analyzed after the desiccated GCL was permeated to ensure that additional cation exchange during permeation was not responsible for the increased hydraulic conductivity. The fractions of bound Ca and Na in the exchange complex after desiccation and permeation were within a factor of 1.1 of the fractions after hydration, indicating that exchange during permeation and after desiccation was not appreciable.

This evidence indicates that cation exchange as a result of subgrade hydration of GCLs coupled with desiccation can cause a large increase in the hydraulic conductivities of GCLs, and may have been the mechanism responsible for the high hydraulic conductivity observed by Meer and Benson (2007). Consequently, GCLs should be protected from desiccation after hydration, which includes prompt placement of cover soil or a leachate collection layer after installation of a geomembrane.

Summary and Conclusions

Laboratory tests were conducted to determine if cation exchange occurs when GCLs used in composite hydraulic barriers hydrate while in contact with a subgrade under the low stress representative of an overlying leachate collection system or cover soil, and if this cation exchange alters the hydraulic conductivity at higher stresses. Hydration experiments simulating conditions in a composite barrier

J. Geotech. Geoenviron. Eng. 2013.139:526-538.

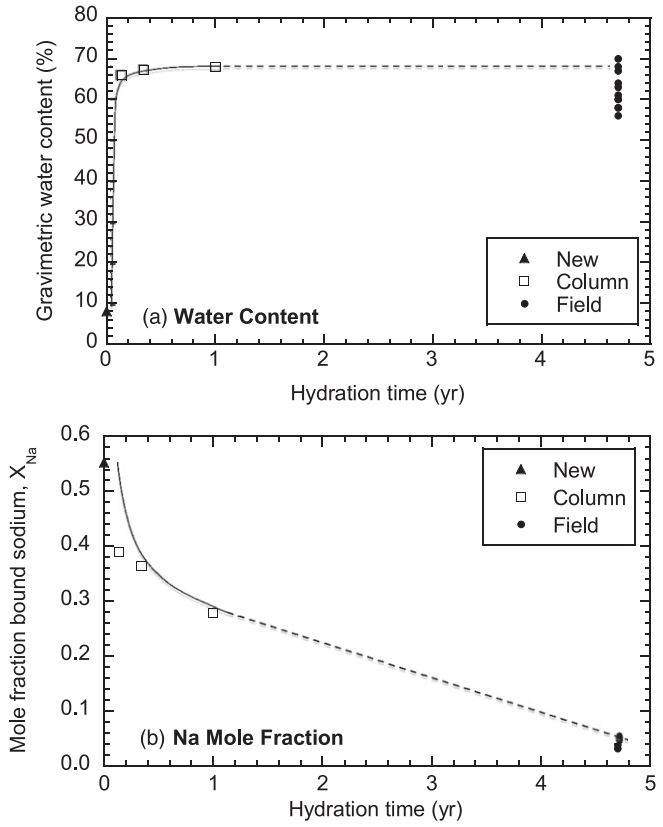

Fig. 11. (a) Gravimetric water content and (b) mole fraction Na in bentonite of GCLs in the large-scale column and exhumed from the field versus hydration time

were conducted using four subgrades ranging from sand to clay with pore waters having cationic strengths ranging from 2.2 to 3.7 mM and a ratio of monovalent to divalent cations (RMD) ranging from 0.007 to 0.12 $M^{1/2}$. After hydration, the hydraulic conductivity of the GCLs was measured over a range of overburden stresses (10–520 kPa) using DI water. The exchange complex and swell index of the bentonite were evaluated prior to testing, after hydration, and when permeation was complete.

Based on the findings of this study, the following conclusions and recommendations are made for GCLs installed in composite barriers:

- GCLs hydrate rapidly on moist subgrades with most of the hydration occurring within 30 days of contact. The average GCL water content after 30 days was 65%, increasing to an average water content of 85% after 365 days.
- Cation exchange occurs when GCLs hydrate on a subgrade as suggested by others. During the first 30 days of hydration, cation exchange is minimal. However, as much as 31% of the Na can be replaced during 1 year of hydration. Given sufficient time, and the presence of Ca or Mg in the subgrade (or in the GCL as calcite), complete replacement of Na by Ca and/or Mg is likely to occur in GCLs in composite barriers when placed against a subgrade.
- Cation exchange during subgrade hydration had no measurable effect on the hydraulic conductivity to DI water for the GCLs evaluated in this study, which were placed on subgrades having water content wet of optimum. Similar conditions have been observed in the field. These findings suggest that subgrades should be compacted at or wet of optimum to minimize the impact of cation exchange during subgrade hydration on the hydraulic conductivity of GCLs. Exceptions may include calcium-rich subgrades, such as those studied by Rowe and Abdelatty (2011) (13.5-mM Ca in pore water). Additional study on the effects of subgrade water content on GCL hydration, cation exchange, and hydraulic conductivity are recommended.
- GCLs exposed to cation exchange during hydration on subgrades must remain moist or their hydraulic conductivity may increase substantially. GCLs installed as part of a composite barrier should be protected by ensuring prompt placement of the cover soil or leachate collection layer after installation of the geomembrane.
- Stress had a significant effect on the hydraulic conductivity of all GCLs tested in this study. Increasing the overburden pressure from 10 to 520 kPa compressed the GCLs and caused a reduction in hydraulic conductivity of at least one order of magnitude. This reduction can be predicted with a power function.
- Dissolution of calcite within the bentonite in a GCL can be a significant factor contributing to replacement of Na by Ca. For the tests in this study, replacement of Na by Ca as a result of calcite dissolution within the GCL was comparable in magnitude to the exchange induced by placement on the subgrade. Similar Ca-for-Na exchange is evident in data from other studies where GCLs were permeated with liquids devoid of Ca. This exchange had no measurable effect on the hydraulic conductivity for the GCLs evaluated in this study. However, at longer time scales existing in the field, replacement of Na by Ca as a result of calcite dissolution in conjunction with exchange from cations in the subgrade pore water could cause increases in hydraulic conductivity.

Acknowledgments

CETCO, the National Science Foundation (Grant No. CMMI-0625850), and the U.S. Department of Energy (DOE) provided financial support for this study. DOE support was provided under Cooperative Agreement No. DE-FC01-06EW07053 entitled "Consortium For Risk Evaluation With Stakeholder Participation III," awarded to Vanderbilt University. The opinions, findings, conclusions, and recommendations expressed herein are those of the authors and do not necessarily represent the views of CETCO, the National Science Foundation, the Department of Energy, or Vanderbilt University.

References

ASTM. (2008). *Annual book of ASTM standards*, Vols. 04.08, 04.09, and 11.01, West Conshohocken, PA.

Benson, C. H., Kucukkirca, I. E., and Scalia, J. (2010). "Properties of geosynthetics exhumed from the final cover at a solid waste landfill." *Geotext. Geomembr.*, 28(6), 536–546.

Benson, C. H., and Meer, S. R. (2009). "Relative abundance of monovalent and divalent cations and the impact of desiccation on geosynthetic clay liners." *J. Geotech. Geoenviron. Eng.*, 135(3), 349–358.

Benson, C. H., Thorstad, P. A., Jo, H. Y., and Rock, S. A. (2007). "Hydraulic performance of geosynthetic clay liners in a landfill final cover." *J. Geotech. Geoenviron. Eng.*, 133(7), 814–827.

Bradshaw, S. L., and Benson, C. H. (2011). "Effect of cation exchange during subgrade hydration and municipal solid waste leachate permeation on the hydraulic conductivity of geosynthetic clay liners." *Geological Engineering Rep. No. 11-09*, Univ. of Wisconsin, Madison, WI.

Daniel, D. E., Bowders, J. J., and Gilbert, R. B. (1997). "Laboratory hydraulic conductivity testing of GCLs in flexible-wall permeameters."

J. Geotech. Geoenviron. Eng. 2013.139:526-538.

Testing and acceptance criteria for geosynthetic clay liners, STP 1308, L. W. Well, ed., ASTM, West Conshohocken, PA, 208–226.
Dreimanis, A. (1962). "Quantitative gasometric determination of calcite and dolomite by using Chittick apparatus." *J. Sediment. Res.*, 32(3), 520–529.
Egloffstein, T. A. (2002). "Bentonite as sealing material in geosynthetic clay liners—Influence of electrolytic concentration, the ion exchange and ion exchange with simultaneous partial desiccation on permeability." *Proc., Int. Geosynthetic Clay Barriers Symp.*, H. Zanzinger, R. M. Koerner, and E. Gartung, eds., Swets and Zeitlinger, Lisse, Netherlands, 141–153.
Grim, R. E. (1968). *Clay mineralogy*, 2nd Ed., McGraw Hall, New York.
Guyonnet, D., et al. (2005). "Geosynthetic clay liners interaction with leachate: Correlation between permeability, microstructure, and surface chemistry." *J. Geotech. Geoenviron. Eng.*, 131(6), 740–749.
Hach Company. (2003). *Method 10031, salicylate method, test 'N tube(TM) vials, HR, 0 to 50.0 mg/L NH3-N*. ⟨https://www.hach.com/fmmimghach?/CODE%3ANITROGENAMM_TNT_HIGH2071%7C1⟩ (Oct. 12, 2006).
James, A. N., Fullerton, D., and Drake, R. (1997). "Field performance of GCL under ion exchange conditions." *J. Geotech. Eng.*, 123(10), 897–901.
Jo, H. Y., Benson, C. H., and Edil, T. B. (2004). "Hydraulic conductivity and cation exchange in non-prehydrated and prehydrated bentonite permeated with weak inorganic salt solutions." *Clays Clay Miner.*, 52(6), 661–679.
Jo, H. Y., Katsumi, T., Benson, C. H., and Edil, T. B. (2001). "Hydraulic conductivity and swelling of nonprehydrated GCLs permeated with single-species salt solutions." *J. Geotech. Geoenviron. Eng.*, 127(7), 557–567.
Kolstad, D. C., Benson, C. H., and Edil, T. B. (2004). "Hydraulic conductivity and swell of nonprehydrated GCLs permeated with multispecies inorganic solutions." *J. Geotech. Geoenviron. Eng.*, 130(12), 1236–1249.
Lee, J. M., Shackelford, C. D., Benson, C. H., Jo, H. Y., and Edil, T. B. (2005). "Correlating index properties and hydraulic conductivity of geosynthetic clay liners." *J. Geotech. Geoenviron. Eng.*, 131(11), 1319–1329.
Likos, W. J., and Wayllace, A. (2010). "Porosity evolution of free and confined bentonites during interlayer hydration." *Clays Clay Miner.*, 58(3), 399–414.
Lin, L.-C., and Benson, C. H. (2000). "Effect of wet-dry cycling on swelling and hydraulic conductivity of geosynthetic clay liners." *J. Geotech. Geoenviron. Eng.*, 126(1), 40–49.
Meer, S. R., and Benson, C. H. (2007). "Hydraulic conductivity of geosynthetic clay liners exhumed from landfill final covers." *J. Geotech. Geoenviron. Eng.*, 133(5), 550–563.
Melchior, S. (2002). "Field studies and excavations of geosynthetic clay barriers in landfill covers." *Proc., Int. Geosynthetic Clay Barriers Symp.*, H. Zanzinger, R. M. Koerner, and E. Gartung, eds., Swets and Zeitlinger, Lisse, Netherlands, 321–330.
Mesri, G., and Olson, R. E. (1971). "Mechanisms controlling the permeability of clays." *Clays Clay Miner.*, 19, 151–158.
Mitchell, J. K., and Soga, K. (2005). *Fundamentals of soil behavior*, 3rd Ed., Wiley, New York.
Moore, D. M., and Reynolds, R. C. Jr. (1989). *X-ray diffraction and the identification of clay minerals*, Oxford University Press, New York.
Norrish, K. (1954). "The swelling of montmorillonites." *Discuss. Faraday Soc.*, 18, 120–134.
Norrish, K., and Quirk, J. P. (1954). "Crystalline swelling of montmorillonite: Use of electrolytes to control swelling." *Nature*, 173, 255–257.
Petrov, R. J., Rowe, R. K., and Quigley, R. M. (1997). "Selected factors influencing GCL hydraulic conductivity." *J. Geotech. Geoenviron. Eng.*, 123(8), 683–695.
Rauen, T. (2007). "Effect of leachate from bioreactor and recirculation landfills on the hydraulic conductivity of geosynthetic clay liners." M.S. thesis, Univ. of Wisconsin, Madison, WI.
Rauen, T., and Benson, C. H. (2008). "Hydraulic conductivity of a geosynthetic clay liner permeated with leachate from a landfill with leachate recirculation." *Proc. of the 1st Pan-American Geosynthetics Conf. and Exhibition, GeoAmericas*, Industrial Fabrics Association International, St. Paul. MN. 76–83.
Rayhani, M. T., Rowe, R. K., Brachman, R. W. I., Take, W. A., and Siemens, G. (2011). "Factors affecting GCL hydration under isothermal conditions." *Geotext. Geomembr.*, 29(6), 525–533.
Rowe, R. K., and Abdelatty, K. (2011). "Effect of a calcium-rich soil on the performance of an overlying GCL." *J. Geotech. Geoenviron. Eng.*, 138(4), 423–431.
Rowe, R. K., Rayhani, M. T., Take, W. A., Siemens, G., and Brachman, R. W. I. (2011). "GCL hydration under simulated daily thermal cycles." *Geosynthet. Int.*, 18(4), 196–205.
Scalia, J., and Benson, C. H. (2010). "Preferential flow in geosynthetic clay liners exhumed from final covers with composite barriers." *Can. Geotech. J.*, 47(10), 1101–1111.
Scalia, J., and Benson, C. H. (2011). "Hydraulic conductivity of geosynthetic clay liners exhumed from landfill final covers with composite barriers." *J. Geotech. Geoenviron. Eng.*, 137(1), 1–13.
Shackelford, C. D., Benson, C. H., Katsumi, T., Edil, T. B., and Lin, L. (2000). "Evaluating the hydraulic conductivity of GCLs permeated with non-standard liquids." *Geotext. Geomembr.*, 18(2–4), 133–161.
Sposito, G. (1981). *The thermodynamics of soil solutions*, Oxford University Press, New York.
Thiel, R., and Criley, K. (2005). "Hydraulic conductivity of partially prehydrated GCLs under high effective confining stress for three real leachates." *GSP 142 waste containment and remediation*, ASCE, Reston, VA.
U.S. Environmental Protection Agency (USEPA). (1991). *MINTEQ version 3.11*, USEPA, Athens, GA.
U.S. Environmental Protection Agency (USEPA). (1996a). "Hydration of GCLs adjacent to soil layers." *Rep. 600/R-96 /149*, USEPA, Washington, DC.
U.S. Environmental Protection Agency (USEPAb). (1996). "Test methods for evaluating solid waste: Physical/chemical methods, method 6010B." *Rep. EPASW-846,* USEPA, Washington, DC.

J. Geotech. Geoenviron. Eng. 2013.139:526-538.

HYDRAULIC CONDUCTIVITY AND SWELL OF NONPREHYDRATED GEOSYNTHETIC CLAY LINERS PERMEATED WITH MULTISPECIES INORGANIC SOLUTIONS

Kolstad, D.C., Benson, C.H. and Edil, T.B., *Journal of Geotechnical and Geo-environmental Engineering,* ASCE, Vol. 130, No. 12, December 2004, pp.1236-1249.

Introduction. This article examines the influence of multispecies inorganic solutions on swelling and hydraulic conductivity of non-prehydrated GCLs containing sodium bentonite. This is a continuation of the research done by Benson, Edil and their students in the area of clays, including GCLs (see CETCO TR-326). Multispecies inorganic solutions were mixed using deionized water, monovalent cation salts (NaCl and/or LiCl) and divalent cation salts ($CaCl_2$ and $MgCl_2$). GCL hydraulic conductivity tests were performed using flexible wall permeameters at an average effective stress of 20 kPa (3 psi) and average head pressure of 2 feet. The GCL hydraulic conductivity tests were run per ASTM D6766 until the influent and effluent electrical conductivity deviated less than 10%. Free swell tests were also conducted per ASTM D6141 using the multispecies inorganic solutions as the test liquid.

Ionic strength and the ratio of monovalent cation concentration to the square root of divalent cation concentration (RMD) in the permeant solution were found to influence swell of the bentonite and hydraulic conductivity of GCLs. A regression model was developed relating hydraulic conductivity of the GCL to ionic strength and the RMD of the permeant solution. The results of this model are expressed in equation 3 and graphically in Figures 7 and 10(a) of the article.

A literature search of leachate chemistry data from different waste containment facilities was also conducted and listed in Table 4. Figure 10(b) plots the ionic strength and RMD of these various leachates onto a corresponding isoperm chart. The chart implies that many municipal solid waste (MSW) landfill leachates and mine waste site leachates, as well as some hazardous waste and fly ash leachates, would result in high (>10^{-7} cm/s) GCL hydraulic conductivities.

Errata. An erratum was published by the authors in the July 2006 issue of ASCE *Journal of Geotechnical and Geo-environmental Engineering*. The following corrections were noted:

- The RMD units in the text, tables and figures should be $M^{1/2}$, not $mM^{1/2}$.
- Equation 3. The correct equation is:

$$\log K_c/\log K_{DI} = 0.965 - 0.976*I + 0.0797*RMD + 0.251*I^{2}* RMD$$

- The fly ash leachate point coordinates from Table 4 are plotted incorrectly in Figure 10(b). According to the data, all but one fly ash point should be between the 10^{-8} and 10^{-9} cm/s isoperm lines.

800.527.9948 Fax 847.577.5566
For the most up-to-date product information, please visit our website, www.cetco.com.

Data Review. Most of the MSW leachate chemistry data listed in Kolstad Table 4 is from prior to 1990. MSW leachate chemistry data for cells built prior to 1990 is not representative of modern MSW landfills because: 1) it was common practice to dispose of industrial waste, hazardous waste and various liquid wastes prior to promulgation of current national solid waste regulations, and 2) samples may not have been taken from controlled collection points because many landfills did not have leachate collection and recovery systems (Bonaparte et al., 2002). The difference between these two time periods in MSW leachate chemistry is quite apparent by segregating pre-1990 and post-1990 data. For those references published *prior to* 1990, the average ionic strength was 0.24 M with an average RMD of 0.22 $M^{1/2}$ and the maximum ionic strength was 0.62 M with a RMD of 0.31 $M^{1/2}$. For those references published *after* 1990, the average ionic strength is 0.12 M with an RMD of 0.16 $M^{1/2}$ and a maximum ionic strength of 0.24 M with a RMD of 0.18 $M^{1/2}$ (Table A).

Table A. MSW Landfill Leachate Chemistry Data.

	Average		Maximum	
	Ionic Strength (M)	RMD ($M^{1/2}$)	Ionic Strength (M)	RMD ($M^{1/2}$)
Kolstad – 17 pre-1990 cases	0.24	0.22	0.62	0.31
Kolstad – 5 post-1990 cases	0.12	0.16	0.24	0.18
EPA Study – 26 post-1990 cases	0.06	0.11	0.22	0.22
Combined 31 post-1990 cases	0.07	0.11	0.24	0.18

The segregated Kolstad data shows that modern MSW leachates (post-1990) have a lower ionic strength than older MSW leachates (pre-1990).

Leachate chemistry data collected from 26 post-1990 MSW landfills as part of a major study by USEPA (Bonaparte et al. 2002) is also presented in Table A. Ionic strengths were estimated from specific conductance per Snoeyink and Jenkins (1980). RMDs were estimated from available calcium, magnesium and sodium concentrations. The MSW leachates in the USEPA study had an average estimated ionic strength of 0.06 M and a RMD of 0.11 $M^{1/2}$. Combining post-1990 cases from both Kolstad and USEPA yields an average ionic strength of 0.07 M and RMD of 0.11 $M^{1/2}$.

Modifying Figure 10(b) to correct the fly ash coordinates and to delete the Kolstad MSW data prior to 1990 yields Figure 1.

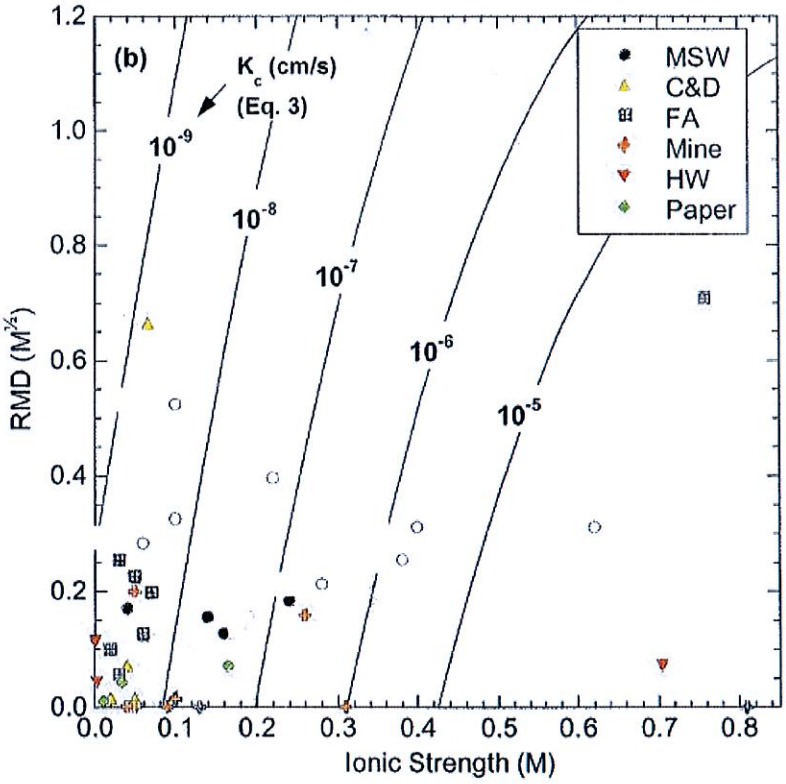

Figure 1. Modified Figure 10(b) from Kolstad et al. 2004 for nonprehydrated GCL permeated at 3 psi average effective stress. When fly ash coordinates are corrected and pre-1990 MSW leachate chemistry data is removed, few leachates cause a significant increase in GCL hydraulic conductivity.

Data Interpretation. The GCL tested in Kolstad's research had a hydraulic conductivity of 9×10^{-10} cm/s when permeated with distilled water. Kolstad Equation 3 predicts the hydraulic conductivity of the nonprehydrated GCL permeated with inorganic chemicals. Using the post-1990 MSW leachate chemistry from Table A, the Kolstad model yields an estimated average nonprehydrated GCL long-term hydraulic conductivity of 6.4×10^{-9} cm/s and a maximum of 1.7×10^{-7} cm/s at 3 psi average effective stress.

However, as noted by the authors, the model expressed in Equation 3 does not take into account 1) higher effective stresses which tend to decrease permeability, 2) prehydration from subgrade or 3) increasing pH over time. The model should be adjusted to account for at least the first two important factors. Petrov (1997) developed the following equation for the effect of confining stress on GCL hydraulic conductivity permeated with distilled water:

$$\log K_{DI} = -8.0068 - 0.5429 \log \sigma$$

Where K_{DI} is in cm/s and σ is in kPa.

Bonaparte et al. found that 74 MSW cells in the USEPA study had maximum heights ranging from 26 to 226 feet, with an average of 90 feet. Assuming a MSW density of 60 pcf (Daniel 1993), the typical effective stress of a MSW liner is 37 psi. Although the expression developed by Petrov is stated to be valid only for effective stress between 3 and 120 kPa (0.4 to 17 psi), the correlation appears to trend linearly. Therefore, it is reasonable to use this expression for 37 psi stress, which is just slightly higher on the logarithmic scale. For an increase in maximum effective stress from 5 psi to 37 psi, the Petrov equation yields a 65% decrease in GCL hydraulic conductivity. Predictions from the Kolstad model, adjusted for post-1990 MSW leachate chemistry data and an effective stress of 37 psi, yield an estimated average nonprehydrated GCL long-term hydraulic conductivity of 2.3×10^{-9} cm/s and a maximum of 6×10^{-8} cm/s for MSW landfills.

Even lower hydraulic conductivity would be expected if the GCL prehydrates from subgrade moisture. Lee and Shackelford (2005) showed that GCL prehydrated with deionized water and then permeated with a 0.1M $CaCl_2$ solution (I = 0.3 M) had a hydraulic conductivity 3 times lower compared to a nonprehydrated GCL. But testing at $CaCl_2$ = 0.05M (I = 0.15M) indicated that the prehydration effect was insignificant. It is possible that prehydration of the GCL will improve long-term hydraulic conductivity at I = 0.24M, the upper end of the MSW ionic strength reported. However, more study in this area is needed.

The highest MSW leachate ionic strength was for young MSW leachate (<5 years). After waste placement ceases and the landfill is capped, methanogenic organisms begin to proliferate in a MSW landfill and the pH begins to approach neutrality as the acids are converted into methane and a bicarbonate buffering system is established during the methane fermentation stage (Bonaparte et al 2002). Concentrations of free divalent cations will decrease with increased pH, due to the solubility of divalent cations (Snoeyink and Jenkins 1980). Consequently, after closure, the ionic strength of the MSW leachate will decrease. Therefore, it can be argued that with GCL prehydration and/or leachate aging that the previously estimated average GCL hydraulic conductivity of 2.3×10^{-9} for MSW landfills is quite conservative.

Giroud (1997) has formulated equations for leakage rates through defects in geomembranes. Under typical MSW landfill conditions; these formulas indicate that the leakage rate through geomembrane defects is controlled by the hydraulic conductivity of the underlying clay. Thus, based upon the estimated GCL long-term hydraulic conductivities stated above, a GM/GCL composite MSW liner would be expected to have a lower leakage rate than a GM/CCL composite MSW liner, where the CCL has a hydraulic conductivity of 10^{-7} cm/s. This is supported by the MSW landfill leakage rate data of GM/GCL and GM/CCL composite liners collected in the USEPA study by Bonaparte et al. (see CETCO TR-316).

Conclusion. In their conclusions Kolstad et al. state that, "high hydraulic conductivities (i.e., $>10^{-7}$ cm/s) are unlikely for nonprehydrated GCLs in base liners in many solid waste containment facilities". Based on the data review compiled above, it is reasonable to refine this conclusion to a) the hydraulic performance of a GCL in a landfill bottom liner will not be significantly affected by a typical modern MSW leachate and that b) high GCL hydraulic conductivities will only occur in certain cases at non-MSW wastes (e.g., hazardous waste, mine waste, fly ash) when the waste leachate contains higher ionic strengths.

800.527.9948 Fax 847.577.5566

References

Bonaparte, R., Daniel, D. E. and Koerner, R. M., Assessment and Recommendations for Optimal Performance of Waste Containment Systems, EPA/600/R-02/099, December 2002, U. S. EPA, ORD, Cincinnati, OH, www.epa.gov/ORD/NRMRL/Pubs/600R02099/600R02099.pdf.

Daniel, D., *Geotechnical Practice for Waste Disposal,* Chapman & Hall, London, 1993.

Giroud, J.P., "Equations for Calculating the Rate of Liquid Migration Through Composite Liners Due to Geomembrane Defects", *Geosynthetics International,* Vol. 4, Nos. 3-4, pp. 335-348, 1997.

Lee, J. and Shackelford, C.D., "Concentration Dependency of the Prehydration Effect for a GCL", *Soils and Foundations,* Japanese Geotechnical Society, Vol. 45, No. 4, 2005.

Meer, S.R. and Benson, C.H., "In-Service Hydraulic Conductivity of GCLs Used in Landfill Covers – Laboratory and Field Studies", Geo Engineering Report No. 04-17, University of Wisconsin at Madison, 2004.

Petrov, R.J., Rowe, R.K., and Quigley, R.M., "Selected Factors Influencing GCL Hydraulic Conductivity", *Journal of Geotechnical and Geoenvironmental Engineering,* ASCE, Vol. 123, No. 8, August 1997, pp. 683-695.

Snoeyink & Jenkins, *Water Chemistry*, John Wiley & Sons Publishers, New York, 1980.

800.527.9948 Fax 847.577.5566

Hydraulic Conductivity and Swell of Nonprehydrated Geosynthetic Clay Liners Permeated with Multispecies Inorganic Solutions

Dale C. Kolstad, M.ASCE[1]; Craig H. Benson, M.ASCE[2]; and Tuncer B. Edil, M.ASCE[3]

Abstract: The influence of multispecies inorganic solutions on swelling and hydraulic conductivity of non-prehydrated geosynthetic clay liners (GCLs) containing sodium bentonite was examined. Ionic strength and the relative abundance of monovalent and divalent cations (RMD) in the permeant solution were found to influence swell of the bentonite, and the hydraulic conductivity of GCLs. Swell is directly related to RMD and inversely related to ionic strength, whereas hydraulic conductivity is directly related to ionic strength and inversely related to RMD. RMD has a greater influence for solutions with low ionic strength (e.g., 0.05 M), whereas concentration effects dominate at high ionic strength (e.g., 0.5 M). No discernable effect of cation species of similar valence was observed in the swell or hydraulic conductivity data for test solutions with similar ionic strength and RMD. A strong relationship between hydraulic conductivity and free swell was found, but the relationship must be defined empirically for a particular bentonite. A regression model relating hydraulic conductivity of the GCL to ionic strength and RMD of the permeant solution was developed. Predictions made with the model indicate that high hydraulic conductivities (i.e., $>10^{-7}$ cm/s) are not likely for GCLs in base liners in many solid waste containment facilities. However, for wastes with stronger leachates or leachates dominated by polyvalent cations, high hydraulic conductivities may occur.

DOI: 10.1061/(ASCE)1090-0241(2004)130:12(1236)

CE Database subject headings: Hydraulic conductivity; Swelling; Inorganic chemicals; Clay liners; Bentonite.

Introduction

Geosynthetic clay liners (GCLs) are factory-manufactured clay liners consisting of a layer of bentonite clay encased by geotextiles or glued to a geomembrane. GCLs have become a popular alternative to compacted clay liners in waste containment applications because of their relatively low cost, ease of installation, perceived resistance to environmental distress (e.g. freeze–thaw and wet–dry cycling), smaller air–space requirements, and low hydraulic conductivity to water ($<10^{-8}$ cm/s). For GCLs that do not contain a geomembrane, bentonite is responsible for the low hydraulic conductivity. Sodium (Na) montmorillonite mineral is the primary component of bentonite, and largely controls the hydraulic conductivity of GCLs (Shackelford et al. 2000).

A variety of studies have shown that the hydraulic conductivity and swelling of bentonite can be affected by inorganic permeant solutions (Alther et al. 1985; Shan and Daniel 1991; Egloffstein 1997, 2001; Quaranta et al. 1997; Ruhl and Daniel 1997; Petrov and Rowe 1997; Shackelford et al. 2000; Jo et al. 2001; Vasko et al. 2001; Ashmawy et al. 2002; Katsumi et al. 2002, 2003; Shan and Lai 2002). The general conclusion of these studies is that the hydraulic conductivity and swelling of GCLs is sensitive to the concentration of the permeant solution and the cation valence. In general, higher hydraulic conductivity and lower swell are obtained in more concentrated solutions or solutions with a preponderance of divalent cations. However, no systematic study has been made regarding how the concentration and relative proportions of monovalent and polyvalent cations in a multispecies (i.e., more than one cation species) solution affect swelling and hydraulic conductivity of bentonite and GCLs.

Several studies have been conducted in soil science regarding the effect of multispecies solutions on the hydraulic conductivity of montmorillonitic soils (Reeve and Bower 1960; McNeal and Coleman 1966; McNeal et al. 1966; Mustafa and Hamid 1975; Malik et al. 1992). However, these studies have focused on increasing the hydraulic conductivity of montmorillonitic soils for land drainage and agricultural applications rather than maintaining low hydraulic conductivity for containment applications. Moreover, none of these studies has focused on clay soils very rich in montmorillonite, such as the Na-bentonites used for GCLs.

This paper discusses how the ionic strength and relative amounts of monovalent and divalent cations in multispecies solutions affect swelling and hydraulic conductivity of nonprehydrated GCLs containing Na-bentonite. The focus is on applications where inorganic solutes are the primary factor affecting hydraulic conductivity (e.g., conventional solid waste containment facilities for municipal, hazardous, or mining wastes) and where complete prehydration (i.e., prehydration by permeation with distilled, deionized, or potable water) is unlikely. The effects of complete prehydration and organic compounds are discussed

[1]Environmental Engineer, Barr Engineering Company, 4700 West 77th St., Minneapolis, MN 55435. E-mail: dkolstad@barr.com

[2]Professor, Dept. of Civil and Environmental Engineering, Univ. of Wisconsin, Madison, WI 53706. E-mail: benson@engr.wisc.edu

[3]Professor, Dept. of Civil and Environmental Engineering, Univ. of Wisconsin, Madison, WI 53706. E-mail: edil@engr.wisc.edu

Note. Discussion open until May 1, 2005. Separate discussions must be submitted for individual papers. To extend the closing date by one month, a written request must be filed with the ASCE Managing Editor. The manuscript for this paper was submitted for review and possible publication on July 23, 2003; approved on April 6, 2004. This paper is part of the ***Journal of Geotechnical and Geoenvironmental Engineering***, Vol. 130, No. 12, December 1, 2004. ©ASCE, ISSN 1090-0241/2004/12-1236–1249/$18.00.

by others (e.g., Shan and Daniel 1991; Petrov and Rowe 1997; Ruhl and Daniel 1997; Shackelford et al. 2000).

Background

Exchangeable Cations, Mobility of Water, and Hydration of Bentonite

A weak interlayer bond allows the montmorillonite crystal layers to separate during hydration as water molecules enter the interlayer space (Grim 1968; van Olphen 1977). Consequently, cations on the interlayer surfaces become exchangeable, which renders the physical properties of Na-montmorillonite susceptible to interactions with the permeant liquid. The degree of exchange depends on the valence, relative abundance, and size of the cations. Generally, cations of greater valence and smaller size replace cations of lower valence and larger size. The preference for replacement is the lyotropic series, which is $Li^+ < Na^+ < K^+ < Rb^+ < Cs^+ < Mg^{2+} < Ca^{2+} < Ba^{2+} < Cu^{2+} < Al^{3+} < Fe^{3+}$ (Sposito 1981; 1989; McBride 1994). Because Na^+ is at the lower end of the lyotropic series, Na-bentonites are prone to cation exchange when permeated with solutions containing divalent or trivalent ions (Sposito 1981).

Water in the pores of bentonite can be considered mobile or immobile. Mobile water is bulk pore water that is free to move under a hydraulic gradient. Immobile water is bound to the external and internal (i.e., interlayer) mineral surfaces by strong electrical forces, and is believed to act as an extension of the solid surface. When the amount of immobile water in the system increases, the hydraulic conductivity of bentonite decreases because the interparticle flow paths for mobile water become more constricted and tortuous. This is especially true in bentonites where swell is constrained (e.g., needle-punched GCLs or GCLs under confining pressure) (Reeve and Ramaddoni 1965; McNeal and Coleman 1966; McNeal et al. 1966; Lagerwerff et al. 1969; Mesri and Olson 1971; Petrov and Rowe 1997; Shackelford et al. 2000; Jo et al. 2001). Changes in the volume of immobile water also cause volume changes in the bentonite (swell occurs as the volume of immobile water increases). Thus swell and hydraulic conductivity are generally inversely related for bentonites (Shackelford et al. 2000; Jo et al. 2001; Ashmawy et al. 2002; Katsumi et al. 2002).

The fraction of the pore water that is immobile is proportional to the number of layers of water molecules hydrating the interlayer surfaces of the montmorillonite particles (McBride 1994). Hydration of montmorillonite in electrolyte solutions occurs in two phases: the crystalline phase and the osmotic phase (Norrish and Quirk 1954; McBride 1994, Zhang et al. 1995; Prost et al. 1998). The crystalline phase occurs first as several molecular layers of water hydrate the interlayer and outer surfaces from the completely dry state. Osmotic hydration occurs when additional water molecules hydrate the interlayer surfaces, resulting in large interlayer distances (McBride 1994). Crystalline hydration generally results in a small expansion of the interlayer space and a limited amount of immobile water, which is manifested at the macroscale as a small amount of swelling (referred to as "crystalline swell") and higher hydraulic conductivity. Osmotic hydration can result in appreciable expansion of the interlayer space, a large fraction of the pore water being bound, and is responsible for the large amount of swelling (referred to as "osmotic swell") and low hydraulic conductivity often associated with Na-bentonites.

When the interlayer cations are monovalent, both crystalline and osmotic hydration occur, allowing the interlayer spacings to become large. However, only crystalline swelling occurs when the interlayer cations are divalent or trivalent, limiting expansion of the interlayer region to approximately 1.96 nm (four layers of water molecules). Strong electrostatic attraction between the montmorillonite sheets and the interlayer cations prevent osmotic swelling when the cations are polyvalent, despite the larger hydration energy associated with polyvalent cations (McBride 1994; 1997; Quirk and Marčelja 1997). Thus, appreciable swelling and lower hydraulic conductivity occur when the interlayer cations are monovalent, whereas very little swelling and higher hydraulic conductivity occur when the cations are divalent or trivalent (Norrish and Quirk 1954; McBride 1994; Wu et al. 1994; Egloffstein 1997, 2001; Onikata et al. 1999; Jo et al. 2001; Ashmawy et al. 2002). In monovalent solutions, the volume of swelling and spacing of the interlayer region is inversely proportional to the square root of the concentration of the solution (Norrish and Quirk 1954; McBride 1994; Zhang et al. 1995; Onikata et al. 1999).

Hydraulic Conductivity to Single-Species Inorganic Solutions

Mesri and Olson (1971) studied the mechanisms controlling the hydraulic conductivity of bentonite when the interlayer cation was sodium or calcium. At similar void ratios, the hydraulic conductivity of Na-bentonite was approximately five times lower than that of the Ca-bentonite. Mesri and Olson (1971) attributed the lower hydraulic conductivity of the Na-bentonite to the presence of immobile water, which resulted in smaller and more tortuous flow paths for mobile water.

Petrov and Rowe (1997) investigated how NaCl solutions of varying concentration affected the hydraulic conductivity of a GCL containing Na-bentonite. Tests were conducted with distilled (DI) water and NaCl solutions having concentrations between 0.1–2.0 M. Hydraulic conductivity of the GCL generally increased as the NaCl concentration increased. At 2.0 M, the hydraulic conductivity was as much as 800 times higher than that with distilled water. For concentrations less than 0.1 M, the hydraulic conductivity was comparable to that obtained with distilled water. Prehydration with at least one pore volume of distilled water tempered the sensitivity of hydraulic conductivity to salt concentration. For 2.0 M NaCl, prehydration with distilled water resulted in a hydraulic conductivity 25 times lower than that obtained by direct permeation with 2.0 M NaCl. Tests conducted over a range of confining stresses (3 to 118 kPa) showed that, at a given concentration, the hydraulic conductivity can vary by a factor of 10 to 50 depending on the effective stress.

Jo et al. (2001) investigated how cation valence and concentration of single-species salt solutions affect free swell and hydraulic conductivity of nonprehydrated GCLs containing Na-bentonite. Salt solutions with cation valences of 1, 2, and 3 and concentrations between 0.005 and 1.0 M were used. All tests were conducted until the physical and chemical termination criteria in ASTM D 6766 were achieved. Permeation with salt solutions having concentrations less than 0.1 M (monovalent) or 0.01 M (divalent or trivalent) yielded hydraulic conductivities similar to those with DI water ($\approx 10^{-9}$ cm/s), regardless of cation valence. For higher concentrations, swell decreased and hydraulic conductivity increased as the concentration or valence increased. Swelling in the presence of monovalent cations followed the order of the hydrated radius (r_h) and the lyotropic series, with Li ($r_h \approx 0.6$ nm) solutions yielding the greatest swell and K (r_h

≈0.3 nm) solutions yielding the lowest swell at a given concentration. In contrast, hydraulic conductivity to the monovalent solutions was insensitive to cation species. No dependence on species was observed for swell or hydraulic conductivity when the solutions contained divalent or trivalent cations. In addition, solutions with trivalent cations resulted in swell and hydraulic conductivity essentially identical to those obtained with solutions having divalent cations at the same concentration.

Jo et al. (2001) conclude that swell and hydraulic conductivity depend more on valence at intermediate concentrations (0.025 M to 0.1 M), whereas concentration dominates at low (0.005 M) and high (1 M) concentrations. They also conclude that hydraulic conductivity and swelling have a strong inverse relationship, and suggest that swell tests can be used as an indicator of adverse chemical interactions that affect the hydraulic conductivity of GCLs.

Hydraulic Conductivity to Multispecies Inorganic Solutions

Reeve and Bower (1960) investigated how sodium adsorption ratio (SAR) of the permeant solution and electrolyte concentration affected the hydraulic conductivity of a sodic (sodium rich) soil with a montmorillonitic clay fraction. SAR is a ratio describing the relative amounts of sodium, calcium, and magnesium in the pore water equilibrated with the soil, and can be written as (McBride 1994):

$$\mathrm{SAR} = \left[\frac{\mathrm{Na}^+}{[(\mathrm{Ca}^{2+} + \mathrm{Mg}^{2+})/2]^{1/2}} \right]_e \quad (1)$$

where the cation (Na^+, Ca^{2+}, Mg^{2+}) concentrations are expressed in meq/L (note: 1 meq/L=1 mN). The soil had a cation exchange capacity (CEC)=8.9 meq/100 g. The permeant solutions were Salton sea water (SAR=57) and diluted Salton sea water with SAR=40, 27.2, 18.2, and 2.2. Reeve and Bower (1960) found that the rate of monovalent for divalent exchange is a function of the divalent cation concentration and SAR of the permeant solution. At a given SAR, solutions with higher ionic strength resulted in more rapid exchange and higher hydraulic conductivity.

McNeal and Coleman (1966) and McNeal et al. (1966) used Na–Ca solutions to investigate how concentration and SAR affect swelling and hydraulic conductivity of Gila clay from New Mexico, USA, which has CEC=41.2 meq/100 g and consists of 29% montmorillonite. Swelling was quantified as the mass of "bound" solution per mass of clay. Test solutions were prepared with NaCl and $CaCl_2$ salts at concentrations of 0.8, 0.2, 0.05, 0.012, and 0.003 mN with SAR=0, 15, 25, 50, 100, and ∞. Specimens for hydraulic conductivity testing were initially equilibrated by permeation with 10 pore volumes of a 0.8 N solution having the same SAR as the test solution, and then were sequentially permeated with test solutions of decreasing concentration.

McNeal et al. (1966) found no appreciable swell in solutions with SAR=0 (all divalent) regardless of concentration, which is consistent with the lack of an osmotic swelling phase when the interlayer contains polyvalent cations (Norrish and Quirk 1954). Measurable swelling began at 0.012 N and SAR=25, and increased as the SAR of the solution increased. Decreases in hydraulic conductivity occurred with decreasing concentration and increasing SAR of the permeant solution. For example, the hydraulic conductivity was 1.5×10^{-5} cm/s for a 0.8 N solution with SAR=0, 5.9×10^{-6} cm/s for a 0.050 N solution with SAR =100, and 1.5×10^{-7} cm/s for a 0.012 N solution with SAR=∞ (all sodium).

McNeal et al. (1966) concluded that salt concentration and SAR affect swelling and hydraulic conductivity of Gila clay in an inverse manner, which was also reported by Jo et al. (2001) for GCLs permeated with single-species solutions. Increasing the concentration or relative abundance of divalent cations (lower SAR) results in less swell and higher hydraulic conductivity. McNeal et al. (1966) postulate that swelling of montmorillonite is the dominant mechanism affecting its hydraulic conductivity because it affects the opening and closing of pores.

Mustafa and Hamid (1975) investigated how electrolyte concentration and SAR of the permeant solution affected the hydraulic conductivity of two montmorillonitic soils, one containing 32% montmorillonite and the other 14% montmorillonite. The hydraulic conductivity of both soils exhibited the same trends with concentration and SAR as reported by McNeal et al. (1966). However, Mustafa and Hamid (1975) indicate that the relationships between swell, hydraulic conductivity, and characteristics of the permeant solution are unique for each soil.

Malik et al. (1992) investigated how mixed Na–Ca solutions of various concentrations affect swelling, dispersion, and flow in two unsaturated clays reported to be montmorillonitic (the montmorillonite content was not reported). NaCl and $CaCl_2$ solutions with SAR=0, 5, 15, 25, and 50 and concentrations of 3.1, 12.5, 50, 200, and 500 mM were used. Their results were also similar to those reported by McNeal et al. (1966); swell of both soils increased and the hydraulic conductivity decreased as the concentration decreased or the SAR increased.

Materials and Methods

Geosynthetic Clay Liner

The GCL used in this study contains granular sodium bentonite encapsulated between a 170 g/m^2 slit-film monofilament woven geotextile and a 206 g/m^2 staple-fiber nonwoven geotextile. The geotextiles are bonded by needle-punching fibers that are thermally fused to the geotextiles. The specific gravity of the bentonite is 2.65, and the average mass of bentonite per area is 4.3 kg/m^2. The initial thickness of the GCL ranges from 5.5 to 6.5 mm, and the average initial gravimetric water content of the bentonite was 9%.

X-ray diffraction showed that the bentonite contains 86% montmorillonite, 3% quartz, 5% tridymite, 3% plagioclase feldspar, 1% K-feldspar, 1% aragonite, 1% illite/mica, and trace amounts of calcite, siderite, clinoptilolite, rutile, and gypsum. The granule size distribution for the GCL (determined by mechanical sieve analysis on the air-dry bentonite) is shown in Fig. 1 along with the granule size distribution for the GCL used by Jo et al. (2001). Both GCLs contain sand-size bentonite granules, but the GCL used in this study has smaller granules.

The CEC and composition of the exchange complex (Ca, Mg, Na, and K) were measured on two samples of bentonite from the GCL using the procedures in *Methods of Soil Analysis* (Spark 1996). Soluble salts were extracted with DI water and exchangeable metals were extracted with ammonium acetate. These replicate measurements yielded CECs of 65.2 and 73.5 meq/100 g and the following exchange complex: Na—56.1 and 40.0 meq/100 g, K—0.6 and 0.8 meq/100 g, Ca—12.0 and 15.7 meq/100 g, Mg—4.0 and 4.8 meq/100 g. Thus, the bentonite used in this study is predominantly Na-montmorillonite.

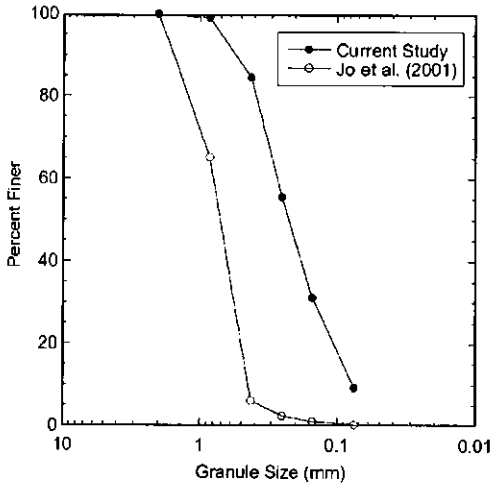

Fig. 1. Granule size distributions for geosynthetic clay liner used in this study and by Jo et al. (2001)

Permeant Liquids

The multispecies salt solutions were prepared with anhydrous inorganic salts (>96% purity) dissociated in DI water. LiCl and NaCl salts were used to investigate the effects of monovalent cations, and $CaCl_2$ and $MgCl_2$ salts were used to investigate the effects of divalent cations. The anionic background (Cl^-) was held constant for all permeant solutions. Type II DI water was used to prepare the solutions and as the reference solution.

A summary of the solutions used in this study is in Table 1. All of the solutions have near neutral pH (6.6 to 8.5). The parameter RMD in Table 1 represents a ratio of the concentrations of monovalent and divalent cations in the permeant solution. RMD is defined as

$$\text{RMD} = \frac{M_M}{\sqrt{M_D}} \tag{2}$$

where M_M=total molarity of monovalent cations; and M_D=total total molarity of divalent cations in the solution. RMD is slightly different from SAR in that RMD characterizes the permeant solution introduced to the soil, whereas SAR generally describes pore water equilibrated with the soil (although SAR has been used to describe solutions by some investigators). RMD also is in terms of molar concentrations (rather than normality), includes all monovalent and divalent cations (SAR is limited to Na, Mg, and Ca) in solution, and does not include a factor of 2 in the denominator (because more than two cations can contribute to M_D).

Solutions having ionic strength (I) ranging from 0.05 to 0.5 M and RMD from 0 to ∞ (all divalent to all monovalent) were used as permeant liquids. These solutions were selected to represent the range of ionic strengths and RMDs expected in leachate from modern disposal facilities for municipal solid waste, hazardous wastes, construction and demolition wastes, fly ash, paper sludge, and mine waste. A review of literature pertaining to the composition of leachates from these wastes is included in Kolstad (2000), and is summarized later in this paper. Most of the solutions were Li–Ca mixtures. However, tests were also conducted with Na–Mg and Li–Na–Ca–Mg mixtures to investigate how cation species affected swell and hydraulic conductivity of the GCL.

Free Swell Tests

Free swell tests were conducted in accordance with ASTM D 5890. Bentonite from the GCL was ground to a fine powder using a mortar and pestle and dry sieved through a No. 200 U.S. standard sieve. The sieved bentonite was air dried for 24 h, and then stored in an airtight container prior to testing. A 100 mL graduated cylinder, accurate to ±0.5 mL, was filled to the 90 mL mark with the test solution. Two grams of sieved bentonite were added to the graduated cylinder in 0.1 g increments. Test solution was then added to the cylinder to reach a final volume of 100 mL by flowing the solution along the cylinder wall so that any particles adhered to the wall would be washed into solution. Swell volume (mL/2 g) was recorded after 24 h, which Jo et al. (2001) report is adequate to establish equilibrium.

Hydraulic Conductivity Tests

Falling head hydraulic conductivity tests with constant tailwater elevation were conducted on the GCL specimens using flexible-wall permeameters in general accordance with ASTM D 5084 and D 6766. An average hydraulic gradient of 100 and effective stress of 20 kPa were applied. Hydraulic gradients this large are uncommon when testing clay soils, but are common when testing GCLs. Large gradients are acceptable when testing GCLs because the differential in effective stress across a thin specimen is not very sensitive to the hydraulic gradient (Shackelford et al. 2000). Aqueous solutions of the inorganic salts (Table 1) were used as the permeant solutions. Backpressure was not used to permit convenient collection of effluent samples for pH and electrical conductivity (EC) testing.

GCL test specimens were prepared by cutting a sample from a GCL panel using a steel cutting ring (105 mm in diameter) and a sharp utility knife following the method described in Daniel et al. (1997). A small amount of test solution was applied along the inner circumference of the ring using a squirt bottle to prevent bentonite loss when removing the specimen from the trimming ring. Excess geotextile fibers were removed from the edge of the specimen with sharp scissors to eliminate potential preferential flow paths between the GCL and flexible membrane (Petrov et al. 1997). Paste prepared with the test solution and bentonite trimmings was delicately placed along the perimeter of the specimen with a small spatula to minimize the potential for sidewall leakage during permeation.

The initial thickness of the GCL specimen was measured to the nearest 0.1 mm with a caliper. Four measurements were made and the average thickness was recorded. The initial weight of the specimen was measured to the nearest 0.01 g. On completion of the hydraulic conductivity test, the specimen was removed from the permeameter and the final thickness and weight were measured in the same manner.

Sidewall leakage and preferential flow paths along the needle-punched fibers are of concern when permeating GCLs with solutions that alter the hydraulic conductivity of bentonite. When relatively high hydraulic conductivities ($>10^{-6}$ cm/s) were obtained, the influent solution was spiked with Rhodamine WT dye (5 mg/L) to stain the flow paths bright red. For all tests that were conducted, the dye tests showed that preferential flow along the needle-punching fibers and the sidewalls did not occur. Jo et al. (2001) report similar findings in their single-species tests on GCLs.

Table 1. Summary of Permeant Solutions

Type of solution	Ionic strength (M)	Monovalent concentration 10^{-2} (M)	Divalent concentration 10^{-2} (M)	RMD ($mM^{1/2}$)	pH	EC (S/m)
Li–Ca	0.05	5.00	0.00	∞	7.4	0.50
		4.35	0.22	0.93	7.6	0.48
		3.33	0.56	0.45	7.7	0.43
		2.00	1.00	0.20	7.2	0.42
		0.00	1.67	0.00	7.8	0.36
Na–Mg		3.33	0.56	0.45	7.4	0.43
Li–Na		3.33	0.56	0.45	7.2	0.43
Ca–Mg		Li(1):Na(3)[a]	Ca(1):Mg(3)[b]			
Li–Ca	0.1	10.0	0.00	∞	6.8	0.88
		8.70	0.44	1.32	7.9	0.87
		8.33	0.56	1.12	8.5	0.88
		7.77	0.77	0.88	8.1	0.87
		6.67	1.11	0.64	7.7	0.86
		5.00	1.67	0.38	7.3	0.80
		2.50	2.50	0.16	7.5	0.77
		1.00	3.00	0.06	7.4	0.72
		0.00	3.33	0.00	7.9	0.70
Na–Mg		8.70	4.35	1.32	6.8	0.87
		6.67	1.11	0.64	6.6	0.86
		1.00	3.00	0.06	7.2	0.73
Li–Na		8.33	0.56	1.12	7.1	0.88
Ca–Mg		Li(3):Na(1)[a]	Ca(3):Mg(1)[b]			
Li–Na		2.50	2.50	0.16	6.5	0.77
Ca–Mg		Li(1):Na(1)[a]	Ca(1):Mg(1)[b]			
Li–Ca	0.2	20.0	0.00	∞	8.1	1.86
		16.7	1.11	1.58	7.2	1.72
		13.3	2.22	0.89	7.1	1.62
		8.00	4.00	0.40	7.2	1.50
		0.00	6.67	0.00	7.2	1.29
Na–Mg		13.3	2.22	0.89	6.7	1.61
Li–Na		8.00	4.00	0.40	7.2	1.50
Ca–Mg		Li(1):Na(3)[a]	Ca(3):Mg(1)[b]			
Li–Ca	0.5	50.0	0.00	∞	8.1	3.45
		38.5	3.85	1.97	7.3	3.46
		31.3	6.25	1.24	8.2	3.29
		20.0	10.0	0.64	8.1	3.03
		0.0	16.7	0.00	7.6	2.74
Na–Mg		31.3	6.25	1.24	7.2	3.30
Li–Na		38.5	3.85	1.97	6.6	3.46
Ca–Mg		Li(3):Na(1)[a]	Ca(1):Mg(3)[b]			
Li–Na		20.0	10.0	0.64	6.9	3.02
Ca–Mg		Li(2):Na(1)[a]	Ca(1):Mg(2)[b]			

Note: RMD=Relative abundance of monovalent and divalent cations; EC=Exchange capacity.

[a]Molar ratio of monovalent cations when two species are present.

[b]Molar ratio of divalent cations when two species are present

The hydraulic conductivity tests were terminated when the termination criteria in ASTM D 5084 and D 6766 were satisfied. The hydraulic conductivity was required to be steady (±25% of the mean with no statistically significant trend for at least four values), the ratio of outflow to inflow was between 0.75 and 1.25 for four consecutive values, and the pH and EC of the influent and effluent deviated less than 10%. A minimum of 2 pore volumes of flow (PVF) was also stipulated, although all tests required more than 2 PVF to satisfy all of the termination criteria (some tests required more than 150 PVF). A pH meter and a portable electrical conductivity probe were used to measure the pH and EC.

Table 2. Summary of Free Swell Data

Ionic strength (M)	RMD $mM^{1/2}$	Free swell (mL/2 g) Li–Ca solutions	Na–Mg solutions	Li–Na–Ca–Mg solutions
0.05	0.93	30.5	—	—
	0.45	24.5	24.5	—
	0.20	22.0	—	—
	0.00	19.0	—	—
0.1	1.32	21.5	21.0	—
	1.12	21.0	—	21.0
	0.88	19.0	—	—
	0.64	17.5	17.5	—
	0.38	14.0	—	—
	0.16	13.5	—	13.0
	0.06	11.5	12.0	—
	0.00	11.0	—	—
0.2	1.67	19.0	—	—
	0.89	15.0	15.5	—
	0.40	12.0	—	12.5
	0.00	9.5	—	—
0.5	1.97	11.5	—	12.0
	1.24	10.5	10.0	—
	0.64	8.5	—	8.5
	0.00	6.5	—	—

Note: Free Swell in distilled water=36.5 mL/2 g; RMD=Relative abundance of monovalent and divalent cations.

Results of Free Swell Tests

Effect of Concentration and Relative Abundance of Monovalent and Divalent Cations

Free swell tests were conducted using solutions with ionic strengths ranging from 0.05 M to 0.5 M and RMD ranging from 0 to 1.97 $mM^{1/2}$. The multispecies solutions were prepared with Li and Ca, Na, and Mg, or Li, Na, Ca, and Mg. Results of the tests are summarized in Table 2.

Free swell is shown as a function of ionic strength in Fig. 2 for the Li–Ca solutions. The data are segregated by solutions that are predominantly divalent (RMD < 0.35 $mM^{1/2}$), solutions with comparable fractions of monovalent and divalent cations (0.35 $mM^{1/2} <$ RMD < 0.90 $mM^{1/2}$), and solutions that are predominantly monovalent (RMD > 0.90 $mM^{1/2}$). Free swell of the bentonite decreases with increasing concentration for each range of RMD. Lower free swell also occurs as the RMD decreases because the presence of more divalent cations suppresses the osmotic component of swelling. RMD also affects the sensitivity to concentration. For the predominantly monovalent solutions (RMD > 0.90 $mM^{1/2}$), the free swell decreases 19 mL/2 g, on average, as the ionic strength is varied between 0.05 to 0.5 M. For the predominantly divalent solutions (RMD < 0.35 $mM^{1/2}$), the free swell decreases 14 mL/2 g, on average, over the same range of ionic strengths.

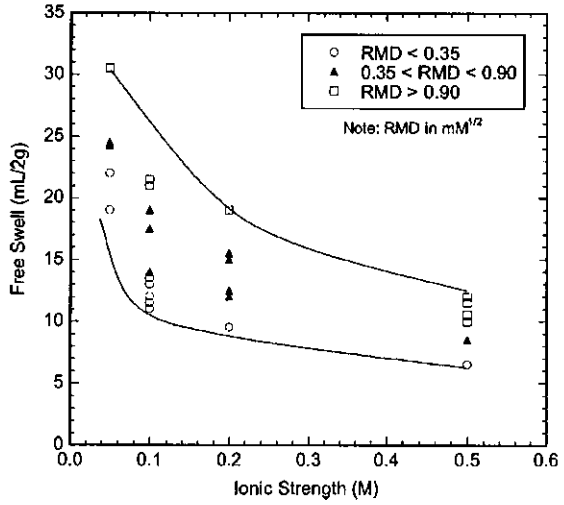

Fig. 2. Free swell of geosynthetic clay liner bentonite as a function of ionic strength for low, intermediate, and high relative abundance of monovalent and divalent cation

The influence of RMD on swell at constant ionic strength is shown in Fig. 3. The relationships are approximately linear, with trend lines fitted to the data using least-squares linear regression. The slope of each trend line reflects the sensitivity of swell to RMD; the intercept is the free swell when the solution only contains divalent cations. When the ionic strength is lower, the trend lines have a larger slope (e.g., slope=12.1 for $I=0.05$ M and 2.6 for $I=0.5$ M), which indicates that RMD has a stronger influence on swelling at low ionic strength and less effect at high ionic strength.

The trends in the free swell tests are consistent with those reported by McNeal et al. (1966) for swelling of Gila clay in mixed Na–Ca solutions. They found a unique relationship between swell and SAR when the concentration was fixed, and that the sensitivity to SAR diminished as the concentration increased. Jo et al. (2001) report similar findings for single species solutions. They found that concentration has a greater effect on free swell for monovalent solutions than divalent solutions.

The sensitivity of free swell to concentration and RMD is

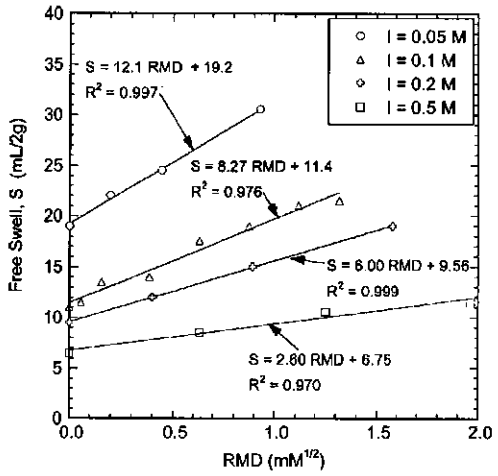

Fig. 3. Free swell of GCL bentonite as a function of RMD for ionic strengths of 0.05, 0.1, 0.2 and 0.5 M

caused by expansion and contraction of the interlayer space as a result of crystalline and osmotic swelling. This effect is illustrated in Fig. 4, which shows basal spacing (i.e., sum of interlayer separation distance and thickness of one montmorillonite layer, also referred to as d_{001}) as a function of ionic strength. The basal spacing was computed using the method in Smalley (1994), which is based on particle geometry, free swell of the bentonite, the thickness of a montmorillonite layer (≈0.9 nm), the basal spacing of Ca-montmorillonite in water (≈1.96 nm), and the free swell of Ca-montmorillonite in water (≈8.0 mL/2 g). The symbol size in Fig. 4 is proportional to RMD (larger symbols for larger RMD). At high ionic strength (0.5 M), the basal spacing (d_{001}) ranges between 1.5 and 2.9 nm, indicating that the swelling is in the crystalline phase ($d_{001} \leq 1.96$ nm) or the low end of the osmotic phase ($d_{001} > 1.96$ nm). In contrast, the basal spacing ranges between 4.5 and 8.6 nm at lower concentration ($I \leq 0.05$ M), which corresponds to crystalline and osmotic swelling ($d_{001} > 1.96$ nm). Moreover, the smallest symbols (lowest RMD)

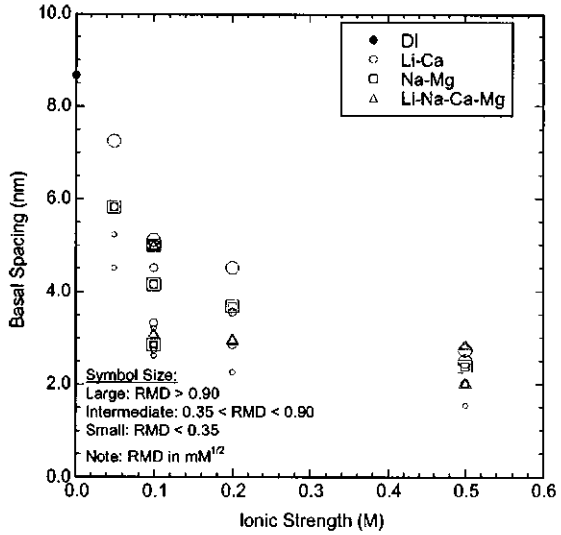

Fig. 4. Free swell of GCL bentonite as a function of computed basal spacing of montmorillonite

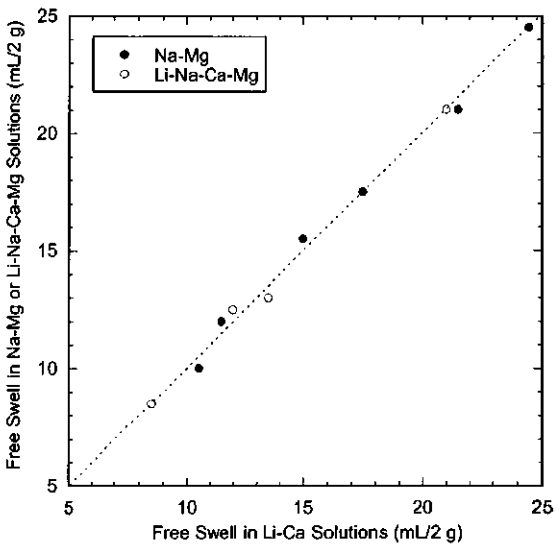

Fig. 5. Comparison of free swell of bentonite in Na–Mg and Li–Na–Ca–Mg solutions to free swell in Li–Ca solutions for solutions prepared with the same ionic strength and RMD

often correspond to the lowest d_{001} for each ionic strength, reflecting suppression of osmotic swelling due to the preponderance of divalent cations.

Effect of Cation Species

The influence of cation species on free swell is illustrated in Fig. 5 using data from the Li–Ca, Na–Mg, and Li–Na–Ca–Mg solutions. Swell in the Na–Mg and Li–Na–Ca–Mg solutions is essentially equal to the swell in the Li–Ca solutions at the same ionic strength and RMD. No discernable effect of cation species is evident. The tendency of divalent cations to suppress osmotic swelling, combined with the insensitivity of free swell to type of divalent cation species (i.e., as in Jo et al. 2001), probably muted any sensitivity to species for the monovalent cations. The single-species tests by Jo et al. (2001) also show that free swell in monovalent solutions is only slightly sensitive to cations species. Thus, free swell is likely to be insensitive to cation species for most monovalent–divalent cation mixtures.

Results of Hydraulic Conductivity Tests

Effect of Concentration and Relative Abundance of Monovalent and Divalent Cations

Hydraulic conductivity tests were conducted using multispecies aqueous solutions listed in Table 1. The ionic strength of the test solutions ranged from 0.05 M to 0.5 M, and the RMD ranged from 0 to 1.97 $mM^{1/2}$. Hydraulic conductivities obtained from these tests are summarized in Table 3.

Hydraulic conductivity is shown in Fig. 6 as a function of ionic strength (I). As in Fig. 2, the solutions have been characterized as primarily divalent (RMD < 0.35 $mM^{1/2}$), comparable mixtures (0.35 $mM^{1/2}$ < RMD < 0.90 $mM^{1/2}$), and primarily monovalent (RMD > 0.90 $mM^{1/2}$). The hydraulic conductivity is sensitive to the composition of the permeant solution, ranging from 5.6×10^{-10} cm/s (I=0.05 M and RMD=0.66 $mM^{1/2}$) to 1.0×10^{-5} cm/s (I=0.5 M and RMD=0), and varies exponentially

Table 3. Summary of Hydraulic Conductivities

Ionic strength (M)	RMD ($mM^{1/2}$)	Hydraulic conductivity (cm/s)		
		Li–Ca solutions	Na–Mg solutions	Li–Na–Ca–Mg solutions
0.05	0.93	5.6×10^{-10}	—	—
	0.45	1.1×10^{-9}	2.1×10^{-9}	—
	0.20	3.0×10^{-9}	—	—
	0.00	9.2×10^{-9}	—	—
0.1	1.32	2.4×10^{-9}	8.9×10^{-10}	—
	1.12	2.3×10^{-9}	—	4.8×10^{-9}
	0.88	3.3×10^{-9}	—	—
	0.64	5.2×10^{-9}	6.5×10^{-9}	—
	0.38	9.3×10^{-9}	—	—
	0.16	9.5×10^{-9}	—	2.1×10^{-8}
	0.06	1.1×10^{-8}	8.5×10^{-9}	—
	0.00	1.3×10^{-8}	—	—
0.2	1.67	2.8×10^{-9}	—	—
	0.89	2.5×10^{-8}	3.4×10^{-8}	—
	0.40	4.9×10^{-8}	—	5.2×10^{-8}
	0.00	1.0×10^{-7}	—	—
0.5	1.97	2.4×10^{-7}	—	9.1×10^{-8}
1.24		8.5×10^{-7}	4.2×10^{-7}	—
0.64		5.0×10^{-6}	—	8.5×10^{-6}
0.00		1.0×10^{-5}	—	—

Note: Hydraulic conductivity to distilled water=9.0×10^{-10} cm/s; RMD=Relative abundance of monovalent and divalent cations.

with ionic strength (linearly on a semilogarithmic graph). The highest hydraulic conductivities at any ionic strength were obtained using the primarily divalent (RMD$<$0.35 $mM^{1/2}$) solutions, and the lowest for the primarily monovalent (RMD$>$0.90 $mM^{1/2}$) solutions.

The effect of RMD at constant ionic strength is shown in Fig. 7. The base-10 logarithm of hydraulic conductivity ($\log_{10}K$) is approximately linearly related to RMD. The trend lines relating

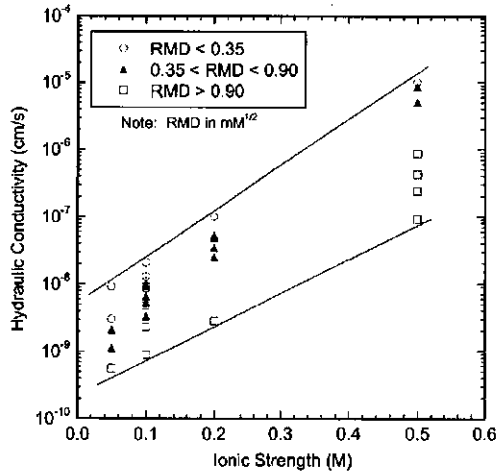

Fig. 6. Hydraulic conductivity of GCL as a function of solution ionic strength for low, intermediate, and high RMD

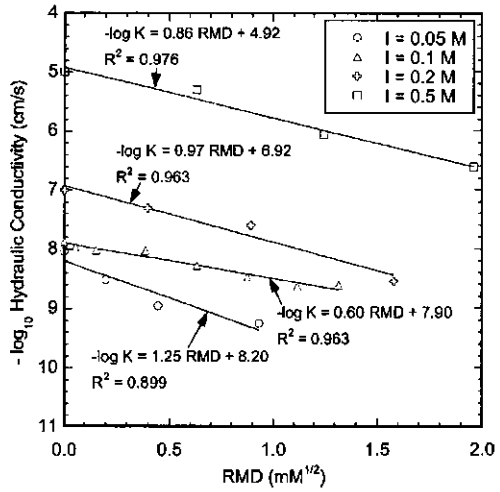

Fig. 7. Hydraulic conductivity of GCL as a function of RMD for ionic strengths of 0.05, 0.1, 0.2, and 0.5 M

$\log_{10}K$ and RMD in Fig. 7 were fit using least-squares linear regression. Their slope describes the sensitivity of hydraulic conductivity to RMD, and the intercept is the hydraulic conductivity to the divalent solution. The hydraulic conductivity exhibits greater sensitivity to RMD at lower ionic strength (i.e., slope $=1.25$ at $I=0.05$ M and 0.86 at $I=0.5$ M). The data for the tests conducted at an ionic strength of 0.1 M are an exception to the trend. The reason for this deviation is unknown.

The trends in Figs. 6 and 7 are comparable to the trends reported by McNeal and Coleman (1966) for Gila clay. They found that the hydraulic conductivity increases with increasing concentration and decreasing SAR, and distinct curves relating hydraulic conductivity to SAR exists when the concentration is fixed. McNeal and Coleman (1966) report that SAR has a stronger influence on hydraulic conductivity at low concentrations, and that the effect of SAR diminishes at high concentrations. Jo et al. (2001) also report similar sensitivity to ionic strength and cation valence for single species solutions. At a given ionic strength, the highest hydraulic conductivities were obtained with divalent or trivalent solutions, and the lowest with monovalent solutions.

A diminished effect of ionic strength and RMD probably would have been observed had much lower or much higher ionic strengths been used. For example, DI water is the limiting case for dilute solutions (in this study, the hydraulic conductivity of the GCL to DI water was 9.0×10^{-10} cm/s). In addition, Jo et al. (2001) report that the hydraulic conductivity of the GCL they tested leveled off between 10^{-5} to 10^{-4} cm/s for ionic strengths greater than 1 M. When the ionic strength is high, osmotic swelling becomes negligible, and the basal spacing is reduced to its smallest value in the hydrated state ($\approx$2 nm). Once this compressed condition is reached, no further increase in hydraulic conductivity can occur. In fact, a decrease in hydraulic conductivity is possible due to the higher viscosity of concentrated solutions (Fernandez and Quigley 1988).

Effect of Cation Species

Li–Ca, Na–Mg, and Li–Na–Ca–Mg solutions having various RMD and ionic strengths were used to investigate how differences in cation species affect the hydraulic conductivity of GCLs

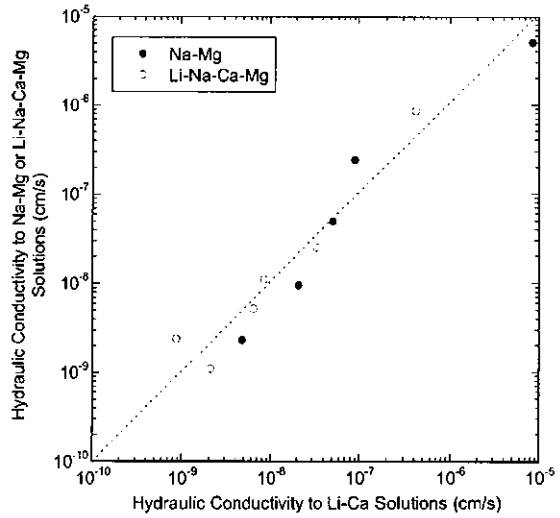

Fig. 8. Comparison of hydraulic conductivities of GCL obtained with Na–Mg and Li–Na–Ca–Mg solutions to hydraulic conductivities obtained with Li–Ca solutions for solutions prepared with the same ionic strength and RMD

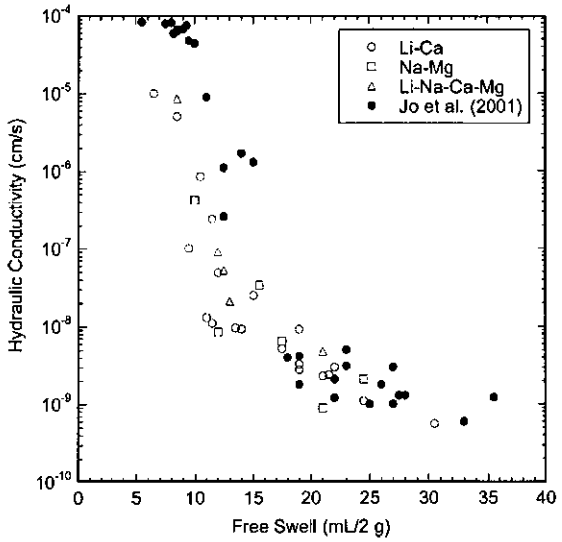

Fig. 9. Hydraulic conductivity of GCL as a function of free swell of bentonite. Test data are from this study and from Jo et al. (2001)

permeated with mixed solutions. Composition of each solution is summarized in Table 1 and the hydraulic conductivities are in Table 3.

Hydraulic conductivities obtained using the Li–Ca solutions are compared with those obtained from the Na–Mg and Li–Na–Ca–Mg solutions in Fig. 8. At comparable ionic strengths and RMD, essentially the same hydraulic conductivities were obtained with the Na–Mg and Li–Na–Ca–Mg solutions as with the Li–Ca solutions. No discernable effect of cation species is apparent. The insensitivity of hydraulic conductivity to cation species is analogous to the insensitivity of free swell to cation species. Differences in preference of the montmorillonite for Ca over Mg and Na over Li appear to have a small effect compared to the effects of RMD and concentration. In addition, Jo et al. (2001) found that the hydraulic conductivity was insensitive to cation species for a given valence.

The insensitivity to cation species evident in Fig. 8, combined with the insensitivity to cation species observed by Jo et al. (2001) for single-species solutions, suggests that the hydraulic conductivity at fixed RMD is likely to be insensitive to cation species in most monovalent–divalent mixtures. Moreover, Jo et al. (2001) found that permeation with single-species solutions containing divalent and trivalent cations yielded essentially the same hydraulic conductivity at a given concentration. Thus, the insensitivity to cation species may extend to multispecies solutions in general, with ionic strength and RMD being the dominant variables controlling hydraulic conductivity. In this case, the denominator of RMD would include the total normality of the polyvalent (valence $\geq +2$) cations in the solution. While this hypothesis is plausible, more testing is needed to confirm its validity.

Practical Implications

Free Swell and Hydraulic Conductivity

Jo et al. (2001) show that a strong relationship exists between free swell of bentonite and the hydraulic conductivity of GCLs exposed to single-species solutions. A similar relationship could be expected for multispecies solutions as well because Figs. 2, 3, 6, and 7 show that ionic strength and RMD affect swell and hydraulic conductivity in a consistent and similar manner. McNeal et al. (1966) also report a strong correlation between swelling and hydraulic conductivity for Gila clay permeated with solutions having different ionic strengths and SAR.

Hydraulic conductivity of the GCL specimens permeated with the multispecies solutions is shown in Fig. 9 as a function of free swell along with the single-species data from Jo et al. (2001). A strong relationship exists between hydraulic conductivity and free swell for both data sets. The slight offset in the two data sets at lower swell volumes (and higher hydraulic conductivities) is most likely due to differences in the granule size distributions of the bentonites and not the use of multispecies versus single species solutions. The GCLs used in both studies were essentially identical, except the bentonite in the GCL used in this study has smaller granules than the bentonite in the GCL used by Jo et al. (2001) (Fig. 1). Mesri and Olson (1971) and McNeal et al. (1966) indicate that bentonites with larger "domains" (quasi-crystals) permit larger flow paths and higher hydraulic conductivity. In addition, Katsumi et al. (2002) show that nonprehydrated GCLs containing bentonite with larger granules are more permeable than GCLs with smaller granules when permeated using stronger ($\geq$0.2 M) salt solutions. Because the granules do not swell appreciably in strong solutions, bentonites with larger granules have larger intergranular pores, and higher hydraulic conductivity. That is, the hydraulic conductivity of granular bentonite permeated with strong solutions follows a similar relationship with particle size as do granular soils; i.e., the hydraulic conductivity increases as the particle size increases, all factors being equal (e.g., Lambe and Whitman 1969; Terzaghi et al. 1996). In contrast, granule size has no effect on free swell, because the bentonite is crushed to pass the No. 200 sieve prior to free swell testing.

McNeal et al. (1966) conclude that swelling of expansive minerals such as montmorillonite is the dominant mechanism affecting the hydraulic conductivity. The results of this study, as well as those in Jo et al. (2001), support this conclusion. The trends shown in Fig. 9 also indicate that free swell tests can be a relatively simple and quick screening method to evaluate the compat-

ibility of GCLs permeated with inorganic salt solutions containing mixtures of cations. Although not a surrogate for chemical compatibility testing (direct testing is needed to demonstrate that a GCL is compatible with a liquid), free swell testing can be used to identify liquids that are incompatible with GCLs. The data in Fig. 9 also illustrate that the relationship between hydraulic conductivity and free swell is bentonite specific, and needs to be identified empirically.

Estimating Hydraulic Conductivity

The approximately linear trends shown in Figs. 6 and 7 suggest that a relatively simple empirical model can be used to estimate hydraulic conductivity of GCLs as a function of ionic strength and RMD. A model relating these parameters was developed using stepwise regression (Draper and Smith 1998) using a significance level of 0.05:

$$\frac{\log K_c}{\log K_{DI}} = 1.085 - 1.097I + 0.0398I^2\ \text{RMD} \qquad (3)$$

In Eq. 3, K_c=hydraulic conductivity to the inorganic chemical solution and K_{DI}=hydraulic conductivity to deionized water. The R^2 for Eq. (3) is 0.967 and the p statistic is less than 0.0001. Eq. (3) is linear in both I and RMD, and the product $I^2 \times$ RMD reflects that the sensitivity to RMD varies nonlinearly with ionic strength (e.g., as in Fig. 7). Eq. (3) is valid for I=0.05–0.5 M and RMD < 2.0 $mM^{1/2}$.

Eq. (3) is based on data from the GCL tested in this study under the state of stress that was employed (effective stress =20 kPa). However, Eq. (3) can be used to *estimate* how inorganic solutions may affect the hydraulic conductivity of other GCLs provided they employ granular Na-bentonite consisting of approximately 80% montmorillonite. Many of the GCLs used in North America today fit this description. Even if the granule size or montmorillonite content differs from those in this study, the relative effects of ionic strength and RMD should be approximately correct. In addition, Petrov and Rowe (1997) show that the hydraulic conductivity of GCLs exhibits similar sensitivity to effective stress regardless of whether DI water or a salt solution is used as the permeant liquid. Thus, Eq. (3) can be used to *estimate* the hydraulic conductivity at different effective stresses if the hydraulic conductivity to DI water at these stresses is known.

A comparison of K_c predicted with Eq. (3) and the measured hydraulic conductivity is shown in Fig. 10(a). The contour lines in Fig. 10 correspond to Eq. (3), whereas the data points correspond to the I and RMD for the tests conducted in this study. Eq. (3) captures the data reasonably well. Hydraulic conductivities predicted with Eq. (3) are also shown as contours in Fig. 10(b) along with points corresponding to I and RMD for actual leachates from a variety of wastes and solid waste disposal facilities reviewed by Kolstad (2000). The ionic strength and RMD of each leachate is summarized in Table 4, along with the data source (literature and regulatory agency reports) and the type of containment facility. The points and contour lines in Fig. 10(b) illustrate what hydraulic conductivity likely would have been had the GCL used in this study been tested with these leachates.

Of the 50 points shown in Fig. 10(b), 37 fall below 10^{-7} cm/s (74%) and 24 fall below 10^{-8} cm/s (48%). Thus, GCLs with high hydraulic conductivities ($>10^{-7}$ cm/s) should not be common in bottom liners where leachates similar to those in Table 4 are likely to be found. Moreover, many of the points in Fig. 10(b) associated with high hydraulic conductivities correspond to "young" (landfill age < 5 yr) municipal solid waste (MSW)

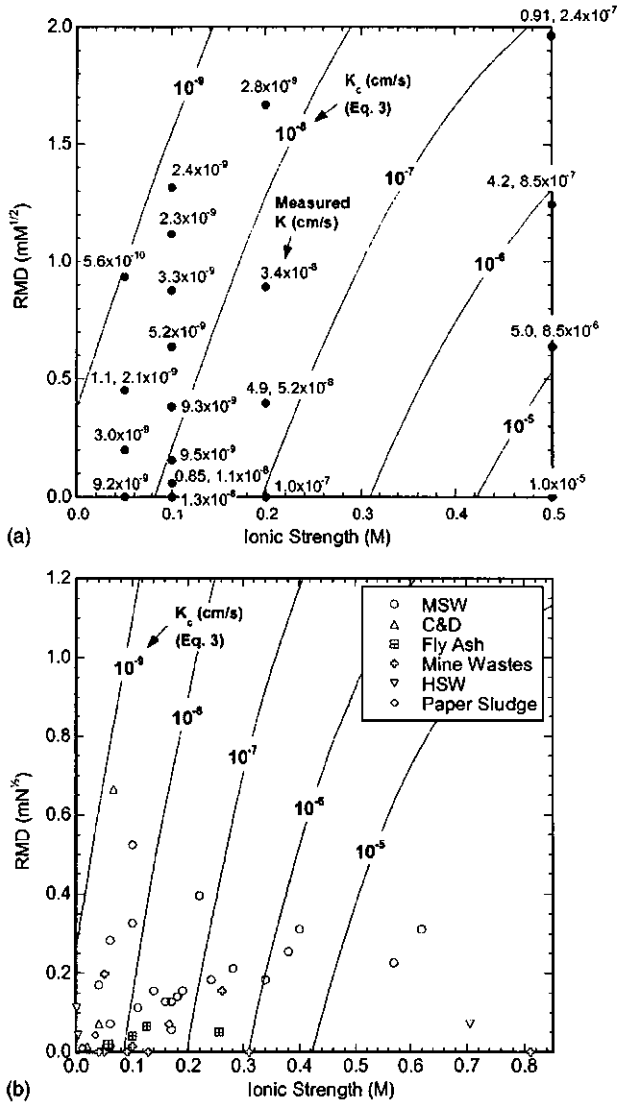

Fig. 10. Contours of hydraulic conductivity as a function of RMD and ionic strength predicted with Eq. (3) along with (a) measured hydraulic conductivities as solid circles and (b) points corresponding to ionic strength and RMD of various leachates. Data from Williams (1975) (I=1.87 M and RMD=0) and Kolstad (2000) (I=1.37 M and RMD=2.52 $mM^{1/2}$) are off the scale in (b).

leachates (Table 4). The composition of MSW leachate changes over time, and thus high hydraulic conductivities may not be realized because of the relatively long time required for a GCL and leachate to reach equilibrium under field conditions (Jo 2003). However, some of the points for mine waste, paper sludge, and fly ash disposal facilities are associated with high hydraulic conductivities, and the composition of leachates from these wastes can be persistent.

Effect of Prehydration

The results of this study pertain specifically to nonprehydrated GCLs. Different results may have been obtained had the GCLs been completely prehydrated by permeation with DI or potable water for several pore volumes of flow. Comparisons between hydraulic conductivities of nonprehydrated and completely prehy-

Table 4. Summary of Ionic Strength and RMD of Various Leachates

Source	Leachate type	Ionic strength (M)	RMD ($mM^{1/2}$)
Ehrig (1983)	Young MSW leachate (<5 yr)	0.28	0.21
Pohland (1980)		0.38	0.25
Tchbanoglous et al. (1993)		0.14	0.16
Chian and DeWalle (1976)		0.17	0.13
Cheremisinoff (1983)		0.22	0.40
Alker et al. (1995)		0.16	0.13
Chian and DeWalle (1975)		0.57	0.23
Chian and DeWalle (1975)		0.62	0.31
Chian and DeWalle (1975)		0.34	0.18
Farquhar (1989)		0.40	0.31
Shams et al. (1994)		0.24	0.18
Ehrig (1983)	Intermediate MSW leachate (5–10 yr)	0.10	0.52
Pohland (1980)		0.10	0.33
Chian and DeWalle (1975)		0.17	0.06
Chian and DeWalle (1975)		0.11	0.11
Farquhar (1989)		0.18	0.14
Chian and DeWalle (1975)	Old MSW leachate (>10 yr)	0.06	0.01
Chian and DeWalle (1975)		0.06	0.28
Farquhar (1989)		0.06	0.07
Alker et al. (1995)		0.04	0.17
Kmet and McGinley (1982)	MSW leachate	0.19	0.16
Ruhl and Daniel (1997)	C and D leachate	0.04	0.17
Kolstad (2000)		0.05	0.01
Kolstad (2000)		0.02	0.01
WMNA (1993)		0.04	0.07
Weber et al. (2002)		0.066	0.66
Kolstad (2000)	Fly ash leachate	0.03	0.25
Kolstad (2000)		0.03	0.06
Kolstad (2000)		0.02	0.10
Kolstad (2000)		0.05	0.23
Kolstad (2000)		0.06	0.13
Kolstad (2000)		0.07	0.20
Kolstad (2000)		0.37	2.52
Kolstad (2000)		0.76	0.71
Al et al. (1994)	Mine process water	0.05	0.00
Shackelford (1998)		0.04	0.00
Jordan et al. (1998)		0.05	0.20

Table 4. (*Continued.*)

Source	Leachate type	Ionic strength (M)	RMD ($mM^{1/2}$)
Williams (1975)	Acidic mine waste drainage	1.87	0.00
Christensen and Laake (1996)		0.13	0.00
Christensen and Laake (1996)		0.09	0.00
Al et al. (1994)		0.81	0.00
Shackelford (1998)		0.31	0.00
Williams (1975)	Pyritic tailings leachate	0.26	0.16
Pettit and Scharer (1999)	Ur rock drainage	0.10	0.01
Kolstad (2000)	Hazardous waste leachate	0.001	0.11
		0.70	0.07
		0.003	0.04
Kolstad (2000)	Paper mill landfill leachate	0.17	0.07
		0.01	0.01
		0.03	0.04

Note: RMD=Relative abundance of monovalent and divalent cations; MSW=Municipal solid waste.

drated GCLs that have been permeated long enough to establish chemical equilibrium between the bentonite solid and the solution show that prehydration by permeation with DI water results in hydraulic conductivities an order of magnitude lower than those obtained without prehydration, even if cation exchange between the mineral surface and the permeant liquid is complete (Petrov and Rowe 1997; Jo et al. 2004).

Although the effect of complete prehydration is significant, complete prehydration is unlikely to occur in the field. Most GCLs in field applications hydrate as water is drawn to the bentonite from an underlying subgrade via vapor diffusion or gradients in matric potential (Daniel et al. 1993, 1998; Katsumi et al. 2003). The prehydration afforded by these processes does not appear to have the same effect as complete prehydration by direct permeation. Vasko et al. (2001) found that the hydraulic conductivity of GCLs prehydrated with DI water via capillary wetting and vapor diffusion and permeated with $CaCl_2$ solutions had essentially the same hydraulic conductivity as nonprehydrated GCLs unless the solution was very strong (concentration >0.1 M). Comparable findings are reported by Katsumi et al. (2003). These observations suggest that hydraulic conductivities reported in this study are likely to be more representative of most field conditions than hydraulic conductivities of completely prehydrated GCLs.

Summary and Conclusions

This study dealt with the influence of multispecies inorganic salt solutions on swelling and hydraulic conductivity of nonprehydrated GCLs. Free swell and hydraulic conductivity tests were conducted on nonprehydrated specimens of a commercially available GCL using DI water and aqueous solutions of LiCl, NaCl, $CaCl_2$, and $MgCl_2$ salts. The relative amounts of monovalent and divalent cations in solution were quantified with the parameter RMD, which is the ratio of the total molarity of monovalent cations to the square root of the total molarity of divalent cations.

Results of the free swell tests show that swell is directly related to RMD and inversely related to ionic strength. RMD has a strong effect on swell in weaker solutions, and a modest effect in strong solutions. Similar findings were obtained from the hydraulic conductivity tests. Hydraulic conductivity was found to be directly related to ionic strength and inversely related to RMD, with RMD having a greater effect on hydraulic conductivity in weaker solutions. Tests were also conducted to determine if cation species affects swell or hydraulic conductivity. No discernable effect of cation species was evident in the free swell or hydraulic conductivity for tests conducted at a given ionic strength and RMD.

A strong relationship between hydraulic conductivity and free swell was found that is analogous to the relationship reported by Jo et al. (2001) for tests conducted using single-species salt solutions. However, the hydraulic conductivity-free swell relationship is not unique, and must be defined empirically for a particular bentonite if free swell tests are to be used for chemical compatibility screening.

The hydraulic conductivity data were also used to develop a regression model relating hydraulic conductivity of the GCL to ionic strength and RMD of the permeant solution. Predictions made with the model indicate that high hydraulic conductivities (i.e., $>10^{-7}$ cm/s) are unlikely for nonprehydrated GCLs in base liners in many solid waste containment facilities. However, for some wastes that transmit stronger leachates or leachates that are dominated by polyvalent cations (e.g., fly ash, paper sludge, and mine wastes), high hydraulic conductivities may be realized provided adequate time exists for the bentonite and leachate to reach chemical equilibrium.

Acknowledgments

Funding for this study was provided in part by the National Science Foundation (Grant No. CMS-9900336). Professor Charles D. Shackelford of Colorado State Univ. provided technical and laboratory assistance during the study along with thoughtful discussion. The writers are grateful for his assistance.

References

Al, T., Blowes, D., and Jambor, J. (1994). "A geochemical study of the main tailings impoundment at the Falconbridge Limited, Kidd Creek Division metallurgical site, Timmins, Ontario," *Environmental chemistry of sulfide mine-wastes*, J. Jambor and D. Blowes, eds., Mineralogical Society of Canada, Ottawa, 333–364.

Alker, S., Sarsby, R., and Howell, R. (1995). "The composition of leachate from waste disposal sites," *Waste disposal by landfill—GREEN '93 Symposium*, Sarsby, R., ed., Balkema, Rotterdam, The Netherlands.

Alther, G., Evans, J., Fang, H., and Witmer, K. (1985). Influence of inorganic permeants upon the permeability of bentonite, *Hydraulic barriers in soil and rock, ASTM STP 874*, A. Johnson, R. Frobel, N. Cavalli, and C. Pettersson, Eds., ASTM, West Conshohocken, Pa., 64–73.

Ashmawy, A., El-Hajji, D., Sotelo, N., and Muhammad, N. (2002), "Hydraulic performance of untreated and polymer-treated bentonite in inorganic landfill leachates." *Clays Clay Miner.*, 50(5), 545–551.

Cheremisinoff, P. (1983). *Leachate from hazardous waste sites*, 1st Ed., Technomic Inc., Lancaster, Pa.

Chian, E., and DeWalle, F. (1975). "Characterization and treatment of leachates generated from landfills," *AIChE Symp. Ser.*, 71(145), 319–327.

Chian, E., and DeWalle, F. (1976). "Sanitary landfill leachates and their leachate treatment." *J. Environ. Eng. Div. (Am. Soc. Civ. Eng.)*, 102(2), 411–431.

Christensen, B., and Laake, M. (1996). "Treatment of acid mine water by sulfate-reducing bacteria; Results from a bench-scale experiment." *Water Res.*, 30(7), 1617–1624.

Daniel, D., Shan, H., and Anderson, J. (1993). Effects of partial wetting on the performance of the bentonite component of a GCL, *Geosynthetics 93*, Industrial Fabrics Assoc. International, St. Paul, MN, 1483–1496.

Daniel, D., Bowders, J., and Gilbert, R. (1997). "Laboratory hydraulic conductivity tests for saturated soils." *Hydraulic conductivity and waste contaminant transport in soil, ASTM STP 1142*, D. Daniel and S. Trautwein, eds., ASTM, West Conshohocken, Pa., 30–78.

Daniel, D., et al. (1998). "Slope stability of geosynthetic clay liner test plots." *J. Geotech. Geoenviron. Eng.*, 124(7), 628–637.

Draper, N., and Smith, H. (1998), *Applied regression analysis*, 3rd Ed., Wiley, New York.

Egloffstein, T. (1997). "Geosynthetic clay liners, part six: Ion exchange," *Geotech. Fabr. Rep.*, 15(5), 38–43.

Egloffstein, T. (2001). "Natural bentonites-influence of the ion exchange and partial desiccation on permeability and self-healing capacity of bentonites used in GCLs." *Geotext. Geomembr.*, 19, 427–444.

Ehrig, R. J. (1983). "Quality and quantity of sanitary landfill leachate." *Waste Manage. Res.*, 1, 53–68.

Farquhar, G. J. (1989). "Leachate: Production and characterization." *Can. J. Civ. Eng.*, 16, 317–325.

Fernandez, F., and Quigley, R. (1988), "Viscosity and dielectric controls on the hydraulic conductivity of clayey soils permeated with water-soluble organics." *Can. Geotech. J.*, 25, 582–589

Grim, R. (1968). *Clay mineralogy*, 2nd Ed., McGraw–Hill, New York, 596.

Jo, H. (2003). "Cation exchange and hydraulic conductivity of geosynthetic clay liners (GCLs) permeated with inorganic salt solutions." PhD dissertation, Univ. of Wisconsin—Madison, Wis.

Jo, H., Benson, C., and Edil, T. (2004). "Hydraulic Conductivity and Cation Exchange in Non-Prehydrated and Prehydrated Bentonite Permeates with Weak Inorganic Salt Solutions," *Clays Clay Miner.*, 52(6), 661–679.

Jo, H., Katsumi, T., Benson, C., and Edil, T. (2001). "Hydraulic conductivity and swelling of nonprehydrated GCLs permeated with single-species salt solutions." *J. Geotech. Geoenviron. Eng.*, 127(7), 557–567.

Jordan, D., Newcomer, R., and Mac Kinnon, R. (1998). "Geochemical transport modeling of tailing pore water." *Tailings and mine waste'98*, Balkema, Amsterdam, 497–506.

Katsumi, T., et al. (2002). "Geosynthetic clay liners against inorganic chemical solutions." *Proc., 2nd Japan–Korea Joint Seminar on Geoenvironmental Engineering*, Kyoto Univ., Kyoto, Japan, 27–32.

Katsumi, T., Ogawa, A., and Fukagawa, R. (2003). "Hydraulic conductivity of prehydrated clay geosynthetic barriers." *Proc., 3rd Korea–Japan Joint Seminar on Geoenvironmental Engineering*, Seoul National Univ., Seoul, pp. 63–68.

Kmet, P., and McGinley, M. (1982). *Chemical characteristics of leachate from municipal solid waste landfills in Wisconsin*, Bureau of Solid Waste Management, Wisconsin Department of Natural Resources, Madison, Wis.

Kolstad, D. (2000). "Compatibility of geosynthetic clay liners (GCLs) with multispecies inorganic solutions." MS thesis, Univ. of Wisconsin—Madison, Wis.

Lagerwerff, J., Nakayama, F., and Fere, M. (1969). "Hydraulic conductivity related to porosity and swelling of soils." *Soil Sci. Soc. Am. Proc.*, 33, 3–11.

Lambe, T., and Whitman, R. (1969), *Soil mechanics*, Wiley, New York.

Malik, M., Mustafa, M. A., and Letey, J. (1992). "Effect of mixed Na/Ca solutions on swelling, dispersion, and transient water flow in unsaturated montmorillonitic soils." *Geoderma*, 52, pp. 17–28.

McBride, M. (1994). *Environmental chemistry of soils*, Oxford University Press, New York, 406.

McBride, M. (1997). "A critique of diffuse double layer models applied to colloid and surface chemistry." *Clays Clay Miner.*, 45(4), 598–608.

McNeal, B., and Coleman, N. (1966). "Effect of solution composition on soil hydraulic conductivity." *Am. J. Soil Sci.*, 30, 308–312.

McNeal, B., Norvell, W., and Coleman, N. (1966). "Effect of solution composition on the swelling of extracted soil clays." *Am. J. Soil Sci.*, 30, 313–317.

Mesri, G., and Olson, R. (1971). "Mechanisms controlling the permeability of clays." *Clays Clay Miner.*, 19, 151–158.

Mustafa, M., and Hamid, K. (1977). "Comparison of two models for predicting the relative hydraulic conductivity of salt-affected swelling soils." *Soil Sci.*, 123, 149–154.

Norrish, K., and Quirk, J. (1954). "Crystalline swelling of montmorillonite, Use of electrolytes to control swelling." *Nature (London)*, 173, 255–257.

Onikata, M., Kondo, M., Hayashi, N., and Yamanaka, S. (1999). "Complex formation of cation exchanged montmorillonites with propylene carbonate: Osmotic swelling in aqueous electrolyte solutions." *Clays Clay Miner.*, 47(5), 672–677.

Pettit, C., and Scharer, J. (1999). "Neutral mine drainage." *Mining and the Environment II Conference Proceedings*, Vol. 2, Sudbury, Ontario. Goldsack, D., Belzile, N., Yearwood, P., and Hall, G., eds., pp. 372–376.

Petrov, R., and Rowe, R. (1997). "Geosynthetic clay liner (GCL)—Chemical compatibility by hydraulic conductivity testing and factors impacting Its performance." *Can. Geotech. J.*, 34, 863–885.

Petrov, R., Rowe, R., and Quigley, R. (1997). "Comparison of laboratory-measured GCL hydraulic conductivity based on three permeameter types." *Geotech. Test. J.*, 20(1), 49–62.

Pohland, F. G. (1980). "Leachate recycle as a landfill management option." *ASME J. Offshore Mech. Arct. Eng.*, 106(6), 1057–1069.

Prost, R., Koutit, T., Benchara, A., and Huard, E. (1998). "State and location of water adsorbed on clay minerals: Consequences of the

hydration and swelling-shrinkage phenomena." *Clays Clay Miner.*, 46(2), pp. 117–131.

Quaranta, J., Gabr, M., and Bowders, J. (1997). "First-exposure performance of the bentonite component of a GCL in a low-pH, calcium-enriched environment." *Testing and acceptance criteria for geosynthetic clay liners, ASTM STP 1308*, L. Well, eds., ASTM, West Conshohocken, Pa., 162–177.

Quirk, J., and Marčelja, S. (1997). "Application of double-layer theories to the extensive crystalline swelling of Li-montmorillonite." *Langmuir*, 13, 6241–6248.

Reeve, R., and Bower, C. (1960). "Use of high-salt waters as a flocculant and source of divalent cations for reclaiming sodic soils." *Soil Sci.*, 90, 139–144.

Reeve, R., and Ramaddoni, G. (1965). "Effect of electrolyte concentration on laboratory permeability and field intake rate of a sodic soil." *Soil Sci.*, 99, 262–266.

Ruhl, J., and Daniel, D. (1997). "Geosynthetic clay liners permeated with chemical solutions and leachates." *J. Geotech. Geoenviron. Eng.*, 123(4), 369–381.

Shackelford, C. (1998). GCL compatibility testing for base liner at the tailings management area for the proposed nicolet minerals company zinc/copper mine, near Crandon, Wisconsin, *Final Rep. Prepared for Foth & Van Dyke and Assoc., Inc.*, Green Bay.

Shackelford, C., Benson, C., Katsumi, T., Edil, T., and Lin, L. (2000). "Evaluating the hydraulic conductivity of GCLs permeated with nonstandard liquids." *Geotext. Geomembr.*, 18, 133–161.

Shams-Khorzani, R., Knox, T., and Brockway, C. (1994). "Sanitary landfill leachate treatment and disposal." *Public Works*, 125(7), 46–49.

Shan, H., and Daniel, D. (1991). "Results of laboratory tests on a geotextile/bentonite liner material." *Geosynthetics 2001*, Industrial Fabrics Assoc. International, St. Paul, Minn., 517–535.

Shan, H., and Lai, Y. (2002). "Effect of hydrating liquid on the hydraulic properties of geosynthetic clay liners." *Geotext. Geomembr.*, 20, 19–38.

Smalley, M. (1994). "Electrical theory of clay swelling." *Langmuir*, 10, 2884–2891.

Spark, D. L. (1996). *Methods of soil analysis, Part 3. Chemical methods*, Soil Science Society of America, Madison, Wis., 1201–1230.

Sposito, G. (1981). *The thermodynamics of soil solutions*, Oxford University Press, New York.

Sposito, G. (1989). *The chemistry of soils*, Oxford University Press, New York.

Tchobanoglous, G., Theisen, H., and Vigil, S. (1993). *Integrated solid waste management*, 1st Ed., McGraw–Hill, New York, 978.

Terzaghi, K., Peck, R., Mesri, G. (1996). *Soil mechanics in engineering practice*, 3rd Ed., Wiley, New York.

Van Olphen, H. (1977). *An introduction to clay colloid chemistry*, 2nd Ed., Wiley, New York.

Vasko, S., Jo, H., Benson, C., Edil, T., and Katsumi, T. (2001). "Hydraulic conductivity of partially prehydrated geosynthetic clay liners permeated with aqueous calcium chloride solutions." *Geosynthetics 2001*, Industrial Fabrics Assoc. International, St. Paul, Minn., 685–699.

Weber, W., Jang, Y., Townsend, T., and Laux, S. (2002). "Leachate from land disposed residential construction waste." *J. Environ. Eng.*, 128(3), 237–245.

Williams, R. (1975). *Waste production and disposal in mining, milling and metallurgical industries*, Millar Freeman Publications.

Waste Management of North America, Inc. (WMNA). (1993). *Construction and demolition landfill leachate characterization study*, WMNA, Naperville, Ill.

Wu, J., Low, P., and Roth, C. (1994). "Effect of 1,4-dioxane on the expansion of montmorillonite layers in a montmorillonite/water system." *Clays Clay Miner.*, 42(2), 109–113.

Zhang, F., Low, P., and Roth, C. (1995). "Effects of monovalent exchangeable cations and electrolytes on the relation between swelling pressure and interlayer distance in montmorillonite." *J. Colloid Interface Sci.*, 173, 34–41.

Errata for "Hydraulic Conductivity and Swell of Nonprehydrated Geosynthetic Clay Liners Permeated with Multispecies Inorganic Solutions" by D. Kolstad, C. Benson, and T. Edil

December 2004, Vol. 130, No. 12, 1236–1249.
DOI: 10.1061/(ASCE)1090.0241(2004)130:12(1236)

Dale C. Kolstad, M.ASCE
Environmental Engineer, Barr Engineering Company, 4700 West 77th St., Minneapolis, MN 55435. E-mail: dkolstad@barr.com

Craig H. Benson, M.ASCE
Professor, Dept. of Civil and Environmental Engineering, Univ. of Wisconsin, Madison, WI 53706. E-mail: benson@engr.wisc.edu

Tuncer B. Edil, M.ASCE
Professor, Dept. of Civil and Environmental Engineering, Univ. of Wisconsin, Madison, WI 53706. E-mail: edil@engr.wisc.edu

The following corrections should be noted.

The units for RMD in the text and graphs in this paper should be $M^{1/2}$ rather than the units of $mM^{1/2}$ shown in the published version. Eq. (3) also contained typographical errors. The correct version is

$$\frac{\log K_c}{\log K_{DI}} = 0.965 - 0.976I + 0.0797\text{RMD} + 0.251I^2\text{RMD} \quad (3)$$

In addition, the plotting positions for the fly ash leachates were reversed in Fig. 10(b) (i.e., the fly ash leachate data were plotted as I versus RMD instead of RMD versus I). A correct version of Fig. 10(b) is presented here. These errors do not affect any of the conclusions or inferences in the paper.

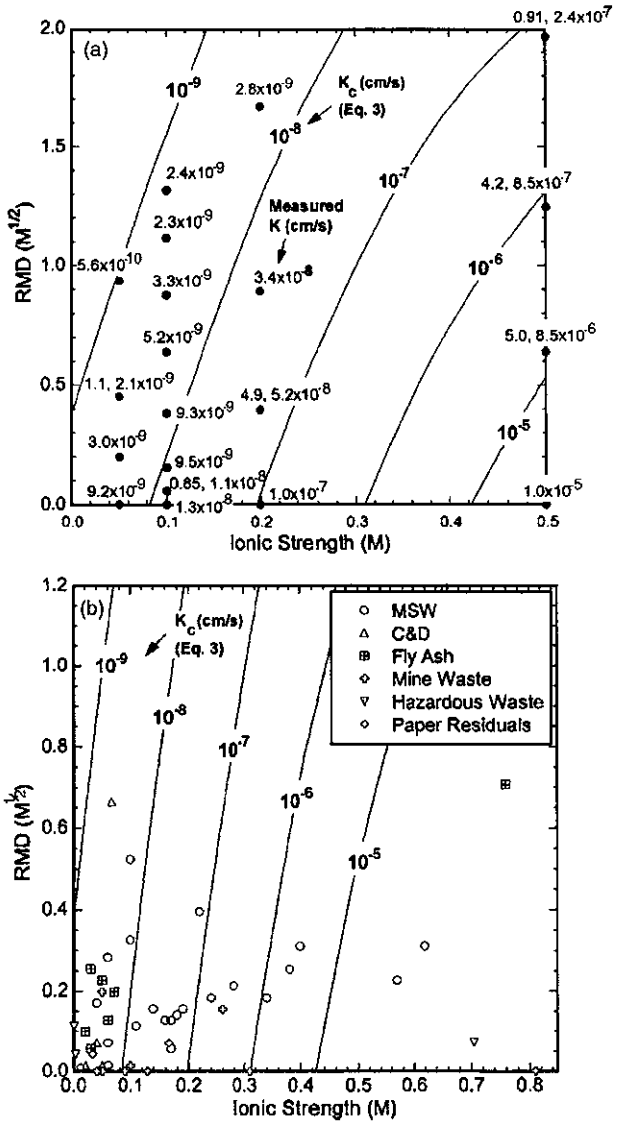

Fig. 10. Contours of hydraulic conductivity as a function of RMD and ionic strength predicted with Eq. (3) along with (a) measured hydraulic conductivities as solid circles and (b) points corresponding to ionic strength and RMD of various leachates. Data from Williams (1975) (I=1.87 M and RMD=0) and Kolstad (2000) (I=1.37 M and RMD=2.52$M^{1/2}$) are off the scale in (b).

HYDRAULIC CONDUCTIVITY OF DESICCATED GEOSYNTHETIC CLAY LINERS

By B. Tom Boardman,[1] Associate Member, ASCE, and David E. Daniel,[2] Member, ASCE

ABSTRACT: Large-scale tests were performed to determine the effect of a cycle of wetting and drying on the hydraulic conductivity of several geosynthetic clay liners (GCLs). The GCLs were covered with 0.6 m of pea gravel and permeated with water. After steady seepage had developed, the water was drained away, and the GCL was desiccated by circulating heated air through the overlying gravel. The drying caused severe cracking in the bentonite component of the GCLs. The GCLs were again permeated with water. As the cracked bentonite hydrated and swelled, the hydraulic conductivity slowly decreased from an initially high value. The long-term, steady value of hydraulic conductivity after the wetting and drying cycle was found to be essentially the same as the value for the undesiccated GCL. It is concluded that GCLs possess the ability to self-heal after a cycle of wetting and drying, which is important for applications in which there may be alternate wetting and drying of a hydraulic barrier (e.g. within a landfill final cover).

INTRODUCTION

The primary purpose of a hydraulic barrier within a bottom liner or final cover system for a waste-containment facility is to minimize infiltration of water or leachate through the hydraulic barrier. Hydraulic barriers in modern landfills are typically composed of a relatively impermeable layer of compacted soil that may be overlain by a geomembrane. A relatively new type of material that may be a useful alternative to a layer of low-permeability compacted soil is a geosynthetic clay liner (GCL). Geosynthetic clay liners are manufactured by sandwiching a thin layer of bentonite between two geotextiles or attaching a layer of bentonite to a geomembrane with an adhesive (Koerner and Daniel 1992; Daniel 1993; Koerner 1994).

It is well known that dry bentonite swells when wetted and shrinks when dried. Shan and Daniel (1991) performed laboratory hydraulic conductivity tests on small samples of one GCL that had been subjected to several wet-dry cycles and reported that severe desiccation cracks developed when the wet GCLs were dried; however the hydraulic conductivity after several wet-dry cycles was the same as the conductivity of the nondisiccated material. These tests were on small laboratory-scale samples and did not include overlapped zones between panels.

The purpose of the research described in this paper was to determine the effect of wetting and drying on the hydraulic conductivity of three large-scale GCLs. Overlapped panels were tested, and, for control, nonoverlapped GCLs were tested, as well. Conclusions are drawn concerning the ability of GCLs to self-heal after a severe wet-dry cycle. These findings are of interest to designers of final cover systems for landfills and site remediation projects, and for designers of landfill liners in areas where drying of a liner can occur.

MATERIALS TESTED

Three commercial products were used in this study to cover the range of types of GCLs available. One material (Bentomat, Colloid Enviromental Technologies Co., Arlington Heights, Ill.), which is a geotextile-encased, needle-punched GCL, is produced by needle-punching two polypropylene geotextiles that contain approximately 4.9 kg/m^2 of loose, granular sodium bentonite between them. After hydration, the bentonite swells around the impermeable fibers to form a hydraulic barrier. The manufacturer recommends that 0.4 kg/m of loose, dry bentonite be placed along the centerline of the overlap when installing the GCL to ensure that the material self-seals along the overlap and forms a continuous barrier. A 100 g/m^2 woven upper geotextile, a 200 g/m^2 nonwoven lower geotextile, and a treated bentonite ("SS" grade) were used in the material tested for this study.

A second material tested (Claymax 200R, Claymax Div., Colloid Environmental Technologies Co.), which is a geotextile encased, adhesive-bonded GCL, is produced by mixing sodium bentonite with an adhesive and sandwiching approximately 4.9 kg/m^2 of bentonite between two geotextiles. A 130 g/m^2 upper, woven geotextile and a 25 g/m^2 lower, openweave, polyester geotextile were used in this study.

The third material tested (Gundseal, GSE Lining Technology, Inc., Houston) is produced by mixing sodium bentonite with an adhesive and attaching approximately 4.9 kg/m^2 of bentonite to a geomembrane. A 0.5-mm-thick, smooth, high-density polyethylene (HDPE) geomembrane constituted the geomembrane component of the GCL used in this study. The GCL was tested with the bentonite side facing downward.

EXPERIMENTAL PROCEDURE

Testing was carried out in rectangular steel tanks measuring 2.4 m in length, 1.2 m in width, and 0.9 m in depth (Estornell and Daniel 1992). A 12-mm-diameter drainage port located in the center of the base of each tank provided an outlet from which water that had passed through the GCL was collected (Fig. 1). Copper tubing led from the drainage port to a collection container located beneath each tank. The container was

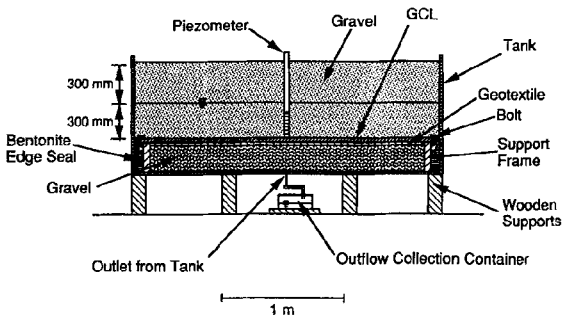

FIG. 1. Tank Used for Experiments

[1]Geotech. Dept., CH2M Hill, 1111 Broadway, Suite 1200, Oakland, CA 94607.

[2]Prof. of Civ. Engrg., Univ. of Texas, Austin, TX 78712.

Note. Discussion open until August 1, 1996. To extend the closing date one month, a written request must be filed with the ASCE Manager of Journals. The manuscript for this paper was submitted for review and possible publication on June 16, 1994. This paper is part of the ***Journal of Geotechnical Engineering***, Vol. 122, No. 3, March, 1996. ©ASCE, ISSN 0733-9410/96/0003-0204–0208/$4.00 + $.50 per page. Paper No. 8674.

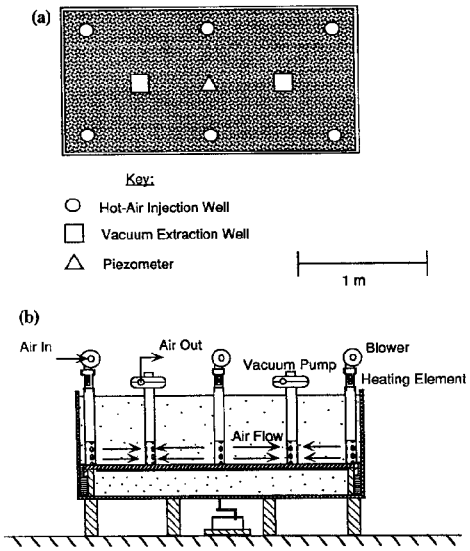

FIG. 2. Arrangement of Six Hot-Air Injection Wells and Two Vacuum Extraction Wells: (a) Plan View; (b) Cross-Sectional View

periodically removed and weighed to determine the quantity of flow through the GCL over a known interval of time.

Each test specimen was cut by hand from rolls supplied by the GCL manufacturer. Through the use of templates, holes spaced about 300 mm apart were cut through the GCL along the edges. The holes were then grommeted, and the GCL attached to a rigid steel frame resting on top of a wood frame located in the bottom of each tank. Attaching the GCL to the steel frame ensured that the GCLs would crack during desiccation rather than shrink dimensionally and pull away from the walls of the tank.

Overlapping samples were installed with a 230-mm-wide overlap, which is within the range recommended by the GCL manufacturers. The centerline of the overlap conincided with the centerline of the tank (lengthwise). In an effort to restrict shrinkage of the GCL in the overlap region, overlapping samples were not attached to the steel frame near the overlap.

After the GCL was attached to the frame, loose, powdered bentonite was then spread along the edge of the installed GCL. The combination of attaching the GCL to the steel frame, and the placement of loose bentonite along the edge of the GCL has been shown to prevent sidewall leakage (LaGatta 1992; Estornell and Daniel 1992). The loose bentonite was approximately 50 mm thick and 75 mm wide. Three gypsum resistivity blocks were then placed in this bentonite edge seal on top of the GCL for all the GCLs tested. The electrical resistivity of the blocks depended on the water content of the gypsum, which in turn was a function of the water content of the surrounding bentonite. The gypsum blocks provided a simple indication of the relative dryness of the bentonite edge seal, which, when coupled with other observations, helped to confirm that complete drying (following a wetting cycle) of the GCL had occurred. After the GCL had been installed, a 25-mm-diameter polyvinyl chloride (PVC) piezometer was placed on top of the GCL in the center of the tank (Fig. 1) to determine the water level in the gravel that would later cover the GCL.

Prior to placement of the gravel above the GCL, eight 100-mm-diameter PVC pipes were placed above the GCL vertically in the pattern shown in Fig. 2. Six of the pipes were used to inject hot air and two pipes were used to extract air from the gravel that was placed over the GCL. Small holes were drilled through all of the pipes every 25 mm along the circumference, and every 25 mm (vertically) along the lower 300 mm of the pipe resulting in the circulation of hot air across the upper surface of the GCL. The lower end of each pipe was sealed with a PVC cap. A 6-mm-thick layer of gravel separated the capped end of each pipe from the upper surface of the GCL.

Once the piezometer, 6 hot-air injection wells, and 2 vacuum extraction wells were in place, the GCL was covered with 600 mm of pea gravel. The GCL was then slowly hydrated with tap water until a final head of water of 300 mm acted on the GCL. The water head was maintained at 300 mm as the GCL was permeated. The dry unit weight of the pea gravel was approximately 15.7 kN/m^3, and the saturated unit weight was 19.5 kN/m^3. The average vertical effective stress was 7.7 kPa during permeation, and the average total vertical stress was 9.6 kPa during drying.

Temperatures were measured in the gravel above the GCL by lowering a thermometer down a piezometer in the center of the tank. After water was drained out of the tank, the temperature in the gravel was approximately 18°C. Air blowers and heating elements were installed on top of the six air injection pipes, and air extraction blowers were installed on top of two pipes (Fig. 2). Once the heating system was turned on, the temperature within the tank slowly rose as the gravel and GCL dried out. The maximum temperature reached during the test ranged from 27°C to 32°C. These values are similar to the in-situ temperatures measured by Corser and Cranston (1991) within a compacted clay liner buried beneath soil cover at an arid site in California. Care was taken not to overheat the gravel or GCL. The time required to dry out the gravel and GCL ranged from 2 to 3 weeks.

It was assumed that if the 50-mm-thick, 75-mm-wide bentonite edge seal was desiccated, then the GCL was desiccated, as well. To confirm this assumption, two tests were conducted in which the GCL was wetted and then dried with the procedure just described. When resistivity readings from the gypsum blocks located in the bentonite edge seal indicated that the bentonite was dry, one test was dismantled and the GCL was examined. The other sample was left undisturbed and was later rehydrated. The bentonite in the excavated GCL, as well as in the edge seal, was dry (water content = 12%) and severely cracked. The typical crack pattern of the bentonite in the GCL is shown in Fig. 3. A photograph is shown in Fig. 4. Due to a limited number of tanks and the time and effort required to set up a single test, only this one tank was dismantled to examine the physical condition of the GCL after desiccation. The gypsum blocks were used to confirm desiccation in the other tests.

Once the gypsum-block readings showed that the bentonite in the edge seal was dry, the GCL was rehydrated with water at a flow rate corresponding to 40 mm/h. The water was added by moving a hose, at the lowest possible flow rate, across the upper surface of the overlying gravel. This wetting rate would correspond to an extreme rainfall event, assuming that the GCL was located at the surface or was buried near the surface under a thin layer of gravel. If soil overlies the GCL, the rate of wetting of the GCL would be much slower. The objective of this study was primarily to determine whether the GCL would swell and self-seal, and not to study the effect of rate of wetting upon the tendency to eventually self-seal.

Hydraulic conductivity readings were then taken every 10–15 min to determine how quickly the desiccated GCL could swell and self-seal. Hydraulic conductivity was computed from measured flow rates, the measured head of water acting on the liner, and the assumed thickness of the GCL. The thickness was determined from laboratory testing (Boardman 1993) and was 12 mm for the fully hydrated GCLs, and 5 mm and 8 mm for Claymax and Bentomat, respectively, for the dried

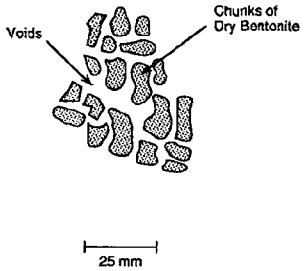

FIG. 3. Crack Pattern Observed in Bentonite Component of Claymax 200R after Wet-Dry Cycle

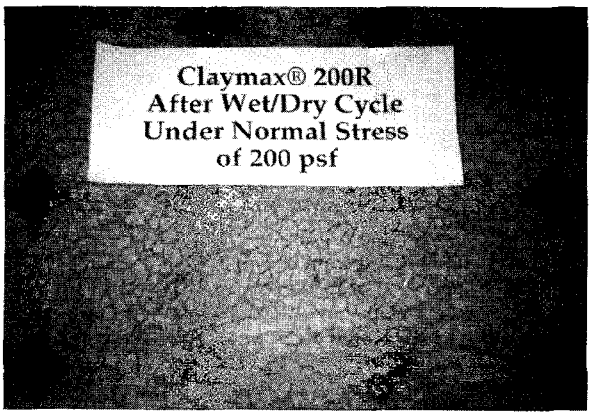

FIG. 4. Cracked Bentonite Component of GCL after Wetting and Drying Cycle (Note: Upper Geotextile Component of GCL Has Been Pulled Back to Reveal Cracking Pattern in Bentonite; 1 psf = 48 Pa)

GCL undergoing initial rehydration. When outflow through the GCL sample stopped after the initial rehydration, the water head was raised in increments of 100 mm to 300 mm over several days. Then the head was kept constant at 300 mm.

When steady flow was reached after rehydration, the water was siphoned out of the tank and the gravel was removed by hand. The GCL was then inspected. The experimental procedure is described in greater detail by Boardman (1993).

RESULTS

Claymax 200R

Two tests were performed on Claymax 200R: one on a intact sample (with no overlap) and the other on overlapping panels.

Intact Sample (No Overlap)

The intact sample was flooded with a water head of 300 mm and was permeated until, after 3 weeks, outflow occurred from the tank and the hydraulic conductivity became steady and equal to 6×10^{-9} cm/s. This compares well with the findings of Lagatta (1992), who measured values of 7 and 8 $\times 10^{-9}$ cm/s on two tests on the same GCL.

The intact sample was desiccated, then rehydrated. Desiccation caused severe cracking within the bentonite of the GCL (Fig. 4). There was flow through the cracked GCL immediately after water was initially introduced. The hydraulic conductivity dropped from its initial peak value of approximately 1×10^{-3} cm/s to a value of 1×10^{-5} cm/s during the first 90 min after the sample was rehydrated (Fig. 5). By the next day, all outflow had ceased. Hydration and swelling of the bentonite in the GCL is assumed to be responsible for the rapid drop in hydraulic conductivity of the bentonite. Although

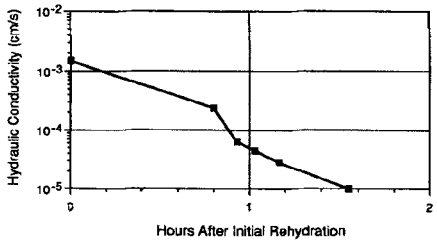

FIG. 5. Short-Term Hydraulic Conductivity versus Time for Initial Stage of Rehydration of Desiccated Claymax 200R (Intact Sample with No Overlap)

some of the large flow could have been through the desiccated edge seal, the fact that the GCL was obviously severely cracked (Fig. 4) and the comparatively massive nature of the edge seal leads the authors to believe that virtually all of the high initial flow was through the GCL, not the edge seal.

The head of water was then slowly increased over the next two days. By the third day after rehydration, outflow resumed. An hydraulic conductivity of 1×10^{-8} cm/s was measured over the next week of permeation (Fig. 6). The final hydraulic conductivity was 1×10^{-8} cm/s, which is similar to the initial value (prior to desiccation) of 6×10^{-9} cm/s. When the test was dismantled, no abnormalities were observed in the GCL; its physical appearance was the same as that of a GCL that had not been desiccated.

The pattern of high initial outflow, followed by no flow, followed by steady low flow was similar to that found by Shan and Daniel (1991) on desiccated, small-scale samples of this same type of GCL. The significance of high initial hydraulic conductivity during the rehydration phase would depend on the specific field application. The desiccated GCL was wetted initially at an input flux of 40 mm/h of water. For a GCL located near the surface and overlain by gravel, the conditions in these experiments would be fairly similar to conditions in the field during a heavy rainstorm. The high initial hydraulic conductivity might or might not be acceptable, depending on the specific application. However, for a GCL that is overlain by soil, e.g., cover soil and topsoil in a final cover system, the water flux reaching the GCL would be much lower than 40 mm/h, which would allow time for the GCL to absorb water and swell before much, if any, water could pass through the GCL. The significance of the high initial hydraulic conductivity upon rehydration of a desiccated GCL will have to be evaluated for each individual project.

Overlapped Panels

The overlapped panels were permeated for 3 weeks prior to desiccation. Some outflow occurred, but steady state conditions were not reached. Experience has shown that many weeks or months of permeation can sometimes be necessary to obtain steady values of hydraulic conductivity for GCLs tested in these tanks (Estornell and Daniel 1992; LaGatta 1992). Rather than delay the wet-dry cycle for weeks or months while waiting for steady flow, it was decided to proceed with the desiccation cycle as the GCL was assumed to be fully hydrated. (Previous experience in similar tests has shown that the GCL is very nearly saturated after 3 weeks of soaking.) The hydraulic conductivity prior to desiccation was assumed to be 7×10^{-9} cm/s, based on nearly identical tests by LaGatta (1992), and the tanks were drained.

The overlapped sample was desiccated, then rehydrated. There was flow through the GCL immediately after the sample was rehydrated. The hydraulic conductivity ranged from 1×10^{-5} to 1×10^{-6} cm/s for the first 3 h after rehydration (Fig. 7). The outflow dropped to essentially zero over the next 2

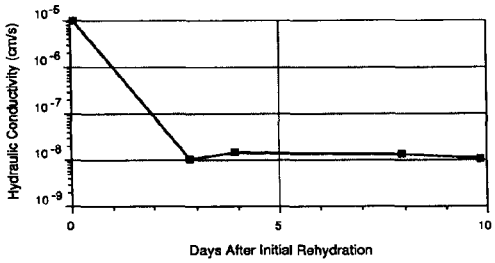

FIG. 6. Long-Term Hydraulic Conductivity versus Time for Rehydration of Desiccated Claymax 200R (Intact Sample with No Overlap)

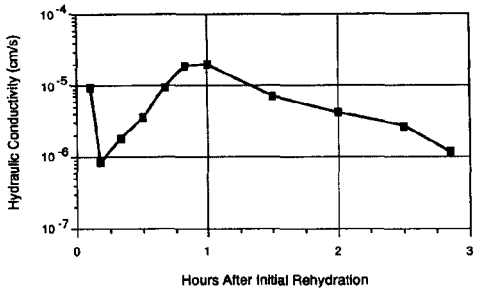

FIG. 7. Short-Term Hydraulic Conductivity versus Time for Initial Stage of Rehydration of Desiccated Claymax 200R (Overlapped Panels)

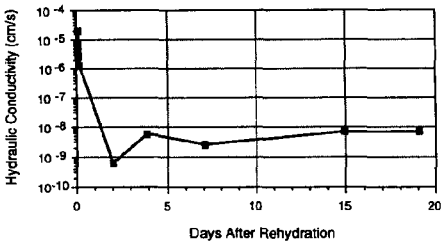

FIG. 8. Long-Term Hydraulic Conductivity versus Time for Rehydration of Desiccated Claymax 200R (Overlapped Panels)

days. As the head of water was increased, the outflow resumed, and the hydraulic conductivity slowly increased to an approximate value of 7×10^{-9} cm/s [same value as measured by LaGatta (1992) for nondesiccated samples] after 19 d of permeation (Fig. 8).

At the completion of the test, the condition of the overlapped panels was examined. The width of the overlap was still 225 mm. The combination of the attachment of the GCL to the steel frame and the compressive stress provided by the overlying gravel prevented the overlapped panels from pulling apart during shrinkage. Experience has shown that wet GCLs will pull apart along the overlap during drying if there is no overburden soil (for instance, during construction, if the GCL is not promptly covered), although the severity of shrinkage in the overlap width depends on the extent of hydration of the bentonite and varies from one type of GCL to another. The overlapping panels appeared to have self-sealed along the overlap in two different ways. First, hydrated bentonite had extruded out of the edges of the upper and lower panels and appeared to form a seal along the lines of contact between the two panels. Second, the thickness of the upper panel increased at the edge of the lower panel (almost as if the upper panel had swelled around the lower panel when both panels were hydrated).

Bentomat

Two sets of tests on Bentomat were performed: one on an intact sample (no overlap) and the other on two overlapping panels.

Intact Sample (No Overlap)

The intact sample was permeated for 3 weeks, but no outflow occurred. A value of hydraulic conductivity prior to desiccation of 1×10^{-9} cm/s was assumed [based on results of tests performed by LaGatta (1992)], and the tanks were drained. The sample was desiccated, then rehydrated. There was no measured outflow through the GCL after two weeks of permeation. After dismantling the test, no abnormalities were found across the surface of the GCL. It was decided not to continue permeating the sample indefinitely due to time constraints and because the practical conclusion was obvious: the wet-dry cycle appeared to cause no deleterious effect on the hydraulic integrity of the sample tested. Perhaps the needle-punched reinforcement of the GCL limited the amount of shrinkage and cracking within the bentonite as the GCL dried.

Overlapped Panels

The hydraulic conductivity of the overlapped panels prior to desiccation did reach steady state and was 1×10^{-9} cm/s. The sample was desiccated and then rehydrated. There was essentially no flow through the GCL immediately after the sample was rehydrated. As the head of water was slowly increased, some flow occurred through the sample. After 10 d of permeation, the hydraulic conductivity was approximately 1×10^{-9} cm/s (Fig. 9), which was the same as the value before desiccation. The wet-dry cycle appeared to cause no increase in the hydraulic conductivity of the GCL.

After completion of the test, the GCL was inspected. The loose bentonite that had been placed along the overlap (per the manufacturer's recommendation) was hydrated and intact, and appeared to have molded into the overlying panel. The width of the overlap was still 225 mm. Bentonite appeared to have extruded out of the edges of both panels along the overlap, which may have helped to limit the amount of flow through the overlap.

Gundseal

One test was performed on overlapping panels of Gundseal. The panels were installed with the geomembrane component facing upwards. An intact sample was not tested because experience has shown that there is no outflow from such tests, given the essentially impermeable nature of the geomembrane component (Estornell and Daniel 1992).

There was no measured outflow through the overlapped panels after three weeks of initial permeation. Since Estornell and Daniel (1992) found no outflow from overlapped panels tested under nearly identical conditions after 5 months of permeation, it was decided to initiate the desiccation process rather than continue to permeate the overlapped GCL panels

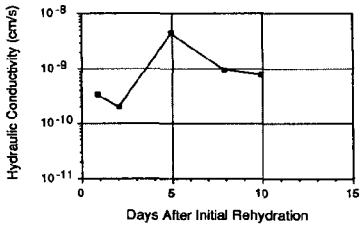

FIG. 9. Long-Term Hydraulic Conductivity versus Time for Rehydration of Desiccated Bentomat (Overlapped Panels)

with water. The tank was drained, and the GCL was desiccated until the resistivity blocks indicated that the bentonite in the edge seal was dry. The sample was then rehydrated. There was no measured outflow through the desiccated sample after another three weeks of permeation.

After the test, the gravel was removed from the tank and the condition of the GCL was observed. The width of the overlap was still 225 mm after the test. The bentonite was hydrated 25 mm to 50 mm into the overlap—the hydrated bentonite in the overlap prevented outflow through the overlap during the period of testing.

CONCLUSIONS

The purpose of this study was to determine the effect of a cycle of wetting and drying on the hydraulic conductivity of large-scale geosynthetic clay liners (GCLs). Each GCL was buried under 600 mm (2 ft) of pea gravel and permeated with water for several weeks. Then the water was removed from the gravel and the GCLs were desiccated by circulating heated air through the gravel using a system of hot air blowers and vacuum pumps. Severe drying and cracking occurred in the bentonite component of the GCLs. After drying, each GCL was slowly rehydrated. The hydraulic conductivity was then monitored to determine the ability of the desiccated GCL to rehydrate and self-seal.

Based on the results of this study, the following conclusions are drawn.

1. The geotextile-encased GCLs (Bentomat and Claymax 200R) swelled and self-sealed upon rehydration, after a cycle of wetting and drying. When the desiccated GCLs were rehydrated, water initially flowed rapidly through most of the desiccated samples, but the bentonite quickly expanded and the hydraulic conductivity decreased as the cracked bentonite began to adsorb water and swell. The long-term, steady value of hydraulic conductivity was essentially the same before and after the desiccation cycle.
2. In tests performed on a GCL containing bentonite attached to a geomembrane (Gundseal), there was no outflow of water either before or after the wetting and drying cycle. Due to the presence of the geomembrane, very little of the GCL actually became hydrated, but the bentonite in the overlapped area did self seal.
3. The wetting and drying cycle did not cause any irreversible shrinkage to occur along the overlap for overlapping samples of any of the GCLs tested. However, samples were partially attached to a rigid, steel frame in these tests, and performance of the materials in the field might be different.
4. Although the bentonite did form open cracks upon drying, the cracks swelled and closed upon wetting. The geosynthetic component of the GCL (geotextile or geomembrane) prevented any intrusion of overlaying pea gravel into the cracks. Designers should be careful that the openings in the geotextile component of the GCL are small enough to prevent the overlying soil from migrating into cracks that develop in the bentonite.
5. The initially high value of hydraulic conductivity of the desiccated GCLs may not be representative of true field conditions because the overlying cover soils would likely adsorb some of the incoming rainfall and cause a more gradual wetting of the GCL. In addition, the rehydration rate of 40 mm/h used in these tests would correspond to an extreme infiltration rate, and the GCL would either have to be overlain by extremely permeable material (e.g., gravel) or buried at extremely shallow depth for a flux of water of 40 mm/h to be applied to the GCL in the field. If the GCL is slowly wetted (which would be the case in many field situations), the GCL would have time to absorb water and to swell without allowing seepage through the GCL. The significance of high initial hydraulic conductivity should be considered on a project-specific basis.

The self-sealing capability of GCL's makes them a viable hydraulic barrier for situations in which the barrier may undergo cyclic wetting and drying, e.g., within a landfill final cover. However, the reader is cautioned not to inappropriately extrapolate the results of these tests. The tests were performed under carefully controlled conditions with a single, severe wetting and drying cycle. Such a severe cycle of wetting and drying is not likely to occur in the field. Numerous but less severe cycles of wetting and drying are more likely to occur in the field. Further research (particular field data) is needed before a final conclusion can be drawn concerning the ability of GCLs to safely withstand numerous wetting and drying cycles under the full range of possible field conditions. Nevertheless, these results are encouraging and suggest that GCLs may be an attractive material to use when some degree of cycling in water content is anticipated within the hydraulic barrier.

ACKNOWLEDGMENTS

The information presented in this paper has been funded wholly or in part by the U.S. Environmental Protection Agency under cooperative agreement CR-815546. This paper has not been subjected to the agency's peer and administrative review. The findings do not necessarily reflect the views of the agency. Mention of trade names or commercial products does not constitute endorsement or recommendation for use.

The writers thank the GCL manufacturers for supplying materials and for cooperating in the research program.

APPENDIX. REFERENCES

Boardman, B. T. (1993). "The potential use of geosynthetic clay liners as final covers in arid regions," MS thesis, Univ. of Texas at Austin, Tex.

Corser, P., and Cranston, M. (1991). "Observations on the long-term performance of composite clay liners and covers." *Proc. Geosynthetic Des. and Perf.*, Vancouver Geotech. Soc., Vancouver, B.C., Canada.

Daniel, D. E. (1993). "Clay liners." *Geotechnical practice for waste disposal*, D. E. Daniel, ed., Chapman and Hall, London, U.K., 137–163.

Estornell, P. M., and Daniel, D. E. (1992). "Hydraulic conductivity of three geosynthetic clay liners." *J. Geotech. Engrg.*, 118(10), 1592–1606.

Koerner, R. M., and Daniel, D. E. (1992). "Better cover-ups," *Civ. Engrg.*, ASCE, 62(5), 55–57.

Koerner, R. M. (1994). *Designing with geosynthetics*, 3rd Ed., Prentice-Hall, Englewood Cliffs, N.J.

LaGatta, M. D. (1992). "Hydraulic conductivity tests on geosynthetic clay liners subjected to differential settlement," MS thesis, Univ. of Texas as Austin, Tex.

Shan, H. Y., and Daniel, D. E. (1991). "Results of laboratory tests on a geotextile/bentonite liner material." *Geosynthetics 91*, Industrial Fabrics Assoc. Int., St. Paul, Minn., 2, 517–535.

HYDRATION OF GCLs ADJACENT TO SOIL LAYERS

An extensive laboratory testing program was undertaken to investigate the potential for hydration of a GCL when placed against a compacted soil layer. Three different GCLs were used to evaluate the effects of hydration time, initial GCL water content, thickness of soil layer and overburden pressure.

Tests were conducted using a low plasticity clay, commonly found in the Cincinnati, Ohio area. Specimens of GCL with a known moisture content, were placed in a specially designed test apparatus, where a soil with a known moisture content was compacted into the base and the GCL was placed on top. The specimen was then loaded with a load platen and allowed to hydrate for a specific amount of time. At the end of the hydration period, the GCL was tested for moisture content. The GCL was left in contact with the soil for periods of 5, 25 and 75 days to define the effect of test duration on the hydration of the GCL.

Test results show that significant increases in the moisture content of a GCL may occur in the first few days of a GCL's contact with a soil stratum. Overburden pressures within the range tested (i.e. 5 to 390 kPa) did not deter the hydration process, but a larger soil thickness resulted in a larger increase in GCL moisture content.

800.527.9948 Fax 847.577.5566

United States
Environmental Protection
Agency

Office of Research and
Development
Washington DC 20460

EPA/600/R-96/149
June 1996

EPA

Report of 1995 Workshop on Geosynthetic Clay Liners

HYDRATION OF GCLs ADJACENT TO SOIL LAYERS

Overview of Testing Program

The authors conducted an extensive laboratory testing program to evaluate the potential for hydration of GCLs placed against a compacted subgrade soil layer. Hydration tests were performed on three different GCL products to evaluate the effects of: (i) test duration (i.e., hydration time); (ii) soil initial water content; (iii) thickness of soil layer; and (iv) overburden pressure. Three commercially-available GCL products, namely, Claymax®, Bentomat®, and Bentofix® were used in the testing program. The soil used in the testing program was obtained from the USEPA GCL Field Test Site at the ELDA-RDF facility in Cincinnati, Ohio. This material is classified as low plasticity clay (CL) based on the Unified Soil Classification System (USCS). Tests were performed on two different soil samples and consistent results were obtained between samples. The results reported herein were obtained from tests on a sample with 99 percent of the soil passing the U.S. No. 200 standard sieve and 33 percent smaller than 2 μm (clay fraction). The liquid limit of the soil is 41 and the plasticity index is 19. The soil has an optimum moisture content (OMC) of 20 percent and a maximum dry unit weight of 16.7 kN/m^3 based on the standard Proctor compaction method (ASTM D 698).

Testing Apparatus and Procedure

Figure 11 shows the apparatus specially designed to conduct the GCL hydration tests. The apparatus consists of a polypropylene mold 75 mm in diameter and 150 mm in height. A geomembrane/GCL/soil composite specimen is placed in the mold and covered with two layers of a thin vapor barrier. A loading platen is placed on the specimen for application of overburden pressure.

To process the soil, it was first passed through a U.S. No. 4 standard sieve. The soil was then moisture conditioned to achieve the desired moisture content. The moist soil was placed in the mold in a loose condition and statically compressed to 50-mm thick lifts. The soil was compacted to a dry unit weight equal to approximately 90 percent of the maximum dry unit weight based on the standard Proctor method (ASTM D 698). Two soil lifts were used giving a total thickness of 100 mm. The GCL and geomembrane specimens were carefully trimmed from the same sheets. The initial moisture content of the GCL was measured by taking a small sample from the same GCL sheet and measuring its weight before and after oven drying. The initial moisture content of the GCLs varied between 15 and 20 percent.

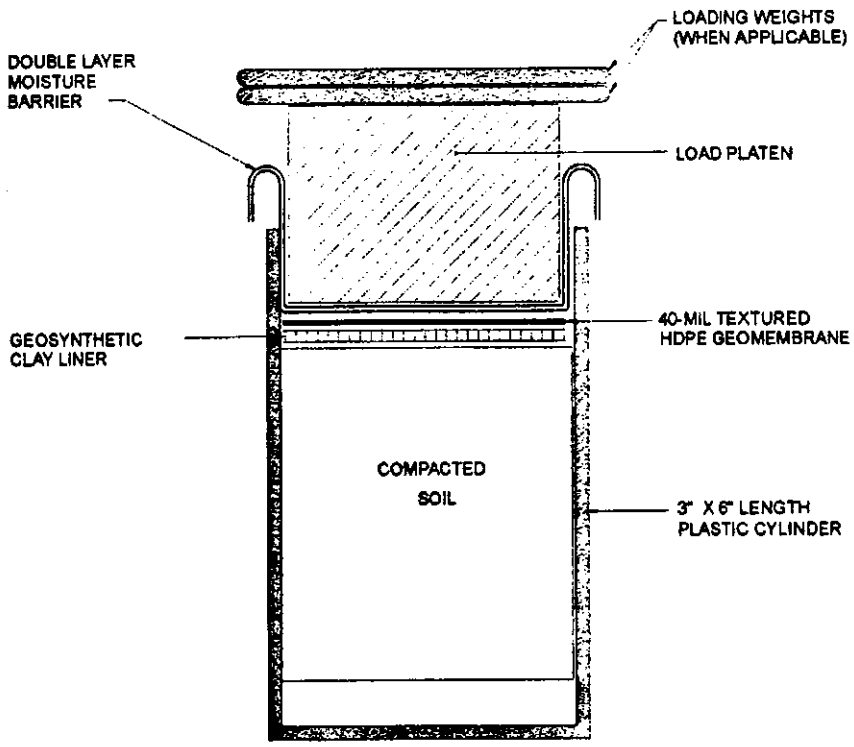

Figure 11. Simplified diagram of GCL hydration test set-up.

The GCL and geomembrane were placed on the soil and covered with the vapor barrier. The side of the GCL placed against the soil was woven in the case of Claymax® and nonwoven for Bentomat® and Bentofix®. Overburden pressure of 10 kPa was applied on the composite specimen utilizing standard weights which were placed on the loading platen. The entire apparatus was then placed in a temperature and humidity controlled room for the desired hydration time period. At the end of the hydration period, the test specimen was removed and the water content of the GCL and soil were measured. The final moisture content of the GCL was measured by weighing the entire GCL specimen before and after oven drying. The final moisture content of the soil was measured as the average water content of three samples obtained from the top, middle, and bottom of the soil specimen.

Testing Conditions and Results

As previously described, test conditions were varied to evaluate the effects of several factors on the hydration of GCLs. To evaluate the effect of test duration, tests were performed where the GCL was in contact with the soil for 5, 25, and 75 days. Soil specimens were compacted to initial moisture contents equal to OMC, 4 percentage points dry of OMC, and 4 percentage points wet of OMC to evaluate the effect of soil initial moisture content on GCL hydration.

Figures 12, 13, and 14 present the results of the hydration tests for the GCL products Claymax®, Bentomat®, and Bentofix®, respectively. These figures show that the moisture content of all three GCLs increased significantly as a result of contact with compacted subgrade soil. The increase in GCL water content was significant after only five days of hydration. With increasing time, GCL water content continued to increase at a decreasing rate. For most tests, GCL water content reached a maximum value after about 25 days of soil contact and for some of the tests water content continued to increase even after 75 days of hydration. It is interesting to note that all three GCL products showed relatively similar behavior. Increases in water content were comparable for the three GCL products despite differences in GCL fabric (i.e., woven vs. nonwoven) and types of bentonite clay used to manufacture the GCLs.

Figures 12, 13, and 14 illustrate the influence of soil subgrade initial moisture content on the hydration of GCLs. From these figures, it is evident that the moisture content of the GCL for any particular hydration time increases as the initial moisture content of the soil increases. These figures also show that a small increase in soil initial moisture content can have a significant impact on GCL moisture content. For example, after 75 days of hydration, the moisture content of Claymax® was approximately 16 percent higher when the initial moisture content of the soil was equal to OMC than when it was 4 percentage points drier than OMC. This behavior is expected because more water is available in the soil for the GCL to hydrate.

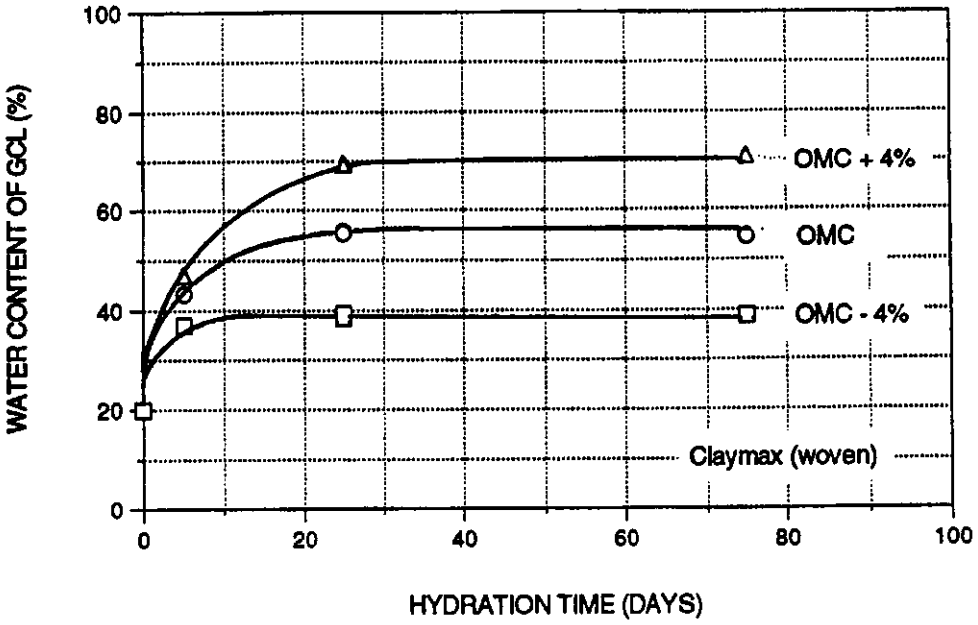

Figure 12. Increase in GCL moisture content due to contact with compacted subgrade soil: Claymax® with woven geotextile against soil.

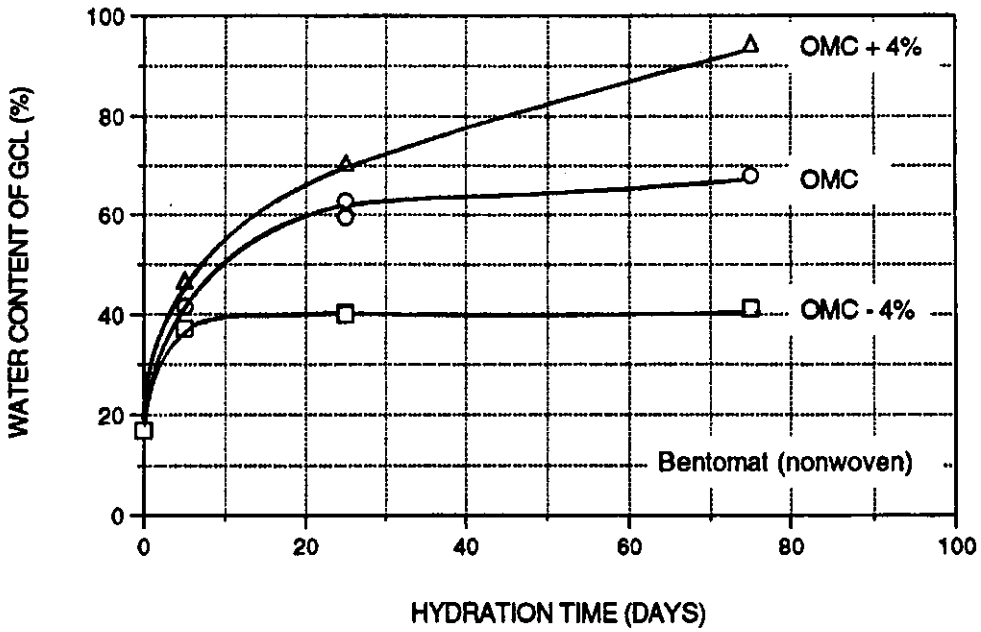

Figure 13. Increase in GCL moisture content due to contact with compacted subgrade soil: Bentomat® with nonwoven geotextile against soil.

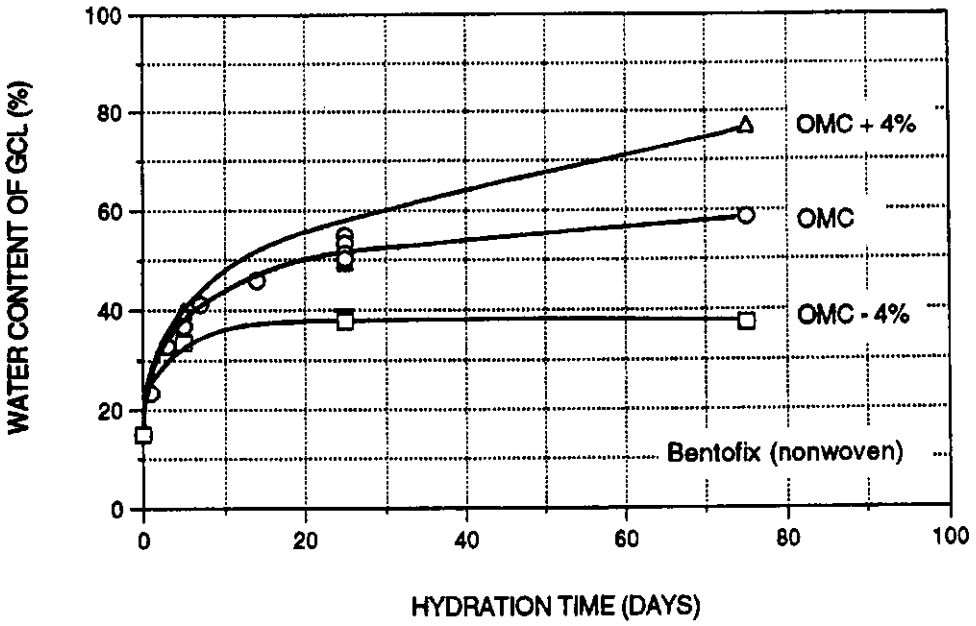

Figure 14. Increase in GCL moisture content due to contact with compacted subgrade soil: Bentofix® with nonwoven geotextile against soil.

The examination of the curves shown in Figures 12, 13, and 14 shows that the time required for the GCL to reach its final moisture content is less in the case of a dry soil than in the case of a wet soil. At the lowest soil initial moisture content tested, GCL moisture content ceased to increase after about 5 to 25 days. At the highest initial moisture content tested, the Bentomat® and Bentofix® GCLs continued to increase in moisture content after 75 days of hydration.

To evaluate the effect of soil layer thickness, specimens were prepared using 50, 100, 150, and 200 mm of soil thickness. Soil initial moisture content was 20 percent and dry unit weight was 14.9 kN/m^3 for all specimens. Figure 15 shows the results of hydration tests for the Bentofix® GCL after 25 days of hydration. The GCL moisture content increased with the increase of the soil layer thickness. However, it appears that only a small change in moisture content increase occurs for thicknesses greater than 100 mm.

The effect of overburden pressure on GCL hydration is illustrated in Figure 16 for the Bentofix® GCL. As shown in this figure, overburden pressure in the range of 5 to 390 kPa did not significantly affect the rate of GCL hydration during the 25-day test duration.

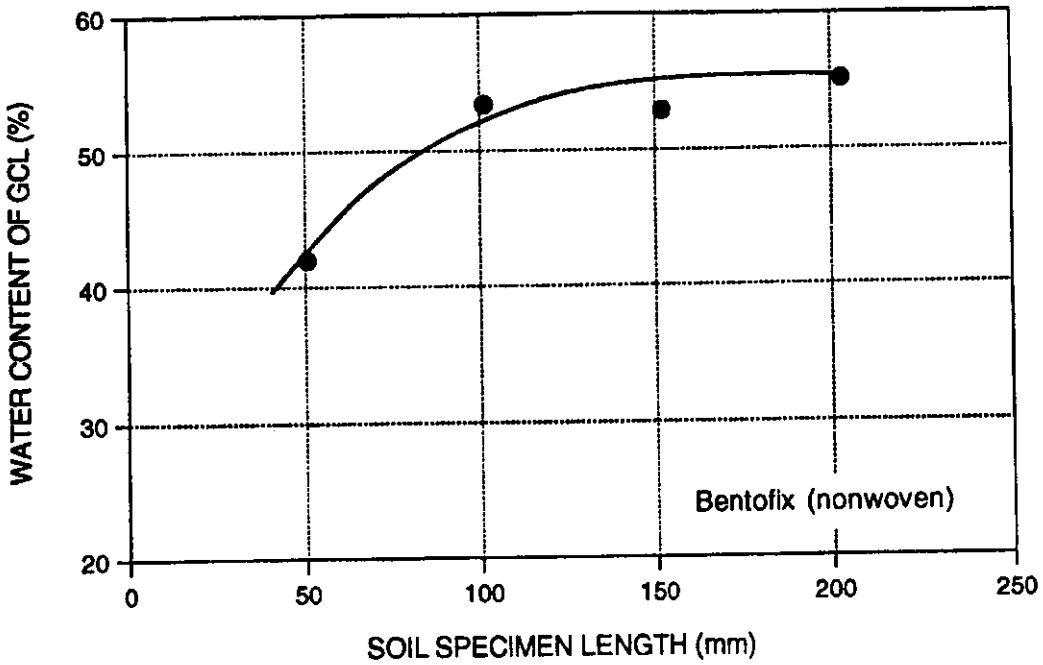

Figure 15. Influence of subgrade soil layer thickness on GCL moisture content.

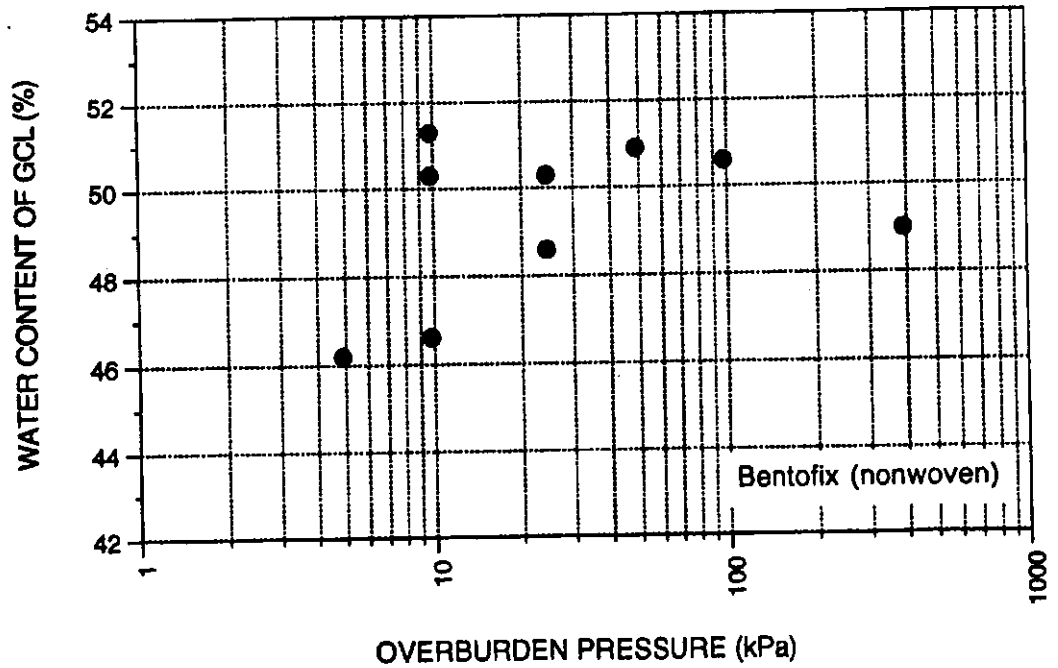

Figure 16. Influence of overburden pressure on the increase in GCL moisture content.

Summary

From the testing program results described above, the following can be concluded:

- GCLs will hydrate when placed in contact with subgrade soils compacted within the range of moisture contents typically found in earthwork construction specifications; this conclusion is consistent with data provided by Daniel et al. [1993]; even for the driest soil (compacted 4 percentage points dry of OMC), GCL moisture contents consistently increased from an initial value in the range of 15 to 20 percent up to about 40 percent within a 100-day period; it should thus be anticipated that GCLs placed even against relatively dry compacted subgrades will undergo substantial hydration;

- given that Daniel et al. [1993] have shown that long-term GCL shear strengths are insensitive to water content for water contents above about 50 percent, stability analyses involving GCLs placed in contact with compacted subgrade soils should be based on hydrated GCL shear strengths;

- significant increases in GCL moisture contents may occur within a few days of GCL contact with a moist soil; the rate of GCL hydration is initially highest and then decreases with increasing time;

- within the range of conditions tested a higher soil moisture content results in a higher GCL moisture content;

- larger soil layer thickness results in a larger increase in GCL moisture content, however, for soil layer thicknesses greater than 100 mm only insignificant increases were observed with increasing soil layer thickness;

- overburden pressure within the range tested (i.e., 5 to 390 kPa) did not influence the hydration process; and

- differences between GCL products tested (i.e., type of bentonite clay and fabric) did not seem to significantly affect the test results.

THE HYDROLOGIC EVALUATION OF LANDFILL PERFORMANCE (HELP) MODEL

ENGINEERING DOCUMENTATION FOR VERSION 3

by

Paul R. Schroeder, Tamsen S. Dozier, Paul A. Zappi,
Bruce M. McEnroe, John W. Sjostrom and R. Lee Peyton
Environmental Laboratory
U.S. Army Corps of Engineers
Waterways Experiment Station
Vicksburg, MS 39180-6199

Interagency Agreement No. DW21931425

Project Officer

Robert E. Landreth
Waste Minimization, Destruction and Disposal Research Division
Risk Reduction Engineering Laboratory
Cincinnati, Ohio 45268

RISK REDUCTION ENGINEERING LABORATORY
OFFICE OF RESEARCH AND DEVELOPMENT
U.S. ENVIRONMENTAL PROTECTION AGENCY
CINCINNATI, OHIO 45268

DISCLAIMER

The information in this document has been funded wholly or in part by the United States Environmental Protection Agency under Interagency Agreement No. DW21931425 to the U.S. Army Engineer Waterways Experiment Station (WES). It has been subjected to WES peer and administrative review, and it has been approved for publication as an EPA document. Mention of trade names or commercial products does not constitute endorsement or recommendation for use.

FOREWORD

Today's rapidly developing and changing technologies and industrial products and practices frequently carry with them the increased generation of materials that, if improperly dealt with, can threaten both public health and the environment. Abandoned waste sites and accidental releases of toxic and hazardous substances to the environment also have important environmental and public health implications. The Risk Reduction Engineering Laboratory assists in providing an authoritative and defensible engineering basis for assessing and solving these problems. Its products support the policies, programs and regulations of the Environmental Protection Agency, the permitting and other responsibilities of State and local governments, and the needs of both large and small businesses in handling their wastes responsibly and economically.

This report presents engineering documentation of the Hydrologic Evaluation of Landfill Performance (HELP) model and its user interface. The HELP program is a quasi-two-dimensional hydrologic model for conducting water balance analyses of landfills, cover systems, and other solid waste containment facilities. The model accepts weather, soil and design data and uses solution techniques that account for the effects of surface storage, snowmelt, runoff, infiltration, evapotranspiration, vegetative growth, soil moisture storage, lateral subsurface drainage, leachate recirculation, unsaturated vertical drainage, and leakage through soil, geomembrane or composite liners. Landfill systems including various combinations of vegetation, cover soils, waste cells, lateral drain layers, low permeability barrier soils, and synthetic geomembrane liners may be modeled. The model facilitates rapid estimation of the amounts of runoff, evapotranspiration, drainage, leachate collection and liner leakage that may be expected to result from the operation of a wide variety of landfill designs. The primary purpose of the model is to assist in the comparison of design alternatives. The model is a tool for both designers and permit writers.

E. Timothy Oppelt, Director
Risk Reduction Engineering Laboratory

ABSTRACT

The Hydrologic Evaluation of Landfill Performance (HELP) computer program is a quasi-two-dimensional hydrologic model of water movement across, into, through and out of landfills. The model accepts weather, soil and design data and uses solution techniques that account for the effects of surface storage, snowmelt, runoff, infiltration, evapotranspiration, vegetative growth, soil moisture storage, lateral subsurface drainage, leachate recirculation, unsaturated vertical drainage, and leakage through soil, geomembrane or composite liners. Landfill systems including various combinations of vegetation, cover soils, waste cells, lateral drain layers, low permeability barrier soils, and synthetic geomembrane liners may be modeled. The program was developed to conduct water balance analyses of landfills, cover systems, and solid waste disposal and containment facilities. As such, the model facilitates rapid estimation of the amounts of runoff, evapotranspiration, drainage, leachate collection, and liner leakage that may be expected to result from the operation of a wide variety of landfill designs. The primary purpose of the model is to assist in the comparison of design alternatives as judged by their water balances. The model, applicable to open, partially closed, and fully closed sites, is a tool for both designers and permit writers.

This report documents the solution methods and process descriptions used in Version 3 of the HELP model. Program documentation including program options, system and operating requirements, file structures, program structure and variable descriptions are provided in a separate report. Section 1 provides basic program identification. Section 2 provides a narrative description of the simulation model. Section 3 presents data generation algorithms and default values used in Version 3. Section 4 describes the method of solution and hydrologic process algorithms. Section 5 lists the assumptions and limitations of the HELP model.

The user interface or input facility is written in the Quick Basic environment of Microsoft Basic Professional Development System Version 7.1 and runs under DOS 2.1 or higher on IBM-PC and compatible computers. The HELP program uses an interactive and a user-friendly input facility designed to provide the user with as much assistance as possible in preparing data to run the model. The program provides weather and soil data file management, default data sources, interactive layer editing, on-line help, and data verification and accepts weather data from the most commonly used sources with several different formats.

HELP Version 3 represents a significant advancement over the input techniques of Version 2. Users of the HELP model should find HELP Version 3 easy to use and should be able to use it for many purposes, such as preparing and editing landfill profiles and weather data. Version 3 facilitates use of metric units, international applications, and designs with geosynthetic materials.

This report should be cited as follows:

> Schroeder, P. R., Dozier, T.S., Zappi, P. A., McEnroe, B. M., Sjostrom, J. W., and Peyton, R. L. (1994). "The Hydrologic Evaluation of Landfill Performance (HELP) Model: Engineering Documentation for Version 3," EPA/600/R-94/168b, September 1994, U.S. Environmental Protection Agency Office of Research and Development, Washington, DC.

This report was submitted in partial fulfillment of Interagency Agreement Number DW21931425 between the U.S. Environmental Protection Agency and the U.S. Army Engineer Waterways Experiment Station, Vicksburg, MS. This report covers a period from November 1988 to August 1994 and work was completed as of August 1994.

CONTENTS

FIGURES

TABLES

ACKNOWLEDGMENTS

The support of the project by the Waste Minimization, Destruction and Disposal Research Division, Risk Reduction Engineering Laboratory, U.S. Environmental Protection Agency, Cincinnati, OH and the Headquarters, U.S. Army Corps of Engineers, Washington, DC, through Interagency Agreement No. DW21931425 is appreciated. In particular, the authors wish to thank the U.S. EPA Project Officer,
Mr. Robert Landreth, for his long standing support.

This document was prepared at the U.S. Army Corps of Engineers Waterways Experiment Station. The final versions of this document and the HELP program were prepared by Dr. Paul R. Schroeder. Dr. Paul R. Schroeder directed the development of the HELP model and assembled the simulation code. Ms. Tamsen S. Dozier revised, tested and documented the evapotranspiration, snowmelt and frozen soil processes.
Mr. Paul A. Zappi revised, assembled and documented the geomembrane leakage processes and the default soil descriptions. Dr. Bruce M. McEnroe revised, tested and documented the lateral drainage process for Version 2, which was finalized in this version. Mr. John W. Sjostrom assembled, tested and documented the synthetic weather generator and the vegetative growth process for Version 2, which was finalized in this version. Dr. R. Lee Peyton developed, revised, tested and documented the slope and soil moisture effects on runoff and curve number. Dr. Paul R. Schroeder developed, tested and documented the remaining processes and the output. Ms. Cheryl Lloyd assisted in the final preparation of the report. The figures used in the report were prepared by Messrs. Christopher Chao, Jimmy Farrell, and Shawn Boelman.

The documentation report and simulation model were reviewed by Dr. Jim Ascough, USDA-ARS-NPA, and Dr. Ragui F. Wilson-Fahmy, Geosynthetic Research Institute, Drexel University. This report has not been subjected to the EPA review and, therefore, the contents do not necessarily reflect the views of the Agency, and no official endorsement should be inferred.

SECTION 1

PROGRAM IDENTIFICATION

PROGRAM TITLE: Hydrologic Evaluation of Landfill Performance (HELP) Model

WRITERS: Paul R. Schroeder, Tamsen S. Dozier, John W. Sjostrom and Bruce M. McEnroe

ORGANIZATION: U.S. Army Corps of Engineers, Waterways Experiment Station (WES)

DATE: September 1994

UPDATE: None Version No.: 3.00

SOURCE LANGUAGE: The simulation code is written in ANSI FORTRAN 77 using Ryan-McFarland Fortran Version 2.44 with assembly language and Spindrift Library extensions for Ryan-McFarland Fortran to perform system calls, and screen operations. The user interface is written in BASIC using Microsoft Basic Professional Development System Version 7.1. Several of the user interface support routines are written in ANSI FORTRAN 77 using Ryan-McFarland Fortran Version 2.44, including the synthetic weather generator and the ASCII data import utilities.

HARDWARE: The model was written to run on IBM-compatible personal computers under the DOS environment. The program requires an IBM-compatible 8088, 80286, 80386 or 80486-based CPU (preferably 80386 or 80486) with an 8087, 80287, 80387 or 80486 math co-processor. The computer system must have a monitor (preferably color EGA or better), a 3.5- or 5.25-inch floppy disk drive (preferably 3.5-inch double-sided, high-density), a hard disk drive with 6 MB of available storage, and 400k bytes or more of available low level RAM. A printer is needed if a hard copy is desired.

AVAILABILITY: The source code and executable code for IBM-compatible personal computers are available from the National Technical Information Service (NTIS). Limited distribution immediately following the initial distribution will be available from the USEPA Risk Reduction Engineering Laboratory, the USEPA Center for Environmental Research Information and the USAE Waterways Experiment Station.

ABSTRACT: The Hydrologic Evaluation of Landfill Performance (HELP) computer program is a quasi-two-dimensional hydrologic model of water movement across, into, through and out of landfills. The model accepts weather, soil and design data and uses solution techniques that account for surface storage, snowmelt, runoff, infiltration, vegetative growth, evapotranspiration, soil moisture storage, lateral subsurface drainage, leachate recirculation, unsaturated vertical drainage, and leakage through soil, geomembrane or composite liners. Landfill systems including combinations of vegetation, cover soils, waste cells, lateral drain layers, barrier soils, and synthetic geomembrane liners may be modeled. The program was developed to conduct water balance analyses of landfills, cover systems, and solid waste disposal facilities. As such, the model facilitates rapid estimation of the amounts of runoff, evapotranspiration, drainage, leachate collection, and liner leakage that may be expected to result from the operation of a wide variety of landfill designs. The primary purpose of the model is to assist in the comparison of design alternatives as judged by their water balances. The model, applicable to open, partially closed, and fully closed sites, is a tool for both designers and permit writers.

The HELP model uses many process descriptions that were previously developed, reported in the literature, and used in other hydrologic models. The optional synthetic weather generator is the WGEN model of the U.S. Department of Agriculture (USDA) Agricultural Research Service (ARS) (Richardson and Wright, 1984). Runoff modeling is based on the USDA Soil Conservation Service (SCS) curve number method presented in Section 4 of the National Engineering Handbook (USDA, SCS, 1985). Potential evapotranspiration is modeled by a modified Penman method (Penman, 1963). Evaporation from soil is modeled in the manner developed by Ritchie (1972) and used in various ARS models including the Simulator for Water Resources in Rural Basins (SWRRB) (Arnold et al., 1989) and the Chemicals, Runoff, and Erosion from Agricultural Management System (CREAMS) (Knisel, 1980). Plant transpiration is computed by the Ritchie's (1972) method used in SWRRB and CREAMS. The vegetative growth model was extracted from the SWRRB model. Evaporation of interception, snow and surface water is based on an energy balance. Interception is modeled by the method proposed by Horton (1919). Snowmelt modeling is based on the SNOW-17 routine of the National Weather Service River Forecast System (NWSRFS) Snow Accumulation and Ablation Model (Anderson, 1973). The frozen soil submodel is based on a routine used in the CREAMS model (Knisel et al., 1985). Vertical drainage is modeled by Darcy's (1856) law using the Campbell (1974) equation for unsaturated hydraulic conductivity based on the Brooks-Corey (1964) relationship. Saturated lateral drainage is modeled by an analytical approximation to the steady-state solution of the Boussinesq equation employing the Dupuit-Forchheimer (Forchheimer, 1930) assumptions. Leakage through geomembranes is modeled by a series of equations based on the compilations by Giroud et al. (1989, 1992). The processes are linked together in a sequential order starting at the surface with a surface water balance; then evapotranspiration from the soil profile; and finally drainage and water routing, starting at the surface with infiltration and then proceeding downward through the landfill profile to the bottom. The solution procedure is applied repetitively for each day as it simulates the water routing throughout the simulation period.

SECTION 2

NARRATIVE DESCRIPTION

The HELP program, Versions 1, 2 and 3, was developed by the U.S. Army Engineer Waterways Experiment Station (WES), Vicksburg, MS, for the U.S. Environmental Protection Agency (EPA), Risk Reduction Engineering Laboratory, Cincinnati, OH, in response to needs in the Resource Conservation and Recovery Act (RCRA) and the Comprehensive Environmental Response, Compensation and Liability Act (CERCLA, better known as Superfund) as identified by the EPA Office of Solid Waste, Washington, DC. The primary purpose of the model is to assist in the comparison of landfill design alternatives as judged by their water balances.

The Hydrologic Evaluation of Landfill Performance (HELP) model was developed to help hazardous waste landfill designers and regulators evaluate the hydrologic performance of proposed landfill designs. The model accepts weather, soil and design data and uses solution techniques that account for the effects of surface storage, snowmelt, runoff, infiltration, evapotranspiration, vegetative growth, soil moisture storage, lateral subsurface drainage, leachate recirculation, unsaturated vertical drainage, and leakage through soil, geomembrane or composite liners. Landfill systems including various combinations of vegetation, cover soils, waste cells, lateral drain layers, low permeability barrier soils, and synthetic geomembrane liners may be modeled. Results are expressed as daily, monthly, annual and long-term average water budgets.

The HELP model is a quasi-two-dimensional, deterministic, water-routing model for determining water balances. The model was adapted from the HSSWDS (Hydrologic Simulation Model for Estimating Percolation at Solid Waste Disposal Sites) model of the U.S. Environmental Protection Agency (Perrier and Gibson, 1980; Schroeder and Gibson, 1982), and various models of the U.S. Agricultural Research Service (ARS), including the CREAMS (Chemical Runoff and Erosion from Agricultural Management Systems) model (Knisel, 1980), the SWRRB (Simulator for Water Resources in Rural Basins) model (Arnold et al., 1989), the SNOW-17 routine of the National Weather Service River Forecast System (NWSRFS) Snow Accumulation and Ablation Model (Anderson, 1973), and the WGEN synthetic weather generator (Richardson and Wright, 1984).

HELP Version 1 (Schroeder et al., 1984a and 1984b) represented a major advance beyond the HSSWDS program (Perrier and Gibson, 1980; Schroeder and Gibson, 1982), which was also developed at WES. The HSSWDS model simulated only the cover system, did not model lateral flow through drainage layers, and handled vertical drainage only in a rudimentary manner. The infiltration, percolation and evapotranspiration routines were almost identical to those used in the Chemicals, Runoff, and Erosion from Agricultural Management Systems (CREAMS) model, which was developed by Knisel (1980) for the U.S. Department of Agriculture (USDA). The runoff and infiltration routines relied heavily on the Hydrology Section of the National Engineering Handbook

(USDA, Soil Conservation Service, 1985). Version 1 of the HELP model incorporated a lateral subsurface drainage model and improved unsaturated drainage and liner leakage models into the HSSWDS model. In addition, the HELP model provided simulation of the entire landfill including leachate collection and liner systems.

Version 1 of the HELP program was tested extensively using both field and laboratory data. HELP Version 1 simulation results were compared to field data for 20 landfill cells from seven sites (Schroeder and Peyton, 1987a). The lateral drainage component of HELP Version 1 was tested against experimental results from two large--scale physical models of landfill liner/drain systems (Schroeder and Peyton, 1987b). The results of these tests provided motivation for some of the improvements incorporated into HELP Version 2.

Version 2 (Schroeder et al., 1988a and 1988b) presented a great enhancement of the capabilities of the HELP model. The WGEN synthetic weather generator developed by the USDA Agricultural Research Service (ARS) (Richardson and Wright, 1984) was added to the model to yield daily values of precipitation, temperature and solar radiation. This replaced the use of normal mean monthly temperature and solar radiation values and improved the modeling of snow and evapotranspiration. Also, a vegetative growth model from the Simulator for Water Resources in Rural Basins (SWRRB) model developed by the ARS (Arnold et al., 1989) was merged into the HELP model to calculate daily leaf area indices. Modeling of unsaturated hydraulic conductivity and flow and lateral drainage computations were improved. Default soil data were improved, and the model permitted use of more layers and initialization of soil moisture content.

In Version 3, the HELP model has been greatly enhanced beyond Version 2. The number of layers that can be modeled has been increased. The default soil/material texture list has been expanded to contain additional waste materials, geomembranes, geosynthetic drainage nets and compacted soils. The model also permits the use of a user-built library of soil textures. Computations of leachate recirculation and groundwater drainage into the landfill have been added. Moreover, HELP Version 3 accounts for leakage through geomembranes due to manufacturing defects (pinholes) and installation defects (punctures, tears and seaming flaws) and by vapor diffusion through the liner based on the equations compiled by Giroud et al. (1989, 1992). The estimation of runoff from the surface of the landfill has been improved to account for large landfill surface slopes and slope lengths. The snowmelt model has been replaced with an energy-based model; the Priestly-Taylor potential evapotranspiration model has been replaced with a Penman method, incorporating wind and humidity effects as well as long wave radiation losses (heat loss at night). A frozen soil model has been added to improve infiltration and runoff predictions in cold regions. The unsaturated vertical drainage model has also been improved to aid in storage computations. Input and editing have been further simplified with interactive, full-screen, menu-driven input techniques.

The HELP model requires daily climatologic data, soil characteristics, and design specifications to perform the analysis. Daily rainfall data may be input by the user,

generated stochastically, or taken from the model's historical data base. The model contains parameters for generating synthetic precipitation for 139 U.S. cities. The historical data base contains five years of daily precipitation data for 102 U.S. cities. Daily temperature and solar radiation data are generated stochastically or may be input by the user. Necessary soil data include porosity, field capacity, wilting point, saturated hydraulic conductivity, and Soil Conservation Service (SCS) runoff curve number for antecedent moisture condition II. The model contains default soil characteristics for 42 material types for use when measurements or site-specific estimates are not available. Design specifications include such things as the slope and maximum drainage distance for lateral drainage layers, layer thicknesses, leachate recirculation procedure, surface cover characteristics and information on any geomembranes.

Figure 1 is a definition sketch for a somewhat typical closed hazardous waste landfill profile. The top portion of the profile (layers 1 through 4) is the cap or cover. The bottom portion of the landfill is a double liner system (layers 6 through 11), in this case composed of a geomembrane liner and a composite liner. Immediately above the bottom composite liner is a leakage detection drainage layer to collect leakage from the primary liner, in this case, a geomembrane. Above the primary liner are a geosynthetic drainage net and a sand layer that serve as drainage layers for leachate collection. The drain layers composed of sand are typically at least 1-ft thick and have suitably spaced perforated or open joint drain pipe embedded below the surface of the liner. The leachate collection drainage layer serves to collect any leachate that may percolate through the waste layers. In this case where the liner is solely a geomembrane, a drainage net may be used to rapidly drain leachate from the liner, avoiding a significant buildup of head and limiting leakage. The liners are sloped to prevent ponding by encouraging leachate to flow toward the drains. The net effects are that very little leachate should leak through the primary liner and virtually no migration of leachate through the bottom composite liner to the natural formations below. Taken as a whole, the drainage layers, geomembrane liners, and barrier soil liners may be referred to as the leachate collection and removal system (drain/liner system) and more specifically a double liner system.

Figure 1 shows eleven layers--four in the cover or cap, one as the waste layers, three in the primary leachate collection and removal system (drain/liner system) and three in the secondary leachate collection and removal system (leakage detection). These eleven layers comprise three subprofiles or modeling units. A subprofile consists of all layers between (and including) the landfill surface and the bottom of the top liner system, between the bottom of one liner system and the bottom of the next lower liner system, or between the bottom of the lowest liner system and the bottom of the lowest soil layer modeled. In the sketch, the top subprofile contains the cover layers, the middle subprofile contains the waste, drain and liner system for leachate collection, and the bottom subprofile contains the drain and liner system for leakage detection. Six subprofiles in a single landfill profile may be simulated by the model.

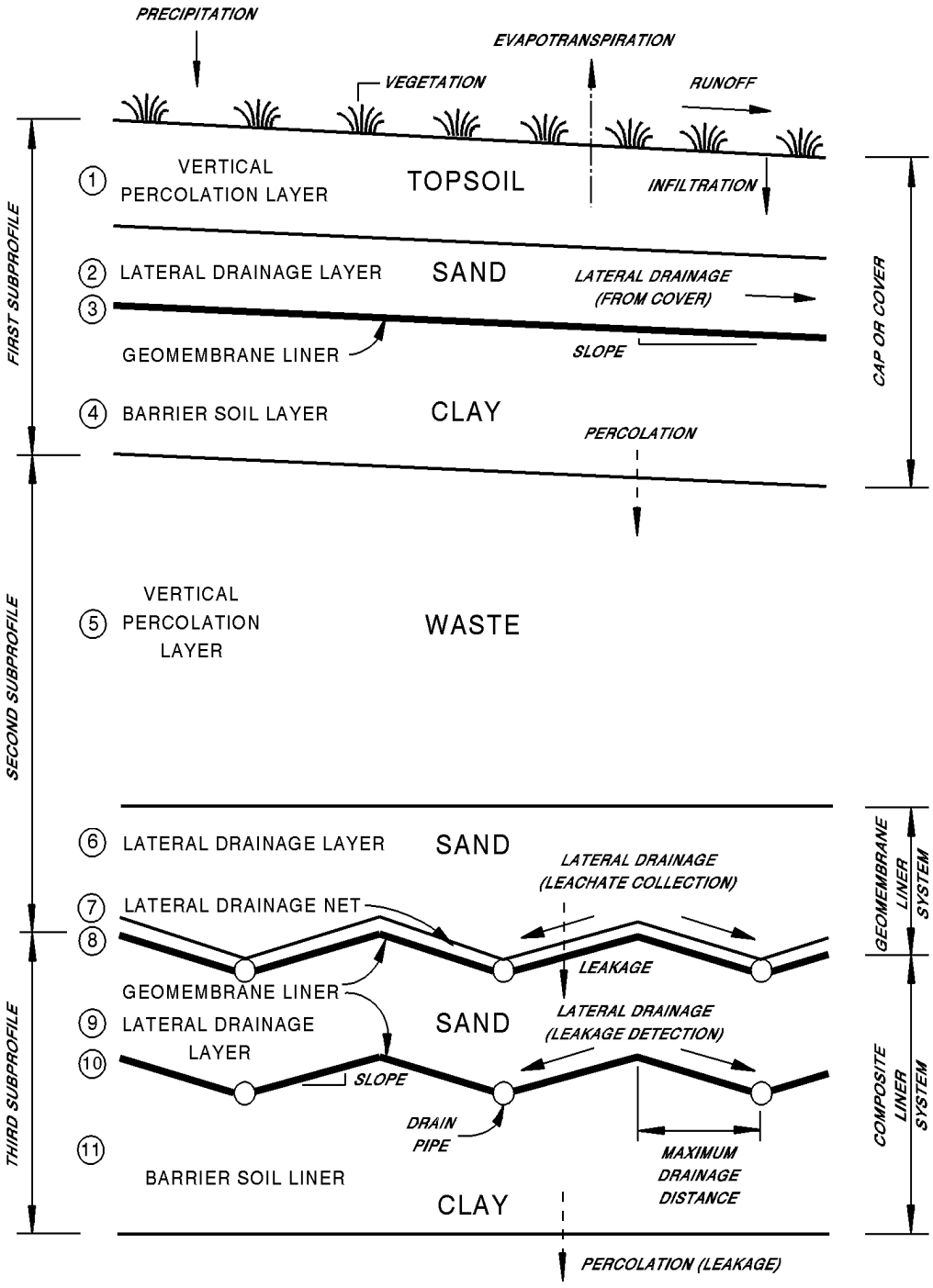

Figure 1. Schematic Profile View of a Typical Hazardous Waste Landfill

The layers in the landfill are typed by the hydraulic function that they perform. Four types are of layers are available: vertical percolation layers, lateral drainage layers, barrier soil liners and geomembrane liners. These layer types are illustrated in Figure 1. The topsoil and waste layers are generally vertical percolation layers. Sand layers above liners are typically lateral drainage layers; compacted clay layers are typically barrier soil liners. Geomembranes are typed as geomembrane liners. Composite liners are modeled as two layers. Geotextiles are not considered as layers unless they perform a unique hydraulic function.

Flow in a vertical percolation layer (e.g., layers 1 and 5 in Figure 1) is either downward due to gravity drainage or extracted by evapotranspiration. Unsaturated vertical drainage is assumed to occur by gravity drainage whenever the soil moisture is greater than the field capacity (greater than the wilting point for soils in the evaporative zone) or when the soil suction of the layer below the vertical percolation layer is greater than the soil suction in the vertical percolation layer. The rate of gravity drainage (percolation) in a vertical percolation layer is assumed to be a function of the soil moisture storage and largely independent of conditions in adjacent layers. The rate can be restricted when the layer below is saturated and drains slower than the vertical percolation layer. Layers, whose primary hydraulic function is to provide storage of moisture and detention of drainage, should normally be designated as vertical percolation layers. Waste layers and layers designed to support vegetation should be designated as vertical percolation layers, unless the layers provide lateral drainage to collection systems.

Lateral drainage layers (e.g., layers 2, 6, 7 and 9 in Figure 1) are layers that promote lateral drainage to collection systems at or below the surface of liner systems. Vertical drainage in a lateral drainage layer is modeled in the same manner as for a vertical percolation layer, but saturated lateral drainage is allowed. The saturated hydraulic conductivity of a lateral drainage layer generally should be greater than 1×10^{-3} cm/sec for significant lateral drainage to occur. A lateral drainage layer may be underlain by only a liner or another lateral drainage layer. The slope of the bottom of the layer may vary from 0 to 40 percent.

Barrier soil liners (e.g., layers 4 and 11 in Figure 1) are intended to restrict vertical flow. These layers should have hydraulic conductivities substantially lower than those of the other types of layers, typically below 1×10^{-6} cm/sec. The program allows only downward flow in barrier soil liners. Thus, any water moving into a liner will eventually percolate through it. The leakage (percolation) rate depends upon the depth of water-saturated soil (head) above the base of the layer, the thickness of the liner and the saturated hydraulic conductivity of the barrier soil. Leakage occurs whenever the moisture content of the layer above the liner is greater than the field capacity of the layer. The program assumes that barrier soil liner is permanently saturated and that its properties do not change with time.

Geomembrane liners (e.g., layers 3, 8 and 10 in Figure 1) are layers of nearly

impermeable material that restricts significant leakage to small areas around defects. Leakage (percolation) is computed to be the result from three sources: vapor diffusion, manufacturing flaws (pinholes) and installation defects (punctures, cracks, tears and bad seams). Leakage by vapor diffusion is computed to occur across the entire area of the liner as a function of the head on the surface of the liner, the thickness of the geomembrane and its vapor diffusivity. Leakage through pinholes and installation defects is computed in two steps. First, the area of soil or material contributing to leakage is computed as a function of head on the liner, size of hole and the saturated hydraulic conductivity of the soils or materials adjacent to the geomembrane liner. Second, the rate of leakage in the wetted area is computed as a function of the head, thickness of soil and membrane and the saturated hydraulic conductivity of the soils or materials adjacent to the geomembrane liner.

SECTION 3

DATA GENERATION AND DEFAULT VALUES

3.1 OVERVIEW

The HELP model requires general climate data for computing potential evapotranspiration; daily climatologic data; soil characteristics; and design specifications to perform the analysis. The required general climate data include growing season, average annual wind speed, average quarterly relative humidities, normal mean monthly temperatures, maximum leaf area index, evaporative zone depth and latitude. Default values for these parameters were compiled or developed from the "Climates of the States" (Ruffner, 1985) and "Climatic Atlas of the United States" (National Oceanic and Atmospheric Administration, 1974) for 183 U.S. cities. Daily climatologic (weather) data requirements include precipitation, mean temperature and total global solar radiation. Daily rainfall data may be input by the user, generated stochastically, or taken from the model's historical data base. The model contains parameters for generating synthetic precipitation for 139 U.S. cities. The historical data base contains five years of daily precipitation data for 102 U.S. cities. Daily temperature and solar radiation data are generated stochastically or may be input by the user.

Necessary soil data include porosity, field capacity, wilting point, saturated hydraulic conductivity, initial moisture storage, and Soil Conservation Service (SCS) runoff curve number for antecedent moisture condition II. The model contains default soil characteristics for 42 material types for use when measurements or site-specific estimates are not available. The porosity, field capacity, wilting point and saturated hydraulic conductivity are used to estimate the soil water evaporation coefficient and Brooks-Corey soil moisture retention parameters. Design specifications include such items as the slope and maximum drainage distance for lateral drainage layers; layer thicknesses; layer description; area; leachate recirculation procedure; subsurface inflows; surface characteristics; and geomembrane characteristics.

3.2 SYNTHETIC WEATHER GENERATION

The HELP program incorporates a routine for generating daily values of precipitation, mean temperature, and solar radiation. This routine was developed by the USDA Agricultural Research Service (Richardson and Wright, 1984) based on a procedure described by Richardson (1981). The HELP user has the option of generating synthetic daily precipitation data rather than using default or user-specified historical data. Similarly, the HELP user has the option of generating synthetic daily mean temperature and solar radiation data rather than using user-specified historical data. The generating routine is designed to preserve the dependence in time, the correlation between variables and the seasonal characteristics in actual weather data at the specified location.

Coefficients for weather generation are available for up to 183 cities in the United States.

Daily precipitation is generated using a Markov chain-two parameter gamma distribution model. A first-order Markov chain model is used to generate the occurrence of wet or dry days. In this model, the probability of rain on a given day is conditioned on the wet or dry status of the previous day. A wet day is defined as a day with 0.01 inch of rain or more. The model requires two transition probabilities: $P_i(W/W)$, the probability of a wet day on day i given a wet day on day i-1; and $P_i(W/D)$, the probability of a wet day on day i given a dry day on day i-1.

When a wet day occurs, the two-parameter gamma distribution function, which describes the distribution of daily rainfall amounts, is used to generate the precipitation amount. The density function of the two-parameter gamma distribution is given by

$$f(p) = \frac{p^{\alpha-1} e^{-p/\beta}}{\beta^{\alpha} \Gamma(\alpha)} \qquad (1)$$

where

$f(p)$ = density function

p = the probability

α *and* β = distribution parameters

Γ = the gamma function of α

e = the base of natural logarithms

The values of P(W/W), P(W/D), α and β vary continuously during the year for most locations. The precipitation generating routine uses monthly values of the four parameters. The HELP program contains these monthly values for 139 locations in the United States. These values were computed by the Agricultural Research Service from 20 years (1951-1970) of daily precipitation data for each location.

Daily values of maximum temperature, minimum temperature and solar radiation are generated using the equation

$$t_i(j) = m_i(j) [\chi_i(j) \cdot c_i(j) + 1] \qquad (2)$$

where

$t_i(j)$ = daily value of maximum temperature (j=1), minimum temperature (j=2), or solar radiation (j=3)

$m_i(j)$ = mean value on day i

$c_i(j)$ = coefficient of variation on day i

$\chi_i(j)$ = stochastically generated residual element for day i

The seasonal change in the means and coefficients of variation is described by the harmonic equation

$$u_i = \bar{u} + C \cos\left[\frac{2\pi}{365}(i - T)\right] \quad (3)$$

where

u_i = value of $m_i(j)$ or $c_i(j)$ on day i

$\bar{u}$ = mean value of u_i

C = amplitude of the harmonic

T = position of the harmonic in days

The Agricultural Research Service computed values of these parameters for the three variables on wet and dry days from 20 years of weather data at 31 locations. The HELP model contains values of these parameters for 184 cities. These values were taken from contour maps prepared by Richardson and Wright (1984).

The residual elements for Equation 2 are generated using a procedure that preserves important serial correlations and cross-correlations. The generating equation is

$$\chi_i(j) = (A \cdot \chi_{i-1}(j)) + (B \cdot \epsilon_i(j)) \quad (4)$$

where

$\chi_i(j)$ = 3 x 1 matrix for day i whose elements are residuals of maximum temperature (j=1), minimum temperature (J=2), and solar radiation (J=3)

$\varepsilon_{i(j)}$ = 3 x 1 matrix of independent random components for item j

A and B = 3 x 3 matrices whose elements are defined such that the new sequences have the desired serial correlation and cross-correlation coefficients

Richardson (1981) computed values of the relevant correlation coefficients from 20 years of weather data at 31 locations. The seasonal and spatial variation in these

correlation coefficients were found to be negligible. The elements of the A and B matrices are therefore treated as constants.

3.3 MOISTURE RETENTION AND HYDRAULIC CONDUCTIVITY PARAMETERS

The HELP program requires values for the total porosity, field capacity, wilting point, and saturated hydraulic conductivity of each layer that is not a liner. Saturated hydraulic conductivity is required for all liners. Values for these parameters can be specified by the user or selected from a list of default values provided in the HELP program. The values are used to compute moisture storage, unsaturated vertical drainage, head on liners and soil water evaporation.

3.3.1 Moisture Retention Parameters

Relative moisture retention or storage used in the HELP model differs from the water contents typically used by engineers. The soil water storage or content used in the HELP model is on a per volume basis (θ), volume of water (V_w) per total (bulk--soil, water and air) soil volume ($V_t = V_s + V_w + V_a$), which is characteristic of practice in agronomy and soil physics. Engineers more commonly express moisture content on a per mass basis (w), mass of water (M_w) per mass of soil (M_s). The two can be related to each other by knowing the dry bulk density (ρ_{db}) and water density (ρ_w), the dry bulk specific gravity (Γ_{db}) of the soil (ratio of dry bulk density to water density), ($\theta = w \cdot \Gamma_{db}$), or the wet bulk density (ρ_{wb}), wet bulk specific gravity (Γ_{wb}) of the soil (ratio of wet bulk density to water density), ($\theta = [w \cdot \Gamma_{wb}] / [1 + w]$).

Total porosity is an effective value, defined as the volumetric water content (volume of water per total volume) when the pores contributing to change in moisture storage are at saturation. Total porosity can be used to describe the volume of active pore space present in soil or waste layers. Field capacity is the volumetric water content at a soil water suction of 0.33 bars or remaining after a prolonged period of gravity drainage without additional water supply. Wilting point is the volumetric water content at a suction of 15 bars or the lowest volumetric water content that can be achieved by plant transpiration (See Section 4.11). These moisture retention parameters are used to define moisture storage and relative unsaturated hydraulic conductivity.

The HELP program requires that the wilting point be greater than zero but less than the field capacity. The field capacity must be greater than the wilting point and less than the porosity. Total porosity must be greater than the field capacity but less than 1. The general relation among moisture retention parameters and soil texture class is shown in Figure 2.

The HELP user can specify the initial volumetric water contents of all non-liner layers. Soil liners are assumed to remain saturated at all times. If initial water contents

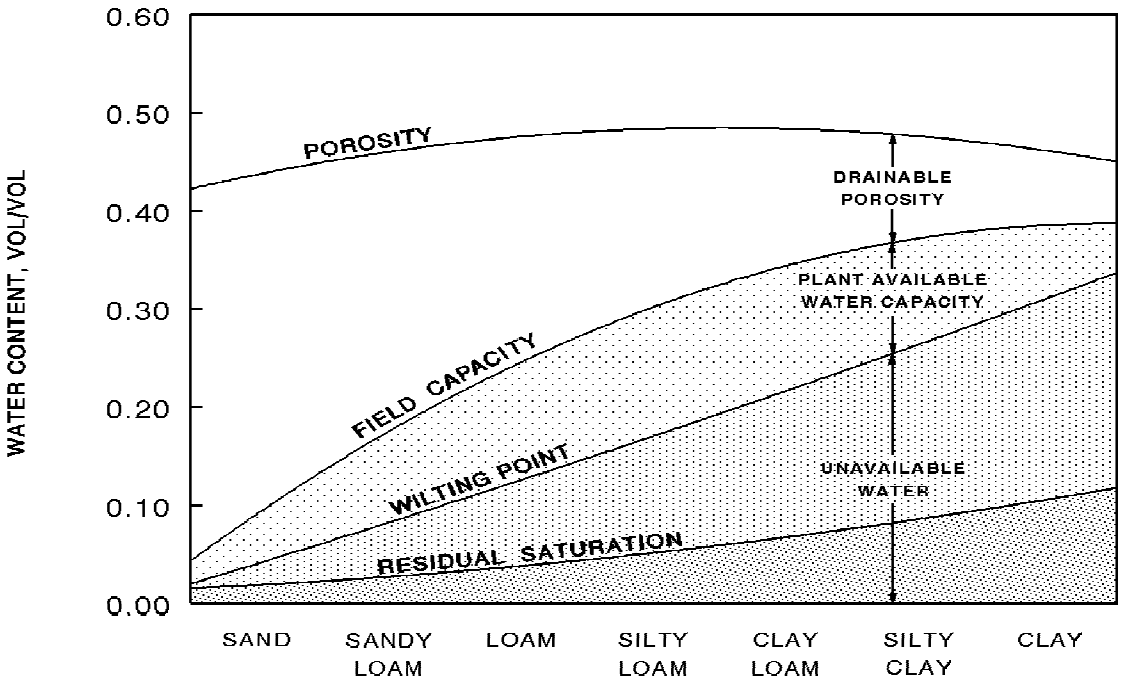

Figure 2. Relation Among Moisture Retention Parameters and Soil Texture Class

are not specified, the program assumes values near the steady-state values (allowing no long-term change in moisture storage) and runs a year of simulation to initialize the moisture contents closer to steady state. The soil water contents at the end of this year are substituted as the initial values for the simulation period. The program then runs the complete simulation, starting again from the beginning of the first year of data. The results of the volumetric water content initialization period are not reported in the output.

3.3.2 Unsaturated Hydraulic Conductivity

Darcy's constant of proportionality governing flow through porous media is known quantitatively as hydraulic conductivity or coefficient of permeability and qualitatively as permeability. Hydraulic conductivity is a function of media properties, such as particle size, void ratio, composition, fabric, degree of saturation, and the kinematic viscosity of the fluid moving through the media. The HELP program uses the saturated and unsaturated hydraulic conductivities of soil and waste layers to compute vertical drainage, lateral drainage and soil liner percolation. The vapor diffusivity for geomembranes is specified as a saturated hydraulic conductivity to compute leakage through geomembranes by vapor diffusion.

Saturated Hydraulic Conductivity

Saturated hydraulic conductivity is used to describe flow through porous media where the void spaces are filled with a wetting fluid (e.g., water). The saturated hydraulic conductivity of each layer is specified in the input. Equations for estimating the hydraulic conductivity for soils and other materials are presented in Appendix A of the HELP Program Version 3 User's Guide.

Unsaturated Hydraulic Conductivity

Unsaturated hydraulic conductivity is used to describe flow through a layer when the void spaces are filled with both wetting and non-wetting fluid (e.g., water and air). The HELP program computes the unsaturated hydraulic conductivity of each soil and waste layer using the following equation, reported by Campbell (1974):

$$K_u = K_s \left[\frac{\theta - \theta_r}{\phi - \theta_r} \right]^{3 + \left(\frac{2}{\lambda}\right)} \tag{5}$$

where

K_u = unsaturated hydraulic conductivity, cm/sec

K_s = saturated hydraulic conductivity, cm/sec

θ = actual volumetric water content, vol/vol

θ_r = residual volumetric water content, vol/vol

ϕ = total porosity, vol/vol

λ = pore-size distribution index, dimensionless

Residual volumetric water content is the amount of water remaining in a layer under infinite capillary suction. The HELP program uses the following regression equation, developed using mean soil texture values from Rawls et al. (1982), to calculate the residual volumetric water content:

$$\theta_r = \begin{cases} 0.014 + 0.25\, WP & for\ WP \geq 0.04 \\ 0.6\, WP & for\ WP < 0.04 \end{cases} \tag{6}$$

where

WP = volumetric wilting point, vol/vol

The residual volumetric water content and pore-size distribution index are constants in the Brooks-Corey equation relating volumetric water content to matrix potential (capillary pressure and adsorptive forces) (Brooks and Corey, 1964):

$$\frac{\theta - \theta_r}{\phi - \theta_r} = \left(\frac{\psi_b}{\psi}\right)^{\lambda} \qquad (7)$$

where

ψ = capillary pressure, bars

ψ_b = bubbling pressure, bars

Bubbling pressure is a function of the maximum pore size forming a continuous network of flow channels within the medium (Brooks and Corey, 1964). Brakensiek et al. (1981) reported that Equation 7 provided a reasonably accurate representation of water retention and matrix potential relationships for tensions greater than 50 cm or 0.05 bars (unsaturated conditions).

The HELP program solves Equation 7 for two different capillary pressures simultaneously to determine the bubbling pressure and pore-size distribution index of volumetric moisture content for use in Equation 7. The total porosity is known from the input data. The capillary pressure-volumetric moisture content relationship is known at two points from the input of field capacity and wilting point. Therefore, the field capacity is inserted in Equation 7 as the volumetric moisture content and 0.33 bar is inserted as the capillary pressure to yield one equation. Similarly, the wilting point and 15 bar are inserted in Equation 7 to yield a second equation. Having two equations and two unknowns (bubbling pressure and pore-size distribution index), the two equations are solved simultaneously to yield the unknowns. This process is repeated for each layer to obtain the parameters for computing moisture retention and unsaturated drainage.

3.3.3 Saturated Hydraulic Conductivity for Vegetated Materials

The HELP program adjusts the saturated hydraulic conductivities of soils and waste layers in the top half of the evaporative zone whenever those soil characteristics were selected from the default list of soil textures. This adjustment, developed for the model from changes in runoff characteristics and minimum infiltration rates as function of vegetation, is made to account for channeling due to root penetration. These adjustments for vegetation are not made for user-specified soil characteristics; they are made only for default soil textures, which assumed that the soil layer is unvegetated and free of continuous root channels that provide preferential drainage paths. The HELP program calculates the vegetated saturated hydraulic conductivity as follows:

$$(K_s)_v = (1.0 + 0.5966\,LAI + 0.132659\,LAI^2 + 0.1123454\,LAI^3 - 0.04777627\,LAI^4 + 0.004325035\,LAI^5)\,(K_s)_{uv} \quad (8)$$

where

$(K_s)_v$ = saturated hydraulic conductivity of vegetated material in top half of evaporative zone, cm/sec

LAI = leaf area index, dimensionless (described in Section 4.11)

$(K_s)_{uv}$ = saturated hydraulic conductivity of unvegetated material in top half of evaporative zone, cm/sec

3.4 EVAPORATION COEFFICIENT

The evaporation coefficient indicates the ease with which water can be drawn upward through the soil or waste layer by evaporation. Using laboratory soil data Ritchie (1972) indicated that the evaporation coefficient (in mm/day$^{0.5}$) can be related to the unsaturated hydraulic conductivity at 0.1 bar capillary pressure (calculated using Equations 5 and 7). The HELP program uses the following form of Ritchie's equation to compute the evaporation coefficient:

$$CON = \begin{cases} 3.30 & (K_u)_{0.1\ bar} \le 0.05\ cm/day \\ 2.44 + 17.19\,(K_u)_{0.1\ bar} & 0.05\ cm/day < (K_u)_{0.1\ bar} < 0.178\ cm/day \\ 5.50 & (K_u)_{0.1\ bar} \ge 0.178\ cm/day \end{cases} \quad (9)$$

where

CON = evaporation coefficient, mm/day$^{0.5}$

$(K_u)_{0.1\ bar}$ = unsaturated hydraulic conductivity at 0.1 bar capillary pressure, cm/sec

The HELP program imposes upper and lower limits on the evaporation coefficient so as not to yield a capillary flux outside of the range for soils reported by Knisel (1980). If the calculated value of the evaporation coefficient is less than 3.30, then it is set equal to 3.30, and if the evaporation coefficient is greater than 5.50, then it is set equal to 5.50. The user cannot enter the evaporation coefficient independently.

Since Equation 9 was developed for soil materials, the HELP program imposes

additional checks on the evaporation coefficient based on the relative field capacity and saturated hydraulic conductivity of each soil and waste layer. Relative field capacity is calculated using the following equation:

$$FC_{rel} = \frac{FC - \theta_r}{\phi - \theta_r} \quad (10)$$

where

FC_{rel} = relative field capacity, dimensionless

FC = field capacity, vol/vol

If the relative field capacity is less than 0.20 (typical of sand), then the evaporation coefficient is set equal to 3.30. Additionally, if the saturated hydraulic conductivity is less than 5×10^{-6} cm/sec (the range of compacted clay), the evaporation coefficient is set equal to 3.30.

3.5 DEFAULT SOIL AND WASTE CHARACTERISTICS

The total density of soil and waste layers can be defined as the mass of solid and water particles per unit volume of the media. The total density of these layers is dependent on the density of the solid particles, the volume of pore space, and the amount of water in each layer. As previously discussed, total porosity can be used to describe the volume of pore space in a soil or waste layer. Therefore, total porosity can be used to indicate the density of soil and waste layers.

The density of soil and waste layers can be increased by compaction, static loading, and/or dewatering of soil and waste layers. Compaction increases density through the application of mechanical energy. Static loading increases density by the application of of the weight of additional soil, barrier, or waste layers. Dewatering increases density by removing pore water and/or reducing the pore pressures in the layer. Dewatering can be accomplished by installing horizontal and/or vertical drains, trenches, water wells, and/or the application of electrical currents. The HELP program provides default values for the total porosity, field capacity, wilting point, and saturated hydraulic conductivity of numerous soil and waste materials as well as geosynthetic materials.

3.5.1 Default Soil Characteristics

Information on default soil moisture retention values for low, moderate, and high-density soil layers is provided in the following sections. High-density soil layers are also described as soil liners. Application of the default soil properties should be limited to

planning level studies and are not intended to replace design level laboratory and field testing programs.

Low-Density Soil Layers

Rawls et al. (1982) reported mean values for total porosity, residual volumetric water content, bubbling pressure, and pore-size distribution index, for the major US Department of Agriculture (USDA) soil texture classes. These values were compiled from 1,323 soils with about 5,350 horizons (or layers) from 32 states. The geometric mean of the bubbling pressure and pore-size distribution index and the arithmetic mean of total porosity and residual volumetric water content for each soil texture class were substituted into Equation 7 to calculate the field capacity (volumetric water content at a capillary pressure of 1/3 bar) and wilting point (volumetric water content at a capillary pressure of 15 bars) of each soil texture class. Rawls et al. (1982) also reported saturated hydraulic conductivity values for each major USDA uncompacted soil texture class. These values were derived from the results of numerous experiments and compared with similar data sets. Default characteristics for the coarse and fine sands (Co and F) were developed by interpolating between Rawls' data.

Freeze and Cherry (1979) reported that typical unconsolidated clay total porosities range from 0.40 to 0.70. Rawls' sandy clay, silty clay, and clay had total porosities of 0.43, 0.48, and 0.47, respectively. Therefore, Rawls' loam and clay soils data are considered to represent conditions typical of minimal densification efforts or low-density soils. Default characteristics for Rawls et al. (1982) low-density soil layers are summarized in Table 1. The USDA soil textures reported in Table 1 were converted to Unified Soil Classification System (USCS) soil textures using a soil classification triangle provided in McAneny et al. (1985). Applicable USDA and USCS soil texture abbreviations are provided in Table 3.

Moderate-Density Soil Layers

Rawls et al. (1982) presented the following form of Brutsaert's (1967) saturated hydraulic conductivity equation:

$$K_s = a \frac{(\phi - \theta_r)^2}{(\psi_b)^2} \frac{\lambda^2}{(\lambda + 1)(\lambda + 2)} \qquad (11)$$

where

K_s = saturated hydraulic conductivity, cm/sec

TABLE 1. DEFAULT LOW DENSITY SOIL CHARACTERISTICS

Soil Texture Class			Total Porosity vol/vol	Field Capacity vol/vol	Wilting Point vol/vol	Saturated Hydraulic Conductivity cm/sec
HELP	USDA	USCS				
1	CoS	SP	0.417	0.045	0.018	1.0×10^{-2}
2	S	SW	0.437	0.062	0.024	5.8×10^{-3}
3	FS	SW	0.457	0.083	0.033	3.1×10^{-3}
4	LS	SM	0.437	0.105	0.047	1.7×10^{-3}
5	LFS	SM	0.457	0.131	0.058	1.0×10^{-3}
6	SL	SM	0.453	0.190	0.085	7.2×10^{-4}
7	FSL	SM	0.473	0.222	0.104	5.2×10^{-4}
8	L	ML	0.463	0.232	0.116	3.7×10^{-4}
9	SiL	ML	0.501	0.284	0.135	1.9×10^{-4}
10	SCL	SC	0.398	0.244	0.136	1.2×10^{-4}
11	CL	CL	0.464	0.310	0.187	6.4×10^{-5}
12	SiCL	CL	0.471	0.342	0.210	4.2×10^{-5}
13	SC	SC	0.430	0.321	0.221	3.3×10^{-5}
14	SiC	CH	0.479	0.371	0.251	2.5×10^{-5}
15	C	CH	0.475	0.378	0.251	2.5×10^{-5}
21	G	GP	0.397	0.032	0.013	3.0×10^{-1}

a = constant representing the effects of various fluid constants and gravity, 21 cm^3/sec

ϕ = total porosity, vol/vol

θ_r = residual volumetric water content, vol/vol

ψ_b = bubbling pressure, cm

λ = pore-size distribution index, dimensionless

A more detailed explanation of Equation 11 can be found in Appendix A of the HELP program Version 3 User's Guide and the cited references.

Since densification is known to decrease the saturated hydraulic conductivity of a soil layer, the total porosity, residual volumetric water content, bubbling pressure, and pore-size distribution index data reported in Rawls et al. (1982) were adjusted by a fraction of a standard deviation and substituted into Equation 11 to reflect this decrease. Examination of Equation 11 and various adjustments to Rawls' reported data indicated that a reasonable representation of moderate-density soil conditions can be obtained by a 0.5 standard deviation decrease in the total porosity and pore-size distribution index and a 0.5 standard deviation increase in the bubbling pressure and residual saturation of Rawls' compressible soils (e.g. loams and clays). These adjustments were substituted into Equations 7 and 11 to determine the total porosity, field capacity, wilting point, and hydraulic conductivity of these soils. The values obtained from these adjustments are thought to represent moderate-density soil conditions typical of compaction by vehicle traffic, static loading by the addition of soil or waste layers, etc. Default characteristics for moderate-density, compressible loams and clays are summarized in Table 2. The USDA soil textures reported in Table 2 were converted to Unified Soil Classification System (USCS) soil textures using information provided in McAneny et al. (1985). Applicable USDA and USCS soil texture abbreviations are provided in Table 3.

High-Density Soil Layers

Similar to moderate-density soil layers, densification produces a high-density, low saturated hydraulic conductivity soil layer or soil liner. Due to the geochemical and low saturated hydraulic conductivity properties of clay, soil liners are typically constructed of compacted clay. Elsbury et al. (1990) indicated that the hydraulic conductivity of clay liners can be impacted by the soil workability, gradation, and swell potential; overburden stress on the liner; liner thickness; liner foundation stability; liner desiccation and/or freeze and thawing; and degree of compaction. Compaction should destroy large soil clods and provide interlayer bonding. The process can be impacted by the lift thickness; soil water content, dry density, and degree of saturation; size of soil clods; soil preparation; compactor type and weight; number of compaction passes and coverage; and construction quality assurance. The HELP program provides default characteristics for clay soil liners with a saturated hydraulic conductivity of $1x10^{-7}$ and $1x10^{-9}$ cm/sec.

Similar to the procedure used to obtain the default moderate-density clay soil properties, Rawls et al.'s (1982) reported total porosity, pore-size distribution index, bubbling pressure, and residual saturation for clay soil layers were adjusted to determine the field capacity and wilting point of the $1x10^{-7}$ cm/sec clay liner. A hydraulic conductivity of $6.8x10^{-8}$ cm/sec was obtained by substituting a 1 standard deviation decrease in Rawls' reported total porosity and pore-size distribution index and a 1 standard deviation increase in Rawls' reported bubbling pressure and residual saturation into Equation 11. These adjustments were substituted into Equation 7 to obtain a field capacity and wilting point representative of the $1x10^{-7}$ cm/sec soil liner.

TABLE 2. MODERATE AND HIGH DENSITY DEFAULT SOILS

Soil Texture Class			Total Porosity vol/vol	Field Capacity vol/vol	Wilting Point vol/vol	Saturated Hydraulic Conductivity cm/sec
HELP	USDA	USCS				
22	L (Moderate)	ML	0.419	0.307	0.180	1.9×10^{-5}
23	SiL (Moderate)	ML	0.461	0.360	0.203	9.0×10^{-6}
24	SCL (Moderate)	SC	0.365	0.305	0.202	2.7×10^{-6}
25	CL (Moderate)	CL	0.437	0.373	0.266	3.6×10^{-6}
26	SiCL (Moderate)	CL	0.445	0.393	0.277	1.9×10^{-6}
27	SC (Moderate)	SC	0.400	0.366	0.288	7.8×10^{-7}
28	SiC (Moderate)	CH	0.452	0.411	0.311	1.2×10^{-6}
29	C (Moderate)	CH	0.451	0.419	0.332	6.8×10^{-7}
16	Liner Soil (High)		0.427	0.418	0.367	1.0×10^{-7}
17	Bentonite (High)		0.750	0.747	0.400	3.0×10^{-9}

3.5.2 Default Waste Characteristics

Table 4 provides a summary of default moisture retention values for various waste layers. Municipal waste properties provided in Tchobanoglous et al. (1977) and Equations 6 and 7 were used to determine the total porosity, field capacity, and wilting point of a well compacted municipal waste. The field capacity and wilting point were calculated using Tchobanoglous et al.'s high and low water content values, respectively. Oweis et al. (1990) provided information on the in-situ saturated hydraulic conductivity of municipal waste. Zeiss and Major (1993) described the moisture flow through

TABLE 3. DEFAULT SOIL TEXTURE ABBREVIATIONS

US Department of Agriculture	Definition
G	Gravel
S	Sand
Si	Silt
C	Clay
L	Loam (sand, silt, clay, and humus mixture)
Co	Coarse
F	Fine
Unified Soil Classification System	**Definition**
G	Gravel
S	Sand
M	Silt
C	Clay
P	Poorly Graded
W	Well Graded
H	High Plasticity or Compressibility
L	Low Plasticity or Compressibility

municipal waste and the effective moisture retention of municipal waste, providing information on waste with dead zones and channeling. In addition, Toth et al. (1988) provided information on compacted coal-burning electric plant ash, Poran and Ahtchi-Ali (1989) provided information on compacted municipal solid waste ash, and Das et al. (1983) provided information on fine copper slag.

The total porosities of the ash and slag wastes were determined using a phase relationship at maximum dry density. The field capacities and wilting points of the ash and slag wastes were calculated using the following empirical equations reported by Brakensiek et al. (1984):

TABLE 4. DEFAULT WASTE CHARACTERISTICS

Waste Identification		Total Porosity vol/vol	Field Capacity vol/vol	Wilting Point vol/vol	Saturated Hydraulic Conductivity cm/sec
HELP	Waste Material				
18	Municipal Waste	0.671	0.292	0.077	1.0×10^{-3}
19	Municipal Waste with Channeling	0.168	0.073	0.019	1.0×10^{-3}
30	High-Density Electric Plant Coal Fly Ash*	0.541	0.187	0.047	5.0×10^{-5}
31	High-Density Electric Plant Coal Bottom Ash*	0.578	0.076	0.025	4.1×10^{-3}
32	High-Density Municipal Solid Waste Incinerator Fly Ash**	0.450	0.116	0.049	1.0×10^{-2}
33	High-Density Fine Copper Slag**	0.375	0.055	0.020	4.1×10^{-2}

* All values, except saturated hydraulic conductivity, are at maximum dry density. Saturated hydraulic conductivity was determined in-situ.

** All values are at maximum dry density. Saturated hydraulic conductivity was determined by laboratory methods.

$$Field\ Capacity = 0.1535 - (0.0018)(\%\ Sand) + (0.0039)(\%\ Clay) + (0.1943)(Total\ Porosity) \quad (12)$$

$$Wilting\ Point = 0.0370 - (0.0004)(\%\ Sand) + (0.0044)(\%\ Clay) + (0.0482)(Total\ Porosity) \quad (13)$$

where 0.05 mm < Sand Particles < 2 mm and Clay Particles < 0.002 mm (McAneny et al. 1985). These equations were developed for natural soils having a sand content between 5 and 70 percent and a clay content between 5 and 60 percent. While the particle size distribution of some of the ash and slag wastes fell outside this range, the effects of this variation on water retention were thought to be minimal. The applicability of these equations to waste materials has not been verified.

The saturated hydraulic conductivities of the ash and slag wastes were taken directly from the references. The saturated hydraulic conductivities of the coal burning electric plant ashes at maximum dry density were determined in-situ and the maximum dry density municipal solid waste incinerator ash and fine copper slag values were determined by laboratory methods. The saturated hydraulic conductivities of various other waste materials are provided in Table 5. Similar to default soils, the HELP program uses Equation 8 to adjust the saturated hydraulic conductivities of the default wastes in the top half of the evaporative zone to account for root penetration.

A more detailed explanation of the calculation procedure used for the ash and slag wastes can be found in Appendix A of the HELP program Version 3 User's Guide. Like the soil properties, the default waste properties were determined using empirical equations developed from soil data. Therefore, these values should not be used in place of a detailed laboratory and field testing program.

TABLE 5. SATURATED HYDRAULIC CONDUCTIVITY OF WASTES

Waste Material	Saturated Hydraulic Conductivity cm/sec*	Reference
Stabilized Incinerator Fly Ash	8.8×10^{-5}	Poran and Ahtchi-Ali (1989)
High-Density Pulverized Fly Ash	2.5×10^{-5}	Swain (1979)
Solidified Waste	4.0×10^{-2}	Rushbrook et al. (1989)
Electroplating Sludge	1.6×10^{-5}	Bartos and Palermo (1977)
Nickel/Cadmium Battery Sludge	3.5×10^{-6}	"
Inorganic Pigment Sludge	5.0×10^{-6}	"
Brine Sludge - Chlorine Production	8.2×10^{-5}	"
Calcium Fluoride Sludge	3.2×10^{-5}	"
High Ash Papermill Sludge	1.4×10^{-6}	Perry and Schultz (1977)

* - Determined by laboratory methods.

3.5.3 Default Geosynthetic Material Characteristics

Table 6 provides a summary of default properties for various geosynthetic materials. The values were extracted from Geotechnical Fabrics Report--1992 Specifiers Guide (Industrial Fabrics Association International, 1991) and Giroud and Bonaparte (1985).

3.6 SOIL MOISTURE INITIALIZATION

The soil moisture of the layers may be initialized by the user or the program. If initialized by the program, the soil moisture is initialized near steady-state using a three step procedure. The first step sets the soil moisture of all liners to porosity or saturation and the moisture of all other layers to field capacity.

In the second step the program computes a soil moisture for each layer below the top liner system. These soil moistures are computed to yield an unsaturated hydraulic conductivity equal to 85% of the lowest effective saturated hydraulic conductivity of all

TABLE 6. DEFAULT GEOSYNTHETIC MATERIAL CHARACTERISTICS

Geosynthetic Material Description		Saturated Hydraulic Conductivity cm/sec
HELP	Geosynthetic Material	
20	Drainage Net (0.5 cm)	$1.0 \times 10^{+1}$
34	Drainage Net (0.6 cm)	$3.3 \times 10^{+1}$
35	High Density Polyethylene (HDPE) Membrane	2.0×10^{-13}
36	Low Density Polyethylene (LDPE) Membrane	4.0×10^{-13}
37	Polyvinyl Chloride (PVC) Membrane	2.0×10^{-11}
38	Butyl Rubber Membrane	1.0×10^{-12}
39	Chlorinated Polyethylene (CPE) Membrane	4.0×10^{-12}
40	Hypalon or Chlorosulfonated Polyethylene (CSPE) Membrane	3.0×10^{-12}
41	Ethylene-Propylene Diene Monomer (EPDM) Membrane	2.0×10^{-12}
42	Neoprene Membrane	3.0×10^{-12}

liner systems above the layer, including consideration for geomembrane liners. If the unsaturated hydraulic conductivity is greater than 5 x 10^{-7} cm/sec or if the computed soil moisture is less than field capacity, the soil moisture is set to equal the field capacity. In all other cases, the computed soil moistures are used.

The third step in the initialization consists of running the model for one year of simulation using the first year of climatological data and the initial soil moistures selected in step 2. At the end of the year of initialization, the soil moistures existing at that point are reported as the initial soil moistures. The simulation is then started using the first year of climatological data again.

3.7 DEFAULT LEAF AREA INDICES AND EVAPORATIVE ZONE DEPTHS

Recommended default values for leaf area index and evaporative depth are given in the program. Figures 3, 4 and 5 show the geographic distribution of the default values for minimum and maximum evaporative depth and maximum leaf area index. The evaporative zone depths are based on rainfall, temperature and humidity data for the climatic regions. The estimates for minimum depths are based loosely on literature values (Saxton et al., 1971) and unsaturated flow model results for bare loamy soils (Thompson and Tyler, 1984; Fleenor, 1993), while the maximum depths are for loamy soils with a very good stand of grass, assuming rooting depths will vary regionally with

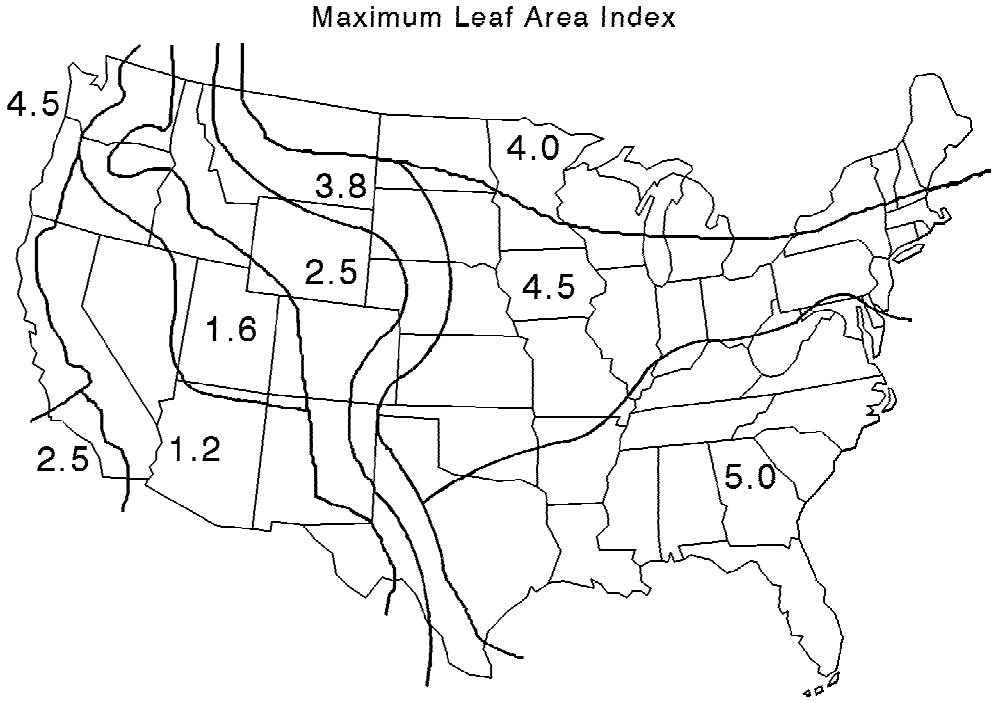

Figure 3. Geographic Distribution of Maximum Leaf Area Index

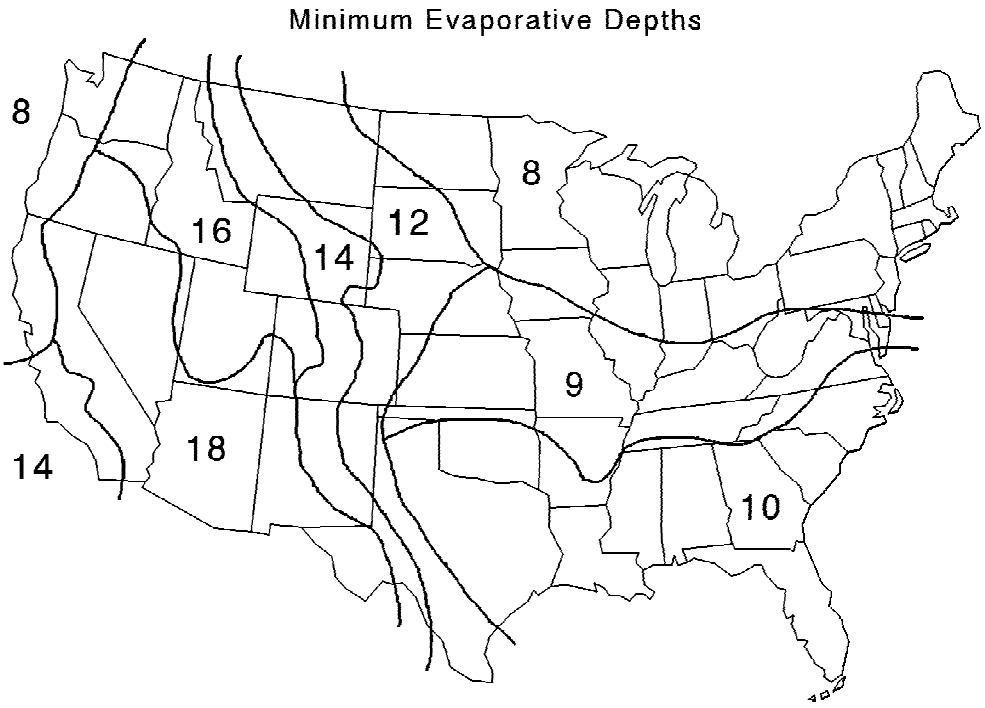

Figure 4. Geographic Distribution of Minimum Evaporative Depth

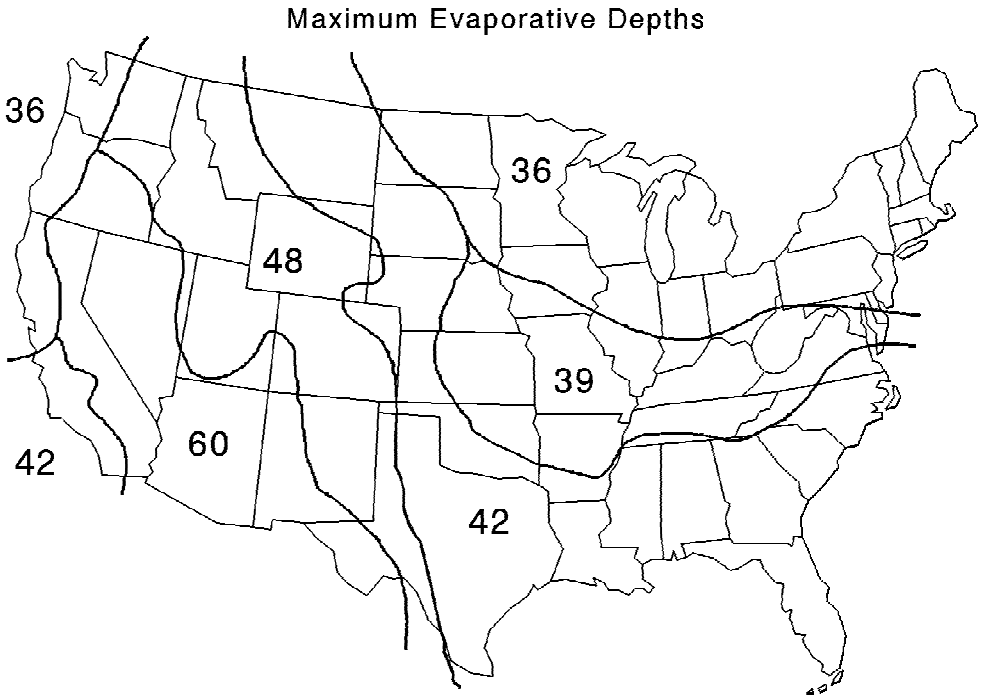

Figure 5. Geographic Distribution of Maximum Evaporative Depth

plant species and climate. The zones and values for the maximum leaf area index are based on recommendations in the documentation for the Simulator for Water Resources in Rural Basins (SWRRB) model (Arnold et al., 1989), considering both rainfall and temperature.

SECTION 4

METHOD OF SOLUTION

4.1 OVERVIEW

The HELP program simulates daily water movement into, through and out of a landfill. In general, the hydrologic processes modeled by the program can be divided into two categories: surface processes and subsurface processes. The surface processes modeled are snowmelt, interception of rainfall by vegetation, surface runoff, and evaporation of water, interception and snow from the surface. The subsurface processes modeled are evaporation of water from the soil, plant transpiration, vertical unsaturated drainage, geomembrane liner leakage, barrier soil liner percolation and lateral saturated drainage. Vegetative growth and frozen soil models are also included in the program to aid modeling of the water routing processes.

Daily infiltration into the landfill is determined indirectly from a surface-water balance. Each day, infiltration is assumed to equal the sum of rainfall and snowmelt, minus the sum of runoff, surface storage and surface evaporation. No liquid water is held in surface storage from one day to the next, except in the snow cover. The daily surface-water accounting proceeds as follows. Snowfall and rainfall are added to the surface snow storage, if present, and then snowmelt plus excess storage of rainfall is computed. The total outflow from the snow cover is then treated as rainfall in the absence of a snow cover for the purpose of computing runoff. A rainfall-runoff relationship is used to determine the runoff. Surface evaporation is then computed. Surface evaporation is not allowed to exceed the sum of surface snow storage and intercepted rainfall. Interception is computed only for rainfall, not for outflow from the snow cover. The snowmelt and rainfall that does not run off or evaporate is assumed to infiltrate into the landfill. Computed infiltration in excess of the storage and drainage capacity of the soil is routed back to the surface and is added to the runoff or held as surface storage.

The first subsurface processes considered are evaporation from the soil and plant transpiration from the evaporative zone of the upper subprofile. These are computed on a daily basis. The evapotranspiration demand is distributed among the seven modeling segments in the evaporative zone.

The other subsurface processes are modeled one subprofile at a time, from top to bottom, using a design dependent time step, varying from 30 minutes to 6 hours. Unsaturated vertical drainage is computed for each modeling segment starting at the top of the subprofile, proceeding downward to the liner system or bottom of the subprofile. The program performs a water balance on each segment to determine the water storage and drainage for each segment, accounting for infiltration or drainage from above, subsurface inflow, leachate recirculation, moisture content and material characteristics.

If the subprofile contains a liner, water-routing or drainage from the segment directly above the liner is computed as leakage or percolation through the liner, and lateral drainage to the collection system, if present. The sum of the lateral drainage and leakage/percolation is first estimated to compute the moisture storage and head on the liner. Using the head, the leakage and lateral drainage is computed and compared to their initial guesses. If the sum of these two outflows is not sufficiently close to the initial estimate, new estimates are generated and the procedure is repeated until acceptable convergence is achieved. The moisture storage in liner systems is assumed to be constant; therefore, any drainage into a liner results in an equal drainage out of the liner. If the subprofile does not contain a liner, the lateral drainage is zero and the vertical drainage from the bottom subprofile is computed in the same manner as the upper modeling segments.

4.2 RUNOFF

The rainfall-runoff process is modeled using the SCS curve-number method, as presented in Section 4 of the National Engineering Handbook (USDA, SCS, 1985). This procedure was selected for four reasons: (1) it is widely accepted, (2) it is computationally efficient, (3) the required input is generally available and (4) it can conveniently handle a variety of soil types, land uses and management practices.

The SCS procedure was developed from rainfall-runoff data for large storms on small watersheds. The development is as follows (USDA, SCS, 1985). Runoff was plotted as a function of rainfall on arithmetic graph paper having equal scales, yielding a curve that becomes asymptotic to a straight line with a 1:1 slope at high rainfall as shown in Figure 6. The equation of the straight-line portion of the runoff curve, assuming no lag between the times when rainfall and runoff begin, is

$$Q = P' - S' \tag{14}$$

where

Q = actual runoff, inches

P' = maximum potential runoff (actual rainfall after runoff starts or actual rainfall when initial abstraction does not occur), inches

S' = maximum potential retention after runoff starts, inches

The following empirical equation was found to describe the relationship among precipitation, runoff and retention (the difference between the rainfall and runoff) at any point on the runoff curve:

$$\frac{F}{S'} = \frac{Q}{P'} \tag{15}$$

where

F = actual retention after runoff starts, inches

= $P' - Q$

Substituting for F,

$$\frac{P' - Q}{S'} = \frac{Q}{P'} \tag{16}$$

If initial abstraction is considered, the runoff curve is translated to the right, as shown in Figure 6, by the amount of precipitation that occurs before runoff begins. This amount of precipitation is termed the initial abstraction, I_a. To adjust Equation 16 for initial abstraction, this amount is subtracted from the precipitation,

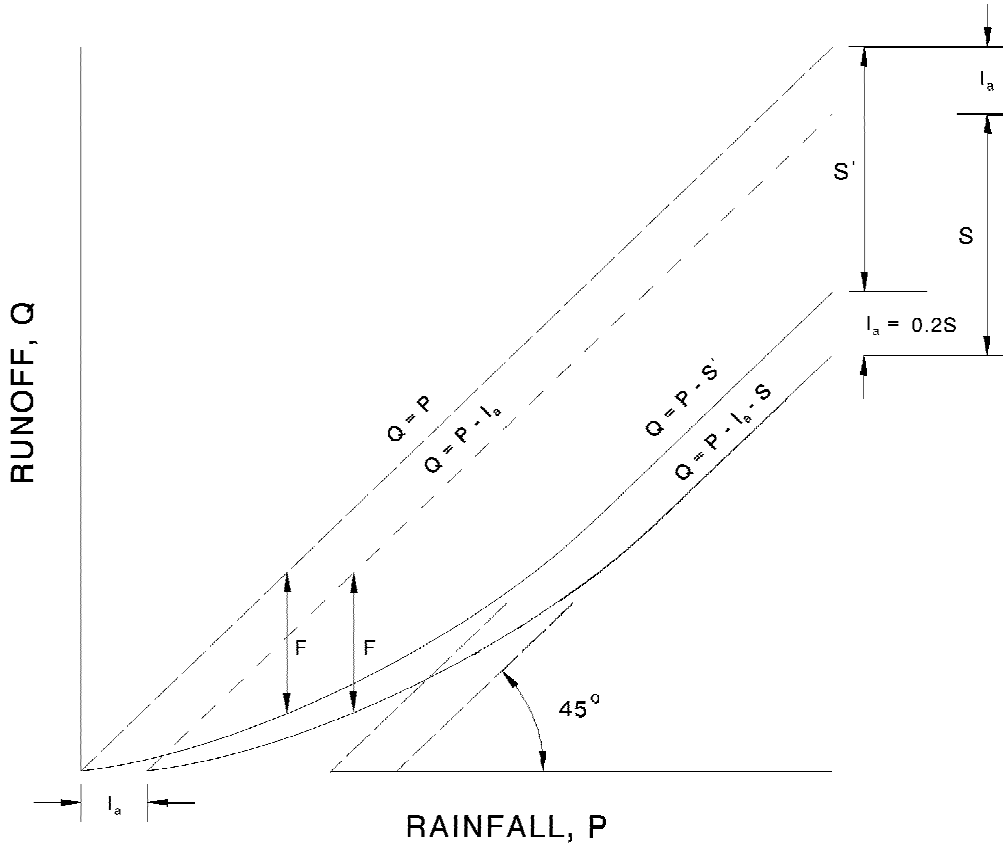

Figure 6. Relation Between Runoff, Precipitation, and Retention

$$P' = P - I_a \tag{17}$$

Equation 16 becomes

$$\frac{P - I_a - Q}{S'} = \frac{Q}{P - I_a} \tag{18}$$

where

P = actual rainfall, inches

I_a = initial abstraction, inches

Figure 6 shows that the two retention parameters, *S'* and *S*, are equal:

$$S = S' \tag{19}$$

Rainfall and runoff data from a large number of small experimental watersheds indicate that, as a reasonable approximation (USDA, SCS, 1985),

$$I_a = 0.2\,S \tag{20}$$

Substituting Equations 19 and 20 into Equation 18 and solving for *Q*,

$$Q = \frac{(P - 0.2\,S)^2}{(P + 0.8\,S)} \tag{21}$$

Performing polynomial division on Equation 21 and dividing both sides of the equation by *S*,

$$\frac{Q}{S} = \frac{P}{S} - 1.2 - \frac{1.0}{\frac{P}{S} + 0.8} \tag{22}$$

Equation 22 is the normalized rainfall-runoff relationship for any *S* and is plotted in Figure 7.

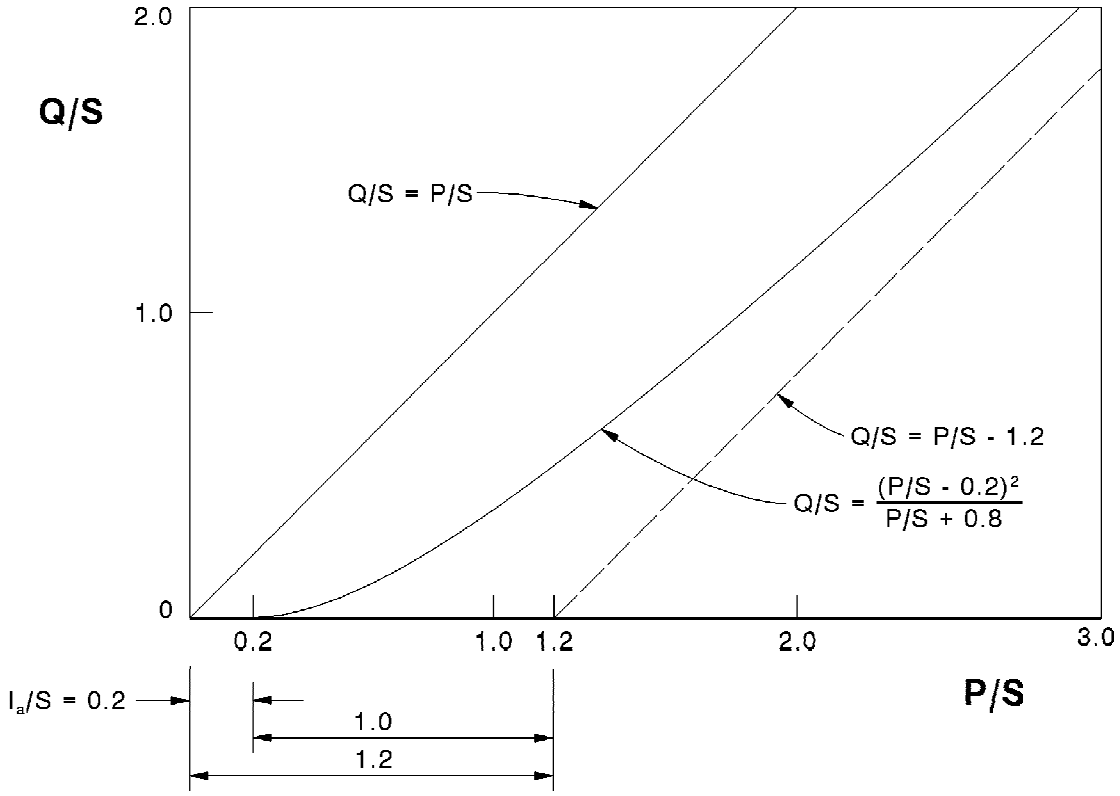

Figure 7. SCS Rainfall-Runoff Relation Normalized on Retention Parameter S

The retention parameter, *S*, is transformed into a so-called runoff curve number, *CN*, to make interpolating, averaging and weighting operations more nearly linear. The relationship between *CN* and *S* is

$$CN = \frac{1000}{S + 10} \tag{23}$$

$$S = \frac{1000}{CN} - 10 \tag{24}$$

The HELP program computes the runoff, Q_i on day *i*, from Equation 21 based on the net rainfall, P_i, on this day. The net rainfall is zero when the mean temperature is less than or equal to 32 °F; is equal to the precipitation when the mean temperature is above 32 °F and no snow cover is present; or is equal to the outflow from the snow cover when

a snow cover is present and the mean temperature is above 32 °F:

$$P_i = \begin{cases} 0.0 & for \quad T_i \le 32\,^\circ F \\ R_i & for \quad T_i > 32\,^\circ F, \quad SNO_{i-1} = 0.0 \\ O_i - EMELT_i & for \quad T_i > 32\,^\circ F, \quad SNO_{i-1} > 0.0 \end{cases} \tag{25}$$

where

P_i = net rainfall and snowmelt available for runoff on day i, inches

R_i = rainfall on day i, inches

O_i = outflow from snow cover subject to runoff on day i, inches

$EMELT_i$ = evaporation of snowmelt on day i, inches

SNO_{i-1} = water equivalence of snow cover at end of day i-1, inches

4.2.1 Adjustment of Curve Number for Soil Moisture

The value of the retention parameter, *S*, for a given soil is assumed to vary with soil moisture as follows:

$$S = \begin{cases} S_{mx}\left[1 - \dfrac{SM - [(FC + WP)/2]}{UL - [(FC + WP)/2]}\right] & for \quad SM > (FC + WP)/2 \\ S_{mx} & for \quad SM \le (FC + WP)/2 \end{cases} \tag{26}$$

where

S_{mx} = maximum value of *S*, inches

SM = soil water storage in the vegetative or evaporative zone, inches

UL = soil water storage at saturation, inches

FC = soil water storage at field capacity (the water remaining following gravity drainage in the absence of other losses), inches

WP = soil water storage at wilting point (the lowest naturally occurring soil water storage), inches.

S_{mx} is the retention parameter, *S*, for a dry condition. It is assumed that the soil water content midway between field capacity and wilting point is characteristic of being dry.

Since soil water is not distributed uniformly through the soil profile, and since the soil moisture near the surface influences infiltration more strongly than soil moisture

located elsewhere, the retention parameter is depth-weighted. The soil profile of the vegetative or evaporative zone depth is divided into seven segments. The thickness of the top segment is set at one thirty-sixth of the thickness of the vegetative or evaporative depth. The thickness of the second segment is set at five thirty-sixths of the thickness of the vegetative or evaporative zone depth. The thickness of each of the bottom five segments is set at one-sixth of the thickness of the vegetative or evaporative zone depth. The user-specified evaporative depth is the maximum depth from which moisture can be removed by evapotranspiration. This depth cannot exceed the depth to the top of the uppermost barrier soil layer. The depth-weighted retention parameter is computed using the following equation (Knisel, 1980):

$$S = \sum_{j=1}^{7} W_j \cdot S_j \tag{27}$$

$$S_j = \begin{cases} S_{mx}\left[1 - \dfrac{SM_j - [(FC_j + WP_j)/2]}{UL_j - [(FC_j + WP_j)/2]}\right] & for \quad SM_j > (FC_j + WP_j)/2 \\ S_{mx} & for \quad SM_j \le (FC_j + WP_j)/2 \end{cases} \tag{28}$$

where

W_j = weighting factor for segment j

SM_j = soil water storage in segment j, inches

UL_j = storage at saturation in segment j, inches

FC_j = storage at field capacity in segment j, inches

WP_j = storage at wilting point in segment j, inches

The weighting factors decrease with the depth of the segment in accordance with the following equation from the CREAMS model (Knisel, 1980):

$$W_j = 1.0159\left[e^{-4.16\frac{D_{j-1}}{EZD}} - e^{-4.16\frac{D_j}{EZD}}\right] \tag{29}$$

where

D_j = depth to bottom of segment j, inches

EZD = vegetative or evaporative zone depth, inches

For the assumed segment thicknesses, this equation gives weighting factors of 0.111, 0.397, 0.254, 0.127, 0.063, 0.032 and 0.016 for segments 1 through 7. The top segment is the highest weighted in a relative sense since its thickness is 1/36 of the evaporative zone depth while the thickness of the second segment is 5/36 and the others are 1/6.

The runoff curve number required as input to the HELP program is that corresponding to antecedent moisture condition II (AMC-II) in the SCS method. AMC-II represents an average soil-moisture condition. The corresponding curve number is denoted CN_{II}. The HELP user can either input a value of CN_{II} directly; input a curve number and have the program adjust it for surface slope conditions; or have the program compute a value based on the vegetative cover type, the default soil type and surface slope conditions.

The value of the maximum moisture retention parameter, S_{mx}, is assumed to equal the value of S for a dry condition, antecedent moisture condition I (AMC-I) in the SCS method (USDA, SCS, 1985). It is assumed that the soil moisture content for this dry condition (a condition where the rainfall in the last five days totaled less than 0.5 inches without vegetation and 1.4 inches with vegetation) is midway between field capacity and wilting point. S_{mx} is related to the curve number for AMC-I, CN_I, as follows:

$$S_{mx} = \frac{1000}{CN_I} - 10 \tag{30}$$

CN_I is related to CN_{II} by the following polynomial (Knisel, 1980):

$$\begin{aligned} CN_I = {} & 3.751 \times 10^{-1} CN_{II} + 2.757 \times 10^{-3} CN_{II}^2 \\ & - 1.639 \times 10^{-5} CN_{II}^3 + 5.143 \times 10^{-7} CN_{II}^4 \end{aligned} \tag{31}$$

4.2.2 Computation of Default Curve Numbers

When the user requests the program to generate and use a default curve number, the program first computes the AMC-II curve number for the specified soil type and vegetation for a mild slope using the following equation:

$$CN_{II_o} = C_o + C_1 \cdot IR + C_2 \cdot IR^2 \tag{32}$$

where

CN_{II_o} = AMC-II curve number for mild slope (unadjusted for slope)

C_O = regression constant for a given level of vegetation

C_1 = regression constant for a given level of vegetation

C_2 = regression constant for a given level of vegetation

IR = infiltration correlation parameter for given soil type

The relationship between CN_{II_o}, the vegetative cover and default soil texture is shown graphically in Figure 8. Table 7 gives values of C_0, C_1 *and* C_2 for the five types of vegetative cover built into the HELP program.

4.2.3 Adjustment of Curve Number for Surface Slope

A regression equation was developed to adjust the AMC-II curve number for surface slope conditions. The regression was developed based on kinematic wave theory where

TABLE 7. CONSTANTS FOR USE IN EQUATION 32

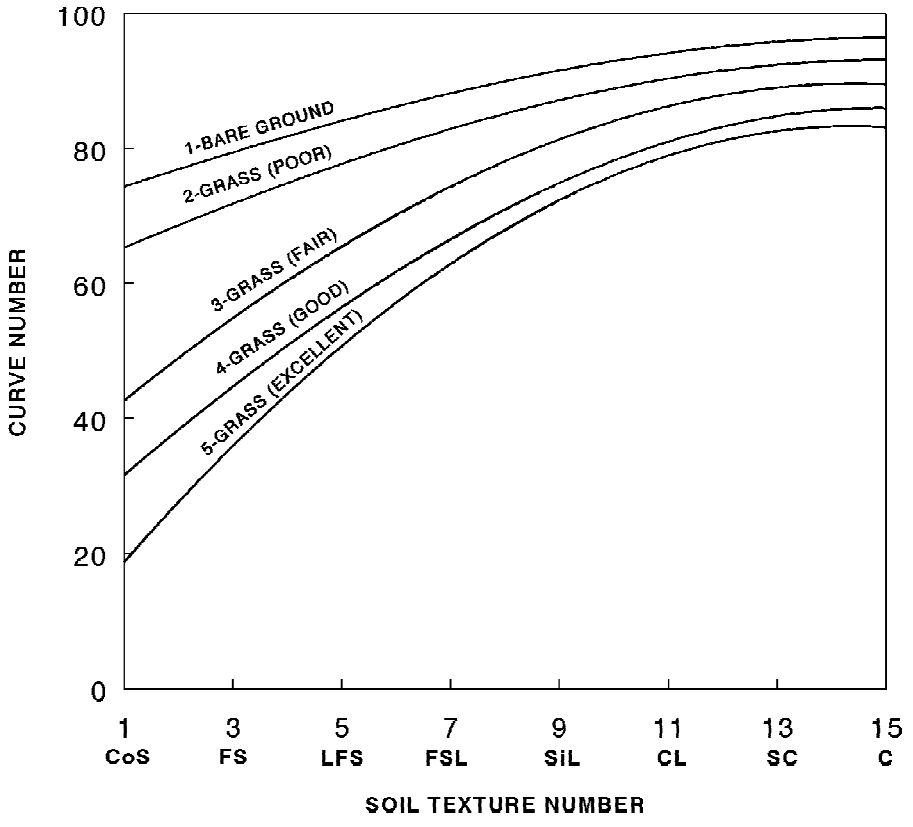

Figure 8. Relation between SCS Curve Number and Default Soil Texture Number for Various Levels of Vegetation

Vegetative Cover	C_0	C_1	C_2
Bare Ground	96.77	-20.80	-54.94
Poor Grass	93.51	-24.85	-71.92
Fair Grass	90.09	-23.73	-158.4
Good Grass	86.72	-43.38	-151.2
Excellent Grass	83.83	-26.91	-229.4

the travel time of runoff from the top of a slope to the bottom of the slope is computed as follows:

$$t_{run} = \frac{1.5}{(i - I)^{1/3}} \left(\frac{L^2}{S} \right)^{1/3} \left(\frac{1.49}{n} \right)^{-2/3} \quad (33)$$

where

t_{run} = runoff travel time (time of concentration), minutes

i = steady-state rainfall intensity (rate), inches/hour

I = steady-state infiltration rate, inches/hour

L = slope length, feet

S = surface slope, dimensionless

n = Manning's roughness coefficient, dimensionless

A decrease in travel time results in less infiltration because less time is available for infiltration to occur.

Using the KINEROS kinematic runoff and erosion model (Woolhiser, Smith, and Goodrich, 1990), hundreds of runoff estimates were generated using different combinations of soil texture class, level of vegetation, slope, slope length, and rainfall depth, duration and temporal distribution. Using these estimates, the curve number that would yield the estimated runoff was calculated from the rainfall depth and the runoff estimate. These curve numbers were regressed with the slope length, surface slope and the curve number that would be generated for the soil texture and level of vegetation placed at a mild slope. The four soil textures used included loamy sand, sandy loam, loam, and clayey loam as specified by saturated hydraulic conductivity, capillary drive, porosity, and maximum relative saturation. Two levels of vegetation were described--a

good stand of grass (bluegrass sod) and a poor stand of grass (clipped range). Slopes of 0.04, 0.10, 0.20, 0.35, and 0.50 ft/ft and slope lengths of 50, 100, 250, and 500 ft were used. Rainfalls of 1.1 inches, 1-hour duration and 2nd quartile Huff distribution and of 3.8 inches, 6-hour duration and balanced distribution were modeled.

The resulting regression equation used for adjusting the AMC-II curve number computed for default soils and vegetation placed at mild slopes, CN_{II_o}, is:

$$CN_{II} = 100 - (100 - CN_{II_o}) \cdot \left(\frac{L^{*2}}{S^*} \right)^{CN_{II_o}^{-0.81}} \quad (34)$$

where

L^* = standardized dimensionless length, (L/500 ft)

S^* = standardized dimensionless slope, (S/0.04)

This same equation is used to adjust user-specified AMC-II curve numbers for surface slope conditions by substituting the user value for CN_{II_o} in Equation 34.

4.2.4 Adjustment of Curve Number for Frozen Soil

When the HELP program predicts frozen conditions to exist, the value of CN_{II} is increased, resulting in a higher calculated runoff. Knisel et al. (1985) found that this type of curve number adjustment in the CREAMS model resulted in improved predictions of annual runoff for several test watersheds. If the CN_{II} for unfrozen soil is less than or equal to 80, the CN_{II} for frozen soil conditions is set at 95. When the unfrozen soil CN_{II} is greater than 80, the CN_{II} is reset to be 98 on days when the program has determined the soil to be frozen. This adjustment results in an increase in CN_I and consequently a decrease in S_{mx} and S' (Equations 19, 26, and 30).

From Equations 19 and 21, it is apparent that as S' approaches zero, Q approaches P. In other words, as S' decreases, the calculated runoff becomes closer to being equal to the net rainfall which is most often, when frozen soil conditions exist, predominantly snowmelt. This will result in a decrease in infiltration under frozen soil conditions, which has been observed in numerous studies.

4.2.5 Summary of Daily Runoff Computation

The HELP model determines daily runoff by the following procedure:

1) Given CN_{II} from input or calculated by Equations 32 or 34, CN_I and S_{mx} are computed once using Equations 31 and 30, respectively.

2) S is computed daily using Equations 27 and 28.

3) The daily runoff resulting from the daily rainfall and snowmelt is computed using Equation 21.

4.3 PREDICTION OF FROZEN SOIL CONDITIONS

In cold regions, the effects of frozen soil on runoff and infiltration rates are significant. Because of the necessary complexity and the particular data requirements of any approach to estimating soil temperatures, the inclusion of a theoretically-based frozen soil model in the HELP program is prohibitive for the purposes of the program. However, for some regions, it is desirable to have some method for predicting the occurrence of frozen soil and the resulting increase in runoff.

Knisel et al. (1985) proposed a rather simple procedure for predicting the existence of frozen soils in the CREAMS model. A modification of that approach has been incorporated into HELP. In the HELP modification, the soil is assumed to enter a frozen state when the average temperature of the previous 30 days first drops below 32 °F. During the time in which the soil is considered to be frozen, the infiltration capacity of the soil is reduced by increasing the calculated runoff. As explained earlier, this is done by increasing the curve number. In addition, other processes are affected such as soil evaporation, vertical drainage in the evaporative zone and groundmelt of snow.

The point in which the soil is no longer considered to be frozen is determined by calculating the length of time required to thaw frozen soil; that is, the number of days in which the soil is to remain frozen after the daily mean air temperature first rises above freezing. The thaw period in days, *DFS*, is a constant for a particular set of climatic data. The thaw period increases with latitude and decreases with solar radiation in the winter at the site and is determined using the following relation.

$$DFS = 35.4 - 0.154\ R_{S(Dec)} \tag{35}$$

where

$R_{S(Dec)}$ = estimate of the normal total solar radiation in December (June in the southern hemisphere) at the selected location, langleys

DFS = estimate of the number of days with mean temperatures above freezing in excess of days with mean temperatures below freezing required to thaw a frozen soil after a thaw is started

$R_{S(Dec)}$ is computed using the maximum daily potential solar radiation for the site in December, $R_{So(Dec)}$, (June in southern hemisphere) (Richardson and Wright, 1984) and the mean daily solar radiation for December (June in southern hemisphere) from the first year

of the user's input data file, $R_{S(1st\ Dec)}$. This estimate is used to provide consistency throughout the simulation and to limit the importance of the first year of solar radiation data. $R_{S(Dec)}$ is computed as follows:

$$R_{S(Dec)} = 0.5 \left[R_{S(1st\ Dec)} + 0.75 \cdot R_{So(Dec)} \right] \quad (36)$$

where

$$R_{So(Dec)} = 711.38\ DD\ [(H \sin|LAT| \sin SD) + (\sin H \cos|LAT| \cos SD)] \quad (37)$$

where

$R_{So(Dec)}$ = average daily potential solar radiation at site in December (June in the southern hemisphere), langleys

DD = $1 + 0.0335 \sin [0.0172 (J + 88.2)]$

J = Julian date, 350 for northern hemisphere and 167 for southern hemisphere

XT = $\arccos [(-\tan |LAT|) (\tan SD)]$

LAT = latitude of site, radians

SD = $0.4102 \sin [0.0172 (J - 80.25)]$

In addition, a counter in the program keeps track of the number of days of below freezing (one is subtracted for each day down to a minimum of zero) or above freezing temperatures (one is added for each day up until a maximum of *DFS* is reached, at which point the soil becomes unfrozen) since the soil became frozen. When the soil freezes for the first time during the season, the counter is set to 0. When a thaw is completed, the counter is reset to (*DFS* + 2)/3, but not less than 3 unless greater than *DFS*. When the counter returns to 0, the soil is refrozen if the average temperature of the previous thirty days is below freezing. As such, the value of the counter also limits the occurrence of a refreeze after a thaw (i.e. the soil is prevented from refreezing immediately following a thaw when the previous 30-day average temperature may not yet have increased to above freezing) (Dozier, 1992).

4.4 SNOW ACCUMULATION AND MELT

Studies have shown that the temperature at which precipitation is equally likely to be rain or snow is in the range of 32 to 36 °F. A delineation temperature of 32 °F is used in the HELP model, that is, when the daily mean temperature is below this value, the program stores precipitation on the surface as snow. Snowmelt is computed using a procedure patterned after portions of the SNOW-17 routine of the National Weather

Service River Forecast System (NWSRFS) Snow Accumulation and Ablation Model (Anderson, 1973). Using this approach, the melt process is divided into that which occurs during nonrain periods and that occurring during rainfall. Rain-on-snow melt is computed using an energy balance approach. To compute the nonrain melt, air temperature is used as an index to energy exchange across the snow-air interface. This is similar to the degree-day method of the Soil Conservation Service (used in Version 2), which uses air temperature as an index to snow cover outflow. The SNOW-17 model uses SI units in all calculations; therefore, the results are converted to English units for compatibility with other HELP routines.

4.4.1 Nonrain Snowmelt

The nonrain snowmelt equation of the SNOW-17 model is computed using the following equation (Knisel, 1980):

$$M_i = \frac{1}{25.4} \left[MF_i \left(T_{c_i} - MBASE \right) - \Delta S_i - F_{m_i} \right] \tag{38}$$

where

M_i = surface melt discharged from the snow cover on day i, inches

MF_i = melt factor for day i, millimeters per °C

T_{c_i} = mean air temperature on day i, °C

$MBASE$ = base temperature below which no melt is produced, 0 °C

ΔS_i = change in storage of liquid water in the snow cover on day i, millimeters

F_{m_i} = portion of the surface melt refrozen during day i, millimeters

In the absence of rain,

$$O_i = M_i \tag{39}$$

where

O_i = outflow from snow cover on day i available for evaporation, runoff, and infiltration, inches

Unlike in version 2, the melt factor, MF, is not constant but varies seasonally due, in large part, to the seasonal variation in solar radiation. In most areas, the variation in the melt factor can be represented by a sine function and is expressed as:

$$MF_i = \left(\frac{MFMAX + MFMIN}{2} \right) + \left[\left(\frac{MFMAX - MFMIN}{2} \right) \sin\left(\frac{2\pi n_i}{366} \right) \right] \quad (40)$$

where

$MFMAX$ = the maximum melt factor, millimeters per day per °C.

$MFMIN$ = the minimum melt factor, millimeters per day per °C.

n_i = number of days since March 21 in northern hemisphere, or since September 21 in southern hemisphere

The maximum melt factor used in Version 3 is 5.2 mm/day-°C and is assumed to occur on June 21 in the northern hemisphere and on December 21 in the southern hemisphere. The minimum melt factor occurs on the reverse of the dates, and its value is 2.0 mm/day-°C. These melt factors are for open areas (Anderson, 1973). At latitudes greater than 50 degrees, the seasonal variation of the melt factor becomes less sinusoidal. Research has shown that at latitudes near 60 degrees the melt factor actually stays at its minimum value for most of the snow season. Therefore, for sites at latitudes above 50 degrees, an adjustment is made to MF_i to represent this gradually "flattening out" of the melt factor during the prolonged winter (Dozier, 1992).

4.4.2 Rain-on-Snow Melt Condition

The rain-on-snow equation is an energy balance equation that makes use of the following assumptions:

1) solar (short-wave) radiation is neglected due to assumed overcast conditions.

2) the incoming long-wave radiation is equal to blackbody radiation at the temperature of the bottom of the cloud cover (assumed to be the mean air temperature).

3) a relative humidity of 90% is assumed.

The daily outflow from a snow cover available for runoff, infiltration and evaporation during a rain-on-snow occurrence may be calculated as the sum of the melt by based on air temperature, latent heat energy transfer based on vapor pressure differences, sensible heat transfer based on air temperature, and advected heat transfer from the mass of rain, less the surface melt that is refrozen by the cold snow cover or stored in the snow cover as a liquid. Taking these assumptions into account and assuming typical values for barometric pressure and wind function, the four energy transfer components and outflow from the snow cover are computed as follows:

$$O_i = \frac{1}{25.4}\left(\frac{Q_{n_i} + Q_{e_i} + Q_{h_i} + Q_{m_i}}{L_f} - F_{m_i} - \Delta S_i\right) \tag{41}$$

where

O_i = outflow from snow cover on day i available for evaporation, runoff, and infiltration, inches

Q_{n_i} = net long-wave radiation transfer on day i, langleys

Q_{e_i} = latent heat energy transfer based on vapor pressure differences, langleys

Q_{h_i} = latent heat energy transfer based on temperature differences, langleys

Q_{m_i} = advected heat transfer from the mass of rain, langleys

L_f = latent heat of fusion for water, 7.97 langleys/millimeters

F_{m_i} = quantity of melt refrozen in snow cover on day i, millimeters

ΔS_f = change in liquid storage in snow cover on day i, millimeters

25.4 = conversion from millimeters to inches

and

$$Q_{n_i} = 1.171 \times 10^{-7}\left[(T_{c_i} + 273)^4 - (T_s + 273)^4\right] \tag{42}$$

$$Q_{e_i} = L_s\,(e_a - e_s)\,f(u) \tag{43}$$

$$Q_{h_i} = L_s\,\gamma\,(T_{c_i} - T_s)\,f(u) \tag{44}$$

$$Q_{m_i} = c\,ROS_i\,T_{c_i} \tag{45}$$

$$f(u) = 0.262 + (0.0391\,u) \tag{46}$$

$$e_{a_i} = 33.8639\,RH\,[(0.00738\,T_{c_i} + 0.8072)^8 - (0.000019)\,|1.8\,T_{c_i} + 48| + 0.001316] \tag{47}$$

where

T_{c_i} = mean air temperature on day i, °C

T_s = snow temperature, 0°C

L_s = latent heat of sublimation for snow, 67.7 langleys/millimeters

e_a = vapor pressure of the atmosphere on day i, millibars (Linsley et al., 1982)

e_s = vapor pressure of the snow cover on day i, 6.11 millibars

$f(u)$ = wind function, dimensionless

u = wind speed, in kilometers/hour (average annual wind speed used in model)

γ = psychometric constant, 0.68 millibars/°C

c = specific heat of water, 0.1 langleys/millimeter-°C

ROS_i = rain on snow cover during day i, millimeters

RH = relative humidity, 0.9

In addition to the surface melt due to heat exchange at the snow-air interface, a small amount of daily heat exchange occurs at the snow-soil interface. The soil heat exchange is not considered directly because the model does not include a soil temperature model. Therefore, this exchange is considered indirectly by the use of a constant daily groundmelt when the ground is not predicted to be frozen. This daily groundmelt, GM_i, for typical landfills with biological activity is estimated to be:

$$GM_i = \begin{cases} 0.2 \ inches & Nonfrozen \ soil \ conditions \\ 0 & Frozen \ soil \ conditions \end{cases} \quad (48)$$

All groundmelt is assumed to infiltrate and is not subject to runoff or evaporation prior to infiltration. The groundmelt on day i may be limited by the quantity of snow available (SNO_{i-1} plus snowfall on day i).

4.4.3 Snowmelt Summary

The SNOW-17 routine differs from the degree-day method in that it accounts for refreezing of melt water due to any heat deficit of the cover and also for the retention and transmission of liquid water in and through the cover. The liquid water in excess of that held within the snow cover becomes outflow or runoff from the snow cover. When rain-on-snow occurs, the quantity of rain is added to the surface melt, from which refreeze and retention in the snow cover may also occur. A positive value for ΔS in Equations 38 and 41 indicates the amount of liquid water in storage within the snow

cover has increased. For further explanation concerning the calculation of ΔS and F_m and the attenuation of excess liquid water, the user is referred to the SNOW-17 documentation (Anderson, 1973).

Naturally the amount of snowmelt is limited by the quantity of snow which is present. The order in which the HELP program determines the amount of snowmelt and remaining snow cover is as follows:

1. The amount of snow available for ablation (surface melt or evaporation) on day i, $AVLSNO_i$, is determined, recognizing that surface melt occurs only at mean daily air temperatures above freezing and that groundmelt occurs only when the soil is not frozen:

$$AVLSNO_i = \begin{cases} SNO_{i-1} + PRE_i - GM_i & for\ T_{C_i} < 0°C \\ SNO_{i-1} - GM_i & for\ T_{C_i} \geq 0°C \end{cases} \quad (49)$$

where

SNO_{i-1} = water storage in the snow cover at the end of day i-1, inches

PRE_i = precipitation on day i, inches

2. The surface melt is calculated using Equations 38 or 41, but is limited to the quantity of available snow:

$$O_i = \begin{cases} 0 & for\ T_{F_i} < 32°F \\ O_i\ from\ Equation\ 36 & for\ PRE_i = 0\ and\ T_{F_i} \geq 32°F \\ O_i\ from\ Equation\ 38 & for\ PRE_i > 0\ and\ T_{F_i} \geq 32°F \\ AVLSNO_i & for\ AVLSNO_i < O_i\ (Eq.\ 36\ or\ 38) \end{cases} \quad (50)$$

3. The quantity of snow remaining after considering all the types of melt is what is available for evaporation (See Surface Evaporation section).

4. The amount of water present in the snow cover at the end of day i, SNO_i, is summed as follows:

$$SNO_i = \begin{cases} SNO_{i-1} + PRE_i - GM_i - ESNO_i & for\ T_{C_i} < 0°C \\ SNO_{i-1} + PRE_i - GM_i - O_i - ESNO_i & for\ T_{C_i} \geq 0°C \end{cases} \quad (51)$$

where

$ESNO_i$ = evaporation of snow in excess of surface melt, O_i, on day i, inches

4.5 INTERCEPTION

Initially during a rainfall event, nearly all rainfall striking foliage is intercepted. However, the fraction of the rainfall intercepted decreases rapidly as the storage capacity of the foliage is reached. The limiting interception storage is approached only after considerable rainfall has reached the ground surface. This process is approximated by the equation:

$$INT_i = INT_{max_i} \left[1 - e^{-\left(\frac{R_i}{INT_{max_i}} \right)} \right] \quad (52)$$

where

INT_i = interception of rainfall by vegetation on day i, inches

INT_{max_i} = interception storage capacity of the vegetation on day i, inches

R_i = rainfall on day i (not including rainfall on snow), inches

Although INT_{max} depends upon vegetation type, growth stage, and wind speed, the data of Horton (1919) and others indicate that 0.05 inches is a reasonable estimate of INT_{max} for a good stand of most types of non-woody vegetation. The HELP program relates INT_{max} to the above ground biomass of the vegetation, CV. This empirical relationship is:

$$INT_{max_i} = \begin{cases} 0.05 \left(\frac{CV_i}{14000} \right) & for\ CV_i < 14000 \\ 0.05 & for\ CV_i \geq 14000 \end{cases} \quad (53)$$

where CV_i is the above ground biomass on day i in kilograms per hectare.

4.6 POTENTIAL EVAPOTRANSPIRATION

The method used in the HELP program for computing evapotranspiration was patterned after the approach recommended by Ritchie (1972). This method uses the concept of potential evapotranspiration as the basis for prediction of the surface and soil water evaporation and the plant transpiration components. The term "potential evapotranspiration" refers to the maximum quantity of evaporation rate that the atmosphere may extract from a plot in a day. A modified Penman (1963) equation is used to calculate the energy available for evapotranspiration.

$$LE_i = PENR_i + PENA_i \tag{54}$$

where

LE_i = energy available on day i for potential evapotranspiration in the absence of a snow cover, langleys

$PENR_i$ = radiative component of the Penman equation on day i, langleys

$PENA_i$ = aerodynamic component of the Penman equation on day i, langleys

The first term of Equation 54 represents that portion of the available evaporative energy due to the radiation exchange between the sun and the earth. The second term expresses the influence of humidity and wind on *LE*. These two components are evaluated as follows:

$$PENR_i = \frac{\Delta_i}{(\Delta_i + \gamma)} R_{n_i} \tag{55}$$

$$PENA_i = \frac{15.36\ \gamma}{(\Delta_i + \gamma)} (1 + 0.1488\ u)(e_{o_i} - e_{a_i}) \tag{56}$$

where

R_{n_i} = net radiation received by the surface on day i, langleys

Δ_i = slope of the saturation vapor pressure curve at mean air temperature on day i, millibars per °C

γ = constant of the wet and dry bulb psychrometer equation, assumed to be constant at 0.68 millibars per °C

u = wind speed at a height of 2 meters, in kilometers/hour (average annual wind speed used in model)

e_{o_i} = saturation vapor pressure at mean air temperature on day i, millibars (computed using Equation 47, where $RH = 1$)

e_{a_i} = mean vapor pressure of the atmosphere on day i, millibars (computed using Equation 47, where RH is the quarterly average dimensionless relative humidity on day i from the input data or on days with precipitation, $RH = 1$)

The value of Δ_i is computed using an equation presented by Jensen (1973):

$$\Delta_i = 1.9993\ [(0.00738\ T_{c_i} + 0.8072)^7 - 0.0005793\ ] \quad (57)$$

where

T_{c_i} = mean air temperature on day i, °C

The net solar radiation received by the earth's surface, R_{n_i}, is the difference between the total incoming and total outgoing radiation and is estimated as follows (Hillel, 1982; Jensen, 1973):

$$R_{n_i} = (1 - \alpha) R_{s_i} - R_{b_i} \quad (58)$$

where

R_{s_i} = incoming global (direct and sky) solar radiation on day i, langleys

α = albedo (reflectivity coefficient of the surface toward short-wave radiation, $\alpha = 0.23$ when there is no snow present; $\alpha = 0.6$ when a snow cover storing more than 5 mm of water exists)

R_{b_i} = the long-wave radiation flux from soil on day i, langleys

R_{b_i} decreases with increasing humidity and cloud cover and is calculated using the following equations (Jensen, 1973):

$$R_{b_i} = R_{bo_i}\left[a_i\left(\frac{R_{s_i}}{R_{so_i}}\right) - b_i\right] \quad (59)$$

where

R_{bo_i} = the maximum outgoing long-wave radiation (assuming a clear day) for day i

R_{so_i} = the maximum potential global solar radiation for day i

a_i *and* b_i = coefficients which are dependent upon the humidity on day i

(for $RH_i < 50\%$, $a_i = 1.2$, $b_i = 0.2$;

for $50\% \leq RH_i < 75\%$, $a_i = 1.1$, $b_i = 0.1$; and

for $RH_i \geq 75\%$, $a_i = 1.0$, $b_i = 0.0$)

The outgoing long-wave radiation (heat loss) on a clear day, R_{bo}, is estimated as follows:

$$R_{bo_i} = 1.171 \times 10^{-7} \left(T_{c_i} + 273 \right)^4 \left(0.39 - 0.05 \sqrt{e_{a_i}} \right) \quad (60)$$

The potential solar radiation for a given day, R_{so}, is calculated using a set of equations from the WGEN model (Richardson and Wright, 1984).

$$R_{so_i} = 711.38 \; DD_i \; [(H_i \sin |LAT| \sin SD_i) + (\sin H_i \cos |LAT| \cos SD_i)] \quad (61)$$

where

LAT = latitude of the location, radians

DD_i = $1 + \{0.0335 \sin [0.0172 \; (J_i + 88.2)]\}$

SD_i = $0.4102 \sin [0.0172 \; (J_i - 80.25)]$

H_i = arc cosine $[(- \tan |LAT|) (\tan SD_i)]$

J_i = the Julian date for day i in northern hemisphere and the Julian date minus 182.5 in the southern hemisphere (negative latitudes)

The potential evapotranspiration is determined by dividing the available energy, LE, by the latent heat of vaporization, L_v (or the latent heat of fusion, L_f, depending on the state of the evaporated water). The latent heat of vaporization is a function of the water temperature. In the HELP model, unless the evaporated water is snow or snowmelt, the mean daily temperature is used to estimate the water temperature and potential evapotranspiration is computed as:

where

E_{o_i} = potential evapotranspiration on day i, in inches

$$E_{o_i} = \frac{LE_i}{25.4\ L_v} \tag{62}$$

$$L_v = \begin{cases} 59.7 - 0.0564\ T_{c_i} & for\ water \\ 67.67 - 0.0564\ T_s & for\ snow \end{cases} \tag{63}$$

L_v = latent heat of vaporization (for evaporating water) or latent heat of fusion (for evaporating snow), langleys per millimeters

T_s = snow temperature, °C

25.4 = conversion from millimeters to inches

4.7 SURFACE EVAPORATION

4.7.1 No Snow Cover

The rate of evapotranspiration from a landfill cover is a function of solar radiation, temperature, humidity, vegetation type and growth stage, water retained on the surface, soil water content and other soil characteristics. Evapotranspiration has three components: evaporation of water or snow retained on foliage or on the landfill surface, evaporation from the soil and transpiration by plants. In the HELP program, the evapotranspiration demand is exerted first on water available at the landfill surface. This available surface water may be either rainfall intercepted by vegetation, ponded water, snowmelt or accumulated snow.

If there is no snow ($SNO_{i-1} = 0$) on the surface at the start of the day and no snowfall ($PRE_i = 0$ and $T_{c_i} \leq 0$°C) during the day or if there is no available snow ($AVLSNO_i = 0$) and no outflow from the snow cover ($O_i = 0$) on day i, the potential evapotranspiration (E_{o_i}) is applied to any calculated interception (INT_i) from rainfall for that day and, partially, to the ponded water. In this situation, the portion of the evaporative demand that is met by the evaporation of surface moisture on day i is given by

$$ESS_i = \begin{cases} E_{o_i} & for\ E_{o_i} \leq INT_i + PW_i(1 - PRF) \\ INT_i + PW_i(1 - PRF) & for\ E_{o_i} > INT_i + PW_i(1 - PRF) \end{cases} \tag{64}$$

where

ESS_i = evaporation of surface moisture, inches

PW_i = water ponded on surface that is unable to run off and is in excess of infiltration capacity, inches

PRF = fraction of area where runoff can potentially occur

If the evaporative demand is less than the calculated interception, the amount of interception is adjusted to equal the evaporative potential.

$$INT_i = E_{o_i} \qquad for\ E_{o_i} < INT_i\ from\ Equation\ 49 \tag{65}$$

4.7.2 Snow Cover Present

If snow is present on the ground after calculating the melt for the day, the program computes an estimated dew-point temperature based on the mean daily temperature for the day, T_{c_i}, and the quarterly average humidity, RH_i, or the existence of precipitation; the dew-point temperature is assumed to equal to the mean daily temperature if precipitation occurred (assumes $RH_i = 1$ if $PRE_i > 0$). If the estimated dew-point temperature is greater than or equal to the temperature of the snow cover, T_s, then the evapotranspiration (evaporation of surface moisture, evaporation of soil moisture, and plant transpiration) is assigned to be zero.

$$ESS_i = 0 \qquad for\ AVLSNO_i - O_i > 0\ \ and\ \ T_{d_i} \geq T_s \tag{66}$$

$$T_{d_i} = (112 - 0.9\ T_{c_i})\ RH_i^{1/8} + 0.1\ T_{c_i} - 112 \tag{67}$$

where T_{d_i} is the estimated dew-point temperature in °C for day i.

If a snow cover existed at the start of the day after discounting the groundmelt ($AVLSNO_i > 0$) and the estimated dew point is lower than the snow temperature, then evaporation of the surface melt available for outflow, O_i, from the snow cover is computed. If the potential evapotranspiration, E_{o_i}, exceeds the surface melt, then the excess evaporative demand is exerted on the snow cover. When evaporating snow or snowmelt, the estimation of the latent heat of vaporization, L_v, by Equation 63 is modified. The temperature of the water is estimated to be 0 °C instead of the mean daily air temperature, T_{c_i}. Therefore, L_v equals 59.7 langleys per millimeter of snowmelt and 67.67 langleys per millimeter of snow water.

Under the conditions just described ($AVLSNO_i > 0$ and $T_{d_i} < T_s$), the daily surface evaporation may consist of a portion of the available melt, O_i; all of the melt and a portion of the snow, SNO_{i-1}; or all of the melt and all of the snow. The following

procedure is then used for calculating surface evaporation:

1. For $O_i > 0$, the potential evaporative energy, LE_i, is reduced by the estimated amount of energy consumed by melting the snow. This lower potential is then exerted on the surface melt outflow. The portion of the surface melt that is evaporated is calculated as:

$$LE'_i = LE_i - 202.4\, O_i \tag{68}$$

$$EMELT_i = \begin{cases} 0 & for\ \ LE'_i \le 0 \\ \dfrac{LE'_i}{25.4\, L_v} & for\ \ 0 < LE'_i < 25.4\, L_v\, O_i \\ O_i & for\ \ LE'_i \ge 25.4\, L_v\, O_i \end{cases} \tag{69}$$

where

$EMELT_i$ = surface melt that is evaporated on day i, inches

LE'_i = potential evaporative energy discounted for surface melt on day i, langleys

2. After allowing for the energy dissipated by the melting of snow at the surface and any evaporation of the melt, the remaining potential evaporative energy is computed as follows:

$$LE''_i = LE'_i - 25.4\, L_v\, O_i \tag{70}$$

where

LE''_i = potential evaporative energy discounted for surface melt and evaporation of surface melt on day i, langleys

3. If there is energy available after any evaporation of surface melt ($LE''_i > 0$), this remaining energy is applied to the snow cover. The amount of evaporated snow, $ESNO_i$, on day i is calculated as follows:

4. The total amount of evaporation of surface moisture, ESS_i, on day i is then calculated as the sum of the evaporated snow and evaporated outflow from the snow cover:

$$ESNO_i = \begin{cases} 0 & for \;\; LE''_i \le 0 \\ \dfrac{LE''_i}{25.4\, L_v} & for \;\; 0 < LE''_i < 25.4\, L_v\, (AVLSNO_i - O_i) \\ AVLSNO_i - O_i & for \;\; LE''_i \ge 25.4\, L_v\, (AVLSNO_i - O_i) \end{cases} \quad (71)$$

$$ESS_i = ESNO_i + EMELT_i \quad (72)$$

where *ESS*, *ESNO*, and *EMELT* are water equivalent in inches.

4.7.3 Remaining Evaporative Demand

The amount of energy remaining available to be applied to subsurface evapotranspiration (i.e., soil water evaporation and plant transpiration) is then the original potential evaporative energy less the energy dissipated in the melt of snow and evaporation of surface water. If snow was available for surface melt or evaporation ($AVLSNO_i > 0$), the remaining energy for subsurface evapotranspiration is:

$$LE_{s_i} = LE_i - 25.4\, (L_f\, O_i + L_v\, EMELT_i + L_v\, ESNO_i) \quad (73)$$

In the absence of a snow cover or snowfall ($AVLSNO_i = 0$), the remaining energy for subsurface evapotranspiration is:

$$LE_{s_i} = LE_i - 25.4\, L_v\, ESS_i \quad (74)$$

where LE_{s_i} is the energy available for potential evapotranspiration of soil water.

The potential evapotranspiration from the soil column in inches is a function of the energy available and the mean air temperature. The potential evapotranspiration from the soil is:

$$ETS_{o_i} = \frac{LE_{s_i}}{25.4\, L_v} \quad (75)$$

where ETS_{o_i} is the potential evapotranspiration of soil water.

4.8 INFILTRATION

In the absence of a snow cover ($AVLSNO_i$ = 0), the infiltration is equal to the sum of rainfall (precipitation at temperatures > 0°C) and groundmelt less the sum of interception (evaporation of surface moisture) and runoff.

$$INF_i = PRE_i + GM_i - INT_i - Q_i \tag{76}$$

In the presence of a snow cover, the infiltration is equal to the sum of outflow from the snow cover and groundmelt less the sum of evaporation of the outflow from the snow cover and runoff.

$$INF_i = O_i + GM_i - EMELT_i - Q_i \tag{77}$$

where INF_i is the infiltration on day i in inches.

Since the runoff is computed using the total rainfall in Equation 21, it is possible for the sum of the runoff and interception to exceed rainfall. Therefore, when the sum of the runoff, Q_i, and interception, INT_i, exceeds the rainfall, PRE_i, the computed runoff is reduced by the excess and the infiltration is assigned the value of the groundmelt, GM_i. It is not possible for the sum of runoff and evaporation of the outflow from the snow cover to exceed the outflow from the snow cover because the evaporation of melt is subtracted from the outflow prior to computation of runoff by Equation 21.

4.9 SOIL WATER EVAPORATION

When the soil is not frozen, any demand in excess of the available surface water is exerted on the soil column first through evaporation of soil water and then through plant transpiration. When the soil is considered frozen, the program assumes that no soil water evaporation or plant transpiration occurs.

The potential soil evaporation is estimated from the following equation based on the work of Penman (1963) when evaporation is not limited by the rate at which water can be transmitted to the surface:

$$ES_{o_i} = \frac{(PENR_i + K_{E_i} PENA_i)\, e^{(-0.000029\, CV_i)}}{25.4\ (59.7 - 0.0564\, T_{c_i})} \tag{78}$$

where

ES_{o_i} = potential evaporation of soil water on day i, inches

$PENR_i$ = radiative component of the Penman equation on day i, langleys

$PENA_i$ = aerodynamic component of the Penman equation on day i, langleys

CV_i = above ground biomass on day i, kg/ha

T_{c_i} = mean air temperature on day i, °C

K_{E_i} = fraction of aerodynamic component contributing to evaporation of soil water

= 1 - 0.0000714 CV_i, but not less than 0

This equation assumes that an above ground biomass of 14,000 kg/ha or more defines a full cover canopy such that the effect of the wind and humidity term, PENA, is negligible in the potential soil evaporation equation.

As patterned after Ritchie (1972), evaporation of soil water occurs in two stages. Stage 1 evaporation demand is controlled only by the available energy, while stage 2 evaporation demand is limited by the rate at which water can be transmitted through the soil to the surface. In stage 1, the rate of evaporation is equal to the potential evaporation from the soil:

$$ES1_i = ES_{o_i} \tag{79}$$

where $ES1_i$ is the stage 1 soil water evaporation rate on day i in inches.

Stage 1 soil water evaporation will continue to occur as long as the cumulative value of the soil water evaporation minus the infiltration is less than the upper limit for stage 1 evaporation. This limit represents the quantity of water that can be readily transmitted to the surface. Cumulative soil water depletion by soil water evaporation is computed as:

$$ES1T_i = \sum_{k=m}^{i} (ES_k - INF_k) \tag{80}$$

where

$ES1T_i$ = cumulative soil water depletion on day i by soil water evaporation, inches

ES_k = soil water evaporation on day k (computed by Equation 90), inches

m = the last day when $ES1T$ was equal to 0

The upper limit of stage 1 evaporation is (Knisel, 1980):

where

U = upper limit of stage 1 evaporation, inches

$$U = \frac{9}{25.4} (CON - 3)^{0.42} \quad (81)$$

CON = evaporation coefficient (Equation 9), millimeters per day$^{0.5}$

When $ES1T_i$ is greater than U, stage 1 evaporation ceases and stage 2 evaporation begins. The following equation is used to compute the stage 2 evaporation rate Ritchie (1972).

$$ES2_i = \frac{1}{25.4} CON [t_i^{0.5} - (t_i - 1)^{0.5}] \quad (82)$$

where

$ES2_i$ = stage 2 soil water evaporation rate for day i, inches

t_i = number of days since stage 1 evaporation ended

Since the daily total of surface and soil water evaporation cannot exceed the daily potential evaporative demand, the evaporation from the soil is limited by the amount of energy available after considering the evaporation of surface water, LE_{s_i}, (i.e., the actual evaporative demand from the soil on day i, ESD_i, cannot exceed the potential evapotranspiration of soil water, ETS_{o_i}). The following equation is used to determine the daily soil water evaporative demand:

$$ESD_i = \begin{cases} ES1_i & for\ ES1T_i < U\ \ and\ \ ES1_i \le ETS_{o_i} \\ ES2_i & for\ ES1T_i \ge U\ \ and\ \ ES2_i \le ETS_{o_i} \\ ETS_{o_i} & for\ ES1T_i < U\ \ and\ \ ES1_i > ETS_{o_i} \\ ETS_{o_i} & for\ ES1T_i \ge U\ \ and\ \ ES2_i > ETS_{o_i} \end{cases} \quad (83)$$

The soil water evaporative demand is then distributed to the soils near the surface, down to a maximum depth for soil water evaporation but not exceeding the evaporative zone depth. The maximum depth is a function of the capillarity of the material, increasing with smaller pore size. Pore size is related to the saturated hydraulic conductivity of a soil. Therefore, the following correlation was developed to estimate the maximum depth of soil water evaporation based on empirical observations:

where

$$SEDMX = 4.6068 \times 1.5952^{-\log_{10} K} \tag{84}$$

K = saturated hydraulic conductivity in the evaporative zone, cm/sec

$SEDMX$ = estimated maximum depth of soil water evaporation, inches

Limits are placed on the depth of soil water evaporation as follows to confine the capillary rise to the zone where a significant upward moisture flux is likely to occur (in top 18 inches for sands and in the top 48 inches for clays):

$$SED = \begin{cases} EZD & for\ EZD \le SEDMX\ and\ EZD \le 48 \\ 48 & for\ EZD \le SEDMX\ and\ EZD > 48 \\ SEDMX & for\ EZD > SEDMX\ and\ 18 \le SEDMX \le 48 \\ 18 & for\ EZD > SEDMX\ and\ SEDMX < 18 \\ 48 & for\ EZD > SEDMX\ and\ SEDMX > 48 \end{cases} \tag{85}$$

where

SED = depth of soil water evaporation, inches

EZD = evaporative zone depth, inches

The soil water evaporation demand is distributed throughout the seven segments in the soil water evaporative depth, *SED*, by the following equation (Knisel, 1980):

$$ESD_i(j) = ESD_i \cdot W(j) \tag{86}$$

where

$ESD_i(j)$ = soil water evaporative demand on segment j on day i, inches

$W(j)$ = weighting factor for segment j, for j = 1 to 7

$$W(j) = 1.0159 \left[e^{-4.16 \frac{D_{j-1}}{SED}} - e^{-4.16 \frac{D_j}{SED}} \right] \qquad for\ D \le SED \tag{87}$$

where

D_j = depth to bottom of segment j, inches; if *D* is greater than *SED*, then *SED* is substituted for *D* in Equation 87

4.10 PLANT TRANSPIRATION

The potential plant transpiration, EP_o, is computed as follows when the mean daily temperature is above 32 °F and the soil is not frozen:

$$EP_{o_i} = \frac{LAI_i}{3} E_{o_i} \tag{88}$$

The actual plant transpiration demand equals the potential plant transpiration except when the daily total of the soil water evaporative demand and potential plant transpiration demand exceeds the potential evapotranspirative demand on the soil water for the day:

$$EPD_i = \begin{cases} EP_{o_i} & for\ EP_{o_i} + ES_i \leq ETS_{o_i} \\ ETS_{o_i} - ES_i & for\ EP_{o_i} + ES_i > ETS_{o_i} \end{cases} \tag{89}$$

where EPD_i is the actual plant transpiration demand in inches on day i.

The plant transpiration demand is distributed throughout the seven segments in the evaporative zone, *EZD*, by the following equation (Knisel, 1980):

$$EPD_i(j) = EPD_i \cdot W(j) \tag{90}$$

where

$EPD_i(j)$ = soil water evaporative demand on segment j on day i, inches

$W(j)$ = weighting factor for segment j, for j = 1 to 7

$$W_j = 1.0159 \left[e^{-4.16 \frac{D_{j-1}}{EZD}} - e^{-4.16 \frac{D_j}{EZD}} \right] \qquad for\ j = 1\ to\ 7 \tag{91}$$

where

D_j = depth to bottom of segment j, inches

4.11 EVAPOTRANSPIRATION

The actual subsurface evapotranspiration on day i, ETS_i, is often less than the sum of the soil water evaporative demand on day i, ESD_i, and the plant transpiration demand on day i, EPD_i, due to a shortage of soil water. The segment demands are then exerted on the soil profile from the surface down. If there is inadequate water storage above the wilting point in the segment to meet the demand, the soil water evapotranspiration from the segment is limited to that storage and the excess (unsatisfied) demand is added to the demand on the next lower segment within the evaporative zone.

The soil water evaporation demand is exerted first from the surface down. The actual soil water evaporation from a segment is equal to the demand, $ESD_i(j)$, plus any excess demand, $ESX(j)$, but not greater than the available water, SM_j - WP_j. The soil water evaporation is

$$ES_i(j) = \begin{cases} ESD_i(j) + ESX(j) & for \quad ESD_i + ESX(j) \le SM(j) - WP(j) \\ SM(j) - WP(j) & for \quad ESD_i + ESX(j) > SM(j) - WP(j) \end{cases} \tag{92}$$

$$ESX(j+1) = ESD_i(j) + ESX(j) - ES_i(j) \tag{93}$$

where

$ES_i(j)$ = soil water evaporation from segment j on day i, inches

The plant transpiration demand is exerted next from the surface down. The actual transpiration from a segment is equal to the demand, $EPD_i(j)$, plus any excess demand, $EPX(j)$, but not greater than the available water, $AW_i(j)$, after extracting the soil water evaporation. The plant transpiration from a segment is also limited to one quarter of the plant available water capacity plus the available drainable water.

$$EP_i(j) = \begin{cases} EPD_i(j) + EPX(j) & for \quad EPD_i(j) + EPX(j) \le AW_i(j) \\ & \quad \& \quad EPD_i(j) + EPX(j) \le EPL_i(j) \\ AW_i(j) & for \quad EPD_i(j) + EPX(j) > AW_i(j) \\ & \quad \& \quad AW_i(j) \le EPL_i(j) \\ EPL_i(j) & for \quad EPD_i(j) + EPX(j) > AW_i(j) \\ & \quad \& \quad AW_i(j) > EPL_i(j) \end{cases} \tag{94}$$

$$EPX(j+1) = EPD_i(j) + EPX(j) - EP_i(j) \tag{95}$$

$$AW_i(j) = SM_i(j) - [ES_i(j) + WP(j)] \tag{96}$$

$$EPL_i(j) = \begin{cases} 0.25\,[FC(j) - WP(j)] & for\ SM_i(j) - ES_i(j) < FC(j) \\ else & \\ SM_i(j) - [ES_i(j) + FC(j)] + 0.25\,[FC(j) - WP(j)] & \end{cases} \tag{97}$$

where

$EP_i(j)$ = plant transpiration from segment j on day i, inches

$EPL_i(j)$ = plant transpiration limit from segment j on day i, inches

$WP(j)$ = wilting point of segment j, inches

$FC(j)$ = field capacity of segment j, inches

The actual evapotranspiration from segment j on day i, $ET_i(j)$, is the sum of the soil water evaporation and the plant transpiration.

$$ET_i(j) = ES_i(j) + EP_i(j) \tag{98}$$

The water extraction profile agrees very well with profiles for permanent grasses measured by Saxton et al. (1971).

The total subsurface evapotranspiration on day i, ETS_i, is the sum of the evapotranspiration from the top seven segments, the evaporative zone.

$$ETS_i = \sum_{j=1}^{7} ET(j) \tag{99}$$

The total evapotranspiration on day i, ET_i, is the sum of the subsurface evapotranspiration and the surface evaporation.

$$ET_i = ETS_i + ESS_i \tag{100}$$

4.12 VEGETATIVE GROWTH

The HELP program accounts for seasonal variation in leaf area index through a general vegetative growth model. This model was extracted from the SWRRB program (Simulator for Water Resources in Rural Basins) developed by the USDA Agricultural Research Service (Arnold et al., 1989). The vegetative growth model computes daily values of total and active above ground biomass based on the maximum leaf area index value input by the user, daily temperature and solar radiation data, mean monthly temperatures and the beginning and ending dates of the growing season. The maximum value of leaf area index depends on the type of vegetation and the quality of the vegetative stand. The program supplies typical values for selected covers; these range from 0 for bare ground to 5.0 for an excellent stand of grass. The default weather data files contain normal mean monthly temperatures and beginning and ending dates of the growing season for 183 locations in the United States.

The vegetative growth model assumes that the vegetative species are perennial and that the vegetation is not harvested. Phenological development of the vegetation is based on the cumulative heat units during the growing season. Vegetative growth starts at the beginning of the growing season and continues during the first 75 percent of the growing season. Growth occurs only when the daily temperature is above the base temperature, assumed to be 0 °C for winter tolerant crops and mixtures of perennial grasses. The heat units for a day is computed as follows.

$$HU_i = T_{c_i} - T_b \tag{101}$$

where

HU_i = heat units on day i, °C-days

T_b = base temperature for plants, 5 °C

The fraction of the growing season that has occurred by day i is equal to the heat unit index on day i. It is computed as follows.

$$HUI_i = \sum_{k=m}^{i} \frac{HU_k}{PHU} \qquad for\ m \le i \le n,\ else\ HUI_i = 0 \tag{102}$$

$$PHU = \sum_{k=m}^{n} HU_k \tag{103}$$

where

HUI_i = heat unit index or fraction of the growing season on day i, dimensionless

PHU = potential heat units in normal growing season, °C-days

m = Julian date of start of growing season

n = Julian date of end of growing season

The daily mean temperature is assumed to vary harmonically as follows for computing *PHU*:

$$T_{c_k} = \overline{TM} + 0.5\,(TM_{\max} - TM_{\min}) \cos\left(2\pi\,\frac{k - 200}{365}\right) \qquad (104)$$

where

T_{c_k} = estimate of normal mean daily temperature on day k, °C

$\overline{TM}$ = mean of the 12 normal mean monthly temperatures, °C

TM_{max} = maximum of the 12 normal mean monthly temperatures, °C

TM_{min} = minimum of the 12 normal mean monthly temperatures, °C

The potential increase in biomass for a day is a function of the interception of radiation energy. The photosynthetic active radiation is estimated as follows.

$$PAR_i = 0.02092\ R_{s_i} \left\{1 - \exp[-0.65\,(LAI_{i-1} + 0.05)]\right\} \qquad (105)$$

where

PAR_i = photosynthetic active radiation, MJ/m^2

R_{s_i} = global solar radiation, langleys

LAI_{i-1} = leaf area index of active biomass at end of day i-1, dimensionless

The leaf area index on day i, LAI_i, is given by the equation

$$LAI_i = \begin{cases} 0 & HUI_i = 0 \\ \dfrac{(LAI_{mx})\ (WLV_i)}{WLV_i + 13360\,exp\,(-0.000608\ WLV_i)} & 0 < HUI_i \le 0.75 \\ 16\,(LAI_{0.75})\,(1 - HUI_i)^2 & HUI_i > 0.75 \end{cases} \qquad (106)$$

where

LAI_{mx} = maximum leaf area index from input, dimensionless

WLV_i = active above-ground biomass on day i, kg/ha

LAI_d = LAI value on day d, (# is the day when vegetation starts declining as estimated as the day when HUI_i = 0.75), dimensionless

The potential increase in biomass during the growing season is

$$DDM_{o_i} = BE \cdot PAR_i \tag{107}$$

where

DDM_{o_i} = potential increase in total biomass on day i, kg/ha

BE = conversion from energy to biomass, 35 kg m^2/ha MJ

The actual increase in biomass may be regulated by water or temperature stress.

$$DDM_i = REG_i \cdot DDM_{o_i} \tag{108}$$

$$REG_i = \min(WS_i, TS_i) \tag{109}$$

where

DDM_i = actual daily increase in total biomass (dry matter) on day i during first 75% of growing season, kg/ha

REG = minimum stress factor for growth regulation (smaller of water stress factor, WS_i, and temperature stress factors, TS_i), dimensionless

The water stress factor, WS_i, is the ratio of the actual transpiration to plant transpiration demand.

$$WS_i = \frac{\sum_{j=1}^{7} EP_i(j)}{\sum_{j=1}^{7} EPD_i(j)} \tag{110}$$

The temperature stress factor, TS_i, is given by the equation

$$TS_i = \begin{cases} 0 & for\ T_{c_i} \le Tb \\ exp\left[\delta\left(\dfrac{To - T_{c_i}}{T_{c_i} - Tb}\right)^2\right] & for\ Tb < T_{c_i} < To \\ exp\left[\delta\left(\dfrac{To - T_{c_i}}{2\,To - (Tb + T_{c_i})}\right)^2\right] & for\ T_{c_i} \ge To \end{cases} \quad (111)$$

$$\delta = \frac{\ln(0.9)}{\left\{\dfrac{To - [(To + Tb)/2]}{(To + Tb)/2}\right\}^2} \quad (112)$$

where

Tb = base temperature for mixture of perennial winter and summer grasses, 5 °C

To = optimal temperature for mixture of perennial winter and summer grasses, 25 °C

As an additional constraint, the temperature stress factor is set equal to zero (and therefore growth ceases) when the daily mean temperature is more than 10 °C below the average annual temperature.

$$TS_i = 0 \qquad when\ T_{c_i} < (\overline{TM} - 10\,^\circ C) \quad (113)$$

The active live biomass is

$$DM_i = \begin{cases} 0 & for\ HUI_i = 0 \\ \sum_{k=m}^{i} DDM_i & for\ 0 < HUI_i \le 0.75 \\ 8\,DM_d\,(1 - HUI_i)^2 & for\ HUI_i > 0.75 \end{cases} \quad (114)$$

where

DM_i = total active live biomass (dry matter) on day i, kg/ha

DM_d = total active live biomass (dry matter) on day d (when HUI_i = 0.75), kg/ha

The root mass fraction of the total active biomass is a function of the heat unit index where the fraction is greatest at the start of the growing season and decreases throughout the season.

$$RF_i = (0.4 - 0.2\ HUI_i) \tag{115}$$

where

RF_i = fraction of total active biomass partitioned to root system on day i, dimensionless

The above ground photosynthetic active biomass is computed as follows:

$$WLV_i = DM_i\ (1.0 - RF_i) \tag{116}$$

where

WLV_i = active above-ground biomass on day i, kg/ha

The program also accounts for plant residue (inactive biomass) in addition to active biomass because inactive biomass also provides shading of the surface and reduces evaporation of soil water. Plant residue is predicted to decay throughout the year as a function of temperature and soil moisture. Plant residue is formed as the active plants go into decline and at the end of the growing season. The decrease in active biomass during the last quarter of the growing season is added to the plant residue. Similarly, at the end of the growing season the active biomass is also added to the plant residue or photosynthetic inactive biomass.

$$RSD_i = \begin{cases} RSD_{i-1}\ (1.0 - DECR_i) & for\ i \le d\ or\ i > n+1 \\ (RSD_{i-1} + DM_{i-1} - DM_i)\ (1.0 - DECR_i) & for\ d < i \le n \\ (RSD_{i-1} + DM_{i-1})\ (1.0 - DECR_i) & for\ i = n+1 \end{cases} \tag{117}$$

where

RSD_n = plant biomass residue on day i, kg/ha

$DECR_i$ = biomass residue decay rate on day i, dimensionless

The plant residue decay rate decreases with moisture contents below field capacity in the evaporative zone, becoming zero at the wilting point. Similarly, the decay rate decreases as the soil temperature at the bottom of the evaporative zone falls below 35 °C and becomes very slow at temperatures below 10 °C, approaching a rate of 0.005. The maximum rate is 0.05. The decay rate is

$$DECR_i = 0.05\ [\min(CDG_i,\ SUT_i)] \tag{118}$$

where

SUT_i = soil moisture factor on plant residue decay, dimensionless

CDG_i = soil temperature factor on plant residue decay, dimensionless

The soil moisture factor on plant residue decay is computed as follows:

$$SUT_i = \begin{cases} 1.0 & for \sum_{j=1}^{7} SM_i(j) \geq \sum_{j=1}^{7} FC(j) \\ \dfrac{\sum_{j=1}^{7} [\,SM_i(j) - WP(j)\,]}{\sum_{j=1}^{7} [\,FC(j) - WP(j)\,]} & for \sum_{j=1}^{7} SM_i(j) < \sum_{j=1}^{7} FC(j) \end{cases} \tag{119}$$

The soil temperature factor on plant residue decay is computed as follows:

$$CDG_i = 0.1 + \frac{0.9\ ST_i(7)}{ST_i(7) + \exp[\,9.93 - 0.312\ ST_i(7)\,]} \tag{120}$$

where

$TS_i(7)$ = soil temperature at bottom of evaporative zone (segment 7), °C

The soil temperature is computed in the manner presented in the SWRRB model (Arnold et al., 1989). The long-term average surface soil temperature is the same as the long-term average air temperature. Changes in temperatures below the surface are dampened by the depth below the surface. The average annual soil temperature is constant throughout the depth, but the difference between the maximum soil temperature and the minimum soil temperature in a year decreases with increasing depth. In addition, the change in the surface soil temperature from day to day is reduced by total above ground biomass (active and inactive) and snow cover.

The total above ground biomass is the sum of the above ground active biomass and the plant residue. This total is used to compute soil temperature for plant decay rate, evaporation of soil water, and interception.

$$CV_i = WLV_i + RSD_i \tag{121}$$

where

CV_i = total above ground biomass on day i, kg/ha

When the normal daily mean temperature is greater than 10 °C all year round, the model assumes that grasses can grow all year. As such, there is no longer a winter dormant period when the active biomass decreases to zero. Therefore, the model assumes that biomass also decays all year in proportion to the quantity of biomass present. Assuming that 20 percent of the biomass is in the root system, the above ground active biomass is computed as follows:

$$WLV_i = 0.8\, BE \cdot PAR_i \cdot REG_i + WLV_{i-1} (1.0 - DECR_i) \tag{122}$$

The growth and decay terms are computed the same as given in Equations 105, 107, 109, 116, and 118. The leaf area index is computed using WLV_i from Equation 122 in Equation 106.

4.13 SUBSURFACE WATER ROUTING

The subsurface water routing proceeds one subprofile at a time, from top to bottom. Water is routed downward from one segment to the next using a storage routing procedure, with storage evaluated at the mid-point of each time step. Mid-point routing provides an accurate and efficient simulation of simultaneous incoming and outgoing drainage processes, where the drainage is a function of the average storage during the time step. Mid-point routing tends to produce relatively smooth, gradual changes in flow conditions, avoiding the more abrupt changes that result from applying the full amount of moisture to a segment at the beginning of the time step. The process is smoothed further by using time steps that are shorter than the period of interest.

Mid-point routing is based on the following equation of continuity for a segment:

$$\Delta Storage = Drainage\ In - DrainageOut - Evapotranspiration + Leachate\ Recirculation + Subsurface\ Inflow \tag{123}$$

$$\Delta SM(j) = 0.5 \{ [DR_i(j) + DR_{i-1}(j)] - [DR_i(j+1) + DR_{i-1}(j+1)] - [ET_i(j) + ET_{i-1}(j)] + [RC_i(j) + RC_{i-1}(j)] + [SI_i(j) + SI_{i-1}(j)] \} \quad (124)$$

$$\Delta SM(j) = SM_i(j) - SM_{i-1}(j) \quad (125)$$

where

$\Delta SM(j)$ = change in storage in segment j, inches

$DR_i(j)$ = drainage into segment j from above during time step i, inches

$SM_i(j)$ = soil water storage of segment j at the mid-point of time step i, inches

$ET_i(j)$ = evapotranspiration from segment j during time step i, inches

$RC_i(j)$ = lateral drainage recirculated into segment j during time step i, inches

$SI_i(j)$ = subsurface inflow into segment j during time step i,inches

Note that segments are numbered from top to bottom and therefore the drainage into segment j+1 from above equals the drainage out of segment j through its lower boundary. This routing is applied to all segments except liners and the segment directly above liners. Drainage into the top segment of the top subprofile is equal to the infiltration from the surface; drainage into the top segment of other subprofiles is equal to the leakage through the liner directly above the subprofile. Water is routed for a whole day in a subprofile before routing water in the next subprofile. The leakage from a subprofile for each time step during the day is totalled and then uniformly distributed throughout the day as inflow into the next subprofile.

The only unknown terms in the water routing equation are $SM_i(j)$ and $DR_i(j+1)$; all other terms have been computed previously or assigned during input. Subsurface inflow is specified during input. Infiltration and evapotranspiration are computed for the day before performing subsurface water routing for the day. Leachate recirculation is known from the calculated lateral drainage for the previous day. The drainage into a segment is known from the calculation of drainage out of the previous segment or from the computation of leakage from the previous subprofile. The two unknowns are solved simultaneously using the continuity and unsaturated drainage equations.

The number of time steps in a day can vary from subprofile to subprofile. A minimum of 4 time steps per day and a maximum of 48 time steps per day can be used. The number of time steps for each subprofile is computed as a function of the design of

the lateral drainage layer in the subprofile and the potential impingement into the lateral drainage layer. The time step is sized to insure that the lateral drainage layer, when initially wetted to field capacity, cannot be saturated in a single time step even in the absence of drainage from the layer.

$$\Delta t = \frac{T(k)\,[POR(k) - FC(k)]}{IR_{max}} \tag{126}$$

$$N = \begin{cases} 4 & for\ \Delta t > 0.25\ days \\ int\left(\frac{1}{\Delta t} + 1\right) & for\ 0.021\ days \le \Delta t \le 0.25\ days \\ 48 & for\ \Delta t < 0.021\ days \end{cases} \tag{127}$$

where

Δt = maximum size of time step, days

$T(k)$ = thickness of lateral drainage layer k, inches

$POR(k)$ = porosity of layer k, vol/vol

$FC(k)$ = field capacity of layer k, vol/vol

IR_{max} = maximum impingement rate into lateral drainage layer, inches/day

N = number of time steps per day, dimensionless

The maximum impingement rate is the lowest saturated hydraulic conductivity of the subprofile layers above the liner, but not greater than maximum daily infiltration (estimated to be about 10 inches/day).

Drainage out of the bottom segment above the liner of a subprofile is the sum of lateral drainage, if a lateral drainage layer, and the leakage or percolation from the segment or the liner of the subprofile. Drainage from this segment is also a function of the soil moisture content of the segment. The soil moisture content, lateral drainage and leakage are solved simultaneously using continuity, lateral drainage and percolation/leakage equations.

The water routing routine does not consider the storage capacity of the lower segments when computing the drainage out of a segment. Therefore, the routine may route more water down than the lower segments can hold and drain. Any water in excess of the storage capacity of a segment (porosity) is routed back up the profile into the segment above the saturated segment. In this way, the water contents of segments are corrected by backing water up from the bottom to the top, saturating segments as the corrections are made. If the entire top subprofile becomes saturated or if water is routed

back to the surface, the excess water is added to the runoff for the day. If runoff is restricted, the excess water is ponded on the surface and subjected to evaporation and infiltration during the next time step.

4.14 VERTICAL DRAINAGE

The rate at which water moves through a porous medium as a saturated flow governed by gravity forces is given by Darcy's law:

$$q = K\,i = K\,\frac{dh}{dl} \tag{128}$$

where

q = rate of flow (discharge per unit time per unit area normal to the direction of flow), inches/day

K = hydraulic conductivity, inches/day

i = hydraulic head gradient, dimensionless

h = piezometric head (elevation plus pressure head), inches

l = length in the direction of flow, inches

This equation is also applicable to unsaturated conditions provided that the hydraulic conductivity is considered a function of soil moisture and that the piezometric head includes suction head.

The HELP program assumes pressure head (including suction) to be constant within each segment of vertical percolation and lateral drainage layers. This assumption is reasonable at moisture contents above field capacity (moisture contents where drainage principally occurs). In circumstances where a layer restricts vertical drainage and head builds up on top of the surface of the layer, as with barrier soil liners and some low permeability vertical percolation layers, the program assumes the pressure head is uniformly dissipated in the low permeability segment. For a given time step these assumptions yield a constant head gradient throughout the thickness of the segment. For vertical percolation layers with constant pressure, the piezometric head gradient in the direction of flow is unity, and the rate of flow equals the hydraulic conductivity:

$$i = \frac{dh}{dl} = 1 \tag{129}$$

$$q = K \tag{130}$$

For low permeability vertical percolation layers and soil liners, the hydraulic head gradient is

$$i = \frac{dh}{dl} = \frac{h_w + l}{l} \tag{131}$$

where

h_w = pressure head on top of layer, inches

The unsaturated hydraulic conductivity is estimated by Campbell's equation (Equation 5). Multiplying the water content terms (θ, θ_r and ϕ) in Equation 5 by the segment thickness yields an equivalent equation with the water content terms expressed in terms of length:

$$K = K_s \left(\frac{SM - RS}{UL - RS} \right)^{3 + \frac{2}{\lambda}} \tag{132}$$

Here, *SM*, *RS*, and *UL* represent the soil water content (θ), residual soil water content (θ_r), and saturated soil water content (ϕ) of the segment, each expressed as a depth of water in inches. The HELP program uses Equation 132 to compute unsaturated hydraulic conductivity.

Based on Equations 130 and 132, the drainage from segment j during the time step i, $DR_i(j+1)$, is as follows:

$$DR_i(j+1) = K_s(j) \cdot i \cdot DT \left[\frac{SM_i(j) - RS(j)}{UL(j) - RS(j)} \right]^{3 + \frac{2}{\lambda(j)}} \tag{133}$$

where

$K_s(j)$ = saturated hydraulic conductivity of segment j, inches/day

DT = the time step size, days

= 1 / N

Rearranging Equation 133 to solve for $SM_i(j)$ and substituting it into Equation 124 for $SM_i(j)$ yields the following non-linear equation for the remaining unknown, $DR_i(j+1)$:

$$DR_i(j+1) = -2[UL(j) - RS(j)] \left[\frac{DR_i(j+1)}{K_s(j)\ i\ DT} \right]^{\frac{\lambda_j}{3\lambda_j+2}} + 2[SM_{i-1}(j) - RS(j)] + DR_{i-1}(j) + DR_i(j) - DR_{i-1}(j+1) - ET_{i-1}(j) - ET_i(j) + RC_{i-1}(j) + RC_i(j) + SI_{i-1}(j) + SI_i(j) \quad (134)$$

The HELP program solves this equation for $DR_i(j+1)$ iteratively using $DR_{i-1}(j+1)$ as its initial guess in the right hand side of Equation 134. If the computed value of $DR_i(j+1)$ is within 0.3 percent of the guess or 0.1 percent of the storage capacity of segment j, the computed value is accepted; else, a new guess is made and the process is repeated until the convergence criteria are satisfied. After $DR_i(j+1)$ is computed, the program computes $SM_i(j)$ using Equation 124. Constraints are placed on the solution of $DR_i(j+1)$ and $SM_i(j)$ so as to maintain these parameters within their physical ranges; 0 to $K_s \cdot DT$ for $DR_i(j+1)$, and $WP(j)$ to $UL(j)$ for $SM_i(j)$.

4.15 SOIL LINER PERCOLATION

The rate of percolation through soil liners depend on the thickness of the saturated material directly above it. The depth of this saturated zone is termed the hydraulic (pressure) head on the soil liner. The average head on the liner is a function of the thicknesses of all segments that are saturated directly above the liner and the moisture content of first unsaturated segment above the liner. The average head on the entire surface of the liner is computed using the following equation:

$$h_w(k)_i = \begin{cases} TS(m) \cdot \dfrac{SM_i(m) - FC(m)}{UL(m) - FC(m)} + \displaystyle\sum_{j=m+1}^{n} TS(j) \\ \quad for\ SM_i(m) > FC(m)\ \ else \\ \displaystyle\sum_{j=m+1}^{n} TS(j) \end{cases} \quad (135)$$

where

$h_w(k)_i$ = average hydraulic head on liner k during time step i, inches

$TS(j)$ = thickness of segment j, inches

m = number of the lowest unsaturated segment in subprofile k

n = number of the segment directly above the soil liner in subprofile k

The percolation rate through a liner soil layer is computed using Darcy's law, as given in Equation 128. As presented in Equation 131, the vertical hydraulic gradient through the soil liner, segment n+1, is

$$\frac{dh}{dl} = \frac{h_w(k) + TS(n+1)}{TS(n+1)} \tag{136}$$

The HELP program assumes that soil liner remains saturated at all times. Percolation is predicted to occur only when there is a positive hydraulic head on top of the liner; therefore, the percolation rate through a soil liner is

$$q_P(k)_i = \begin{cases} 0 & for\ h_w(k)_i = 0 \\ K_s(n+1)\,\dfrac{h_w(k)_i + TS(n+1)}{TS(n+1)} & for\ h_w(k)_i > 0 \end{cases} \tag{137}$$

where

$q_P(k)_i$ = percolation rate from subprofile k during time step i, inches/day

4.16 GEOMEMBRANE LINER LEAKAGE

In Version 3 of the HELP program geomembrane liners are identified as individual layers in the landfill profile. The geomembranes can be used alone as a liner or in conjunction with low permeability soil to form a composite liner. The soil would be defined as a soil liner in a separate layer. The program permits the membrane to be above, below or between high, medium or low permeability soils. Leakage is calculated for intact sections of geomembrane and for sections with pinholes or installation defects.

Giroud and Bonaparte (1989) defined composite liners as a low permeability soil liner covered with a geomembrane. However, composite liner design schemes can include various combinations of geomembranes, geotextiles, and soil layers. Therefore, in this section a composite liner is defined to be a liner system composed of one or more geomembranes and a low permeability soil, possibly separated by a geotextile. The HELP program defines a geomembrane as a thin "impervious" sheet of plastic or rubber used as a liquid barrier. Geotextiles are defined as flexible, porous fabrics of synthetic fibers used for cushioning, separation, reinforcement, and filtration.

The geomembrane component of a composite liner virtually eliminates leakage except in the area of defects, punctures, tears, cracks and bad seams. The low permeability soil component increases the breakthrough time and provides physical strength. In contact with a geomembrane the low permeability soil decreases the rate of leakage through the

hole in the geomembrane. As such, the two components of a composite liner complement each other. Geomembrane and soil liners also have complimentary physical and chemical endurance properties.

Giroud and Bonaparte (1989) provided a detailed summary of procedures for calculating leakage through composite liners. Methods described in this section were derived from Giroud and Bonaparte's work, summarizing also the work of Brown et al. (1987), Jayawickrama et al. (1988) and Fukuoka (1985, 1986). In these procedures Giroud and Bonaparte (1989) assumed that the hydraulic head acting on the landfill liners and the depth of liquid on these liners are equivalent since the effects of velocity head are relatively small for landfill liners.

4.16.1 Vapor Diffusion Through Intact Geomembranes

Intact geomembranes are liners or sections of liners without any manufacturing or installation defects, that is without any holes. Since the voids between the molecular chains of geomembrane polymers are extremely narrow, leakage through intact geomembranes is likely only at the molecular level, regardless of whether transport is caused by liquid or vapor pressure differences. Therefore, transport of liquids through intact sections of composite liners is controlled by the rate of water vapor transport through the geomembrane. The hydraulic conductivities of the adjacent soil layers are much higher than the permeability of the geomembrane and therefore do not affect the leakage through intact sections of geomembranes.

A combination of Fick's and Darcy's laws results in a relationship between geomembrane water vapor diffusion coefficient, obtained from water vapor transmission tests, and "equivalent geomembrane hydraulic conductivity". Giroud and Bonaparte (1989) recommended using the term "equivalent hydraulic conductivity" since water transport through intact geomembranes is not described truly by Darcy's law for transport through porous media. The following equation for water transport through intact geomembranes was developed by substituting this relationship into Fick's law:

$$WVT = diffusivity \cdot \Delta p = \frac{permeability \cdot \Delta p}{T_g} \qquad Fick's\ law \tag{138}$$

$$q_L = \frac{WVT}{\rho} = K_s \frac{\Delta h}{T_g} \qquad Darcy's\ law \tag{139}$$

where

WVT = water vapor transmission, g/cm^2-sec

Δp = vapor pressure difference, mm Hg

T_g = thickness of geomembrane, cm

q_L = geomembrane leakage rate, cm/sec

ρ = density of water, g/cm^3

K_g = equivalent saturated hydraulic conductivity of geomembrane, cm/sec

Δh = hydraulic head difference, cm H_2O

Expressing Δp in terms of hydraulic head, Δh, diffusivity (also known as permeance or coefficient of diffusion) and hydraulic conductivity are related as follows:

$$K_g = \frac{diffusivity \cdot T_g}{\rho} \tag{140}$$

Equation 139 applies to the diffusion of water through the geomembrane induced by hydraulic head or vapor pressure differences. The program applies Darcy's law to geomembrane liners in the same manner as for soil liners (Equation 137). Diffusivity is expressed in the program as equivalent hydraulic conductivity. Table 8 provides default "equivalent hydraulic conductivities" for geomembranes of various polymer types. Leakage through intact sections of geomembranes is computed as follows:

$$q_{L_1}(k)_i = \begin{cases} 0 & for\ h_g(k)_i = 0 \\ K_g(k)\,\dfrac{h_g(k)_i + T_g(k)}{T_g(k)} & for\ h_g(k)_i > 0 \end{cases} \tag{141}$$

where

$q_{L_1}(k)_i$ = geomembrane leakage rate by diffusion during time step i, inches/day

$K_g(k)$ = equivalent saturated hydraulic conductivity of geomembrane in subprofile k, inches/day

$h_g(k)_i$ = average hydraulic head on geomembrane liner in subprofile k during time step i, inches

$T_g(k)$ = thickness of geomembrane in subprofile k, inches

4.16.2 Leakage Through Holes in Geomembranes

Properly designed and constructed geomembrane liners are seldom installed completely free of flaws as evident from leakage flows and post installation leak tests.

TABLE 8. GEOMEMBRANE DIFFUSIVITY PROPERTIES*

Geomembrane Material	Coefficient of Migration, cm^2/sec	Equivalent Hydraulic Conductivity, cm/sec
Butyl Rubber	$2x10^{-11}$	$1x10^{-12}$
Chlorinated Polyethylene (CPE)	$6x10^{-11}$	$4x10^{-12}$
Chlorosulfonated Polyethylene (CSPE) or Hypalon	$5x10^{-11}$	$3x10^{-12}$
Epichlorohydrin Rubber (CO)	$3x10^{-9}$	$2x10^{-10}$
Elasticized Polyolefin	$1x10^{-11}$	$8x10^{-13}$
Ethylene-Propylene Diene Monomer (EPDM)	$2x10^{-11}$	$2x10^{-12}$
Neoprene	$4x10^{-11}$	$3x10^{-12}$
Nitrile Rubber	$5x10^{-10}$	$3x10^{-11}$
Polybutylene	$7x10^{-12}$	$5x10^{-13}$
Polyester Elastomer	$2x10^{-10}$	$2x10^{-11}$
Low-Density Polyethylene (LDPE)	$5x10^{-12}$	$4x10^{-13}$
High-Density Polyethylene (HDPE)	$3x10^{-12}$	$2x10^{-13}$
Polyvinyl Chloride (PVC)	$2x10^{-10}$	$2x10^{-11}$
Saran Film	$9x10^{-13}$	$6x10^{-14}$

* From Giroud and Bonaparte (1985)

Geomembrane flaws can range in size from pinholes that are generally a result of manufacturing flaws such as polymerization deficiencies to larger defects resulting from seaming errors, abrasion, and punctures occurring during installation. Giroud and Bonaparte (1989) defines pinhole-sized flaws to be smaller than the thickness of the geomembrane. Since geomembrane liner thicknesses are typically 40 mils or greater, the HELP program assigns the diameter of pinholes to be 40 mils or 0.001 m (defect area = $7.84x10^{-7}$ m^2). Giroud and Bonaparte (1989) indicates that pinhole flaws are more commonly associated with the original, less sophisticated, geomembrane manufacturing

techniques. Current manufacturing and polymerization techniques have made pinhole flaws less common. Giroud and Bonaparte (1989) defined installation defect flaws to be of a size equal to or larger than the thickness of the geomembrane. Based on 6 case studies that produced consistent results, Giroud and Bonaparte (1989) recommended using a defect area of 1 cm^2 (20 x 5 mm) for conservatively high predictions of liner leakage on projects with intensive quality assurance/quality control monitoring during liner construction. Therefore, the HELP program uses a defect area of 1 cm^2. Finally, the HELP program user must define the flaw density or frequency (pinholes or defects/acre) for each geomembrane liner. Giroud and Bonaparte (1989) recommended using a flaw density of 1 flaw/acre for intensively monitored projects. A flaw density of 10 flaws/acre or more is possible when quality assurance is limited to spot checks or when environmental difficulties are encountered during construction. Greater frequency of defects may also result from poor selection of materials, poor foundation preparation and inappropriate equipment as well as other design flaws and poor construction practices.

Geosyntec (1993) indicated that geomembranes may undergo deterioration due to aging or external elements such as chemicals, oxygen, micro-organisms, temperature, high-energy radiation, and mechanical action (i.e., foundation settlement, slope failure, etc.). Although geomembrane deterioration can create geomembrane flaws or increase the size of existing flaws, the HELP program does not account for this time-dependent deterioration in the liner.

The liquid that passes through a geomembrane hole will flow laterally between the geomembrane and the flow limiting (controlling) layer of material adjacent to the geomembrane, unless there is perfect contact between the geomembrane and the controlling soil or free flow from the hole. The space between the geomembrane and the soil is assumed to be uniform. The size of this space depends on the roughness of the soil surface, the soil particle size, the rugosity and stiffness of the geomembrane, and the magnitude of the normal stress (overburden pressure) that tends to press the geomembrane against the soil. The HELP program ranks the contact between a geomembrane and soil as perfect, excellent, good, poor, and worst case (free flow). The HELP program also permits designs where a geomembrane is separated from a low permeability soil by a geotextile. The leakage is controlled by the hydraulic transmissivity of the gap or geotextile between the geomembrane and the soil. This interfacial flow between the geomembrane and soil layer covers an area called the wetted area. The hole in the geomembrane is assumed to be circular and the interfacial flow is assumed to be radial; therefore, the wetted area is circular. Giroud and Bonaparte (1989); Bonaparte et al. (1989); and Giroud et al. (1992) examined steady-state leakage through a geomembrane liner for all of these qualitative levels of contact and provided either theoretical or empirical solutions for the leakage rate and the radius of interfacial flow. Leakage and wetted area are dependent on the static hydraulic head on the liner; the hydraulic conductivity and thickness of the surrounding soil, waste, or geotextile layers; the size of the flaw; and the contact (interface thickness) between the geomembrane and the controlling soil layer.

The HELP program designates the controlling soil layer as either high, medium or low permeability. High is a saturated hydraulic conductivity greater than or equal to $1x10^{-1}$ cm/sec; medium is greater than or equal to $1x10^{-4}$ cm/sec and less than $1x10^{-1}$ cm/sec; and low is less than $1x10^{-4}$ cm/sec. The low permeability layers are assumed to remain saturated in the wetted area throughout the simulation. As mentioned earlier, geomembranes are geosynthetics with a very low cross-plane hydraulic conductivity (See Table 8). On the other hand, geotextiles are geosynthetics with a high cross-plane hydraulic conductivity and high in-plane transmissivity (See Table 9). The fabrics can help minimize damage to the membrane by the surrounding soil or waste layers. The in-plane transmissivity of geotextiles used as geomembrane cushions is used to compute the radius of interfacial flow and leakage through a geomembrane separated from the controlling soil by a geotextile.

Worst Case (Free Flow) Leakage

Giroud and Bonaparte (1989) theoretically examined free flow through a geomembrane surrounded by infinitely pervious media such as air or high permeability soil or waste layers (Brown et al., 1987). However, Giroud and Bonaparte (1989) cautioned that if the leachate head on the geomembrane liner is very small, surface tensions in the surrounding high permeability layers could prevent free flow through the geomembrane flaw. With time, leachate-entrained, fine-grained particles can clog the high permeability layers, greatly reducing the permeability of these layers and possibly preventing free flow. Free flow is assumed whenever the layers above and below the geomembrane have high permeability.

TABLE 9. NEEDLE-PUNCHED, NON-WOVEN GEOTEXTILE PROPERTIES [*]

Applied Compressive Stress, kPa	Resulting Geotextile Thickness, cm	In-Plane Flow		Cross-Plane Flow
		Geotextile Transmissivity, cm^2/sec [**]	Horizontal Hydraulic Conductivity, cm/sec	Vertical Hydraulic Conductivity, cm/sec
1 to 8	0.41	0.3	0.7	0.4
100	0.19	0.04	0.2	---
200	0.17	0.02	0.1	---

[*] Geotechnical Fabrics Report--1992 Specifiers Guide (Industrial Fabrics Association International, 1991), and Giroud and Bonaparte (1985).

[**] Transmissivity = horizontal hydraulic conductivity x thickness.

Pinholes. Giroud and Bonaparte (1989) concluded that percolation through pinholes surrounded by high permeability layers can be considered as flow through a pipe and recommended using Poiseuille's equation. Therefore, the HELP program uses the following form of Poiseuille's equation to predict free flow leakage through geomembrane pinholes:

$$q_{L_2}(k)_i = \frac{(86{,}400)\ \pi\ n_2(k)\ \rho_{15}\ g\ h_g(k)_i\ d_2^4}{(4{,}046.9)\ (128)\ \eta_{15}\ T_g(k)} \quad (142)$$

$$q_{L_2}(k)_i = \frac{1.775 \times 10^{-4}\ n_2(k)\ h_g(k)_i}{T_g(k)} \quad (143)$$

where

$q_{L_2}(k)_i$ = leakage rate through pinholes in subprofile k during time step i, inches/day

86,400 = units conversion, 86,400 seconds per day

$n_2(k)$ = pinhole density in subprofile k, #/acre

ρ_{15} = density of water at 15°C = 999 kg/m^3

g = gravitational constant, 386.1 inches/sec^2

d_2 = diameter of a pinhole, 0.001 meters

4,046.9 = units conversion, 4,046.9 m^2/acre

η_{15} = dynamic viscosity of water at 15°C = 0.00114 kg/m sec

$T_g(k)$ = thickness of geomembrane in subprofile k, inches

1.775 x 10^{-4} = constant, 1.775 x 10^{-4} inches acre/day

Installation Defects. Giroud and Bonaparte (1989) also concluded that leakage through defects in geomembranes surrounded by high permeability layers can be considered as flow through an orifice and recommended using Bernoulli's equation. Therefore, the HELP program uses the following form of Bernoulli's equation to predict free flow leakage through geomembrane defects:

$$q_{L_3}(k)_i = \frac{86{,}400\ C_B\ n_3(k)\ a_3\ \sqrt{2\ g\ h_g(k)_i}}{4046.9} \quad (144)$$

$$q_{L_3}(k)_i = 0.0356\ n_3(k)\ \sqrt{h_g(k)_i} \quad (145)$$

where

$q_{L_3}(k)_i$ = leakage rate through defects in subprofile k during time step i, inches/day

C_B = head loss coefficient for sharp edged orifices, 0.6

$n_3(k)$ = installation defect density for subprofile k, #/acre

a_3 = defect area, 0.0001 m^2

$h_g(k)_i$ = average hydraulic head on geomembrane liner in subprofile k during time step i, inches

0.0356 = constant, 0.0356 $inches^{0.5}$ acre/day

Perfect Liner Contact

Perfect geomembrane liner contact means that there is no gap or interface between the geomembrane liner and controlling soil or waste layer. Perfect contact is not common but can be achieved if the geomembrane is sprayed directly onto a compacted, fine-grained soil or waste layer or if the geomembrane and controlling layers are manufactured together. Problems associated with the installation of spray-on liners (e.g. application, polymerization, etc.) has limited their use. Perfect liner contact results in only vertical percolation through the controlling layer below the liner flaw; however, both vertical and horizontal flow can occur in the layer opposite the controlling soil or waste layer.

Giroud and Bonaparte (1989) indicated that a lower bound estimate of leakage for perfect contact conditions can be estimated using Darcy's law assuming vertical flow through the controlling layer only in the area below the hole. An upper bound prediction can be obtained by assuming radial flow in the controlling layer and integrating Darcy's law in spherical coordinates to obtain the following equation:

$$Q_h = \frac{\pi\ K_s\ h_g\ d_o}{1 - \dfrac{0.5\ d_o}{T_s}} \quad (146)$$

where

Q_h = leakage rate through pinholes and installation defects, m^3/sec

K_s = saturated hydraulic conductivity of soil layer, m/sec

h_g = hydraulic head on geomembrane, m

d_o = diameter of the geomembrane flaw, m

T_s = thickness of soil layer, m

A geomembrane flaw diameter of 0.1 cm is used for pinhole flaws. Considering the density of pinholes, converting units and assuming $d/T_s \approx 0$, the leakage rate for pinholes in geomembrane with perfect contact is

$$q_{L_2}(k)_i = \frac{\pi \; n_2(k) \; K_s(k) \; h_g(k)_i \; 0.04}{6{,}272{,}640} \tag{147}$$

where

$q_{L_2}(k)_i$ = leakage rate through pinholes in subprofile k during time step i, inches/day

$n_2(k)$ = pinhole density in subprofile k, #/acre

$K_s(k)$ = saturated hydraulic conductivity of soil layer at the base of subprofile k, inches/day

$h_g(k)_i$ = average hydraulic head on liner in subprofile k during time step i, inches

0.04 = diameter of a pinhole, 0.04 inches

6,272,640 = units conversion, 6,272,640 square inches per acre

Since the area of defect flaws was identified to be 1 cm^2, an equivalent defect diameter was calculated to be 1.13 cm. Considering the density of installation defects and converting units, the leakage rate for installation defects in geomembrane with perfect contact is

$$q_{L_3}(k)_i = \frac{\pi \; n_3(k) \; K_s(k) \; h_g(k)_i \; 0.445}{6{,}272{,}640 \left[1 - \frac{(0.5) \; (0.445)}{T_s(k)} \right]} \tag{148}$$

where

$q_{L_3}(k)_i$ = leakage rate through installation defects in subprofile k during time step i, inches/day

$n_3(k)$ = installation defect density in subprofile k, #/acre

0.445 = diameter of an installation defect, 0.445 inches

$T_s(k)$ = thickness of soil layer at base of subprofile k, inches

Interfacial Flow

Problems associated with the installation of geomembrane liners typically causes an interface or gap to develop between the installed geomembrane liner and the adjacent materials. Even with a large overburden pressure on the geomembrane liner, gaps exist due to geomembrane wrinkles from installation; clods, large particle size and irregularities in the subsoil; and the stiffness of the geomembrane preventing the liner from filling the small voids between soil particles. However, the thickness of the interface is dependent on the effective stress on the liner. Percolation through geomembrane flaws typically involves radial flow through the interface and vertical flow through the controlling layer (See Figure 9). This flow also occurs in reverse when the controlling layer is placed over the geomembrane (See Figure 10). Layer erosion and consolidation can increase the interface thickness over time; however, such increases are not considered in the HELP program.

The head acting on the geomembrane liner decreases from a maximum at the edge of the geomembrane flaw to zero at the edge of the wetted area. Flow through the interface and controlling layer completely dissipates the leachate head or, as with intact liners, the total head on the liner. The leachate is assumed to flow radially until this head is dissipated; this radial distance is called the wetted area.

Giroud and Bonaparte (1989) indicated that the interfacial flow is dependent on the hydraulic transmissivity (thickness) of the air or geotextile cushion occupying the interface, the hydraulic head on the geomembrane, the hydraulic conductivity of the controlling soil layer, and the size of the geomembrane flaw. Vertical flow through the controlling layer is dependent on the hydraulic conductivity of the layer, the hydraulic gradient on the layer at various locations in the wetted area, and the area of the wetted area.

Giroud and Bonaparte (1989) and Giroud et al. (1992) used Darcy's law for flow through a porous media, considering both radial and interfacial flow, and developed the following equation, modified for flow per unit area and temperature corrected, for estimating leakage through circular flaws in geomembranes with interfacial flow.

$$q_h = K_s \, i_{avg} \, n \, \pi \, R^2 \left(\frac{\eta_{20}}{\eta_{15}} \right) \tag{149}$$

where

q_h = interfacial flow leakage rate through flawed geomembrane, m/sec

K_s = saturated hydraulic conductivity of controlling soil layer, m/sec

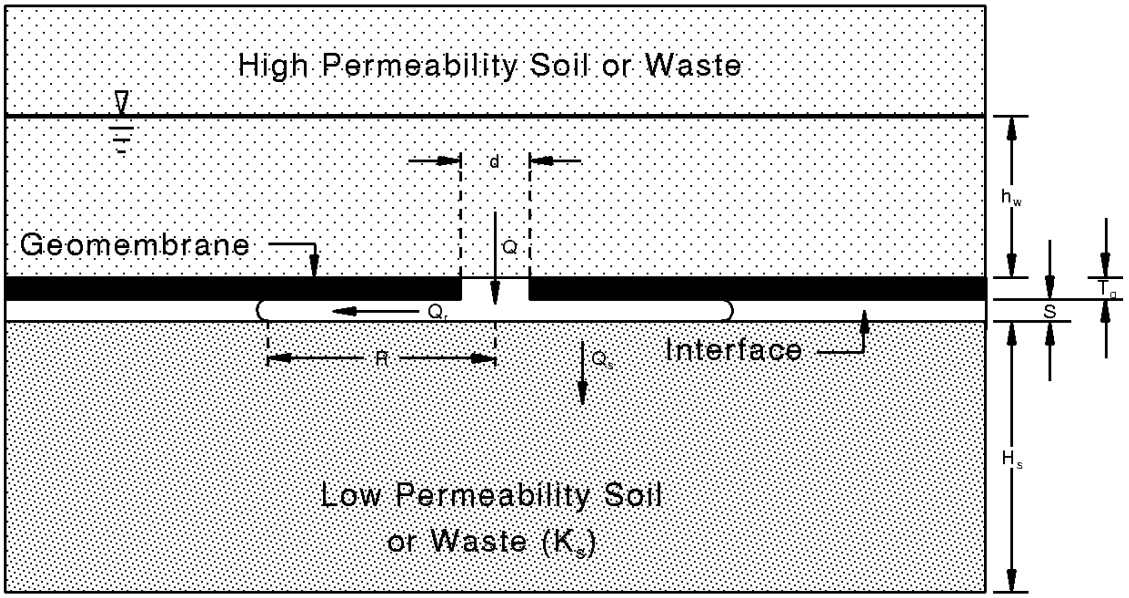

Figure 9. Leakage with Interfacial Flow Below Flawed Geomembrane

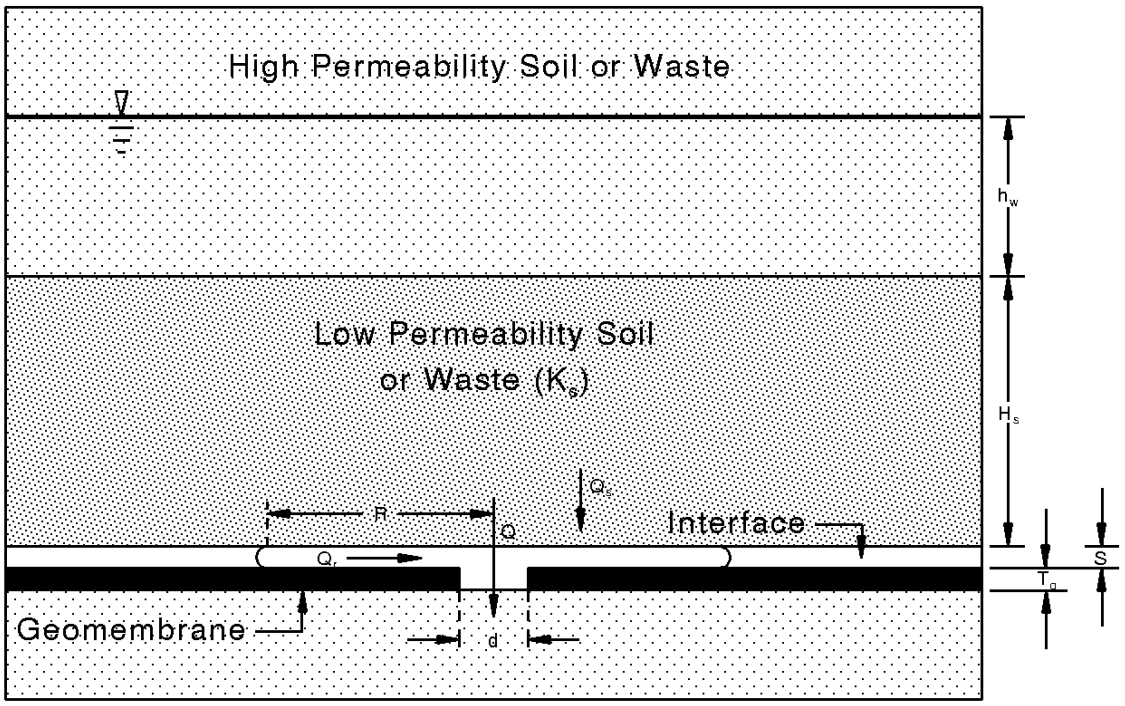

Figure 10. Leakage with Interfacial Flow Above Flawed Geomembrane

i_{avg} = average hydraulic gradient on wetted area of controlling soil layer, dimensionless

n = density of flaws, # per m^2

R = radius of wetted area or interfacial flow around a flaw, m

η_{20} = absolute viscosity of water at 20°C, 0.00100 kg/m-sec

η_{15} = absolute viscosity of water at 15°C, 0.00114 kg/m-sec

Since the U.S. Geological Survey defined hydraulic conductivity, in Meinzer units, as the number of gallons per day of water passing through 1 ft^2 of medium under a unit hydraulic gradient (1 ft/1 ft) at a temperature of 60°F (15°C) (Viessman et al., 1977; Linsley et al., 1982), Equation 149 was corrected to reflect an absolute water viscosity at 15°C (Giroud and Bonaparte, 1989).

Giroud et al. (1992) developed the following equation to describe the average hydraulic gradient on the geomembrane; a description of the development is presented in the following paragraphs.

$$i_{avg} = 1 + \left[\frac{h_g}{2\ T_s \ln\left(\frac{R}{r_o}\right)} \right] \tag{150}$$

where

h_g = total hydraulic head on geomembrane, m

T_s = thickness of controlling soil layer, m

r_o = radius of a geomembrane flaw, m

Methods for calculating the wetted area radius for various liner contact conditions and design cases are presented in the following sections.

The HELP program applies Equations 149 and 150 as follows:

$$q_{L_{2,3}}(k)_i = \left(\frac{0.00100}{0.00114}\right) \left[\frac{K_s(k)\ i_{avg_{2,3}}(k)_i\ n_{2,3}(k)\ \pi\ R_{2,3}(k)_i^2}{6{,}276{,}640} \right] \tag{151}$$

$$i_{avg_{2,3}}(k)_i = 1 + \left[\frac{h_g(k)_i}{2\ T_s(k)\ \ln\left(\frac{R_{2,3}(k)_i}{r_{o_{2,3}}} \right)} \right] \quad (152)$$

where

$q_{L_{2,3}}(k)_i$ = leakage rate through pinholes (2) or installation defects (3) with interfacial flow in subprofile k during time step i, inches/day

$K_s(k)$ = saturated hydraulic conductivity of controlling soil layer in subprofile k, inches/day

$i_{avg_{2,3}}(k)_i$ = average hydraulic gradient on wetted area of controlling soil layer from pinholes (2) or installation defects (3) in subprofile k during time step i, dimensionless

$n_{2,3}(k)$ = density of pinholes (2) or defects (3) in subprofile k, #/acre

$R_{2,3}(k)_i$ = radius of wetted area or interfacial flow around a pinhole (2) or an installation defect (3) in subprofile k during time step i, inches

6,272,640 = units conversion, 6,272,640 square inches per acre

$r_{o_{2,3}}$ = radius of flaw; pinhole r_{o_2} = 0.02 inches; defect r_{o_3} = 0.22 inches

$h_g(k)_i$ = average hydraulic head on liner in subprofile k during time step i, inches

$T_s(k)$ = thickness of soil layer at base of subprofile k, inches

Geotextile Interface

Giroud and Bonaparte (1989) assumed a unit hydraulic gradient for vertical flow through the controlling layer (i.e., Equation 149 without the i_{avg} term) and applied the principle of conservation of mass to the radial and vertical flow through the geomembrane. They integrated the resulting equation and developed the following equation for estimating the radius of the wetted area:

$$R = \left[\frac{4\ h_g\ \theta_{int}}{K_s \left[2\ \ln\left(\frac{R}{r_o} \right) + \left(\frac{r_o}{R} \right)^2 - 1 \right]} \right]^{\frac{1}{2}} \quad (153)$$

where

θ_{int} = hydraulic transmissivity of the interface or geotextile, m^2/sec

However, assuming a unit hydraulic gradient indicates that the depth of saturated material on the geomembrane is substantially smaller than the thickness of the controlling layer. This was a limitation of Giroud and Bonaparte's (1989) method for estimating geomembrane liner leakage. However, Giroud et al. (1992) used a simplified and conservative form of Equation 153, the principle of conservation of mass for flow through the two layers, and integrated the resulting equation to obtain an equation similar in form to Darcy's law (Q = Kia). The hydraulic gradient term in the resulting equation was identified as the average hydraulic gradient on the geomembrane liner and is provided in Equation 150.

Equation 153 is solved iteratively by using ($h_g + r_o$) as the initial guess and then substituting the computed R into the right hand side until it converges. Equation 151 is also limited by the fact that the thickness between the installed geomembrane liner and the controlling layer is not easily determined, especially for multiple design cases. However, Giroud and Bonaparte (1989) provided information on the hydraulic transmissivity (loaded thickness times in-plane hydraulic conductivity) of geotextile cushion under a variety of effective stresses (See Table 9). Therefore, the HELP program only uses Equation 153 to estimate the leakage through flaws in geomembrane liners installed with geotextile cushions. The cushion is assumed to completely fill the interface between the liner and controlling layer. For other liner design cases, Giroud and Bonaparte (1989); Bonaparte et al. (1989); and Giroud et al. (1992) used laboratory and field data and theoretically based equations to develop semi-empirical and empirical equations for estimating the wetted area radius for excellent, good, and poor contact between the geomembrane liner and controlling layer.

Pinholes. The HELP program applies Equation 153 for computing the radius of the wetted area of leakage from pinholes and through a geotextile interface and a controlling soil layer as given in Equation 154 for each time step and each subprofile. The radius is then used in Equation 152 to compute the average hydraulic gradient. The radius and average hydraulic gradient is then used in Equation 151 to compute the leakage rate for pinholes.

$$R_2(k)_i = \left[\frac{4\ h_g(k)_i\ \theta_{int}(k)}{K_s(k) \left\{ \left[2\ \ln\left(\frac{R_2(k)_i}{0.02} \right) \right] + \left(\frac{0.02}{R_2(k)_i} \right)^2 - 1 \right\}} \right]^{\frac{1}{2}} \qquad (154)$$

where

$\theta_{int}(k)$ = hydraulic in-plane transmissivity of the geotextile in subprofile k, $inches^2$/day

Installation Defects. The HELP program applies Equation 153 for computing radius of leakage from installation defects and through a geotextile interface and a controlling soil layer as follows:

$$R_3(k)_i = \left[\frac{4 \; h_g(k)_i \; \theta_{int}(k)}{K_s(k) \left\{ \left[2 \ln\left(\frac{R_3(k)_i}{0.22} \right) \right] + \left(\frac{0.22}{R_3(k)_i} \right)^2 - 1 \right\}} \right]^{\frac{1}{2}} \qquad (155)$$

This radius is then used in Equation 152 to compute the average hydraulic gradient. The radius and average hydraulic gradient is then used in Equation 151 to compute the leakage rate for installation defects.

Excellent Liner Contact

Excellent liner contact is achieved under three circumstances. Medium permeability soils and materials are typically cohesionless and therefore generally are able to conform to the geomembrane, providing excellent contact. The second circumstance is for very well prepared low permeability soil layer with exceptional geomembrane placement typically achievable in the laboratory, small lysimeters or small test plots. The third circumstance is by the use of a geosynthetic clay liner (GCL) adjacent to the geomembrane with a good foundation. The GCL, upon wetting, will swell to fill the gap between the geomembrane and the foundation, providing excellent contact.

Medium Permeability Controlling Soil. Giroud and Bonaparte (1989) indicated that if a geomembrane liner is installed with a medium permeability material (saturated hydraulic conductivity greater than or equal to $1x10^{-4}$ cm/sec and less than $1x10^{-1}$ cm/sec) above the geomembrane as the controlling soil layer, the flow to the geomembrane flaw will be impeded by the medium permeability layer and the leakage through the flaw will be less than free flow leakage. Similarly, if medium permeability material below the geomembrane acts as the controlling soil layer, the flow from the flaw will be impeded by the medium permeability layer and leakage will also be less than free flow. Whenever a medium permeability soil acts as the controlling soil layer, the contact is modeled as excellent. However, even with excellent contact, there will be some level of flow between the geomembrane and medium permeability layer. Bonaparte et al. (1989) used a theoretical examination of the flow in the interface between the medium permeability soil and the geomembrane liner to develop several empirical approaches that averaged the logarithms of the perfect contact leakage and free flow leakage predictions to obtain the following equation for the radius of convergence of leakage to a flaw in a geomembrane placed on high permeability material and overlain by medium permeability material:

$$R = 0.97\ a_o^{0.38}\ h_g^{0.38}\ K_s^{-0.25} \quad (156)$$

where

R = radius of interfacial flow around a geomembrane flaw, m

a_o = geomembrane flaw area, 7.84×10^{-7} m^2 for pinholes and 0.0001 m^2 for installation defects

h_g = total hydraulic head on geomembrane, m

K_s = saturated hydraulic conductivity of controlling soil layer, m/sec

This equation is also used to calculate the wetted radius of interfacial flow for geomembranes overlain by high permeability soil and underlain by medium permeability soil. This radius, as it is actually computed below in Equations 157 or 155, is then used in Equation 152 to compute the average hydraulic gradient. The radius and average hydraulic gradient are then used in Equation 151 to compute the leakage rate for geomembrane flaws.

Pinholes. By inserting the pinhole area, converting units and simplifying, Equation 156 is converted to the following equation for radius of interfacial flow from pinholes in geomembranes with medium permeability controlling soil layers.

$$R_2(k)_i = 0.0494\ h_g(k)_i^{0.38}\ K_s(k)^{-0.25} \quad (157)$$

where

$R_2(k)_i$ = radius of wetted area or interfacial flow around a pinhole in subprofile k during time step i, inches

$K_s(k)$ = saturated hydraulic conductivity of controlling soil layer in subprofile k, inches/day

$h_g(k)_i$ = average hydraulic head on liner in subprofile k during time step i, inches

Installation Defects. By inserting the installation defect area, converting units and simplifying, Equation 156 is converted to the following equation for radius of interfacial flow from installation defects in geomembranes with medium permeability controlling soil layers.

$$R_3(k)_i = 0.312\ h_g(k)_i^{0.38}\ K_s(k)^{-0.25} \quad (158)$$

where

$R_3(k)_i$ = radius of wetted area or interfacial flow around a pinhole in subprofile k during time step i, inches

Low Permeability Controlling Soil. Giroud and Bonaparte (1989) indicated that, when a geomembrane liner is installed on or under a low-permeability soil or waste layer, excellent geomembrane liner contact can be obtained if the liner is flexible and without wrinkles and the controlling layer is well compacted, flat, and smooth; has not been deformed by rutting due to construction equipment; and has no clods or cracks. Excellent contact is also possible when using a GCL with a good foundation as the low permeability soil layer. Using the theoretical techniques previously mentioned and laboratory data, Brown et al. (1987) developed charts for estimating the leakage rate through circular flaws in geomembrane liners for what Giroud and Bonaparte (1989) defined to be excellent liner contact. Leakage rates predicted using these charts are dependent on the flaw surface area, the saturated hydraulic conductivity of the controlling soil or waste layer, and the total leachate head on the geomembrane. Giroud and Bonaparte (1989) summarized and extrapolated or interpolated the data in these charts and developed the following equation for the wetted area radius with excellent liner contact with low permeability soil (saturated hydraulic conductivity less than 1×10^{-4} cm/sec); units are as in Equation 156:

$$R = 0.5\ a_o^{0.05}\ h_g^{0.5}\ K_s^{-0.06} \tag{159}$$

This radius, as it is actually computed below in Equations 160 or 161, is then used in Equation 152 to compute the average hydraulic gradient. The radius and average hydraulic gradient are then used in Equation 151 to compute the leakage rate for geomembrane flaws.

Pinholes. By inserting the pinhole area, converting units and simplifying, Equation 159 is converted to the following equation for radius of leakage from pinholes in geomembranes with excellent contact with low permeability controlling soil layers.

$$R_2(k)_i = 0.0973\ h_g(k)_i^{0.5}\ K_s(k)^{-0.06} \tag{160}$$

Installation Defects. By inserting the installation defect area, converting units and simplifying, Equation 159 is converted to the following equation for radius of leakage from installation defects in geomembranes with excellent contact with low permeability controlling soil layers.

$$R_3(k)_i = 0.124\ h_g(k)_i^{0.5}\ K_s(k)^{-0.06} \quad (161)$$

Good Liner Contact

Using the equations for perfect and excellent liner contact and free-flow percolation through geomembrane liners, Giroud and Bonaparte (1989) developed leakage rate curves for a variety of conditions (i.e., leachate head, saturated hydraulic conductivity, etc.). The worst case field leakage was arbitrarily defined to be midway between free-flow and excellent contact leakage estimates. The area between worst case field leakage and excellent contact leakage was arbitrarily divided into thirds and defined as good and poor field leakage. However, due to the lengthy calculations required to estimate good and poor liner leakage, Giroud and Bonaparte (1989) developed empirical equations to predict leakage through geomembrane liners under good and poor field conditions. These equations are discussed in the following paragraphs.

Giroud and Bonaparte (1989) indicated that good geomembrane liner contact can be defined as a geomembrane, installed with as few wrinkles as possible, on an adequately compacted, low-permeability layer with a smooth surface. Similar to Equations 156 and 159, Giroud and Bonaparte (1989) observed families of approximately parallel linear curves when plotting the leakage rate as a function of total head on the geomembrane liner, geomembrane flaw area, and saturated hydraulic conductivity of the controlling soil or waste layer. Giroud and Bonaparte (1989) concluded that the leakage rate through damaged geomembranes is approximately proportional to equations of the form $a_o^y\ h_g^x\ K_s^z$. Therefore, Giroud and Bonaparte (1989) proposed the following equation for determining the wetted area radius for good liner contact:

$$R = 0.26\ a_o^{0.05}\ h_g^{0.45}\ K_s^{-0.13} \quad (162)$$

This radius, as it is actually computed below in Equations 163 or 164, is then used in Equation 152 to compute the average hydraulic gradient. The radius and average hydraulic gradient are then used in Equation 151 to compute the leakage rate for geomembrane flaws. Similar to Equation 159, Equation 162 has the limitation that the saturated hydraulic conductivity of the controlling soil layer must be less than $1x10^{-4}$ cm/sec. Equation 162 is valid only in units of meters and seconds.

Pinholes. Inserting pinhole area, performing units conversion and simplifying, Equation 162 is converted for radius of leakage from pinholes in geomembranes with good contact with low permeability controlling soil layers as follows:

$$R_2(k)_i = 0.174\ h_g(k)_i^{0.45}\ K_s(k)^{-0.13} \quad (163)$$

Installation Defects. By inserting the installation defect area, converting units and simplifying, Equation 162 is converted to the following equation for radius of leakage from installation defects in geomembranes with good contact with low permeability controlling soil layers.

$$R_3(k)_i = 0.222\ h_g(k)_i^{0.45}\ K_s(k)^{-0.13} \quad (164)$$

Poor Liner Contact

Giroud and Bonaparte (1989) indicated that poor geomembrane liner contact can be defined as a geomembrane, installed with a certain number of wrinkles, on a poorly compacted, low-permeability soil or waste layer, with a surface that does not appear smooth. Similar to Equation 162, Giroud and Bonaparte (1989) proposed the following equation for determining the radius of leakage through a geomembrane for poor contact with a low permeability controlling soil layer:

$$R = 0.61\ a_o^{0.05}\ h_g^{0.45}\ K_s^{-0.13} \quad (165)$$

This radius, as it is actually computed below in Equations 166 or 167, is then used in Equation 152 to compute the average hydraulic gradient. The radius and average hydraulic gradient are then used in Equation 151 to compute the leakage rate for geomembrane flaws. Similar to Equations 159 and 162, Equation 165 has the limitation that the saturated hydraulic conductivity of the controlling soil layer must be less than $1x10^{-4}$ cm/sec. Equation 165 is valid using units of meters and seconds.

Pinholes. By inserting pinhole area, performing units conversion and simplifying, Equation 165 is converted to the following equation for radius of leakage from pinholes in geomembranes with poor contact with low permeability controlling soil layers.

$$R_2(k)_i = 0.174\ h_g(k)_i^{0.45}\ K_s(k)^{-0.13} \quad (166)$$

Installation Defects. By inserting the installation defect area, converting units and simplifying, Equation 165 is converted to the following equation for radius of leakage

from installation defects in geomembranes with poor contact with low permeability controlling soil layers.

$$R_3(k)_i = 0.521\ h_g(k)_i^{0.45}\ K_s(k)^{-0.13} \quad (167)$$

4.17 GEOMEMBRANE AND SOIL LINER DESIGN CASES

As previously mentioned, the HELP program simulates leakage through both the intact and damaged portions of geomembrane liners. Leakage through geomembrane flaws (pinholes and defects) is modeled for various liner contact conditions. The minimum level of leakage will occur through an intact geomembrane liner. The total leakage is the sum of leakage through (1) intact geomembrane sections and (2) pinhole-size and (3) defect-size geomembrane flaws.

$$q_{L_T} = q_{L_1} + q_{L_2} + q_{L_3} \quad (168)$$

The HELP program insures that the total leakage through the geomembrane and controlling layers is not greater than the volume of drainable water. The program also checks to insure that the leakage rate is not greater than the product of the hydraulic gradient and the saturated hydraulic conductivity of the controlling layer.

Giroud and Bonaparte (1989) and Giroud et al. (1992) developed their equations for intact geomembranes, geomembranes surrounded by highly-pervious materials, and composite liners; defined as a geomembrane installed over a low-permeable soil liner and covered by a drainage layer. However, various other liner design cases are possible and, although the equations were not specifically designed to address these designs, similar physical conditions indicated that these equations would be applicable to other liner design cases. However, the applicability of these equations to other liner designs has not been fully verified.

Geomembrane liners are frequently installed with various defects that increase as design and installation monitoring efforts decrease. Therefore, the HELP program user must identify the liner contact condition (perfect, excellent, good, poor, or worst case) for each damaged geomembrane liner. The user must also identify the hydraulic conductivity of the controlling layer and the geomembrane flaw type (pinhole or defect) and density. The user must also identify the thickness and equivalent hydraulic conductivity of the geomembrane for the intact portions of the liner. In some cases, the user will have to identify the geotextile cushion thickness and in-plane hydraulic transmissivity.

Based on the design of the geomembrane liner system (layer type, saturated hydraulic conductivity, and location of controlling soil layer), the HELP program can compute leakage for 6 different geomembrane liner design cases (See Figures 11 through 16).

These design cases are discussed in the following sections.

Design Case 1. Geomembrane liner Design Case 1 consists of a geomembrane installed between two highly permeable soil or waste layers (See Figure 11). The program uses the free flow equations (Equation 143 for pinholes and Equation 145 for installation defects) to calculate the leakage rate through flaws. The vapor diffusion equation (Equation 141) is used to calculate the leakage rate through the intact portion of the geomembrane liner. The damaged and intact leakage estimates are then added together to predict the total leakage through the geomembrane liner.

Design Case 2. Geomembrane liner Design Case 2 consists of three design scenarios: 1) a geomembrane liner installed on top of a highly permeable layer and overlaid by a medium permeability layer; 2) a geomembrane liner installed on top of a medium permeability layer and overlaid by a highly permeable layer; and 3) a geomembrane liner installed between two medium permeability layers (See Figure 12). Three levels of contact (perfect, excellent, or worst case) between the geomembrane and medium permeability layer are allowed for this design case. The program uses Equations 147 and 148 to calculate the perfect contact leakage rate through pinholes and installation defects, respectively. Equations 151, 152, 157 (for pinholes) and 158 (for installation defects) are used to calculate the excellent contact leakage rate. As in Design Case 1, free flow equations (Equation 143 for pinholes and Equation 145 for installation defects) are used to calculate the worst case contact leakage rate. Finally, the vapor diffusion equation (Equation 141) is used to calculate the leakage rate through the intact portion of the geomembrane liner for all three scenarios and levels of contact. The damaged and intact leakage estimates are subsequently added together to predict the total leakage through the geomembrane liner.

Design Case 3. Geomembrane liner Design Case 3 consists of a geomembrane overlying a low permeability layer (either a soil liner or vertical percolation layer), which is the controlling soil layer (See Figure 13). The geomembrane may be covered with either a high permeability, medium permeability, or low permeability soil or waste layer

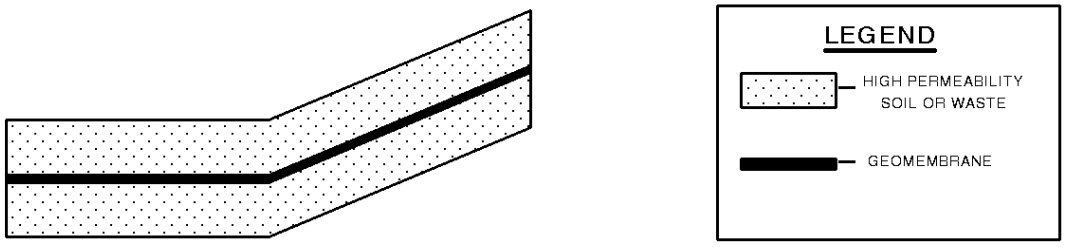

Figure 11. Geomembrane Liner Design Case 1

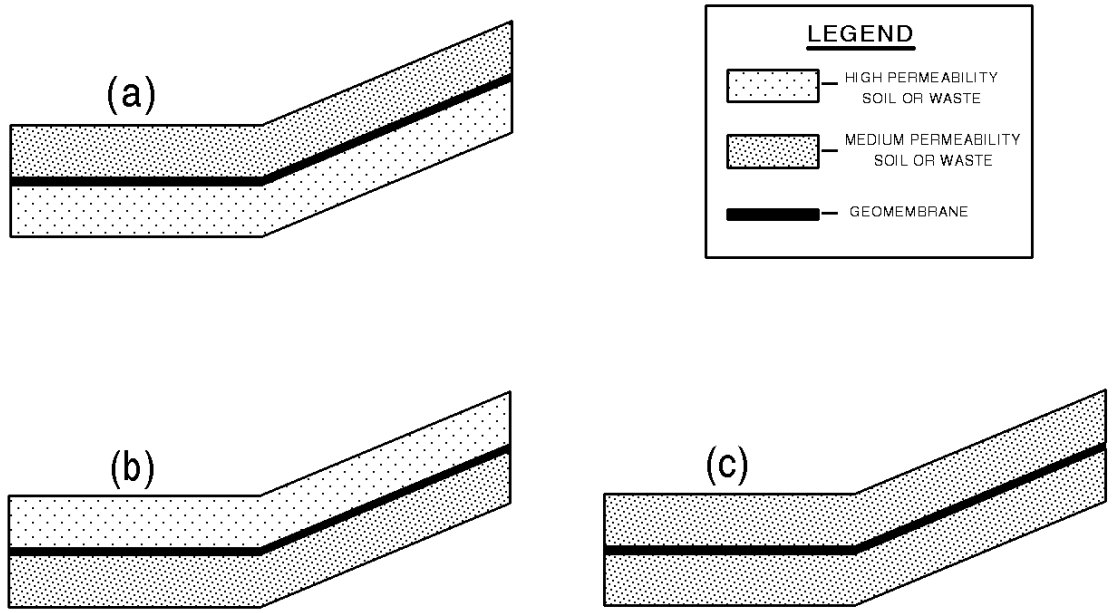

Figure 12. Geomembrane Liner Design Case 2

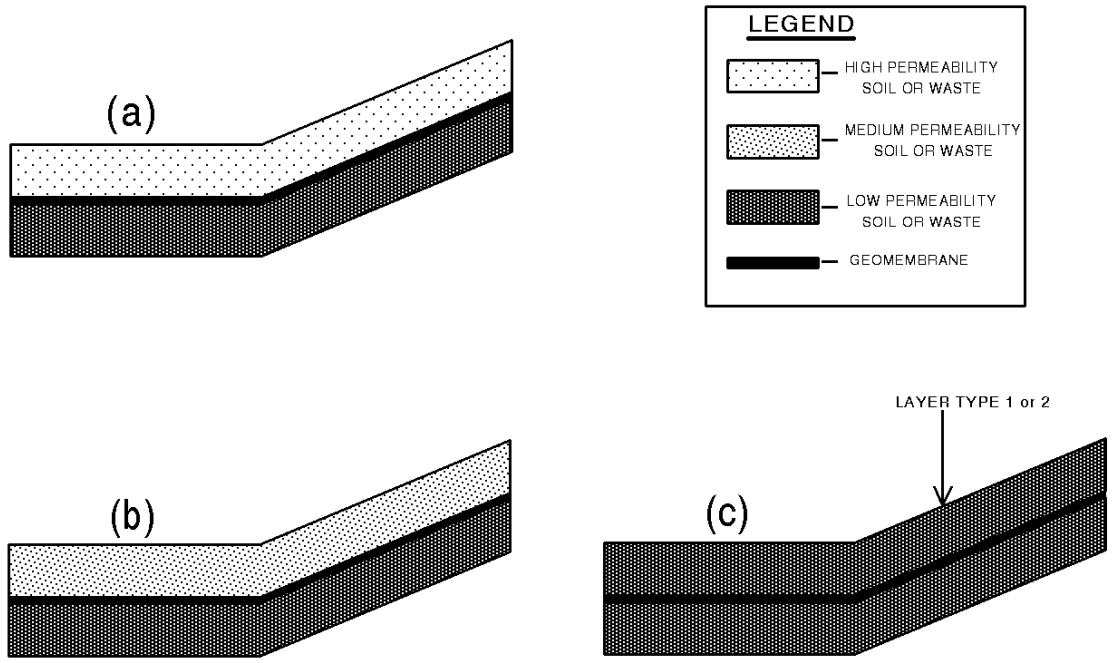

Figure 13. Geomembrane Liner Design Case 3

designated as either a vertical percolation or lateral drainage layer. The level of contact between the geomembrane and low permeability controlling soil layer may be defined as perfect, excellent, good, poor, or worst case. The program uses Equations 147 and 148 to calculate the perfect contact leakage rate through pinholes and installation defects, respectively. Equations 151 and 152 are used to calculate the interfacial flow leakage rate and hydraulic head gradient for excellent, good and poor levels of contact. Equations 160, 163 and 166 are used to calculate the radius of interfacial flow from pinholes respectively for excellent, good and poor levels of contact. Equations 161, 164 and 167 are used to calculate the radius of interfacial flow from installation defects respectively for excellent, good and poor levels of contact. As in Design Case 1, free flow equations (Equation 143 for pinholes and Equation 145 for installation defects) are used to calculate the worst case contact leakage rate. Finally, the vapor diffusion equation (Equation 141) is used to calculate the leakage rate through the intact portion of the geomembrane liner for all levels of contact. The damaged and intact leakage estimates are subsequently added together to predict the total leakage through the geomembrane liner.

Design Case 4. Geomembrane liner Design Case 4 is simply the inverse of Design Case 3 (See Figure 14); the low permeability controlling soil layer overlies the geomembrane. The same soil and layer types and levels of contacts may be used. The same equations as described for Design Case 3 are used to calculate leakage for the various contacts and flaw sizes. This geomembrane liner design case is the exact inverse of that considered

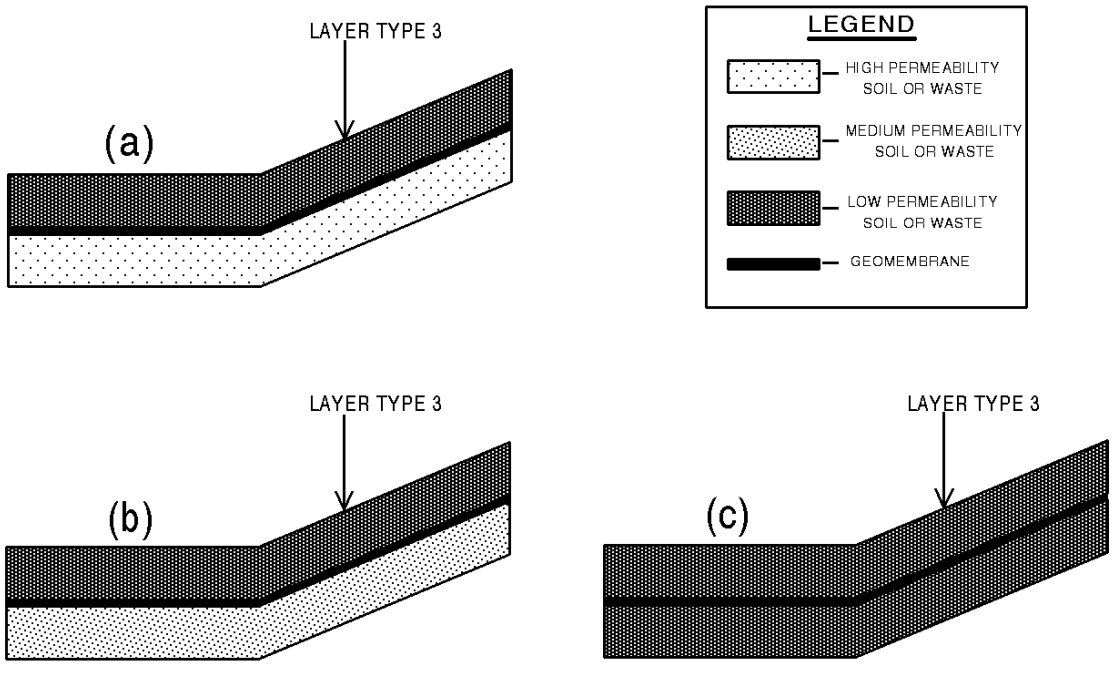

Figure 14. Geomembrane Liner Design Case 4

by Giroud and Bonaparte (1989). However, since the total head loss for leakage through damaged geomembrane liners is assumed to occur through the interface and controlling layer, the equations proposed by Giroud and Bonaparte (1989) should apply as well for the inverted case. However, the total head on the geomembrane for this design case and Design Case 6 is equal to the sum of the leachate depth in the layer above the liner system and the thickness of saturated soil liner above the geomembrane as shown in Figure 10; the hydraulic head is the total thickness of continuously saturated soil or waste above the geomembrane. In Design Cases 1, 2, 3 and 5, the total head is just the depth of saturated material above the liner system as shown in Figure 9.

Design Case 5. As shown in Figure 15, geomembrane liner Design Case 5 consists of eight scenarios that have a geotextile cushion placed between the geomembrane liner and the controlling soil layer. The controlling soil layer may be composed of medium or low permeability soil. The controlling soil layer may be above or below the geomembrane, but, if above, the controlling soil layer cannot be a soil liner. The geotextile is not connected to the leachate collect system, which would cause them to act as a drainage layer. The geotextile functions solely as a liner cushion and defines the interfacial flow between the geomembrane and controlling soil layer. Assuming the cushion completely fills the interface, Equations 151, 152, 154 (for pinholes) and 155 (for installation defects) are used to estimate the leakage rate as a function of the hydraulic in-plane transmissivity of the geotextile. Table 9 provides hydraulic transmissivity values, at several compressive stresses, for needle-punched, non-woven geotextiles. Recall that the hydraulic transmissivity of geotextiles is greatly affected by the applied compressive stress and the degree of clogging.

Design Case 6. Geomembrane liner Design Case 6 consists of a geomembrane liner installed on a high, medium, or low permeability soil or waste layer with a geotextile cushion separating the geomembrane and a overlying soil liner (layer type 3). (See Figure 16). Similar to Design Case 5, the program uses Equations 151, 152, 154 (for pinholes) and 155 (for installation defects) to estimate the leakage rate as a function of the hydraulic in-plane transmissivity of the geotextile. However, as in Design Case 4, the total head on the geomembrane is equal to the sum of the continuously saturated material above the liner system and the thickness of the soil liner above the geomembrane.

Flow through the geotextile cushion in either Design Case 5 or 6 can increase the geomembrane liner leakage due to an increase in the wetted area and possibly creating a connection between the geomembrane flaw and controlling layer macropores. On the other hand, laboratory tests have shown that a needlepunched, nonwoven geotextile cushion installed between a geomembrane liner and controlling layer can decrease leakage if the effective stress on the liner or controlling layer is adequate to push the geotextile into irregularities in the controlling layer (worst case and possibly poor contact cases). This prevents free lateral flow between the liner and controlling layer. However, the beneficial effects of geotextile cushions may be limited to cases of poor design and

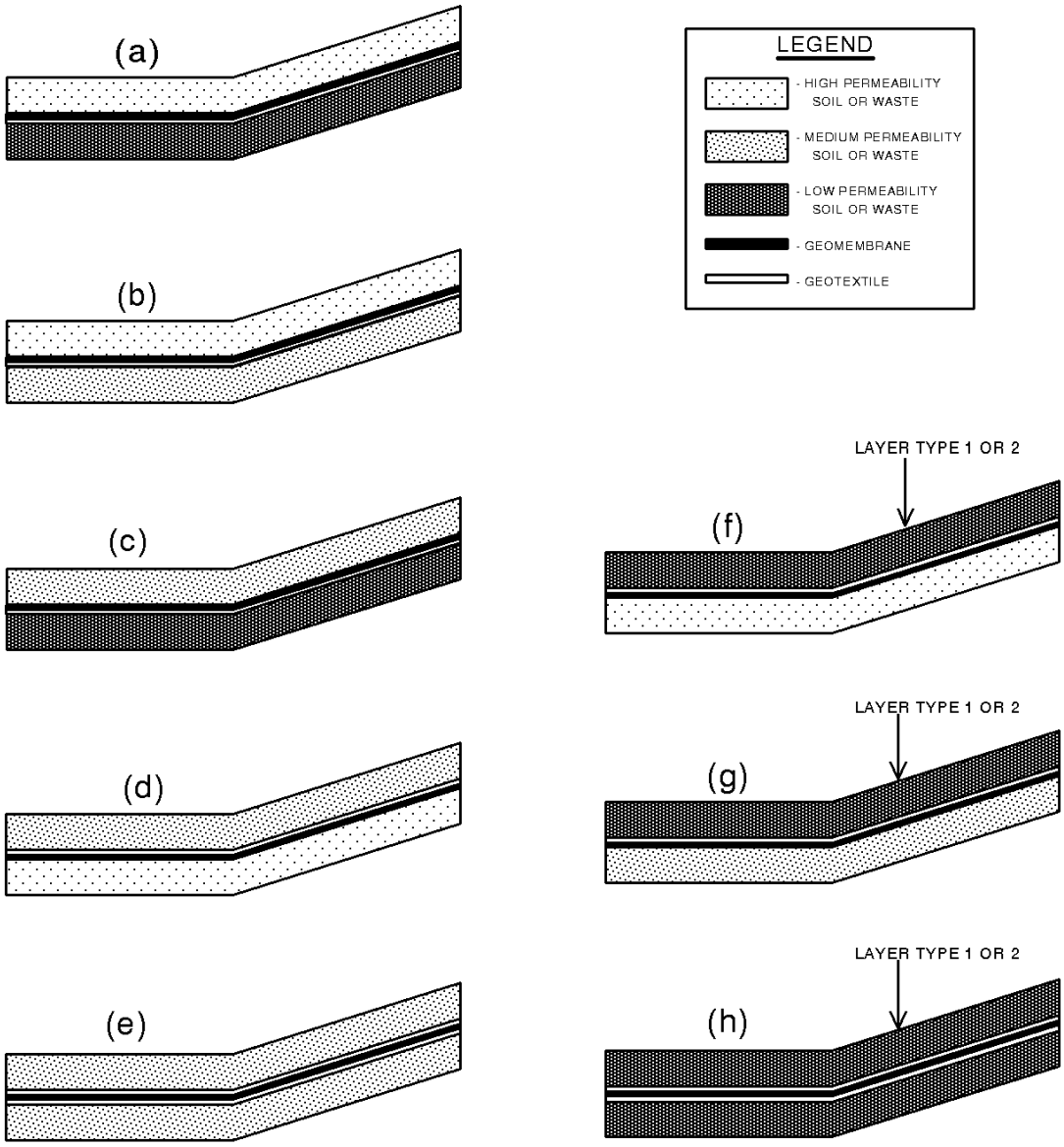

Figure 15. Geomembrane Liner Design Case 5

installation.

4.18 LATERAL DRAINAGE

Unconfined lateral drainage from porous media is modeled by the Boussinesq equation (Darcy's law coupled with the continuity equation), employing the Dupuit-Forcheimer (D-F) assumptions. The D-F assumptions are that, for gravity flow to a shallow sink, the flow is parallel to the liner and that the velocity is in proportion to the

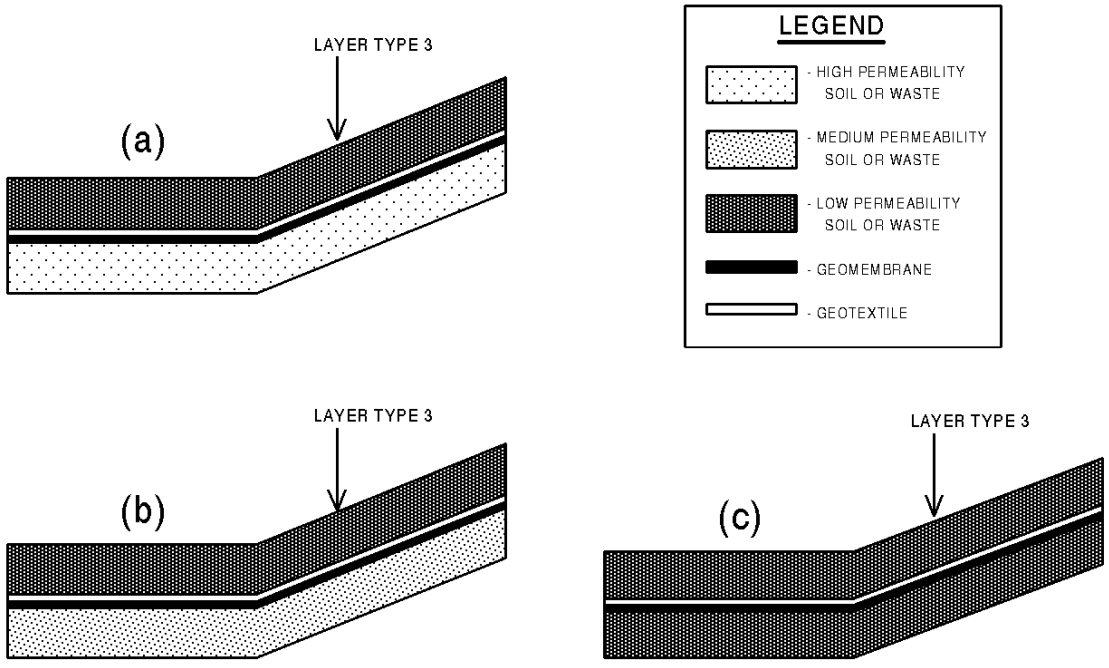

Figure 16. Geomembrane Liner Design Case 6

slope of the water table surface and independent of depth of flow (Forcheimer, 1930). These assumptions imply the head loss due to flow normal to the liner is negligible, which is valid for drain layers with high hydraulic conductivity and for shallow depths of flow, depths much shorter than the length of the drainage path. The Boussinesq equation may be written as follows (See Figure 17 for definition sketch):

$$f \frac{\partial h}{\partial t} = K_D \frac{\partial}{\partial l} \left[(h - l \sin \alpha) \frac{\partial h}{\partial l} \right] + R \qquad (169)$$

where

f = drainable porosity (porosity minus field capacity), dimensionless

h = elevation of phreatic surface above liner at edge of drain, cm

t = time, sec

K_D = saturated hydraulic conductivity of drain layer, cm/sec

l = distance along liner surface in the direction of drainage, cm

α = inclination angle of liner surface

R = net recharge (impingement minus leakage), cm/sec

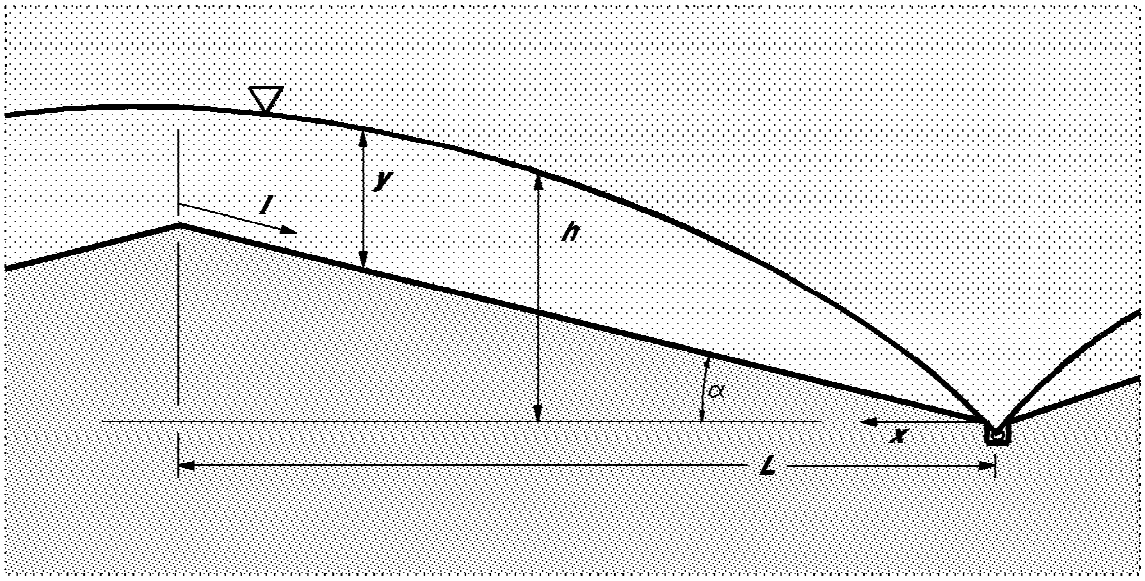

Figure 17. Lateral Drainage Definition Sketch

Where the saturated zone directly above the liner extends into more than one modeling segment, the saturated hydraulic conductivity, K_D, is assigned the weight-averaged saturated hydraulic conductivity of the saturated zone.

$$K_D = \frac{\sum_{j=n}^{m} K_s(j) \cdot d(j)}{y} \qquad where \quad y = \sum_{j=n}^{m} d(j) \tag{170}$$

where

$K_s(j)$ = saturated hydraulic conductivity of segment j, cm/sec

$d(j)$ = thickness of saturated soil in segment j, cm

m = number of the lowest unsaturated segment in subprofile

n = number of the segment directly above the liner in subprofile

y = depth of saturated lateral drainage (h - x *tan* α), cm

x = horizontal distance from drain, cm

The lateral drainage submodel assumes that the relationship between lateral drainage rate and average saturated depth for steady flow approximates the overall relationship for an unsteady drainage event. For steady flow, the lateral drainage rate is equal to the net recharge.

$$\frac{\partial h}{\partial t} = 0 \qquad \frac{dQ_D}{dx} = R \qquad Q_{D_o} = R \cdot L \qquad q_D = \frac{Q_{D_o}}{L} \tag{171}$$

where

Q_D = lateral drainage rate per unit width of drain at any x, cm^2/sec

Q_{D_o} = lateral drainage rate into collector pipe at drain, $x = 0$, (flow rate per unit length of collector), cm^2/sec

L = length of the horizontal projection of the liner surface (maximum drainage distance) cm

q_D = lateral drainage rate at drain in flow per unit area of landfill, cm/sec

Translating the axis from l (parallel to the liner) to x (horizontal) and substituting for R, the steady lateral drainage equation is described as follows:

$$R = \frac{Q_{D_o}}{L} = q_D = K_D \cos^2 \alpha \frac{d}{dx}\left(y \frac{dh}{dx}\right) \tag{172}$$

After expressing h in terms of y and expanding, Equation 171 can be rewritten as follows:

$$y \frac{d^2 y}{dx^2} + \left(\frac{dy}{dx}\right)^2 + (\tan \alpha) \frac{dy}{dx} = \frac{q_D}{K_D \cos^2 \alpha} \tag{173}$$

Nondimensionally, it can be rewritten as follows:

$$y^* \frac{d^2 y^*}{dx^{*2}} + \left(\frac{dy^*}{dx^*}\right)^2 + (\tan \alpha) \frac{dy^*}{dx^*} = \frac{q_D^*}{\cos^2 \alpha} \tag{174}$$

where

x^* = x / L , nondimensional horizontal distance

y^* = y / L , nondimensional depth of saturation above liner

q_D^* = q_D / K_D , nondimensional lateral drainage rate

Assuming a unit hydraulic gradient in the direction of flow at the drain, the boundary conditions for Equation 174 are

$$\frac{dy^*}{dx^*} = \frac{1}{\cos\alpha} - \tan\alpha \qquad at \quad x^* = 0 \tag{175}$$

$$y^* \left(\frac{dy^*}{dx^*} + \tan\alpha \right) = 0 \qquad at \quad x^* = 1 \tag{176}$$

An alternative boundary condition is used for shallow saturated depths and small lateral drainage rates [$q_D^* \leq 0.4(\sin^2\alpha)$]. For values of $q_D^* > 0.4(\sin^2\alpha)$, the depth of saturated drainage media at the upper end of the liner is greater than 0.

$$y^* = \frac{q_D^*}{\cos^2\alpha} \tag{177}$$

Equation 177 can be solved analytically for the two limiting cases by simplifying, employing the boundary conditions and integrating from $x^* = 0$ to $x^* = 1$. For small drain rates or shallow saturated depths, such that $q_D^* < 0.4(\sin^2\alpha)$ or $\bar{y}^* < 0.2 \tan\alpha$ ($\bar{y}^*$ = average depth of saturation above the entire liner),

$$\bar{y}^* = \frac{q_D^*}{2\,(\sin\alpha)\,(\cos\alpha)} \qquad for \quad q_D^* < 0.4\,\sin^2\alpha$$

$$or \tag{178}$$

$$q_D^* = 2\,(\sin\alpha)\,(\cos\alpha)\,\bar{y}^* \qquad for \quad \bar{y}^* < 0.2\,\tan\alpha$$

For large drainage rates, such that $q_D^* \gg 0.4(\sin^2\alpha)$ or $\bar{y}^* \gg 0.2 \tan\alpha$,

Equation 174 was solved numerically for a wide range of values of the parameters, q_D^* and α. The nondimensional average depth of saturation on top of the liner ($\bar{y}^*$) was computed numerically for each solution. Analysis of these solutions showed that the

$$\bar{y}^{*} = \frac{\pi \sqrt{q_D^{*}}}{4 \cos\alpha} \qquad for \quad q_D^{*} \gg 0.4 \sin^2\alpha$$

$$or \qquad (179)$$

$$q_D^{*} = \left(\frac{4 \bar{y}^{*} \cos\alpha}{\pi} \right)^2 \qquad for \quad \bar{y}^{*} \gg 0.2 \tan\alpha$$

relationship among q_D, y, L, K, and α is closely approximated by the following equation which converges to the analytical solutions for small drainage rates (Equation 178) and large drainage rates (Equation 179).

$$\bar{y}^{*} = \frac{\pi \sqrt{q_D^{*}}}{4 \cos\alpha} \left(\frac{2 \sqrt{0.4}}{\pi} \right) \left(\frac{q_D^{*}}{0.4 \sin^2\alpha} \right)^{\left[\frac{1}{2 \ln\left(\frac{2\sqrt{0.4}}{\pi} \right)} \right]} \qquad for \quad q_D^{*} \geq 0.4 \sin^2\alpha \qquad (180)$$

This two-part function (Equations 179 and 180) is continuous and smooth and matches the closed-form, asymptotic solutions for the cases where $\bar{y}^{*} \ll \tan\alpha$ and $\bar{y}^{*} \gg \tan\alpha$. The estimate of q_D^{*} given by Equations 178 and 180 is within one percent of the value obtained by solving Equation 174 numerically. Equations 178 and 180 are used to compute q_D in the lateral drainage submodel. The equations are applied iteratively along with the liner leakage or percolation equations and storage equation to solve concurrently for the average depth of saturation, the liner leakage or percolation and the average depth of saturation above the liner during each time period. The process is repeated for each subprofile with a lateral drainage layer for every time step.

4.19 LATERAL DRAINAGE RECIRCULATION

The lateral drainage from any subprofile may be collected or recirculated. If collected, that fraction of the drainage is removed from the landfill and the quantity is reported as a volume collected. If recirculated, that fraction of the drainage from the subprofile is stored during the day and then uniformly distributed the next day throughout the specified layer. The recirculation is then applied in the vertical water routing procedure using Equations 124 and 134. Recirculation can be distributed to any layer that is not a liner.

where

$RC_i(j)$ = recirculation into segment j during a timestep on day i, inches

$$RC_i(j) = \frac{1}{N(k_j)} \sum_{k=1}^{nk} \sum_{n=1}^{N(k)} \frac{FRC(k,j)\ q_D(k)_{i-1,n}}{N(k)} \qquad (181)$$

$N(k_j)$ = number of timesteps in a day for subprofile k containing segment j

k = number of the subprofile

nk = total number of subprofiles in the landfill

n = number of the timestep in day i-1

$N(k)$ = total number of timesteps in a day for subprofile k, day^{-1}

$FRC(k,j)$ = fraction of the lateral drainage from subprofile k that is recirculated to segment j

$q_d(k)_{i-1,n}$ = lateral drainage rate from subprofile k during timestep n on day i-1, inches/day

4.20 SUBSURFACE INFLOW

Subsurface inflow is treated as steady, uniform seepage into a layer. Inflow may be specified for any layer. If the inflow for a liner is specified, the inflow is added to the inflow into the next lower layer that is not a liner. If inflow is specified for a liner system that is on the bottom of the landfill profile, the inflow is added to the inflow of the first layer above the liner system. The subsurface inflow is then applied in the vertical water routing procedure using Equations 124 and 134. The inflow is specified for each layer in the input. The inflow is specified as the volume per year per unit area, which is then simply converted by the program to a volume per time step based on a unit area. Volume per unit area is used throughout the program for storage and flows.

4.21 LINKAGE OF SUBSURFACE FLOW PROCESSES

The drainage rate out of a subprofile must equal the sum of lateral drainage rate and the leakage rate through the liner system. The subsurface water routing, liner leakage and lateral drainage calculations are linked as follows:

1. Water is routed through the subprofile from top to bottom by unsaturated vertical drainage using Equation 134.

2. The total drainage rate out of the segment directly above the liner system is initially assumed to be the same as in the previous time step. Excess water is backed up through the subprofile as necessary.

3. The average depth of saturation above the liner system and the effective lateral hydraulic conductivity of the saturated zone are computed using Equation 135. The depth or head is only an estimate since it is based on estimated drainage out of the subprofile.

4. Lateral drainage and liner leakage or percolation are computed using Equation 178 or 180 for lateral drainage, Equation 137 for soil liner percolation, and Equations 141, 143, 145, 147, 148, 151, 152, 154, 155, 157, 158, 160, 161, 163, 164, 166, 167 or 168 for geomembrane liner leakage. The estimated saturated depth is used in these computations.

5. A new estimate of the average depth of saturation is generated by updating the water storage using the computed lateral drainage and percolation/leakage. If the new estimate is within the larger of 5 percent or 0.01 inches of the original estimate, then the updated water storage and the computed rates are accepted. If not, the original and new estimate are averaged to generate a new estimate and steps 4 and 5 are repeated until the convergence criterion is met. If the estimated and computed total drainage are greater than the available gravity water (storage in excess of field capacity), then the total drainage is assigned the value of the gravity water. Then, the leakage and lateral drainage volumes are proportional to the relative rates, and the depth of saturation is computed by Equation 178 using the assigned lateral drainage rate.

6. The procedure is repeated for each time step in a day, and the lateral drainage volumes are summed as are the liner leakage/percolation volumes for the subprofile before beginning computations for the next subprofile. The daily lateral drainage is then partitioned to removal and recirculation as specified in the input. The liner leakage/percolation is assigned as drainage into the next subprofile or out of the landfill. The depths of saturation for time steps during the day are averaged and reported as average daily head.

SECTION 5

ASSUMPTIONS AND LIMITATIONS

5.1 METHODS OF SOLUTION

The modeling procedures documented in the previous section are necessarily based on many simplifying assumptions. Most of these are stated in the sections documenting the individual procedures. Generally, these assumptions are reasonable and consistent with the objectives of the program when applied to standard landfill designs. However, some of these assumptions may not be reasonable for unusual designs. The major assumptions and limitations of the program are summarized below.

Precipitation on days when the mean air temperature is below freezing is assumed to occur as snow. Snowmelt is assumed to be a function of energy from air temperature, solar radiation and rainfall. Solar radiation effects are included in an empirical melt factor. In addition, groundmelt is assumed to occur at a constant rate of 0.5 mm/day as long as the ground is not frozen. Snow and snowmelt are subject to evaporation prior to runoff and infiltration. The program does not consider the effects of aspect angle or drifting in its accounting of snow behavior.

Prediction of frozen soil conditions is a simple, empirical routine based on antecedent air temperatures. Thaws are based on air temperatures and climate data. Soils while frozen are assumed to be sufficiently wet so as to impede infiltration and to promote runoff. Similarly, no evapotranspiration and drainage are permitted from the evaporative zone while frozen.

Runoff is computed using the SCS method based on daily amounts of rainfall and snowmelt. The program assumes that areas adjacent to the landfill do not drain onto the landfill. The time distribution of rainfall intensity is not considered. The program cannot be expected to give accurate estimates of runoff volumes for individual storm events on the basis of daily rainfall data. However, because the SCS rainfall-runoff relationship is based on considerable daily field data, long-term estimates of runoff should be reasonable. One would expect the SCS method to underestimate runoff from short duration, high intensity storms; larger curve numbers could be used to compensate if most of the precipitation is from short duration, high intensity storms. The SCS method does not explicitly consider the length and slope of the surface over which overland flow occurs; however, a routine based on a kinematic wave model was developed to account for surface slope and length.

Potential evapotranspiration is modeled by an energy-based Penman method. As applied, the program uses average quarterly relative humidity and average annual wind speed. It is assumed that these data yield representative monthly results. Similarly, the program assumes that the relative humidity is 100% on days when precipitation occurs.

The program uses an albedo of 0.23 for soils and vegetation and 0.60 for snow. The actual evapotranspiration is a function of other data, also. The solar radiation and temperature data are often synthetically generated. The vegetation data is generated by a vegetative growth model. The evaporative zone depth is assumed to be constant throughout the simulation period. However, outside of the growing season, the actual depth of evapotranspiration is limited to the maximum depth of evaporation of soil water, which is a function of the soil saturated hydraulic conductivity.

Vegetative growth is based on a crop growth model. Growth is assumed to occur during the first 75% of the growing season based on heating units. Recommendations for the growing season are based primarily for summer grasses and assume that the growing season is that portion of the year when the temperature is above 50 to 55 °F. However, the user may specify a more appropriate growing season for different vegetation. The optimal growth temperature and the base temperature are based on a mixture of winter and summer perennial grasses. It is assumed that other vegetation have similar growth constraints and conditions. It is further assumed that the vegetation is not harvested.

The HELP program assumes Darcian flow for vertical drainage through homogeneous, temporally uniform soil and waste layers. It does not consider preferential flow through channels such as cracks, root holes or animal burrows. As such, the program will tend to overestimate the storage of water during the early part of the simulation and overestimate the time required for leachate to be generated. The effects of these limitations can be minimized by specifying a larger effective saturated hydraulic conductivity and a smaller field capacity. The program does increase the effective saturated hydraulic conductivity of default soils for vegetation effects.

Vertical drainage is assumed to be driven by gravity alone and is limited only by the saturated hydraulic conductivity and available storage of lower segments. If unrestricted, the vertical drainage rate out of a segment is assumed to equal the unsaturated hydraulic conductivity of the segment corresponding to its moisture content, provided that moisture content is greater than the field capacity or the soil suction of the segment is less than the suction of the segment directly below. The unsaturated hydraulic conductivity is computed by Campbell hydraulic equation using Brooks-Corey parameters. It is assumed that all materials conducting unsaturated vertical drainage have moisture retention characteristics that can be well represented by Brooks-Corey parameters and the Campbell equation. The pressure or soil suction gradient is ignored when applying the Campbell equation; therefore, the unsaturated drainage and velocity of the wetting front may be underestimated. This is more limiting for dry conditions in the lower portion of the landfill; the effects of this limitation can be reduced by specifying a larger saturated hydraulic conductivity. For steady-state conditions, this limitation has little or no effect.

The vertical drainage routine does not permit capillary rise of water from below the evaporative zone depth. Evapotranspiration is not modeled as capillary rise, but rather as a distributed extraction that emulates capillary rise. This is limiting for dry conditions where the storage of water to satisfy evaporative demand is critical and for designs where

the depth to the liner is shallow. This limitation can be reduced by increasing the field capacity in the evaporative zone and the evaporative zone depth.

Percolation through soil liners is modeled by Darcy's law, assuming free drainage from the bottom of the liner. The liners are assumed to be saturated at all times, but leakage occurs only when the soil moisture of the layer above the liner is greater than the field capacity. The program assumes that an average hydraulic head can be computed from the soil moisture and that this head is applied over the entire surface of the liner. As such, when the liner is leaking, the entire liner is leaking at the same rate. The liners are assumed to be homogeneous and temporally uniform.

Leakage through geomembrane is modeled by a family of theoretical and empirical equations. In all cases, leakage is a function of hydraulic head. The program assumes that holes in the geomembrane are dispersed uniformly and that the average hydraulic head is representative of the head at the holes. The program further assumes that the holes are predominantly circular and consist of two sizes. Pinholes are assumed to be 1 mm in diameter while installation defects are assumed to have an cross-sectional area of 1 cm^2. It is assumed that holes of other shapes and sizes could be represented as some quantity of these characteristic defects. Leakage through holes in geomembranes is often restricted by an adjacent layer or soil or material termed the controlling soil layer. Materials having a saturated hydraulic conductivity greater than or equal to $1x10^{-1}$ cm/sec are considered to be a high permeability material; materials having a saturated hydraulic conductivity greater than or equal to $1x10^{-4}$ cm/sec but less than $1x10^{-1}$ cm/sec are considered to be a medium permeability material; and materials having a saturated hydraulic conductivity less than $1x10^{-4}$ cm/sec are considered to be a low permeability material. The program assumes that no aging of the liner occurs during a simulation.

The lateral drainage model is based on the assumption that the lateral drainage rate and average saturated depth relationship that exists for steady-state drainage also holds for unsteady drainage. This assumption is reasonable for leachate collection, particularly for closed landfills where drainage conditions should be fairly steady. Where drainage conditions are more variable, such as in the cover drainage system, the lateral drainage rate is underestimated when the saturated depth is building and overestimated when the depth is falling. Overall, this assumption causes the maximum depth to be slightly overestimated and the maximum drainage rate to be slightly underestimated. The long-term effect on the magnitude of the water balance components should be small. As with leakage or percolation through liners, the average saturated depth is computed from the gravity water and moisture retention properties of the drain layer and other layers when the drain layer is saturated. The program assumes that horizontal and vertical saturated hydraulic conductivity to be of similar magnitude and that the horizontal value is specified for lateral drainage layer.

Subsurface inflow is assumed to occur at a constant rate and to be uniformly distributed spatially throughout the layer, despite entering the side. This assumption causes a delay in its appearance in the leachate collection and more rapid achievement of steady-state moisture conditions. This limitation can be minimized by dividing the

landfill into sections where inflow occurs and sections without inflow.

Leachate recirculation is assumed to be uniformly distributed throughout the layer by a manifold or distribution system. Leachate collected on one day for recirculation is distributed steadily throughout the following day.

5.2 LIMITS OF APPLICATION

The model can simulate water routing through or storage in up to twenty layers of soil, waste, geosynthetics or other materials for a period of 1 to 100 years. As many as five liner systems, either barrier soil, geomembrane or composite liners, can be used. The model has limits on the order that layers can be arranged in the landfill profile. Each layer must be described as being one of four operational types: vertical percolation, lateral drainage, barrier soil liner or geomembrane liner. The model does not permit a vertical percolation layer to be placed directly below a lateral drainage layer. A barrier soil liner may not be placed directly below another barrier soil liner. A geomembrane liner may not be placed directly below another geomembrane liner. Three or more liners, barrier soil or geomembrane, cannot be placed adjacent to each other. The top layer may not be a barrier soil or geomembrane liner. If a liner is not placed directly below the lowest lateral drainage layer, the lateral drainage layers in the lowest subprofile are treated by the model as vertical percolation layers. If a geomembrane liner is specified as the bottom layer, the soil or material above the liner is assumed to be the controlling soil layer. No other restrictions are placed on the order of the layers.

The lateral drainage equation was developed and tested for the expected range of hazardous waste landfill design specifications. The ranges examined for slope and maximum drainage length of the drainage layer were 0 or 30 percent and 25 to 2000 feet; however, the formulation of the equations indicates that the range of the slope could be extended readily to 50 percent and the length could be extended indefinitely.

Several relations must exist between the moisture retention properties of a material. The porosity, field capacity and wilting point can theoretically range from 0 to 1 in units of volume per volume, but the porosity must be greater than the field capacity, and the field capacity must be greater than the wilting point. The general relation between soil texture class and moisture retention properties is shown in Figure 2.

The initial soil moisture content cannot be greater than the porosity or less than the wilting point. If the initial moisture contents are initialized by the program, the moisture contents are set near the steady-state values. However, the moisture contents of layers below the top liner system or cover system are specified too high for arid and semi-arid locations and too low for very wet locations, particularly when thick profiles are being modeled.

Values for the maximum leaf area index may range from 0 for bare ground to 5.0 for

an excellent stand of grass. Greater leaf area indices may be used but have little impact on the results. Detailed recommendations for leaf area indices and evaporative depths are given in the program. For numerical stability, the minimum evaporative zone depth should be at least 3 inches.

The program computes the evaporation coefficient for the cover soils based on their soil properties. The default values for the evaporation coefficient are based on experimental results reported by Ritchie (1972) and others. The model imposes upper and lower limits of 5.50 and 3.30 for the evaporation coefficient so as not to exceed the range of experimental data.

The program performs water balance analysis for a minimum period of one year. All simulations start on the January 1 and end on December 31. The condition of the landfill, soil properties, thicknesses, geomembrane hole density, maximum level of vegetation, etc., are assumed to be constant throughout the simulation period. The program cannot simulate the actual filling operation of an active landfill. Active landfills are modeled a year at a time, adding a yearly lift of material and updating the initial moisture of each layer for each year of simulation.

REFERENCES

Anderson, E. (1973). "National Weather Service river forecast system--snow accumulation and ablation model," Hydrologic Research Laboratory, National Oceanic and Atmospheric Administration, Silver Spring, MD.

Arnold, J. G., Williams, J. R., Nicks, A. D., and Sammons, N. B. (1989). "SWRRB, a simulator for water resources in rural basins," Agricultural Research Service, USDA, Texas A&M University Press, College Station, TX.

Bartos, M. J., and Palermo, M. R. (1977). "Physical and engineering properties of hazardous industrial wastes and sludges," Technical Resource Document EPA-600/2-77-139, US Army Engineer Waterways Experiment Station, Vicksburg, MS.

Bonaparte, R., Giroud, J. P., and Gross, B. A. (1989). "Rates of leakage through landfill liners," *Proceedings of geosynthethetics 1989 conference*, GeoServices Inc., San Diego, CA.

Brakensiek, D. L., Engleman, R. L., and Rawls, W. J. (1981). "Variation within texture classes of soil water parameters," *Transactions of the American Society of Agricultural Engineers* 24(2), 335-339.

Brakensiek, D. L., Rawls, W. J., and Stephenson, G. R. (1984). "Modifying SCS hydrologic soil groups and curve numbers for rangeland soils," *American Society of Agricultural Engineers* Paper No. PNR-84-203.

Brooks, R. H. and Corey, A. T. (1964). "Hydraulic properties of porous media," Hydrology Paper No. 3, Colorado State University, Fort Collins, CO. 27 pp.

Brown, K. W., Thomas, J. C., Lytton, R. L., Jayawikrama, P., and Bahrt, S. C. (1987). "Quantification of leak rates through holes in landfill liners," Technical Resource Document EPA/600/S2-87-062, US Environmental Protection Agency, Cincinnati, OH.

Brutsaert, W. (1967). "Some methods of calculating unsaturated permeability," *Transactions of the American Society of Agricultural Engineers* 10(3), 400-404.

Campbell, G. S. (1974). "A simple method for determining unsaturated hydraulic conductivity from moisture retention data," *Soil Science* 117(6), 311-314.

Darcy, H. (1856). *Les fontaines publique de la ville de Dijon*. Dalmont, Paris. As cited by Hillel, D. (1982). *Introduction to soil physics*. Academic Press, New York.

Das, B. M., Tarquin, A. J., and Jones, A. D. (1983). "Geotechnical properties of a copper slag," Transportation Research Record 941, Transportation Research Board, National Academy of Sciences, Washington, D.C.

Dozier, T. S. (1992). "Examination and modification of three surface hydrologic processes in the HELP model," M.S. thesis, Mississippi State University, Mississippi State, MS.

Elsbury, B. R., Daniel, D. E., Sraders, G. A., and Anderson, D. C. (1990). "Lessons learned from compacted clay liner," *Journal of Geotechnical Engineering* 116(11).

Fleenor, B. (1993). "Examination of vertical water movement HELP Beta Version 3 versus RMA42," M.S. thesis, University of California, Davis, CA.

Forchheimer, P. (1930). *Hydraulik*. 3rd ed., Teuber, Leipzig and Berlin. As cited by Hillel, D. (1982). *Introduction to soil physics*. Academic Press, New York.

Freeze, R. A., and Cherry, J. A. (1979). *Groundwater*. Prentice-Hall, Englewood Cliffs, NJ.

Fukuoka, M. (1985). "Outline of large scale model test on waterproof membrane," Unpublished Report, Japan.

Fukuoka, M. (1986). "Large scale permeability tests for geomembrane-subgrade system," *Proceedings of the third international conference on geotextiles, volume 3*," Balkema Publishers, Rotterdam, The Netherlands.

Geosyntec Consultants. (1993). "Long-term performance of high density polyethylene cap at Chem-Nuclear's proposed Illinois low-level radioactive waste disposal facility - original and revision," Boynton Beach, FL.

Giroud, J. P., Badu-Tweneboah, K., and Bonaparte, R. (1992). "Rate of leakage through a composite liner due to geomembrane defects," *Geotextiles and Geomembranes* 11(1), 1-28.

Giroud, J. P., and Bonaparte, R. (1985). "Waterproofing and drainage: Geomembranes and synthetic drainage layers." *Geotextiles and geomembranes-- definitions, properties, and design - selected papers, revisions, and comments*, 2nd ed., Industrial Fabrics Association International, St. Paul, MN.

Giroud, J. P., and Bonaparte, R. (1989). "Leakage through liners constructed with geomembrane liners--parts I and II and technical note," *Geotextiles and Geomembranes* 8(1), 27-67, 8(2), 71-111, 8(4), 337-340.

Giroud, J. P., Khatami, A., and Badu-Tweneboah, K. (1989). "Evaluation of the rate of leakage through composite liners," *Geotextiles and Geomembranes* 8(4), 337-340.

Hillel, D. (1982). *Introduction to soil physics*. Academic Press, New York.

Horton, R. E. (1919). "Rainfall interception," *Monthly Weather Review* 47(9), 603-623.

Industrial Fabrics Association International. (1991). "Geotextile fabrics report-- 1992 specifiers guide," Volume 9, Number 9, St. Paul, MN.

Jayawickrama, P. W., Brown, K. W., Thomas, J. C., and Lytton, R. L. (1988). "Leakage rates through flaws in membrane liners," *Journal of Environmental Engineering* 114(6).

Jensen, M. E., ed. (1973). *Consumptive use of water and irrigation water requirements*. American Society of Civil Engineers, New York.

Knisel, W. G., ed. (1980). "CREAMS, a field scale model for chemical runoff and erosion from agricultural management systems. Vols. I, II, and III" Conservation Report 26, USDA-SEA. 643 pp.

Knisel, W. G., Moffitt, D. C., and Dumper, T. A. (1985). "Representing seasonally frozen soil with the CREAMS model," *American Society of Agricultural Engineering* 28 (September - October), 1487-1492.

Linsley, R. K., Kohler, M. A., and Paulhus, J. L. H. (1982). *Hydrology for engineers*. 3rd ed., McGraw-Hill, New York. 508 pp.

McAneny, C. C., Tucker, P. G., Morgan, J. M., Lee, C. R., Kelley, M. F., and Horz, R. C. (1985). "Covers for uncontrolled hazardous waste sites," Technical Resource Document EPA/540/2-85/002, US Army Engineer Waterways Experiment Station, Vicksburg, MS.

National Oceanic and Atmospheric Administration. (1974). *Climatic atlas of the United States.* US Department of Commerce, Environmental Science Services Administration, Nation Climatic Center, Ashville, NC. 80 pp.

Oweis, I. S., Smith, D. A., Ellwood, R. B., and Greene, D. S. (1990). "Hydraulic characteristics of municipal refuse," *Journal of Geotechnical Engineering* 116(4), 539-553.

Penman, H. L. (1963). "Vegetation and hydrology," Technical Comment No. 53, Commonwealth Bureau of Soils, Harpenden, England.

Perrier, E. R., and Gibson, A. C. (1980). "Hydrologic simulation on solid waste disposal sites," Technical Resource Document EPA-SW-868, US Environmental Protection

Agency, Cincinnati, OH. 111 pp.

Perry, J. S., and Schultz, D. I. (1977). "Disposal and alternate uses of high ash paper-mill sludge." *Proceedings of the 1977 national conference on treatment and disposal of industrial wastewaters and residues*, University of Houston, Houston, TX.

Poran, C. J., and Ahtchi-Ali, F. (1989). "Properties of solid waste incinerator fly ash," *Journal of Geotechnical Engineering* 115(8), 1118-1133.

Rawls, W. J., Brakensiek, D. L., and Saxton, K. E. (1982). "Estimation of soil water properties," *Transactions of the American Society of Civil Engineers*. pp. 1316-1320.

Richardson, C. W. (1981). "Stochastic simulation of daily precipitation, temperature, and solar radiation," *Water Resources Research* 17(1), 182-190.

Richardson, C. W., and Wright, D. A. (1984). "WGEN: A model for generating daily weather variables," ARS-8, Agricultural Research Service, USDA. 83 pp.

Ritchie, J. T. (1972). "A model for predicting evaporation from a row crop with incomplete cover," *Water Resources Research* 8(5), 1204-1213.

Ruffner, J. A. (1985). *Climates of the states, National Oceanic and Atmospheric Administration narrative summaries, tables, and maps for each state, volume 1 Alabama - New Mexico and volume 2 New York - Wyoming and territories*. Gale Research Company, Detroit, MI. 758 pp. and 1572 pp.

Rushbrook, P. E., Baldwin, G., and Dent, C. B. (1989). "A quality-assurance procedure for use at treatment plants to predict the long-term suitability of cement-based solidified hazardous wastes deposited in landfill sites." *Environmental Aspects of Stabilization and Solidification of Hazardous and Radioactive Wastes*, ASTM STP 1033, P. L. Cote' and T. M. Gilliam, eds., American Society for Testing and Materials, Philadelphia, PA.

Saxton, K. E., Johnson, H. P., and Shaw, R. H. (1971). "Modeling evapotranspiration and soil moisture." *Proceedings of american society of agricultural engineers 1971 winter meeting*, St. Joseph, MI. No. 71-7636.

Schroeder, P. R., and Gibson, A. C. (1982). "Supporting documentation for the hydrologic simulation model for estimating percolation at solid waste disposal sites (HSSWDS)," Draft Report, US Environmental Protection Agency, Cincinnati, OH. 153 pp.

Schroeder, P. R., Morgan, J. M., Walski, T. M., and Gibson, A. C. (1984a). "The hydrologic evaluation of landfill performance (HELP) model, volume I, user's guide for

version 1," Technical Resource Document EPA/530-SW-84-009, US Environmental Protection Agency, Cincinnati, OH. 120 pp.

Schroeder, P. R., Gibson, A. C., and Smolen, M. D. (1984b). "The hydrologic evaluation of landfill performance (HELP) model, volume II, documentation for version 1," Technical Resource Document EPA/530-SW-84-010, US Environmental Protection Agency, Cincinnati, OH. 256 pp.

Schroeder, P. R., and Peyton, R. L. (1987a). "Verification of the hydrologic evaluation of landfill performance (HELP) model using field data," Technical Resource Document, EPA 600/2-87-050, US Environmental Protection Agency, Cincinnati, OH. 163 pp.

Schroeder, P. R., and Peyton, R. L. (1987b). "Verification of the lateral drainage component of the HELP model using physical models," Technical Resource Document, EPA 600/2-87-049, US Environmental Protection Agency, Cincinnati, OH. 117 pp.

Schroeder, P. R., Peyton, R. L., McEnroe, B. M., and Sjostrom, J. W. (1988a). "The hydrologic evaluation of landfill performance (HELP) model: Volume III. User's guide for version 2," Internal Working Document EL-92-1, Report 1, US Army Engineer Waterways Experiment Station, Vicksburg, MS. 87 pp.

Schroeder, P. R., McEnroe, B. M., Peyton, R. L., and Sjostrom, J. W. (1988b). "The hydrologic evaluation of landfill performance (HELP) model: Volume IV. Documentation for version 2," Internal Working Document EL-92-1, Report 2, US Army Engineer Waterways Experiment Station, Vicksburg, MS. 72 pp.

Swain, A. (1979). "Field studies of pulverized fuel ash in partially submerged conditions." *Proceedings of the symposium of the engineering behavior of industrial and urban fill*, The Midland Geotechnical Society, University of Birmingham, Birmingham, England, pp. D49-D61.

Tchobanoglous, G., Theisen, H., and Eliassen, R. (1977). *Solid wastes: engineering principles and management issues*. McGraw-Hill, New York.

Thompson, F. L., and Tyler, S. W. (1984). "Comparison of Two Groundwater Flow Models--UNSAT1D and HELP," EPRI CS-3695, Topical Report, October, Prepared by Battelle, Pacific Northwest Laboratories, for Electric Power Research Institute, Palo Alto, CA, 71 pp.

Toth, P. S., Chan, H. T., and Cragg, C. B. (1988). "Coal ash as a structural fill, with special reference to the Ontario experience," *Canadian Geotechnical Journal* 25, 694-704.

USDA, Soil Conservation Service. (1985). *National engineering handbook, section 4,*

hydrology. US Government Printing Office, Washington, D.C.

Viessman, W. Jr., Knapp, J. W., Lewis, G. L., and Harbaugh, T. E. (1977). *Introduction to hydrology*. 2nd ed., Harper and Row Publishers, New York.

Woolhiser, D. A., Smith, R. E., and Goodrich, D. C. (1990). "KINEROS, a kinematic runoff and erosion model: Documentation and user manual," ARS-77, US Department ofAgriculture, Agricultural Research Service, 130 pp.

Zeiss, C., and Major, W. (1993). "Moisture flow through municipal solid waste: patterns and characteristics," *Journal of Environmental Systems* 22(3), 211-232.

Hydraulic Conductivity and Swell of Nonprehydrated Geosynthetic Clay Liners Permeated with Multispecies Inorganic Solutions

Dale C. Kolstad, M.ASCE[1]; Craig H. Benson, M.ASCE[2]; and Tuncer B. Edil, M.ASCE[3]

Abstract: The influence of multispecies inorganic solutions on swelling and hydraulic conductivity of non-prehydrated geosynthetic clay liners (GCLs) containing sodium bentonite was examined. Ionic strength and the relative abundance of monovalent and divalent cations (RMD) in the permeant solution were found to influence swell of the bentonite, and the hydraulic conductivity of GCLs. Swell is directly related to RMD and inversely related to ionic strength, whereas hydraulic conductivity is directly related to ionic strength and inversely related to RMD. RMD has a greater influence for solutions with low ionic strength (e.g., 0.05 M), whereas concentration effects dominate at high ionic strength (e.g., 0.5 M). No discernable effect of cation species of similar valence was observed in the swell or hydraulic conductivity data for test solutions with similar ionic strength and RMD. A strong relationship between hydraulic conductivity and free swell was found, but the relationship must be defined empirically for a particular bentonite. A regression model relating hydraulic conductivity of the GCL to ionic strength and RMD of the permeant solution was developed. Predictions made with the model indicate that high hydraulic conductivities (i.e., $>10^{-7}$ cm/s) are not likely for GCLs in base liners in many solid waste containment facilities. However, for wastes with stronger leachates or leachates dominated by polyvalent cations, high hydraulic conductivities may occur.

DOI: 10.1061/(ASCE)1090-0241(2004)130:12(1236)

CE Database subject headings: Hydraulic conductivity; Swelling; Inorganic chemicals; Clay liners; Bentonite.

Introduction

Geosynthetic clay liners (GCLs) are factory-manufactured clay liners consisting of a layer of bentonite clay encased by geotextiles or glued to a geomembrane. GCLs have become a popular alternative to compacted clay liners in waste containment applications because of their relatively low cost, ease of installation, perceived resistance to environmental distress (e.g. freeze–thaw and wet–dry cycling), smaller air–space requirements, and low hydraulic conductivity to water ($<10^{-8}$ cm/s). For GCLs that do not contain a geomembrane, bentonite is responsible for the low hydraulic conductivity. Sodium (Na) montmorillonite mineral is the primary component of bentonite, and largely controls the hydraulic conductivity of GCLs (Shackelford et al. 2000).

A variety of studies have shown that the hydraulic conductivity and swelling of bentonite can be affected by inorganic permeant solutions (Alther et al. 1985; Shan and Daniel 1991; Egloffstein 1997, 2001; Quaranta et al. 1997; Ruhl and Daniel 1997; Petrov and Rowe 1997; Shackelford et al. 2000; Jo et al. 2001; Vasko et al. 2001; Ashmawy et al. 2002; Katsumi et al. 2002, 2003; Shan and Lai 2002). The general conclusion of these studies is that the hydraulic conductivity and swelling of GCLs is sensitive to the concentration of the permeant solution and the cation valence. In general, higher hydraulic conductivity and lower swell are obtained in more concentrated solutions or solutions with a preponderance of divalent cations. However, no systematic study has been made regarding how the concentration and relative proportions of monovalent and polyvalent cations in a multispecies (i.e., more than one cation species) solution affect swelling and hydraulic conductivity of bentonite and GCLs.

Several studies have been conducted in soil science regarding the effect of multispecies solutions on the hydraulic conductivity of montmorillonitic soils (Reeve and Bower 1960; McNeal and Coleman 1966; McNeal et al. 1966; Mustafa and Hamid 1975; Malik et al. 1992). However, these studies have focused on increasing the hydraulic conductivity of montmorillonitic soils for land drainage and agricultural applications rather than maintaining low hydraulic conductivity for containment applications. Moreover, none of these studies has focused on clay soils very rich in montmorillonite, such as the Na-bentonites used for GCLs.

This paper discusses how the ionic strength and relative amounts of monovalent and divalent cations in multispecies solutions affect swelling and hydraulic conductivity of nonprehydrated GCLs containing Na-bentonite. The focus is on applications where inorganic solutes are the primary factor affecting hydraulic conductivity (e.g., conventional solid waste containment facilities for municipal, hazardous, or mining wastes) and where complete prehydration (i.e., prehydration by permeation with distilled, deionized, or potable water) is unlikely. The effects of complete prehydration and organic compounds are discussed

[1]Environmental Engineer, Barr Engineering Company, 4700 West 77th St., Minneapolis, MN 55435. E-mail: dkolstad@barr.com

[2]Professor, Dept. of Civil and Environmental Engineering, Univ. of Wisconsin, Madison, WI 53706. E-mail: benson@engr.wisc.edu

[3]Professor, Dept. of Civil and Environmental Engineering, Univ. of Wisconsin, Madison, WI 53706. E-mail: edil@engr.wisc.edu

Note. Discussion open until May 1, 2005. Separate discussions must be submitted for individual papers. To extend the closing date by one month, a written request must be filed with the ASCE Managing Editor. The manuscript for this paper was submitted for review and possible publication on July 23, 2003; approved on April 6, 2004. This paper is part of the ***Journal of Geotechnical and Geoenvironmental Engineering***, Vol. 130, No. 12, December 1, 2004. ©ASCE, ISSN 1090-0241/2004/12-1236–1249/$18.00.

J. Geotech. Geoenviron. Eng. 2004.130:1236-1249.

by others (e.g., Shan and Daniel 1991; Petrov and Rowe 1997; Ruhl and Daniel 1997; Shackelford et al. 2000).

Background

Exchangeable Cations, Mobility of Water, and Hydration of Bentonite

A weak interlayer bond allows the montmorillonite crystal layers to separate during hydration as water molecules enter the interlayer space (Grim 1968; van Olphen 1977). Consequently, cations on the interlayer surfaces become exchangeable, which renders the physical properties of Na-montmorillonite susceptible to interactions with the permeant liquid. The degree of exchange depends on the valence, relative abundance, and size of the cations. Generally, cations of greater valence and smaller size replace cations of lower valence and larger size. The preference for replacement is the lyotropic series, which is $Li^+ < Na^+ < K^+ < Rb^+ < Cs^+ < Mg^{2+} < Ca^{2+} < Ba^{2+} < Cu^{2+} < Al^{3+} < Fe^{3+}$ (Sposito 1981; 1989; McBride 1994). Because Na^+ is at the lower end of the lyotropic series, Na-bentonites are prone to cation exchange when permeated with solutions containing divalent or trivalent ions (Sposito 1981).

Water in the pores of bentonite can be considered mobile or immobile. Mobile water is bulk pore water that is free to move under a hydraulic gradient. Immobile water is bound to the external and internal (i.e., interlayer) mineral surfaces by strong electrical forces, and is believed to act as an extension of the solid surface. When the amount of immobile water in the system increases, the hydraulic conductivity of bentonite decreases because the interparticle flow paths for mobile water become more constricted and tortuous. This is especially true in bentonites where swell is constrained (e.g., needle-punched GCLs or GCLs under confining pressure) (Reeve and Ramaddoni 1965; McNeal and Coleman 1966; McNeal et al. 1966; Lagerwerff et al. 1969; Mesri and Olson 1971; Petrov and Rowe 1997; Shackelford et al. 2000; Jo et al. 2001). Changes in the volume of immobile water also cause volume changes in the bentonite (swell occurs as the volume of immobile water increases). Thus swell and hydraulic conductivity are generally inversely related for bentonites (Shackelford et al. 2000; Jo et al. 2001; Ashmawy et al. 2002; Katsumi et al. 2002).

The fraction of the pore water that is immobile is proportional to the number of layers of water molecules hydrating the interlayer surfaces of the montmorillonite particles (McBride 1994). Hydration of montmorillonite in electrolyte solutions occurs in two phases: the crystalline phase and the osmotic phase (Norrish and Quirk 1954; McBride 1994, Zhang et al. 1995; Prost et al. 1998). The crystalline phase occurs first as several molecular layers of water hydrate the interlayer and outer surfaces from the completely dry state. Osmotic hydration occurs when additional water molecules hydrate the interlayer surfaces, resulting in large interlayer distances (McBride 1994). Crystalline hydration generally results in a small expansion of the interlayer space and a limited amount of immobile water, which is manifested at the macroscale as a small amount of swelling (referred to as "crystalline swell") and higher hydraulic conductivity. Osmotic hydration can result in appreciable expansion of the interlayer space, a large fraction of the pore water being bound, and is responsible for the large amount of swelling (referred to as "osmotic swell") and low hydraulic conductivity often associated with Na-bentonites.

When the interlayer cations are monovalent, both crystalline and osmotic hydration occur, allowing the interlayer spacings to become large. However, only crystalline swelling occurs when the interlayer cations are divalent or trivalent, limiting expansion of the interlayer region to approximately 1.96 nm (four layers of water molecules). Strong electrostatic attraction between the montmorillonite sheets and the interlayer cations prevent osmotic swelling when the cations are polyvalent, despite the larger hydration energy associated with polyvalent cations (McBride 1994; 1997; Quirk and Marčelja 1997). Thus, appreciable swelling and lower hydraulic conductivity occur when the interlayer cations are monovalent, whereas very little swelling and higher hydraulic conductivity occur when the cations are divalent or trivalent (Norrish and Quirk 1954; McBride 1994; Wu et al. 1994; Egloffstein 1997, 2001; Onikata et al. 1999; Jo et al. 2001; Ashmawy et al. 2002). In monovalent solutions, the volume of swelling and spacing of the interlayer region is inversely proportional to the square root of the concentration of the solution (Norrish and Quirk 1954; McBride 1994; Zhang et al. 1995; Onikata et al. 1999).

Hydraulic Conductivity to Single-Species Inorganic Solutions

Mesri and Olson (1971) studied the mechanisms controlling the hydraulic conductivity of bentonite when the interlayer cation was sodium or calcium. At similar void ratios, the hydraulic conductivity of Na-bentonite was approximately five times lower than that of the Ca-bentonite. Mesri and Olson (1971) attributed the lower hydraulic conductivity of the Na-bentonite to the presence of immobile water, which resulted in smaller and more tortuous flow paths for mobile water.

Petrov and Rowe (1997) investigated how NaCl solutions of varying concentration affected the hydraulic conductivity of a GCL containing Na-bentonite. Tests were conducted with distilled (DI) water and NaCl solutions having concentrations between 0.1–2.0 M. Hydraulic conductivity of the GCL generally increased as the NaCl concentration increased. At 2.0 M, the hydraulic conductivity was as much as 800 times higher than that with distilled water. For concentrations less than 0.1 M, the hydraulic conductivity was comparable to that obtained with distilled water. Prehydration with at least one pore volume of distilled water tempered the sensitivity of hydraulic conductivity to salt concentration. For 2.0 M NaCl, prehydration with distilled water resulted in a hydraulic conductivity 25 times lower than that obtained by direct permeation with 2.0 M NaCl. Tests conducted over a range of confining stresses (3 to 118 kPa) showed that, at a given concentration, the hydraulic conductivity can vary by a factor of 10 to 50 depending on the effective stress.

Jo et al. (2001) investigated how cation valence and concentration of single-species salt solutions affect free swell and hydraulic conductivity of nonprehydrated GCLs containing Na-bentonite. Salt solutions with cation valences of 1, 2, and 3 and concentrations between 0.005 and 1.0 M were used. All tests were conducted until the physical and chemical termination criteria in ASTM D 6766 were achieved. Permeation with salt solutions having concentrations less than 0.1 M (monovalent) or 0.01 M (divalent or trivalent) yielded hydraulic conductivities similar to those with DI water ($\approx 10^{-9}$ cm/s), regardless of cation valence. For higher concentrations, swell decreased and hydraulic conductivity increased as the concentration or valence increased. Swelling in the presence of monovalent cations followed the order of the hydrated radius (r_h) and the lyotropic series, with Li ($r_h \approx 0.6$ nm) solutions yielding the greatest swell and K (r_h

J. Geotech. Geoenviron. Eng. 2004.130:1236-1249.

≈ 0.3 nm) solutions yielding the lowest swell at a given concentration. In contrast, hydraulic conductivity to the monovalent solutions was insensitive to cation species. No dependence on species was observed for swell or hydraulic conductivity when the solutions contained divalent or trivalent cations. In addition, solutions with trivalent cations resulted in swell and hydraulic conductivity essentially identical to those obtained with solutions having divalent cations at the same concentration.

Jo et al. (2001) conclude that swell and hydraulic conductivity depend more on valence at intermediate concentrations (0.025 M to 0.1 M), whereas concentration dominates at low (0.005 M) and high (1 M) concentrations. They also conclude that hydraulic conductivity and swelling have a strong inverse relationship, and suggest that swell tests can be used as an indicator of adverse chemical interactions that affect the hydraulic conductivity of GCLs.

Hydraulic Conductivity to Multispecies Inorganic Solutions

Reeve and Bower (1960) investigated how sodium adsorption ratio (SAR) of the permeant solution and electrolyte concentration affected the hydraulic conductivity of a sodic (sodium rich) soil with a montmorillonitic clay fraction. SAR is a ratio describing the relative amounts of sodium, calcium, and magnesium in the pore water equilibrated with the soil, and can be written as (McBride 1994):

$$\mathrm{SAR} = \left[\frac{\mathrm{Na}^+}{[(\mathrm{Ca}^{2+} + \mathrm{Mg}^{2+})/2]^{1/2}} \right]_e \quad (1)$$

where the cation (Na^+, Ca^{2+}, Mg^{2+}) concentrations are expressed in meq/L (note: 1 meq/L = 1 mN). The soil had a cation exchange capacity (CEC) = 8.9 meq/100 g. The permeant solutions were Salton sea water (SAR = 57) and diluted Salton sea water with SAR = 40, 27.2, 18.2, and 2.2. Reeve and Bower (1960) found that the rate of monovalent for divalent exchange is a function of the divalent cation concentration and SAR of the permeant solution. At a given SAR, solutions with higher ionic strength resulted in more rapid exchange and higher hydraulic conductivity.

McNeal and Coleman (1966) and McNeal et al. (1966) used Na–Ca solutions to investigate how concentration and SAR affect swelling and hydraulic conductivity of Gila clay from New Mexico, USA, which has CEC = 41.2 meq/100 g and consists of 29% montmorillonite. Swelling was quantified as the mass of "bound" solution per mass of clay. Test solutions were prepared with NaCl and $CaCl_2$ salts at concentrations of 0.8, 0.2, 0.05, 0.012, and 0.003 mN with SAR = 0, 15, 25, 50, 100, and ∞. Specimens for hydraulic conductivity testing were initially equilibrated by permeation with 10 pore volumes of a 0.8 N solution having the same SAR as the test solution, and then were sequentially permeated with test solutions of decreasing concentration.

McNeal et al. (1966) found no appreciable swell in solutions with SAR = 0 (all divalent) regardless of concentration, which is consistent with the lack of an osmotic swelling phase when the interlayer contains polyvalent cations (Norrish and Quirk 1954). Measurable swelling began at 0.012 N and SAR = 25, and increased as the SAR of the solution increased. Decreases in hydraulic conductivity occurred with decreasing concentration and increasing SAR of the permeant solution. For example, the hydraulic conductivity was 1.5×10^{-5} cm/s for a 0.8 N solution with SAR = 0, 5.9×10^{-6} cm/s for a 0.050 N solution with SAR = 100, and 1.5×10^{-7} cm/s for a 0.012 N solution with SAR = ∞ (all sodium).

McNeal et al. (1966) concluded that salt concentration and SAR affect swelling and hydraulic conductivity of Gila clay in an inverse manner, which was also reported by Jo et al. (2001) for GCLs permeated with single-species solutions. Increasing the concentration or relative abundance of divalent cations (lower SAR) results in less swell and higher hydraulic conductivity. McNeal et al. (1966) postulate that swelling of montmorillonite is the dominant mechanism affecting its hydraulic conductivity because it affects the opening and closing of pores.

Mustafa and Hamid (1975) investigated how electrolyte concentration and SAR of the permeant solution affected the hydraulic conductivity of two montmorillonitic soils, one containing 32% montmorillonite and the other 14% montmorillonite. The hydraulic conductivity of both soils exhibited the same trends with concentration and SAR as reported by McNeal et al. (1966). However, Mustafa and Hamid (1975) indicate that the relationships between swell, hydraulic conductivity, and characteristics of the permeant solution are unique for each soil.

Malik et al. (1992) investigated how mixed Na–Ca solutions of various concentrations affect swelling, dispersion, and flow in two unsaturated clays reported to be montmorillonitic (the montmorillonite content was not reported). NaCl and $CaCl_2$ solutions with SAR = 0, 5, 15, 25, and 50 and concentrations of 3.1, 12.5, 50, 200, and 500 mM were used. Their results were also similar to those reported by McNeal et al. (1966); swell of both soils increased and the hydraulic conductivity decreased as the concentration decreased or the SAR increased.

Materials and Methods

Geosynthetic Clay Liner

The GCL used in this study contains granular sodium bentonite encapsulated between a 170 g/m^2 slit-film monofilament woven geotextile and a 206 g/m^2 staple-fiber nonwoven geotextile. The geotextiles are bonded by needle-punching fibers that are thermally fused to the geotextiles. The specific gravity of the bentonite is 2.65, and the average mass of bentonite per area is 4.3 kg/m^2. The initial thickness of the GCL ranges from 5.5 to 6.5 mm, and the average initial gravimetric water content of the bentonite was 9%.

X-ray diffraction showed that the bentonite contains 86% montmorillonite, 3% quartz, 5% tridymite, 3% plagioclase feldspar, 1% K-feldspar, 1% aragonite, 1% illite/mica, and trace amounts of calcite, siderite, clinoptilolite, rutile, and gypsum. The granule size distribution for the GCL (determined by mechanical sieve analysis on the air-dry bentonite) is shown in Fig. 1 along with the granule size distribution for the GCL used by Jo et al. (2001). Both GCLs contain sand-size bentonite granules, but the GCL used in this study has smaller granules.

The CEC and composition of the exchange complex (Ca, Mg, Na, and K) were measured on two samples of bentonite from the GCL using the procedures in *Methods of Soil Analysis* (Spark 1996). Soluble salts were extracted with DI water and exchangeable metals were extracted with ammonium acetate. These replicate measurements yielded CECs of 65.2 and 73.5 meq/100 g and the following exchange complex: Na—56.1 and 40.0 meq/100 g, K—0.6 and 0.8 meq/100 g, Ca—12.0 and 15.7 meq/100 g, Mg—4.0 and 4.8 meq/100 g. Thus, the bentonite used in this study is predominantly Na-montmorillonite.

J. Geotech. Geoenviron. Eng. 2004.130:1236-1249.

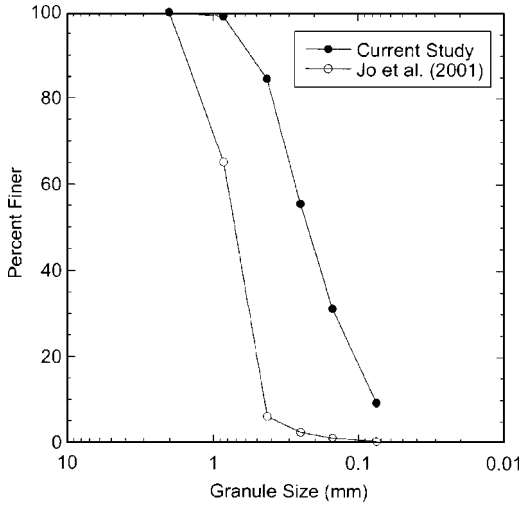

Fig. 1. Granule size distributions for geosynthetic clay liner used in this study and by Jo et al. (2001)

Permeant Liquids

The multispecies salt solutions were prepared with anhydrous inorganic salts (>96% purity) dissociated in DI water. LiCl and NaCl salts were used to investigate the effects of monovalent cations, and $CaCl_2$ and $MgCl_2$ salts were used to investigate the effects of divalent cations. The anionic background (Cl^-) was held constant for all permeant solutions. Type II DI water was used to prepare the solutions and as the reference solution.

A summary of the solutions used in this study is in Table 1. All of the solutions have near neutral pH (6.6 to 8.5). The parameter RMD in Table 1 represents a ratio of the concentrations of monovalent and divalent cations in the permeant solution. RMD is defined as

$$\text{RMD} = \frac{M_M}{\sqrt{M_D}} \tag{2}$$

where M_M=total molarity of monovalent cations; and M_D=total total molarity of divalent cations in the solution. RMD is slightly different from SAR in that RMD characterizes the permeant solution introduced to the soil, whereas SAR generally describes pore water equilibrated with the soil (although SAR has been used to describe solutions by some investigators). RMD also is in terms of molar concentrations (rather than normality), includes all monovalent and divalent cations (SAR is limited to Na, Mg, and Ca) in solution, and does not include a factor of 2 in the denominator (because more than two cations can contribute to M_D).

Solutions having ionic strength (I) ranging from 0.05 to 0.5 M and RMD from 0 to ∞ (all divalent to all monovalent) were used as permeant liquids. These solutions were selected to represent the range of ionic strengths and RMDs expected in leachate from modern disposal facilities for municipal solid waste, hazardous wastes, construction and demolition wastes, fly ash, paper sludge, and mine waste. A review of literature pertaining to the composition of leachates from these wastes is included in Kolstad (2000), and is summarized later in this paper. Most of the solutions were Li–Ca mixtures. However, tests were also conducted with Na–Mg and Li–Na–Ca–Mg mixtures to investigate how cation species affected swell and hydraulic conductivity of the GCL.

Free Swell Tests

Free swell tests were conducted in accordance with ASTM D 5890. Bentonite from the GCL was ground to a fine powder using a mortar and pestle and dry sieved through a No. 200 U.S. standard sieve. The sieved bentonite was air dried for 24 h, and then stored in an airtight container prior to testing. A 100 mL graduated cylinder, accurate to ±0.5 mL, was filled to the 90 mL mark with the test solution. Two grams of sieved bentonite were added to the graduated cylinder in 0.1 g increments. Test solution was then added to the cylinder to reach a final volume of 100 mL by flowing the solution along the cylinder wall so that any particles adhered to the wall would be washed into solution. Swell volume (mL/2 g) was recorded after 24 h, which Jo et al. (2001) report is adequate to establish equilibrium.

Hydraulic Conductivity Tests

Falling head hydraulic conductivity tests with constant tailwater elevation were conducted on the GCL specimens using flexible-wall permeameters in general accordance with ASTM D 5084 and D 6766. An average hydraulic gradient of 100 and effective stress of 20 kPa were applied. Hydraulic gradients this large are uncommon when testing clay soils, but are common when testing GCLs. Large gradients are acceptable when testing GCLs because the differential in effective stress across a thin specimen is not very sensitive to the hydraulic gradient (Shackelford et al. 2000). Aqueous solutions of the inorganic salts (Table 1) were used as the permeant solutions. Backpressure was not used to permit convenient collection of effluent samples for pH and electrical conductivity (EC) testing.

GCL test specimens were prepared by cutting a sample from a GCL panel using a steel cutting ring (105 mm in diameter) and a sharp utility knife following the method described in Daniel et al. (1997). A small amount of test solution was applied along the inner circumference of the ring using a squirt bottle to prevent bentonite loss when removing the specimen from the trimming ring. Excess geotextile fibers were removed from the edge of the specimen with sharp scissors to eliminate potential preferential flow paths between the GCL and flexible membrane (Petrov et al. 1997). Paste prepared with the test solution and bentonite trimmings was delicately placed along the perimeter of the specimen with a small spatula to minimize the potential for sidewall leakage during permeation.

The initial thickness of the GCL specimen was measured to the nearest 0.1 mm with a caliper. Four measurements were made and the average thickness was recorded. The initial weight of the specimen was measured to the nearest 0.01 g. On completion of the hydraulic conductivity test, the specimen was removed from the permeameter and the final thickness and weight were measured in the same manner.

Sidewall leakage and preferential flow paths along the needle-punched fibers are of concern when permeating GCLs with solutions that alter the hydraulic conductivity of bentonite. When relatively high hydraulic conductivities ($>10^{-6}$ cm/s) were obtained, the influent solution was spiked with Rhodamine WT dye (5 mg/L) to stain the flow paths bright red. For all tests that were conducted, the dye tests showed that preferential flow along the needle-punching fibers and the sidewalls did not occur. Jo et al. (2001) report similar findings in their single-species tests on GCLs.

J. Geotech. Geoenviron. Eng. 2004.130:1236-1249.

Table 1. Summary of Permeant Solutions

Type of solution	Ionic strength (M)	Monovalent concentration 10^{-2} (M)	Divalent concentration 10^{-2} (M)	RMD ($mM^{1/2}$)	pH	EC (S/m)
Li–Ca	0.05	5.00	0.00	∞	7.4	0.50
		4.35	0.22	0.93	7.6	0.48
		3.33	0.56	0.45	7.7	0.43
		2.00	1.00	0.20	7.2	0.42
		0.00	1.67	0.00	7.8	0.36
Na–Mg		3.33	0.56	0.45	7.4	0.43
Li–Na Ca–Mg		3.33 Li(1):Na(3)[a]	0.56 Ca(1):Mg(3)[b]	0.45	7.2	0.43
Li–Ca	0.1	10.0	0.00	∞	6.8	0.88
		8.70	0.44	1.32	7.9	0.87
		8.33	0.56	1.12	8.5	0.88
		7.77	0.77	0.88	8.1	0.87
		6.67	1.11	0.64	7.7	0.86
		5.00	1.67	0.38	7.3	0.80
		2.50	2.50	0.16	7.5	0.77
		1.00	3.00	0.06	7.4	0.72
		0.00	3.33	0.00	7.9	0.70
Na–Mg		8.70	4.35	1.32	6.8	0.87
		6.67	1.11	0.64	6.6	0.86
		1.00	3.00	0.06	7.2	0.73
Li–Na Ca–Mg		8.33 Li(3):Na(1)[a]	0.56 Ca(3):Mg(1)[b]	1.12	7.1	0.88
Li–Na Ca–Mg		2.50 Li(1):Na(1)[a]	2.50 Ca(1):Mg(1)[b]	0.16	6.5	0.77
Li–Ca	0.2	20.0	0.00	∞	8.1	1.86
		16.7	1.11	1.58	7.2	1.72
		13.3	2.22	0.89	7.1	1.62
		8.00	4.00	0.40	7.2	1.50
		0.00	6.67	0.00	7.2	1.29
Na–Mg		13.3	2.22	0.89	6.7	1.61
Li–Na Ca–Mg		8.00 Li(1):Na(3)[a]	4.00 Ca(3):Mg(1)[b]	0.40	7.2	1.50
Li–Ca	0.5	50.0	0.00	∞	8.1	3.45
		38.5	3.85	1.97	7.3	3.46
		31.3	6.25	1.24	8.2	3.29
		20.0	10.0	0.64	8.1	3.03
		0.0	16.7	0.00	7.6	2.74
Na–Mg		31.3	6.25	1.24	7.2	3.30
Li–Na Ca–Mg		38.5 Li(3):Na(1)[a]	3.85 Ca(1):Mg(3)[b]	1.97	6.6	3.46
Li–Na Ca–Mg		20.0 Li(2):Na(1)[a]	10.0 Ca(1):Mg(2)[b]	0.64	6.9	3.02

Note: RMD=Relative abundance of monovalent and divalent cations; EC=Exchange capacity.

[a]Molar ratio of monovalent cations when two species are present.

[b]Molar ratio of divalent cations when two species are present

The hydraulic conductivity tests were terminated when the termination criteria in ASTM D 5084 and D 6766 were satisfied. The hydraulic conductivity was required to be steady (±25% of the mean with no statistically significant trend for at least four values), the ratio of outflow to inflow was between 0.75 and 1.25 for four consecutive values, and the pH and EC of the influent and effluent deviated less than 10%. A minimum of 2 pore volumes of flow (PVF) was also stipulated, although all tests required more than 2 PVF to satisfy all of the termination criteria (some tests required more than 150 PVF). A pH meter and a portable electrical conductivity probe were used to measure the pH and EC.

J. Geotech. Geoenviron. Eng. 2004.130:1236-1249.

Table 2. Summary of Free Swell Data

Ionic strength (M)	RMD $mM^{1/2}$	Free swell (mL/2 g)		
		Li–Ca solutions	Na–Mg solutions	Li–Na–Ca–Mg solutions
0.05	0.93	30.5	—	—
	0.45	24.5	24.5	—
	0.20	22.0	—	—
	0.00	19.0	—	—
0.1	1.32	21.5	21.0	—
	1.12	21.0	—	21.0
	0.88	19.0	—	—
	0.64	17.5	17.5	—
	0.38	14.0	—	—
	0.16	13.5	—	13.0
	0.06	11.5	12.0	—
	0.00	11.0	—	—
0.2	1.67	19.0	—	—
	0.89	15.0	15.5	—
	0.40	12.0	—	12.5
	0.00	9.5	—	—
0.5	1.97	11.5	—	12.0
	1.24	10.5	10.0	—
	0.64	8.5	—	8.5
	0.00	6.5	—	—

Note: Free Swell in distilled water=36.5 mL/2 g; RMD=Relative abundance of monovalent and divalent cations.

Results of Free Swell Tests

Effect of Concentration and Relative Abundance of Monovalent and Divalent Cations

Free swell tests were conducted using solutions with ionic strengths ranging from 0.05 M to 0.5 M and RMD ranging from 0 to 1.97 $mM^{1/2}$. The multispecies solutions were prepared with Li and Ca, Na, and Mg, or Li, Na, Ca, and Mg. Results of the tests are summarized in Table 2.

Free swell is shown as a function of ionic strength in Fig. 2 for the Li–Ca solutions. The data are segregated by solutions that are predominantly divalent (RMD < 0.35 $mM^{1/2}$), solutions with comparable fractions of monovalent and divalent cations (0.35 $mM^{1/2} <$ RMD < 0.90 $mM^{1/2}$), and solutions that are predominantly monovalent (RMD > 0.90 $mM^{1/2}$). Free swell of the bentonite decreases with increasing concentration for each range of RMD. Lower free swell also occurs as the RMD decreases because the presence of more divalent cations suppresses the osmotic component of swelling. RMD also affects the sensitivity to concentration. For the predominantly monovalent solutions (RMD > 0.90 $mM^{1/2}$), the free swell decreases 19 mL/2 g, on average, as the ionic strength is varied between 0.05 to 0.5 M. For the predominantly divalent solutions (RMD < 0.35 $mM^{1/2}$), the free swell decreases 14 mL/2 g, on average, over the same range of ionic strengths.

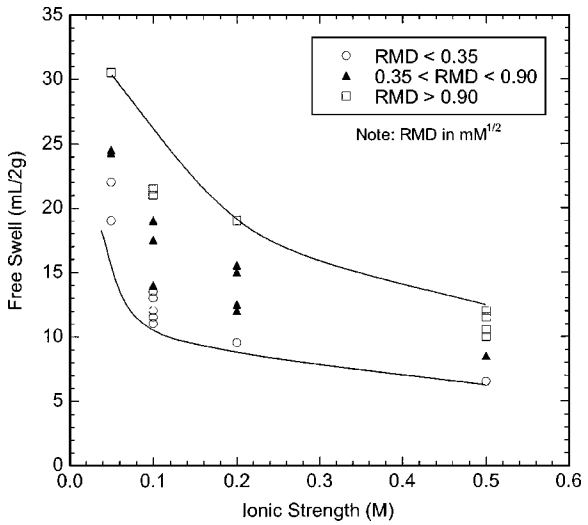

Fig. 2. Free swell of geosynthetic clay liner bentonite as a function of ionic strength for low, intermediate, and high relative abundance of monovalent and divalent cation

The influence of RMD on swell at constant ionic strength is shown in Fig. 3. The relationships are approximately linear, with trend lines fitted to the data using least-squares linear regression. The slope of each trend line reflects the sensitivity of swell to RMD; the intercept is the free swell when the solution only contains divalent cations. When the ionic strength is lower, the trend lines have a larger slope (e.g., slope=12.1 for $I=0.05$ M and 2.6 for $I=0.5$ M), which indicates that RMD has a stronger influence on swelling at low ionic strength and less effect at high ionic strength.

The trends in the free swell tests are consistent with those reported by McNeal et al. (1966) for swelling of Gila clay in mixed Na–Ca solutions. They found a unique relationship between swell and SAR when the concentration was fixed, and that the sensitivity to SAR diminished as the concentration increased. Jo et al. (2001) report similar findings for single species solutions. They found that concentration has a greater effect on free swell for monovalent solutions than divalent solutions.

The sensitivity of free swell to concentration and RMD is

J. Geotech. Geoenviron. Eng. 2004.130:1236-1249.

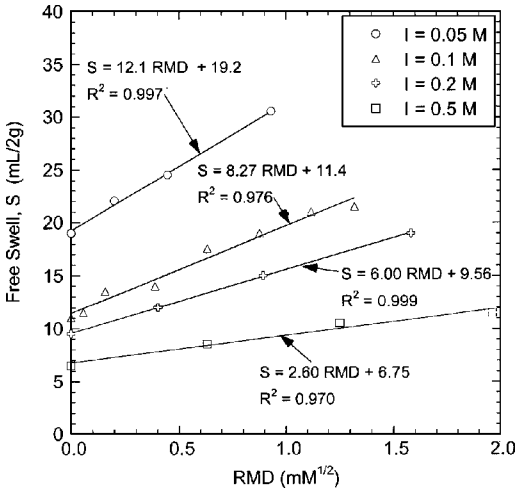

Fig. 3. Free swell of GCL bentonite as a function of RMD for ionic strengths of 0.05, 0.1, 0.2 and 0.5 M

caused by expansion and contraction of the interlayer space as a result of crystalline and osmotic swelling. This effect is illustrated in Fig. 4, which shows basal spacing (i.e., sum of interlayer separation distance and thickness of one montmorillonite layer, also referred to as d_{001}) as a function of ionic strength. The basal spacing was computed using the method in Smalley (1994), which is based on particle geometry, free swell of the bentonite, the thickness of a montmorillonite layer ($\approx$0.9 nm), the basal spacing of Ca-montmorillonite in water ($\approx$1.96 nm), and the free swell of Ca-montmorillonite in water ($\approx$8.0 mL/2 g). The symbol size in Fig. 4 is proportional to RMD (larger symbols for larger RMD). At high ionic strength (0.5 M), the basal spacing (d_{001}) ranges between 1.5 and 2.9 nm, indicating that the swelling is in the crystalline phase ($d_{001} \leq 1.96$ nm) or the low end of the osmotic phase ($d_{001} > 1.96$ nm). In contrast, the basal spacing ranges between 4.5 and 8.6 nm at lower concentration ($I \leq 0.05$ M), which corresponds to crystalline and osmotic swelling ($d_{001} > 1.96$ nm). Moreover, the smallest symbols (lowest RMD)

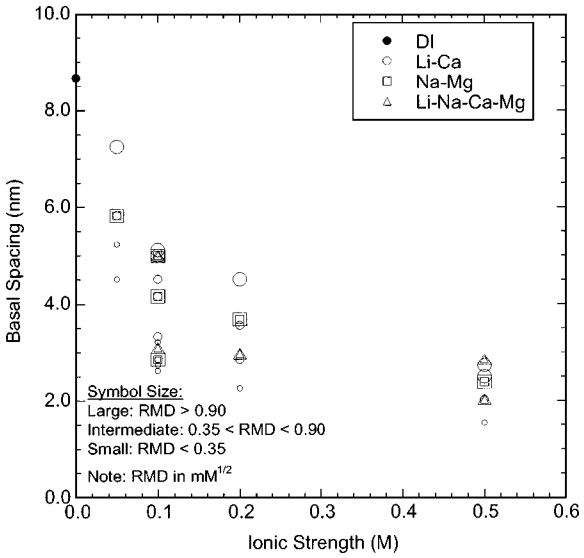

Fig. 4. Free swell of GCL bentonite as a function of computed basal spacing of montmorillonite

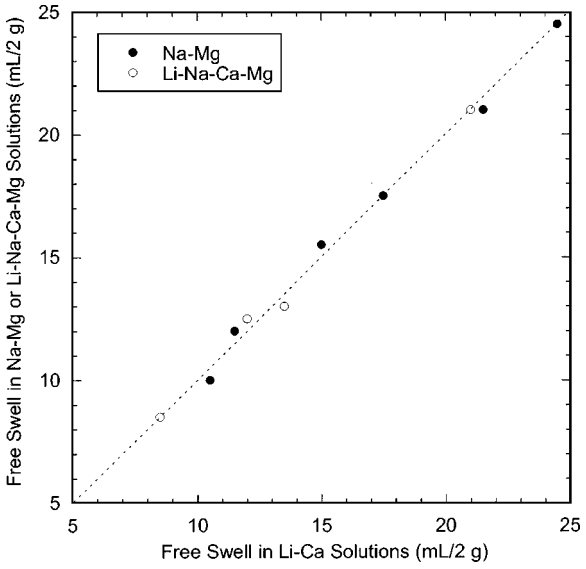

Fig. 5. Comparison of free swell of bentonite in Na–Mg and Li–Na–Ca–Mg solutions to free swell in Li–Ca solutions for solutions prepared with the same ionic strength and RMD

often correspond to the lowest d_{001} for each ionic strength, reflecting suppression of osmotic swelling due to the preponderance of divalent cations.

Effect of Cation Species

The influence of cation species on free swell is illustrated in Fig. 5 using data from the Li–Ca, Na–Mg, and Li–Na–Ca–Mg solutions. Swell in the Na–Mg and Li–Na–Ca–Mg solutions is essentially equal to the swell in the Li–Ca solutions at the same ionic strength and RMD. No discernable effect of cation species is evident. The tendency of divalent cations to suppress osmotic swelling, combined with the insensitivity of free swell to type of divalent cation species (i.e., as in Jo et al. 2001), probably muted any sensitivity to species for the monovalent cations. The single-species tests by Jo et al. (2001) also show that free swell in monovalent solutions is only slightly sensitive to cations species. Thus, free swell is likely to be insensitive to cation species for most monovalent–divalent cation mixtures.

Results of Hydraulic Conductivity Tests

Effect of Concentration and Relative Abundance of Monovalent and Divalent Cations

Hydraulic conductivity tests were conducted using multispecies aqueous solutions listed in Table 1. The ionic strength of the test solutions ranged from 0.05 M to 0.5 M, and the RMD ranged from 0 to 1.97 $mM^{1/2}$. Hydraulic conductivities obtained from these tests are summarized in Table 3.

Hydraulic conductivity is shown in Fig. 6 as a function of ionic strength (I). As in Fig. 2, the solutions have been characterized as primarily divalent ($RMD < 0.35$ $mM^{1/2}$), comparable mixtures (0.35 $mM^{1/2} < RMD < 0.90$ $mM^{1/2}$), and primarily monovalent ($RMD > 0.90$ $mM^{1/2}$). The hydraulic conductivity is sensitive to the composition of the permeant solution, ranging from 5.6×10^{-10} cm/s ($I = 0.05$ M and $RMD = 0.66$ $mM^{1/2}$) to 1.0×10^{-5} cm/s ($I = 0.5$ M and $RMD = 0$), and varies exponentially

J. Geotech. Geoenviron. Eng. 2004.130:1236-1249.

Table 3. Summary of Hydraulic Conductivities

Ionic strength (M)	RMD ($mM^{1/2}$)	Hydraulic conductivity (cm/s)		
		Li–Ca solutions	Na–Mg solutions	Li–Na–Ca–Mg solutions
0.05	0.93	5.6×10^{-10}	—	—
	0.45	1.1×10^{-9}	2.1×10^{-9}	—
	0.20	3.0×10^{-9}	—	—
	0.00	9.2×10^{-9}	—	—
0.1	1.32	2.4×10^{-9}	8.9×10^{-10}	—
	1.12	2.3×10^{-9}	—	4.8×10^{-9}
	0.88	3.3×10^{-9}	—	—
	0.64	5.2×10^{-9}	6.5×10^{-9}	—
	0.38	9.3×10^{-9}	—	—
	0.16	9.5×10^{-9}	—	2.1×10^{-8}
	0.06	1.1×10^{-8}	8.5×10^{-9}	—
	0.00	1.3×10^{-8}	—	—
0.2	1.67	2.8×10^{-9}	—	—
	0.89	2.5×10^{-8}	3.4×10^{-8}	—
	0.40	4.9×10^{-8}	—	5.2×10^{-8}
	0.00	1.0×10^{-7}	—	—
0.5	1.97	2.4×10^{-7}	—	9.1×10^{-8}
1.24		8.5×10^{-7}	4.2×10^{-7}	—
0.64		5.0×10^{-6}	—	8.5×10^{-6}
0.00		1.0×10^{-5}	—	—

Note: Hydraulic conductivity to distilled water $=9.0\times10^{-10}$ cm/s; RMD = Relative abundance of monovalent and divalent cations.

with ionic strength (linearly on a semilogarithmic graph). The highest hydraulic conductivities at any ionic strength were obtained using the primarily divalent ($RMD < 0.35\ mM^{1/2}$) solutions, and the lowest for the primarily monovalent ($RMD > 0.90\ mM^{1/2}$) solutions.

The effect of RMD at constant ionic strength is shown in Fig. 7. The base-10 logarithm of hydraulic conductivity ($\log_{10}K$) is approximately linearly related to RMD. The trend lines relating

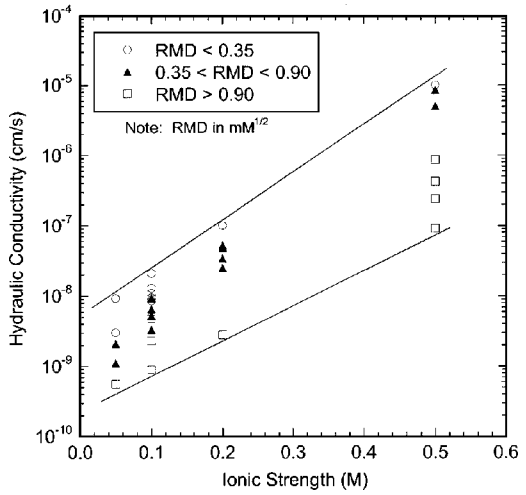

Fig. 6. Hydraulic conductivity of GCL as a function of solution ionic strength for low, intermediate, and high RMD

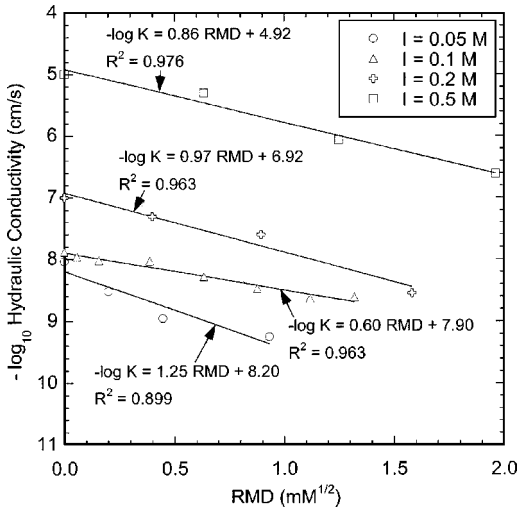

Fig. 7. Hydraulic conductivity of GCL as a function of RMD for ionic strengths of 0.05, 0.1, 0.2, and 0.5 M

$\log_{10}K$ and RMD in Fig. 7 were fit using least-squares linear regression. Their slope describes the sensitivity of hydraulic conductivity to RMD, and the intercept is the hydraulic conductivity to the divalent solution. The hydraulic conductivity exhibits greater sensitivity to RMD at lower ionic strength (i.e., slope $=1.25$ at $I=0.05$ M and 0.86 at $I=0.5$ M). The data for the tests conducted at an ionic strength of 0.1 M are an exception to the trend. The reason for this deviation is unknown.

The trends in Figs. 6 and 7 are comparable to the trends reported by McNeal and Coleman (1966) for Gila clay. They found that the hydraulic conductivity increases with increasing concentration and decreasing SAR, and distinct curves relating hydraulic conductivity to SAR exists when the concentration is fixed. McNeal and Coleman (1966) report that SAR has a stronger influence on hydraulic conductivity at low concentrations, and that the effect of SAR diminishes at high concentrations. Jo et al. (2001) also report similar sensitivity to ionic strength and cation valence for single species solutions. At a given ionic strength, the highest hydraulic conductivities were obtained with divalent or trivalent solutions, and the lowest with monovalent solutions.

A diminished effect of ionic strength and RMD probably would have been observed had much lower or much higher ionic strengths been used. For example, DI water is the limiting case for dilute solutions (in this study, the hydraulic conductivity of the GCL to DI water was 9.0×10^{-10} cm/s). In addition, Jo et al. (2001) report that the hydraulic conductivity of the GCL they tested leveled off between 10^{-5} to 10^{-4} cm/s for ionic strengths greater than 1 M. When the ionic strength is high, osmotic swelling becomes negligible, and the basal spacing is reduced to its smallest value in the hydrated state ($\approx$2 nm). Once this compressed condition is reached, no further increase in hydraulic conductivity can occur. In fact, a decrease in hydraulic conductivity is possible due to the higher viscosity of concentrated solutions (Fernandez and Quigley 1988).

Effect of Cation Species

Li–Ca, Na–Mg, and Li–Na–Ca–Mg solutions having various RMD and ionic strengths were used to investigate how differences in cation species affect the hydraulic conductivity of GCLs

J. Geotech. Geoenviron. Eng. 2004.130:1236-1249.

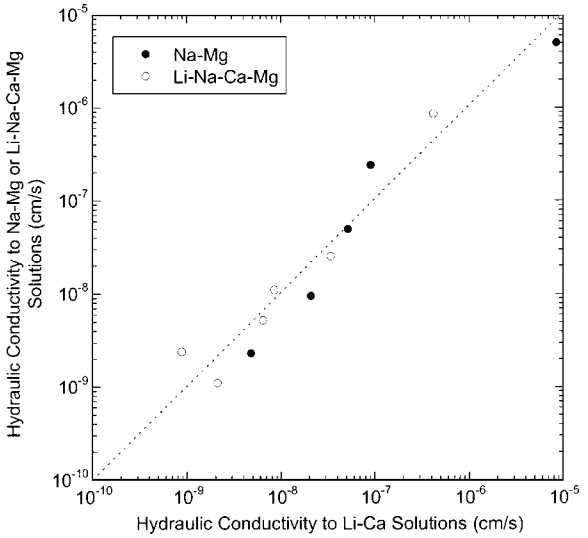

Fig. 8. Comparison of hydraulic conductivities of GCL obtained with Na–Mg and Li–Na–Ca–Mg solutions to hydraulic conductivities obtained with Li–Ca solutions for solutions prepared with the same ionic strength and RMD

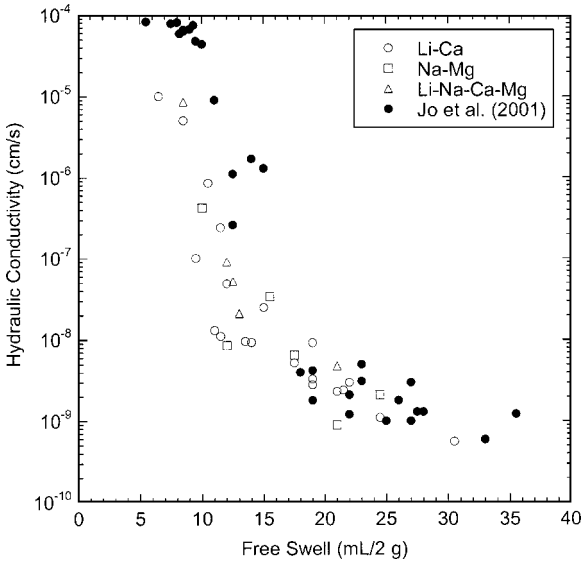

Fig. 9. Hydraulic conductivity of GCL as a function of free swell of bentonite. Test data are from this study and from Jo et al. (2001)

permeated with mixed solutions. Composition of each solution is summarized in Table 1 and the hydraulic conductivities are in Table 3.

Hydraulic conductivities obtained using the Li–Ca solutions are compared with those obtained from the Na–Mg and Li–Na–Ca–Mg solutions in Fig. 8. At comparable ionic strengths and RMD, essentially the same hydraulic conductivities were obtained with the Na–Mg and Li–Na–Ca–Mg solutions as with the Li–Ca solutions. No discernable effect of cation species is apparent. The insensitivity of hydraulic conductivity to cation species is analogous to the insensitivity of free swell to cation species. Differences in preference of the montmorillonite for Ca over Mg and Na over Li appear to have a small effect compared to the effects of RMD and concentration. In addition, Jo et al. (2001) found that the hydraulic conductivity was insensitive to cation species for a given valence.

The insensitivity to cation species evident in Fig. 8, combined with the insensitivity to cation species observed by Jo et al. (2001) for single-species solutions, suggests that the hydraulic conductivity at fixed RMD is likely to be insensitive to cation species in most monovalent–divalent mixtures. Moreover, Jo et al. (2001) found that permeation with single-species solutions containing divalent and trivalent cations yielded essentially the same hydraulic conductivity at a given concentration. Thus, the insensitivity to cation species may extend to multispecies solutions in general, with ionic strength and RMD being the dominant variables controlling hydraulic conductivity. In this case, the denominator of RMD would include the total normality of the polyvalent (valence $\geq +2$) cations in the solution. While this hypothesis is plausible, more testing is needed to confirm its validity.

Practical Implications

Free Swell and Hydraulic Conductivity

Jo et al. (2001) show that a strong relationship exists between free swell of bentonite and the hydraulic conductivity of GCLs exposed to single-species solutions. A similar relationship could be expected for multispecies solutions as well because Figs. 2, 3, 6, and 7 show that ionic strength and RMD affect swell and hydraulic conductivity in a consistent and similar manner. McNeal et al. (1966) also report a strong correlation between swelling and hydraulic conductivity for Gila clay permeated with solutions having different ionic strengths and SAR.

Hydraulic conductivity of the GCL specimens permeated with the multispecies solutions is shown in Fig. 9 as a function of free swell along with the single-species data from Jo et al. (2001). A strong relationship exists between hydraulic conductivity and free swell for both data sets. The slight offset in the two data sets at lower swell volumes (and higher hydraulic conductivities) is most likely due to differences in the granule size distributions of the bentonites and not the use of multispecies versus single species solutions. The GCLs used in both studies were essentially identical, except the bentonite in the GCL used in this study has smaller granules than the bentonite in the GCL used by Jo et al. (2001) (Fig. 1). Mesri and Olson (1971) and McNeal et al. (1966) indicate that bentonites with larger "domains" (quasi-crystals) permit larger flow paths and higher hydraulic conductivity. In addition, Katsumi et al. (2002) show that nonprehydrated GCLs containing bentonite with larger granules are more permeable than GCLs with smaller granules when permeated using stronger ($\geq$0.2 M) salt solutions. Because the granules do not swell appreciably in strong solutions, bentonites with larger granules have larger intergranular pores, and higher hydraulic conductivity. That is, the hydraulic conductivity of granular bentonite permeated with strong solutions follows a similar relationship with particle size as do granular soils; i.e., the hydraulic conductivity increases as the particle size increases, all factors being equal (e.g., Lambe and Whitman 1969; Terzaghi et al. 1996). In contrast, granule size has no effect on free swell, because the bentonite is crushed to pass the No. 200 sieve prior to free swell testing.

McNeal et al. (1966) conclude that swelling of expansive minerals such as montmorillonite is the dominant mechanism affecting the hydraulic conductivity. The results of this study, as well as those in Jo et al. (2001), support this conclusion. The trends shown in Fig. 9 also indicate that free swell tests can be a relatively simple and quick screening method to evaluate the compat-

J. Geotech. Geoenviron. Eng. 2004.130:1236-1249.

ibility of GCLs permeated with inorganic salt solutions containing mixtures of cations. Although not a surrogate for chemical compatibility testing (direct testing is needed to demonstrate that a GCL is compatible with a liquid), free swell testing can be used to identify liquids that are incompatible with GCLs. The data in Fig. 9 also illustrate that the relationship between hydraulic conductivity and free swell is bentonite specific, and needs to be identified empirically.

Estimating Hydraulic Conductivity

The approximately linear trends shown in Figs. 6 and 7 suggest that a relatively simple empirical model can be used to estimate hydraulic conductivity of GCLs as a function of ionic strength and RMD. A model relating these parameters was developed using stepwise regression (Draper and Smith 1998) using a significance level of 0.05:

$$\frac{\log K_c}{\log K_{DI}} = 1.085 - 1.097I + 0.0398I^2 \text{ RMD} \quad (3)$$

In Eq. 3, K_c=hydraulic conductivity to the inorganic chemical solution and K_{DI}=hydraulic conductivity to deionized water. The R^2 for Eq. (3) is 0.967 and the p statistic is less than 0.0001. Eq. (3) is linear in both I and RMD, and the product $I^2 \times$RMD reflects that the sensitivity to RMD varies nonlinearly with ionic strength (e.g., as in Fig. 7). Eq. (3) is valid for I=0.05–0.5 M and RMD$<$2.0 mM$^{1/2}$.

Eq. (3) is based on data from the GCL tested in this study under the state of stress that was employed (effective stress =20 kPa). However, Eq. (3) can be used to *estimate* how inorganic solutions may affect the hydraulic conductivity of other GCLs provided they employ granular Na-bentonite consisting of approximately 80% montmorillonite. Many of the GCLs used in North America today fit this description. Even if the granule size or montmorillonite content differs from those in this study, the relative effects of ionic strength and RMD should be approximately correct. In addition, Petrov and Rowe (1997) show that the hydraulic conductivity of GCLs exhibits similar sensitivity to effective stress regardless of whether DI water or a salt solution is used as the permeant liquid. Thus, Eq. (3) can be used to *estimate* the hydraulic conductivity at different effective stresses if the hydraulic conductivity to DI water at these stresses is known.

A comparison of K_c predicted with Eq. (3) and the measured hydraulic conductivity is shown in Fig. 10(a). The contour lines in Fig. 10 correspond to Eq. (3), whereas the data points correspond to the I and RMD for the tests conducted in this study. Eq. (3) captures the data reasonably well. Hydraulic conductivities predicted with Eq. (3) are also shown as contours in Fig. 10(b) along with points corresponding to I and RMD for actual leachates from a variety of wastes and solid waste disposal facilities reviewed by Kolstad (2000). The ionic strength and RMD of each leachate is summarized in Table 4, along with the data source (literature and regulatory agency reports) and the type of containment facility. The points and contour lines in Fig. 10(b) illustrate what hydraulic conductivity likely would have been had the GCL used in this study been tested with these leachates.

Of the 50 points shown in Fig. 10(b), 37 fall below 10^{-7} cm/s (74%) and 24 fall below 10^{-8} cm/s (48%). Thus, GCLs with high hydraulic conductivities ($>10^{-7}$ cm/s) should not be common in bottom liners where leachates similar to those in Table 4 are likely to be found. Moreover, many of the points in Fig. 10(b) associated with high hydraulic conductivities correspond to "young" (landfill age$<$5 yr) municipal solid waste (MSW)

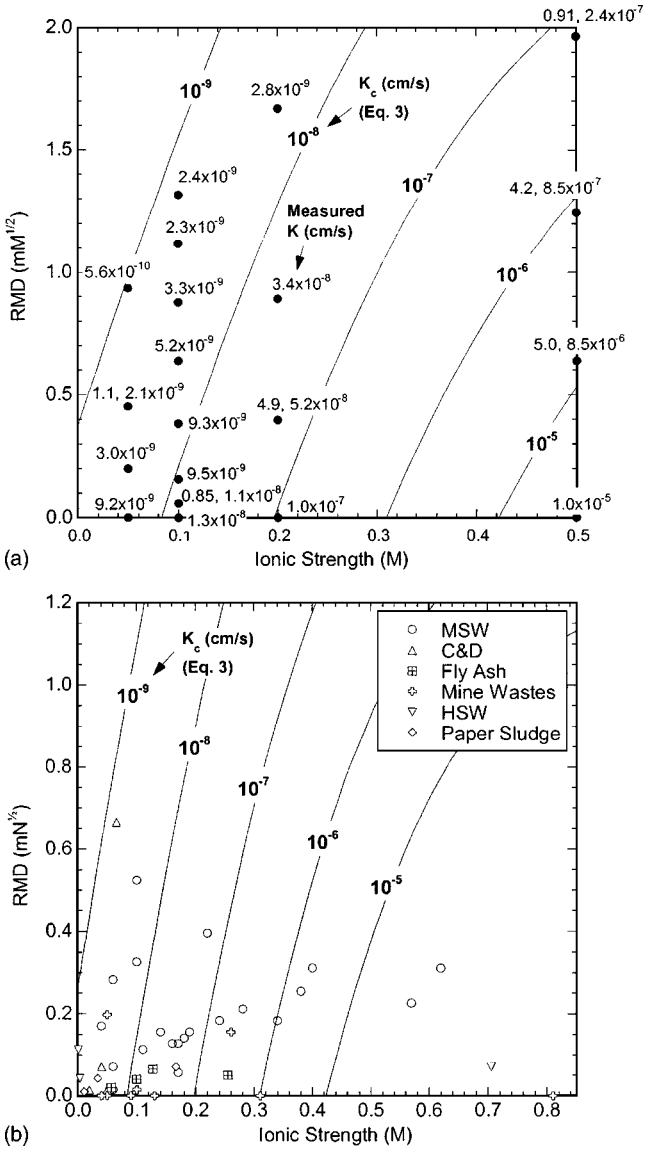

Fig. 10. Contours of hydraulic conductivity as a function of RMD and ionic strength predicted with Eq. (3) along with (a) measured hydraulic conductivities as solid circles and (b) points corresponding to ionic strength and RMD of various leachates. Data from Williams (1975) (I=1.87 M and RMD=0) and Kolstad (2000) (I=1.37 M and RMD=2.52 mM$^{1/2}$) are off the scale in (b).

leachates (Table 4). The composition of MSW leachate changes over time, and thus high hydraulic conductivities may not be realized because of the relatively long time required for a GCL and leachate to reach equilibrium under field conditions (Jo 2003). However, some of the points for mine waste, paper sludge, and fly ash disposal facilities are associated with high hydraulic conductivities, and the composition of leachates from these wastes can be persistent.

Effect of Prehydration

The results of this study pertain specifically to nonprehydrated GCLs. Different results may have been obtained had the GCLs been completely prehydrated by permeation with DI or potable water for several pore volumes of flow. Comparisons between hydraulic conductivities of nonprehydrated and completely prehy-

J. Geotech. Geoenviron. Eng. 2004.130:1236-1249.

Table 4. Summary of Ionic Strength and RMD of Various Leachates

Source	Leachate type	Ionic strength (M)	RMD ($mM^{1/2}$)
Ehrig (1983)	Young MSW leachate (<5 yr)	0.28	0.21
Pohland (1980)		0.38	0.25
Tchbanoglous et al. (1993)		0.14	0.16
Chian and DeWalle (1976)		0.17	0.13
Cheremisinoff (1983)		0.22	0.40
Alker et al. (1995)		0.16	0.13
Chian and DeWalle (1975)		0.57	0.23
Chian and DeWalle (1975)		0.62	0.31
Chian and DeWalle (1975)		0.34	0.18
Farquhar (1989)		0.40	0.31
Shams et al. (1994)		0.24	0.18
Ehrig (1983)	Intermediate MSW leachate (5–10 yr)	0.10	0.52
Pohland (1980)		0.10	0.33
Chian and DeWalle (1975)		0.17	0.06
Chian and DeWalle (1975)		0.11	0.11
Farquhar (1989)		0.18	0.14
Chian and DeWalle (1975)	Old MSW leachate (>10 yr)	0.06	0.01
Chian and DeWalle (1975)		0.06	0.28
Farquhar (1989)		0.06	0.07
Alker et al. (1995)		0.04	0.17
Kmet and McGinley (1982)	MSW leachate	0.19	0.16
Ruhl and Daniel (1997)		0.04	0.17
Kolstad (2000)	C and D leachate	0.05	0.01
Kolstad (2000)		0.02	0.01
WMNA (1993)		0.04	0.07
Weber et al. (2002)		0.066	0.66
Kolstad (2000)	Fly ash leachate	0.03	0.25
Kolstad (2000)		0.03	0.06
Kolstad (2000)		0.02	0.10
Kolstad (2000)		0.05	0.23
Kolstad (2000)		0.06	0.13
Kolstad (2000)		0.07	0.20
Kolstad (2000)		0.37	2.52
Kolstad (2000)		0.76	0.71
Al et al. (1994)	Mine process water	0.05	0.00
Shackelford (1998)		0.04	0.00
Jordan et al. (1998)		0.05	0.20

J. Geotech. Geoenviron. Eng. 2004.130:1236-1249.

Table 4. (*Continued.*)

Source	Leachate type	Ionic strength (M)	RMD ($mM^{1/2}$)
Williams (1975)	Acidic mine waste drainage	1.87	0.00
Christensen and Laake (1996)		0.13	0.00
Christensen and Laake (1996)		0.09	0.00
Al et al. (1994)		0.81	0.00
Shackelford (1998)		0.31	0.00
Williams (1975)	Pyritic tailings leachate	0.26	0.16
Pettit and Scharer (1999)	Ur rock drainage	0.10	0.01
Kolstad (2000)	Hazardous waste leachate	0.001	0.11
		0.70	0.07
		0.003	0.04
Kolstad (2000)	Paper mill landfill leachate	0.17	0.07
		0.01	0.01
		0.03	0.04

Note: RMD = Relative abundance of monovalent and divalent cations; MSW = Municipal solid waste.

drated GCLs that have been permeated long enough to establish chemical equilibrium between the bentonite solid and the solution show that prehydration by permeation with DI water results in hydraulic conductivities an order of magnitude lower than those obtained without prehydration, even if cation exchange between the mineral surface and the permeant liquid is complete (Petrov and Rowe 1997; Jo et al. 2004).

Although the effect of complete prehydration is significant, complete prehydration is unlikely to occur in the field. Most GCLs in field applications hydrate as water is drawn to the bentonite from an underlying subgrade via vapor diffusion or gradients in matric potential (Daniel et al. 1993, 1998; Katsumi et al. 2003). The prehydration afforded by these processes does not appear to have the same effect as complete prehydration by direct permeation. Vasko et al. (2001) found that the hydraulic conductivity of GCLs prehydrated with DI water via capillary wetting and vapor diffusion and permeated with $CaCl_2$ solutions had essentially the same hydraulic conductivity as nonprehydrated GCLs unless the solution was very strong (concentration >0.1 M). Comparable findings are reported by Katsumi et al. (2003). These observations suggest that hydraulic conductivities reported in this study are likely to be more representative of most field conditions than hydraulic conductivities of completely prehydrated GCLs.

Summary and Conclusions

This study dealt with the influence of multispecies inorganic salt solutions on swelling and hydraulic conductivity of nonprehydrated GCLs. Free swell and hydraulic conductivity tests were conducted on nonprehydrated specimens of a commercially available GCL using DI water and aqueous solutions of LiCl, NaCl, $CaCl_2$, and $MgCl_2$ salts. The relative amounts of monovalent and divalent cations in solution were quantified with the parameter RMD, which is the ratio of the total molarity of monovalent cations to the square root of the total molarity of divalent cations.

Results of the free swell tests show that swell is directly related to RMD and inversely related to ionic strength. RMD has a strong effect on swell in weaker solutions, and a modest effect in strong solutions. Similar findings were obtained from the hydraulic conductivity tests. Hydraulic conductivity was found to be directly related to ionic strength and inversely related to RMD, with RMD having a greater effect on hydraulic conductivity in weaker solutions. Tests were also conducted to determine if cation species affects swell or hydraulic conductivity. No discernable effect of cation species was evident in the free swell or hydraulic conductivity for tests conducted at a given ionic strength and RMD.

A strong relationship between hydraulic conductivity and free swell was found that is analogous to the relationship reported by Jo et al. (2001) for tests conducted using single-species salt solutions. However, the hydraulic conductivity-free swell relationship is not unique, and must be defined empirically for a particular bentonite if free swell tests are to be used for chemical compatibility screening.

The hydraulic conductivity data were also used to develop a regression model relating hydraulic conductivity of the GCL to ionic strength and RMD of the permeant solution. Predictions made with the model indicate that high hydraulic conductivities (i.e., $>10^{-7}$ cm/s) are unlikely for nonprehydrated GCLs in base liners in many solid waste containment facilities. However, for some wastes that transmit stronger leachates or leachates that are dominated by polyvalent cations (e.g., fly ash, paper sludge, and mine wastes), high hydraulic conductivities may be realized provided adequate time exists for the bentonite and leachate to reach chemical equilibrium.

J. Geotech. Geoenviron. Eng. 2004.130:1236-1249.

Acknowledgments

Funding for this study was provided in part by the National Science Foundation (Grant No. CMS-9900336). Professor Charles D. Shackelford of Colorado State Univ. provided technical and laboratory assistance during the study along with thoughtful discussion. The writers are grateful for his assistance.

References

Al, T., Blowes, D., and Jambor, J. (1994). "A geochemical study of the main tailings impoundment at the Falconbridge Limited, Kidd Creek Division metallurgical site, Timmins, Ontario," *Environmental chemistry of sulfide mine-wastes*, J. Jambor and D. Blowes, eds., Mineralogical Society of Canada, Ottawa, 333–364.

Alker, S., Sarsby, R., and Howell, R. (1995). "The composition of leachate from waste disposal sites," *Waste disposal by landfill—GREEN '93 Symposium*, Sarsby, R., ed., Balkema, Rotterdam, The Netherlands.

Alther, G., Evans, J., Fang, H., and Witmer, K. (1985). Influence of inorganic permeants upon the permeability of bentonite, *Hydraulic barriers in soil and rock, ASTM STP 874*, A. Johnson, R. Frobel, N. Cavalli, and C. Pettersson, Eds., ASTM, West Conshohocken, Pa., 64–73.

Ashmawy, A., El-Hajji, D., Sotelo, N., and Muhammad, N. (2002), "Hydraulic performance of untreated and polymer-treated bentonite in inorganic landfill leachates." *Clays Clay Miner.*, 50(5), 545–551.

Cheremisinoff, P. (1983). *Leachate from hazardous waste sites*, 1st Ed., Technomic Inc., Lancaster, Pa.

Chian, E., and DeWalle, F. (1975). "Characterization and treatment of leachates generated from landfills," *AIChE Symp. Ser.*, 71(145), 319–327.

Chian, E., and DeWalle, F. (1976). "Sanitary landfill leachates and their leachate treatment." *J. Environ. Eng. Div. (Am. Soc. Civ. Eng.)*, 102(2), 411–431.

Christensen, B., and Laake, M. (1996). "Treatment of acid mine water by sulfate-reducing bacteria; Results from a bench-scale experiment." *Water Res.*, 30(7), 1617–1624.

Daniel, D., Shan, H., and Anderson, J. (1993). Effects of partial wetting on the performance of the bentonite component of a GCL, *Geosynthetics 93*, Industrial Fabrics Assoc. International, St. Paul, MN, 1483–1496.

Daniel, D., Bowders, J., and Gilbert, R. (1997). "Laboratory hydraulic conductivity tests for saturated soils." *Hydraulic conductivity and waste contaminant transport in soil, ASTM STP 1142*, D. Daniel and S. Trautwein, eds., ASTM, West Conshohocken, Pa., 30–78.

Daniel, D., et al. (1998). "Slope stability of geosynthetic clay liner test plots." *J. Geotech. Geoenviron. Eng.*, 124(7), 628–637.

Draper, N., and Smith, H. (1998), *Applied regression analysis*, 3rd Ed., Wiley, New York.

Egloffstein, T. (1997). "Geosynthetic clay liners, part six: Ion exchange," *Geotech. Fabr. Rep.*, 15(5), 38–43.

Egloffstein, T. (2001). "Natural bentonites-influence of the ion exchange and partial desiccation on permeability and self-healing capacity of bentonites used in GCLs." *Geotext. Geomembr.*, 19, 427–444.

Ehrig, R. J. (1983). "Quality and quantity of sanitary landfill leachate." *Waste Manage. Res.*, 1, 53–68.

Farquhar, G. J. (1989). "Leachate: Production and characterization." *Can. J. Civ. Eng.*, 16, 317–325.

Fernandez, F., and Quigley, R. (1988), "Viscosity and dielectric controls on the hydraulic conductivity of clayey soils permeated with water-soluble organics." *Can. Geotech. J.*, 25, 582–589

Grim, R. (1968). *Clay mineralogy*, 2nd Ed., McGraw–Hill, New York, 596.

Jo, H. (2003). "Cation exchange and hydraulic conductivity of geosynthetic clay liners (GCLs) permeated with inorganic salt solutions." PhD dissertation, Univ. of Wisconsin—Madison, Wis.

Jo, H., Benson, C., and Edil, T. (2004). "Hydraulic Conductivity and Cation Exchange in Non-Prehydrated and Prehydrated Bentonite Permeates with Weak Inorganic Salt Solutions," *Clays Clay Miner.*, 52(6), 661–679.

Jo, H., Katsumi, T., Benson, C., and Edil, T. (2001). "Hydraulic conductivity and swelling of nonprehydrated GCLs permeated with single-species salt solutions." *J. Geotech. Geoenviron. Eng.*, 127(7), 557–567.

Jordan, D., Newcomer, R., and Mac Kinnon, R. (1998). "Geochemical transport modeling of tailing pore water." *Tailings and mine waste'98*, Balkema, Amsterdam, 497–506.

Katsumi, T., et al. (2002). "Geosynthetic clay liners against inorganic chemical solutions." *Proc., 2nd Japan–Korea Joint Seminar on Geoenvironmental Engineering*, Kyoto Univ., Kyoto, Japan, 27–32.

Katsumi, T., Ogawa, A., and Fukagawa, R. (2003). "Hydraulic conductivity of prehydrated clay geosynthetic barriers." *Proc., 3rd Korea–Japan Joint Seminar on Geoenvironmental Engineering*, Seoul National Univ., Seoul, pp. 63–68.

Kmet, P., and McGinley, M. (1982). *Chemical characteristics of leachate from municipal solid waste landfills in Wisconsin*, Bureau of Solid Waste Management, Wisconsin Department of Natural Resources, Madison, Wis.

Kolstad, D. (2000). "Compatibility of geosynthetic clay liners (GCLs) with multispecies inorganic solutions." MS thesis, Univ. of Wisconsin—Madison, Wis.

Lagerwerff, J., Nakayama, F., and Fere, M. (1969). "Hydraulic conductivity related to porosity and swelling of soils." *Soil Sci. Soc. Am. Proc.*, 33, 3–11.

Lambe, T., and Whitman, R. (1969), *Soil mechanics*, Wiley, New York.

Malik, M., Mustafa, M. A., and Letey, J. (1992). "Effect of mixed Na/Ca solutions on swelling, dispersion, and transient water flow in unsaturated montmorillonitic soils." *Geoderma*, 52, pp. 17–28.

McBride, M. (1994). *Environmental chemistry of soils*, Oxford University Press, New York, 406.

McBride, M. (1997). "A critique of diffuse double layer models applied to colloid and surface chemistry." *Clays Clay Miner.*, 45(4), 598–608.

McNeal, B., and Coleman, N. (1966). "Effect of solution composition on soil hydraulic conductivity." *Am. J. Soil Sci.*, 30, 308–312.

McNeal, B., Norvell, W., and Coleman, N. (1966). "Effect of solution composition on the swelling of extracted soil clays." *Am. J. Soil Sci.*, 30, 313–317.

Mesri, G., and Olson, R. (1971). "Mechanisms controlling the permeability of clays." *Clays Clay Miner.*, 19, 151–158.

Mustafa, M., and Hamid, K. (1977). "Comparison of two models for predicting the relative hydraulic conductivity of salt-affected swelling soils." *Soil Sci.*, 123, 149–154.

Norrish, K., and Quirk, J. (1954). "Crystalline swelling of montmorillonite, Use of electrolytes to control swelling." *Nature (London)*, 173, 255–257.

Onikata, M., Kondo, M., Hayashi, N., and Yamanaka, S. (1999). "Complex formation of cation exchanged montmorillonites with propylene carbonate: Osmotic swelling in aqueous electrolyte solutions." *Clays Clay Miner.*, 47(5), 672–677.

Pettit, C., and Scharer, J. (1999). "Neutral mine drainage." *Mining and the Environment II Conference Proceedings*, Vol. 2, Sudbury, Ontario. Goldsack, D., Belzile, N., Yearwood, P., and Hall, G., eds., pp. 372–376.

Petrov, R., and Rowe, R. (1997). "Geosynthetic clay liner (GCL)—Chemical compatibility by hydraulic conductivity testing and factors impacting Its performance." *Can. Geotech. J.*, 34, 863–885.

Petrov, R., Rowe, R., and Quigley, R. (1997). "Comparison of laboratory-measured GCL hydraulic conductivity based on three permeameter types." *Geotech. Test. J.*, 20(1), 49–62.

Pohland, F. G. (1980). "Leachate recycle as a landfill management option." *ASME J. Offshore Mech. Arct. Eng.*, 106(6), 1057–1069.

Prost, R., Koutit, T., Benchara, A., and Huard, E. (1998). "State and location of water adsorbed on clay minerals: Consequences of the

J. Geotech. Geoenviron. Eng. 2004.130:1236-1249.

hydration and swelling-shrinkage phenomena." *Clays Clay Miner.*, 46(2), pp. 117–131.
Quaranta, J., Gabr, M., and Bowders, J. (1997). "First-exposure performance of the bentonite component of a GCL in a low-pH, calcium-enriched environment." *Testing and acceptance criteria for geosynthetic clay liners, ASTM STP 1308*, L. Well, eds., ASTM, West Conshohocken, Pa., 162–177.
Quirk, J., and Marčelja, S. (1997). "Application of double-layer theories to the extensive crystalline swelling of Li-montmorillonite." *Langmuir*, 13, 6241–6248.
Reeve, R., and Bower, C. (1960). "Use of high-salt waters as a flocculant and source of divalent cations for reclaiming sodic soils." *Soil Sci.*, 90, 139–144.
Reeve, R., and Ramaddoni, G. (1965). "Effect of electrolyte concentration on laboratory permeability and field intake rate of a sodic soil." *Soil Sci.*, 99, 262–266.
Ruhl, J., and Daniel, D. (1997). "Geosynthetic clay liners permeated with chemical solutions and leachates." *J. Geotech. Geoenviron. Eng.*, 123(4), 369–381.
Shackelford, C. (1998). GCL compatibility testing for base liner at the tailings management area for the proposed nicolet minerals company zinc/copper mine, near Crandon, Wisconsin, *Final Rep. Prepared for Foth & Van Dyke and Assoc., Inc.*, Green Bay.
Shackelford, C., Benson, C., Katsumi, T., Edil, T., and Lin, L. (2000). "Evaluating the hydraulic conductivity of GCLs permeated with nonstandard liquids." *Geotext. Geomembr.*, 18, 133–161.
Shams-Khorzani, R., Knox, T., and Brockway, C. (1994). "Sanitary landfill leachate treatment and disposal." *Public Works*, 125(7), 46–49.
Shan, H., and Daniel, D. (1991). "Results of laboratory tests on a geotextile/bentonite liner material." *Geosynthetics 2001*, Industrial Fabrics Assoc. International, St. Paul, Minn., 517–535.
Shan, H., and Lai, Y. (2002). "Effect of hydrating liquid on the hydraulic properties of geosynthetic clay liners." *Geotext. Geomembr.*, 20, 19–38.
Smalley, M. (1994). "Electrical theory of clay swelling." *Langmuir*, 10, 2884–2891.
Spark, D. L. (1996). *Methods of soil analysis, Part 3. Chemical methods*, Soil Science Society of America, Madison, Wis., 1201–1230.
Sposito, G. (1981). *The thermodynamics of soil solutions*, Oxford University Press, New York.
Sposito, G. (1989). *The chemistry of soils*, Oxford University Press, New York.
Tchobanoglous, G., Theisen, H., and Vigil, S. (1993). *Integrated solid waste management*, 1st Ed., McGraw–Hill, New York, 978.
Terzaghi, K., Peck, R., Mesri, G. (1996). *Soil mechanics in engineering practice*, 3rd Ed., Wiley, New York.
Van Olphen, H. (1977). *An introduction to clay colloid chemistry*, 2nd Ed., Wiley, New York.
Vasko, S., Jo, H., Benson, C., Edil, T., and Katsumi, T. (2001). "Hydraulic conductivity of partially prehydrated geosynthetic clay liners permeated with aqueous calcium chloride solutions." *Geosynthetics 2001*, Industrial Fabrics Assoc. International, St. Paul, Minn., 685–699.
Weber, W., Jang, Y., Townsend, T., and Laux, S. (2002). "Leachate from land disposed residential construction waste." *J. Environ. Eng.*, 128(3), 237–245.
Williams, R. (1975). *Waste production and disposal in mining, milling and metallurgical industries*, Millar Freeman Publications.
Waste Management of North America, Inc. (WMNA). (1993). *Construction and demolition landfill leachate characterization study*, WMNA, Naperville, Ill.
Wu, J., Low, P., and Roth, C. (1994). "Effect of 1,4-dioxane on the expansion of montmorillonite layers in a montmorillonite/water system." *Clays Clay Miner.*, 42(2), 109–113.
Zhang, F., Low, P., and Roth, C. (1995). "Effects of monovalent exchangeable cations and electrolytes on the relation between swelling pressure and interlayer distance in montmorillonite." *J. Colloid Interface Sci.*, 173, 34–41.

J. Geotech. Geoenviron. Eng. 2004.130:1236-1249.

Hydraulic Conductivity of Geosynthetic Clay Liners Exhumed from Landfill Final Covers

Stephen R. Meer[1] and Craig H. Benson[2]

Abstract: Samples of geosynthetic clay liners (GCLs) from four landfill covers were tested for water content, swell index, hydraulic conductivity, and exchangeable cations. Exchange of Ca and Mg for Na occurred in all of the exhumed GCLs, and the bentonite had a swell index similar to that for Ca or Mg bentonite. Hydraulic conductivities of the GCLs varied over 5 orders of magnitude regardless of cover soil thickness or presence of a geomembrane. Hydraulic conductivity was strongly related to the water content at the time of sampling. Controlled desiccation and rehydration of exhumed GCLs that had low hydraulic conductivity (10^{-9} to 10^{-7} cm/s) resulted in increases in hydraulic conductivity of 1.5–4 orders of magnitude, even with overburden pressure simulating a 1-m-thick cover. Comparison of these data with other data from the United States and Europe indicates that exchange of Ca and/or Mg for Na is likely to occur in the field unless the overlying cover soil is sodic (sodium rich). The comparison also shows that hydraulic conductivities on the order of 10^{-6} to 10^{-4} cm/s should be expected if exchange occurs coincidently with dehydration, and the effects of dehydration are permanent once the water content of the GCL drops below approximately 100%. Evaluation of the field data also shows that covering a GCL with a soil layer 750–1,000 mm thick or with a geomembrane overlain by soil does not ensure protection against ion exchange or large increases in hydraulic conductivity.

DOI: 10.1061/(ASCE)1090-0241(2007)133:5(550)

CE Database subject headings: Geosynthetics; Linings; Clays; Hydraulic conductivity; Swelling; Landfills.

Introduction

Geosynthetic clay liners (GCLs) are factory-made clay liners that consist of a layer of bentonite sandwiched between two geotextiles that are held together by needle punching, stitching, or adhesives. In some cases, a geomembrane is included in addition to or in lieu of the geotextiles. The key component of a GCL is the sodium (Na) bentonite, which has a hydraulic conductivity $\approx 10^{-9}$ cm/s when permeated with deionized (DI) or tap water under stresses typical in final covers (Shan and Daniel 1991; Shackelford et al. 2000; Jo et al. 2001; 2005; Kolstad et al. 2004). GCLs present an attractive alternative to compacted clay liners as the hydraulic barrier layer in landfill cover systems because of their low hydraulic conductivity (10^{-9} cm/s), ease of installation, and limited thickness (Bouazza 2002). However, the bentonite in GCLs is sensitive to chemical interactions with the hydrating liquid, and ion exchange that occurs in bentonite can significantly alter its physical properties (Shan and Daniel 1991; Gleason et al. 1997; Ruhl and Daniel 1997; Shackelford et al. 2000; Jo et al. 2001, 2004; Vasko et al. 2001; Kolstad et al. 2004).

Recent studies have suggested that, under some circumstances, the combined effects of ion exchange and physical dehydration can significantly increase the hydraulic conductivity of a GCL (Melchior 1997, 2002; Lin and Benson 2000; Benson et al. 2006), rendering the GCL ineffective as a hydraulic barrier. However, field data confirming these effects have been limited. The focus of this study was to determine the hydraulic conductivity of GCLs used in four landfill final covers and to investigate field conditions influencing the hydraulic conductivity. GCLs from each cover were exhumed and tested for saturated hydraulic conductivity, water content, swell index, and composition of the exchange complex (the collection of cations adsorbed on the clay surface). Samples of the overlying cover soil from each field site were also tested for carbonate content, cations in the pore water, and index properties. Data from these tests were evaluated in conjunction with data reported by others to draw inferences regarding the likelihood of cation exchange and increases in hydraulic conductivity. Methods commonly assumed to protect GCLs from ion exchange and increases in hydraulic conductivity are also evaluated in the context of the field data.

Background

Laboratory Studies on Effects of Wet–Dry Cycling and Ion Exchange

Lin and Benson (2000) studied the effects of wet–dry cycling on the swell of bentonite and the hydraulic conductivity of a needle-punched GCL hydrated with DI water and a 12.5 mM $CaCl_2$ solution representing the pore water of vegetated surface layers in Wisconsin. A needle-punched GCL with a dry mass per unit area of 7.5 kg/m^2 was used. Hydraulic conductivity tests were con-

[1]Staff Engineer, Sigma Environmental Services, Inc., 1300 West Canal St., Milwaukee, WI 53233. E-mail: smeer@thesigmagroup.com

[2]Professor and Kellet Fellow, Geological Engineering, Univ. of Wisconsin-Madison, 1415 Engineering Dr., Madison, WI 53706. E-mail: benson@engr.wisc.edu

Note. Discussion open until October 1, 2007. Separate discussions must be submitted for individual papers. To extend the closing date by one month, a written request must be filed with the ASCE Managing Editor. The manuscript for this paper was submitted for review and possible publication on July 12, 2006; approved on November 29, 2006. This paper is part of the ***Journal of Geotechnical and Geoenvironmental Engineering***, Vol. 133, No. 5, May 1, 2007. ©ASCE, ISSN 1090-0241/2007/5-550–563/$25.00.

J. Geotech. Geoenviron. Eng. 2007.133:550-563.

ducted on GCL specimens that were repeatedly permeated and then allowed to air dry until the mass ceased changing (gravimetric water content ≈15–20%). Swell tests were conducted on bentonite that had been wetted and dried. Swelling decreased to levels typical of Ca bentonite within 4–5 wet–dry cycles for all specimens hydrated with the $CaCl_2$ solution, whereas swell of specimens hydrated with DI water increased slightly as the number of wet–dry cycles increased. All specimens retained low (10^{-9} cm/s) hydraulic conductivity through four wet–dry cycles. During the remaining wet–dry cycles, the specimen permeated with DI water retained low hydraulic conductivity, but all specimens permeated with $CaCl_2$ showed increases in hydraulic conductivity of approximately 3 orders of magnitude ($>10^{-6}$ cm/s). Lin and Benson (2000) conclude that the increase in hydraulic conductivity was the result of ion exchange in conjunction with dehydration of the bentonite, the latter giving rise to desiccation cracks that did not swell shut during rewetting.

Sporer and Gartung (2002) conducted wet–dry cycling on GCLs containing Na or Ca bentonite. The GCLs were hydrated with DI water or 9 mM $CaCl_2$ under a normal stress of 15 kPa, and then were dried under the same confining stress until the water content was ≈10–15%. Water content after each wetting cycle was determined and the bentonite was inspected visually for cracks after the final cycle. Sporer and Gartung (2002) report that desiccation impacts subsequent rehydration, reducing the hydrated water content by approximately 10–20% depending on the water used for hydration (DI water or $CaCl_2$ solution). No cracks were visible in the bentonite hydrated with DI water, but cracks were present in the bentonite permeated with the $CaCl_2$ solution. Hydraulic conductivity tests were also conducted on two GCLs containing Ca bentonite that had undergone one wet–dry cycle or no cycling. The hydraulic conductivity of the specimen that had undergone a single wet–dry cycle was 1 order of magnitude lower than the specimen that was not dried.

Field Studies of Hydraulic Properties of Geosynthetic Clay Liners in Landfill Final Covers

James et al. (1997) exhumed an adhesive-bonded GCL containing Na bentonite to determine why a cover with a GCL was leaking excessively. The GCL was placed on compacted clay and was overlain by a 150-mm-thick layer of gravel and a 300-mm-thick surface layer. The exhumed GCL contained finely cracked zones and had an average gravimetric water content of 116%. Na in the GCL was extensively replaced by Ca. The montmorillonite fraction of the bentonite in the exhumed GCL contained 10.3 $cmol^+$/kg Na and 81.6 $cmol^+$/kg Ca, on average, whereas 60.4 $cmol^+$/kg Na and 40.9 $cmol^+$/kg Ca were present when the GCL was new. Calcite in the bentonite (2%), rainfall percolating through overlying calcareous soil, and the water used to initially hydrate the GCL (Ca concentration ≈0.003 M) were suggested as the source of the Ca involved in exchange. Hydraulic conductivity tests were not conducted on the exhumed GCL.

Melchior (1997, 2002) studied five GCLs containing Na bentonite installed in a landfill cover near Hamburg, Germany. Two of the GCLs were underlain by a pan lysimeter (50×10 m) for measuring percolation. Three GCLs were installed in observation plots (3×2 m) without a lysimeter. A composite GCL containing a geomembrane was included in one of the observation plots, with the geomembrane oriented upward. All GCLs were covered with 150 mm of sandy gravel overlain by a 300-mm-thick surface layer of topsoil. For the conventional GCLs, daily percolation rates from the lysimeters were as high as 15 mm/day, and the average annual percolation rate ranged between 188 and 222 mm/year after 4 years. Root penetration of the GCL occurred within 5 months of installation, and extensive cracking of the bentonite was observed in slightly more than 1 year, with some cracks as wide as 2 mm. Moreover, complete exchange of Ca for Na occurred and the swell index of the bentonite was comparable to that of Ca bentonite. Hydraulic conductivities ranged between 1×10^{-5} and 3×10^{-4} cm/s and water contents ranged between 55 and 100% (average=60%). Desiccation cracks were observed in GCLs having a water content <100%. Properties of the composite GCL were notably different. Less cation exchange occurred in the composite GCL, and the bentonite retained had higher water content and swell index. However, cation exchange was not eliminated by the geomembrane.

Egloffstein (2001, 2002) summarizes the properties of GCLs exhumed from landfill covers in Germany. Gravimetric water contents of the GCLs ranged from 40 to 120% and complete exchange of Ca for Na occurred within as little as 2 years. Egloffstein (2002) reports that the GCLs had hydraulic conductivities on the order of 10^{-5} cm/s when first permeated, but the hydraulic conductivity decreased to approximately 10^{-7} cm/s after approximately 20 days. An effective stress of 20 kPa was applied during the hydraulic conductivity tests. No information was provided regarding the permeant liquid.

Egloffstein (2001) also conducted a long-term hydraulic conductivity test on a new specimen of GCL that was initially permeated with DI water and then with a $CaCl_2$ solution. Permeation with the Ca solution caused the hydraulic conductivity to increase to 3×10^{-8} cm/s, which is considerably lower than the hydraulic conductivity of the exhumed specimens. Based on this observation, Egloffstein (2001) concludes that the higher hydraulic conductivities of exhumed GCLs are due to ion exchange combined with desiccation cracks that do not seal during rehydration, as suggested by Lin and Benson (2000). Egloffstein (2002) also reports that desiccation cracks in GCLs are finer and more abundant in needle-punched GCLs than in stitch-bonded GCLs. Egloffstein (2001) also suggests that the confining pressure afforded by 750 mm or more of cover soil is sufficient to seal desiccation cracks and prevent large increases in hydraulic conductivity, but provides no data to support this hypothesis.

Wagner and Schnatmeyer (2002) evaluated a landfill cover design containing a needle-punched GCL with Na bentonite at a field site in Luxembourg. Percolation from the cover was recorded with a 45-m^2 pan lysimeter over a 2-year period. The GCL was placed on a layer of sand and overlain by 250 mm of coarse electric furnace slag and 750 mm of silty sand. The slag provided lateral drainage at the surface of the GCL, and the sand and slag formed capillary breaks on both sides of the GCL that maintained moisture within the bentonite. Percolation collected in the lysimeter was minimal during the first year and 6 mm during the second year. Daily percolation rates typically were five times higher during the second year than the first year, and the peak daily percolation rate was 0.072 mm/day.

Mansour (2001) exhumed GCLs from a test section consisting of a 660-mm-thick surface layer of well-graded sandy soil with fines overlying a conventional GCL (characteristics not described) located in a semiarid area of California. The exhumation was conducted 5 years after the test section was constructed. Tests conducted on the exhumed GCL using DI water as the permeant liquid at a confining stress of 35 kPa yielded a hydraulic conductivity of 1.9×10^{-9} cm/s. Water content of the GCL was not reported, but the swell index was determined to be 33 mL/2 g, on average. These properties were reported as nearly

J. Geotech. Geoenviron. Eng. 2007.133:550-563.

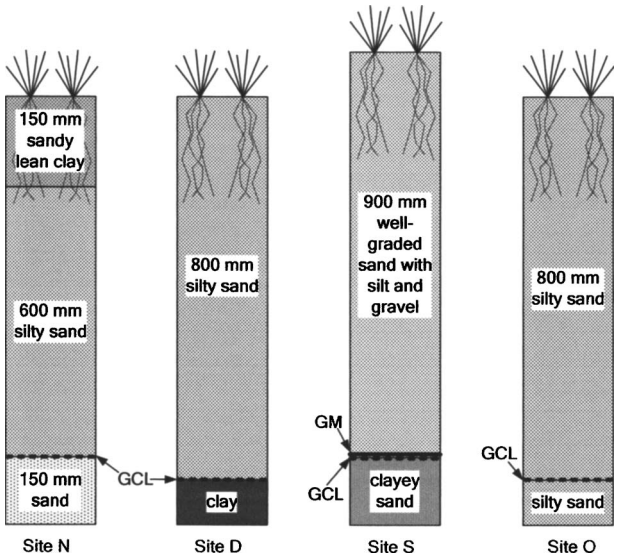

Fig. 1. Profiles of final covers at the field sites

identical to those measured on the GCL when it was installed. Analysis of soluble salts in the surface layer and the GCL indicated that the pore water in both materials was dominated by Na. The sodic (sodium rich) condition of the surface layer probably prevented cation exchange in the GCL, as evinced by the absence of change in swell index (Benson et al. 2006).

Henken-Mellies et al. (2002) conducted a 3-year field test of a GCL containing Ca bentonite in a landfill cover system underlain by a pan lysimeter. A geocomposite drainage layer was placed directly above the GCL and was overlain by a 1-m-thick surface layer. The average leakage rate for the 3-year observation period was 5.4 mm/year, although daily percolation rates as high as 1.7 mm/day (608 mm/year) were recorded. Henken-Mellies et al. (2002) also indicate that sensors installed in the GCL showed that the water content of the bentonite changed considerably, even with 1,000 mm of soil overlying the GCL. Higher water contents generally were observed in the spring and early summer, whereas lower water contents were observed over the rest of the year.

Mackey and Olsta (2004) exhumed GCLs from two landfills (A and B) on the coast of Florida where the final cover consisted of a surface layer overlying a needle-punched GCL. Both had been in service for more than 5 years. Clean sand (610–810 mm thick) was used for the cover soil at Landfill A and silty sand (460–860 mm thick) was used for the cover soil at Landfill B. Shell fragments (a potential source of Ca) were found in the surface layer at both sites. The bentonite was moist at both sites (water contents were not reported) and analysis of exchangeable cations showed that nearly all of the Na had been replaced by Ca and Mg at both sites. The swell index at both sites ranged between 7.5 and 14 mL/2 g, which is consistent with Ca and Mg being the dominant exchangeable cations. Hydraulic conductivity of the GCL exhumed from Landfill A ranged between 8.5×10^{-9} and 6.4×10^{-6} cm/s, with lower hydraulic conductivities being reported for tests conducted by the GCL manufacturer (average$=1.4\times10^{-8}$ cm/s) than independent laboratories (average$=1.2\times10^{-6}$ cm/s). Lower hydraulic conductivities were reported for the GCL exhumed from Landfill B (3.5×10^{-9} to 2.3×10^{-8} cm/s).

Benson et al. (2006) describe a case history of a final cover over a coal-ash landfill containing a GCL with Na bentonite. The GCL was covered with 760 mm of vegetated silty sand and underlain with two gravel-filled lysimeters to monitor percolation. Higher than anticipated percolation rates (up to 450 mm/year) were recorded within 4–15 months after installation of the GCL. The GCL was subsequently replaced with a composite GCL laminated with a polyethylene geofilm. Low percolation rates (2.6–4.1 mm/year) were maintained by the composite GCL for more than 5 years. Samples of the conventional GCL exhumed from the cover had hydraulic conductivities on the order of 5×10^{-6} cm/s. The high hydraulic conductivities were attributed to exchange of Ca and Mg for Na combined with dehydration of the bentonite. Ca and Mg from the surface layer were responsible for the cation exchange that occurred.

Table 1. Description of Covers at Field Sites

	Site			
Property	N	D	S	O
Location	Wisconsin	Wisconsin	Wisconsin	Georgia
Geosynthetic clay liner bonding	Needle punched	Adhesive bonded	Needle punched	Adhesive bonded (top deck); needle punched (slopes)
Installation date	11/1997	9/1991	9/1998	4/1997
Sampling date	7/2002	10/2002	10/2002	12/2002
Service life (year)	4.6	11.1	4.1	5.6
Surface layer thickness (mm)	750	800	900	800 (top deck) 400 (slopes)

Materials

GCLs

GCLs were exhumed from covers at four landfills. Three of the landfills are located in Wisconsin, and one is located in Georgia. The cover profiles at each site are illustrated in Fig. 1, and descriptions of each site are summarized in Table 1. None of the GCLs were laminated with a geomembrane (GM), but at one landfill (S), the GCL was overlain by a geomembrane to form a composite barrier. At each landfill, one or more test pits were excavated to a depth near the GCL in the cover profile. When the excavation approached the GCL, the remaining cover soil was removed by hand to prevent damage to the GCL. Once the GCL was exposed, samples were cut into square specimens (300×300 mm) using a razor knife and sealed in plastic for subsequent testing.

Tests were also conducted on a new (never in-service) GCL provided by a manufacturer. The new GCL contained granular Na bentonite encased by two geotextiles (a slit-film woven geotextile and a nonwoven geotextile) bonded by needle punching. The mass per unit area of air-dry bentonite in the GCL was 4.3 kg/m^2, the initial air-dry thickness of the GCL ranged from 5.8 to 7.0 mm, and the average initial air-dry water content of the bentonite was 7%. Bentonite in the GCL consisted of sand-size granules (0.075–2.0 mm). The clay-size fraction (particles finer than 0.002 mm) was 87%, the liquid limit was 504, and the plasticity index was 465.

J. Geotech. Geoenviron. Eng. 2007.133:550-563.

Table 2. Properties of Cover Soils from Field Sites and Alternate Cover Assessment Program Sites

Site	Soil type	Water content (%)	Paste pH	$CaCO_3$ content (%)
N	Sandy lean clay (upper 150 mm)	11	7.4	2.6
	Silty sand (lower 600 mm)	13	7.2	2.2
S (surface layer)	Well-graded sand with silt and gravel	19	5.6	1.0
S (subgrade)	Clayey sand	13	5.1	1.0
D	Silty sand	24	5.8	1.0
O (top deck)	Silty sand	20	5.2	1.4
O (slope)	Silty sand	21	5.0	1.3
Alternate Cover Assessment Program D	Lean clay	—	7.9	0.9
Alternate Cover Assessment Program F	Sandy silt	—	7.8	1.9
Alternate Cover Assessment Program V	Silty sand with gravel	—	8.0	1.9
Alternate Cover Assessment Program A	Clayey sand	—	7.2	0.5

Although the new GCL was not identical to the GCLs used at each of the landfills, most of the GCLs used in North America contain bentonite from similar sources and have similar hydraulic properties, with hydraulic conductivities to DI water typically falling within 9×10^{-10} to 3×10^{-9} cm/s for stresses typical of covers (Shackelford et al. 2000; Thiel et al. 2001; Kolstad et al. 2004; Jo et al. 2001, 2004, 2005; Lee and Shackelford 2005). The new GCL was also provided by the same manufacturer that supplied the GCLs to each of the sites in this study. Therefore, except for bonding method, the new GCL used in this study is believed to be reasonably representative of the GCLs initially installed in the field.

Cover Soils

Grab samples of the overlying cover soils at each site were collected for particle size analysis (ASTM D 422, see ASTM 2004) and calcium carbonate content following the method described in Radd (1978). Paste pH was also measured following the method described in Sobek et al. (1978). Properties of the cover soils are summarized in Table 2. Four additional cover soils from the Alternative Cover Assessment Program (ACAP) (Albright et al. 2004, 2006) were also tested for comparative purposes, as was the subgrade soil from one of the field sites (Site S). Index properties of the ACAP soils and the subgrade from Site S are also summarized in Table 2. The cover soils are fine textured, ranging from silty sands to clays, have near neutral pH (5.1–8.0), and low carbonate content.

Methods

Cover Soil Elution Tests

Elution tests were conducted on the cover soils using a batch procedure and a column procedure. The batch procedure was conducted following the procedures described in ASTM D 6141 (ASTM 2004) using a solution mimicking synthetic rainwater as the eluent (see subsequent discussion for composition) with a liquid-to-solid ratio of 1.3. The mixture was blended using a high-speed mixer. The resulting slurry was sealed, allowed to equilibrate for 24 h, and then vacuum filtered using a Buchner funnel and Whatman GF-F filter paper. Concentrations of Ca, Mg, Na, and K in the test liquid were measured using atomic absorption spectroscopy (AAS) following USEPA Method 200.7.

Column elution tests were conducted on the cover soils in rigid-wall permeameters similar to those described in ASTM D 5856 (ASTM 2004). Specimens were prepared by compaction in a stainless steel compaction mold (diameter=105 mm, height=75 mm) to a dry unit weight corresponding to 85% relative compaction per standard Proctor. Both ends of the specimen were covered with disks of nonwoven geotextile, and a porous stone was placed on top of the upper geotextile to distribute the influent water. Synthetic rainwater was allowed to slowly drip (2 mL/h) onto the porous stone to simulate the slow unsaturated infiltration that might occur in the field. Effluent from the column was analyzed for concentrations of Ca, Mg, Na, and K by AAS, as described previously.

Ionic composition of the synthetic rainwater was based on an analysis of rainwater chemistry from 18 locations in North America, Europe, and Asia (Meer and Benson 2004). The analysis showed that average rainwater has an ionic strength of 0.8 mM, RMD of 0.02 $M^{1/2}$, and pH 7.1, on average, with Ca, Na, and NH_4 being the dominant cations. RMD is defined as $M_m/M_d^{1/2}$, where M_m=total molarity of monovalent cations and M_d=total molarity of polyvalent cations, and represents the relative abundance of monovalent and polyvalent cations in a solution. For inorganic aqueous permeant solutions, ionic strength and RMD

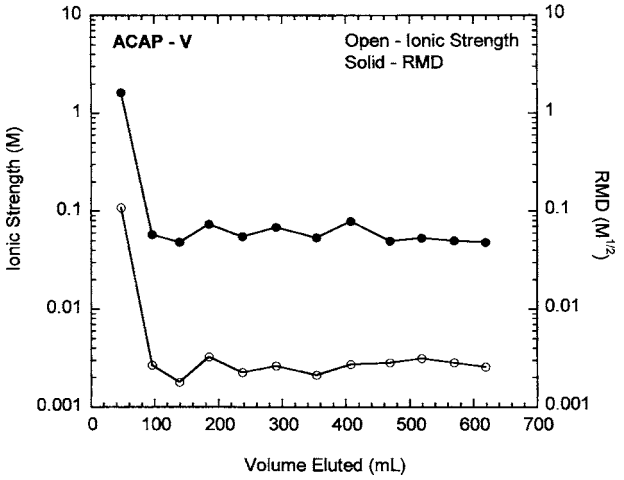

Fig. 2. Ionic strength and RMD for the leachate from column tests on surface layer soil from alternate cover assessment program (Site V)

J. Geotech. Geoenviron. Eng. 2007.133:550-563.

Table 3. Steady-State Ionic Strength and RMD from Column Elution Tests on Cover Soils

Site	Location	Column		Batch	
		Ionic strength (M)	RMD ($M^{1/2}$)	Ionic strength (M)	RMD ($M^{1/2}$)
S	Surface layer	0.0005	0.0075	0.0005	0.0140
S	Subgrade	0.0009	0.0250	0.0007	0.0154
D	Surface layer	0.0006	0.0110	0.0004	0.0210
O	Surface layer (top deck)	0.0010	0.0600	0.0009	0.0535
O	Surface layer (slopes)	0.0011	0.0350	0.0009	0.0192
N	Surface layer (upper)	0.0042	0.0060	0.0010	0.0102
N	Surface layer (lower)	0.0015	0.0050	0.0009	0.0252
Alternate Cover Assessment Program D	Surface layer	0.0004	0.0180	0.0172	1.910
Alternate Cover Assessment Program F	Surface layer	0.0037	0.0950	0.0028	0.0713
Alternate Cover Assessment Program V	Surface layer	0.0028	0.0500	0.0015	0.0789
Alternate Cover Assessment Program A	Surface layer	0.0040	0.0300	0.0032	0.0299

are master variables controlling the hydraulic conductivity of GCLs for pH between 2 and 12 (Jo et al. 2001; Kolstad et al. 2004). The synthetic rainwater was prepared by dissolving NaCl and $CaCl_2$ salts in DI water to create a solution having the ionic strength and RMD noted above. NH_4 was not included to minimize the potential for chemical instability of the influent.

An example of how the ionic strength and RMD of the effluent varied is shown in Fig. 2 as a function of eluted volume (all data compiled in Meer and Benson 2004). The ionic strength and RMD typically decreased quickly and then leveled off, with steady ionic strength and RMD being obtained within 200 mL of elution. The steady ionic strengths and RMDs obtained from the column tests are summarized in Table 3 along with the ionic strengths and RMDs obtained from the batch tests. The column and batch test data are compared in Fig. 3.

The data from the batch and column tests are comparable. Ionic strengths from the column tests are slightly higher than those from the batch tests (1.5 times, on average) and the RMD is slight lower (0.85 times, on average). Thus, the batch test provides a relatively simple and expedient method to generate a test liquid representative of flow-through conditions. Graphs were also prepared to determine if ionic strength or RMD could be correlated to the $CaCO_3$ content of the cover soils. No trend with $CaCO_3$ content was observed for ionic strength or RMD.

Swell Index Tests

Swell index tests were conducted on bentonite from the new GCL and the exhumed GCLs according to methods described in ASTM D 5890 (ASTM 2004). Tests were conducted with DI water on all of the GCLs. Leachate obtained from the batch elution tests on the cover soils was also used to conduct swell index tests on bentonite from the new GCL. Tests were conducted with the batch test leachate to determine whether swell index tests can be used to assess compatibility of GCLs with cover soils. Results of the swell index tests are summarized in Table 4 (new GCL) and Table 5 (exhumed GCLs).

Hydraulic Conductivity Tests

Hydraulic conductivity tests were conducted on the GCLs in flexible-wall permeameters according to methods described in ASTM D 5084 using the falling headwater-constant tailwater

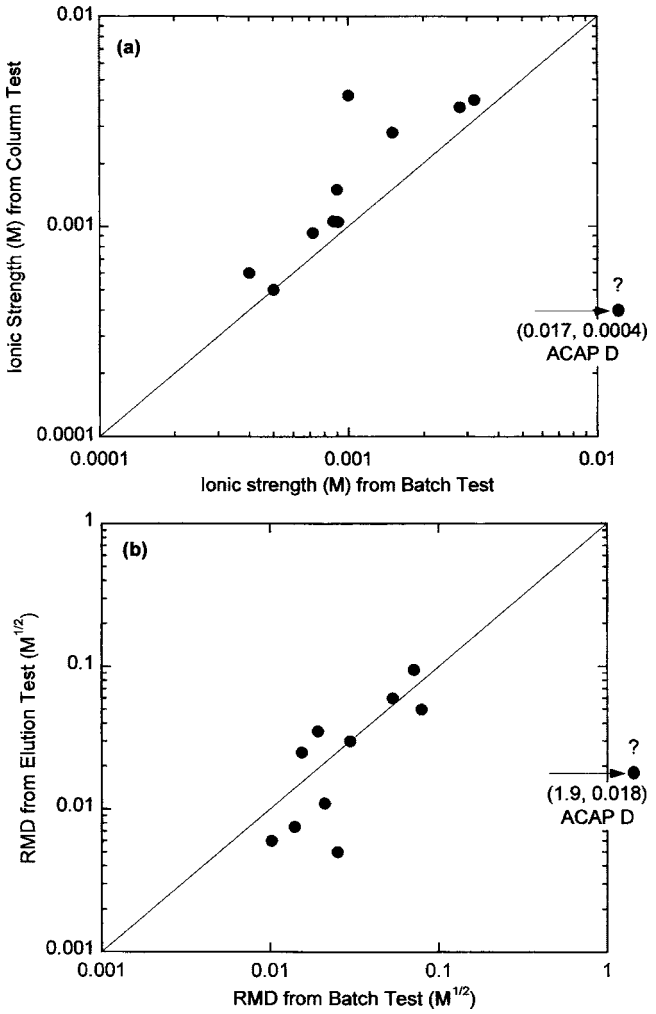

Fig. 3. Comparison of ionic strength (a) and RMD (b) from column and batch elution tests on cover soils using synthetic rainwater as the eluent

J. Geotech. Geoenviron. Eng. 2007.133:550-563.

Table 4. Swell Index of Sodium Bentonite from New Geosynthetic Clay Liner in Liquid Produced by ASTM D 6141 Batch Tests Conducted with Cover Soils from Field Sites

Site	Soil used in batch test	Swell index (mL/2 g)
N	Surface layer—upper 150 mm	30
N	Surface layer—lower 600 mm	30
D	Surface layer	28
O	Surface layer—top deck	29
O	Surface layer—side slope	29
S	Surface layer	28
S	Subgrade	29
New geosynthetic clay liner	No soil—deionized water	35

method. An average hydraulic gradient of 100 and an average effective stress of 20 kPa were applied. Backpressure was not used to simulate field-satiated conditions. The hydraulic gradient that was used is higher than that in the field, but is typical of hydraulic gradients used when testing GCLs. Because GCLs are thin, relatively high hydraulic gradients can be used without the excessive increases in effective stress that are encountered when testing compacted clays with higher hydraulic gradients (Shackelford et al. 2000).

GCL test specimens were prepared using the method described in Jo et al. (2001). A razor knife was used to cut the GCL along the outer circumference of a stainless steel cutting ring with a sharpened edge. To prevent loss of bentonite around the perimeter, a small volume of permeant liquid was applied to the GCL along the inner circumference of the cutting ring prior to cutting. After the specimen was removed from the cutting ring, excess

Table 5. Physical and Chemical Properties of Geosynthetic Clay Liners

Site ID[a] and sample number	Exhumed water content (%)	Post-test water content (%)	Swell index (mL/2 g)	Hydraulic conductivity (cm/s)	Exchange complex (mole fraction)			
					Na	Ca	Mg	K
New geosynthetic clay liner	—	209.1	36	1.2×10^{-9}	0.74	0.22	0.03	0.02
New geosynthetic clay liner	—	202.3	34	1.7×10^{-9}	0.65	0.27	0.03	0.05
N-1	30.9	55.0	9.5	4.3×10^{-5}	0.06	0.73	0.16	0.05
N-2	39.8	52.0	8.0	8.2×10^{-5}	0.03	0.70	0.18	0.08
N-3	44.5	73.0	8.0	6.0×10^{-5}	0.02	0.71	0.20	0.07
N-4	51.4	51.4	—	1.7×10^{-5}	0.02	0.74	0.18	0.05
N-5	38.4	44.0	—	1.2×10^{-6}	0.06	0.71	0.20	0.03
N-6	55.1	54.0	8.0	1.2×10^{-5}	0.03	0.71	0.21	0.05
N-7	48.8	42.0	—	1.5×10^{-6}	—	—	—	—
N-8	32.5	53.0	—	8.1×10^{-6}	—	—	—	—
N-9	52.0	47.0	—	2.1×10^{-5}	—	—	—	—
N-10	55.7	67.0	—	1.0×10^{-4}	—	—	—	—
N-11	58.5	60.0	—	9.1×10^{-5}	—	—	—	—
N-12	38.3	60.1	—	7.2×10^{-5}	—	—	—	—
N-12	—	—	—	4.6×10^{-5}	—	—	—	—
N-13	44.3	60.8	—	2.0×10^{-5}	—	—	—	—
N-14	53.4	53.4	—	1.9×10^{-5}	—	—	—	—
D-1	182.1	155.1	11.0	2.9×10^{-8}	0.15	0.72	0.12	0.01
D-2	170.2	135.9	—	3.0×10^{-8}	0.02	0.78	0.18	0.02
D-3	204.2	179.0	—	1.1×10^{-7}	0.03	0.78	0.18	0.01
D-4	165.9	179.0	10.5	7.5×10^{-8}	0.04	0.70	0.21	0.04
S-1	57.9	68.5	—	5.1×10^{-5}	0.21	0.68	0.09	0.01
S-2	59.2	94.4	9.5	9.4×10^{-5}	0.18	0.66	0.13	0.02
S-3	60.9	90.4	9.3	1.6×10^{-4}	0.29	0.61	0.09	0.01
S-4	60.8	98.0	—	1.3×10^{-4}	0.22	0.65	0.11	0.02
O-1[b]	98.5	102.0	—	1.2×10^{-4}	—	—	—	—
O-2	94.9	103.7	6.9	4.0×10^{-5}	0.11	0.53	0.19	0.18
O-3	108.0	118.1	9.2	5.2×10^{-9}	0.29	0.43	0.21	0.07
O-4	99.1	115.3	—	2.6×10^{-8}	0.09	0.75	0.12	0.04
O-5[c]	59.4	81.0	—	1.4×10^{-4}	0.16	0.56	0.17	0.12
O-6	61.4	72.7	—	7.5×10^{-5}	—	—	—	—
O-7	82.0	95.2	—	1.5×10^{-6}	—	—	—	—
O-8	86.1	96.1	—	1.8×10^{-8}	—	—	—	—

[a]Letter designates site.

[b]Needle-punched geosynthetic clay liner.

[c]Adhesive-bonded geosynthetic clay liner.

J. Geotech. Geoenviron. Eng. 2007.133:550-563.

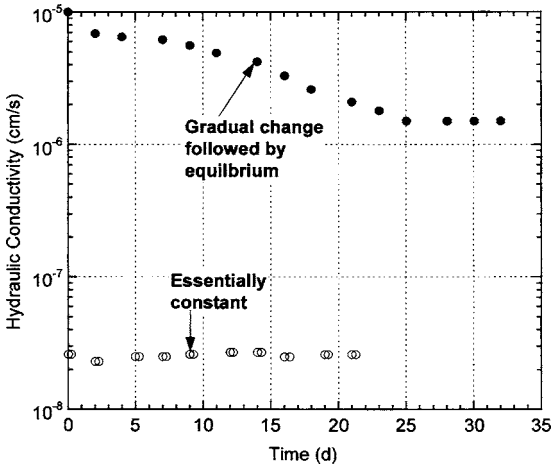

Fig. 4. Hydraulic conductivity records typifying the range of behavior observed in the hydraulic conductivity tests on exhumed geosynthetic clay liners. Data in this graph are from tests conducted on geosynthetic clay liners from Site 0.

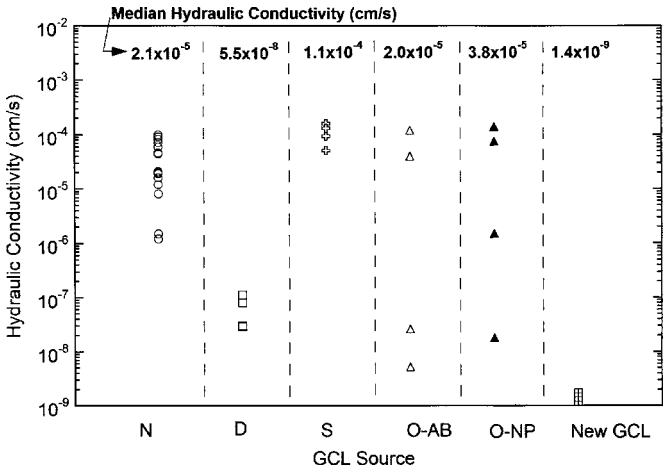

Fig. 5. Hydraulic conductivities of exhumed geosynthetic clay liners. Geosynthetic clay liners at Site O were adhesive bonded or needle punched. The geosynthetic clay liners from Sites N and D were adhesive bonded and the geosynthetic clay liners from Site S was needle punched. Hydraulic conductivity of new geosynthetic clay liners included for comparison.

geotextile fibers along the edge of the GCL were removed with scissors, and bentonite paste was applied around the perimeter to reduce the potential for sidewall leakage.

A 10 mM $CaCl_2$ solution was used as the permeant liquid, as suggested in ASTM D 5084 for regions with hard tap water (e.g., Madison, Wis.). Egloffstein (2001, 2002), Lin and Benson (2000), and Benson et al. (2006) have used similar solutions when permeating GCLs used for landfill cover applications. To evaluate the importance of the permeant liquid, comparative hydraulic conductivity tests were conducted using DI water as the permeant liquid on a GCL exhumed from Site S. The hydraulic conductivity obtained with DI water (1.4×10^{-5} cm/s) was 3.6 times lower than the lowest hydraulic conductivity (5.1×10^{-5} cm/s) measured from Site S specimens using 10 mM $CaCl_2$ solution as the permeant liquid. Thus, the choice of permeant liquid is believed to have only a modest effect on hydraulic conductivity. Benson et al. (2006) also conducted tests on exhumed GCLs with a pore water percolate and 10 mM $CaCl_2$ solution, and found similar hydraulic conductivities were obtained using both liquids. The lack of sensitivity to the permeant liquid reflects the abundance of exchangeable Ca in the exhumed GCLs (discussed subsequently).

Hydraulic conductivities of the GCLs are summarized in Table 5. Typical permeation times ranged between 20 and 45 days, even though the termination criteria in ASTM D 5084 generally were met in much shorter periods. Longer permeation times were used to determine if decreases in hydraulic conductivity would occur as reported by Egloffstein (2002). Two types of behavior were observed during the hydraulic conductivity tests on the exhumed GCLs (see examples in Fig. 4). For most of the tests on the exhumed GCLs, the hydraulic conductivity remained essentially constant from the beginning of the test. However, for some of the test specimens, the hydraulic conductivity increased or decreased gradually during the test period, and then stabilized. All tests were conducted long enough so that steady hydraulic conductivity was obtained and inflow equaled outflow, as defined in ASTM D 5084.

If specimens had high hydraulic conductivity ($>10^{-6}$ cm/s), rhodamine WT dye (5 mg/L) was added to the permeant liquid to verify that sidewall leakage was not occurring as recommended by Jo et al. (2001). No indication of sidewall leakage was found in any of the tests. The effluent lines were also inspected periodically for bentonite particles that may have piped from the GCL. No bentonite particles were observed visually in the effluent.

Soluble Salts and Exchangeable Cations

Exchangeable cations present on the bentonite of the exhumed GCLs and the new GCL were determined by extraction using the ammonium acetate method (Thomas 1982). Each test was conducted with 10 g of dry bentonite crushed to pass a No. 20 U.S. standard sieve. Chemical analysis of the extracts was conducted by AAS, as described previously. Mole fractions of exchangeable Na, K, Ca, and Mg are summarized in Table 5.

Results and Discussion

Hydraulic Conductivity

Hydraulic conductivities of the exhumed GCLs are shown in Fig. 5. The median hydraulic conductivity of the GCL from each site is also shown along the top of the graph (Fig. 5). The exhumed GCLs have a broad range of hydraulic conductivities, spanning nearly five orders of magnitude (5.2×10^{-9} to 1.6×10^{-4} cm/s). Greater variability was obtained at sites where GCL samples were taken from multiple test pits (2 orders of magnitude at Site N, nearly 5 orders of magnitude at Site O) than those where the GCLs were obtained from single test pits (less than 1 order of magnitude for Sites D and S). All of the exhumed GCLs also have higher hydraulic conductivity than the new GCL (1.2×10^{-9} to 1.7×10^{-9} cm/s). For example, the median hydraulic conductivity of the GCL from Site D (5.5×10^{-8} cm/s), which has lowest overall hydraulic conductivity of the four sites, is 39 times higher than the median hydraulic conductivity of the new GCL (1.4×10^{-9} cm/s).

At Site O, a needle-punched GCL was used on the side slopes and an adhesive-bonded GCL was used on the top deck. Comparison of the hydraulic conductivities (Fig. 5, Table 5) indicates that there is no apparent difference between the hydraulic conduc-

J. Geotech. Geoenviron. Eng. 2007.133:550-563.

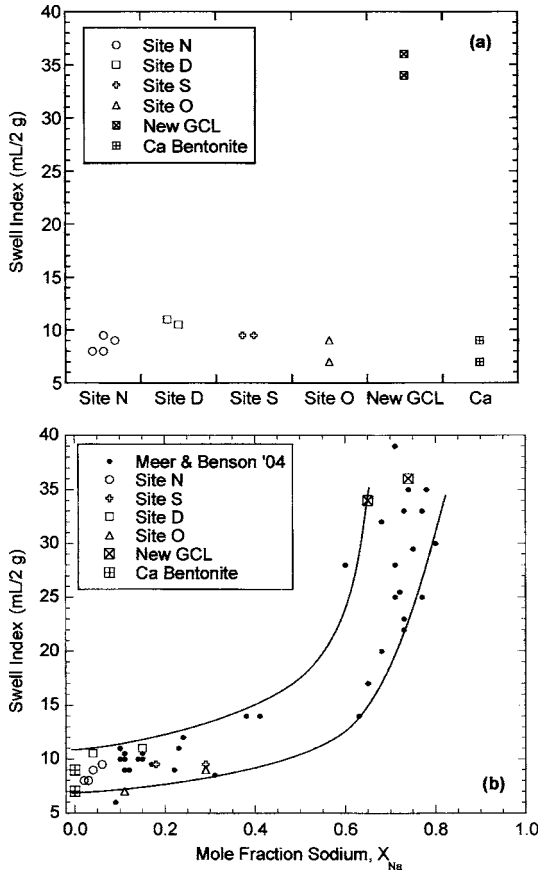

Fig. 6. Box plots of index swell of bentonite from exhumed geosynthetic clay liners, new geosynthetic clay liners, and Ca bentonite: (a) index swell versus mole fraction of exchangeable sodium (b). Smooth curve and solid points in (b) are from parametric laboratory tests conducted by Meer and Benson (2004). Index swell of Ca bentonite is from Jo et al. (2004).

tivity of the needle-punched (labeled O-NP) or adhesive-bonded (labeled O-AB) GCLs at Site O. Both types of GCL had hydraulic conductivities near the upper end ($\sim 1 \times 10^{-4}$ cm/s) and the lower end ($\sim 3 \times 10^{-8}$ cm/s) of the range. A *t* test was conducted on the data at the 5% significance level to confirm that the two sets of hydraulic conductivities are similar. The data were transformed logarithmically prior to testing, so that the assumption of normality in the *t* test would be satisfied. A *p* statistic of 0.66 was obtained, indicating that there is no statistically significant difference between the hydraulic conductivity of both data sets at the 5% level ($0.66 \geqslant 0.05$). The similarity of the hydraulic conductivities of the needle-punched and adhesive-bonded GCLs (collected from the slopes and top deck, respectively) also suggests that the slope had no systematic effect on hydraulic conductivity of the GCL.

Swell Index and Exchangeable Cations

The swell index data are shown in Fig. 6(a). DI water was used as the hydrating liquid for these swell tests; thus, ion exchange did not occur during these tests and the data in Fig. 6(a) reflect the swell index of the bentonite in its in-service condition. Swell indices for the new GCL are also shown in Fig. 6(a) along with swell indices for Ca bentonite reported by Jo et al. (2004) for bentonite from the new GCL homoionized following the procedure in Mesri and Olson (1971). For each site, there is little variability (<4 mL/2 g) in the swell index of the exhumed GCLs and all of the swell indices fall within a narrow range (6.9–11.0 mL/2 g). The swell indices for the exhumed GCLs are similar to those for the calcium bentonite (6–10 mL/2 g) and much lower than the swell index for the new GCL (34–36 mL/2 g).

The exchangeable cation data, summarized in Table 5, are consistent with the low swell indices for the exhumed GCLs shown in Fig. 6(a). For all of the exhumed GCLs, much of the Na originally sorbed to the bentonite has been replaced primarily by Ca, but also by Mg. The Na mole fraction of the exhumed GCLs ranges from 0.02 to 0.29 (average=0.11), the Ca mole fraction ranges from 0.43 to 0.78 (average of 0.68), and the Mg mole fraction ranges from 0.09 to 0.21 (average=0.16). In contrast, for the new GCL, the Na mole fraction is 0.65–0.74, the Ca mole fraction is 0.22–0.27, and the Mg mole fraction is 0.03. The preponderance of exchangeable Ca and Mg in the exhumed GCLs is not surprising given that the leachates from the column tests on the cover soils contained primarily divalent cations ($0.0050 < \text{RMD} < 0.095\ \text{M}^{1/2}$). The abundance of divalent exchangeable cations in these GCLs is also consistent with the findings reported by James et al. (1997), Melchior (1997, 2002), Egloffstein (2001, 2002), Mackey and Olsta (2004), and Benson et al. (2006).

The correspondence between swell index and mole fraction of exchangeable Na is shown in Fig. 6(b). Also included are data from Meer and Benson (2004), which span a broad range of Na mole fraction, and the data from Jo et al. (2004) for Ca bentonite. Meer and Benson (2004) created bentonites with varying Na and Ca mole fractions by batch mixing bentonite from the new GCL with aqueous solutions having varying concentrations of Na and Ca. Replacement of Na by Ca (i.e., a decrease in the Na mole fraction) corresponds directly to a decrease in swell index. Moreover, when the Na mole fraction is less than 0.3, the bentonite has a swell index comparable to that of fully exchanged Ca bentonite. Thus, complete replacement of Na by divalent cations is not necessary for a bentonite to have the swelling properties of Ca bentonite.

The least amount of cation exchange occurred in the GCL from Site S (Na mole fraction=0.18–0.29). The presence of the geomembrane above the GCL at Site S probably slowed the exchange process, as was also observed by Melchior (2002), but the GCL at Site S was also in service for the shortest time (4.1 years) of all GCLs exhumed. Despite the reduction in exchange, the geomembrane was ineffective in protecting the GCL from alterations in hydraulic conductivity. In fact, the GCL from Site S had the highest median hydraulic conductivity of all the GCLs that were sampled. The source of the exchanging cations at Site S is also unclear, considering that the overlying geomembrane probably blocked most of the cations migrating from the overlying cover soils. Diffusion from the underlying subgrade may have been responsible for the exchange, as the leachate from the column tests on the subgrade soil was primarily divalent ($\text{RMD}=0.025\ \text{M}^{1/2}$). The distance over which diffusion would need to occur in the GCL is short enough (<10 mm) to permit influx of sufficient Ca and Mg within 4.1 years to provide the mass required for near complete exchange. However, the contributions of diffusion have not been confirmed experimentally, and additional study is needed to determine if diffusion from the underlying subgrade was a key factor contributing to exchange.

J. Geotech. Geoenviron. Eng. 2007.133:550-563.

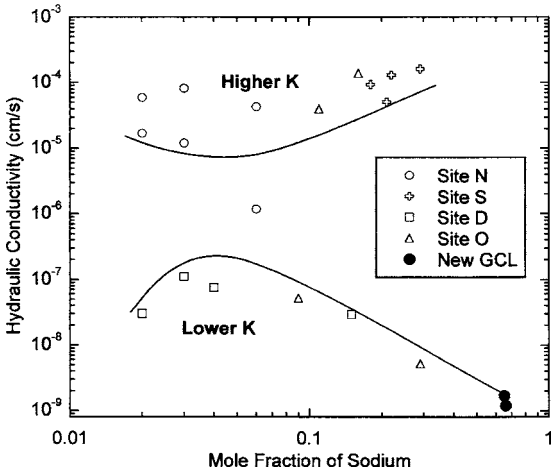

Fig. 7. Hydraulic conductivity of exhumed geosynthetic clay liner and new geosynthetic clay liner versus Na mole fraction in the exchange complex of the bentonite

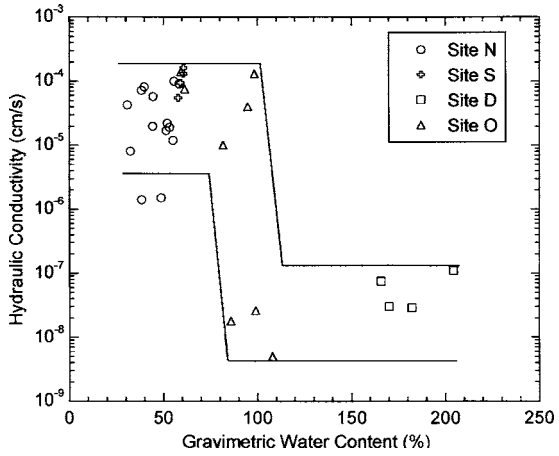

Fig. 8. Hydraulic conductivity of exhumed geosynthetic clay liners versus gravimetric water content at the time of exhumation

Hydraulic Conductivity and Exchangeable Cations

Hydraulic conductivity versus mole fraction of exchangeable Na is shown in Fig. 7 for the exhumed GCLs and the new GCL. There is no apparent relationship between hydraulic conductivity and Na mole fraction, although the lowest hydraulic conductivities correspond to the highest Na mole fraction (and are for the new GCL). However, all of the GCLs (except the new GCL) have swell indices comparable to that of Ca bentonite and a Na mole fraction low enough (<0.3) to result in swelling properties similar to Ca bentonite. Thus, because the Na mole fraction was low on all of the exhumed GCLs, a strong relationship between Na mole fraction and hydraulic conductivity should not be expected.

Except for one point, the data can be segregated into two groups regardless of the Na mole fraction: GCLs with higher hydraulic conductivity ($>10^{-5}$ cm/s) and GCLs with lower hydraulic conductivity ($<10^{-7}$ cm/s) (Fig. 7). The lower hydraulic conductivities are similar to those obtained from long-term hydraulic conductivity tests conducted by Egloffstein (2001) and Jo et al. (2005) using dilute Ca solutions (10 mM). Their tests, which were conducted long enough for complete replacement of Na by Ca under continuously saturated conditions, show that the long-term equilibrium hydraulic conductivity of saturated bentonite to dilute Ca solutions is approximately 2×10^{-8} cm/s for stresses similar to those observed in covers. In fact, a very long-term hydraulic conductivity test on a specimen of the new GCL that was continuously permeated over a period of 4.4 years and 1,108 pore volumes of flow with a 10 mM $CaCl_2$ solution yielded a hydraulic conductivity of 2.3×10^{-8} cm/s (Benson et al. 2006). Thus, the very high hydraulic conductivities of some of the exhumed GCLs must be caused by other factors in conjunction with ion exchange.

Hydraulic Conductivity and Water Content

Lin and Benson (2000), Egloffstein (2001, 2002), and Benson et al. (2006) suggest that the high hydraulic conductivities of GCLs exhumed from covers is due to replacement of Ca and Mg for Na combined with dehydration of the bentonite. For example, Lin and Benson (2000) found that Ca-for-Na exchange combined with desiccation resulted in hydraulic conductivities comparable to those in the group of higher hydraulic conductivities shown in Fig. 7.

Dehydration induces two physical changes in saturated bentonite that alter hydraulic conductivity: (1) removal of strongly bound water molecules in the interlayer region present from the initial hydration when Na was the dominant exchangeable cation; and (2) formation of desiccation cracks that do not heal during rehydration, due to the low swelling capacity of Ca and Mg bentonites. Strongly bound water molecules in the interlayer are responsible for the lower hydraulic conductivity of bentonites that have undergone Ca-for-Na exchange by permeation with dilute solutions (Jo et al. 2004, 2006; Benson et al. 2006). Removing these water molecules results in irreversible shrinkage of bentonite granules, resulting in larger intergranular pores and higher hydraulic conductivity (Benson et al. 2006). Similarly, desiccation cracks act as preferential flow paths that also contribute to higher hydraulic conductivity.

Hydraulic conductivity of the GCLs is shown in Fig. 8 as a function of gravimetric water content of the bentonite at the time of sampling. There is an abrupt change in hydraulic conductivity that occurs when the gravimetric water content is approximately 80–100%. GCLs with gravimetric water contents less than 85% typically have high hydraulic conductivities (10^{-6} to 10^{-4} cm/s), whereas GCLs with gravimetric water contents greater than 100% have lower hydraulic conductivities (10^{-8} to 10^{-7} cm/s). The GCLs exhumed by Melchior (2002) that contained desiccation cracks also had gravimetric water contents less than 100%. In contrast, water contents exceeding 200% were obtained for the new GCL (Table 5).

Comparison of the gravimetric water contents following termination of the hydraulic conductivity tests with the water contents at the time of exhumation (Table 5) indicates that this segregation of the data set remained after the specimens were permeated. GCLs with high hydraulic conductivity typically had gravimetric water contents less than approximately 125%. The largest increase in gravimetric water content during permeation was 37%, in most cases the gravimetric water content increased 10–15%, and in some cases the gravimetric water content decreased. Moreover, none of the exhumed GCLs had gravimetric water contents comparable to the new GCL. Thus, the dehydration effect is per-

J. Geotech. Geoenviron. Eng. 2007.133:550-563.

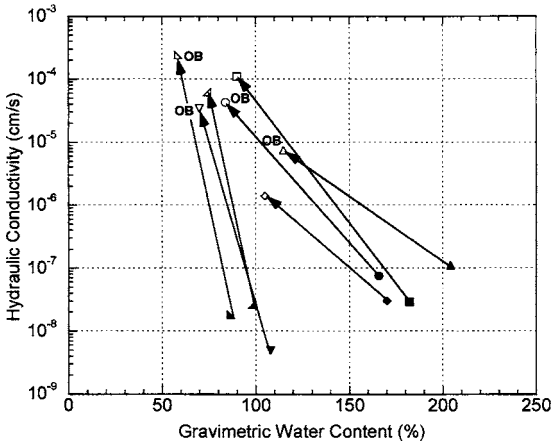

Fig. 9. Hydraulic conductivity of exhumed geosynthetic clay liners as a function of gravimetric water content before and after a controlled desiccation treatment. Solid symbol corresponds to in situ water content (before condition). Open symbol is water content after controlled desiccation. The label OB indicates that 20 kPa stress was applied during desiccation.

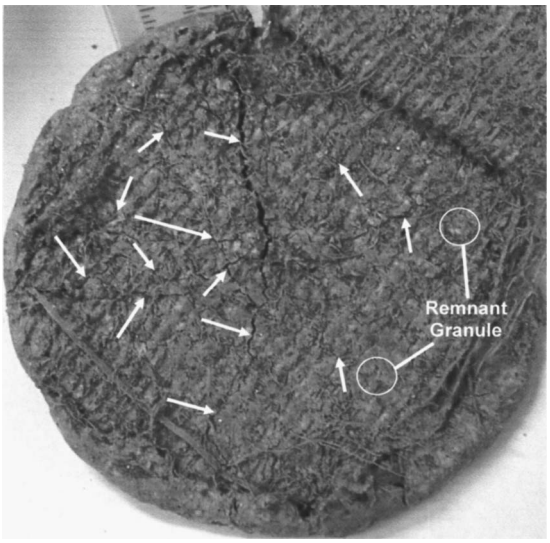

Fig. 10. Exposed surface of bentonite in exhumed geosynthetic clay liner desiccated to water content of 75% and then rehydrated and permeated. Note desiccation cracks in bentonite (white arrows) and examples of remnant bentonite granules.

manent, which is expected given that Ca and Mg bentonites do not undergo osmotic swelling during hydration (Norrish and Quirk 1954).

The importance of maintaining water within the bentonite is also evident in the thickness of the GCLs, which is an index of the degree of swelling of the bentonite. The GCL from Site D, which had the highest water content and the lowest median hydraulic conductivity (5.5×10^{-8} cm/s), was thicker (average=13.4 mm) than the GCLs from Site N (average =6.0 mm) and Site S (average=9.0 mm), which had the lowest water contents (<60%) and the highest hydraulic conductivities (median hydraulic conductivity $>10^{-5}$ cm/s). The exhumed GCLs from Site O with high hydraulic conductivity also were somewhat thinner than the GCLs with low hydraulic conductivity (7.5 versus 8.6 mm, on average).

The abrupt change in hydraulic conductivity shown in Fig. 8 suggests that there is a critical gravimetric water content below which the hydraulic conductivity remains high after the bentonite rehydrates. Thus, exhumed GCLs that had low hydraulic conductivity (10^{-7} to 10^{-9} cm/s) were subjected to a controlled desiccation treatment to achieve water contents between 58 and 90% or between 105 and 115% (i.e., above and below 100%). After drying, the specimens were repermeated (only one dry–wet cycle was applied). To determine if overburden pressure had any influence on the effect of desiccation, four exhumed GCLs having low hydraulic conductivity (10^{-7} to 10^{-9} cm/s) were dried under an overburden pressure of 20 kPa (applied dead load) to simulate the stress applied by approximately 1 m of cover soil. Hydraulic conductivities of these specimens are shown in Fig. 9 as a function of the gravimetric water content (exhumed water content or water content after desiccation treatment). Specimens that had overburden pressure applied during desiccation are labeled as "OB" in Fig. 9.

Controlled desiccation resulted in an increase in hydraulic conductivity in all cases. Desiccation to gravimetric water contents greater than 100% caused an increase in hydraulic conductivity of 1–2 orders of magnitude, whereas desiccation to gravimetric water contents less than 100% increased the hydraulic conductivity by 3–4 orders of magnitude. Thus, a critical water content below which the hydraulic conductivity did not change was not identified. Nevertheless, these findings suggest that drying to a lower water content has a more dramatic effect on hydraulic conductivity.

The increase in hydraulic conductivity during controlled desiccation was unaffected by the application of overburden pressure, regardless of the range of water contents used for drying (Fig. 9). The hydraulic conductivity following desiccation ranged from 8.0×10^{-6} to 2.4×10^{-4} cm/s for specimens that had overburden pressure applied during desiccation, whereas the specimens dried without overburden pressure had hydraulic conductivities ranging from 1.3×10^{-6} to 1.1×10^{-4} cm/s. A t test conducted at the 5% significance level on the logarithmically transformed data confirmed that the hydraulic conductivities of the specimens desiccated with and without overburden pressure were not statistically different ($p=0.57\gg0.05$). Moreover, a specimen that was desiccated to a gravimetric water content of 105% without overburden pressure applied had lower hydraulic conductivity (1.3×10^{-6} cm/s) than a specimen desiccated to water content of 115% (8.0×10^{-6} cm/s) with overburden pressure applied (Fig. 9). Thus, application of overburden pressure corresponding to 1 m of soil appears insufficient to prevent large increases in hydraulic conductivity during drying.

Formation of desiccation cracks appears to be a key factor contributing to the increase in hydraulic conductivity. A specimen of GCL from Site O (exhumed gravimetric water content=99%, hydraulic conductivity=2.6×10^{-8} cm/s) was desiccated to a gravimetric water content of 75%. Following desiccation, the hydraulic conductivity increased to 6.2×10^{-5} cm/s. After removal of the specimen from the permanent, the upper geotextile was carefully peeled back, and the bentonite examined for signs of structural changes due to desiccation. A photograph of the specimen illustrating the desiccation cracks (noted with white arrows) is shown in Fig. 10. Remnant bentonite granules are also evident in the photograph, suggesting that intergranule flow may also have contributed to the high hydraulic conductivity.

J. Geotech. Geoenviron. Eng. 2007.133:550-563.

Table 6. Field Hydraulic Conductivity, Cover System, and Other Related Data from Literature and This Study

Source	Cover thickness (mm)	Service life (years)	Mole fraction sodium	Mole fraction calcium	Swell index (mL/2 g)	Hydraulic conductivity (cm/s)[a]
James et al. (1997)	450	1.5	0.16	0.69	NR	NR
Melchior (2002)	450	2.0	0.09	0.80	11	1.5×10^{-4} [b]
	450	4.0	0.04	0.81	9	3.5×10^{-5} [b]
	450	2.0	0.05	0.70	8	9.4×10^{-4} [b]
	450	4.0	0.02	0.83	7	1.0×10^{-5} [b]
Mansour (2001)	660	5.0	NR	NR	33	1.9×10^{-9} [b]
Mackey and Olsta (2004)	610–810	7.2	0.01	0.64	8.3	1.2×10^{-6} [c]
						1.4×10^{-8} [d]
	460–860	5.5	0.02	0.49	10.8	1.1×10^{-8}
Wagner and Schnatmeyer (2002)	1000	2.0	NR	NR	NR	8.3×10^{-8} [e]
Henken-Mellies et al. (2002)	1000	3.0	NR	NR	NR	2.3×10^{-6} [e]
Benson et al. (2006)	760	4.1	0.10	0.67	12	5.0×10^{-5} [b]
	760	2.0	0.09	0.55	8	4.8×10^{-5} [b]
This study—Site N	750	4.6	0.04	0.72	9	3.9×10^{-5} [b]
This study—Site D	800	11.1	0.06	0.74	11	6.2×10^{-8} [b]
This study—Site S	900	4.1	0.22	0.65	10	1.1×10^{-4} [b]
This study—Site O	800	5.6	0.16	0.56	8	4.7×10^{-5} [b]

[a]NR=not reported in previous study.

[b]Mean reported hydraulic conductivities measured on exhumed geosynthetic clay liners.

[c]Hydraulic conductivity of exhumed geosynthetic clay liner reported by independent testing laboratory.

[d]Hydraulic conductivity of exhumed geosynthetic clay liner reported by geosynthetic clay liner manufacturer.

[e]Computed based on peak daily percolation rate assuming unit gradient flow.

Practical Implications

Anticipated Field Conditions

Data from previous field studies are summarized in Table 6 along with the data from this study. Service life of the GCL, swell index of the bentonite, and mole fractions of exchangeable cations on the bentonite (if available) are reported in Table 6 along with hydraulic conductivities. Data from Egloffstein (2001, 2002) are not included in Table 6, because too little information was provided in these publications to complete the table entries reliably.

Hydraulic conductivity of the GCL in the field study conducted by Henken-Mellies et al. (2002) was computed from the reported peak daily percolation rate. A unit hydraulic gradient was used in the computations, because a geocomposite drainage layer having hydraulic conductivity several orders of magnitude higher than the overlying cover soils was placed above the GCL. Hydraulic conductivity of the GCL in the study by Wagner and Schnatmeyer (2002) was also computed using a unit hydraulic gradient and the peak daily percolation rate because of the lateral drainage provided by the coarse slag placed above the GCL.

The data summarized in Table 6 suggest that increases in the hydraulic conductivity of GCLs used in covers may be common, and that the contributing factors are cation exchange combined with desiccation (or lack of initial hydration, as discussed in the following section). The data reported in other studies generally are consistent with this conclusion (the exception being the study by Mansour 2001). Of the 15 GCLs included in Table 6, 9 have hydraulic conductivities greater than 10^{-5} cm/s, and 11 are greater than 10^{-6} cm/s. Four GCLs have hydraulic conductivities on the order of 10^{-8} cm/s. One GCL has a hydraulic conductivity less than 10^{-8} cm/s (Mansour 2001), and only this GCL has a hydraulic conductivity comparable to that of a new GCL ($\approx 2\times10^{-9}$ cm/s). Moreover, the soil placed over this GCL was sodic (Mansour 2001; Benson et al. 2006), which is atypical of most surficial soils (Sposito 1989), as is illustrated by the low RMDs of the column test leachates (Table 3).

Except for the site described by Mansour (2001), the sites having GCLs with lower hydraulic conductivity ($\approx10^{-8}$ cm/s, or lower) tend to be in wet and humid areas or have been in service for only a short period. The sites evaluated by Mackey and Olsta (2004) are on the coast of Florida, and Site D in the present study is located in a densely wooded area in northern Wisconsin that is surrounded by wetlands. Desiccation at these sites probably is less likely than at other sites. The study by Wagner and Schnatmeyer (2002) was only conducted for 2 years and even in this short duration, the hydraulic conductivity of the GCL had already reached 8.3×10^{-8} cm/s. If Wagner and Schnatmeyer (2002) had conducted their study over a longer period of time, higher hydraulic conductivity of the GCL may have been realized.

Protective Methods

Egloffstein (2001, 2002) recommends that at least 750 mm of cover soil (and preferably 1,000 mm) be placed above a GCL to prevent the changes in hydraulic conductivity associated with cation exchange and dehydration. Egloffstein (2002) suggests that GCLs covered with surface layers this thick are under sufficient overburden pressure to prevent large changes in hydraulic conductivity and will have long-term hydraulic conductivities of approximately 10^{-8} cm/s even if Ca replaces Na on the bentonite. Lin and Benson (2000) indicate that a geomembrane can be used to protect GCLs from desiccation and changes in hydraulic conductivity caused by cation exchange combined with desiccation.

Review of the data in Table 6 indicates that neither of these recommendations may be adequate to ensure that the low hydrau-

J. Geotech. Geoenviron. Eng. 2007.133:550-563.

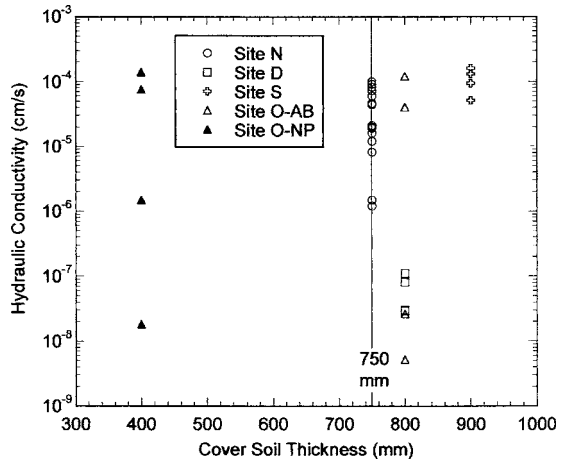

Fig. 11. Hydraulic conductivities of exhumed geosynthetic clay liners as a function of the thickness of the surface layer. Vertical line corresponds to Egloffstein's recommended minimum thickness (750 mm) to prevent changes in hydraulic conductivity caused by cation exchange and dehydration.

lic conductivity of a GCL is maintained. Hydraulic conductivities exceeding 10^{-6} cm/s were obtained for seven of the nine cases in Table 6 that have cover soils at least 750 mm thick, and the hydraulic conductivities exceeding 10^{-6} cm/s include the GCL evaluated by Henken-Mellies et al. (2002), which was overlain by 1,000 mm of soil. In addition, the highest hydraulic conductivity was obtained for Site S, which was covered with 900 mm of soil and a geomembrane. As illustrated in Fig. 11, there is no relationship between cover soil thickness and hydraulic conductivity of the exhumed GCLs. Whether any cover soil thickness is adequately protective remains unknown and deserves further study.

The data from Site S illustrate that covering a GCL with a geomembrane does not necessarily preclude increases in hydraulic conductivity or cation exchange, as this GCL had the highest median hydraulic conductivity of all the GCLs evaluated in this study, a Na mole fraction between 0.18 and 0.22, and a Ca mole fraction between 0.61 and 0.68. The reasons why the GCL from Site S were so permeable has not been determined conclusively, and the generality of this finding is unknown (only one site with a geomembrane over the GCL was evaluated). However, one possible explanation is that minimal hydration of the GCL occurred beneath the geomembrane before cation exchange occurred, a condition known to preclude osmotic swelling of the bentonite (Norrish and Quirk 1954; Jo et al. 2004; Kolstad et al. 2004). Consequently, water molecules were not bound in the interlayer and low hydraulic conductivity may never have been achieved, even when the GCL was first hydrating. Rapid exchange relative to the rate of hydration is known to result in bentonite having a hydraulic conductivity on the order of 10^{-5} cm/s for stresses typical of covers (Jo et al. 2005), which is similar to the hydraulic conductivity of the GCL at Site S.

Uncertainty exists regarding the mechanism responsible for exchange at Site S. However, as mentioned previously, the exchangeable Ca and Mg on the bentonite may have originated in the subgrade and migrated upward into the GCL via diffusion. The high hydraulic conductivity of the GCL at Site S may also have implications for linear applications where a composite liner consisting of a geomembrane overlying a GCL is placed on a subgrade soil where divalent cations are predominant.

Evaluating Compatibility of Cover Soils with Swell Index Tests

The batch elution procedure described in ASTM D 6141 is one method of creating synthetic pore water for evaluating the compatibility of cover soils and GCLs. The ASTM D 6141 batch test produced leachates having similar ionic strength as the elution tests when synthetic rainwater was used as the eluent. The leachate from ASTM D 6141 also had RMDs similar to, but slightly higher than the RMDs produced by the elution tests (average ratio of RMD for batch test to column test of 1.17). Thus, ASTM D 6141 appears to be a reasonable method to create synthetic pore water. More research is necessary, however, to verify that the ASTM D 6141 batch test with synthetic rainwater yields pore waters typical of field conditions.

The eluent from ASTM D 6141 is often used as the hydrating liquid for swell index tests to diagnose the compatibility of cover soils and bentonite in GCLs. As shown in Table 4, the swell indices for the batch test liquids range between 28 and 30 mL/2 g. This range is slightly lower than swell index of the new GCL in DI water (34–36 mL/2 g), but is not atypical of swell indices associated with Na bentonites (Jo et al. 2001; Kolstad et al. 2004; Katsumi and Fukagawa 2005; Lee and Shackelford 2005; Lee et al. 2005). In contrast, bentonite from GCLs exhumed from the field sites had swell indices ranged between 7 and 11 mL/2 g (Table 5), which are typical of Ca bentonite. This comparison, along with the hydraulic conductivities reported in Table 5, suggests that swell index tests conducted using the leachate from ASTM D 6141 batch tests are not reliable indicators of incompatibility between a GCL and a cover soil.

Summary and Conclusions

GCL samples were exhumed from four landfills and tested for water content, swell index, saturated hydraulic conductivity, and exchangeable cations. Tests were also conducted on a new GCL that had never been in service. Samples of the overlying cover soil from each landfill were also obtained and subjected to batch and column elution tests.

Most of the exchangeable Na initially on the bentonite in the exhumed GCLs was replaced by Ca and Mg, and the bentonites had swell indices typical of Ca bentonite (~10 mL/2 g). Hydraulic conductivities of the exhumed GCLs varied over a wide range (5.2×10^{-9} to 1.6×10^{-4} cm/s), and exhibited no relationship with cover soil thickness or mole fraction of exchangeable Na. Very high hydraulic conductivities (5.6×10^{-5} to 1.6×10^{-4} cm/s) were even obtained for a GCL that had been covered by a geomembrane and 900 mm of soil. The exchangeable cations, swell indices, and hydraulic conductivities of the exhumed GCLs in this study are similar to those reported in several other field studies in the United States and Europe. The similarity of these findings suggests that Ca-for-Na exchange in the bentonite of GCLs is likely to occur at most field sites (unless the overlying soil is sodic, which is unusual) and that large increases in hydraulic conductivity are likely to occur, unless the water content of the GCL can be maintained above 100%. None of the conventional means assumed to protect a GCL (cover soil at least 750 mm thick, overlying geomembrane) appears effective in preventing large increases in hydraulic conductivity.

Hydraulic conductivity of the exhumed GCLs was strongly related to the gravimetric water content at the time of sampling. GCLs with gravimetric water contents less than 85% had high

J. Geotech. Geoenviron. Eng. 2007.133:550-563.

hydraulic conductivities (10^{-6} to 10^{-4} cm/s), whereas GCLs with gravimetric water contents greater than 100% had lower hydraulic conductivities (10^{-8} to 10^{-7} cm/s). Controlled desiccation of exhumed GCLs that had low hydraulic conductivity (10^{-9} to 10^{-7} cm/s) resulted in increases in hydraulic conductivity of 1.5–4 orders of magnitude, even with an applied overburden pressure simulating 1 m of cover soil. The results of the controlled desiccation treatment indicate that desiccation (or lack of hydration) is a key factor controlling the hydraulic conductivity of GCLs once Ca-for-Na exchange has occurred.

If GCLs are to be considered as effective hydraulic barrier layers in landfill cover systems, the ability to protect GCLs from ion exchange and desiccation must be demonstrated. The hydraulic conductivity data reported in the literature for GCLs used in landfill covers, in conjunction with the data from this study, imply that commonly used protective measures (cover soil thickness >750 mm, overlying geomembrane) may be inadequate in many cases. Moreover, the common test method used to assess compatibility between bentonite and cover soils (i.e., ASTM D 6141) is unable to discriminate between conditions that cause long-term alterations in the exchange complex and hydraulic conductivity of GCLs. These findings indicate that more research is needed regarding installation methods that will ensure rapid hydration of GCLs, protective measures that will prevent dehydration, and test methods that can be used to diagnose whether a GCL is likely to undergo large increases in hydraulic conductivity when used in a landfill cover.

Acknowledgments

Financial support for this study was provided by the U.S. Environmental Protection Agency (USEPA) (Contract No. 2C-R361-NAEX) and through the U.S. National Science Foundation (NSF) under Grant No. CMS-9900336. David Carson was the project manager for the portion funded by USEPA. This paper has not been reviewed by the USEPA or NSF. Endorsement by either organization is not implied and should not be assumed.

References

Albright, W., et al. (2004). "Field water balance of landfill final covers." *J. Environ. Qual.*, 33(6), 2317–2332.

Albright, W., et al. (2006). "Field performance of three compacted clay landfill covers." *Vadose Zone J.*, 5(6), 1157–1171.

ASTM. (2004). *Annual Book of ASTM standards*, Vols. 04.09 I and II, ASTM, West Conshohocken, Pa.

Benson, C., Thorstad, P., Jo, H., and Rock, S. (2006). "Case history: Hydraulic performance of geosynthetic clay liners in a landfill final cover." *J. Geotech. Geoenviron. Eng.*, in press.

Bouazza, A. (2002). "Geosynthetic clay liners." *Geotext. Geomembr.*, 20, 3–17.

Egloffstein, T. (2001). "Natural bentonites-influence of the ion exchange and partial desiccation on permeability and self-healing capacity of bentonites used in GCLs." *Geotext. Geomembr.*, 19, 427–444.

Egloffstein, T. (2002). "Bentonite as sealing material in geosynthetic clay liners-influence of the electrolytic concentration, the ion exchange and ion exchange with simultaneous partial desiccation on permeability." *Clay geosynthetic barriers*, H. Zanzinger, R. Koerner, and E. Gartung, eds., Swets and Zeitlinger, Lesse, 141–153.

Gleason, M. M., Daniel, D. E., and Eykholt, G. R. (1997). "Calcium and sodium bentonite for hydraulic containment applications." *J. Geotech. Geoenviron. Eng.*, 123(5), 438–445.

Henken-Mellies, W., Zanzinger, H., and Gartung, E. (2002). "Long-term field test of a clay geosynthetic barrier in a landfill cover system." *Clay geosynthetic barriers*, H. Zanzinger, R. Koerner, and E. Gartung, eds., 303–309.

James, A. N., Fullerton, D., and Drake, R. (1997). "Field performance of GCL under ion exchange conditions." *J. Geotech. Geoenviron. Eng.*, 123(10), 897–901.

Jo, H., Benson, C., and Edil, T. (2006). "Rate-limited cation exchange in thin bentonitic barrier layers." *Can. Geotech. J.*, 43, 370–391.

Jo, H., Benson, C., and Edil, T. (2004). "Hydraulic conductivity and cation exchange in nonprehydrated and prehydrated bentonite permeated with weak inorganic salt solutions." *Clays Clay Miner.*, 52(6), 661–679.

Jo, H. Y., Benson, C. H., Shackelford, C. D., Lee, J.-M., and Edil, T. B. (2005). "Long-term hydraulic conductivity of a geosynthetic clay liner permeated with inorganic salt solutions." *J. Geotech. Geoenviron. Eng.*, 131(4), 405–417.

Jo, H., Katsumi, T., Benson, C., and Edil, T. (2001). "Hydraulic conductivity and swelling of nonprehydrated GCLs permeated with single-species salt solutions." *J. Geotech. Geoenviron. Eng.*, 127(7), 557–567.

Katsumi, T., and Fukagawa, R. (2005). "Factors affecting the chemical compatibility and the barrier performance of GCLs." *Proc., 16th Int. Conf. on Soil Mechanics and Geotechnical Engineering*, Millpress Science, Rotterdam, The Netherlands, 2285–2288.

Kolstad, D., Benson, C., and Edil, T. (2004). "Hydraulic conductivity and swell of nonprehydrated geosynthetic clay liners permeated with multispecies inorganic solutions." *J. Geotech. Geoenviron. Eng.*, 130(12), 1236–1249.

Lee, J., and Shackelford, C. (2005). "Impact of bentonite quality on hydraulic conductivity of geosynthetic clay liners." *J. Geotech. Geoenviron. Eng.*, 131(1), 64–77.

Lee, J., Shackelford, C., Benson, C., Jo, H., and Edil, T. (2005). "Correlating index properties and hydraulic conductivity of geosynthetic clay liners." *J. Geotech. Geoenviron. Eng.*, 131(11), 1319–1329.

Lin, L., and Benson, C. (2000). "Effect of wet-dry cycling on swelling and hydraulic conductivity of GCLs." *J. Geotech. Geoenviron. Eng.*, 126(1), 40–49.

Mackey, R., and Olsta, J. (2004). "Performance of geosynthetic clay liners used in two landfill closures in a coastal area of Florida." *Advances in Geosynthetic Clay Liners Technology: 2nd Symp.*, STP 1456, R. Mackey and K. von Maugeuge, eds., ASTM, West Conshohocken, Pa., 53–71.

Mansour, R. (2001). "GCL performance in semi-arid climate conditions." *Proc., Sardinia 2001, 8th Int. Waste Management and Landfill Symp.*, T. Christensen, R. Cossu, and R. Stegmann, eds., CISA, Cagliari, Italy, 219–226.

Meer, S., and Benson, C. (2004). "In-Service Hydraulic Conductivity of GCLs in Landfill Covers: Laboratory and Field Studies." *Rep. No. EPA/600/R-05/148*, U.S. Environmental Protection Agency, Washington, D.C.

Melchior, S. (2002). "Field studies and excavations of geosynthetic clay barriers in landfill covers." *Clay geosynthetic barriers*, H. Zanzinger, R. Koerner, and E. Gartung, eds., Swets and Zeitlinger, Lesse, 321–330.

Melchior, S. (1997). "In situ studies on the performance of landfill caps." *Proc., Int. Containment Technology Conf.*, Florida State Univ., Tallahassee, Fla., 365–373.

Mesri, G., and Olsen, R. (1971). "Mechanisms controlling the permeability of clays." *Clays Clay Miner.*, 19, 151–158.

Norrish, K., and Quirk, J. (1954). "Crystalline swelling of montmorillonite, use of electrolytes to control swelling." *Nature (London)*, 173, 255–257.

Radd, A. (1978). *Manual on soil sampling and methods of analysis*, 2nd Ed., Canadian Soc. Soil Science, Ottawa, 86–98.

Ruhl, J., and Daniel, D. (1997). "Geosynthetic clay liners permeated with chemical solutions and leachates." *J. Geotech. Geoenviron. Eng.*, 123(4), 369–381.

J. Geotech. Geoenviron. Eng. 2007.133:550-563.

Shackelford, C., Benson, C., Katsumi, T., Edil, T., and Lin, L. (2000). "Evaluating the hydraulic conductivity of geosynthetic clay liners permeated with non-standard liquids." *Geotext. Geomembr.*, 18, 133–162.

Shan, H., and Daniel, D. (1991). "Results of laboratory tests on a geotextile/bentonite liner material." *Proc., Geosynthetics '91*, Industrial Fabrics Assoc. Int., St. Paul, Minn., 517–535.

Sobek, A., Schuller, W., Freeman, J., and Smith, R. (1978). "Field and laboratory methods applicable to overburden and mine soils." *Rep. No. EPA 600/2-78-054*, U.S. Environmental Protection Agency, Washington, D.C.

Sporer, H., and Gartung, E. (2002). "Examinations on the self-healing capacity of geosynthetic clay liners." *Clay geosynthetic barriers*, H. Zanzinger, R. Koerner, and E. Gartung, eds., 339–344.

Sposito, G. (1989). *The chemistry of soils*. Oxford Univ., New York.

Thiel, R., Daniel, D., Erickson, R., Kavazanjian, E., and Giroud, J. (2001). *The GSE GundSeal GCL design manual*, GSE Lining Technology, Inc., Houston.

Thomas, G. (1982). "Exchangeable Cations." *Methods of soil analysis. Part 2. Chemical and microbiological properties*, 2nd Ed., A. Page, R. Miller, and D. Keeney, eds., Soil Science of America, Madison, Wis., 167–179.

Vasko, S., Jo, H., Benson, C., Edil, T., and Katsumi, T. (2001). "Hydraulic conductivity of partially prehydrated geosynthetic clay liners permeated with aqueous calcium chloride solutions." *Proc., Geosynthetics 2001*, Industrial Fabrics Assoc. Int., St. Paul, Minn., 685–699.

Wagner, J., and Schnatmeyer, C. (2002). "Test field study of different cover sealing systems for industrial dumps and polluted sites." *Appl. Clay Sci.*, 21, 99–116.

J. Geotech. Geoenviron. Eng. 2007.133:550-563.

Geotextiles and Geomembranes 29 (2011) 525–533

Contents lists available at ScienceDirect

Geotextiles and Geomembranes

journal homepage: www.elsevier.com/locate/geotexmem

Factors affecting GCL hydration under isothermal conditions

M.T. Rayhani [a], R.K. Rowe [b,*], R.W.I. Brachman [b], W.A. Take [b], G. Siemens [c]

[a] Department of Civil and Environmental Engineering, Carleton University, Ottawa, Canada
[b] Geotechnical and Geoenvironmental Engineering, GeoEngineering Centre at Queen's—RMC, Queen's Univ., Kingston, Canada K7L 3N6
[c] GeoEngineering Centre at Queen's-RMC, Department of Civil Engineering, Royal Military College of Canada, Kingston, Canada

ARTICLE INFO

Article history:
Received 30 April 2010
Received in revised form
18 February 2011
Accepted 7 March 2011
Available online 23 July 2011

Keywords:
Geosynthetic clay liner
Hydration
Silty sand
Sand

ABSTRACT

The hydration of different GCLs from the pore water of the underlying foundation soil is investigated for isothermal conditions at room temperature. Results are reported for three different reinforced (needle punched) GCL products. Both a silty sand (SM) and sand (SP) foundation soil are examined. GCL hydration is shown to be highly dependant on the initial moisture content of the foundation soil. GCLs on a foundation soil with a moisture content close to field capacity hydrated to a moisture content essentially the same as if immersed in water while those on soil at an initial moisture content close to residual only hydrated to a gravimetric moisture content of 30–35%. The method of GCL manufacture is shown to have an effect on the rate of hydration and the final moisture content. The presence or absence of a small (2 kPa) seating pressure is shown to affect the rate of hydration but not the final moisture content. The GCL hydration did not change significantly irrespective of whether a nonwoven cover or woven carrier GCL rested on the foundation soil.

1. Introduction

Geosynthetic clay liners (GCLs) are often used as part of composite liners with a geomembrane liner placed over the GCL (e.g., Rowe et al., 2004; Guyonnet et al., 2009). GCLs have been found to be highly effective for preventing groundwater contamination provided that: (a) they are adequately hydrated (Petrov and Rowe, 1997), (b) the overlap between the panels is maintained (Rowe, 2005), (c) they are not subjected to excessive desiccation combined with cation exchange (Benson et al., 2010), or (d) internal erosion of the bentonite (Rowe and Orsini, 2003; Dickinson and Brachman, 2010). After placement, the GCL takes up water from the underlying soil and provided that it hydrates before contact with leachate, it is usually a very good barrier to advective transport of contaminants (Rowe, 2007). However while the performance of these GCLs as liners is known to depend, at least in part, on the degree of hydration that has occurred before it comes into contact with the contaminants to be contained (Petrov and Rowe, 1997), the rate of hydration of a GCL placed on an underlying subsoil has received very little attention and it is largely an article of faith that they will be adequately hydrated by the time they need to perform their containment function. Daniel et al. (1993) and Eberle and von Maubeuge (1997) have reported limited data for GCLs placed on sand. The former paper showed that, when placed on sand at 3% gravimetric moisture content, an initially air dry GCL reached 88% moisture content after 40–45 days. The latter paper showed that when placed over sand with a moisture content of 8–10%, an initially air dry GCL reached a moisture content of 100% in less than 24 h and 140% after 60 days. However these tests were on different foundation soils with water retention curves, different moisture contents and different GCLs and it is not clear to what extent the properties of the specific foundation soil and GCL affected the rate of hydration.

It is known that both the method of GCL manufacture (Rowe, 2007; Beddoe et al., 2011) and type of bentonite used (Bouazza et al., 2006) can both influence the performance of a GCL. For example, Beddoe et al. (2011) demonstrated that the water retention curve for a GCL was a function of how it was manufactured. Also, Bouazza et al. (2006) showed large differences in transport of liquids or gas between granular and powdered bentonite during the initial hydration of a GCL. Gates et al. (2009) reported that GCLs with fine grained (powdered) bentonite took up water faster and formed an effective seal sooner than coarse granular bentonite due to larger surface area of the bentonite particles.

The speed of hydration is important in terms of both assessing how fast the composite liner system must be covered with soil/waste if one aims to minimize damage due to shrinkage and wetting and drying cycles (e.g., Thiel et al., 2006; Gassner, 2009; Rowe et al., 2010, 2011; Bostwick et al., 2010), to minimize the

* Corresponding author. Tel.: +1 613 533 6933; fax: +1 613 533 6934.
E-mail addresses: mrayhani@connect.carleton.ca (M.T. Rayhani), kerry@civil.queensu.ca (R.K. Rowe), brachman@civil.queensu.ca (R.W.I. Brachman), andy.take@civil.queensu.ca (W.A. Take), Greg.Siemens@rmc.ca (G. Siemens).

0266-1144/$ – see front matter © 2011 Elsevier Ltd. All rights reserved.
doi:10.1016/j.geotexmem.2011.06.001

potential for desiccation cracking due to heat generated by the waste (Rowe, 2005), or to be confident that the GCL is adequately hydrated before coming into contact with the contaminant to be contained in applications such as leachate ponds or landfills. Thus, the objective of this paper is to investigate the effect of the subgrade moisture content and GCL manufacture on the rate of moisture uptake of GCLs from an underlying soil.

2. Material properties

2.1. Geosynthetic clay liners

Three different types of GCLs from two different manufacturers were examined in this study. They included Bentofix NSL (GCL1 in this paper) and NWL (GCL2) and Bentomat DN (GCL3). The basic characteristics of the GCLs are summarized in Table 1. The GCLs differed in the type of carrier geotextiles, the size of bentonite granules, and the manufacturing treatment. All GCLs contained granular sodium bentonite with similar smectite content and swell index but GCL3 had a higher cation exchange capacity than GCLs1 and 2 (Table 2). GCL3 contained coarse grained bentonite with D_{60} of 1.1 mm, while other GCLs contained fine grain bentonite with D_{60} of about 0.35 mm.

2.2. Soil characteristics

Silty sand (SM) from the Queen's composite geosynthetic liner experimental field site in Godfrey Ontario (Brachman et al., 2007) was used as primary foundation soil examined. The particle size distribution of the soil obtained using ASTM D 422 is given in Fig. 1. This data indicates that the soil is silty sand with 35% passing the 0.075 mm sieve. The fines were non-plastic. Standard Proctor compaction tests (ASTM D 698) gave a maximum dry density of about 1.83 Mg/m^3 at an optimum moisture content of 11.4% (Fig. 2).

A series of tests also were performed on a poorly graded sand (SP, ASTM D 2487) with 5% fines to investigate the influence of soil type on GCL hydration. Its Standard Proctor maximum dry density (ASTM D 698) was 1.89 Mg/m^3 at an optimum moisture content of 10.3%. The grain size distribution of the sand as well as its compaction parameters are shown in Figs. 1 and 2. Fig. 3 shows the estimated soil water retention curves (based on the data point function in GeoStudio, 2007) for the silty sand and sand.

3. Method

Polyvinyl chloride (PVC) cells 150 mm in diameter and 500 mm high were constructed to investigate the closed-system (i.e., constant mass of moisture) hydration of various GCLs from foundation soil pore water. Each cell was filled with a foundation soil, with height of about 450 mm, at a known void ratio and moisture content as described below, sealed, and allowed to come to moisture equilibrium. Then a GCL sample (initial thickness of 6–9 mm) was placed on top of the soil, and the system was sealed again (with just enough headspace to allow swelling as the GCL hydrated) (Fig. 4). The test cells were opened weekly and the GCL was removed, thickness measured, weighed, and returned to the column to track the evolution of hydration with time (several months). A laser measurement technique was used to track the change in GCL thickness due to swelling of the bentonite during hydration.

Bulk samples of Godfrey silty sand were mixed with water to bring its moisture content (w_{fdn}) to 10%, 16% and 21%, which correspond to the lower, average, and higher moisture content observed during GCL installation at the Godfrey field site (Brachman et al. 2007).The moisture content of 21% is approximately field capacity for the silty sand. A series of tests with subsoil samples at a much drier initial moisture content of 5% were also conducted to study GCL hydration at moisture contents corresponding to the residual degree of saturation.

Experiments on sand foundations were performed at moisture contents of 10% and 2%, to investigate hydration behavior at the standard Proctor optimum and the residual degree of saturation, respectively for this soil.

At the beginning of the test, GCL samples were taken from the roll at its initial moisture content, cut to a diameter of 150 mm, and placed on the foundation soil. Full details of the initial moisture contents of each GCL specimen and foundation soil investigated in this study are presented in Table 3. After installation, a geomembrane was placed on top of the GCL to minimize potential evaporation into the headspace above the GCL. A steel seating block of 25 mm thickness was then placed over the geomembrane to apply a 2 kPa stress to encourage contact between the GCL and the foundation soil. To investigate the effect of contact on the time rate of hydration of the GCL, one test (PM-1, Table 3) was conducted without this surcharge being applied. The experiments were conducted under isothermal conditions at 22 °C.

Tap water with an average calcium concentration of 30–40 mg/L was used as the pore fluid in the foundation soil.

4. Results and discussion

4.1. Typical results

The measured GCL moisture contents (w) for all tests are reported in Table 4 for regular time periods up to 30 weeks. In this

Table 2
Properties of bentonite in GCLs tested.

GCL	Grain Size Distribution (mm)				Smectite Content (%)[a]	Swell Index (ml/2g)[b]	Cation Exchange capacity (meq/100g)[b]
	D_{10}	D_{30}	D_{60}	D_{90}			
GCL1	0.1	0.28	0.35	0.65	50–55	26	80
GCL2	0.15	0.3	0.35	0.7	50–55	24	80
GCL3	0.4	0.65	1.1	1.7	53–58	23	100

[a] Data from Bostwick L,E, (2009).
[b] Tests performed by M. Hosney, Queen's University.

Table 1
Properties of the reinforced GCLs examined.

GCL	Total dry mass/area (g/m^2)	Initial moisture content, w (%)	Carrier GT		Cover GT		Layer Connection	Average peel strength (N)	Designation in this paper
			Type	Mass (g/m^2)	Type	Mass (g/m^2)			
NSL	4628–5650	7	W	120–126	NW	216–258	NPTT	94 ± 16	GCL1
NWL	3486–5068	7	SRNW	230–253	NW	200–224	NPTT	260 ± 17	GCL2
DN	4307–5145	8–10	NW	200–283	NW	226–263	NP	219 ± 30	GCL3

W = Woven, NW = Nonwoven, SRNW = Scrim reinforced nonwoven, NP = Needle punched, NPTT = Needle punched and thermally treated; The Geotextile masses were measured by D.N. Arnepalli, Queen's University. Peel strength tests performed by M. Hosney, Queen's University.

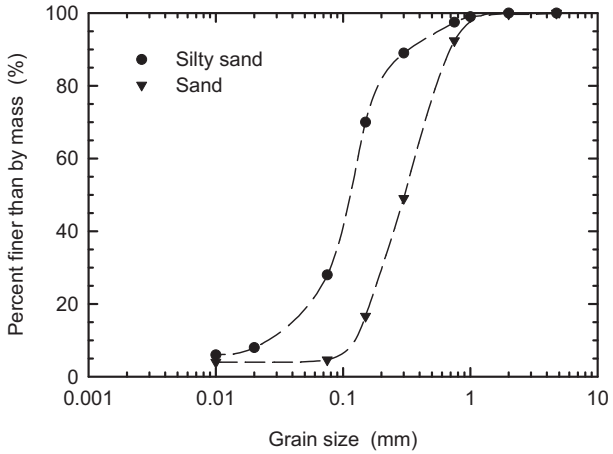

Fig. 1. Grain size distributions for the foundation soils examined.

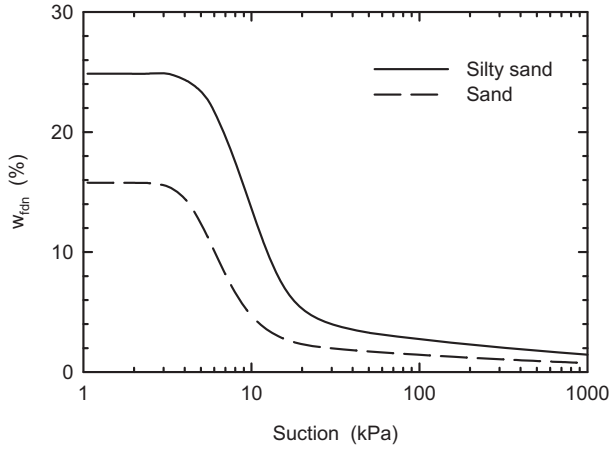

Fig. 3. Estimated water retention curves for the foundation soils examined.

paper, all moisture contents reported are gravimetric moisture contents (i.e., mass of water/mass of solids). Typical results for three tests conducted on GCL1, GCL2 and GCL3 are shown in Fig. 5. These were all obtained with the silty sand foundation soil at an initial moisture content of $w_{fdn} = 16\%$. All three showed a rapid increase in moisture content over the first 10 weeks, reaching gravimetric moisture contents of between about 80 and 100%. After 10 weeks, the rate of moisture uptake decreased and the GCLs reached essentially steady-state conditions with the foundation soil after 30 weeks, beyond which there was no significant (less than 4%) further increase in moisture content when allowed to hydrate for up to 70 weeks.

Recognizing that the hydration of GCLs may be expected to be different for different products (e.g., GCL3 is different to GCL1 and GCL2 in Fig. 5), the measured moisture contents (w) are normalized in this paper by their hydration potential, w_{ref}, under specified conditions, which is defined here to be the moisture content to which a GCL will hydrate when immersed in water while being subjected to a 2 kPa confining stress. This is a reference moisture content that represents the maximum moisture content to which the GCL is likely to hydrate at a nominal stress of 2 kPa. These were measured (based on five replicates) to be 140% (±4%), 115% (±3%) and 150% (±5%) for GCLs1–3, respectively. Fig. 6 shows the results from Fig. 5 when normalized by w_{ref} for each GCL. In the remainder of this paper, GCL hydration results are presented in terms of w/w_{ref}.

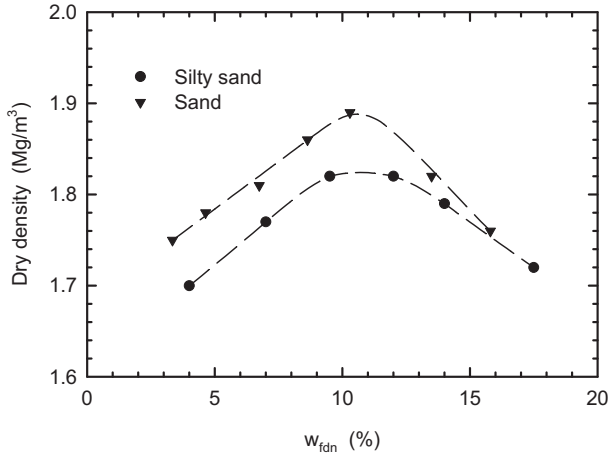

Fig. 2. Standard Proctor compaction results for the foundation soils examined.

4.2. Effect of foundation soil moisture content on GCL hydration

Normalized moisture content results from tests conducted with the silty sand soil prepared at four different moisture contents (5%, 10%, 16% and 21%) are presented in Fig. 7. These four moisture contents ranged from near field capacity to the residual moisture content (i.e., near the wilting point). In each case the moisture content of the GCL increases from its initial moisture content as it comes into equilibrium with the foundation soil. As expected the rate of hydration increases with increasing foundation soil moisture content. Interestingly, about half of the ultimate moisture uptake occurs in the first week and typically more than 70% of the uptake occurred in the first 5 weeks. The time to reach the final equilibrium moisture content depended on both the product and subsoil moisture content. The quickest water uptake occurred in GCL2 placed on the silty sand at 21% moisture content; in this case the GCL achieved 97% of its final equilibrium moisture content in 5 weeks. GCLs1 and 3 placed on silty sand at 21% moisture content

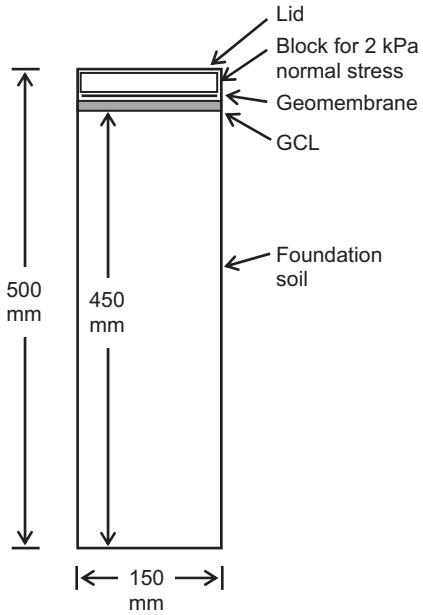

Fig. 4. Schematic of apparatus used for isothermal hydration.

Table 3
Experimental details: Subgrade dry density was 1.65 Mg/m^3 for all cases. Subgrade was Godfrey silty sand (SM) and seating load was 2 kPa unless otherwise noted.

GCL type	GCL		Initial Subgrade w (%)	GT component of GCL in contact with underlying soil	Test
	w (%)	Total Dry mass/area (g/m^2)			
GCL1	7.5	4752	5	W	PM14
GCL1	7.5	4771	10	W	PM15
GCL1	7.0	4709	16	W	PM5
GCL1	7.0	4628	16	NW cover	PM6
GCL1	6.0	5650	21	W	PM12
GCL2	5.8	4437	5	SRNW	PM16
GCL2	5.8	5068	10	SRNW	PM17
GCL2	2.6	3486	16	SRNW	PM7
GCL2	8.8	4877	16	SRNW	PM9
GCL2	6.6	4585	16	NW cover	PM3
GCL2	8.1	4627	21	SRNW	PM13
GCL2	6.3	4771	2[a]	SRNW	PM18
GCL2	6.3	4409	10[a]	SRNW	PM19
GCL3	5.0	4846	5	NW carrier	PM4
GCL3	8.3	5063	10	NW carrier	PM10
GCL3	9.0	5044	16	NW carrier	PM2
GCL3	6.4	4974	16	NW cover	PM8
GCL3	8.3	5145	21	NW carrier	PM11
GCL3[b]	8.4	4307	16	NW carrier	PM1

[a] Sand (SP) subgrade.
[b] No seating load.

achieved about 90% in of their final equilibrium moisture content in 5 weeks.

The ultimate moisture content attained by the GCL is a function of the moisture available in the foundation soil. As shown in Table 4, increasing the moisture content of the foundation soil results in an increase in the equilibrium moisture content of the GCL. The equilibrium moisture content of GCLs placed on foundation soil at 5% ranges between 24% and 55% of the reference moisture content (Fig. 8 and Table 4). GCLs placed on the silty sand at 21% moisture content attained 100% of the reference water content.

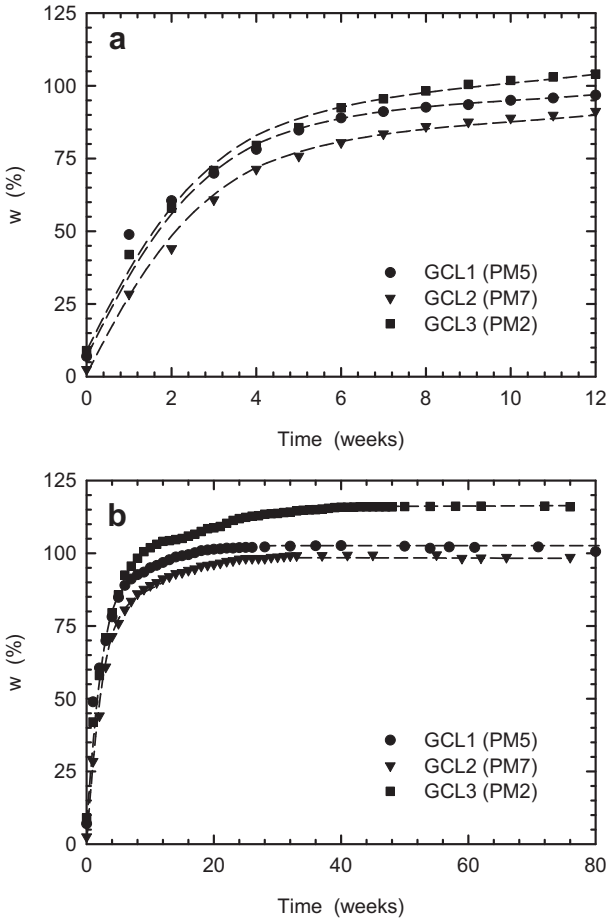

Fig. 5. Effect of GCL type on GCL hydration. Silty sand subgrade, w_{fdn} = 16%. (a) hydration in first 12 weeks, and (b) hydration for more than a year.

Table 4
Moisture content of GCLs after different elapsed times. All test on Godfrey silty sand (SM) with carrier geotextile on subgrade and 2 kPa seating pressure unless noted otherwise.

GCL	Initial subgrade w (%)	GCL Moisture Content, w (%)							w/w_{ref} after week				Test
		Initial (%)	1 day(%)	1 week (%)	5 weeks (%)	10 weeks (%)	20 weeks (%)	30 weeks (%)	5 (%)	10 (%)	20 (%)	30 (%)	
GCL1	5	7.5	12	23	35	35	34	34	25	25	24	24	PM14
GCL1	10	7.5	18	38	73	80	86	86	52	57	62	62	PM15
GCL1	16	7	22	45	84	95	101	102	60	68	72	73	PM5
GCL1	16	7	22	42	73	90	102	105	52	64	73	75	PM6[a]
GCL1	21	6	30	80	128	141	141	141	91	100	100	100	PM12
GCL2	5	5.8	12	22	37	38	39	40	32	33	34	34	PM16
GCL2	10	5.8	15	36	72	79	85	85	63	69	74	74	PM17
GCL2	16	2.6	21	44	80	89	97	99	68	76	83	85	PM7[b]
GCL2	16	8.8	24	45	76	81	86	88	66	70	75	77	PM9
GCL2	16	6.6	20	45	77	85	87	89	67	74	76	77	PM3[a]
GCL2	21	8.1	30	63	112	116	116	116	97	100	100	100	PM13
GCL2	2	6.3	11	22	30	31	31	31	26	27	27	27	PM18[c]
GCL2	10	6.3	19	51	79	86	87	90	68	75	76	78	PM19[c]
GCL3	5	5	13	31	48	62	76	83	32	41	50	55	PM4
GCL3	10	8.3	22	36	75	91	99	102	50	61	66	68	PM10
GCL3	16	9	20	42	86	102	109	114	57	68	73	76	PM2
GCL3	16	6.4	19	38	79	103	115	120	53	68	77	80	PM8[a]
GCL3	21	8.3	35	91	134	141	149	149	89	94	99	99	PM11
GCL3	16	8.4	19	33	53	83	93	119	33	52	58	74	PM1[d]

w_{ref} = 140% for GCL1, w_{ref} = 115% for GCL2 and w_{ref} = 150% for GCL3.
[a] Cover geotextile in contact with subgrade for these tests.
[b] Very low mass per unit area for this case.
[c] Sand (SP) for PM18 and 19.
[d] No seating load.

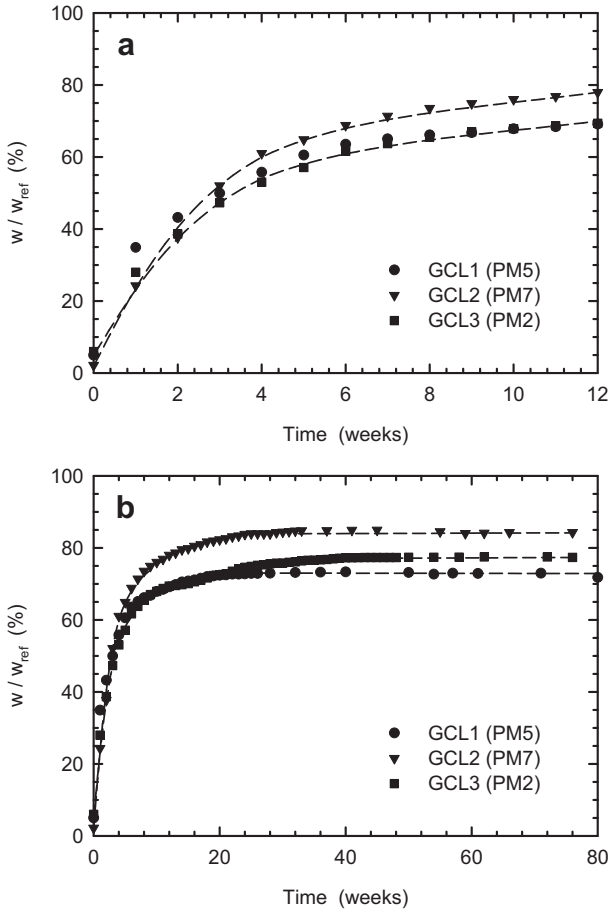

Fig. 6. Effect of GCL type on normalized hydration (w/w_{ref}). Silty sand subgrade, w_{fdn} = 16%. (a) hydration in first 12 weeks, and (b) hydration for more than a year.

4.3. Effect of GCL manufacture on hydration

The method of GCL manufacture affected the moisture uptake by the GCLs both when immersed in water and resting on the silty sand foundation soil. All GCL contained Wyoming bentonite with swell indices between 23 and 26 mL/2 g, similar smectite content but cation exchange capacity of 80 meq/100 g for GCLs1 and 2 and 100 meq/100 g for GCL3 (Table 2). When immersed in water with a 2 kPa seating pressure, the constraint imposed by the good anchorage of the needle punched fibers by the scrim-reinforcement and thermal treatment of the carrier geotextile for GCL2 (peel strength 260 N, Table 1) limited the swelling and the moisture content stabilized at about 115% (with a slight variation). Even though it was thermally treated, the woven carrier in GCL1 (peel strength 94 N, Table 1) provided much less effective anchorage and hence was less effective at constraining swelling and the moisture content stabilized at 140%. The least effective anchorage of fibers was for GCL3 (peel strength 219 N, Table 1) which stabilized at moisture content of about 150%. Despite the much higher peel strength, GCL3 hydrated to slightly higher moisture content (w_{ref}) than GCL1.

This finding is similar to that of Petrov et al. (1997), Lake and Rowe (2000a,b) and Beddoe et al. (2011) who reported that improved anchorage of the needle-punching restricted the GCL swell, lowered bulk GCL void ratios and consequently gave (other factors being equal): (a) lower hydraulic conductivity, (b) lower diffusion coefficients, and (c) less difference between the wetting and drying water retention curves. This is especially true for GCL2;

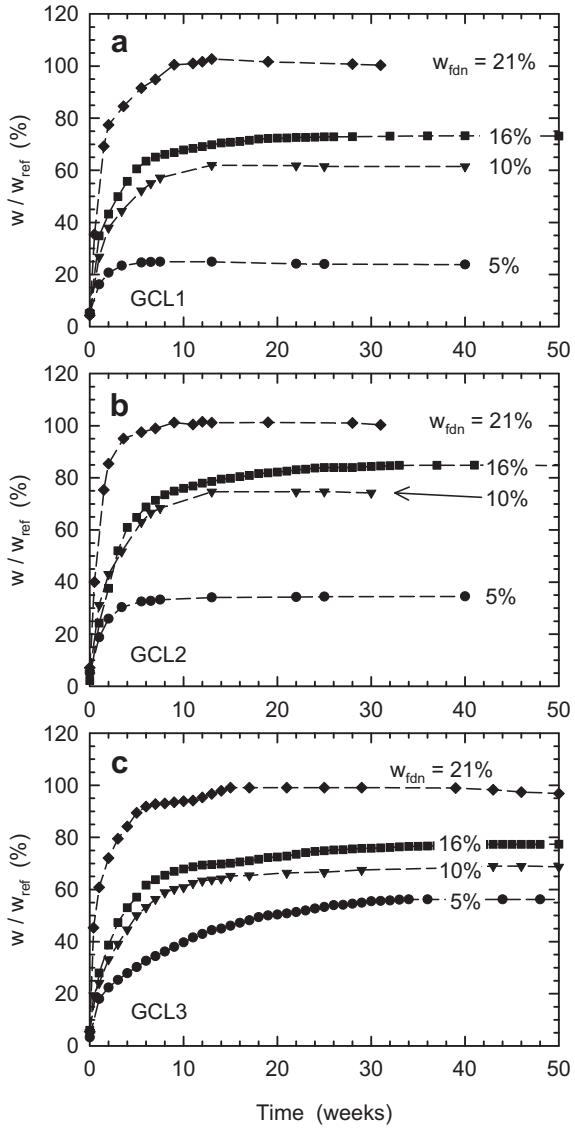

Fig. 7. Effect of initial subgrade moisture content (w_{fdn}) on normalized GCL hydration (w/w_{ref}). Silty sand subgrade.

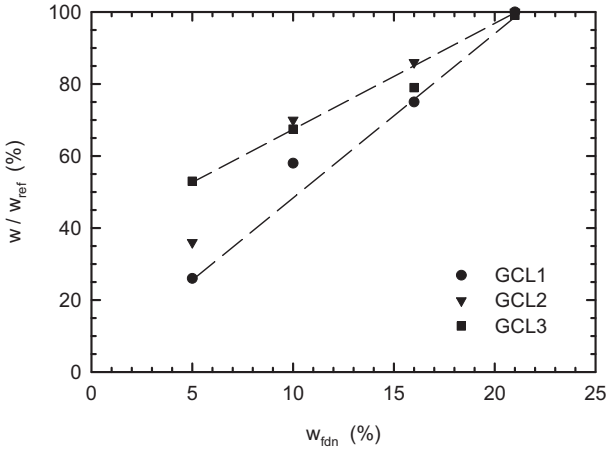

Fig. 8. Effect of initial subgrade moisture content (w_{fdn}) on GCL normalized hydration (w/w_{ref}). Silty sand subgrade after 30 weeks.

in this study and that by Beddoe et al. (2011) the performance of GCL1 was closer to that of GCL3 than GCL2 and this is attributed to the better anchorage achieved with the scrim reinforce nonwoven in GCL2 than for either GCL1 and GCL3.

When placed on the silty sand foundation soil at essentially field capacity (21%), all three GCLs hydrated to equilibrium moisture contents in excess of 99% of the reference value (Table 4). The time taken to reach about 95% of the reference values was about 3.5 weeks for GCL2, 7 weeks for GCL1 and about 10 weeks for GCL3. Of particular note in terms of the effect of method of GCL manufacture is the change in thickness of the GCL as it hydrates (Table 5). On this foundation soil with ample water to fully hydrate the GCL, the final hydrated thickness was 10.4, 8.2 and 10.9 mm and this represents an increase from the initially air dry state of 22%, 6% and 18% for GCL1–GCL3 respectively. This difference is manifest by a lower bulk void ratio for the hydrated GCL2 than the other two GCLs (Table 5) which can be expected to result in improved performance as noted above for the water hydrated samples. This is the result of the much better anchorage of the needle punched fibers afforded by the thermal treatment of the nonwoven carrier of GCL2 than was evident for either the other two GCLs. The improved bulk void ratio of GCL2 compared to GCL3 is consistent with the earlier findings of Petrov et al. (1997) and Lake and Rowe (2000a,b). However in their tests the GCL with a thermally treated woven carrier (product NS) provided much better anchorage of the thermally treated woven carrier in the presently tested product (NSL). The NSL product was manufatured to be a "lighter" (hence the "L") version of the NS with less material so that it would be more competitive in markets where GCLs are primarily selected based on price. What is apparent here is that the changes made to achieve a reduction in cost has also resulted in some reduction in hydration performance relative to the former NS product and its current companion product (GCL2). The improved hydration performance of GCL2 to GCL1 from the same manufacturer as well as compared to GCL3 from a different manufacturer is consistent with other studies (e.g. Beddoe et al., 2011). This highlights the importance of manufacture and changes that can occur over time even with the same manufacturer.

4.4. Effect of small confining stress on GCL hydration

All but one of the tests reported in this paper were conducted with a 2 kPa confining stress on top of the GCL. The small confining stress was applied to improve experimental repeatability by reducing the potential for zones of poor contact between the GCL and foundation soil. Fig. 9 shows results from the one test conducted with zero confining stress. These values were normalized by a reference moisture content of 160%, obtained when immersed in water with no confining stress. Without the small confining stress, the rate of moisture uptake from the foundation soil was slower and it took 30–35 weeks before reaching a similar moisture content as when the 2 kPa pressure was used.

4.5. Effect of GCL mass per unit area on hydration

Although GCLs have a minimum average roll value certified by the manufacturer, there can be considerable variability in the mass per unit area of samples taken from the same roll as is evident from the range given in Table 1. To investigate the influence of GCL mass per unit area on the rate of hydration, two samples of GCL2 with mass per unit area of 3490 g/m^2 (PM7) and 4880 g/m^2 (PM9) were examined under otherwise similar conditions. There was a small difference in the moisture uptake between the two tests (Table 4 and Fig. 10) with the higher mass per unit area sample initially taking up moisture faster but then coming to a final equilibrium moisture content slightly lower than that for the lower mass per unit area sample. The ratio of equilibrium moisture content to the reference value (w/w_{ref}) was about 86% for the specimen with the lower mass per unit area and about 77% for that with the higher mass of bentonite per unit area. Thus the mass per unit area appears to have some small effect on hydration but further testing would be required to investigate the mechanism by which this is achieved.

4.6. Effect of GCL placement on hydration

GCLs are commonly placed with the carrier geotextile in contact with the foundation soil and this was the normal case considered in

Table 5
GCL thickness (mm) with time of hydration and 30 week bulk void ratio.

GCL type	Initial sub grade w (%)	Initial thickness (mm)	1 week	5 weeks	10 weeks	20 weeks	30 weeks	Bulk void ratio at 30 weeks	Tests
GCL1	5	6.2	6.2	6.4	7.0	7.3	7.7	2.70	PM14
GCL1	10	7.0	7.0	7.4	7.7	8.0	8.2	2.93	PM15
GCL1	16	6.2	6.9	7.5	8.0	8.1	8.2	2.95	PM5
GCL1	16	6.2	6.4	6.5	6.7	7.4	8.0	2.92	PM6[a]
GCL1	21	8.5	8.9	9.4	9.6	10.4	10.4	3.28	PM12
GCL2	5	6.0	6.0	6.1	6.4	6.9	6.9	2.30	PM16
GCL2	10	6.8	6.8	7.0	7.2	7.9	7.9	2.41	PM17
GCL2	16	6.0	6.1	6.4	6.8	6.8	6.8	2.81	PM7[b]
GCL2	16	7.0	7.2	7.8	7.9	8.0	8.0	2.63	PM9
GCL2	16	7.0	7.2	7.5	7.8	7.8	8.0	2.75	PM3[a]
GCL2	21	7.7	7.8	8.0	8.2	8.5	8.5	3.00	PM13
GCL2	2	6.1	6.1	6.2	6.4	6.6	6.6	1.99	PM18[c]
GCL2	10	6.1	6.2	6.5	7.0	7.6	7.6	2.66	PM19[c]
GCL3	5	7.9	8.0	8.4	8.5	8.6	8.6	2.74	PM4
GCL3	10	9	9.2	9.3	9.3	9.4	9.4	3.05	PM10
GCL3	16	7.8	8.0	8.1	8.6	8.8	9.2	3.00	PM2
GCL3	16	9	9.2	9.6	10.4	10.5	10.5	3.53	PM8[a]
GCL3	21	9.2	9.8	10.4	10.5	10.8	10.9	3.64	PM11
GCL3	16	7.8	7.9	8.0	8.1	8.5	8.7	3.24	PM1[d]

[a] Cover geotextile in contact with subgrade for these test.
[b] Very low mass per unit area for this case.
[c] Concrete sand (PM18 and 19).
[d] No seating load.

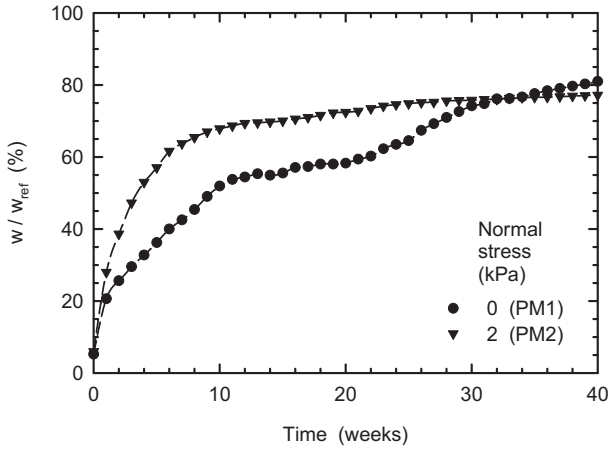

Fig. 9. Effect of normal stress on normalized hydration (w / w_{ref}) for GCL 3. Silty sand subgrade, w_{fdn} = 16%.

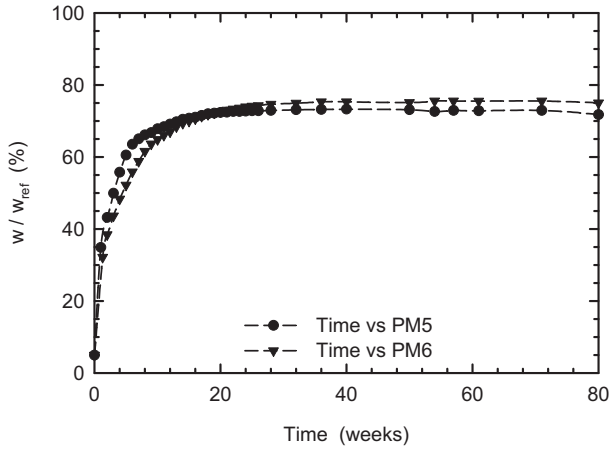

Fig. 11. Effect of geotextile in contact with subgrade on normalizesd hydration (w/w_{ref}) for GCL1. Silty sand subgrade, w_{fdn} = 16%.

this study. To assess what, if any, effect this may have on the hydration of the GCL, three tests (PM6, PM3 and PM8 in Tables 3 and 4) were conducted with the cover geotextile directly on the foundation soil. The results for GCL1 (Table 4 and Fig. 11) show that little difference in the equilibrium water content and rate of hydration can be observed despite the differences in geotextile type (W versus NW) in contact with the subsoil. Similar results were observed for GCL2 (PM5 and PM6) and GCL3 (PM2 and PM8). This suggests that the mode of hydration is not dependent on the type of geotextile which is placed in contact with the foundation soil.

4.7. Influence of soil type on GCL hydration

To examine the effect of foundation soil type (and hence the water retention curve), one test was conducted for GCL2 placed on sand for comparison with silty sand. Fig. 12 shows the moisture uptake for the two soils at initial 10% moisture content. The rate of hydration was slightly higher for the sand than for the silty sand. The GCL moisture uptake of about 60% of the reference value (w/w_{ref}) occurred in the first 2 weeks on sand, while it took about 5 weeks on the silty sand. However, the time to reach the final equilibrium moisture content was similar for both foundation soils. The difference in rate of hydration of the GCL is attributed to the complex unsaturated behavior of the foundation soil-GCL interaction. At lower suctions the sand will have a higher unsaturated conductivity and will allow initial passage of water to the GCL faster than the silty sand. As the GCL extracts water from the soil and the soil suction increases the unsaturated conductivity of the sand dips below that of the silty sand which allows the GCL on the silty sand to catch up. From the water retention curves, the sand has

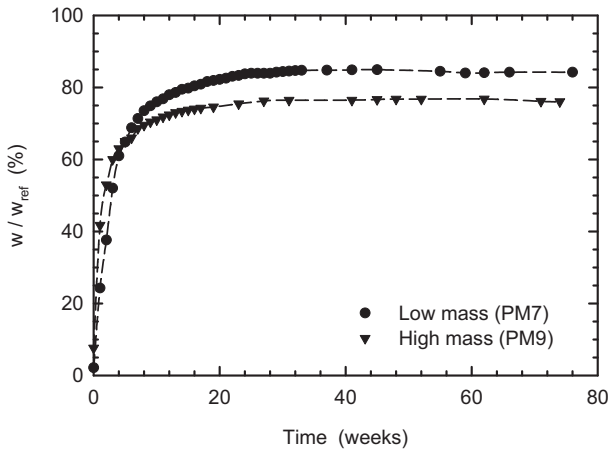

Fig. 10. Effect of mass per unit area on normalized hydration (w/w_{ref}) for GCL2. Silty sand subgrade, w_{fdn} = 16%.

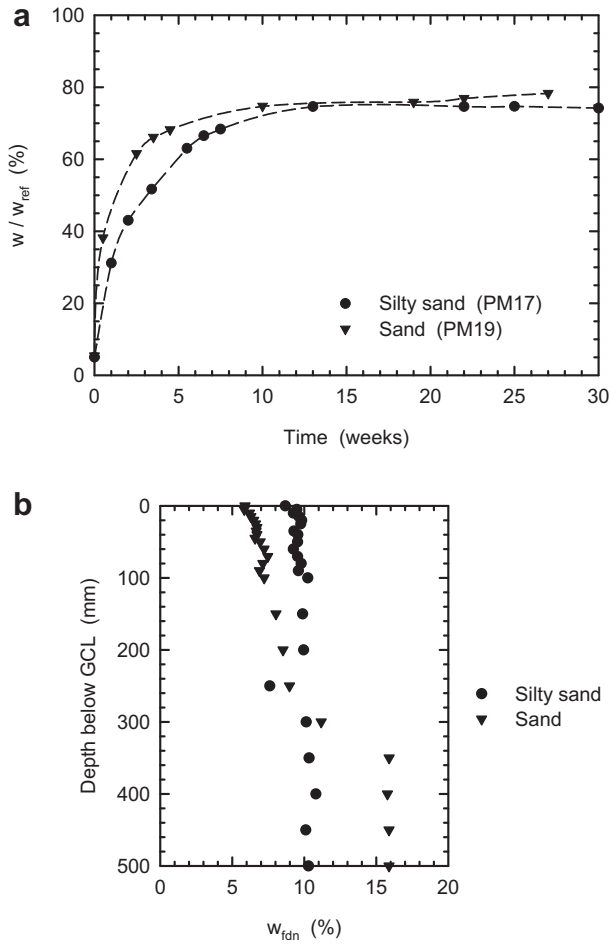

Fig. 12. Effect of subgrade soil type on GCL2 hydration w_{dfn} = 10%. (a) (w/w_{ref}) with time and (b) equilibrium subgrade water content.

a lower suction compared with the silty sand at similar water contents, however the sand is a free-draining material. Therefore although the average moisture content was 10%, downward moisture migration occurred during the period before placement of the GCL and subsequently. As a consequence, the final moisture at the soil-GCL interface was closer to 6% for the sand compared with about 9% in the silty sand. Comparing the water retention curves in Fig. 3 this in turn should still lead to a slightly higher equilibrium moisture content for the GCL placed on top of sand. However GCL2 has a very flat water retention curve (Beddoe et al., 2011) in the low suction region and therefore the changes in suction did not result in any significant changes in moisture content.

4.8. Comparison with findings from previous studies

Daniel et al. (1993) investigated the hydration of an adhesive bonded GCL consisting of 3.5-mm-thick layer of sodium bentonite mixed with an adhesive and attached to a geomembrane (Gundseal) placed on a foundation sand ($D_{10} = 0.2$ mm, $D_{60} = 0.5$ mm, $D_{85} = 0.7$ mm) at initial sand moisture contents between 1% and 17%. These adhesive bonded GCLs were observed to hydrate to GCL moisture contents of approximately 75% and 155% when on sand at 2% and 10% moisture content, respectively (after 6 weeks). The sand used in the experiments of Daniel et al. (1993) is similar to the one used in the present study ($D_{10} = 0.15$ mm, $D_{60} = 0.38$ mm, $D_{85} = 0.6$ mm) in which needle punched GCL2 was observed to hydrate to moisture contents of 30% and 79% after 5 weeks of equilibration with sand foundations at 2% and 10% moisture contents (PM18 & PM19, Table 4). This large difference in moisture content between the adhesive bonded GCL and the needle punched GCL illustrates the higher degree of confinement (and resistance to large increases in void ratio) provided by needle punched GCL.

Eberle and von Maubeuge (1997) reported that a needle punched GCL placed with a well graded sand (90% passing 4.75 mm sieve and at an initial moisture content of 8–10%) both above and below it, achieved a moisture content of 100% in less than 24 h and 140% after 60 days under isothermal conditions (23 °C). These results indicate that the rate of hydration in these experiments were significantly higher than the present study (e.g. PM10, 15, 17, 19 in Table 4). This significant difference in GCL moisture uptake is probably due to a combination of factors but in particular (a) the presence of powdered bentonite in their GCL compared with granular bentonite in the present study, and (b) hydration from two sides in their experiment compared with from only one side in the current study (which simulates a GCL in a composite liner).

5. Conclusions

The hydration of different GCLs from the pore water of the underlying foundation soil in a closed-system was investigated for isothermal conditions at room temperature 22 °C. Three different reinforced (needle punched) GCL products were tested for hydration from both an underlying silty sand (SM) and sand (SP) foundation soil for time periods up to 70 weeks.

Of the factors examined, the initial water content of the silty sand foundation layer had the greatest impact on the rate of GCL hydration and the steady-state GCL moisture content. GCLs placed on a foundation soil with an initial moisture content close to field capacity hydrated to moisture contents that were essentially the same as if the GCL was immersed in water. In contrast, GCLs on soil at initial moisture content close to their residual moisture content (5% for the silty sand and 2% for the sand considered) only hydrated to a gravimetric moisture content of 30–35%, which is only about a quarter of the value achieved immersed in water.

The method of GCL manufacture was also found to have a significant effect on the rate of GCL hydration and the steady-state GCL moisture content at low foundation moisture contents because of the difference in confinement of the bentonite afforded by the combination of different carrier geotextiles and the presence/absence of thermal treatment of the needle punched fibers.

It was also found that the presence or absence of a small (2 kPa) seating pressure (which affects the intimacy of contact between the GCL and foundation soil) affected the rate of hydration but not the final moisture content. Due to the differences in the water retention curves of the different foundation soil, a GCL placed on a sand (SP) demonstrated faster hydration and slightly higher final moisture content than when on a silty sand (SM) with same initial moisture content. For the particular GCLs tested, hydration did not change significantly irrespective of whether the cover or carrier GCL rested on the foundation soil, suggesting that the water retention characteristics of the GCL are not affected by placement orientation.

The results are for the specific materials and conditions tested and should not be directly used for significantly different conditions without independent verification.

Acknowledgements

This study was financially supported by the Natural Science and Engineering Research Council of Canada (NSERC), the Ontario Centres of Excellence, and Terrafix Geosynthetics Inc. The research was conducted using equipment funded by the Canada Foundation for Innovation (CFI) and the Ontario Ministry of Research and Innovation. The writers are grateful to their industrial partners, Terrafix Geosynthetics Inc., Solmax International, Ontario Ministry of Environment, AECOM, AMEC Earth and Environmental, Golder Associates Ltd., and the CTT group, however the views expressed herein are those of the writers and not necessarily those of our partners.

References

ASTM D 2487, 2005a. ASTM Standard 04.08. Standard Practice for Classification of Soils for Engineering Purposes (Unified Soil Classification System). ASTM, West Conshohocken, PA, USA, pp. 249–260.

ASTM D 422, 2005b. ASTM Standard 04.08. Standard test method for particle size analysis of soils. ASTM, West Conshohocken, PA, USA, pp. 10–17.

ASTM D 698, 2005c. ASTM Standard 04.08. Standard test methods for laboratory compaction characteristics on soil using standard effort. ASTM, West Conshohocken, PA, USA, pp. 80–90.

Beddoe, R.A., Take, W.A., Rowe, R.K., 2011. Water retention behaviour of geosynthetic clay liners, ASCE. Journal of Geotechnical and Geoenvironmental Engineering. doi:10.1061/(ASCE)GT.1943-5606.0000526 Published online March 2, 2011.

Benson, C.H., Kucukkirca, I.E., Scalia, J., 2010. Properties of geosynthetics exhumed from a final cover at a solid waste landfill. Geotextiles and Geomembranes 28 (6), 536–546.

Bostwick, L.E. (2009). Laboratory study of geosynthetic clay liner shrinkage when subjected to wet/dry cycles. M.Sc. Thesis, Queen's University, Kingston.

Bostwick, L.E., Rowe, R.K., Take, W.A., Brachman, R.W.I., 2010. Anisotropy and directional shrinkage of geosynthetic clay liners. Geosynthetics International 17 (3), 1–14.

Bouazza, A., Gates, W.P., Abuel-Naga, H., 2006. Factors impacting liquid and gas flow through geosynthetic clay liners. Geosynthetics – Recent Developments, Geosynthetics – Recent Developments, 9. Indian International Geosynthetics Society, New Delhi, pp. 19–146.

Brachman, R.W.I., Rowe, R.K., Take, W.A., Arnepalli, N., Chappel, M.J., Bostwick, L.E., and Beddoe, R. 2007. Queen's composite geosynthetic liner experimental site, 60th Canadian Geotechnical Conference, Ottawa, October, 2135–2142.

Daniel, D.E., Shan, H.Y., Anderson, J.D., 1993. Effects of partial wetting on the performance of the bentonite component of a geosynthetic clay liner. In: Proceedings of Geosynthetics '93. IFAI, Vancouver, B.C., pp. 1483–1496. March 30–April 1.

Dickinson, S., Brachman, R.W.I., 2010. Permeability and internal erosion of a GCL beneath coarse gravel. Geosynthetics International 17 (3), 112–123.

Eberle, M.A. and von Maubeuge, K. 1997. Measuring the In-Situ Moisture Content of Geosynthetic Clay Liners (GCLs) Using Time Domain Reflectometry (TDR), 6th Int. Conf. on Geosynthetics, Atlanta, 1: 205–210.

Gassner, F., 2009. Field observation of GCL shrinkage at a site in Melbourne Australia. Geotextiles and Geomembranes 27 (5), 406–408.
Gates, W.P, Hornsey, W.P., and Buckley, J.L. 2009. Geosynthetic clay liners-Is the key component being overlooked? Proceeding of GIGSA GeoAfrica 2009 Conference, Cape Town.
GeoStudio, 2007. Version 7.16, Build 4840. Geo-Slope International Ltd.
Guyonnet, D., Touze-Foltz, N., Norotte, V., Pothier, C., Didier, G., Gailhanou, H., Blanc, P., Warmont, F., 2009. Performance-based indicators for controlling geosynthetic clay liners in landfill applications. Geotextiles and Geomembranes 27 (5), 321–331.
Lake, C.B., Rowe, R.K., 2000a. Swelling characteristics of needlepunched, thermally treated GCLs. Geotextiles and Geomembranes 18 (2), 77–102.
Lake, C.B., Rowe, R.K., 2000b. Diffusion of sodium and chloride through geosynthetic clay liners. Geotextiles and Geomembranes 18 (2), 102–132.
Petrov, R.J., Rowe, R.K., 1997. Geosynthetic clay liner compatibility by hydraulic conductivity testing: factors impacting performance. Canadian Geotechnical Journal 34 (6), 863–885.
Petrov, J.R., Rowe, R.K., Quigley, R.M., August 1997. Selected factors influencing GCL hydraulic conductivity. Journal of Geotechnical and Geoenvironmental Engineering, 683–695.
Rowe, R.K., 2005. Long-term performance of contaminant barrier system. Geotechnique 55 (9), 631–678.
Rowe, R.K., 2007. Advances and remaining challenges for geosynthetics in geoenvironmental engineering applications, 23rd manual rocha lecture. Soils and Rocks 30 (1), 3–30.
Rowe, R.K., Orsini, C., 2003. Effect of GCL and subgrade type on internal erosion in GCLs. Geotextiles and Geomembranes 21 (1), 1–24.
Rowe, R.K., Bostwick, L.E., Thiel, R., 2010. Shrinkage characteristics of heat-tacked GCL seams. Geotextiles and Geomembranes 28 (4), 352–359.
Rowe, R.K., Quigley, R.M., Brachman, R.W.I., Booker, J.R. (2004). Barrier Systems for Waste Disposal Facilities, Taylor & Francis Books Ltd (E & FN Spon) London, 587p.
Rowe, R.K., Bostwick, L.E., Take, W.A., 2011. Effect of GCL properties on shrinkage when subjected to wet-dry cycles. Journal of Geotechnical and Geoenvironmental Engineering. doi:10.1061/(ASCE)GT.1943-5606.0000522 ASCE.
Thiel, R., Giroud, J.P., Erickson, R., Criley, K. and Bryk, J. 2006. Laboratory measurements of GCL shrinkage under cyclic changes in temperature and hydration conditions, 8th International Conference on Geosynthetics, Yokohama, Japan 1:21–44.

Effect of GCL Properties on Shrinkage When Subjected to Wet-Dry Cycles

R. Kerry Rowe, F.ASCE[1]; L. E. Bostwick[2]; and W. A. Take[3]

Abstract: The potential shrinkage of eight different geosynthetic clay liners (GCLs) subjected to wetting and drying cycles is examined. It is shown that the initial (e.g, off-the-roll) moisture content may affect the initial shrinkage but did not notably affect the final equilibrium shrinkage. For GCLs with granular bentonite and wetted to a moisture content of about 60% (or greater) in the hydration phase, the actual moisture content did not appear to affect the magnitude of the final equilibrium shrinkage. However, it did affect the rate of shrinkage. Specimens brought to about 100% moisture content in each cycle reached a constant shrinkage value much faster than those brought to about 60% in each wetting cycle. GCLs containing powdered bentonite generally shrank more than those containing granular bentonite. All of the powdered bentonite specimens continued a slow accumulation of strain with increasing cycles, even up to 75 cycles. The shrinkage of a needle-punched GCL with a thermally treated scrim-reinforced nonwoven carrier geotextile and granular bentonite was less than that for a needle-punched GCL with a simple nonwoven carrier and granular bentonite. For some products, there was considerable variability in GCL shrinkage for specimens from the same roll and tested under nominally identical conditions, whereas for other products, the variability was relatively small. The shrinkage strain required to cause the loss of a 150–300 mm panel overlap is shown to be able to be mobilized in about five wet-dry cycles in the experiments reported. **DOI: 10.1061/(ASCE)GT.1943-5606.0000522.**

CE Database subject headings: Shrinkage; Bentonite; Hydration; Dewatering; Moisture.

Author keywords: GCL; Shrinkage; Bentonite.

Introduction

The primary function of a geosynthetic clay liner (GCL) in a composite liner is to minimize leakage through any holes in the overlying geomembrane (Rowe 2005; Saidi et al. 2008). Many factors can affect the performance of GCLs used alone or as part of composite liners (e.g., Benson et al. 2010a; Dickinson and Brachman 2010); however, one aspect that has received very little attention is the effect of overlaps of GCL panels. Historically, the GCL has typically been installed in panels with a 150 mm overlap of the panels with powdered bentonite between the overlaps to ensure good hydraulic behavior (Cooley and Daniel 1995; Benson et al. 2004). The overlying geomembrane is typically covered with soil once installed, but sometimes it is left exposed to the atmosphere for operational reasons for periods ranging from months to years. Leaving composite liners uncovered has resulted in five reported cases of needle-punched GCL panel movement in which the initial 150 mm overlap had been lost and significant gaps between panels have been observed (Thiel and Richardson 2005; Koerner and Koerner 2005a, b; Thiel et al. 2006). These cases corresponded to composite liners both on side slopes and the landfill base and exposure periods of 2 months to 5 years. Panel separations of 300 and 450 mm were observed after only two months of exposure for two needle-punched GCLs on a base with 4° slope. In another case, a separation of 1,200 mm occurred after 36 months of exposure on a 34° slope (Thiel et al. 2006). However, there is also a published case (Gassner 2009) in which a needle-punched GCL experienced only 50 mm of shrinkage during 18 months of exposure on a 18° slope. Instances of panel separation in the field occurred over a range of environmental conditions (such as temperature, humidity, and type of subsoil).

The objective of this paper is to examine the effect that the type of GCL may have on the magnitude of shrinkage in an experimental program that represents a significant extension of the work of Thiel et al. (2006). The various features of different products, such as the type of carrier geotextile and the type and granularity of the bentonite, were systematically examined to assess the role the effect that these variables may have on GCL shrinkage when subjected to wet-dry cycles in the laboratory.

Background Information

There has been relatively little research into the shrinkage of GCL panels. Although the problem of field shrinkage of high-moisture-content, unreinforced GCLs has long been known, it was not expected to occur with reinforced (i.e., needle-punched) products (Mackey 1997; Thiel et al. 2006). Indeed, Koerner and Koerner (2005a, b) stated that field drying alone of a high-moisture-content reinforced GCL was not known to cause shrinkage. Following the recognition of the panel separation issue, a laboratory

[1]Professor and Canada Research Chair in Geotechnical and Geoenvironmental Engineering, GeoEngineering Centre Queen's-RMC, Dept. of Civil Engineering, Queen's Univ., Kingston, ON, Canada K7L 3N6 (corresponding author). E-mail: kerry@civil.queensu.ca

[2]Engineer, Stantec, Ottawa, ON, Canada. E-mail: laura.bostwick@stantec.com

[3]Associate Professor, GeoEngineering Centre Queen's-RMC, Dept. of Civil Engineering, Queen's Univ., Kingston, ON, Canada, K7L 3N6. E-mail: andy.take@civil.queensu.ca

Note. This manuscript was submitted on July 20, 2009; approved on February 8, 2011; published online on February 10, 2011. Discussion period open until April 1, 2012; separate discussions must be submitted for individual papers. This paper is part of the ***Journal of Geotechnical and Geoenvironmental Engineering***, Vol. 137, No. 11, November 1, 2011. ©ASCE, ISSN 1090-0241/2011/11-1019–1027/$25.00.

Table 1. Properties of Needle-Punched GCLs Examined

Product	Average dry mass (g/m^2)	Range of dry mass (g/m^2)	Range of initial moisture contents (%)	Cover GT	Average cover GT mass (g/m^2)	Carrier GT	Average carrier GT mass (g/m^2)	Bentonite granularity and type	Thermally treated?
GCL1	4970	4880–5060	< 1–7	NW	240	W	120	Fine, A	Yes
GCL2	4380	3690–5010	3–65	NW	230	NWSR	260	Fine, A	Yes
GCL3	5550	5100–6030	0–19	NW	280	W	130	Coarse, A	No
GCL4	4870	4510–5170	5–72	NW	260	NW	230	Coarse, A	No
GCL5	5380	5360–5410	10	NW	410	NWSR	500	Powdered, A	Yes
GCL6	4740	4710–4780	11	NW	310	NWSR	440	Powdered, B	Yes
GCL7	4860	4860–4870	11–12	NW with bentonite	410	W	220	Powdered, C	Yes
GCL8	4680	4670–4690	9–10	NW	240	W	140	Powdered, B	Yes

Note: NW, nonwoven; W, woven; NWSR, scrim-reinforced nonwoven; GT, geotextile.

testing program was initiated by Thiel et al. (2006). In their experiments, GCLs nominally similar to GCL1–GCL4 examined in this study (Table 1) were subjected to wet-dry cycling and their shrinkage monitored. Following this study, it was concluded that wet-dry cycling had the potential to cause shrinkage in the GCL to the degree observed in the field. Thiel et al. (2006) also showed that geotextiles alone exhibit very little shrinkage (maximum of 2.4%). However, with one exception, the study by Thiel et al. was limited to one specimen per product.

Thiel et al. (2006) did test one product type (GCL2) twice, although these tests were not strictly identical because they were on two versions of the product with one having a much greater needle-punching density and significantly higher peel strength than the other. After 40 cycles in these tests, there was substantial variation in the accumulated shrinkage (12.9 and 19.2% for GCLs with construction similar to GCL2 but peel strengths of 2 and 0.8 kN/m, respectively). However, it is not possible to tell from these data whether this difference was due to the significantly different peel strengths or was a reflection of potential sample variability because, in general, there was a poor correlation between the amount of shrinkage and the peel strength of the different products. For example, the maximum shrinkage (23%) was for a product similar to GCL4 having a peel strength of 2 kN/m, followed by 20.6% for a product similar to GCL3 (peel strength 1 kN/m), then 19.2% for a product similar to GCL2 with peel strength of 0.8 kN/m, then 14.5% for a product similar to GCL1 (peel strength 0.3 kN/m), and the lowest was 12.9% for a product similar to GCL2 with peel strength of 2 kN/m. Thiel et al.'s tests focused primarily on illustrating that wet-dry cycles could accumulate sufficient shrinkage to explain panel separation. The test for the GCL4 gave 23% shrinkage (equivalent to just over 1,000 mm in the field), which could explain all but one of the field cases of panel separation observed for that product.

Testing Program

Materials

It is well known that the type of bentonite can affect its swelling (and shrinkage) and interaction with different permeants (e.g., Rowe et al. 2004; Katsumi et al. 2008; Benson et al. 2010b; Gates and Bouazza 2010; Hornsey et al. 2010; Lange et al. 2010; Rosin-Paumier et al. 2010; Shackelford et al. 2010). Thus, eight different GCL products were examined in this study. Four (two containing coarse granular bentonite and two containing fine granular bentonite) were manufactured for the North American market, while four others, consisting of powdered bentonite, were manufactured in Europe. The four North American products used in this study have been previously examined for GCL shrinkage (Thiel et al. 2006; Bostwick et al. 2007, 2008, 2010; Rowe et al. 2010), with a comparison between test results provided for GCLs without heat tacking in Bostwick et al. (2010); to the writers' knowledge, the powdered European products have not previously been examined in cyclic wet-dry shrinkage tests. This study also reports a far more extensive study than that reported in conference papers by Thiel et al. (2006) or Bostwick et al. (2007, 2008). A summary of the products examined is given in Table 1 and details of bentonite grain size classification are given in Fig. 1. Peel test and swell index values are given in Table 2.

Three different types of bentonite were examined. Bentonite type A was a Wyoming sodium bentonite used in both the North American and the European products, in all three granularities (Table 1). As reported by the supplier, bentonite type B was also sodium bentonite but not Wyoming sodium bentonite, and C was a blend of sodium bentonites from different sources (including Wyoming sodium bentonite). The swell indexes are given in Table 2 for the bentonite used in each GCL. The swell index of the type A bentonite used in the various GCLs was fairly consistent for a given roll of GCL but varied between 23 and 32 mL/g from product to product (probably reflecting variability in the bentonite provided from nominally the same source from time to time). The swell index for bentonite B was 24–25 mL/g and C was 28 mL/g.

Test Specimens

Both restrained (R) and unrestrained (UR) specimens were tested. Preliminary tests by Bostwick et al. (2008) demonstrated that this factor does not significantly impact the final maximum shrinkage.

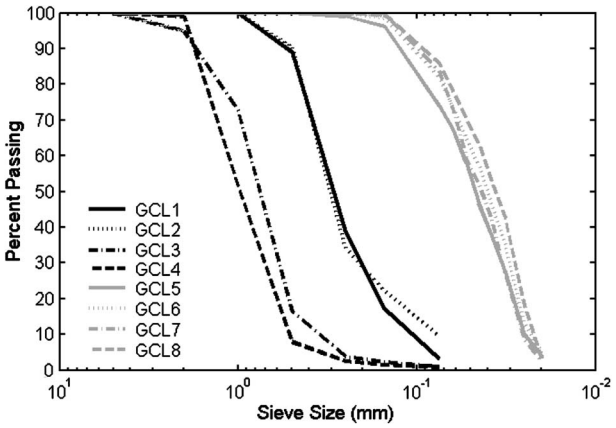

Fig. 1. Grain-size analysis of bentonites from various GCL products

J. Geotech. Geoenviron. Eng. 2011.137:1019-1027.

Table 2. Peel Strengths of Needle-Punched GCLs Examined and Swell Index

Product	Average peak peel strength (N)	Standard deviation of average peak peel strength (N)	Average bonding peel strength (kN/m)	Standard deviation of average bonding peel strength (kN/m)	Mean swell index (mL/2 g)	Standard deviation of swell index (mL/2 g)
GCL1	93.8	16.5	0.66	0.09	25.3	0.4
GCL2	260	16.8	2.37	0.12	22.6	0.5
GCL3	204	35.7	1.51	0.26	32.2	0.3
GCL4	219	29.6	1.78	0.28	23.2	0.3
GCL5	207	33.7	1.51	0.19	27.1	0.3
GCL6	224	16.9	1.71	0.09	24.3	0.6
GCL7	97.0	14.2	0.73	0.06	27.7	0.3
GCL8	54.0	4.2	0.41	0.04	25.3	0.6

Each specimen, whether restrained or unrestrained, had a testing area of 550 by 350 mm; this was further reduced to an area of interest of 500 by 300 mm by drawing a 25 mm border on all sides of the specimen. By analyzing only the area of interest, edge effects were avoided.

After specimens were cut and prepared, they were placed on individual smooth aluminum baking pans. Unrestrained specimens were allowed to move freely on the pan, while restrained specimens were held down with 25-mm-wide clamps at either end. Circular control markers, used for calibration during photogrammetric analysis, were also added to the pans. An example of a restrained specimen is shown in Fig. 2.

Testing Process

Once the initial conditions of each specimen were recorded (e.g., water content, mass per unit area, and measurements at grid lines), the specimens were wet with a specified amount of water. An 8 L commercial garden sprayer was used to apply the water in a uniform manner across the specimen. The amount of water varied according to the specimen being tested, as noted subsequently.

In test series I, 500 g of water was added to reproduce the base-case test conditions adopted by Thiel et al. (2006), which was selected on the basis of a target moisture content of about 65% because this was reported by Daniel et al. (1993) to be a typical water content reached through moisture uptake from soil. However, because the mass per unit area of the specimens tested varied widely, the application of a constant mass of water meant that, in fact, moisture content varied and generally was not 65%. Thus, in test series II, the amount of water was selected to give a target water content of 60% of specimen dry mass after moisture uptake. Two additional test series (III and IV) examined the effect of adding extra water during the hydration phase; these test series were conducted concurrently with test series I and II. In test series III, specimens were wet with 1,000 g of water. In test series IV, the amount of water added was selected such that it would bring the specimens to a target water content equal to 100% of specimens' dry mass.

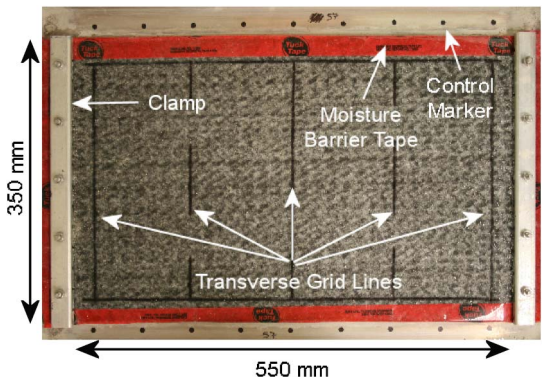

Fig. 2. Setup of restrained pan tests

Following the wetting process, specimens were allowed to hydrate for 8 h in a temperature-controlled room at 20°C. During this period, the specimens were covered with moisture-barrier plastic to prevent moisture loss to the atmosphere.

The subsequent drying phase, which lasted 15 h, took place in ovens set to 60°C. This temperature was on the basis of that used by Thiel et al. (2006) to approximate the temperature that can be reached by a black geomembrane exposed to solar radiation. Pelte et al. (1994) measured a maximum geomembrane temperature of 70°C in the field. At the completion of the drying phase, the samples had reached an average moisture content of slightly less than 1%. The handling phase took approximately 1 h, resulting in a total cycle length of 24 h.

The described experiments were not intended to give the expected shrinkage strains under field conditions, but rather to indicate the effect of variables examined on the maximum amount of shrinkage that might be expected under extreme exposure conditions. For the GCL to shrink, it must first uptake moisture, lose it, and then uptake it again. In this paper, the GCLs were wetted with spray from a water bottle. However, in the field, GCL moisture uptake will be partly because of uptake from the soil and partly because of condensation of water evaporated from the GCL. The experiments reported herein approximate the latter mechanism. The uptake of moisture from the soil and its dependence on the water-retention curve and the water content of the foundation soil as well as the water-retention curve for the GCL is not examined in the present study.

Strain Measurement

Definition of Specimen Strain

For restrained specimens, the restraint caused specimens to neck (Thiel et al. 2006; Bostwick et al. 2007, 2008), and hence, the maximum strain occurred near the midpoint of the specimen. To minimize the risk of a single point measurement giving excessive and unrepresentative strain, strain in restrained specimens was expressed as the average strain on the basis of measurements 100 mm to either side of the maximum individual value. This is termed the maximum strain.

For unrestrained specimens, the lack of restraint meant that no necking occurred; therefore, all shrinkage on unrestrained specimens was expressed as the average shrinkage along the entire length of the specimen for the transverse (across-roll) direction and across the entire width of the specimen for the longitudinal (roll) direction.

J. Geotech. Geoenviron. Eng. 2011.137:1019-1027.

This paper does not specifically address the possible effect of anisotropic shrinkage on overall shrinkage behavior. Bostwick et al. (2010) demonstrated that there is no apparent variability in longitudinal and transverse shrinkage for GCL2. GCL4 often exhibited preferential shrinkage in the longitudinal direction; however, this was not always the case and this was likely due to the considerable variability in the distribution of bentonite within a single sample of GCL4.

Hand Measurements

During testing, hand measurements were taken of each of the specimens following every drying cycle. Measurements were taken at each of the grid lines, and were only taken within the area of interest; this resulted in five measurements per cycle for restrained specimens, and 10 measurements per cycle for unrestrained specimens. This allowed an approximate measurement of strain as testing progressed. These measurements were only used as a check on the primary method of measurement—image analysis as is subsequently discussed. Final hand measurements are given by Bostwick (2009).

Image Analysis

A 10 megapixel (MP) digital SLR camera was used to capture digital images of each specimen at the end of both the hydration and the drying portions of the imposed moisture cycles. These images were used to calculate shrinkage deformation using the program GeoPIV (White et al. 2003).

The first stage of the image-based deformation measurement analysis is the definition of the regions to be tracked. In the software GeoPIV, these regions (or patches) consist of a small portion of the original matrix comprising the initial image. These 64×64 pixel square patches were selected to form 51 pairs on each specimen, coincident with the border lines. Each patch consists of its own unique distribution of pixel color intensity; to enhance the contrast on products with white geotextiles, black paint was applied to the specimen. The uniqueness of each patch made it traceable throughout the series of images, thus allowing movement to be calculated. A series of control markers was drawn on each pan to provide static reference points, which allowed precise calibration of the pans using close-range photogrammetry.

According to White et al. (2003), GeoPIV is capable of a precision up to 0.1 pixels. Thus, the error in an analysis is dependent on the resolution of the photograph taken. Photographs taken with a 10 MP camera, with dimensions of $3{,}588 \times 2{,}592$ pixels and, thus, a resolution of approximately 0.17 mm/pixel, have an approximate error of 0.02 mm. The conversion of this error to percent strain depends on the gauge length being studied. For a transverse-strain measurement with a gauge length of 300 mm, the approximate error would be 0.006%.

Discussion of Test Results

Effect of Initial Moisture Content

One of the differences between different GCL products is the initial off-the-roll moisture content. For example, for GCL2, a typical value is less than 10%, whereas GCL4 is typically 15–30%. The initial moisture content for some specimens used in these tests was around 5–7%, which indicates that some drying occurred during storage; these specimens may have undergone an unintended first drying relative to the off-the-roll moisture content prior to being cut.

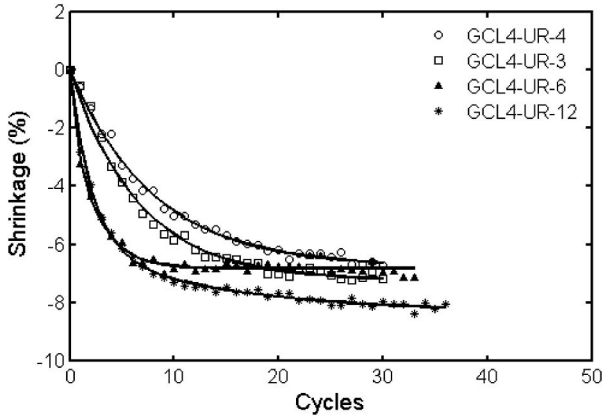

Fig. 3. Effect of initial moisture content on shrinkage of GCL4

To examine the effect of the initial water content at the start of the first wetting/drying cycle for GCL4 (which typically has a relatively high off-the-roll moisture content), water was added prior to testing to artificially raise the moisture content from the off-the-roll value stored in the lab (5% for GCL4-UR-4) to initial values of 19% (GCL4-UR-3), 64% (GCL4-UR-12), and 72% (GCL4-UR-6) to cover an extreme range of possible initial conditions. These specimens were allowed to equilibrate prior to the addition of 500 g of water used in the wetting phase. Fig. 3 and Table 3 demonstrate that although there was a wide range in observed shrinkage values for these four samples, there does not appear to be any strong correlation on the basis of the initial moisture content (at least for GCL4, which came with the highest off-the-roll moisture contents). As shown in Table 3, the average moisture content following drying was independent of the initial moisture content. Thus, in these experiments, the drying portion of the cycle is sufficient to negate the effects of initial moisture content, returning the specimens to the same moisture content for the second and subsequent cycles. While a higher initial moisture content might increase the shrinkage in the very first cycle (as is evident from Fig. 3) and, hence, the accumulated strain in the first few cycles, after a number of cycles, the effect is lost and at equilibrium there is no apparent effect. Indeed, the highest strain (8.2%) was not for the specimen with the highest initial water content, and the lowest final equilibrium strain (6.6–6.8%) was for specimens with the lowest and highest initial water contents (Table 3). However, the difference in the first few cycles could be of practical importance for GCLs only left exposed for a few wet/dry cycles. The strain after five cycles was 3.2–3.8% for the specimens with low initial water content and 6.1–6.2% for the specimens with higher initial water contents.

To put the noted strains in context, for typical 4.4–4.7 m wide GCL rolls, and assuming adjacent rolls shrink in a similar manner, a shrinkage of 3.2–3.4% would give panel separation for a 150 mm overlap and shrinkage of 6.4–6.8% would give panel separation for a 300 mm overlap. Thus, for a 150 mm panel overlap, separation of GCL4 could occur after only a couple of cycles if the GCL had developed a water content above 100% prior to the first drying cycles, or after as few as five cycles if the moisture content was in the range of 50–80%. This may be a contributing factor to the fact that GCL4, which starts with a higher initial water content, has shown panel separation after only a few months exposure on a flat (4%) slope in the field (Thiel et al. 2006).

Effect of Extra Added Water

Thiel et al. (2006) noted that reducing the amount of water added from the original 500 to 300 mL resulted in approximately 25% less

J. Geotech. Geoenviron. Eng. 2011.137:1019-1027.

Table 3. Effect of Initial Moisture Content on Final Shrinkage Magnitude

Sample	Dry mass per unit area (g/m^2)	Initial moisture content (%)	Target moisture content—first cycle (%)	Average moisture content after drying (%)	Final shrinkage (%)	Shrinkage after five cycles (%)
GCL4-UR-4	4,960	5	58	0.6	6.6	3.2
GCL4-UR-3	4,510	19	77	0.6	7.2	3.8
GCL4-UR-12	5,100	64	115	0.5	8.2	6.2
GCL4-UR-6	4,870	72	125	0.5	6.8	6.1

Note: For typical range of panel widths, shrinkage required for loss of 150 and 300 mm panel overlap would be 3.2–3.4% and 6.4–6.8%, respectively.

shrinkage for GCL2. To examine this issue further, a series of experiments was undertaken in which more water was added during the hydration process. For series III, 1,000 g was added instead of 500 g (series I); in series IV, the water content was raised to 100% of the dry mass compared to the usual 60% in series II (Table 4).

For GCL1 (Fig. 4), the extra water did not cause a change in the final magnitude of shrinkage. It did, however, increase the rate of shrinkage in the early cycles—the specimen hydrated with extra water reached its shrinkage equilibrium much faster than those hydrated with the standard 500 g.

There did not appear to be a change in either the rate or the magnitude of shrinkage for GCL2 (Fig. 5). This is the same product tested for the effect of water content by Thiel et al. (2006), and they concluded that less water resulted in less shrinkage. These two findings may both be valid [i.e., reducing the wet-cycle water content from about 60% to 35–40% (at or below the typical plastic limit) resulted in less shrinkage, but increasing it to about 100% did not increase shrinkage relative to that for 60%] because 300 mL of water may not have been sufficient to uniformly hydrate the entire specimen to 35–40%. The experience gained during testing has shown that it is more difficult to uniformly apply smaller amounts of water to a specimen. Bostwick (2009) showed that for identical amounts of hydration water, a specimen that had been wetted unevenly, leaving areas unhydrated, can experience less shrinkage than a specimen that has been wetted evenly.

For GCL4 (Fig. 6), the effect of additional moisture was examined for both unrestrained and restrained specimens. Bostwick (2009) showed that longitudinal restraint does not greatly affect final shrinkage (as is also confirmed in Fig. 6 with the UR specimens only giving slightly less final shrinkage than the R specimens). There appeared to be an increase in both the initial rate of shrinkage and the final equilibrium shrinkage with extra water, although there was considerable difference in final shrinkage among the specimens with 60% water added even though they were tested under nominally identical conditions. Thus, it is possible that the difference in equilibrium strain between the control specimens and the specimens with extra water added could be a result of specimen variability, although the increase in shrinkage from 60% to 100% water content for early cycles is significant. As was found when examining the effect of initial water content (Table 3 and Fig. 3), the initial rate of shrinkage for the specimens with extra water appears to be higher than for those wetted with the standard amount of water.

Application of the Student *t*-test to the data on the percentage of total shrinkage after five cycles shows that the addition of extra hydration water does increase the rate of shrinkage at the 0.025 significance level. This could be important in field applications in which the number of cycles is limited. The shrinkage after five cycles ranged from 4.8 to 9.1%, depending on the GCL and water added in these experiments. This would, theoretically, be sufficient to give panel separation for a 150 mm overlap in all cases and panel separation for a 300 mm overlap in about 40% of the cases examined (Table 4) after five wet-dry cycles. That said, care should be exercised in interpreting the results given in Table 4. Even when

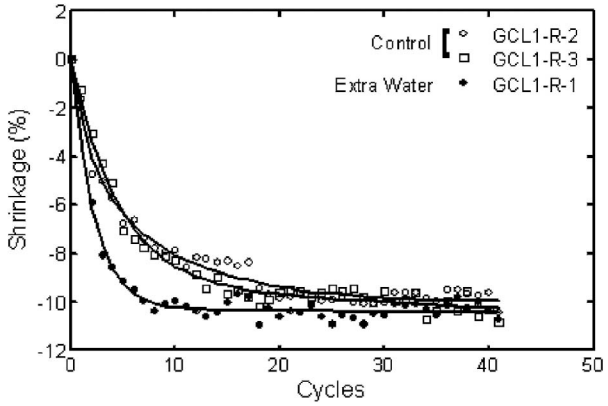

Fig. 4. Effect of additional hydration water on GCL shrinkage (GCL1)

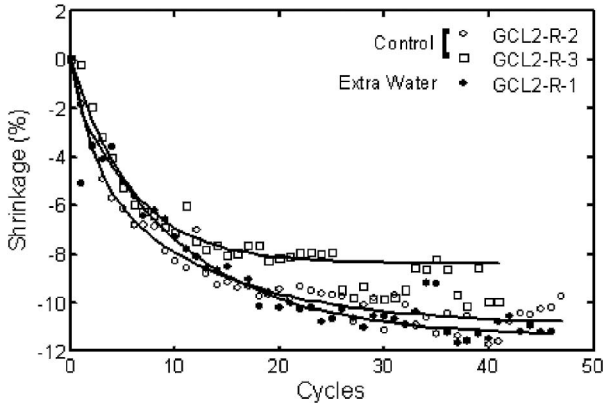

Fig. 5. Effect of additional hydration water on shrinkage of GCL2

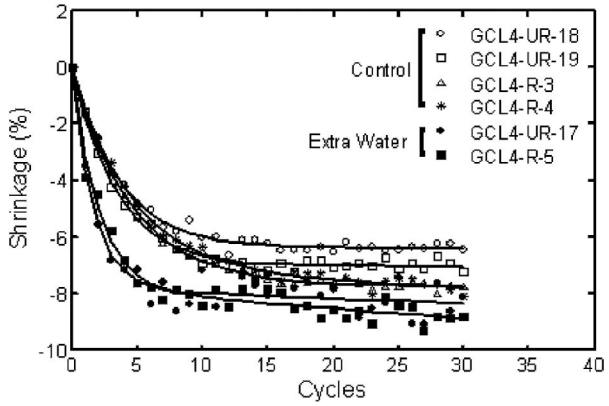

Fig. 6. Effect of additional hydration water on shrinkage of GCL4

J. Geotech. Geoenviron. Eng. 2011.137:1019-1027.

Table 4. Effect of Extra Hydration Water on GCL Shrinkage

Sample	Type of test—series	Dry mass per unit area (g/m^2)	Water added (% dry mass)	Final transverse shrinkage (%)	Transverse shrinkage after five cycles (%)	Percentage of final shrinkage after five cycles (%)
GCL1-R-2	Control—I	5,060	51	10.0	6.4	64
GCL1-R-3	Control—I	4,880	53	10.2	6.4	63
GCL1-R-1	Extra water—III	4,970	105	10.4	9.2	88
GCL2-R-2	Control—I	4,610	58	10.8	6.1	56
GCL2-R-3	Control—I	4,800	59	8.4	4.9	58
GCL2-R-1	Extra water—III	4,200	123	11.3	5.1	45
GCL4-UR-18	Control—II	4,570	60	6.4	4.8	75
GCL4-UR-19	Control—II	4,640	60	7.0	5.4	77
GCL4-R-3	Control—II	4,890	60	7.8	5.2	67
GCL4-R-4	Control—II	5,080	60	7.8	4.9	63
GCL4-UR-17	Extra water—IV	4,850	100	8.3	7.5	90
GCL4-R-5	Extra water—IV	4,910	100	8.9	7.3	82

they have consistent initial conditions in terms of moisture content, different GCLs will experience different suction cycles because of their different water-retention curves. Beddoe et al. (2010) provided a methodology for establishing the water-retention curve for GCLs, which was used by Beddoe (2009) and Beddoe et al. (2011) to examine the water-retention curves under both wetting and drying conditions for GCLs 1–4.

The findings of Beddoe et al. (2011) indicate that GCL2 had a substantially different gravimetric water-retention curve than the other three products. The water-retention curves of Beddoe et al. (2011) measured along a wetting path indicate that 60% gravimetric moisture content corresponds to a suction of 150–300 kPa, depending on the GCL product. The much higher target gravimetric moisture content of 100% corresponds to an equilibrium suction of approximately 5–60 kPa, again depending on the GCL product. Thus, as a result of the practical testing decision of applying consistent gravimetric moisture cycles for all samples in this study, GCL2 will be more fully hydrated during the swelling phase of each cycle, and therefore subjected to a larger suction cycle than the other GCLs at the same water content. Thus, in these tests, GCL2 is subject to the most severe conditions in which, as in the field with similar foundation conditions, GCL2 is likely to be at a lower water content than the other GCLs and, hence, is likely to experience less shrinkage in wet-dry cycles.

Effect of Bentonite Granularity and Type

The GCLs tested in this study contained bentonite with three different granularities (Fig. 1)—coarse granular (two products), fine granular (two products), and powdered (four products). The granular bentonite specimens all had Wyoming bentonite and were produced in North America. Of the four powdered bentonite specimens produced for the European market, only one was a Wyoming bentonite (denoted as type A), although the other bentonites (types B and C) were also sodium bentonite. These bentonite types were compared to see what effect, if any, this variable had on shrinkage. The comparisons were grouped by carrier geotextile type so that this variable did not influence the interpretation of the results. To simplify graphs, only the results for specimens showing the greatest and least shrinkage are plotted for granular products.

For the scrim-reinforced products (Fig. 7), the initial shrinkage over the first five cycles was very similar for all cases. However, after about five cycles, GCL6 (powdered bentonite type B, test series III) exhibited much greater shrinkage than GCL5 (test series III) and GCL2 (test series I). After about 10–15 cycles, GCL5 (powdered Wyoming bentonite) exhibited greater shrinkage than GCL2 (fine granular Wyoming bentonite). Nominally, GCL5 and GCL6 have the same cover and carrier geotextiles, differing only in the type of bentonite (although the average mass per unit area of the geotextile for GCL5 was greater than for GCL6).

For the GCLs with nonwoven/woven cover/carrier geotextiles (Fig. 8), GCL7 (powdered type C bentonite with extra bentonite impregnated in the complete cover layer, resulting in a higher geotextile weight; test series III) initially gave the lowest shrinkage. For GCL1 (test series I) and GCL3 (with the granular Wyoming bentonite, test series I), the shrinkage leveled off after about 25 cycles;

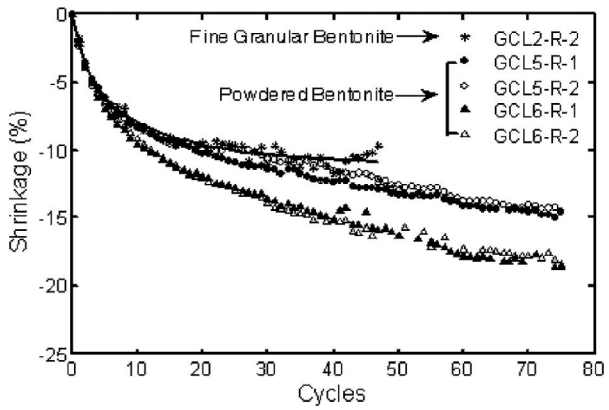

Fig. 7. Effect of bentonite particle size on shrinkage (nonwoven/nonwoven scrim-reinforced cover/carrier)

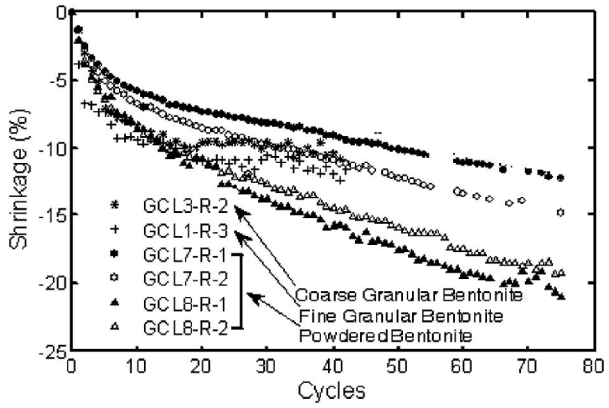

Fig. 8. Effect of bentonite particle size on shrinkage (nonwoven/woven cover/carrier)

J. Geotech. Geoenviron. Eng. 2011.137:1019-1027.

Table 5. Summary of Properties and Final Shrinkage for GCLs with Powdered Bentonite

Sample	Bentonite type	Carrier GT	Cover GT	Maximum transverse shrinkage (%)	Average (%)	Shrinkage after five cycles (%)
GCL5-R-1	A	NWSR	NW	14.8	14.8	6.2
GCL5-R-2				14.7		6.6
GCL6-R-1	B	NWSR	NW	18.8	18.5	7.0
GCL6-R-2				18.1		6.6
GCL7-R-1	C	W	NW with bentonite	12.3	13.6	4.4
GCL7-R-2				14.8		5.0
GCL8-R-1	B	W	NW	20.5	19.9	6.2
GCL8-R-2				19.3		6.5

however, for GCL7, shrinkage kept increasing. GCL8 (type B bentonite, test series III) initially exhibited shrinkage similar to GCL1 and GCL3, but after about 15 cycles, it continued to accumulate shrinkage strains at a significant rate, whereas for the other two GCLs, the shrinkage accumulation began to level off. Thus, after many cycles, the GCLs with powdered bentonite exhibited very different total shrinkage behavior than that observed with either the fine or coarse granular bentonite (Figs. 7 and 8). The GCLs with granular bentonite reached a relatively constant shrinkage by about 30 cycles, whereas the GCLs with the powdered bentonite had not reached a relatively constant shrinkage after 75 cycles. As a consequence, the GCLs with the powdered bentonite also experienced much higher shrinkage, up to 20% in some cases. Although powdered bentonite specimens tend to shrink more than granular bentonite specimens, there is still a large variability even among products with the same bentonite grain size (Table 5).

Although it is of scientific interest to observe the difference in the behavior between the different GCLs after many cycles, the relevance of this to actual field situations must be questioned unless the composite liner is left uncovered for very considerable periods of time. Because it will generally take considerable time for the GCL to rehydrate to 60% moisture content after drying, the first 5–10 cycles are likely most relevant to field situations for GCLs resting on typical foundation soils. At 10 cycles, the magnitude of the shrinkage for the powdered and granular bentonite products were similar.

GCLs 5 and 6 have very similar properties except for the type of bentonite. Bentonite type A (Wyoming bentonite) in GCL5 gave less shrinkage than bentonite type B in GCL6. GCL6 experienced less shrinkage than GCL8, which also contained bentonite type B (although it had a different carrier geotextile). GCL7 (bentonite type C) had additional bentonite impregnated into the cover layer. After the completion of 75 cycles, GCL8 exhibited the highest shrinkage of all the GCLs examined; however, there did not appear to be a great difference between GCLs 6 and 8, which had similar shrinkage curves and contained the same type of bentonite (type B).

Effect of GCL Type

Although all products contained a nonwoven cover geotextile, the carrier geotextile ranged from woven (W), nonwoven (NW), and nonwoven scrim reinforced (NWSR). A comparison between the otherwise similar GCL2 (NW/NWSR) and GCL1 (NW/W) is given in Fig. 9. To simplify the graphs, only the results for specimens showing the greatest and least shrinkage for each of the products are included; in addition, individual data points have been removed for clarity. In these specific tests, there is no statistically significant difference between the product with the nonwoven scrim-reinforced geotextile and the product with the woven geotextile (Bostwick 2009), on the basis of the results of a Student *t*-test. However, this does not necessarily mean that they will perform the same in the field, and this observation should be viewed with considerable caution as will be subsequently explained.

There does not appear to be a statistically significant difference (Bostwick 2009) between GCL3 (NW/W) and GCL4 (NW/NW), as may be appreciated from Fig. 10. This is consistent with instances of field shrinkage because both Thiel and Richardson (2005) and Koerner and Koerner (2005a, b) reported that both GCL3 and GCL4 had suffered loss of panel overlaps.

There is high variability between specimens from the same GCL roll (which was especially significant for GCL4), even when care is taken to only compare specimens tested under as near-identical conditions as practical. Also, the dry unit weights of the various geotextiles in each of the products differs, which may affect shrinkage.

In investigating possible solutions to the problem of GCL panel separation, Koerner and Koerner (2005a, b) recommended that if a

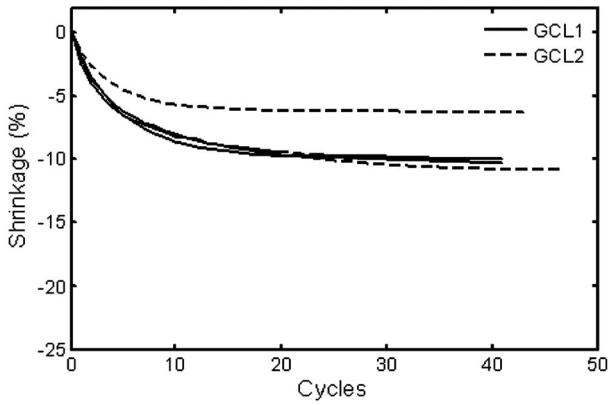

Fig. 9. Comparison of maximum and minimum shrinkage curves—fine granular bentonite

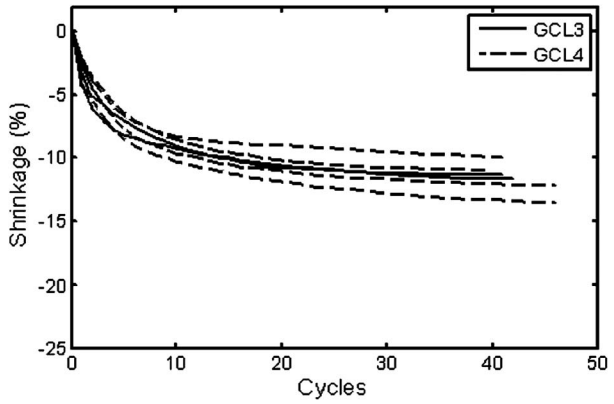

Fig. 10. Comparison of shrinkage curves—coarse granular bentonite

J. Geotech. Geoenviron. Eng. 2011.137:1019-1027.

Table 6. Effect of Scrim Reinforcement on GCL Shrinkage

Sample	Water added (% dry mass)	Transverse shrinkage (%)	Shrinkage after five cycles (%)	Sample	Water added (% dry mass)	Transverse shrinkage (%)	Shrinkage after five cycles (%)
GCL2-R-2	58	10.8	6.1	GCL4-R-1	45	13.5	8.4
GCL2-R-3	59	8.4	4.9	GCL4-R-2	49	12.1	7.6
GCL2-R-4	64	10.7	4.1	GCL4-UR-1	51	10.0	6.6
GCL2-R-5	60	10.0	5.1	GCL4-UR-2	55	11.0	6.4
GCL2-R-6	59	9.8	5.3				
GCL2-UR-1	60	9.1	3.7				
GCL2-UR-2	70	10.5	4.0				
GCL2-UR-3	52	6.2	4.5				
Average	60	9.4	4.7	Average	50	11.7	7.3
Standard deviation	5	1.5	0.8	Standard deviation	4	1.5	0.9

Note: Each sample had 500 g of water added to it; differences in water content as a percentage of dry mass is a result of the differences in sample dry mass.

NW/NW product is used, it should be accompanied by scrim reinforcement. In addition, laboratory shrinkage tests by Thiel et al. (2006) showed that a GCL with scrim reinforcement shrank less than a simple NW/NW product. The results of a comparison between GCL2 and GCL4 tested under nominally identical conditions are given in Table 6. Although there is a large range of shrinkage for both products, on average, GCL4 shrank more than GCL2 (the scrim-reinforced, thermally treated product). A one-tailed Student *t*-test confirmed that this result is statistically significant (Bostwick 2009). However, the maximum shrinkages of 10.8% (GCL2) and 13.5% (GCL4) are less than those found by Thiel et al. (2006) of 12.8% (GCL2) and 23.0% (GCL4) for tests that were nominally identical. The difference for GCL2 is modest (10.8% versus 12.8%), but for GCL4 it is large (12.8% versus 23%), suggesting that there is much greater variability from roll to roll for GCL4 than for GCL2.

Both GCL1 and GCL3 had a woven carrier geotextile, with the major differences being the bentonite granularity (GCL1 with fine granules, GCL3 with coarse granules) and the heat treatment of GCL1. On the basis of the data, GCL3 did shrink more than GCL1 at a statistically significant level (Bostwick 2009), indicating that either the bentonite granularity or the heat treatment may play a factor in GCL shrinkage.

Conclusions

Shrinkage of eight different GCLs subjected to wetting and drying cycles was examined. On the basis of specific experiments conducted and GCLs tested, the following conclusions were reached:

1. Higher initial moisture content results in higher initial shrinkage and accumulated shrinkage during the first five cycles. The effect of the initial moisture content diminished with number of cycles and did not notably affect the magnitude of the final equilibrium shrinkage after many cycles.
2. For GCLs with granular bentonite and wetted to a moisture content of about 60% (or greater) in the hydration phase, the actual moisture content did not appear to affect the magnitude of the final equilibrium shrinkage (i.e., after many cycles). However, it did affect the rate of shrinkage. Specimens brought to about 100% moisture content in each cycle reached a constant shrinkage value much faster than those brought to about 60% in each wetting cycle.
3. The difference in the accumulation of shrinkage strain in the first five cycles because of higher initial water content (conclusion 1 above) or higher hydrated water content (conclusion 2 above) could have important implications in the field where the number of cycles is limited. The former will depend on the moisture content of the as-delivered GCL (with it being much higher for some GCL products than for other GCLs). For the same thermal exposure conditions, the latter will depend on the initial moisture content of the underlying foundation layer, the water-retention curve of the foundation layer, and the water-retention curve of the GCL, which may vary from product to product (Beddoe et al. 2011).
4. For GCLs with Wyoming bentonite, the bentonite particle size affected the magnitude of the shrinkage, with the GCLs containing fine granular bentonite shrinking the least and those with powdered bentonite the most. All the powdered bentonite specimens continued to show a slow accumulation of strain with increasing cycles up to at least 75 cycles, although the strains in the most critical early stages were similar to those with granular bentonite. Thus, over the range examined, the bentonite grain size will not significantly affect the GCL performance with respect to panel separation unless the GCL is subjected to a very large number of wet-dry cycles.
5. The shrinkage of a needle-punched GCL with a thermally treated scrim-reinforced nonwoven carrier geotextile and granular bentonite was less than that for a needle-punched GCL with a simple nonwoven carrier and granular bentonite.
6. For some products, there was considerable variability in GCL shrinkage for specimens from the same roll and tested under nominally identical conditions, whereas for other products, the variability was relatively small. For example, a comparison of results from this study with those reported by Thiel et al. (2006) for nominally identical experimental conditions and products showed that while the difference for one product was modest (10.8% versus 12.8%), for another it was large (12.8% versus 23%).
7. The shrinkage strain required to cause the loss of 150–300 mm panel overlap could be mobilized in about five wet-dry cycles in the experiments reported.

The results from the experiments reported in this paper should not be viewed as expected values of shrinkage strains under field conditions, but rather as an indication of the effect of certain variables and the maximum amount of shrinkage that might be expected under extreme exposure conditions. For the GCL to shrink, it must first uptake moisture, lose it, and then uptake it again. In these laboratory tests, this was achieved by wetting from a spray water bottle. However, in the field, GCL moisture uptake will be from (1) the soil and (2) possible condensation of water evaporated from the GCL. The uptake of moisture will depend on the water-retention curve and the water content of the foundation soil at the time the GCL is placed and the water-retention curve for the GCL.

J. Geotech. Geoenviron. Eng. 2011.137:1019-1027.

Beddoe et al. (2011) showed that in terms of moisture uptake, there is a significant difference between the water-retention curves of different products. The effect of this is not reflected in the current study in which all GCLs were brought to a similar nominal water content or had a similar amount of moisture added in the same time period. Because the rate of cyclic accumulation of shrinkage strains was observed to be a function of the moisture content cycle imposed on a GCL sample, it is therefore likely that the magnitude of shrinkage achieved in the field will be a function of (1) the water-retention characteristics of the GCL and subsoil and (2) the magnitude, duration, and number of moisture cycles. When these factors are considered, there may be greater differences between the shrinkage observed for different products than is evident from this study. In addition, although the temperature of the ovens was chosen to correspond to temperatures measured in the field beneath a geomembrane, the testing process could not exactly replicate the water-vapor pressure experienced by field-installed GCLs.

Acknowledgments

The study reported herein was financially supported by the Natural Sciences and Engineering Research Council of Canada (NSERC), the Ontario Centres of Excellence, and Terrafix Geosynthetics Inc. The writers are grateful to their industrial partners, Terrafix Geosynthetics Inc, Solmax International, Ontario Ministry of Environment, AECOM (Gartner Lee Ltd.), AMEC Earth and Environmental, Golder Associates Ltd., and CTT Group, for their input during the study. The funding for the equipment used was provided by the Canada Foundation for Innovation, the Ontario Innovation Trust and NSERC. The writers also gratefully acknowledge Khaled Abdelatty for providing CEC values, Mohammed Hosney for providing swell index values, and NAUE GmbH for providing the mineralogical analyses of the bentonite from the GCLs tested. Grain size analysis of the powdered bentonite was performed by Dr. D.N. Singh, IIT Bombay. The value of discussions with Dr. R.W.I. Brachman and Messers K. von Maubeuge, B. Herlin, B. Kennedy, and R. Thiel is gratefully acknowledged.

References

Beddoe, R. (2009). "Establishing the water retention behaviour of geosynthetic clay liners." M.Sc. thesis, Queen's Univ., Kingston, ON, Canada.

Beddoe, R. A., Take, W. A., and Rowe, R. K. (2010). "Development of suction measurement techniques to quantify the water retention behaviour of GCLs." *Geosynth. Int.*, 17(5), 301–312.

Beddoe, R. A., Take, W. A., and Rowe, R. K. (2011). "Water retention behaviour of geosynthetic clay liners." *J. Geotech. Geoenviron. Eng.*, 10.1061/(ASCE)GT.1943-5606.0000526 (Mar. 2, 2011).

Benson, C. H., Jo, H. Y., and Abichou, T. (2004). "Forensic analysis of excessive leakage from lagoons lined with a composite GCL." *Geosynth. Int.*, 11(3), 242–252.

Benson, C. H., Kucukkirca, I. E., and Scalia, J. (2010a). "Properties of geosynthetics exhumed from a final cover at a solid waste landfill." *Geotext. Geomembr.*, 28(6), 536–546.

Benson, C. H., Ören, A. H., and Gates, W. P. (2010b). "Hydraulic conductivity of two geosynthetic clay liners permeated with a hyperalkaline solution." *Geotext. Geomembr.*, 28(2), 206–218.

Bostwick, L. E. (2009). "Laboratory study of geosynthetic clay liner shrinkage when subjected to wet/dry cycles." M.Sc. thesis, Queen's Univ., Kingston, ON, Canada.

Bostwick, L. E., Rowe, R. K., Take, W. A., and Brachman, R. W. I. (2007). "The effect of sample size on shrinkage of a non scrim reinforced geosynthetic clay liner." *60th Canadian Geotechnical Conf.*, Canadian Geotechnical Society, Richmond, BC, Canada, 2123–2128.

Bostwick, L. E., Rowe, R. K., Take, W. A., and Brachman, R. W. I. (2008). "Observations of the dimensional stability of four GCL products under combined thermal and moisture cycles." *Geoamericas 2008*, Industrial Fabrics Association Int. (IFAI), Roseville, MN, 435–443.

Bostwick, L. E., Rowe, R. K., Take, W. A., and Brachman, R. W. I. (2010). "Anisotropy and directional shrinkage of geosynthetic clay liners." *Geosynth. Int.*, 17(3), 157–170.

Cooley, B. H., and Daniel, D. E. (1995). "Seam performance of overlapped geosynthetic clay liners." *Geosynthetics '95*, Industrial Fabrics Association Int. (IFAI), Roseville, MN, 691–705.

Daniel, D. E., Shan, H. Y., and Anderson, J. D. (1993). "Effects of partial wetting on the performance of the bentonite component of a geosynthetic clay liner." *Geosynthetics '93*, Vancouver, BC, Canada, 1483–1496.

Dickinson, S., and Brachman, R. W. I. (2010). "Permeability and internal erosion of a GCL beneath coarse gravel." *Geosynth. Int.*, 17(3), 112–123.

Gassner, F. (2009). "Field observation of GCL shrinkage at a site in Melbourne, Australia." *Geotext. Geomembr.*, 27(5), 406–408.

Gates, W. P., and Bouazza, A. (2010). "Bentonite transformations in strongly alkaline solutions." *Geotext. Geomembr.*, 28(2), 219–225.

Hornsey, W. P., Scheirs, J., Gates, W. P., and Bouazza, A. (2010). "The impact of mining solutions/liquors on geosynthetics." *Geotext. Geomembr.*, 28(2), 191–198.

Katsumi, T., Ishimori, H., Onikata, M., and Fukagawa, R. (2008). "Long-term barrier performance of modified bentonite materials against sodium and calcium permeant solutions." *Geotext. Geomembr.*, 26(1), 14–30.

Koerner, R. M., and Koerner, G. R. (2005a). "In-situ separation of GCL panels beneath exposed geomembranes." *GRI White Paper #5*, Geosynthetic Institute, Folsom, PA.

Koerner, R. M., and Koerner, G. R. (2005b). "In-situ separation of GCL panels beneath exposed geomembranes." *Geotech. Fabr. Rep.*, 23(5), 34–39.

Lange, K., Rowe, R. K., and Jamieson, H. (2010). "The potential role of geosynthetic clay liners in mine water treatment systems." *Geotext. Geomembr.*, 28(2), 199–205.

Mackey, R. (1997). "Geosynthetic clay liners, part five: Design, permitting and installation concerns." *Geotech. Fabr. Rep.*, 15(1), 34–38.

Pelte, T., Pierson, P., and Gourc, J. P. (1994). "Thermal analysis of geomembranes exposed to solar radiation." *Geosynth. Int.*, 1(1), 21–44.

Rosin-Paumier, S., et al. (2010). "Swell index, oedopermeametric, filter press and rheometric tests for identifying the qualification of bentonites used in GCLs." *Geosynth. Int.*, 17(1), 1–11.

Rowe, R. K. (2005). "Long-term performance of contaminant barrier systems." *Geotechnique*, 55(9), 631–678.

Rowe, R. K., Bostwick, L. E., and Thiel, R. (2010). "Shrinkage characteristics of heat-tacked GCL seams." *Geotext. Geomembr.*, 28(4), 352–359.

Rowe, R. K., Quigley, R. M., Brachman, R. W. I., and Booker, J. R. (2004). *Barrier systems for waste disposal facilities*, Taylor & Francis Books, London, 587.

Saidi, F., Touze-Foltz, N., and Goblet, P. (2008). "Numerical modelling of advective flow through composite liners in case of two interacting adjacent square defects in the geomembrane." *Geotext. Geomembr.*, 26(2), 196–204.

Shackelford, C. D., Sevick, G. W., and Eykhol, G. R. (2010). "Hydraulic conductivity of geosynthetic clay liners to tailings impoundment solutions." *Geotext. Geomembr.*, 28(2), 149–162.

Thiel, R., Giroud, J. P., Erickson, R., Criley, K., and Bryk, J. (2006). "Laboratory measurements of GCL shrinkage under cyclic changes in temperature and hydration conditions." *Eighth International Conf. on Geosynthetics*, Vol. 1, Ios Press, Fairfax, VA, 21–44.

Thiel, R., and Richardson, G. (2005). "Concern for GCL shrinkage when installed on slopes." *JGRI-18 at GeoFrontiers*, GII Publications, Folsom, PA, 2.31.

White, D. J., Take, W. A., and Bolton, M. D. (2003). "Soil deformation measurement using particle image velocimetry (PIV) and photogrammetry." *Geotechnique*, 53(7), 619–631.

J. Geotech. Geoenviron. Eng. 2011.137:1019-1027.

Hydraulic Conductivity of Geosynthetic Clay Liners Exhumed from Landfill Final Covers with Composite Barriers

Joseph Scalia IV, S.M.ASCE[1]; and Craig H. Benson, F.ASCE[2]

Abstract: Geosynthetic clay liners (GCLs) were exhumed from composite barriers, (i.e., geomembrane over GCL) in final covers at four sites after 4.7 to 6.7 years to evaluate the in-service condition. Monovalent bound cations were replaced by divalent cations in all GCLs, with near complete exchange at two-thirds of the sampling locations. Hydraulic conductivity was measured using two dilute solutions commonly used as permeant water: standard water (SW, $0.01M$ $CaCl_2$ solution) and type II deionized water (DW). Hydraulic conductivities to SW varied over four orders of magnitude, whereas identical specimens (i.e., from same sample) had hydraulic conductivities to DW consistently $\leq 3\times10^{-10}$ m/s. Higher hydraulic conductivities and sensitivity to permeant water did not correspond directly to the amount of cation exchange. Exhumed GCLs with higher gravimetric higher water contents (>50%) exhibited a gel structure indicative of osmotic hydration and had lower hydraulic conductivities to both SW and DW, regardless of the amount of sodium (Na) replaced by divalent cations. These GCLs with higher water contents were placed on subgrade having water content in excess of optimum water content (standard Proctor). Conditions that promote rapid hydration and osmotic swell in a GCL are recommended to ensure that a GCL in a composite barrier maintains low hydraulic conductivity ($\leq 5\times10^{-11}$ m/s), even if the native Na is ultimately replaced by divalent cations. Subgrade with water content ≥ optimum water content is recommended.

DOI: 10.1061/(ASCE)GT.1943-5606.0000407

CE Database subject headings: Geosynthetics; Clay liners; Landfills; Hydraulic conductivity; Barriers; Composite materials; Water content.

Author keywords: Geosynthetic clay liner; Landfill; Final cover; Hydraulic conductivity; Cation exchange; Hydration; Osmotic swell; Crystalline swell; Preferential flow.

Introduction

Geosynthetic clay liners (GCLs) are factory-manufactured hydraulic barriers containing sodium (Na) bentonite that are used in waste containment systems to control the migration of liquids and gases. In a final cover, a new GCL typically has a saturated hydraulic conductivity of approximately 10^{-11} m/s (Shan and Daniel 1991; Shackelford et al. 2000; Jo et al. 2001, 2005; Kolstad et al. 2004). Recent studies on GCLs exhumed from final covers have shown, however, that the low hydraulic conductivity of GCLs is not necessarily maintained throughout the service life of a final cover. For example, hydraulic conductivities in the range of 10^{-7} to 10^{-6} m/s have been reported for GCLs exhumed from final covers after 2.0–11.0 years of service (Melchior 2002; Benson et al. 2007; Meer and Benson 2007).

The high hydraulic conductivities observed in exhumed GCLs have been attributed to loss of swelling capacity of the bentonite coupled with formation of cracks and other macroscopic features during dehydration. During rewetting, swelling of the bentonite is insufficient to seal off these features, which results in high hydraulic conductivity. The loss of swelling capacity is caused by replacement of Na bound to the clay surface by calcium (Ca) and magnesium (Mg), which prevents osmotic swelling in the interlayer of montmorillonite (the primary clay mineral in bentonite). Water entering the GCL from overlying cover soils has been suggested as the primary source of the Ca^{2+} and Mg^{2+} (Melchior 2002; Benson et al. 2007; Meer and Benson 2007; Benson and Meer 2009).

Lin and Benson (2000) hypothesized that GCLs deployed in composite barrier layers, (i.e., GCL overlain by a geomembrane, GM) are unlikely to experience cation exchange and wet-dry cycling, and thus will retain low hydraulic conductivity. However, this hypothesis has remained largely unverified because field data regarding the condition of GCLs in composite barriers are scant and conflicting. Melchior (2002) exhumed a GCL comprised of granular bentonite laminated with a high-density polyethylene (HDPE) geofilm from a final cover test section in Germany 5 years after construction (the GM was oriented upward). The mole fraction of bound Na^+ decreased from 0.65 to 0.55 while the GCL was in service, whereas near complete replacement of Na^+ (2 to 4% Na^+ remaining on the exchange complex) was observed in adjacent GCLs without geofilm or an overlying GM. In contrast, Meer and Benson (2007) exhumed GCL samples from a composite barrier layer (GCL overlain by 1.5 mm textured HDPE GM) in a final cover in Wisconsin that had been in service for 4.1 years. Hydraulic conductivity of the GCL ranged from 5.1×10^{-7} to 1.3×10^{-6} m/s when permeating with $0.01M$ $CaCl_2$, more than four orders-of-magnitude higher than the hydraulic conductivity

[1]Graduate Research Assistant, Geological Engineering, Univ. of Wisconsin, Madison, WI 53706 (corresponding author). E-mail: scalia@wisc.edu

[2]Wisconsin Distinguished Professor and Chair, Geological Engineering, Univ. of Wisconsin, Madison, WI 53706. E-mail: chbenson@wisc.edu

Note. This manuscript was submitted on July 22, 2009; approved on June 9, 2010; published online on June 29, 2010. Discussion period open until June 1, 2011; separate discussions must be submitted for individual papers. This paper is part of the ***Journal of Geotechnical and Geoenvironmental Engineering***, Vol. 137, No. 1, January 1, 2011. ©ASCE, ISSN 1090-0241/2011/1-1–13/$25.00.

of a new GCL. Ca^{2+} and Mg^{2+} replaced at least 55% of the Na^{+} originally in the GCL and the swell index (SI) of the bentonite was comparable to Ca-bentonite. Meer and Benson (2007) hypothesized that the cation exchange was due to upward diffusion of divalent cations from the subgrade.

Despite these conflicting reports regarding the in situ GCL condition, composite barriers containing GCLs have performed well as hydraulic barriers in a broad variety of climates. For example, Benson et al. (2007) reported average annual percolation rates between 2.6 and 4.1 mm/year over a 6-year period for a cover containing a GCL laminated with geofilm in a humid continental climate. Similarly, Albright et al. (2004) reported percolation rates ranging from 0 to <0.1 mm/year for two final covers constructed with composite barriers containing a GCL overlain by a HDPE GM that had service lives between 4 and 5 years in arid and semiarid climates (the study described herein includes the GCLs from Albright et al. 2004, and they are shown to be altered). Nevertheless, despite the good performance record, understanding these alterations may be important when making inferences regarding long-term performance.

In this study, GCLs in composite barriers were exhumed from four sites after being in service for 4.7 to 6.7 years. At two of the sites, GCLs were exhumed from test sections simulating covers with composite barriers that were constructed as part of the U.S. EPA Alternative Cover Assessment Program (ACAP) (Albright et al. 2004). GCLs were also exhumed from actual final covers at two municipal solid waste (MSW) landfills that employed composite barrier layers. All GCL samples were tested for saturated hydraulic conductivity, water content, SI, and bound and soluble cations. GCLs were permeated with a $0.01M$ $CaCl_2$ solution, which is recommended in ASTM D5084-03 for regions with hard tap water (e.g., Madison, Wisconsin, United States) and is commonly referred to as standard water (SW). Some GCLs were also permeated with DW, including GCLs where high hydraulic conductivity was obtained with SW. Water content and soluble cations in the subgrade were also determined for interpretive purposes.

Background

GCLs containing Na-bentonite typically have hydraulic conductivities ranging from 6×10^{-12} to 2×10^{-11} m/s when permeated with dilute aqueous solutions using conventional test methods and under stresses characteristic of final covers (Petrov and Rowe 1997; Shackelford et al. 2000; Jo et al. 2001; Kolstad et al. 2004; Meer and Benson 2007). Na-bentonite in GCLs has low hydraulic conductivity because much of the water in the bentonite is bound to the clay mineral surface and unavailable for flow (Mesri and Olson 1971; Mitchell 1993; Shang et al. 1994). The association of water molecules with the clay surface during hydration is manifested as swelling, which seals off macroscopic flow paths that can control hydraulic conductivity. Thus, hydraulic conductivity of a GCL and bentonite swell is often related (Shackelford et al. 2000; Jo et al. 2001; Kolstad et al. 2004; Benson and Meer 2009).

Swelling of bentonite occurs in two distinct phases: the crystalline phase and the osmotic phase (Norrish and Quirk 1954). Crystalline swelling occurs first as water molecules move into the interlayer space hydrating the mineral surface and associated cations. Crystalline swelling causes the interlayer to separate by a distance corresponding to several water molecules (McBride 1994). Completion of crystalline swelling corresponds to a gravimetric water content in bentonite of approximately 35% (Mooney et al. 1952; Norrish and Quirk 1954; Martin 1960; Guyonnet et al. 2005). Osmotic swelling follows crystalline swelling as water molecules flow into the interlayer region in response to the concentration gradient between the interlayer region and the free pore water.

Osmotic swelling can produce far greater swell than crystalline swelling alone (McBride 1994), and is responsible for the high swelling capacity and low hydraulic conductivity of Na-bentonite in DW. The magnitude of osmotic swell is a function of the ionic strength of the pore water, with greater swell occurring when the pore water is more dilute (Norrish and Quirk 1954; McBride 1994; Kolstad et al. 2004; Jo et al. 2005). Bentonites that have undergone osmotic swell generally have water contents exceeding 35%, and in many cases have water contents in excess of 100%. Osmotic swelling only occurs, however, when cations occupying the interlayer space during hydration are predominantly monovalent. When divalent cations are predominant, only crystalline swelling occurs during hydration (Norrish and Quirk 1954; McBride 1994; Guyonnet et al. 2005).

Chemical interactions that affect swelling concurrently affect hydraulic conductivity. Interactions that prevent osmotic swell (e.g., replacement of monovalent cations by divalent cations prior to osmotic swell) result in high hydraulic conductivity, whereas interactions that promote osmotic swell (e.g., permeation by dilute pore water with monovalent cations) result in low hydraulic conductivity (Jo et al. 2001; Kolstad et al. 2004). Bentonites that have already undergone osmotic swelling can retain relatively low hydraulic conductivity under stresses typical of covers (10–30 kPa), even if the Na^{+} is subsequently replaced by divalent cations, provided that the bentonite is not desiccated. For example, Egloffstein (2001, 2002) permeated Na-bentonite GCLs with a $0.3M$ $CaCl_2$ solution after 20 days of permeation with DW (which promoted osmotic swelling). After 3 years, at which time complete exchange of Na^{+} for Ca^{2+} was assumed, the hydraulic conductivity of the GCL was only 3×10^{-10} m/s. Similarly, Jo et al. (2005) showed that permeation of Na-bentonite GCLs with dilute $CaCl_2$ solutions (<40 mM) that are known to induce osmotic swelling resulted in hydraulic conductivity less than 6×10^{-10} m/s even though more than 94 pore volumes of flow passed through the bentonite and all of the Na^{+} was replaced by Ca^{2+}. Lee et al. (2005) show that replacement of Na^{+} by Ca^{2+} in GCLs initially prehydrated with DW (promoting osmotic swell) and then permeated with dilute $CaCl_2$ solutions results in hydraulic conductivities no greater than 3.5×10^{-10} m/s. Similar results have been reported by Gleason et al. (1997) and Shackelford et al. (2000) for Na-bentonites permeated with dilute solutions of divalent cations mimicking soil eluents.

GCLs manufactured with Na-bentonite that have undergone osmotic swelling can retain low hydraulic conductivity even with a preponderance of bound divalent cations because water molecules associated with osmotic swelling are strongly associated with the clay surface (Jo et al. 2005). Osmotic pressures associated with concentration differences in the interlayer and the bulk pore water during exchange have insufficient energy to remove these tightly bound water molecules (Jo et al. 2005; Benson and Meer 2009). However, if these water molecules are extracted by a source with greater energy, much higher hydraulic conductivities may be realized because montmorillonites containing primarily divalent cations do not undergo osmotic swelling when rehydrated (Meer and Benson 2007). This is the reason why a GCL that has undergone replacement of Na^{+} by divalent cations coupled with desiccation can be many orders of magnitude more permeable, (e.g., 10^{-7} m/s) than a new GCL (Melchior 2002; Lin

J. Geotech. Geoenviron. Eng. 2011.137:1-13.

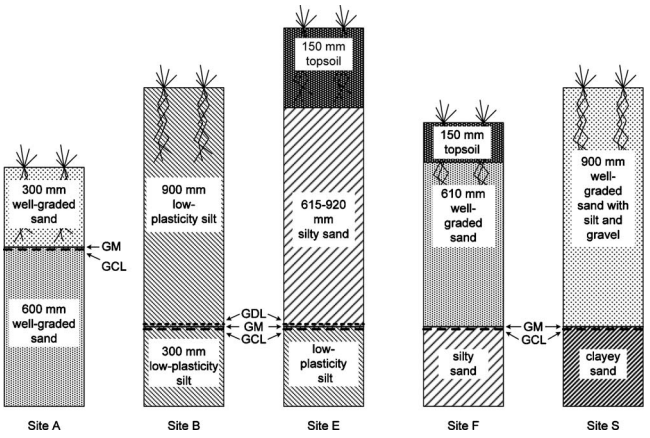

Fig. 1. Profiles of final covers at landfills where GCLs were exhumed. GM=geomembrane, GCL=geosynthetic clay liner, and GDL=geosynthetic drainage layer. Site S originally described in Meer and Benson (2007).

and Benson 2000, Egloffstein 2001; Benson et al. 2007; Benson and Meer 2009). Similarly, rapid exchange relative to the rate of hydration induced by permeation with a concentrated solution of divalent cations (effectively producing Ca-bentonite prior to full osmotic hydration) yields hydraulic conductivities on the order of 10^{-7} m/s (Jo et al. 2005).

Replacement of Na^+ by Ca^{2+} and Mg^{2+} while GCLs are in service is well documented. Downward percolation of pore water containing Ca^{2+} and Mg^{2+} from overlying cover soils is generally cited as the source of divalent cations for exchange (Egloffstein 2001; Melchior 2002; Meer and Benson 2007; Benson et al. 2007). However, Meer and Benson (2007) showed extensive replacement of Na^+ by Ca^{2+} and Mg^{2+} in a GCL exhumed from a composite barrier layer, and attributed the exchange to diffusion of divalent cations into the GCL from the subgrade. Bradshaw (2008) has also shown that divalent cations migrate into GCLs covered by a GM during and after the initial hydration on a subgrade. However, the extent of exchange that commonly occurs in the field in GCLs covered with a GM has not been well documented.

Exhumation of GCLS and Subgrades

GCLs were exhumed from final covers at four sites where they had been used in a composite barrier layer. Two of the sites (A and B) were located in semiarid to arid regions in states on the west coast of the United States; the other two (E and F) were located in the humid continental climate of the midwestern United States (based on climate definitions in McKnight and Hess 2007). At Sites E and F, samples were exhumed from two adjacent areas that had been constructed at different times. These areas are identified as Site E-01 (Site E, 2001 installation), Site E-02 (Site E, 2002 installation), Site F-03 (Site F, 2003 installation), and Site F-05 (Site F, 2005 installation). All of the GCLs were originally comprised of natural Na-bentonite in granules sandwiched between two geotextiles bonded by needle punching. The cover profile at each landfill is shown in Fig. 1 and the geographic location, service life, and cover thickness are summarized in Table 1. Site S in Fig. 1 and Table 1 is from Meer and Benson (2007). Performance data for Sites A and B are described in Albright et al. (2004).

All GCLs were sampled in accordance with ASTM D6072-08, with a minimum of six square samples (0.3×0.3 m) collected at each site. Soils overlaying the composite barrier layer were removed from an area approximately 4×4 m using a tracked excavator until the excavation was within approximately 0.15 m of the uppermost geosynthetic layer. The remaining soil was then removed by hand. Rectangular sections (2×2 m) of geocomposite drainage layer (if present) and GM were removed from the floor of each test pit by cutting the perimeter with a sharp utility knife. No visible defects were observed in any of the overlying GMs. Thus, all of the GCLs were isolated hydraulically from the overlying cover soils.

The perimeter of each GCL sample was cut with a sharp utility knife while the GCL remained on the subgrade [Fig. 2(a)]. GCL surrounding the sampling area was pulled back, and a rigid PVC plate (0.3×0.3 m) was slid under the sample [Fig. 2(b)]. The GCL sample was then wrapped with plastic sheeting to prevent loss of moisture, placed in a plastic tub, and covered with at least 0.1 m of loose soil for protection during transport and storage. A bulk sample of the subgrade immediately beneath the GCL sample (<20-mm depth) was also collected for determination of water content, particle-size distribution, and chemical analysis of the pore water.

No recommendation is made in ASTM D6072-08 as to how a plated GCL sample should be transported post exhumation, but prior to permeation. One concern is the impact of stress relief prior to testing. To assess this issue, two alternate stress states were tested using split samples from Sites B and E. One state consisted of burying plated GCLs beneath at least 0.5 m of soil in a large plastic tub (henceforth referred to as "with overburden pressure"). The other method consisted of storing the GCLs in a shallow plastic tub beneath a thin (<0.15-m depth) soil layer (henceforth referred to as "without overburden pressure"). Duplicate samples collected adjacently were used for this evaluation.

Hydraulic conductivity tests were conducted on the duplicate samples using methods described subsequently. A comparison of hydraulic conductivities obtained for both stress states is shown in

Table 1. Description of Covers at Field Sites

	Site						
	West Coast		Midwest				Wisconsin
Property location	A	B	E		F		S[a]
Installation date	May 2002	November 2000	August 2001	September 2002	August 2003	July 2005	September 1998
Sampling date	March 2007	August 2007	June 2007	June 2007	August 2008	August 2008	October 2002
Service life (year)	4.9	6.7	5.8	4.7	4.9	3.1	4.1
Surface layer thickness (mm)	300	900	915–1,145	915–1,220	760		900

[a]Meer and Benson (2007).

J. Geotech. Geoenviron. Eng. 2011.137:1-13.

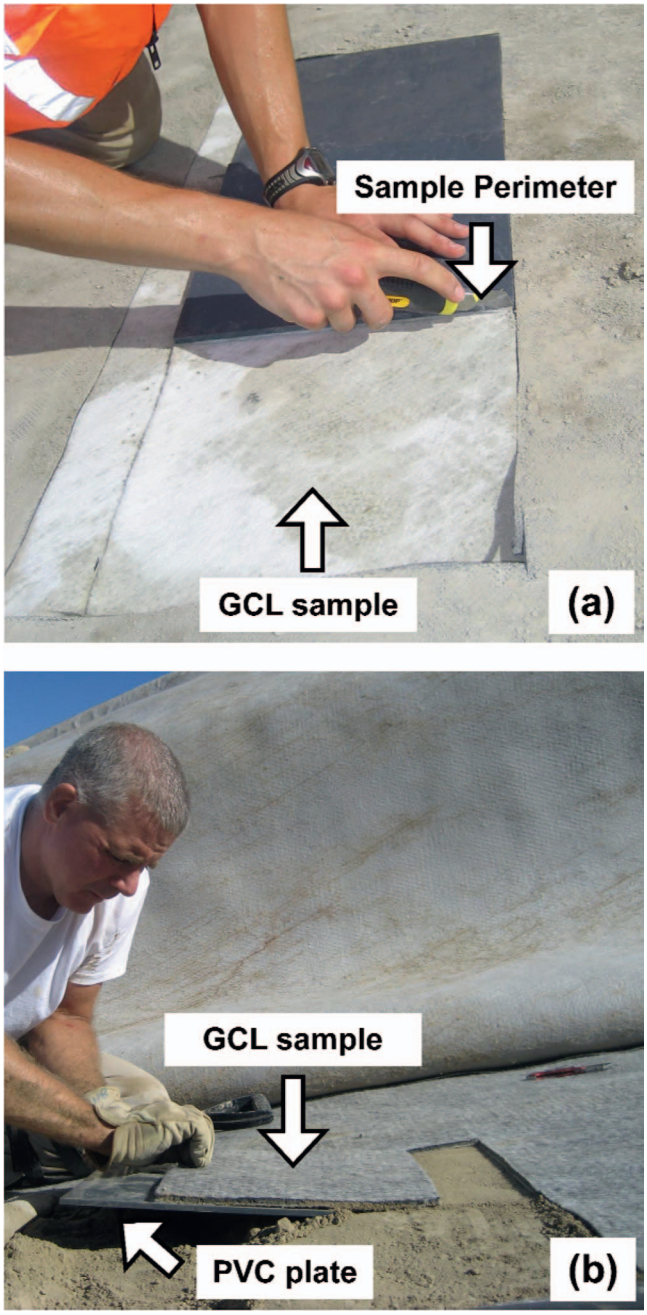

Fig. 2. (Color) Exhumation of GCL samples: (a) cutting around perimeter with razor knife; (b) delicately sliding sample onto rigid plastic plate

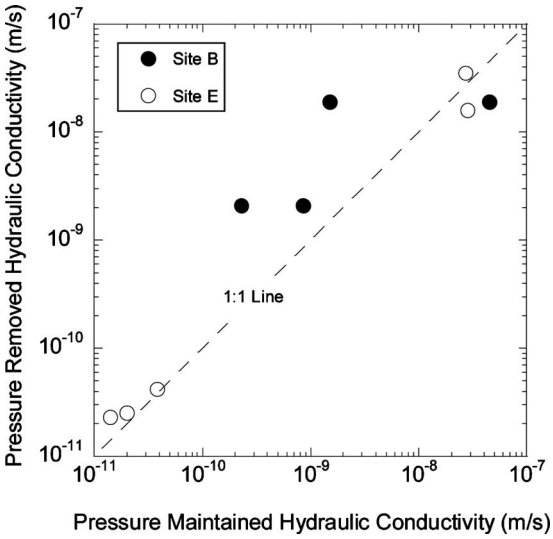

Fig. 3. Hydraulic conductivity of exhumed GCLs with and without overburden pressure prior to permeation

Fig. 3. No bias is evident in the hydraulic conductivities, although three of the four specimens from Site B had higher hydraulic conductivity when transported without overburden pressure applied. A *t*-test was performed on the data at a 5% significance level to confirm that the two sets of hydraulic conductivities were statistically similar. The data were transformed logarithmically prior to testing so that the assumption of normality in the *t*-test would be satisfied. A *p*-statistic of 0.17 was calculated, indicating that there was no statistically significant difference between the hydraulic conductivities of both data sets at the 5% level (0.17 $>$0.05). Overall, hydraulic conductivities from GCLs with overburden pressure were slightly higher (1.1 times, on average) than comparable hydraulic conductivities from GCLs without overburden pressure. However, this difference in hydraulic conductivities is small relative to the overall variation in hydraulic conductivity (three orders of magnitude).

Test Methods

Hydraulic Conductivity

Hydraulic conductivity tests were conducted on GCL specimens in flexible-wall permeameters following the procedures in ASTM D5084-03 and ASTM D6766-06. The hydraulic conductivities are summarized in Table 2. The falling headwater-constant tailwater method was employed. Backpressure was not applied to represent the field condition. The average effective stress was selected to represent the in situ condition, and ranged between 15 and 24 kPa depending on the cover thickness. An average hydraulic gradient of 125 was applied to all specimens. This hydraulic gradient is higher than in the field, but is typical for GCL testing. In addition, Shackelford et al. (2000) showed that hydraulic gradient has negligible impact on the hydraulic conductivity of GCLs when the hydraulic gradient is less than 500.

Specimens having a diameter of 152 mm were cut from the GCL field samples using a razor knife. The GCL sample was retained on the rigid plastic sampling plate during cutting to avoid disturbing any structure within the bentonite. After cutting, geotextile fibers around the perimeter were trimmed back with scissors. Thickness of the GCL specimen was then measured with calipers at six equidistant points around the GCL perimeter and the mass of the specimen was recorded. A frosting of bentonite paste, composed of new Na-bentonite hydrated in the permeant water, was applied to the perimeter of the specimen to prevent sidewall leakage.

Two permeant waters were employed: 0.01*M* $CaCl_2$ solution, which is suggested in ASTM D5084-03 for areas with hard tap water, (e.g., Madison, Wis., United States, where the laboratory tests were conducted) and type II DW. All GCL samples were permeated with SW. A portion of the GCLs were tested with DW, particularly those GCLs with high hydraulic conductivity to SW. Solutions similar to SW have been used extensively for permeat-

Table 2. Physical and Chemical Properties of Exhumed GCLs

Site id	Swell index (mL/2 g)	Water content (%)	Hydraulic conductivity (m/s) SW[b]	Hydraulic conductivity (m/s) DW[b]	Exchange complex (mole fraction)[a] Na^+	K^+	Ca^{2+}	Mg^{2+}
New[a]	[c]36	—	1.2×10^{-11} [c]	1.1×10^{-11}	[c]0.74	[c]0.02	[c]0.22	[c]0.03
	[c]34	—	1.7×10^{-11} [c]	1.0×10^{-11}	[c]0.65	[c]0.02	[c]0.27	[c]0.03
	20.5	53	1.1×10^{-11}	—	0.32	0.01	0.48	0.18
	18.0	55	1.0×10^{-11}	—	0.33	0.01	0.49	0.17
	22.0	53	9.3×10^{-12}	—	0.39	0.01	0.43	0.17
Site A	19.8	56	1.3×10^{-11}	1.0×10^{-11}	0.35	0.01	0.47	0.16
	13.0	53	1.5×10^{-11}	—	0.25	0.01	0.57	0.17
	20.5	61	1.2×10^{-11}	—	0.30	0.01	0.50	0.19
	20.0	57	1.4×10^{-11}	—	0.29	0.01	0.51	0.19
	16.5	59	1.6×10^{-11}	—	0.34	0.01	0.49	0.16
	12.0	22	1.8×10^{-8}	—	0.37	0.03	0.41	0.20
	14.0	21	2.0×10^{-8}	—	0.45	0.03	0.52	0.00
	20.0	21	4.1×10^{-9}	—	0.52	0.03	0.29	0.16
	16.5	21	1.5×10^{-8}	—	0.59	0.03	0.24	0.14
Site B	16.0	17	2.3×10^{-9}	—	0.46	0.03	0.33	0.18
	14.0	20	8.5×10^{-9}	—	0.46	0.03	0.33	0.18
	17.0	18	2.1×10^{-9}	2.0×10^{-11}	0.43	0.03	0.35	0.19
	13.0	19	4.5×10^{-8}	—	0.41	0.02	0.37	0.20
	15.0	20	1.5×10^{-9}	—	0.54	0.03	0.28	0.15
	18.0	21	1.9×10^{-8}	—	0.52	0.03	0.29	0.16
	8.0	70	4.7×10^{-11}	—	0.06	0.01	0.71	0.21
	8.0	64	4.2×10^{-11}	—	0.06	0.01	0.70	0.22
Site E-01	10.0	58	4.0×10^{-11}	—	0.05	0.01	0.69	0.25
	10.0	60	2.3×10^{-11}	—	0.05	0.02	0.72	0.22
	8.0	58	1.3×10^{-8} [d]	—	0.05	0.01	0.70	0.25
	10.0	56	1.6×10^{-7} [d]	—	0.06	0.02	0.66	0.26
	10.0	56	1.3×10^{-7} [d]	2.5×10^{-10}	0.03	0.01	0.70	0.26
	11.0	63	2.1×10^{-8} [d]	—	0.04	0.00	0.71	0.25
Site E-02	9.0	60	1.5×10^{-8} [d]	—	0.04	0.01	0.69	0.25
	11.0	68	3.3×10^{-11}	—	0.05	0.01	0.67	0.27
	10.0	67	3.2×10^{-11}	—	0.05	0.01	0.69	0.25
	8.0	61	3.7×10^{-11}	—	0.05	0.02	0.72	0.21
	8.0	61	6.5×10^{-9} [d]	8.9×10^{-11}	0.03	0.03	0.95	0.00
Site F-03	10.0	61	2.6×10^{-9} [d]	9.3×10^{-11}	0.01	0.03	0.96	0.00
	10.0	65	3.3×10^{-9} [d]	1.2×10^{-10}	0.01	0.02	0.97	0.00
	13.0	43	3.8×10^{-9}	1.3×10^{-11}	0.14	0.03	0.83	0.00
Site F-05	12.0	46	2.1×10^{-7}	1.4×10^{-11}	0.14	0.04	0.83	0.00
	13.0	45	1.1×10^{-8}	1.3×10^{-11}	0.13	0.03	0.84	0.00

[a]Only major cations satisfying the CEC are presented.

[b]SW = standard water (0.01*M* $CaCl_2$); DW = deionized water.

[c]Tests conducted by Meer and Benson (2007).

[d]Preferential flow observed.

ing GCLs exhumed from final covers (Egloffstein 2001, 2002; Lin and Benson 2000; Benson et al. 2007; Meer and Benson 2007). Both solutions generally are considered to be nonreactive permeant waters that result in the same hydraulic conductivity for GCLs (Shackelford et al. 2000; Jo et al. 2001; Kolstad et al. 2004). However, DW was used to ensure that the permeant water would not be a source of cations for exchange reactions.

Hydraulic conductivity tests were conducted until the termination criteria stipulated in ASTM D5084-03 were met. For specimens that exhibited high hydraulic conductivity ($>10^{-9}$ m/s), rhodamine WT dye (5 mg/L) was added to the influent liquid at the conclusion of testing to determine if sidewall leakage was occurring. No indication of sidewall leakage was found in any test. The effluent lines and effluent were also monitored throughout testing for bentonite particle migration. No particles were observed in the effluent lines and effluent.

SI

SI of bentonite from the GCLs was measured using 2 g of oven-dry bentonite removed from each GCL sample. Methods described in ASTM D5890-04 were followed. All tests were

Table 3. Arithmetic Mean Water Content, TCM, and MDR of Exhumed GCLs

	Water content (%)		TCM ($cmol^+/kg$) [a]		MDR[b]	
Site	Mean	Std. dev.	Mean	Std. dev.	Mean	Std. dev.
A	52	3	5.5	0.9	0.96	0.02
B	20	2	9.2	0.6	0.99	0.01
E-01	62	5	2.6	1.0	0.85	0.10
E-02	59	5	2.8	1.5	0.77	0.19
F-03	63	2	2.5	0.5	0.70	0.02
F-05	45	2	8.4	0.4	0.95	0.00

[a]TCM=total charge of soluble cations per mass of soil solid.

[b]MDR=ratio of the total charge of monovalent soluble cations relative to the total charge of divalent soluble cations.

conducted with DW as the hydrating solution. Duplicate tests were performed for each sample, but the SI were identical. The SI of each sample is summarized in Table 2.

Soluble Cations, Bound Cations, and Cation Exchange Capacity

Soluble cations (SC), bound cations (BC), and cation exchange capacity (CEC) were determined following the procedures in ASTM D7503-10. Chemical analysis of extracts from the SC and BC tests was conducted using inductively coupled plasma-optimal emission spectroscopy (ICP-OES) following USEPA Method 6010 B (U.S. EPA 2007). BC mole fractions of the major exchangeable cations (Na^+, K^+, Ca^{2+}, and Mg^{2+}) for each GCL sample are presented in Table 2. BC mole fractions were calculated as the ratio of total charge per unit mass of bentonite associated with a particular cation to the CEC.

Strength and relative abundance of SC (cations that can be released by rinsing with water) were quantified by the total soluble cation charge per mass (TCM) and the ratio of monovalent-to-divalent cations (MDR). TCM is defined as the total charge of monovalent and divalent SC per mass of soil solid. MDR is the ratio of the total charge of monovalent SC relative to the total charge of divalent SC. The average TCM and MDR of bentonite from each site is presented in Table 3. These charge and mass-based metrics associated with the bentonite solid are analogous to the ionic strength (I) and ratio of monovalent-to-divalent cations (RMD) used to describe the characteristics of permeant water (Kolstad et al. 2004). MDR is also analogous to the sodium adsorption ratio (SAR), which describes the relative abundance of Na^+, Ca^{2+}, and Mg^{2+} cation in pore water in equilibrium with the soil solid (McBride 1994). Because TCM and MDR are mass-based metrics, their use precludes the need for a dilution correction to account for differences in liquid-to-solid ratio between the field and in laboratory extracts.

Subgrade Soils

Water contents (ASTM D422-07) and Unified Soil Classification System (USCS) classifications (ASTM D2487-06) of the subgrade soils are summarized in Table 4. Water content of the subgrade varied between sites from 2.3% (Site B) to 15.9% (Site F-03). Sites located in arid climates (Sites A and B) had lower subgrade water contents (2.3–9.8%) than the sites in continental climates (Sites E and F) (8.5–15.9%). The subgrade soils range from well-graded sand (Site A) to low plasticity silt (Site B).

Pore water in the subgrade was characterized using a batch test method similar to the procedure described in ASTM D6141-04. Meer and Benson (2007) indicated that this method "provides a relatively simple and expedient method to generate a test liquid representative of flow-through conditions." DW was used as the eluent with a liquid-to-solid ratio of 1.3. The soil-water mixture was placed in a sealed 250-mL bottle and rotated for 24 h. The solution was then separated by centrifugation and vacuum filtered through 0.45-μm filter paper. Concentrations of major cations (Ca^{2+}, Mg^{2+}, Na^+, and K^+) in the eluent were measured by ICP-OES following U.S. EPA Method 6010 B (U.S. EPA 2007) and used to compute the TCM and MDR for each subgrade soil (Table 4).

Table 4. USCS Classification (ASTM D2487-06) and Arithmetic Mean Water Content (ASTM D422-07), TCM, and MDR of Subgrade Soils

		Water content (%)		TCM[a] ($cmol^+/kg$)		MDR[b]	
Site	Soil classification	Mean	Std. dev.	Mean	Std. dev.	Mean	Std. dev.
A	SW	9.8	0.0	0.73	0.09	0.74	0.08
B	ML	2.3	0.2	0.97	0.12	0.76	0.03
E-01	ML-CL	14.2	1.6	0.63	0.08	0.62	0.08
E-02		14.9	1.2	0.58	0.15	0.64	0.07
F-03	SM	15.9	0.0	0.46	0.09	0.52	0.02
F-05		8.5	0.0	1.20	0.15	0.76	0.04

[a]TCM=total charge of soluble cations per mass of soil solid.

[b]MDR=ratio of the total charge of monovalent soluble cations relative to the total charge of divalent soluble cations.

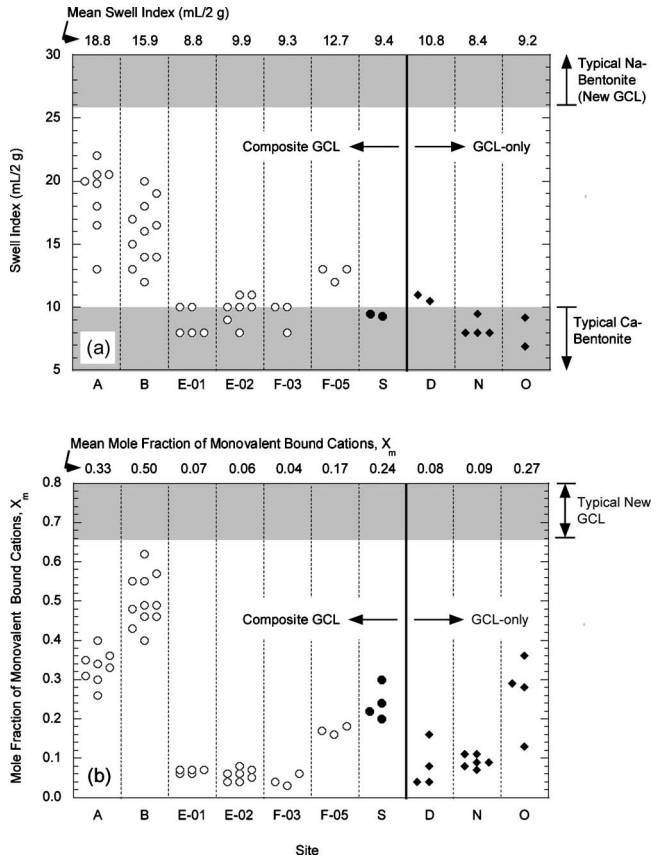

Fig. 4. (a) Swell index in deionized water; (b) mole fraction monovalent bound cations for GCL-only and composite GCL covers. Data are from this study (open symbols) and Meer and Benson (2007) (closed symbols).

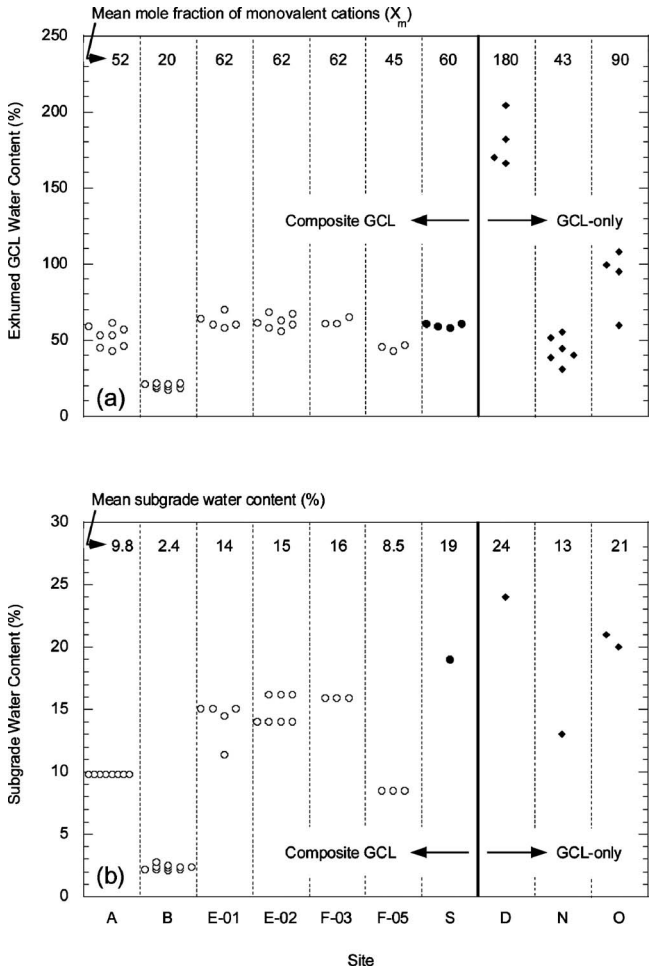

Fig. 5. (a) Gravimetric water content of exhumed GCLs; (b) subgrades for covers where GCLs were in composite barriers or the sole barrier layer. Data are from this study (open symbols) and Meer and Benson (2007) (closed symbols).

Results

GCL Water Content and Cation Exchange

SI and the mole fraction of monovalent cations (X_m) of the exhumed GCLs are shown in Fig. 4 along with the data from Meer and Benson (2007) for a GCL in a composite barrier (Site S) and GCLs that were the sole barrier layer in a final cover (Sites D, N, and O). Swell indices typical of Ca-bentonite (5–10 mL/2 g) and Na-bentonite (26–36 mL/2 g) are denoted in Fig. 4(a), and the X_m typical of a new GCL (>0.65) is marked in Fig. 4(b). Cation exchange and loss of swell are common and extensive in GCLs deployed in composite barriers. At four of the six sampling locations, the GCLs exhumed from composite barriers had SI near those typical of Ca-bentonite (7–11 mL/2 g) and concurrently low X_m (i.e., bound cations predominantly divalent). These SI and X_m are congruent with those for the GCLs exhumed by Meer and Benson (2007). Two of the six sampling locations (locations A and B) in this study had SI and X_m falling between the SI and X_m for Na- and Ca-bentonite, even though all of the GCLs in this study were covered with a GM.

GCLs installed in composite barrier layers are protected from downward percolation of overlying soil eluents. However, cation exchange and loss of swell from multivalent cations is not prevented by the overlying GM, and is limited in only some cases. Multivalent cations may still enter the GCL by advective transport from underlying soil pore water during hydration, diffusion from underlying soil pore water, or a combination of both mechanisms (Meer and Benson 2007; Bradshaw 2008). Given the similarity of the SI and X_m of the GCLs exhumed in this study and those in Meer and Benson (2007), transport of cations from the subgrade appears to be as equally important as downward percolation of soil eluent. Eventually, GCLs in most composite barriers probably will undergo complete cation exchange and have swell indices typical of Ca-bentonite once sufficient divalent cations migrate into the GCL.

Water content of exhumed GCLs is shown in Fig. 5(a) along with the data from Meer and Benson (2007). GCLs exhumed from composite barriers exhibit less overall variation in water content (20–63%) than the GCLs not covered by a GM (43–180%), that were reported in Meer and Benson (2007). At a given site, the water content varies by at most 12 percentage points for GCLs in composite barriers, compared to 49 percentage points for GCLs used as the sole barrier layer in Meer and Benson (2007). Moreover, the average water content varies between 45 and 62% for six of the seven sampling locations, where the GCL was part of a composite barrier, but between 43 and 180% for the GCLs used without a GM described in Meer and Benson (2007). More consistent in situ water content in composite barrier GCLs was likely a result of the overlying GM eliminating wet-dry cycling of the GCL.

Water content of the exhumed GCLs varies systematically

J. Geotech. Geoenviron. Eng. 2011.137:1-13.

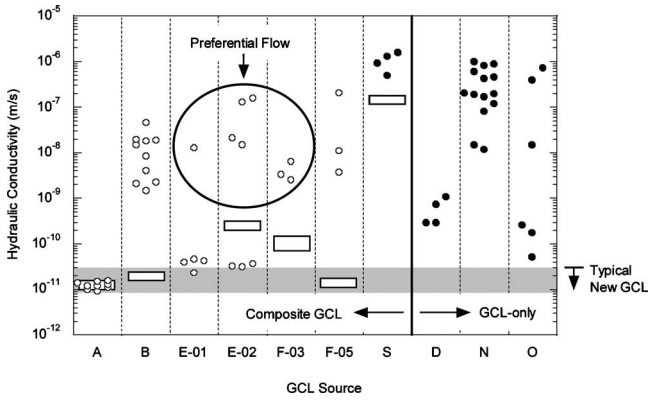

Fig. 6. Hydraulic conductivity of exhumed GCLs from covers where GCLs were in composite barriers or the sole barrier layer. Data are from this study (open symbols) and Meer and Benson (2007) (closed symbols). Circles are hydraulic conductivity to SW; open boxes are hydraulic conductivity to DW.

with the water content of the subgrade, as shown in Fig. 5(b). For example, the driest exhumed GCLs (Site B) were installed on the driest subgrade (water content=2.4%) and the wettest exhumed GCLs (Site D) were installed on the wettest subgrade (water content=24%). Subgrades underlying composite barriers in this study tended to have lower water contents than subgrades underlying GCLs installed as the sole barrier, (i.e., from Meer and Benson 2007). Lower subgrade water content is likely a result of the GM preventing downward percolation.

Hydraulic Conductivity

Hydraulic conductivities of the GCLs exhumed in this study are shown in Fig. 6 along with hydraulic conductivities of GCLs exhumed by Meer and Benson (2007). Hydraulic conductivities of the GCLs exhumed in this study range nearly five orders of magnitude (9.3×10^{-11} to 1.3×10^{-6} m/s). For GCLs permeated with SW, high hydraulic conductivities ($>10^{-9}$ m/s) were obtained at all but one site. Additionally, when permeated with SW, many of the GCLs from composite barriers and those GCLs serving as the sole barrier layer have comparable hydraulic conductivity, except a greater number of GCLs exhumed in this study had hydraulic conductivities to SW close to 10^{-11} m/s. In contrast, the GCLs exhumed in this study had lower hydraulic conductivity to DW than those exhumed by Meer and Benson (2007).

Lower hydraulic conductivities were obtained in most cases when GCLs were permeated with DW rather than SW (Fig. 6). For example, the hydraulic conductivity to SW at Site B ranged between 2×10^{-9} and 5×10^{-8} m/s, whereas the hydraulic conductivity to DW ranged from 2×10^{-11} to 3×10^{-11} m/s. However, at Site A, essentially the same hydraulic conductivity was obtained with SW and DW ($\approx1\times10^{-11}$ m/s). Meer and Benson (2007) (e.g., Site S in Fig. 6) and Benson et al. (2007) did not find similar sensitivity to water type. For the GCLs that they exhumed, GCLs having high hydraulic conductivity to SW also had high hydraulic conductivity to DW.

Because actual pore waters contain a mixture of cations (Meer and Benson 2007; Benson and Meer 2009; Scalia and Benson 2010a), the actual hydraulic conductivity of the GCLs exhumed in this study probably exists between the hydraulic conductivities to SW and DW. However, a definitive inference regarding the actual in-service hydraulic conductivity is not possible. Nevertheless, the sensitivity to water type and the high hydraulic conductivity to SW, both of which are atypical of a new GCL, indicate that covering a GCL with a GM does not preclude alteration of the GCL while the GCL is in service. If alteration to the GCLs had not occurred in situ, permeation with SW and DW would have yielded essentially the same hydraulic conductivity, as observed with new GCLs.

After terminating the hydraulic conductivity tests, GCLs with high hydraulic conductivity were permeated with dye to detect if preferential flow was occurring. Preferential flow was observed in the GCLs from Site F-03 and Site E that had high hydraulic conductivities (see call out in Fig. 6). Preferential flow in GCLs from Site E occurred along nearly all of the bundles of needle-punched fibers and was concomitant with dark mineral precipitates (see Scalia and Benson 2010b). For Site F-03, preferential flow in the GCLs also occurred along bundles of needle-punched fibers. However, only 5% of the bundles of needle-punched fibers transmitted preferential flow at Site F-03. GCLs exhibiting preferential flow behaved differently than the other GCLs exhumed in this study and are separated out of the remaining discussion in this paper. They are described in greater detail in Scalia and Benson (2010b).

Hydraulic conductivities of the GCLs are shown in Fig. 7 as a function of SI [Fig. 7(a)] and X_m [Fig. 7(b)]. New GCLs permeated with SW and GCLs from Site S permeated with SW and DW by Meer and Benson (2007) are also shown in Fig. 7. Data from GCLs that did not exhibit preferential flow fall into two bands corresponding to higher hydraulic conductivity and lower hydraulic conductivity. The band with higher hydraulic conductivity shows strong sensitivity to SI and X_m, whereas the band with lower hydraulic conductivity has much less sensitivity to SI and X_m. Higher hydraulic conductivities correspond almost exclusively to GCLs permeated with SW [one data point for DW from Meer and Benson (2007) is in this region], whereas lower hydraulic conductivities correspond to data from GCLs permeated with either SW or DW.

Effect of Subgrade Condition

The relationship between hydraulic conductivity to SW and exhumed water content is shown in Fig. 8(a). When the GCLs with preferential flow are excluded, low hydraulic conductivity is obtained consistently when the water content of the GCL exceeds 50%. For lower water contents, the hydraulic conductivity consistently is higher than 10^{-9} m/s. Meer and Benson (2007) report a similar step relationship, except the transition occurred at a water content of 85%. The data from Site S from Meer and Benson (2007) and the GCLs with preferential flow in this study do not follow this trend.

The relationship between water content of the exhumed GCL and the subgrade water content is shown in Fig. 8(b). Water content of GCLs increases as the water content of the subgrade increases, as has also been shown in laboratory studies (Daniel 1993; U.S. EPA 1996; Thiel and Criley 2005). Subgrade water content also influenced the soluble and bound cations in the bentonite, as shown in Fig. 9. GCLs that had lower TCM [Fig. 9(a)] and lower X_m [Fig. 9(b)] were from subgrades having higher water content. Most importantly, when the GCLs with preferential flow are excluded, low hydraulic conductivity ($<5\times10^{-11}$ m/s) to SW was achieved consistently when the subgrade water content was at least 10%.

Water content of the exhumed GCLs is shown as a function of water content of the subgrade relative to optimum water content

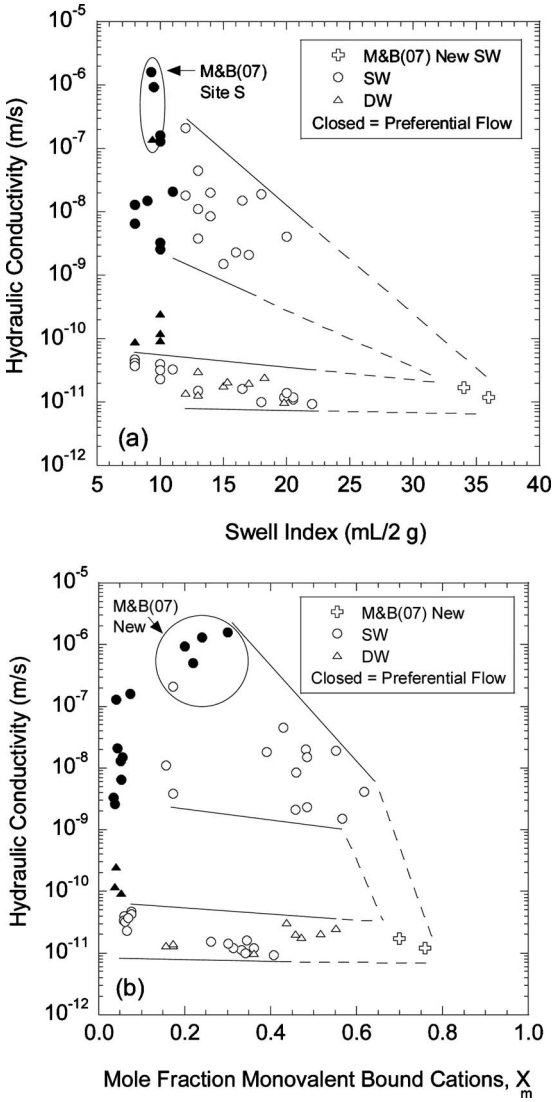

Fig. 7. Hydraulic conductivity to standard water (SW) versus: (a) swell index in deionized water (DW); (b) mole fraction bound sodium for exhumed GCLs from composite barriers. Data for new GCL are from Meer and Benson (2007).

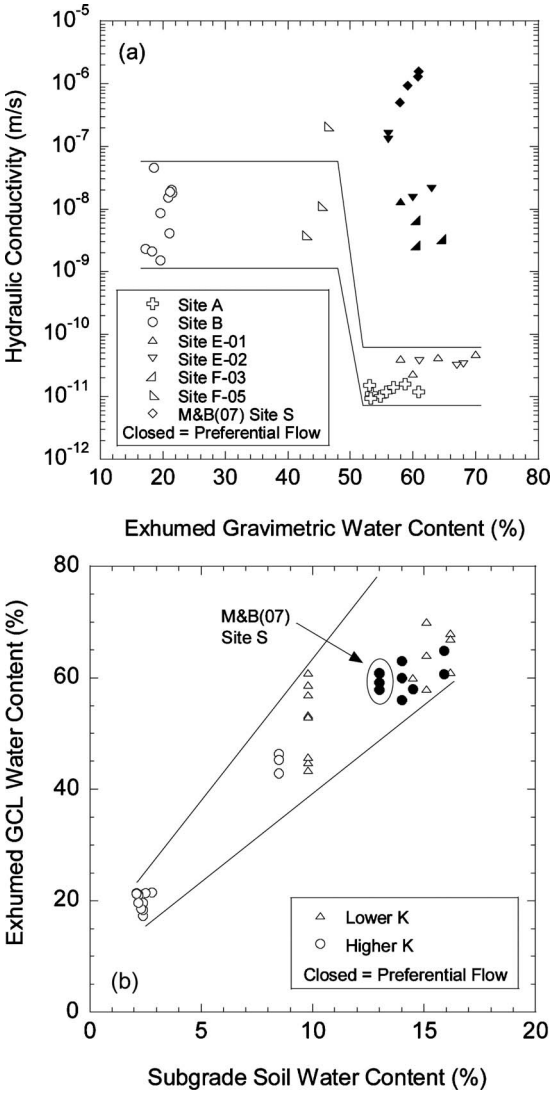

Fig. 8. (a) Hydraulic conductivity (K) of exhumed GCLs to standard water versus water content; (b) water content of exhumed GCLs versus corresponding water content of subgrade. GCLs with lower K had $K < 5 \times 10^{-11}$ m/s, whereas GCLs with higher K had $K > 1 \times 10^{-9}$ m/s.

(OWC, standard Proctor) in Fig. 10. Data from by U.S. EPA (1996) and Bradshaw (2008) are also included in Fig. 10. Both U.S. EPA (1996) and Bradshaw (2008) examined GCL hydration from an underlying compacted subgrade. The duration of these laboratory hydration studies was limited to 75 days (U.S. EPA 1996) and 90 days (Bradshaw 2008). While this duration is much less than the hydration period for the field samples in this study, the duration was sufficient to achieve essentially complete GCL hydration (Daniel 1993; U.S. EPA 1996; Thiel and Criley 2005; Bradshaw 2008). As shown in Fig. 10, water content of the GCLs increases as the water content of the subgrade relative to OWC increases. When the water content of the subgrade soil exceeds OWC, the hydrated GCLs consistently have water contents >50%, which corresponds to the range associated with osmotic swell and low hydraulic conductivity.

The subgrade also influences soluble cations in the bentonite (Fig. 11). TCM of the GCL increases as TCM of the subgrade increases [Fig. 11(a)], but the relative abundance of monovalent and divalent cations in the GCL (as indicated by MDR) is nearly independent of the relative abundance in the subgrade [Fig. 11(b)]. The GCLs with preferential flow are an exception; MDRs for these GCLs are comparable to MDRs of the subgrade, which may indicate that these GCLs are closer to equilibrium than those without preferential flow (perhaps due to preferential flow). Most importantly, when GCLs with preferential flow are excluded, low hydraulic conductivity to SW is consistently obtained when the GCL TCM is ≤ 7 cmol$^+$/kg and the subgrade TCM is ≤ 0.8 cmol$^+$/kg. More dilute pore water in the GCL (lower TCM) promotes osmotic swelling of the bentonite, and therefore lower hydraulic conductivity to SW even if the Na^+ on the bentonite has been replaced by divalent cations.

Discussion

The aforementioned results have shown that GCLs in composite barriers are altered by their environment even though they are covered by a GM. When GCLs that exhibit preferential flow paths

J. Geotech. Geoenviron. Eng. 2011.137:1-13.

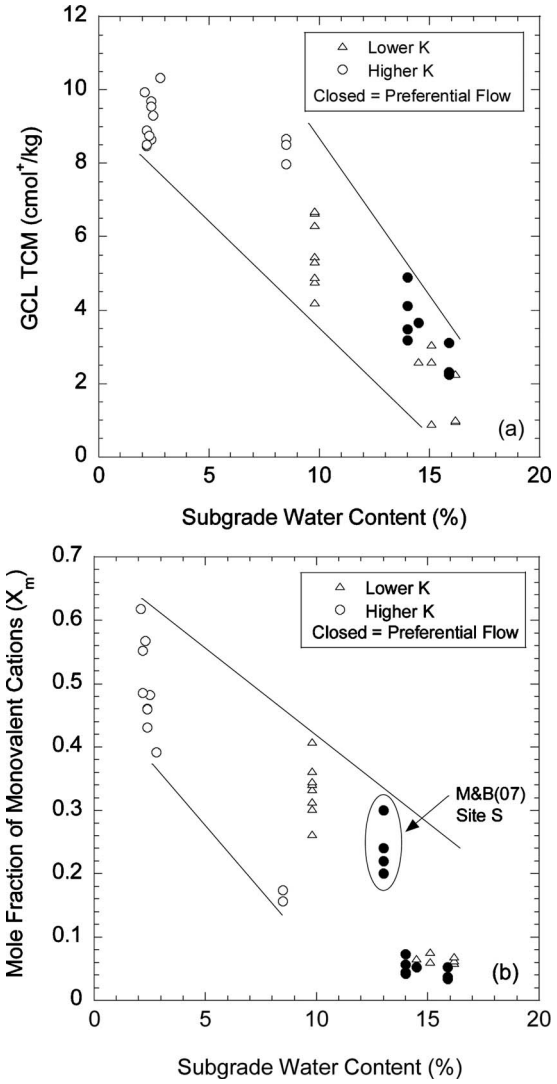

Fig. 9. (a) Total soluble cation charge per mass (TCM); (b) mole fraction of monovalent cations of GCL versus water content of subgrade. GCLs with lower hydraulic conductivity (K) had $K<5\times10^{-11}$ m/s, whereas GCLs with higher K had $K>1\times10^{-9}$ m/s.

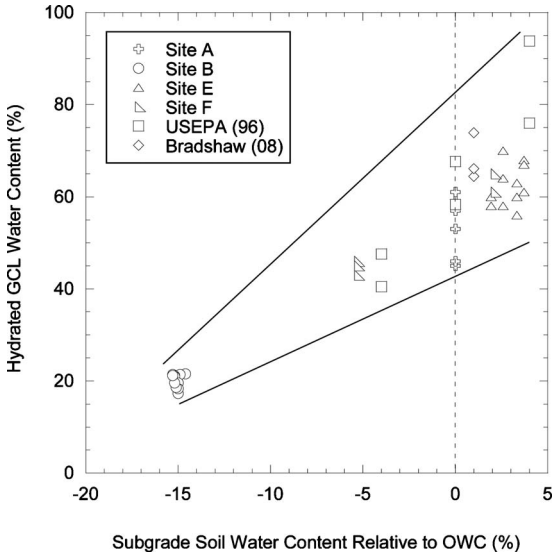

Fig. 10. Water content of GCLs at exhumation as a function of subgrade water content relative to optimum water content (OWC, standard Proctor)

are excluded, GCLs in composite barriers that are hydrated sufficiently on a moist subgrade with modest TCM have low hydraulic conductivity ($<5\times10^{-11}$ m/s) and are insensitive to water type. In contrast, GCLs that do not hydrate sufficiently and/or hydrate on a subgrade with lower water content and higher TCM can have high hydraulic conductivity to SW and can be very sensitive to water type (Figs. 8 and 11).

This behavior is in marked contrast to new GCLs, which have essentially identical hydraulic conductivities to SW and DW when permeated for durations similar to the tests conducted in this study (<30 days) (Jo et al. 2001, 2005; Kolstad et al. 2004). Moreover, the GCLs exhumed in this study have hydraulic conductivities to SW as much as four orders of magnitude higher than the hydraulic conductivity reported for new GCLs after very long-term permeation with solutions similar to SW ($\sim2\times10^{-10}$ m/s) that result in complete replacement of Na^+ by Ca^{2+} and/or Mg^{2+} (Egloffstein 2001; Jo et al. 2005; Benson et al. 2007). These findings indicate that alterations that occur within composite barriers can introduce unique sensitivity to GCLs, and suggest that the sensitivity is affected by the hydration state.

In a composite barrier, hydration of the GCL occurs gradually over a period of approximately 30 days as water migrates upward from the subgrade in the liquid and vapor phases (Daniel 1993; U.S. EPA 1996; Bradshaw 2008). The amount of hydration depends on the water content of the subgrade (Daniel 1993; U.S. EPA 1996; Bradshaw 2008). If the subgrade is sufficiently moist to induce osmotic swelling of the bentonite, (i.e., water content at least 35%) before divalent cations from the subgrade replace the Na^+, the swollen structure of the bentonite will be retained and permeation with SW or DW will yield low hydraulic conductivity (even if divalent cations in the permeant water replace Na^+ in the bentonite). For example, at Sites A and E, the GCL had a water content >53% and hydraulic conductivities to DW and SW in the range of 9×10^{-12} to 5×10^{-11} m/s, even though divalent cations replaced 48% of the Na^+ (on average) at Site A and 90% at Site E (GCLs with preferential flow at Site E excluded). Moreover, when exhumed, the GCLs at Sites A and E exhibited the gel-like consistency of bentonite that had undergone osmotic swell [Fig. 12(a)], as described in Guyonnet et al. (2005). Pore water in the subgrade at Sites A and E (Table 4) was also more dilute (TCM <0.8 $cmol^+/kg$), which promotes osmotic swell.

In contrast, if the subgrade has insufficient moisture to promote or complete osmotic swell, and divalent cations replace a substantial portion of the Na^+ in the bentonite, then the hydraulic conductivity of the GCL to SW can be orders of magnitude higher because osmotic swell is precluded as Ca^{2+} in SW replaces the remaining Na^+ in the bentonite. For example, the GCLs from Site B and Site F-05 had water content <46%, substantial replacement of Na^+ by divalent cations, high hydraulic conductivity to SW, and a granular structure characteristic of a GCL that had not undergone osmotic swell [Fig. 12(b)]. Pore water in these subgrades was also more concentrated (TCM >0.8 $cmol^+/kg$, Table 4). As a result, pore water in the GCL will be more concentrated [Fig. 11(b)], which will suppress osmotic swell.

The GCLs from Site S in Meer and Benson (2007) and the GCLs from Sites E and F with preferential flow are exceptions. These data cluster in Figs. 8(a) and 11(b) and are inconsistent with data for the other GCLs. The GCL from Site S also did not have the gel-like consistency associated with bentonite that had

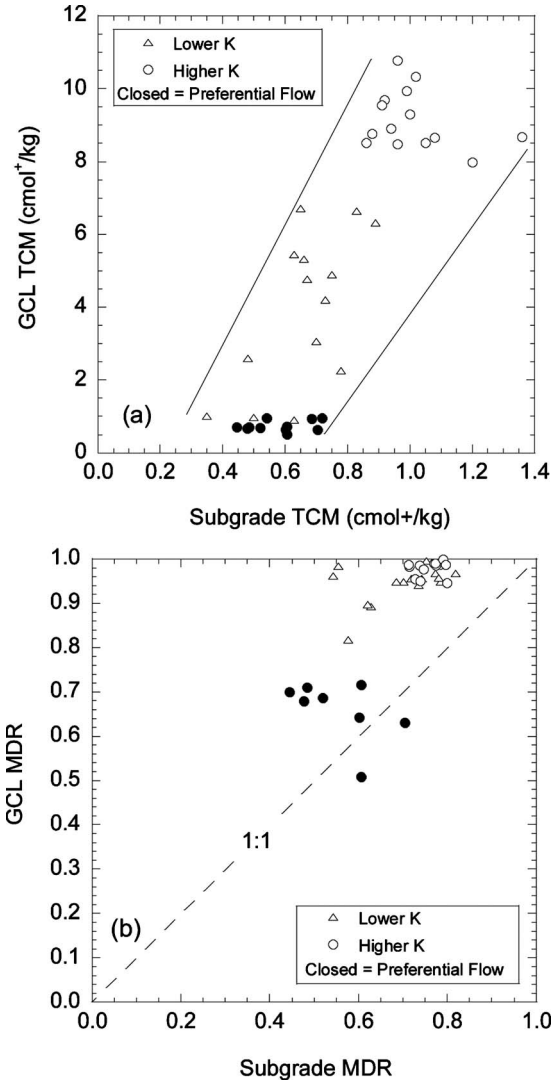

Fig. 11. (a) Total soluble cation charge per mass (TCM) of GCL versus TCM of subgrade; (b) monovalent-to-divalent cation ratio (MDR) of GCL versus MDR of subgrade. GCLs with lower hydraulic conductivity (K) had $K < 5 \times 10^{-11}$ m/s, whereas GCLs with higher K had $K > 1 \times 10^{-9}$ m/s.

undergone osmotic swell and contained cracks typically associated with wet-dry cycling [Fig. 13(a)]. This GCL may have undergone hydration, cation exchange, and then dehydration, even though the GCL was overlain by a GM (e.g., if cover soil was not placed on the GM promptly). However, information regarding the installation and service life of the GCL at Site S is insufficient to confirm whether this sequence of processes could have occurred. Because the GCL from Site S had relatively low X_m and SI (Fig. 4), cracks in the bentonite probably did not swell shut during permeation and acted as preferential flow paths. Consequently, the GCL had similar hydraulic conductivity to SW and DW (Fig. 6).

The GCLs with preferential flow paths from Sites E and F are highly unusual and are different from those at Site S. These GCLs had distinct preferential flow occur along bundles of needle-punched fibers [Fig. 13(b)]. Mechanisms causing these flow paths were beyond the scope of this study, but cation exchange as water from the subgrade is wicked upward through bundles of needle-punched fibers is a likely cause (Scalia and Benson 2010b). Conditions causing this phenomenon have not yet been indentified. However, the bentonite adjacent to the needle-punching fibers did not exhibit the gel-like structure associated with osmotic swell. Remnant granules and inter-granule pores were visible [Fig. 13(b)].

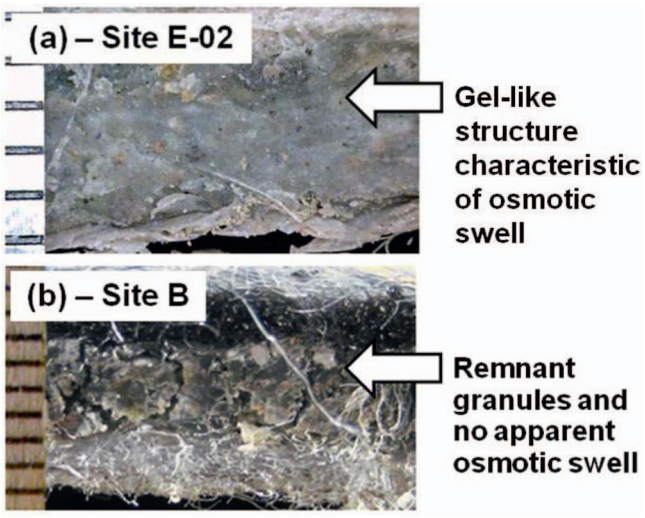

Fig. 12. (Color) (a) Cross sections of exhumed GCLs from Site E-02; (b) Site B. Vertical scale in millimeters.

Conclusions and Recommendations

GCLs were exhumed from final covers with composite barriers at four sites after 4.7–6.7 years of service. Hydraulic conductivity of the GCLs was measured using standard water (SW, 10 mM $CaCl_2$ solution) and type II DW to represent a typical permeant water and nonreactive permeant water. GCLs were also tested for SI, w, BC, SC, and CEC. Subgrade soils were exhumed and evaluated for pore-water composition, w, and particle size distribution.

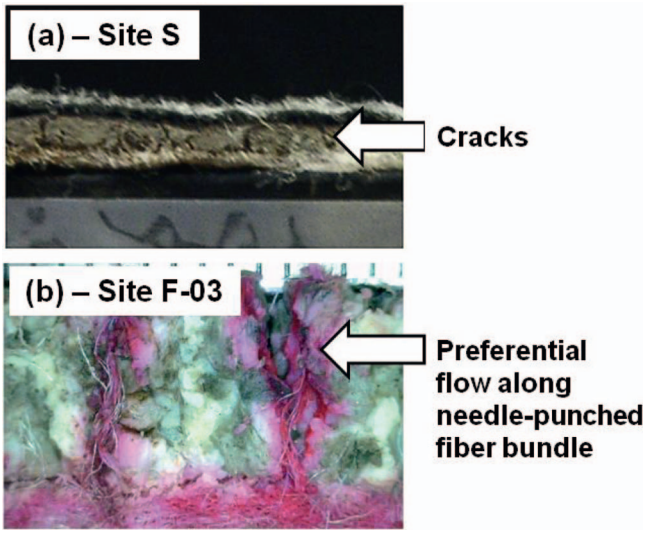

Fig. 13. (Color) (a) Cross sections of exhumed GCLs from Site S; (b) Site F-03. Photo of GCL from Site S is from Meer (2004). Photo of GCL from Site F-03 is after permeation with rhodamine WT dye. Horizontal scale in millimeters.

J. Geotech. Geoenviron. Eng. 2011.137:1-13.

Based on the findings from these analyzes, the following conclusions and recommendations are made regarding GCLs deployed in final covers with composite barriers:

1. In most environments, divalent cations likely will replace the native Na^+ in GCLs deployed in composite barriers. Exchange appears to occur more rapidly and completely when the GCL is installed on a subgrade with higher water content.
2. The hydraulic conductivity of GCLs exhumed from composite barriers can be sensitive to the type of permeant water. GCLs hydrated to water content in excess of 50% tended to have low hydraulic conductivity regardless of the amount of Na^+ replaced by divalent cations or the type of permeant water. Therefore, conditions that promote rapid hydration to a water content $>50\%$ are recommended to ensure that a GCL has low hydraulic conductivity regardless of the type of pore water migrating through the GCL.
3. The water content of GCLs exhumed from composite barriers was directly related to the water content of the subgrade underlying the GCL. Subgrades with water contents above 10% or in excess of optimum water content were associated with GCLs that had higher water contents ($>50\%$) at exhumation and low hydraulic conductivity regardless of type of permeant water.
4. GCLs with more dilute pore water (lower GCL TCM) were associated with subgrades with more dilute pore water (lower subgrade TCM). GCLs without preferential flow that had low hydraulic conductivity regardless of water type were exhumed from subgrades having $\text{TCM} < 0.8\ \text{cmol}^+/\text{kg}$.
5. Preferential flow was observed in some GCLs along bundles of needle-punched fibers. These GCLs had higher hydraulic conductivity to SW and DW and essentially complete replacement of Na^+ by divalent cations. The mechanisms underlying preferential flow in these GCLs have not yet been identified. However, bentonite surrounding the needle-punched fibers in these GCLs did not exhibit the gel-like appearance of bentonite that had undergone osmotic swell.
6. Subgrade placed in excess of OWC is recommended to ensure rapid hydration and osmotic swell in GCLs used in composite barriers. Provided that desiccation is prevented, GCLs placed under these conditions are likely to maintain low hydraulic conductivity ($\leq 5 \times 10^{-11}$ m/s) to dilute permeant waters even after complete exchange of divalent for monovalent cations has occurred.

While these findings illustrate that GCLs in composite barriers are altered by their environment, field data indicate that final covers containing composite barriers with a GCL function very well. Percolation rates less than approximately 4 mm/year have been reported in continental climates, and near zero percolation has been reported in semi-arid and arid climates.

Acknowledgments

A consortium consisting of the National Science Foundation (Grant No. CMMI-0625850), the U.S. Nuclear Regulatory Commission, the U.S. Environmental Protection Agency, the U.S. Department of Energy, the Environmental Research and Education Foundation, Colloid Environmental Technologies Corporation, Veolia Environmental Services, and Waste Connections, Inc. provided financial support for this study. This support is gratefully acknowledged. The findings and recommendations in this report are solely those of the writers, and do not necessarily represent the policies or opinions of the sponsors. Endorsement by the sponsors is not implied and should not be assumed.

References

Albright, W. H., et al. (2004). "Field water balance of landfill final covers." *J. Environ. Qual.*, 33(6), 2317–2332.

Benson, C. H., and Meer, S. R. (2009). "Relative abundance of monovalent and divalent cations and the impact of desiccation on geosynthetic clay liners." *J. Geotech. Geoenviron. Eng.*, 135(3), 349–358.

Benson, C. H., Thorstad, P. A., Jo, H., and Rock, S. A. (2007). "Hydraulic performance of geosynthetic clay liners in a landfill final cover." *J. Geotech. Geoenviron. Eng.*, 133(7), 814–827.

Bradshaw, S. L. (2008). "Effect of cation exchange during subgrade hydration and leachate permeation." M.S. thesis, Univ. of Wisconsin, Madison, Wis.

Daniel, D. E. (1993). "Clay liners." *Geotech. Practice for Waste Disposal*, Chap. 7, Chapman & Hall, London, 137–163.

Egloffstein, T. A. (2001). "Natural bentonites-influence of the ion exchange and partial desiccation on permeability and self-healing capacity of bentonites used in GCLs." *Geotext. Geomembr.*, 19, 427–444.

Egloffstein, T. A. (2002). "Bentonite as sealing material in geosynthetic clay liners-influence of the electrolytic concentration, the ion exchange and ion exchange with simultaneous partial desiccation on permeability." *Clay geosynthetic barriers*, H. Zanzinger, R. Koerner, and E. Gartung, eds., Swets and Zeitlinger, Lisse, The Netherlands, 141–153.

Gleason, M. H., Daniel, D. E., and Eykholt, G. R. (1997). "Calcium and sodium bentonite for hydraulic containment applications." *J. Geotech. Eng.*, 118(5), 438–445.

Guyonnet, D., et al. (2005). "Geosynthetic clay liner interaction with leachate: Correlation between permeability, microstructure, and surface chemistry." *J. Geotech. Geoenviron. Eng.*, 131(6), 740–749.

Jo, H., Benson, C. H., Shackelford, C. D., Lee, J., and Edil, T. B. (2005). "Long-term hydraulic conductivity of a non-prehydrated geosynthetic clay liner permeated with inorganic salt solutions." *J. Geotech. Geoenviron. Eng.*, 131(4), 405–417.

Jo, H., Katsumi, T., Benson, C. H., and Edil, T. B. (2001). "Hydraulic conductivity and swelling of nonprehydrated GCLs permeated with single-species salt solutions." *J. Geotech. Geoenviron. Eng.*, 127(7), 557–567.

Kolstad, D. C., Benson, C. H., and Edil, T. D. (2004). "Hydraulic conductivity and swell of nonprehydrated GCLs permeated with multispecies inorganic solutions." *J. Geotech. Geoenviron. Eng.*, 130(12), 1236–1249.

Lee, J., Shackelford, C. D., Benson, C. H., Jo, H., and Edil, T. B. (2005). "Correlating index properties and hydraulic conductivity of geosynthetic clay liners." *J. Geotech. Geoenviron. Eng.*, 131(11), 1319–1329.

Lin, L., and Benson, C. H. (2000). "Effect of wet-dry cycling on swelling and hydraulic conductivity of GCLs." *J. Geotech. Geoenviron. Eng.*, 126(1), 40–49.

Martin, R. T. (1960). "Adsorbed water on clay: A review." *Proc., 9th Nat. Conf. on Clays and Clay Minerals*, Clay Minerals Society, Lafayette, Ind.

McBride, M. B. (1994). *Environmental chemistry of soils*, Oxford University Press, New York.

McKnight, T. L., and Hess, D. (2007). *Physical geography: A landscape appreciation*, 9th Ed., Prentice-Hall, Upper Saddle River, N.J.

Meer, S. R. (2004). "In-service hydraulic conductivity of GCLs in landfill covers: Laboratory and field studies." M.S. thesis, Univ. of Wisconsin, Madison, Wis.

Meer, S. R., and Benson, C. H. (2007). "Hydraulic conductivity of geosynthetic clay liners exhumed from landfill final covers." *J. Geotech. Geoenviron. Eng.*, 133(5), 550–563.

Melchior, S. (2002). "Field studies and excavations of geosynthetic clay barriers in landfill covers." *Clay geosynthetic barriers*, H. Zanzinger,

R. M. Koerner, and E. Gartung, eds. Swets and Zeitlinger, Lisse, The Netherlands, 321–330.
Mesri, G., and Olson, R. E. (1971). "Mechanisms controlling the permeability of clays." *Clays Clay Miner.*, 19, 151–158.
Mitchell, J. K. (1993). *Fundamentals of soil behavior*, 2nd Ed., Wiley, New York.
Mooney, R. W., Keenan, A. G., and Wood, L. A. (1952). "Adsorption of water vapor by montmorillonite. II. Effect of exchangeable ions and lattice swelling as measured by X-ray diffraction." *J. Am. Chem. Soc.*, 74(6), 1371–1374.
Norrish, K., and Quirk, J. P. (1954). "Crystalline swelling of montmorillonite, use of electrolytes to control swelling." *Nature*, 173, 255–257.
Petrov, R. J., and Rowe, R. K. (1997). "Geosynthetic clay liner (GCL)—Chemical compatibility by hydraulic conductivity testing and factors impacting its performance." *Can. Geotech. J.*, 34, 863–885.
Scalia, J. and Benson C.H. (2010a). "Effect of permeant water on the hydraulic conductivity of exhumed GCLs." *Geotech. Test. J.*, 33(3), 1–11.
Scalia, J., and Benson, C. H. (2010b). "Preferential flow in geosynthetic clay liners exhumed from final covers with composite barriers." *Can. Geotech. J.*, 47(10), 1101–1111.
Shackelford, C. D., Benson, C. H., Katsumi, T., Edil, T. B., and Lin, L. (2000). "Evaluating the hydraulic conductivity of GCLs permeated with non-standard liquids." *Geotext. Geomembr.*, 18, 133–161.
Shan, H., and Daniel, D. E. (1991). "Results of laboratory tests on a geotextile/bentonite liner material." *Proc., Geosynthetic '91*, Industrial Fabrics Association International, St. Paul, Minn., 517–535.
Shang, J. Q., Lo, K. Y., and Quigley, R. M. (1994). "Quantitative determination of potential distribution in Stern-Guoy double-layer mode." *Can. Geotech. J.*, 31, 624–636.
Thiel, R. S., and Criley, K. (2005). "Hydraulic conductivity of partially prehydrated GCLs under high effective confining stress for three real leachates." *Waste containment and remediation, GSP 142*, ASCE, Reston, Va.
U.S. EPA. (1996). "Hydration of GCLs adjacent to soil layers." *Rep. No. 600/R-96 /149*, Office of Research and Development, Washington, D.C.
U.S. EPA. (2007). *Method 6010B: Inductively coupled plasma-atomic emission spectrometry, physical/chemical methods SW846*, 3rd Ed., Office of Solid Waste and Emergency Response, Washington, D.C.

Technical Paper by R.S. Thiel and K. Criley

HYDRAULIC CONDUCTIVITY OF A GCL UNDER VARIOUS HIGH EFFECTIVE CONFINING STRESSES FOR THREE DIFFERENT LEACHATES

ABSTRACT: Reinforced GCL samples were partially pre-hydrated on native damp subgrade soils for several weeks, and were then tested for hydraulic conductivity using three different leachates under a variety of effective confining stresses. The samples were received with an initial moisture content of approximately 35%, and gained in moisture content at a rate of about 1% per day over a three week period while sitting in an unconfined condition on a silty-sand material in a closed container. The subgrade soil had a moisture content of 27%, with a negligible change in moisture content over this period The samples tested with MSW leachate were tested under effective stresses of 240, 480, and 720 kPa. The samples tested with MSW-incinerator ash leachate were tested under effective stresses of 180, 360, and 530 kPa. The samples tested with pulp & paper waste leachate were tested under effective stresses of 165, 340, and 475 kPa. All of the results showed decreasing hydraulic conductivity with increasing effective stress with the ash leachate being the most sensitive to effective stress, and the pulp&paper leachate being the least sensitive. The results correlate fairly well with data previously published in the literature regarding the hydraulic conductivity of GCLs at different effective stresses when permeated with tap water and a calcium-chloride solution. The hydraulic conductivity of the GCL to all of the leachates tended to level off to a common value of about 2×10^{-12} m/s at effective stresses above 475 kPa. Some interesting results are presented in the paper showing the effects of changing the effective confining stresses during the tests.

KEYWORDS: Geosynthetic clay liner, hydraulic conductivity, leachate

AUTHOR: R.S. Thiel, Vice President, Vector Engineering, Inc., 143E Spring Hill Dr., Grass Valley, California, 95945, USA, Telephone: 1/530-272-2448, Telefax: 1/530-272-8533, E-mail: richard@rthiel.com; K. Criley, Laboratory Manager, Vector Engineering, Inc., 143E Spring Hill Dr., Grass Valley, California, 95945, USA, Telephone: 1/530-272-2448, Telefax: 1/530-272-8533, E-mail: criley@vectoreng.com.

PUBLICATION: *Geosynthetics International* is published by the Industrial Fabrics Association International, 1801 County Road B West, Roseville, Minnesota 55113-4061, USA, Telephone: 1/612-222-2508, Telefax: 1/612-631-9334. *Geosynthetics International* is registered under ISSN 1072-6349.

DATES: Original manuscript received December, 2002, revised manuscript received _ and accepted _. Discussion open until _.

REFERENCE: Thiel, R.S., and Criley, K. [DATE], "Hydraulic Conuctivity of a GLC Under Various High Effective Confining Stresses for Three Different Leachates", *Geosynthetics International*, Vol. _, No. _, pp. _-_.

1. INTRODUCTION

The scope of this paper relates to the hydraulic conductivity of a geosynthetic clay liner (GCL) subjected to various normal loads and three different liquids (waste leachates) having different dissolved chemical compositions.

Estimates and calculations regarding leakage rates through intact geosynthetic clay liners (GCLs) are directly related to the assumed hydraulic conductivity of the bentonite clay. The hydraulic conductivity of the sodium bentonite clay component of GCLs is based on fluid flow through a porous medium, in accordance with Darcy's Law, and is typically measured by ASTM D 5084. When the GCL is placed as a primary liquid barrier without a geomembrane, liquid flow rate through the GCL would generally be estimated by Darcy's law as:

$$Q = kiA$$

where q = liquid flux in units of $m^3/s/m^2$; k = hydraulic conductivity of the GCL in units of m/s; i = hydraulic gradient across the GCL, and A = area of the GCL normal to the flow in units of m^2. This equation assumes that the GCL is the predominant barrier, and that planar-series effects of other layers are negligible in the cross-plane hydraulic conductivity.

If the GCL is used as part of a composite liner in contact with a geomembrane, the liquid flow rate through a defect in the geomembrane is generally estimated using the "Giroud equation" as follows:

$$Q = C\,[1 + 0.1(h_w / t)^{0.95}]\; a^{0.1}\, h_w^{0.9}\, k^{0.74} \qquad (3.1)$$

where: C = a constant related to the quality of the intimate contact between the geomembrane and underlying clay liner; h_w = head of liquid on top of the geomembrane (m); t = thickness of the soil component of the composite liner (m); a = area of defect in geomembrane (m^2).

In either case, it can be seen that the value of the GCL hydraulic conductivity, k, is a predominant factor in controlling the leakage rate. The hydraulic conductivity of sodium bentonite is affected by two principal variables: (1) the level of normal or effective stress applied to the GCL, and (2) chemical alterations caused by different permeating liquids that change the hydraulic conductivity of the sodium bentonite. This paper reports the results of laboratory testing that explores the combined effects of both of these two variables.

2. BACKGROUND DISCUSSION RELATED TO EFFECTS OF EFFECTIVE STRESS

Effective stress is a significant variable that controls the behavior of bentonite. It decreases both hydraulic conductivity, and the susceptibility of bentonite to chemical alterations (discussed in Section 3). Increasing the effective stress on a GCL decreases the void ratio (or porosity) within the bentonite layer, which tends to lower its hydraulic conductivity. This tendency toward decreased hydraulic conductivity in response to increased effective stress is a basic characteristic of virtually all soils and other porous materials.

Figure 1 shows the relationship between hydraulic conductivity to water and effective stress for several types of GCLs as reported by Dr. Dave Daniel (Thiel et al., 2001). The differences in hydraulic conductivity between various GCLs are minimal, except at very low effective stresses where internally reinforced and non-internally reinforced GCLs behave slightly different in response to variations in effective stresses. The GCLs that have internal reinforcement (e.g., geotextile-encased, needlepunched GCLs) tend to have lower hydraulic conductivity with minimal confinement because as the bentonite hydrates and swells, the needlepunched fibers hold the encasing geotextiles together, thereby providing confinement and effective stress upon the bentonite. At high normal stresses, the differences in hydraulic conductivity between the various commercial GCLs tend to be subtle.

3. BACKGROUND DISCUSSION RELATED TO EFFECTS OF CHEMICAL INTERACTIONS

3.1 General Parameters Affecting Bentonite Hydraulic Conductivity

Chemical interactions and their effect on the hydraulic conductivity of sodium bentonite in GCLs have been studied by several researchers and evaluated for numerous projects. Four chemical-interaction parameters can influence the hydraulic conductivity of bentonite: 1) dielectric constant of permeating liquid, 2) salt concentration of the permeating liquid, 3) predominant cation of the bentonite vs. those in the permeating liquid, and 4) pH of the permeating liquid.

- The dielectric constant of the permeating liquid. Water-based (aqueous) liquids all have a dielectric constant of ≈ 80, but organic liquids such as gasoline have a much lower dielectric constant (often in the range of 1 to 5). The lower the dielectric constant of the liquid in the bentonite, the less the swelling mechanisms of the bentonite are activated, and the higher is its hydraulic conductivity. Bentonites tend to swell and to be impermeable when contacted by fresh water, but not when they are contacted by chemicals such as gasoline, jet or diesel fuel, or solvents such as trichloroethylene or acetone that have a low dielectric constant. Nearly all organic liquids have a much lower dielectric constant than water, so they can therefore cause potentially large increases in

the hydraulic conductivity of bentonite. Dilute organics (for example, a few parts per million of organics dissolved in water), however, do not significantly alter the dielectric constant of water, do not impede swelling in bentonite, and do not threaten to increase its hydraulic conductivity.

- The salt concentration of the permeating liquid. Bentonites swell the most, and tend to maintain the lowest hydraulic conductivity, when contacted by typical ground- or tap-water. Salt concentrations in the tens or hundreds of parts per million are not particularly high and do not tend to greatly alter hydraulic conductivity. However, concentrations in the thousands or tens of thousands of parts per million may be sufficiently high to negatively effect significant changes in hydraulic conductivity. For example, ordinary bentonite does not swell much when mixed with seawater. If a GCL were used to contain seawater, the hydraulic conductivity of the GCL would be relatively high because of the high salt concentration in seawater. The concentration of salt in seawater is about 30,000 parts per million. In general, salt concentrations in the tens of parts per million, and perhaps up to several hundred parts per million (depending on the type of salt – see the discussion below), are not sufficiently large to pose a serious threat to GCLs in most applications. When concentrations are of a thousand parts per million or more, they become large enough to cause concern. For concentrations less than about 500 parts per million, it is the type of salt rather than the concentration that is critical.

- The cations. Perhaps the most important factor affecting the hydraulic conductivity of GCLs from a practical standpoint is the type of cation in the bentonite and the charge (called *valence*) of that cation relative to the cations in the permeating liquid. Cations are positively charged ions, and the ones most commonly found in the ground in significant concentrations exist as salt, such as NaCl. The key cations typically found in GCLs are Na^{+}, K^{+}, Ca^{++}, Mg^{++}, and Al^{+++} (sodium, potassium, calcium, magnesium, and aluminum, respectively). With bentonites, the higher the positive charge of the cation, the more permeable the bentonite. Thus, the most beneficial cations in the water are sodium and potassium, which both have a charge of +1. The least favorable cations are the polyvalent cations, which have a charge of +2 or more. Several polyvalent cations are found in soils, but calcium tends to produce by far the most significant adverse effects on bentonite swelling. The reason sodium bentonite is used in GCLs is that with sodium in the bentonite, hydraulic conductivity tends to be extremely low. If the sodium is replaced by calcium, the hydraulic conductivity can increase as much as one to two orders of magnitude. Thus, if a GCL is permeated with a calcium-rich liquid in the field, its hydraulic conductivity may increase significantly, and its sealing capacity be reduced to the point that the GCL may fail to meet the designer's expectations. Cation replacement is a potentially serious issue that should be evaluated carefully. A good discussion of the basic principles of cation exchange in GCLs can be found in Egloffstein (1997).

- The pH of the permeating liquid. The pH of the permeating liquid can also affect the hydraulic conductivity of bentonite. In cases of extremely acidic or caustic liquids (i.e., pH less than 2 or greater than 13), the liquid may be sufficiently aggressive to literally

dissolve some of the bentonite clay. If the clay is dissolved, the liquid can "eat through" the GCL and dramatically increase hydraulic conductivity. However, liquids with this capability are rare. More common are less extreme ranges of pH. Also, the greater the amount of dissolved material in the leachate, the less bentonite is affected directly by pH because the dissolved ions are much more significant than pH itself.

3.2 Other Studies

Landfill leachates can alter the hydraulic conductivity of GCLs. Ruhl and Daniel (1997) present test data on five different GCL products using several different permeant liquids, three different conditions of hydration, and an effective confining stress of 35 kPa. These GCLs maintained low hydraulic conductivity (generally $< 2\times10^{-11}$ m/s) whether they were permeated with simulated hazardous waste leachate, real MSW leachate, or simulated fly ash leachate. The hydraulic conductivity of the GCLs was not adversely affected when real leachate was used as compared to tap water. The GCLs had a relatively high hydraulic conductivity when permeated with a strong calcium solution or strong acids and bases.

Rowe (1998) suggests that the real leachate used by Ruhl and Daniel had a low concentration of cations, and he reports test values for a synthetic leachate that was modeled to have a composition quite similar to that of real leachate from the Keele Valley Landfill. (The chemical composition of the MSW leachates used by Ruhl and Daniel (1997) and by Rowe (1998) are summarized in Table 1). Rowe's results showed that, under a relatively low effective stress of 36 kPa, the hydraulic conductivity of the GCL increased by approximately a factor of 6 when permeated with the synthetic leachate as compared to tap water. However, Ruhl and Daniel (1997) found that while a synthetic leachate did cause increases in hydraulic conductivity, the real MSW leachate did not. One factor to bear in mind is that although real leachates may contain calcium and other conductivity-increasing chemicals, they also contain suspended solids (including biologically active materials) that tend to plug the pores of the bentonite and reduce hydraulic conductivity. Impacts from actual leachates may vary considerably from one leachate to another. Some of the subtleties of testing are discussed in Section 6.

Table 1. Comparison of Leachate Constituent Concentrations (mg/l unless otherwise stated).

Chemical Constituent	Leachate Used By Ruhl and Daniel (1997)	Simulated Leachate Used by Rowe (1998)	Landfill Leachates Used in the Present Study		
			MSW Landfill Leachate	Ash Landfill Leachate	Pulp&Paper Landfill Leachate
Sodium	368	1615	2900	5060	4350
Potassium	N/A	354	188	3170	331
Calcium	112	1224	337	8170	105
Magnesium	100	473	359	311	374
Chloride	520	4414	5600	33000	3000
Ammonia (NH4)	N/A	618	260	16	94
BiCarb. (HCO3)	N/A	4876	2500	7	7670
SO4	N/A	137	55	800	120
TDS	1800	N/A	11000	50000	12000
TOC	312	N/A	310	30	460
PH (pH units)	7	6.2	8.5	7.0	7.6

N/A = Not available

As mentioned in the previous subsection, the effective stress placed on sodium bentonite influences hydraulic conductivity. Effective stress has a major impact on the susceptibility of GCLs to alterations caused by cation exchange. This issue was limitedly explored by Dave Daniel (Thiel et al., 2001) and is illustrated in Figure 2 for a geotextile-encased GCL that was permeated with either distilled water or a 0.125 molar solution of $CaCl_2$ (5,000 mg/l of calcium). In the tests using $CaCl_2$, a worst-case condition was employed of hydration with the same $CaCl_2$ solution that was used for permeation. At low effective stress, the GCL was about three orders of magnitude more permeable to the calcium chloride solution than to distilled water. However, at an effective stress of about 400 kPa, the hydraulic conductivity was about the same for water as for the calcium chloride solution. Although calcium tends to cause shrinkage of the bentonite and the development of a more permeable fabric of bentonite particles, the application of a high effective stress was presumed to squeeze the bentonite particles together strongly enough to prevent deleterious alterations in the arrangement of bentonite particles.

4. OUTLINE OF LABORATORY INVESTIGATION

The laboratory investigations presented in this paper were performed to determine the hydraulic conductivity of GCLs when permeated with three different types of waste leachate under various effective stresses. The duration of the testing ranged from approximately 4-11 weeks and was dictated by project and laboratory constraints. The material that was tested was a double-nonwoven needlepunched GCL provided by CETCO, having an average bentonite mass per unit area of 4,170 g/m^2. The following three leachates were provided:

- Leachate from a "standard" large MSW landfill.
- Leachate from incinerator ash that was created from burning MSW.
- Leachate from a forest-products landfill whose waste consisted primarily of pulp & paper sludge and boiler ash from a paper mill. This is referred to as pulp&paper (P&P) leachate.

A summary of the more pertinent constituents is presented in Table 1 to allow side-by-side comparisons. Laboratory testing was performed in accordance with ASTM D5084. Table 2 presents a matrix showing the effective stress applied to the various specimens, time periods of testing, and estimated number of pore volumes passed through the specimens.

4.1 Bentonite Pre-hydration on Subgrade Soils

In the field GCLs will generally be in place on a natural soil subgrade for weeks, if not months, before there is an opportunity for exposure to leachate. Work by Daniel et al. (1993) has shown that the high matric-suction of bentonite will cause it to undergo substantial hydration under these conditions even with relatively dry natural subgrade soils. This phenomenon was simulated in the current test program by placing the as-received GCL samples on project-specific subgrade soils representing two of the projects for which the testing was being performed. The soil was a silty-sand with a natural water content of approximately 27%. The gain in water content versus time for the GCL samples is presented in Figure 3. The samples tested with the MSW and incinerator ash leachates were removed from the subgrade soil after 3 weeks. The samples tested with the P&P leachate were left on the subgrade soil an additional 2 weeks before commencing hydraulic conductivity testing.

4.2 Permeability Testing – General Procedure

The samples were tested for hydraulic conductivity in triaxial pressure cells in accordance with ASTM D5084. All of the samples were backpressure saturated using their respective leachates as the saturating fluid. Table 2 presents details related to effective pressures, and hydraulic gradients used during the testing. For purposes of calculating the conductivity during testing, the initial thickness of the samples was used. The conductivity was corrected using the final sample thickness that was determined after testing. The permeability tests were conducted using the falling-head, rising-tailwater method (Method C). Hydraulic gradients vary during the testing for this method. For this test program the gradients ranged from 10 to 500. The higher gradients were used where the samples exhibited lower hydraulic conductivity so that meaningful test results could be obtained in a reasonable period of time. Although this range of gradients exceeds the maximum gradient of 30 recommended by ASTM D5084, data published by Shackelford et al. (2000) and others have reported that higher gradients are acceptable for testing GCLs. The main reason that higher gradients might be acceptable for GCLs is that the variation in effective stress due to the hydraulic gradient across a specimen is far less for thin GCLs than for thicker soil specimens. The range of hydraulic gradients used in the test program described herein is considered quite appropriate and representative of the standard of practice applied to GCLs.

The effective pressures were selected unique to the landfills for which the studies were being performed, and were therefore not the same pressures for each of the three leachates. The original intent of the work was to evaluate the hydraulic performance of the GCL material to each of the leachates at pre-selected effective pressures that were to be held constant. The pressures selected for the basic testing program are presented on Table 2. During the testing of the MSW and incinerator-ash leachates, however, there was a compressor failure and accidental pressure changes occurred that led to further investigation on the results of pressure changes. The series of pressure changes that occurred with the MSW and incinerator ash leachates (either accidentally or intentionally) are described in the Section 5.

4.3 Measurement of Specimen Thickness

The test method for hydraulic conductivity requires measurement or estimation of the specimen thickness, *t*. The reported hydraulic conductivity values in ASTM test method D5084 are directly proportional to the measured or assumed values of *t*. Normally, with soil specimens prepared for this test method, *t* is measured before and after the test with a calipers or other direct-measuring device. With fabric-supported GCLs the measurement is complicated by the presence of the geotextiles. The assumed value of *t* used to calculate the hydraulic conductivity of a GCL is intended to represent the thickness of the bentonite portion of the GCL. The thickness of the entire GCL specimens may or may not be representative of the value *t* depending on whether or not the bentonite extrudes into all of the pore spaces of the geotextiles, or only a portion of them. Limited guidance provided in ASTM D5887 suggests that the geotextiles could be cut away from the tested specimen and the thickness of the remaining bentonite measured directly with calipers. For purposes of this study, the hydraulic conductivity values were calculated using values of *t* wherein the thickness of the geotextile was subtracted from the total specimen thickness by the method described in the following paragraph. Note that Table 2 reports the assumed thickness of the bentonite, and the footnote at the bottom gives the average thickness of the textiles that would be added to the assumed bentonite thickness to obtain the total end-of-test specimen thicknesses, if desired.

First a 0.1 m round duplicate GCL specimen was cut from the sample next to the test specimen. The upper and lower textiles were carefully separated by cutting the connecting needle-punched fibers with a razor knife. The bentonite was carefully removed taking care to avoid additional damage to the textiles. With the bentonite removed, the halves were placed on top of each other between two 0.1 m diameter steel calibration spacers. The assembly was placed in a load frame and compressed using a 72 kPa stress. The total height of the spacer with the compressed textile was measured with a caliper in three places 120° apart. The compressed textile thickness was determined by subtracting the known calibration spacer thickness.

The same thickness measurement procedure using the steel calibration spacers was then performed on each of the hydraulic conductivity test specimens both before and after the hydraulic conductivity tests were performed. The values of *t* for each of the test specimens was calculated by subtracting the predetermined textile thicknesses from the total specimen thicknesses.

Table 2. Summary of hydraulic conductivity test parameters and results.

SAMPLE DESCRIPTION:	MSW-1	MSW-2	MSW-3	ASH-1	ASH-2	ASH-3	PPL-1	PPL-2	PPL-3
Water content as recevied. %	41	34	38	39	36	42	34	39	36
Water content, after prehydration %	61	55	58	59	57	66	67	70	66
Initial Hydrated Thickness, "L", mm	5.9	5.7	5.5	5.0	6.0	5.0	6.2	5.7	5.7
Effective confining stress, kPa	239	478	718	177	359	527	165	338	476
Test Time, days	14	13	13	6	13	13	27	27	27
Estimated Pore Volumes [(c)]	2.7	2.1	0.2	4.7	46	0.7	1.5	1.8	1.7
Hydraulic Conductivity, m/sec. [(a)]	6E $^{-12}$	1E $^{-12}$	4E $^{-13}$	5E $^{-8}$	3E $^{-11}$	9E $^{-13}$	6E $^{-12}$	1E $^{-12}$	1E $^{-12}$
AIR COMPRESSOR FAILURE									
New Effective confining Stress, kPa	SAME	SAME	SAME	SAME	SAME	SAME	**TEST**		
Additional Test Time, days	36	39	35	16	19	36	**STARTED AFTER**		
Hydraulic Conductivity, m/sec. [(a)]	3E $^{-12}$	1E $^{-12}$	5E $^{-13}$	3E $^{-8}$	3E $^{-11}$	2E $^{-12}$	**COMPRESSOR FAILURE**		
EFFECTIVE CONFINING STRESS CHANGED									
New Effective confining Stress, kPa	478	239	239	NA	718	359			
Additional Test Time, days	16	25	33	NA	44	32	**NOT**		
Hydraulic Conductivity, m/sec. [(a)]	1E $^{-12}$	3E $^{-13}$	4E $^{-13}$	NA	2E $^{-10}$	3E $^{-12}$	**INCREASED**		
Final Thickness, "L", mm	3.0	2.1	2.6	3.8	2.1	3.0	4.4	3.0	3.0
Final water content, %	109	93	101	71	48	92	91	79	70
Gradiant Range	370-50	500-400	360-230	280-90	510-10	360-70	185-90	250-150	310-220
Total Test Time, (conductivity) days	66	77	81	22	76	81	27	27	27

NOTES:

a) Hydraulic conductivities are based on the final measured bentonite thickness obtained by subtracting the measured textile thickness from the over-all, end of test specimen thickness.

b) The average textile thickness which was subtracted from the total end-of-test specimen thickness was 3 mm

c) The estimated pore volume is based on the end of test bentonite thickness.

5. RESULTS

5.1 General Trends

A summary of the hydraulic conductivity results after 3 to 6+ weeks of testing at the selected effective stresses are presented graphically in Figure 4. The results reported by Daniel (shown in Figures 1 and 2) are repeated on Figure 4 for comparison. The results from the current program show a similar pattern to the results reported by Daniel, and indicate that the relationship between hydraulic conductivity and effective confining stress is specific to a given liquid chemistry, but that at effective pressures greater than 400 to 500 kPa the hydraulic conductivity of a GCL is independent of the liquid. Relative to each of the liquids tested, the following results can be stated:

- For the P&P leachate, the GCL hydraulic conductivity behavior is similar to that of tap water.
- For MSW leachate the hydraulic conductivity at the 240-kPa load is approximately three times higher than for tap water. At the higher effective stresses that were tested of 480 and 720 kPa the results appear that they might be slightly greater than that of tap water, but for all practical purposes could be considered equal to that of tap water.
- The incinerator ash leachate is definitely the most aggressive and the GCLs hydraulic conductivity with it shows the highest sensitivity to effective stress. It appears even more aggressive than the $CaCl_2$ solution results reported by Daniel (Thiel et al., 2001). Even so, at an effective stress of 500 kPa the results with the ash leachate were equivalent to the results for the other leachates.

5.2 Variation of Testing Pressures

After approximately 12 to 13 days of testing the MSW and incinerator ash leachates there was an air compressor failure. This had the effect of reducing the effective pressure to near zero for a period of approximately 24 hours. During this time the samples would have had the opportunity to swell, absorb more leachate, and possibly more easily allow chemical degradation of the bentonite. In the interest of investigating the effects of pressure changes, the testing was continued to see what would happen to the hydraulic conductivity. Due to the uncontrolled volume swings and potential leaks in the system during the compressor failure, the hydraulic conductivity readings in the period of time for several days after the compressor failure are not considered valid. Eventually, the samples re-stabilized under the original pressure. With the exception of test nos. ASH-2, ASH-3, and MSW-1 all of the measured hydraulic conductivities returned to the pre-failure readings and some even decreased. The specimen for ASH-3 increased in hydraulic conductivity only very slightly. A summary of the results are presented in Table 2, and the hydraulic conductivity values vs. time and pressure-change events are shown in Figure Nos. 5-13.

After the experience of the compressor failure and re-stabilization, there was still enough leachate to continue running the samples for one to two more weeks. A decision was made to intentionally change the effective confining stresses and note the effects. The effective stress was doubled (increased by 100%) on test nos. MSW-1 and ASH-2; reduced by 32% on test no. ASH-3; reduced by 50% on test no. MSW-2; and reduced by 66% on test no. MSW-3.

Test no. MSW-1 behaved as might have been predicted. That is, the hydraulic conductivity showed a decreasing trend after increasing the effective pressure. This cause-and-effect conclusion may not be so clear, however, when the results for test nos. MSW-2 and MSW-3 are examined. In these cases, the effective stress was decreased. Initially after the decrease in effective stress the hydraulic conductivity increased, as would be expected. After several days, however, and until the end of the tests, the final hydraulic conductivity decreased to below its starting value, which is exactly the opposite of what would have been predicted. Part of this phenomenon may be due to biological activity, as discussed later.

Test no. ASH-2 appeared unaffected by an increase in effective stress, and towards the end of the test showed possible signs of hydraulic conductivity increases. The test was terminated too early, in the opinion of the authors, to allow any conclusion regarding the final trend in the hydraulic conductivity caused by the last few data points.

Results for test no. ASH-3 were only slightly affected by the decrease in effective stress. The higher hydraulic conductivity value for the last data point would be considered an outlier, and cannot be considered statistically significant to establish any trend at the end of the test. The test had to be terminated at that point for logistical reasons.

6. DISCUSSION

The testing described in this paper was run up to 10 times longer than standard hydraulic conductivity testing that is performed on a production basis. Even so, the testing described herein would not be considered “long-term”. Shackelford et al. (2000) have suggested that “long-term” testing of GCLs might require on the order of 30 pore volumes of liquid to be confident that chemical equilibrium is achieved. They also suggested that chemical properties of the influent and effluent could be measured (e.g. pH, conductivity, and concentration of various ions) for further verification that equilibrium had been achieved. There were no provisions to measure the chemical properties of the effluent in this study, although that would be a good recommendation for future studies.

One of the subtleties of long-term hydraulic conductivity testing is the potential problem with bacteria buildup on the specimens. This condition may lead to a decrease in the apparent hydraulic conductivity. This may be the reason that the hydraulic conductivity decreased even after the effective stress was decreased for the MSW leachate test nos. 2 and 3. This phenomenon might tend to occur more often with landfill leachates that are rich in certain nutrients. Many laboratory technicians can testify to the odor that is experienced when the tests

are finished and cells are taken apart as being indicative of organic activity. Additionally, black stains are a common observation, seen on filter papers, textiles, and membranes surrounding specimens after long term testing. If the bacteria occur in the laboratory, there is a good chance it may also occur in the field, and artificial sterilization during testing may not be representative of field conditions. Adding chemicals to kill the bacteria can have the influence of altering the leachate chemistry and hydraulic conductivity.

Leachates that are high in salt content can influence flow when the temperature changes and re-crystallization of the salts occurs. As biological and chemical reactions tend to increase landfill and leachate temperatures, a decrease in temperature may occur as the leachate travels away from the center of chemical activity towards the liner containment system, causing temperatures to decrease and crystallization to occur, blocking pore space. Some sodium, calcium, and magnesium salt solutions may start to re-crystallize.

Long term tests can also allow air and gas to migrate, grow, or evolve into the pore water of the specimen causing de-saturation. Air may be a result of chemical reaction or from the apparatus back-pressure. As specimens become unsaturated, their hydraulic conductive values tend to become lower.

The calculations of pore volumes and of hydraulic conductivity from the test data are significantly influenced by the estimation of *t*. Consolidation during the test, and changes in the effective stresses during testing, changes the specimen thicknesses during the course of the test. How these changes occur during the course of testing, and how the effect of the geotextiles is taken into account, are subjects for future investigation.

7. CONCLUSIONS

The following conclusions were derived from the limited laboratory test data described in this paper:

- The hydraulic conductivity of a GCL is a function of effective confining stress. The relationship is fluid-specific.
- For the test durations described in this paper, the following relative hydraulic conductivity results were observed for a GCL that was saturated and permeated with the following leachates:
    - Leachate derived from the waste stream of a mixed newspaper recycling and kraft pulp & paper mill appeared to result in hydraulic conductivities that were essentially the same as those obtained from tap water over the range of effective stresses tested.

  - Leachate derived from an MSW landfill appeared to result in a hydraulic conductivity that was approximately three times greater than tap water at an effective stress of 240 kPa, but was essentially the same as that obtained from tap water at effective stresses greater than 475 kPa.

  - Leachate derived from an ash landfill, whose waste was obtained from incinerating MSW, appeared to result in hydraulic conductivities that ranged from approximately 5,000 times greater than that obtained with tap water at effective stresses below 200 kPa, to a value that was essentially the same as that obtained from tap water at effective stresses greater than 500 kPa.

  - The measured hydraulic conductivity of sodium-bentonite GCLs appears to be independent of the fluid chemistry at effective stresses greater than 400 to 500 kPa.

  - The results presented in this study show trends consistent with data previously reported by Daniel.

- After initial conditions stabilized in the hydraulic conductivity tests, short-term perturbations of effective stress during further testing did not appear to substantially affect the results within the time frames and number of pore volumes investigated in this study.

- The duration of testing, and consequently the number of pore-volumes of leachate that permeated through the GCL specimens, was limited in the present study such that it may not be considered to represent long-term results. Additional investigations having more pore-volumes of fluid transfer through GCL samples are needed to assess the true long-term performance of GCLs when permeated with non-standard liquids.

- Long-term testing programs may need to address practical testing issues related to bacteria buildup in the samples, and gas accumulation in the permeating liquids.

ACKNOWLEDGEMENTS

The authors are grateful to Chris Haynes of Weyerhaeuser Corporation for use of hydraulic conductivity data generated for their projects.

REFERENCES

ASTM D5084, "*Standard Test Methods for Measurement of Hydraulic Conductivity of Saturated Porous Materials Using a Flexible Wall Permeameter*", Annual Book of ASTM Standards, Vol. 04.08, American Society for Testing and Materials, West Conshohocken, Pennsylvania, USA.

Daniel, D.E., Shan, H.Y., and Anderson, J.D., 1993, "Effects of Partial Wetting on the Performance of the Bentonite Component of a Geosynthetic Clay Liner", *Proceedings of Geosynthetics '93 Conference*, Vancouver, B.C., Industrial Fabrics Association International, Roseville, MN, pp. 1483-1496.

Egloffstein, T., 1997, "Geosynthetic Clay Liners, Part Six: Ion Exchange", *Geotechnical Fabrics Report*, Vol. 15, No. 5, June/July, pp. 38-43.

Rowe, R.K., 1998, "Geosynthetics and the Minimization of Contaminant Migration through Barrier Systems Beneath Solid Waste", *Proceedings of the Sixth International Conference on Geosynthetics,* IFAI, Atlanta, GA, March 25-29, pp. 27-102.

Ruhl, J.L. and Daniel, D.E., 1997, "Geosynthetic Clay Liners Permeated with Chemical Solutions and Leachate", *Journal of Geotechnical and Geoenvironmental Engineering*, ASCE, Vol. 123, No. 4, pp. 369-381.

Shackelford, C.D., Benson, C.H., Katsumi, T., Edil, T.B., and Lin, L., 2000, "Evaluating the Hydraulic Conductivity of GCLs Permeated with Non-standard Liquids", *Geotextiles and Geomembranes*, V18, pp. 133-161.

Thiel, R., Daniel, D.E., Erickson, R., Kavazanjian, E., and Giroud, J.P. (2001) *GundSeal GCL Design Manual*. Published by GSE, Houston, TX.

NOTATIONS

Basic SI units are given in parentheses.

a	=	area of defect in geomembrane (m^2)
A	=	cross sectional area of fluid flow (m^2)
C	=	constant related to the quality of the intimate contact between the geomembrane and underlying clay liner (dimensionless)
h_w	=	head of liquid on top of the geomembrane (m)
i	=	fluid gradient (dimensionless)
k	=	hydraulic conductivity of soil or geosynthetic to a particular fluid (m/s)
Q	=	volumetric flow rate (m^3/s)

t = thickness of soil component of composite liner (m)

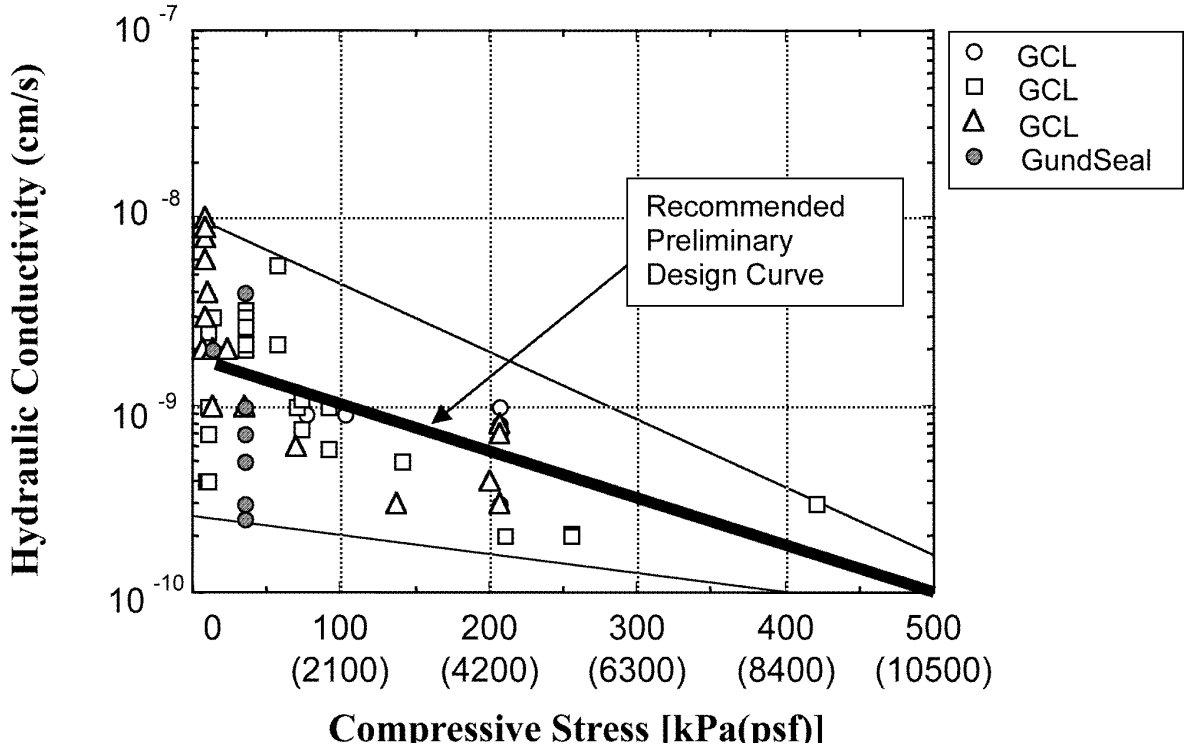

Figure 1. Hydraulic Conductivity as a Function of Effective Confining Stress. (from Thiel et al., 2001) ***[Note: Hydraulic conductivity units are presented in non-SI units of cm/s because the figure was obtained from the original reference. This is being corrected.]***

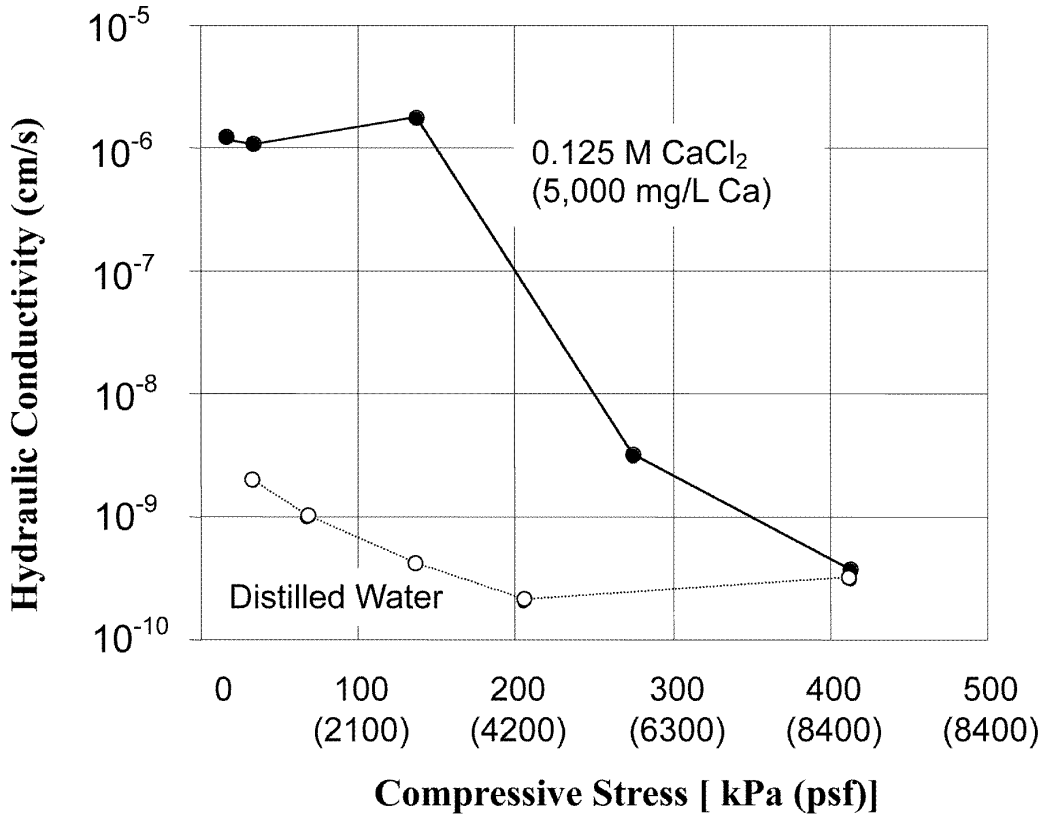

Figure 2. Influence of Effective Stress on the Hydraulic Conductivity of GCLs Permeated with Distilled Water or with a Very Strong Calcium Solution (from Thiel et al., 2001) ***[Note: Hydraulic conductivity units are presented in non-SI units of cm/s because the figure was obtained from the original reference. This is being corrected.]***

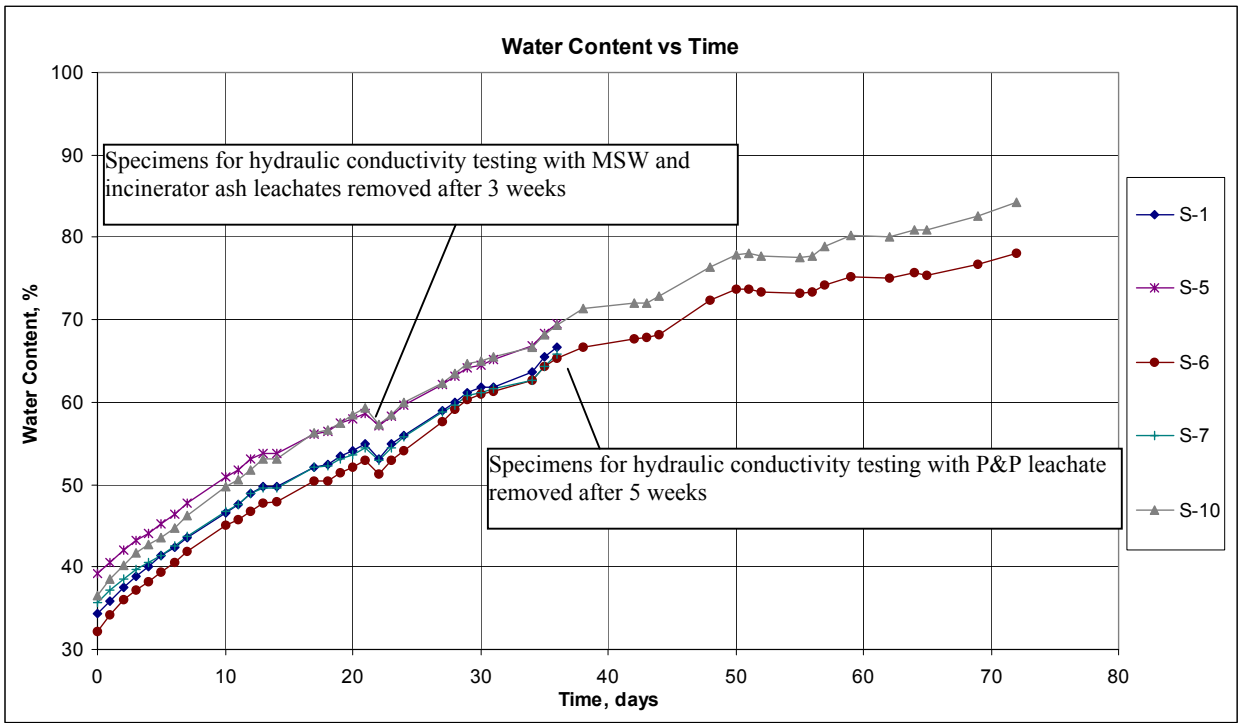

Figure 3. Water Content vs. Time for GCL Samples on Silty Sand Soil with Soil wc = 27%

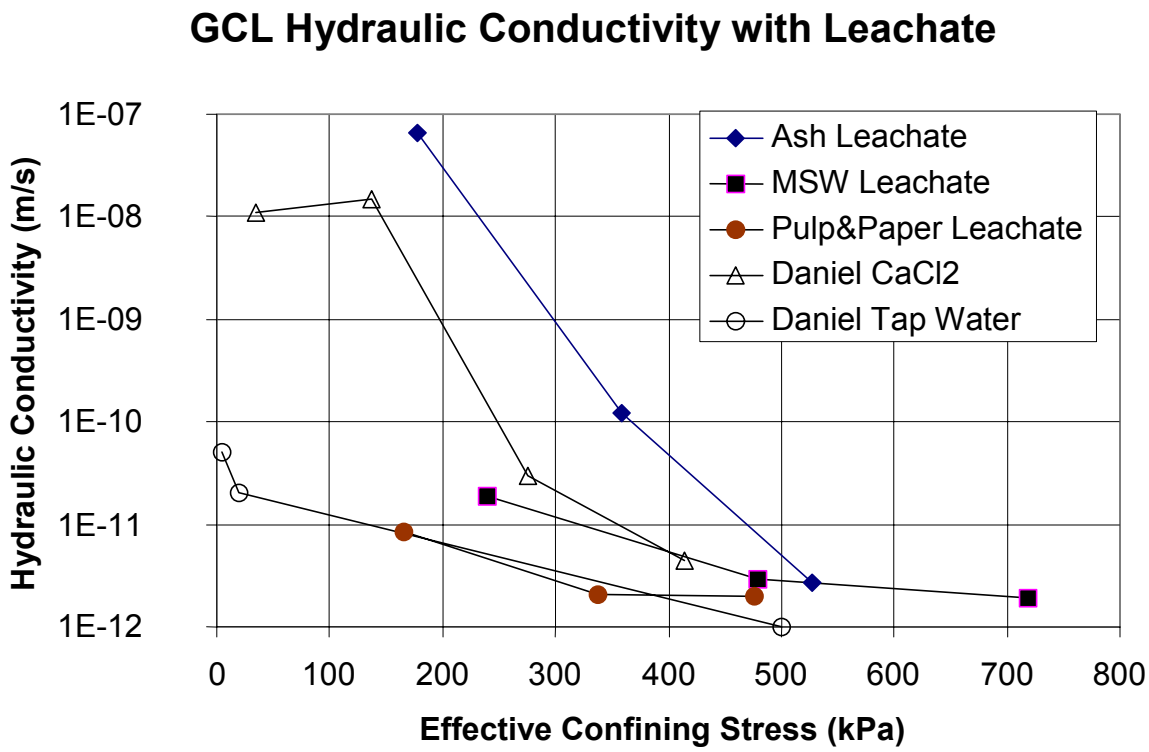

Figure 4. Summary Results for Hydraulic Conductivity of GCL vs. Effective Confining Stress for Three Different Leachates.

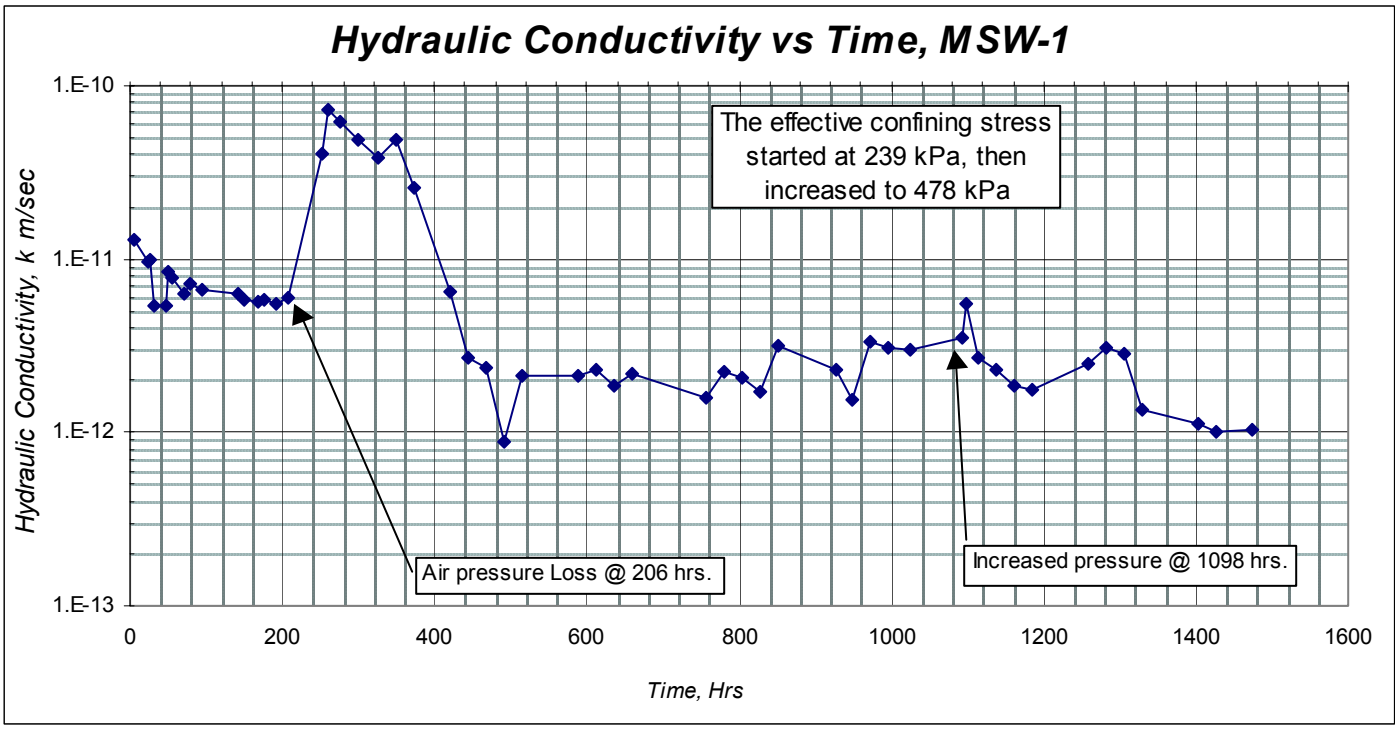

Figure 5. Time vs. hydraulic conductivity for specimen MSW-1 tested with MSW leachate at low initial effective stress (239 kPa).

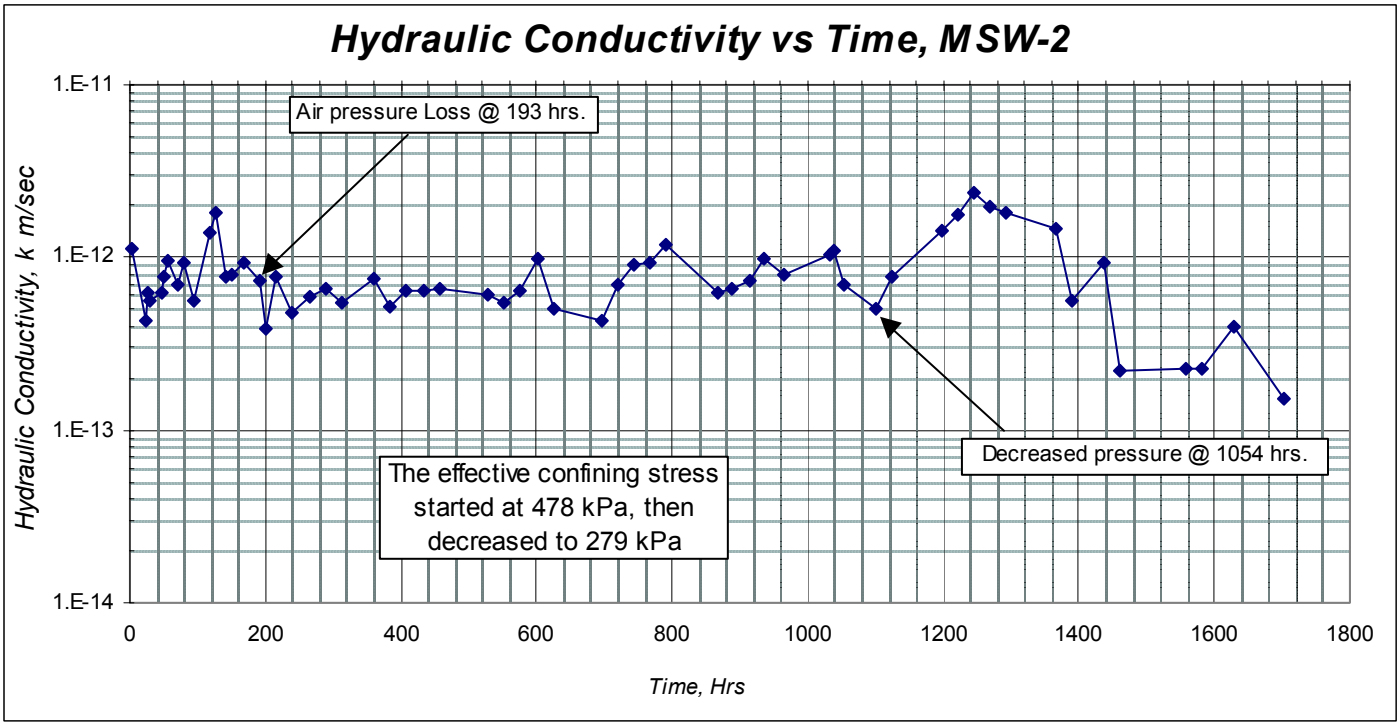

Figure 6. Time vs. hydraulic conductivity for specimen MSW-2 tested with MSW leachate at medium initial effective stress (478 kPa).

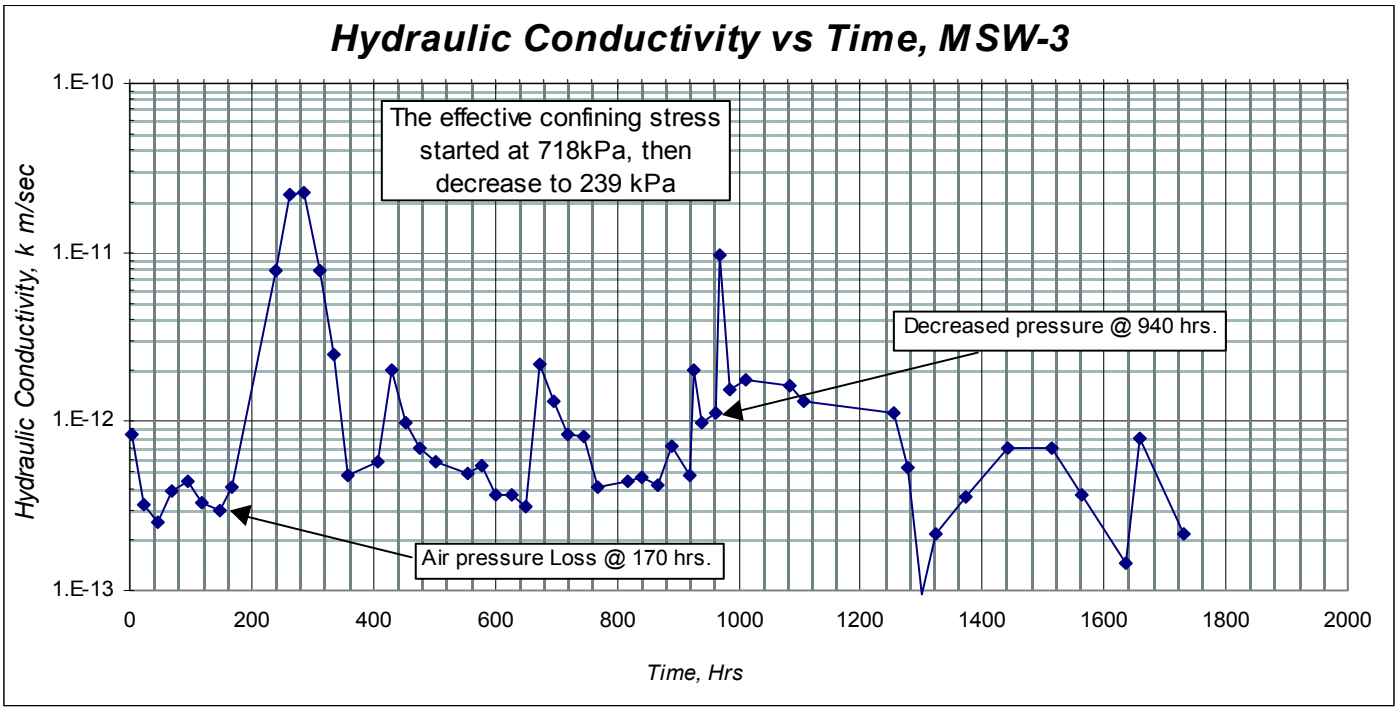

Figure 7. Time vs. hydraulic conductivity for specimen MSW-3 tested with MSW leachate at high initial effective stress (718 kPa).

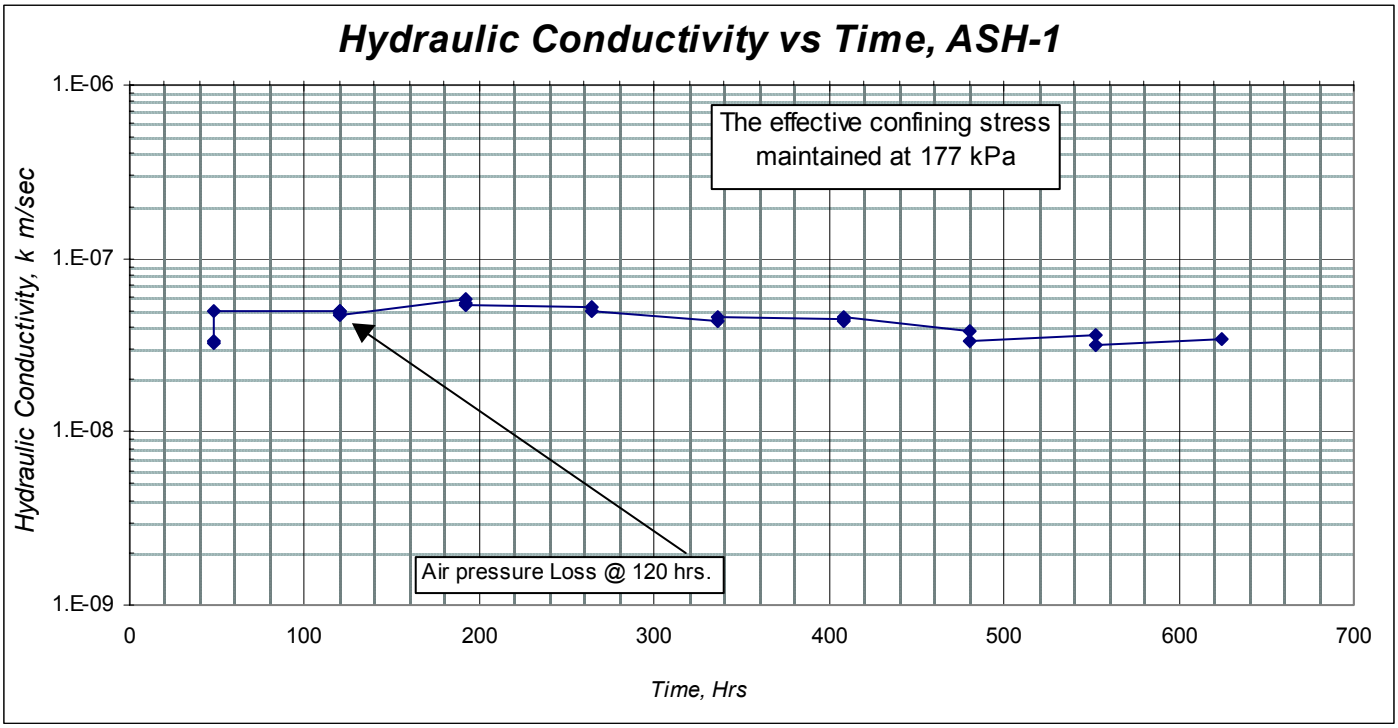

Figure 8. Time vs. hydraulic conductivity for specimen ASH-1 tested with incinerator ash leachate at low initial effective stress (177 kPa).

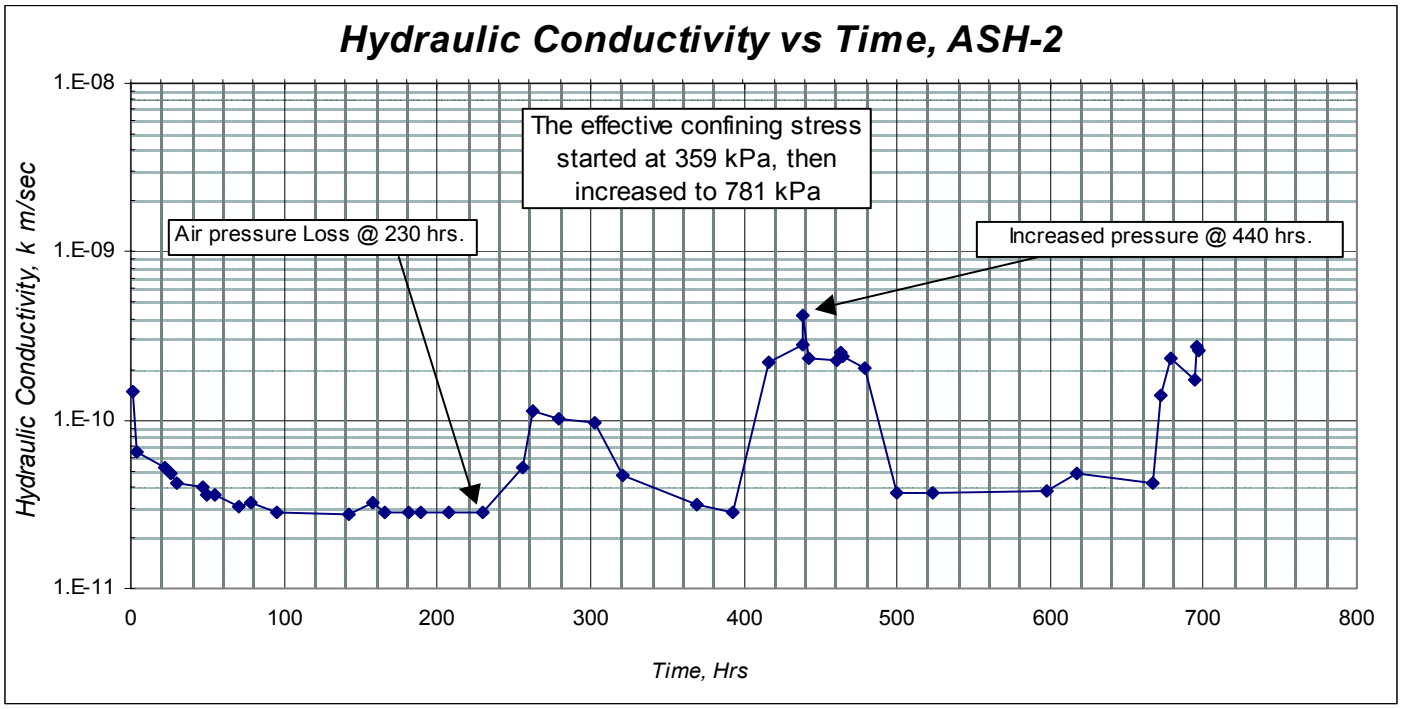

Figure 9. Time vs. hydraulic conductivity for specimen ASH-2 tested with incinerator ash leachate at medium initial effective stress (359 kPa).

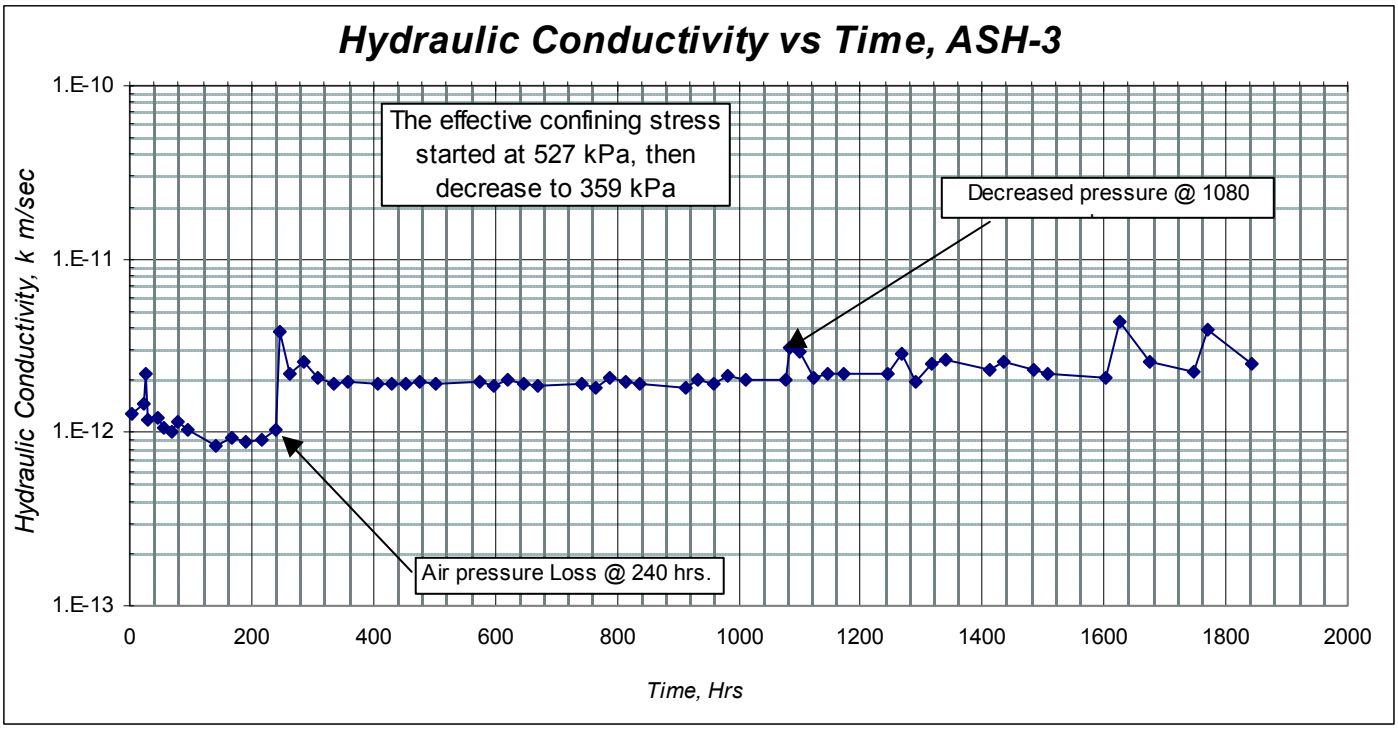

Figure 10. Time vs. hydraulic conductivity for specimen ASH-2 tested with incinerator ash leachate at high initial effective stress (527 kPa).

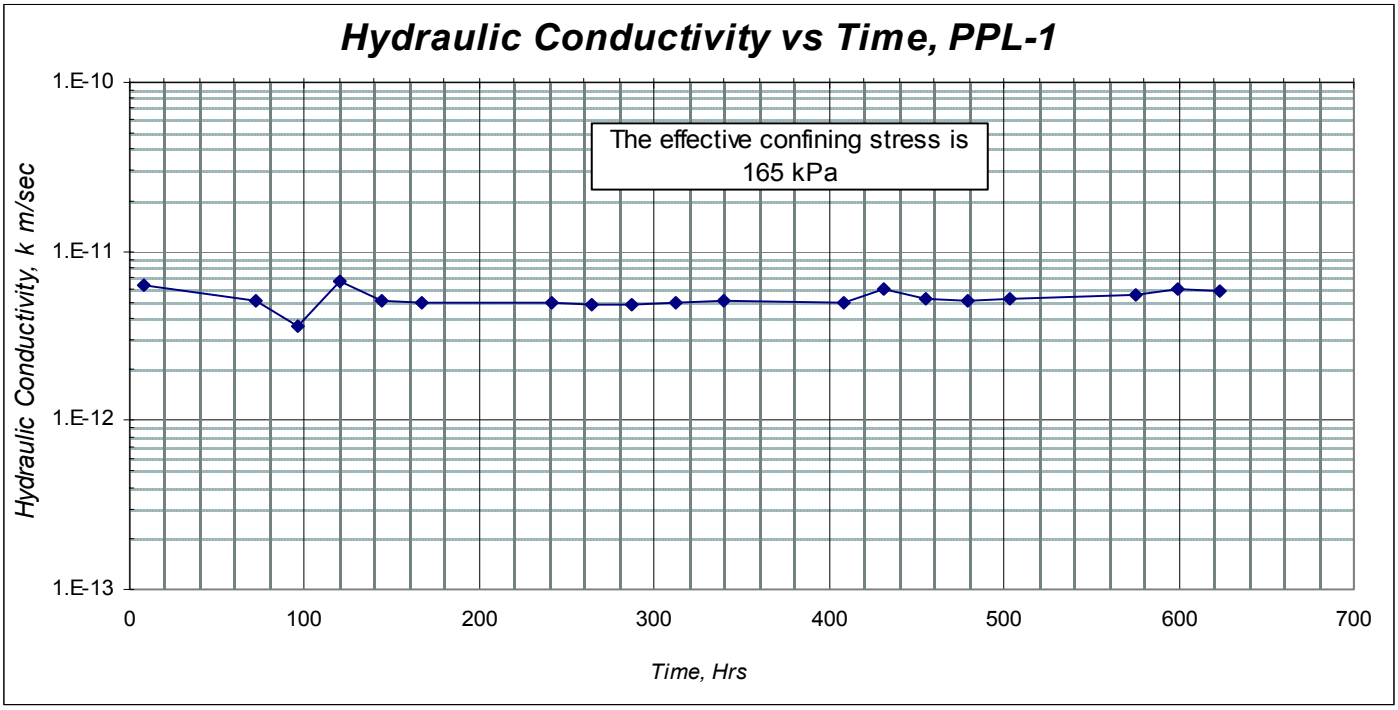

Figure 11. Time vs. hydraulic conductivity for specimen PPL-1 tested with pulp&paper waste leachate at low initial effective stress (165 kPa).

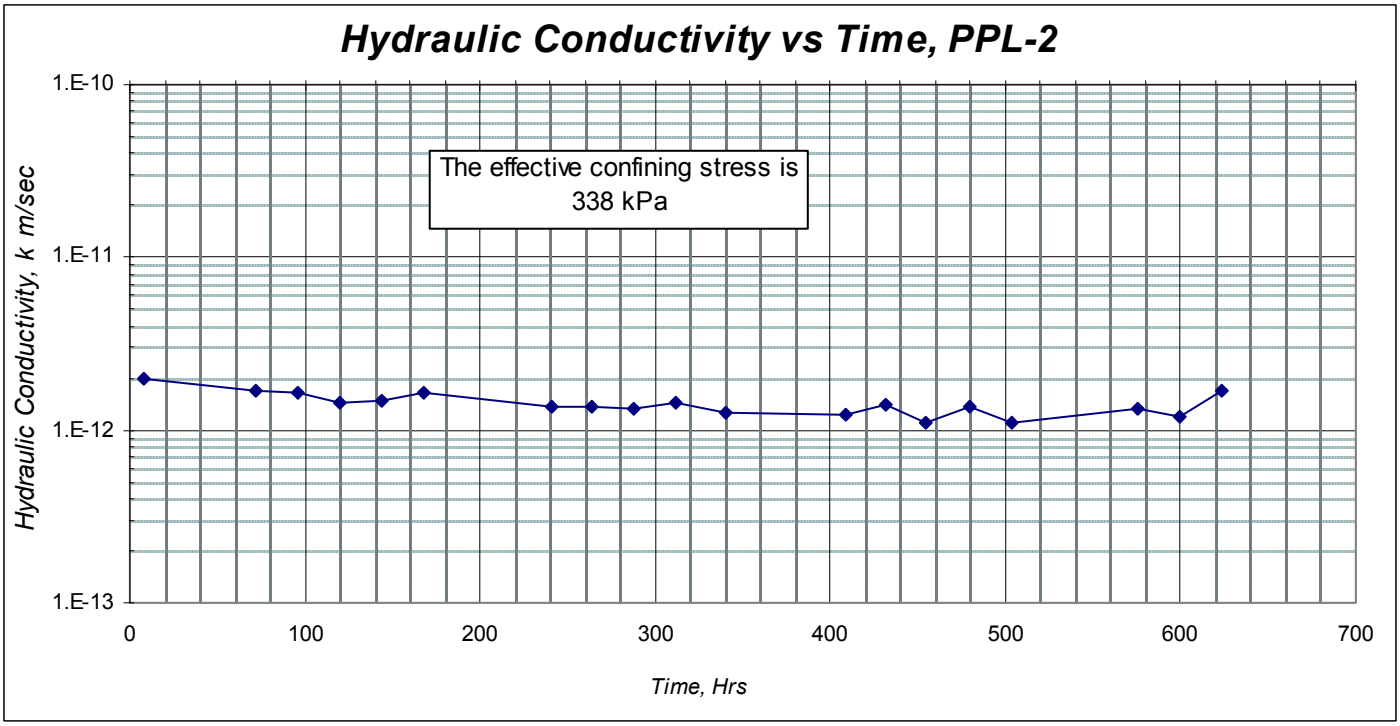

Figure 12. Time vs. hydraulic conductivity for specimen PPL-2 tested with pulp&paper waste leachate at medium initial effective stress (338 kPa).

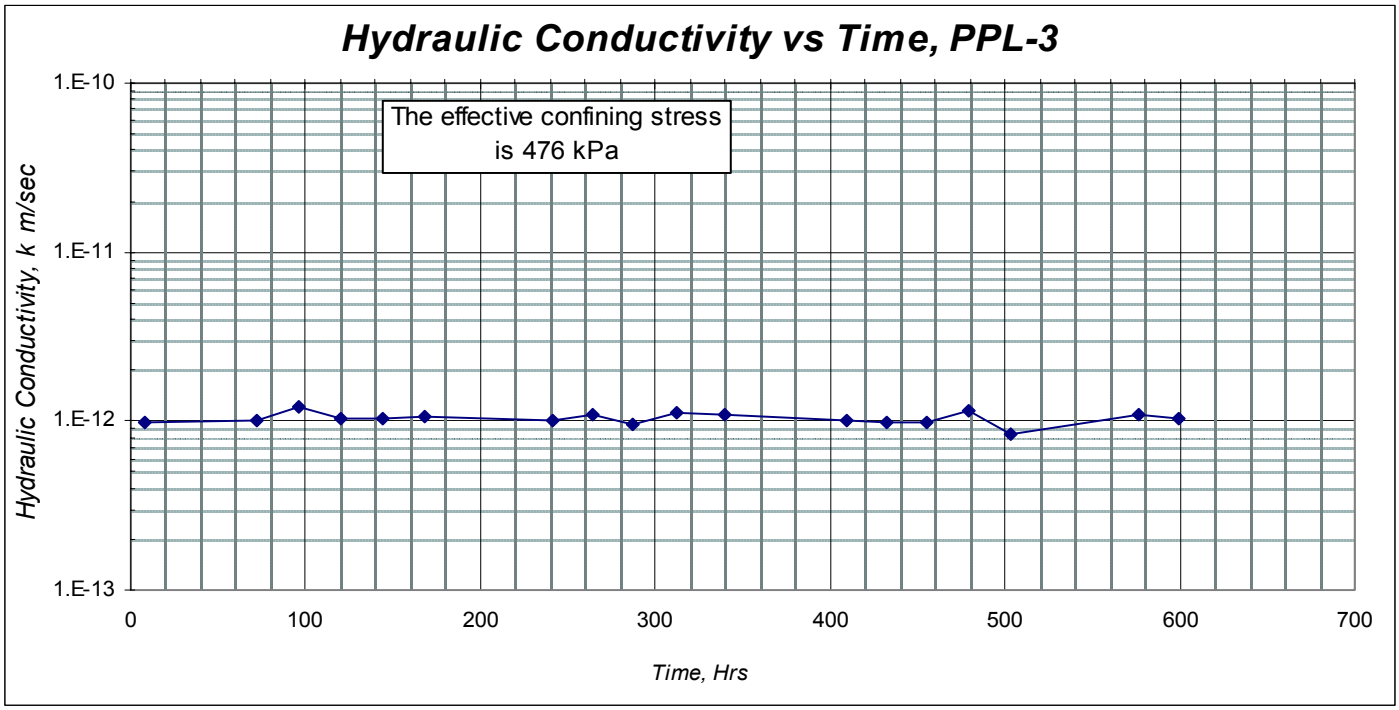

Figure 13. Time vs. hydraulic conductivity for specimen PPL-3 tested with pulp&paper waste leachate at medium initial effective stress (476 kPa).